UNIVERSITY OF SOUTHAMPTON

FACULTY OF NATURAL AND ENVIRONMENTAL SCIENCES

Centre for Biological Sciences

Exploring the Roles of Membrane Proteins in Manganese Homeostasis of Higher Plants

by

Emily Christobel Farthing

Thesis for the degree of Doctor of Philosophy

September 2016

UNIVERSITY OF SOUTHAMPTON

ABSTRACT

Thesis for the degree of Doctor of Philosophy

Exploring the Roles of Membrane Proteins in Manganese Homeostasis of Higher Plants

Emily Christobel Farthing

Manganese (Mn) is an essential heavy metal micronutrient in plant growth and development, but becomes toxic when present in excess, with potential agricultural yield losses under both nutritional extremes. Membrane transporters play a key role in enabling plant growth under Mn deficiency and toxicity. This study directly compares the roles of members from different ubiquitous transporter families in Mn homeostasis: Group 8/9 members of the Metal Tolerance Proteins (MTPs), At MTP8–MTP11; At ECA3, a P_{2A}-type ATPase; and Natural Resistance Associated Macrophage Proteins, At NRAMP1 and At NRAMP2.

MTP8 plays a significant role in Mn detoxification at the tonoplast, conferring Mn hypertolerance when overexpressed; it is also the only Group 8/9-MTP involved in alleviating Mn/iron antagonism. A role in Mn detoxification is also assigned to MTP10, identified through comparison of novel double and triple *mtp* knockout mutants. Expression in yeast provides evidence that these proteins can transport Mn, with greater Mn tolerance conferred by MTP8 and MTP10 than MTP11.

ECA3 is also shown to play a minor role in conferring tolerance to Mn toxicity *in planta*, but this is only apparent when MTP11 is non-functional; its major role appears to lie in alleviating Mn deficiency. This thesis also clarifies the disputed subcellular localisations of ECA3 and MTP11, demonstrating targeting to the trans- and cis-Golgi, respectively. Additionally, NRAMP2 is shown to alleviate Mn deficiency at the cis-Golgi. Characterisation of double and triple mutants has begun to clarify the relative contribution of NRAMP1, NRAMP2 and ECA3 in Mn deficiency. The use of mutants in this study has also highlighted the antagonistic effects of calcium in Mn homeostasis.

Overall, this study provides a more comprehensive understanding of how key transporters function together in Mn homeostasis, identifying targets that may be useful for crop improvement.

Table of Contents

Table (of Conte	ntsi
List of	Tables	vii
List of	Figures .	ix
DECLA	RATION	OF AUTHORSHIPxvii
Ackno	wledgen	nentsxix
Definit	tions and	d Abbreviationsxx
Chapte	er 1:	General Introduction 1
1.1	Eleme	nts of Plant Nutrition1
	1.1.1	Macronutrients and micronutrients are both essential for plant nutrition:
	1.1.2	Plant development and function is highly influenced by Mn availability .2
1.2	Manga	anese nutrition for human health10
1.3	The us	se of membrane transporters in Mn homeostasis of higher plants10
	1.3.1	Acquisition from the soil: lessons learnt from iron uptake11
	1.3.2	Cytoplasmic detoxification of Mn13
	1.3.3	Cation Diffusion Facilitators (or Metal Tolerance Proteins) transport
		divalent metal cations from the cytoplasm16
	1.3.4	P2A-type ATPases are calcium pumps with an affinity for manganese20
	1.3.5	NRAMPs are important transporters of Mn and other divalent metal
		cations32
1.4	Regula	ation of heavy metal homeostasis35
1.5	Potent	tial application of knowledge37
1.6	Overa	Il Aims of the Project38
Chapte	er 2:	Materials and Methods 42
2.1	Plant g	growth and materials42
	2.1.1	Growth conditions for soil-grown Arabidopsis thaliana and Triticum
		aestivum42
	2.1.2	Generating double mutants in Arabidopsis42
	2.1.3	Isolating stably transformed Arabidopsis lines44

	2.1.4	Metal Tolerance Assays in Arabidopsis thaliana	.44
	2.1.5	Metal Tolerance Assays in Triticum aestivum	.48
2.2	Bacteria	I and yeast growth and materials	.48
	2.2.1	Culture of Bacteria	.48
	2.2.2	Preparation of Chemically Competent E. coli	.48
	2.2.3	Preparation of Electro-competent Agrobacterium	.50
	2.2.4	Transformation of Competent Bacteria	.50
	2.2.5	Purification of plasmid DNA from bacterial cells	.51
	2.2.6	Growth of Saccharomyces cerevisiae	.51
	2.2.7	S. cerevisiae transformation	.51
	2.2.8	Metal assays in <i>S. cerevisiae</i>	.52
2.3	Molecul	ar methods and techniques	.53
	2.3.1	Extraction of RNA from Arabidopsis thaliana and Triticum aestivum	.53
	2.3.2	cDNA synthesis	.53
	2.3.3	Reverse Transcriptase PCR (RT-PCR) and gel electrophoresis	.53
	2.3.4	Quantitative PCR (qPCR) to Assess Gene Expression	.54
	2.3.5	Generating expression clones and constructs	.56
2.4	Localisa	tion studies	.60
	2.4.1	Transient expression in tobacco	.60
	2.4.2	Observation of fluorescence	.60
2.5	Bioinfor	matics	.62
Chapte	er 3:	Bioinformatics and Mutant Analysis to Investigate the Metal Toleran	ice
	Protei	ns	65
3.1	Introduc	ction and Aims	.65
	3.1.1	Bioinformatics	.67
	3.1.2	Use of mutants as a tool for investigating transporter function	.68
	3.1.3	Ethyl methanesulfonate mutagenesis and forward genetics	.69
	3.1.4	Artificial microRNA (amiRNA) as a tool for downregulation	.69
	3.1.5	Downregulating wheat genes with RNAi	.73
	3.1.6	Aims	.74

3.2	Results	75
	3.2.1	Bioinformatic analysis of At MTP8 – MTP1175
	3.2.2	Using Genevestigator for expression analysis of At MTP8-1175
	3.2.3	Isolating T-DNA insertion mutants for At MTP8-1185
	3.2.4	MTP8 and MTP11 are essential for alleviating Mn toxicity in Arabidopsis89
	3.2.5	954-12 is an EMS mutant with a similar phenotype to mtp8 insertion
		mutants102
	3.2.6	Exploring the possibility that MTP9 and MTP10 share a functional
		redundancy109
	3.2.7	Generating an RNAi knockdown mutant for Ta MTP8 and MTP8.1113
3.3	Discussi	ion118
	3.3.1	Identifying homologous proteins in more agriculturally relevant species 118
	3.3.2	Predicted expression patterns of At MTP8 – 11120
	3.3.3	At MTP8 and At MTP11 are essential for manganese homeostasis121
	3.3.4	Mn toxicity is exacerbated by lower Ca availability122
	3.3.5	MTP8 is the key Arabidopsis Mn-MTP involved in alleviating Mn/Fe
		antagonism123
Chapt	er 4:	Functional analysis of MTPs using transgenic plants125
4.1	Introdu	ction and Aims125
	4.1.1	Transgenic plants as a tool for overexpression and complementation
	4.1.1	studies
	4.1.2	Determination of subcellular localisation to investigate protein function 126
	4.1.3	Aims
4.2		
4.2	Results	127
	4.2.1	Cloning of Arabidopsis group 8/9 MTPs127
	4.2.2	Phenotypic analysis of stably transformed Arabidopsis lines128
	4.2.3	Determining subcellular localisation with stable and transient expression
		in Arabidopsis and tobacco143

	4.3.1	Overexpression of At MTP8 confers marked tolerance to Mn via	
		vacuolar sequestration1	L47
	4.3.2	At MTP11 and At MTP10 localise to different parts of the Golgi1	L50
	4.3.3	Os MTP11 restores the Mn-dependent phenotype of Arabidopsis	
		mtp11-3	l51
Chapte	er 5:	Functional analysis of MTPs using heterologous expression in yeast 1	L 53
5.1	Introduc	ction and Aims1	153
	5.1.1	Using yeast mutants to investigate MTP transport ability	153
	5.1.2	Site-directed mutagenesis to determine functionally important residue	es155
	5.1.3	Aims	L57
5.2	Results.		L57
	5.2.1	Generating yeast expression clones for At MTP8 and MTP11	157
	5.2.2	At MTP8, MTP10 and MTP11 function as Mn transporters when	
		expressed in yeast1	L59
	5.2.3	At MTP8, MTP10 and MTP11 target Golgi-like compartments in yeast1	L59
	5.2.4	Identifying potentially important residues for Mn-MTP function1	L66
	5.2.5	Generating site-directed mutants for At MTP8 and At MTP11 and	
		assessing their effect on function and specificity	L70
	5.2.6	Modelling the potential tertiary structure of At MTP8	L75
5.3	Discussion	on1	l81
	5.3.1	At MTP8, At MTP10 and At MTP11 target the Golgi when expressed in	I
		yeast1	181
	5.3.2	MTP8 and MTP10 are strong Mn transporters1	L84
	5.3.3	DxxxD domains play important roles in Mn-MTP function1	L85
Chapte	er 6:	The Roles of At ECA3, At NRAMP1 and At NRAMP2 in Mn Deficiency	189
6.1	Introduc	ction and Aims1	189
	6.1.1	Aims1	L90
6.2	Results.	1	190
	6.2.1	Three nramp1 mutants display different levels of sensitivity to Mn	
		deficiency1	190

	6.2.2	At NRAMP2 is involved in alleviating Mn deficiency	.197
	6.2.3	At NRAMP2 targets the cis-Golgi when expressed in tobacco	.201
	6.2.4	Elucidating the function of ECA3 in Mn homeostasis	.206
	6.2.5	Exploring the contribution of At ECA3, At NRAMP1 and At NRAMP2 i	n
		Mn deficiency	.212
6.3	Discussi	on	217
	6.3.1	The intermediate sensitivity of nramp1-2 to Mn-deficiency may be d	ue
		to translation of a truncated At NRAMP1	217
	6.3.2	NRAMP2 is involved in alleviating Mn deficiency at the cis-Golgi	221
	6.3.3	At ECA3 is a transporter with a major role in alleviating Mn deficience	у,
		and a minor role in Mn toxicity	.221
	6.3.4	Exploring the relative importance of At NRAMP1, At NRAMP2 and At	ţ
		ECA3 in Mn homeostasis	223
Chapt	er 7:	General Discussion	.227
7.1	At MTP	8, MTP10 and MTP11 all contribute to Mn tolerance	227
	7.1.1	At MTP8 sequesters excess Mn into the vacuole	227
	7.1.2	At MTP10 and At MTP11 detoxify Mn at different subcompartments	of
		the Golgi	.228
7.2	Suscept	ibility to Mn depends on Ca availability	229
7.3	At ECA3	B, At NRAMP1 and At NRAMP2 play major roles in Mn deficiency	230
7.4	An upda	ated overview of Mn homeostasis in the plant cell	230
7.5	Potentia	al applications of knowledge and future outlook	233
Apper	ndix A		237
	Reference		239

List of Tables

Table 1.1. Critical leaf sufficiency and toxicity concentrations of essential mineral elements in
non-hyperaccumulating crop species6
Table 1.2. Summary of characterised Metal Tolerance Proteins (MTPs) from plants20
Table 1.3. Examples of different types of putative calcium (Ca) transporters identified in
Arabidopsis thaliana26
Table 1.4. Key members of the NRAMP family that have been characterised to the level of
transport specifity and subcellular localisation32
Table 2.1. Accession numbers and mutant lines used in this project42
Table 2.2. Primers used to confirm zygosity of single and double <i>mtp</i> insertion mutants44
Table 2.3. Comparison of nutrient concentrations in basal-strength media
Table 2.4. Concentrations of Lombnaes nutrient solution
Table 2.5. Summary of bacterial strains used in this report48
Table 2.6. Genotypes and growth requirements of S. cerevisaie strains used
Table 2.7. Typical PCR conditions when using Biomix Red Taq or <i>Pfu</i> as polymerase54
Table 2.8. Typical PCR parameters when using Biomix Red Taq or <i>Pfu</i> as polymerase54
Table 2.9. Primers used to amplify coding sequences from cDNA for cloning into pENTR/D-TOPO
vector. 57
Table 2.10. Destination vectors used in this report57
Table 2.11. Primers used to generate site-directed mutation for At MTP8 and MTP1158
Table 2.12. Primers used to amplify RNAi to target either Ta MTP8 or MTP8.158
Table 2.13. Primers and templates involved in 4-PCR strategy to amplify amiRNA from PRS300
60
Table 2.14. Sequences of primrs I-IV to amplify MTP9 amiRNA constructs from pRS30060
Table 2.15. Components of PCRs to amplify amiRNA from pRS30060

Table 3.1. Analysis of At Mn-MTP protein sequences	74
Table 3.2. At Mn-MTP protein sequence similarity and identity	74
Table 3.3. Top 10 conditions that cause an upregulation in expression of At MTP8	76
Table 3.4. Homologous Mn MTPs identified in different cereal species	80
Table 3.5. Identification of Mn-MTP homeologues in <i>Triticum aestivum</i>	80
Table 5.1 Impact of different mutations on metal transport ability of At MTP8 and At M	/TP11
when expressed in metal-sensitive yeast mutants	179

List of Figures

Figure 1.1. Elements in Plant Nutrition
Figure 1.2. Inhibition of plant growth under Mn extremes
Figure 1.3. Strategies for iron (Fe) uptake from the soil by plants12
Figure 1.4. Metal homeostasis in a typical plant cell.
Figure 1.5. Proposed structure of Ec YiiP, the <i>E. coli</i> Zn-transporting Cation Diffusion Facilitator.
Figure 1.6. Phylogenetic relationship of land plant Metal Tolerance Proteins (MTPs)18
Figure 1.7. Two proposed detoxification mechanisms have been proposed for At MTP1123
Figure 1.8. Approximate values for Ca concentrations across a typical plant cell24
Figure 1.9. Phylogenetic tree of P-type ATPases in plant species
Figure 1.10. Post-Albers mechanism of pumping by P-type ATPases, using the rabbit SERCA1a as
an example29
an example
Figure 1.11. Phylogenetic relationship of NRAMP transporters
Figure 1.11. Phylogenetic relationship of NRAMP transporters
Figure 1.11. Phylogenetic relationship of NRAMP transporters
Figure 1.11. Phylogenetic relationship of NRAMP transporters
Figure 1.11. Phylogenetic relationship of NRAMP transporters
Figure 1.11. Phylogenetic relationship of NRAMP transporters
Figure 1.11. Phylogenetic relationship of NRAMP transporters

Figure 3.9. Confi	rmation of <i>mtp8-2 mtp11-1</i> and <i>mtp8-2 mtp10-1</i> double mutants at F	
Figure 3.10. Con	firmation of mtp8-2 mtp10-1 mtp11-1 triple mutant at RNA level	86
Figure 3.11. The	Mn-dependent phenotype of mtp11 can be induced at lower Mn	
	concentrations when there is less Ca available in the growth media.	88
Figure 3.12. The	mtp8 mutants are sensitive to elevated Mn under different Ca regime	es 89
Figure 3.13. Inse	rtion mutants for mtp8-2 and mtp11-1 display sensitive phenotypes t	o Mn
	under the low Ca regime.	90
Figure 3.14. The	mtp8 mtp11 double mutant displays an additive Mn-dependent pher	notype
	under the low Ca regime	92
Figure 3.15. The	mtp8 mtp11 double mutant displays an additive Mn-dependent pher	notype
	under the basal Ca regime.	93
Figure 3.16. Gro	wth pattern of the mtp10 mtp11 double mutant at elevated Mn	94
Figure 3.17. The	mtp8-2 mtp10-1 double mutant does not display an additive phenoty	pe on
	elevated Mn.	95
Figure 3.18. The	mtp8 mtp10 mtp11 triple mutant displays a strong additive Mn-depe	ndent
	phenotype under the low Ca regime	96
Figure 3.19. The	mtp8 mtp10 mtp11 triple mutant displays an additive Mn-dependent	t
	phenotype under the basal Ca regime.	97
Figure 3.20. Sing	le mutants <i>mtp8-2, mtp11-1</i> and <i>mtp10-1</i> do not display sensitive ph	enotypes
	under Fe or Zn extremes.	98
Figure 3.21. <i>mtp</i>	8-1 and mtp8-2 are sensitive to Fe deficiency under higher pH	99
Figure 3.22. Stur	nted and chlorotic phenotype of mtp8-2 and mtp8-2 mtp11-1 under lo	ow Fe. hig
	рН	
Figure 3 23 Stur	nted and chlorotic phenotype of mtp8-2 and mtp8-2 mtp10-1 under lo	w Fo hig
. 16u1 C J.2J. J.UI	pH	
Fig 2 24 6:		
Figure 3.24. Stur	nted and chlorotic phenotype of mtp8-2, mtp8-2 mtp10-1 and mtp8-2 mtp11-1 mutants under low Fe. high pH	•

Figure 3.25. Chlorotic phenotype of <i>mtp8</i> mutants on soil limed to pH 7.2104
Figure 3.26. The <i>mtp9-1</i> single mutant does not display a chlorotic phenotype on limed soil.10
Figure 3.27. The 954-12 EMS mutant displays a similar Mn-sensitivity to mtp8-2106
Figure 3.28. EMS mutant 954-12 displays similar phenotype to <i>mtp8-2</i> under low Fe, high pH.
Figure 3.29. Chlorotic phenotype of <i>mtp8-2</i> insertion mutant and 954-12 EMS mutant on soil
limed to pH 7.2
Figure 3.30. Mn-dependent phenotype of F2 generation 954-12 Col0 WT and 954-12 <i>mtp8-2</i> crosses.
Figure 3.31. The insertion mutant <i>mtp9-1</i> is not sensitive to Mn
Figure 3.32. Generation of amiRNA constructs to target At <i>MTP9</i>
Figure 3.33. Cloning strategy to generate concatenated RNAi hairpin targeting Ta <i>MTP8</i> and <i>MTP8.1</i> in wheat
Figure 3.34. Analysis of wheat RNAi samples targeting Ta MTP8 and MTP8.1
Figure 4.1. Cloning process to generate p35S::At MTP8 construct for plant expression127
Figure 4.2. Cloning steps for At MTP9 and MTP11
Figure 4.3. Segregation ratio analysis to achieve homozygous stably transformed Arabidopsis
seedlings at T3 generation, using p35S::At MTP8 in Columbia-8 wild type as a example129
Figure 4.4. Confirmation of transgenic Arabidopsis lines transformed with At MTP8 and At MTP11
Figure 4.5 Confirmation of transgenic Arabidopsis lines transformed with Os MTP11::GFP.131
Figure 4.6. Overexpression of MTP8 confers hypertolerance in WT Arabidopsis
Figure 4.7. Overexpression of MTP8::GFP confers hypertolerance in WT Arabidopsis134
Figure 4.8. Overexpression of At MTP8 confers hypertolerance to low Fe induced by high pH

Figure 4.9. Expression of At MTP8 complements the Mn-sensitivity of <i>mtp8-2.</i>
Figure 4.10. Expression of Os MTP11 rescues the Mn-sensitivity of <i>mtp11-3</i> 137
Figure 4.11. Expression of Os MTP11::GFP rescues the Mn-sensitivity of <i>mtp11-3</i>
Figure 4.12. Over-expression of At MTP11 in Columbia-0 WT does not enhance Mn tolerance
under low Ca regime139
Figure 4.13. Over-expression of Os MTP11 in Columbia-0 WT does not enhance Mn tolerance 140
Figure 4.14. At MTP8 localises to the tonoplast in stably transformed Arabidopsis143
Figure 4.15. Time-lapse of MTP8::GFP forming trans-vacuolar strands in tobacco cells144
Figure 4.16. Co-expression of At MTP8 with ST::RFP and LT16b::mOrange2 in tobacco145
Figure 4.17. Punctate expression of At MTP11 in Arabidopsis
Figure 4.18. At MTP11 targets the cis-Golgi when transiently expressed in tobacco148
Figure 4.19. MTP10::GFP targets the trans-Golgi <i>in planta</i> .
Figure 4.20. Os MTP11 targets the trans-Golgi when expressed in Arabidopsis and tobacco.150
Figure 5.1. Schematic illustrating use of yeast transport mutants for investigating protein
function154
Figure 5.2. Generation of yeast expression vectors for MTP8157
Figure 5.3. Functional analysis of At MTP8, MTP10 and MTP11 in the Mn-sensitive
Saccharomyces cerevisiae mutant pmr1159
Figure 5.4. Functional analysis of At MTP8, MTP10 and MTP11 in the Fe-sensitive mutant ccc1,
and Zn- and Co-sensitive mutant zrc1 cot1160
Figure 5.5. Functional analysis of At MTP8, MTP10 and MTP11 in the Fe deficiency-sensitive
Saccharomyces cerevisiae mutant fet3 fet4161
Figure 5.6. At MTP8, MTP10 and MTP11 are all expressed at intracellular membranes in yeast.
Figure 5.7. At MTP8 expression overlaps with that of Golgi marker when expressed in yeast.163

Figure 5.8. At MTP11 expression overlap with that of Golgi marker when expressed in yeast.164

Figure 5.9. Output of consensus prediction programmes available at ARAMEMNON database.
Figure 5.10. Multiple sequence alignment of At MTP8, At MTP9, At MTP10 and At MTP11.167
Figure 5.11. Multiple sequence alignment of At MTP8, At MTP11 and At MTP1168
Figure 5.12. Hypothetical membrane topology of At MTP8170
Figure 5.13. Hypothetical membrane topology of At MTP11171
Figure 5.14. Hypothetical membrane topology of A) At MTP9 and B) At MT10172
Figure 5.15. Generation of At MTP8 and At MTP11 site-directed mutants173
Figure 5.16. Functional analysis of At MTP8 and site-directed mutants in the Mn-sensitive
Saccharomyces cerevisiae mutant pmr1175
Figure 5.17. Functional analysis of At MTP11 and site-directed mutants in the Mn-sensitive
Saccharomyces cerevisiae mutant pmr1176
Figure 5.18. Functional analysis of At MTP8 and MTP11 site-directed mutants in the Zn- and Co-
sensitive Saccharomyces cerevisiae mutant zrc1 cot1
Figure 5.19. Functional analysis of At MTP8 and At MTP11 site-directed mutants in the Fe-
sensitive Saccharomyces cerevisiae mutant ccc1178
Figure 5.20. Comparison of Ec YiiP with At MTP8.
Figure 5.21. Predicted tertiary structure of Ec YiiP, At MTP8 and At MTP11 generated using
Swissmodel (Biasini, et al., 2014) with Ec YiiP as a homology model template.
182
Figure 6.1. Alignment of At NRAMP1 with Staphylococcus capitis DMT (Sca DMT) and E. coli
MntH, two prokaryotic NRAMP homologs
Figure 6.2. At NRAMP1 genomic structure and predicted protein topology191
Figure 6.3. Sensitivity to Mn deficiency of three different <i>nramp1</i> mutants, when grown
hydroponically and exposed to Mn deficiency from day 0
Figure 6.4. Sensitivity to Mn deficiency of three different <i>nramp1</i> mutants, when grown
hydroponically and exposed to Mn deficiency from day 29

Figure 6.5. NRAMP1 transcript exists at the 3' end of nramp1-2 but not of nramp1-1194
Figure 6.6. Mn deficiency phenotypes of two <i>nramp1</i> mutants when grown on plates under two
Ca regimes.
Figure 6.7. Alignment of At NRAMP1 and At NRAMP2197
Figure 6.8. Isolation of T-DNA insertion mutants for <i>nramp2</i>
Figure 6.9. Sensitivity of <i>nramp2-1</i> to Mn deficiency
Figure 6.10. Sensitivity of <i>nramp2-1</i> is specific to Mn-deficiency
Figure 6.11. Amplification and cloning of At NRAMP2
Figure 6.12. NRAMP2 targets the cis-Golgi network when transiently expressed in tobacco.203
Figure 6.13. Mn deficiency phenotypes of two <i>eca3</i> mutants when grown on plates under two
Ca regimes.
Figure 6.14. Differential Mn-deficient phenotype of eca3-1 1 when exposed to treatment at
different stages of development206
Figure 6.15. Pattern of At ECA3 (At1g10130) expression in Arabidopsis plants across a range of
developmental stages207
Figure 6.16. Additive phenotype of eca3-2 mtp11-1 under Mn toxicity when grown under
standard Ca conditions
Figure 6.17. Additive phenotype of <i>eca3-2 mtp11-1</i> under Mn toxicity when grown under low Ca
conditions209
Figure 6.18. ECA3 targets the trans-Golgi network when transiently expressed in tobacco. 211
Figure 6.19. Comparison of eca3-1, nramp1-1 and nramp2-1 single mutants under Mn
deficiency
Figure 6.20. Confirmation of <i>nramp1-1, nramp1-2</i> and <i>eca3-1</i> double mutants at RNA level.213
Figure 6.21. Confirmation of <i>eca3-1 nramp1-1 nramp2-1</i> triple mutant at RNA level214
Figure 6.22. Additive sensitivity of eca3-1, nramp1-1 and nramp2-1 double mutants under Mn
deficiency216

Figure 6.23. Comparison of <i>nramp1-1 nramp2-1 eca3-1</i> double	e and triple mutants under Mn
deficiency.	217
Figure 6.24. Proposed model of At NRAMP1, At NRAMP2 and	At ECA3 contributing to alleviating
Mn deficiency	222
Figure 7.1. Schematic for subcellular localisation of transporte	ers characterised in this study.230

DECLARATION OF AUTHORSHIP

I, Emily Christobel Farthing

declare that this thesis and the work presented in it are my own and has been generated by me as the result of my own original research.

Exploring the Roles of Membrane Proteins in Manganese Homeostasis of Higher Plants

I confirm that:

- This work was done wholly or mainly while in candidature for a research degree at this University;
- 2. Where any part of this thesis has previously been submitted for a degree or any other qualification at this University or any other institution, this has been clearly stated;
- 3. Where I have consulted the published work of others, this is always clearly attributed;
- 4. Where I have quoted from the work of others, the source is always given. With the exception of such quotations, this thesis is entirely my own work;
- 5. I have acknowledged all main sources of help;

7. None of this work has been published before submission.

6. Where the thesis is based on work done by myself jointly with others, I have made clear exactly what was done by others and what I have contributed myself;

Signed:	 	 	

Date:	
Date.	

Acknowledgements

Firstly, a sincere Thank You to my supervisor, Dr. Lorraine Williams, for your endless support, guidance and encouragement, and always pushing me a little further. This would not have been possible without you. Thank you to the Gerald Kerkut Trust and a Vice Chancellor's Scholarship for funding, and providing me with the opportunity to perform this research. Thank you to my examiners, Dr. Declan Doyle and Dr. Tony Miller.

Thank you to all past and present members of the LEW lab and surrounding lab space (especially llectra, Tania, Przemek, Nancy, Kerry, Nick, Zul, Adam, Franz and Jon) for providing a great work environment, motivation and enthusiastic discussion. In particular, thank you to Kerry Peaston and Tania Garcia Becerra, for your invaluable technical help, expertise and training in certain areas of this project. Thank you also to my array of helpful undergraduates, especially Shannon Turberville, Jon Griffin, Kate Henbest and Isabel Morgan.

Thank you also to Mike Cotton, for help with Arabidopsis growth and harvest. To Dr. Mark Willett, for expertise and advice with confocal microscopy, which ended up being my favourite part of data collection. Thanks also to our collaborators at NIAB, Cambridge, especially Emma Wallington and Rhian Howells, for advice and expertise in generating the wheat RNAi constructs, and for performing wheat transformation. Thank you to Dr. C. Gourlay (University of Kent) for providing fluorescent yeast strains and the pAG425galDsRed vector for yeast confocal microscopy. Thank you to Adrian King for showing me real-life examples of manganese deficiency in barley and wheat at Blackford Hall.

A set of acknowledgements would not be complete without a gushy list of thanks to all my friends and colleagues who have provided support along the way: to the 2012 cohort and members of BSPS and B85, you have all made for a lovely supportive network to work alongside and have fun with. To the cake club for providing more reasons to look forward to a Friday. To the Welbeck housemates I have had the pleasure of living with over the last four years. Thanks to Rachel, Cat and Lyssia for providing endless tea, ears and shoulders, and to my Chandler's Ford friends for entertaining conversation.

Undertaking this PhD has been a marathon, not a sprint, and it has come with its ups and downs. Thank you, thank you, to my incredible parents, for your unwavering support and for always believing in me, and to Will, I am so proud to have you as a little (big) brother. Thank you to Ben the Human, you have been so supportive, encouraging and patient, especially over the last few months, and for always providing me with chocolate buttons. Thank you also to my wonderful Grandparents, and to Ro, for your love and encouragement, and to Digby, for reminding me to appreciate the simple things. I could not have done this without any of you.

Finally, this thesis is dedicated to the memory of Grandad and Bran. Wish you were here.

Definitions and Abbreviations

Zn	Zinc	GAL	Galactose Promoter
Fe	Iron	EMS	Ethyl Methanesulfonate
Mn	Manganese	RISC	RNA-Induced Silencing Complex
Cd	Cadmium	siRNA	Small Interfering RNA
Со	Cobalt	h	Hour
Ca	Calcium	DMF	<i>N,N</i> -Dimethylfomamide
PSII	Photosystem II	bp	Base Pairs
ROS	Reactive Oxygen Species	rRNA	Ribosomal RNA
SOD	Super Oxide Dismutase	gDNA	Genomic DNA
MTP	Metal Tolerance Protein	cDNA	Complementary DNA
CDF	Cation Diffusion Facilitator	Hyg	Hygromycin
ECA	ER-type Ca ²⁺ -ATPase	RT-PCR	Reverse-Transcriptase
	_		Polymerase Chain Reaction (PCR)
ACA	Autoinhibited Ca ²⁺ -ATPase	qPCR	Quantitative PCR
CAX	Cation/Anion Exchanger	amiRNA	Artificial microRNA
CCX	Cation Calcium Exchanger	RNAi	RNA interference
VIT	Vacuolar Iron Transporter	BSA	Bovine Serum Albumin
ZIP	Zrt- Irt-related Protein	LB	Luria Broth
NRAMP	Natural Resistance Associated	SC	Synthetic Complete
	Macrophage Protein		
PMR	Plasma Membrane ATPase Related	Col	Columbia
GFP	Green Fluorescent Protein	Ws	Wassilewskija
YFP	Yellow Fluorescent Protein	FW	Fresh Weight
mRFP	Monomeric Red Fluorescent Protein	ANOVA	Analysis of Variance
IRT	Iron-Regulated Transporter	Tukey's HSD	Tukey's test for Honest
			Significant Difference
HMA	Heavy Metal ATPase	SE	Standard Error
DMT	Divalent Metal Transporter	½ MS	Half-strength Murashige and
			Skoog
PVC	Pre-Vacuolar Compartment	MH	Modified Hoaglands
TMD	Transmembrane Domain	CTM	Consensus Transport Motif
CTD	Cytoplasmic Domain	TGN	Trans-Golgi network
At	Arabidopsis thaliana	CGN	Cis-Golgi network
Os	Oryza sativa (rice)	Та	Triticum aestivum (bread wheat)
Hv	Hordeum vulgare (barley)	Cs	Cucumbis sativa (cucumber)

Chapter 1: General Introduction

1.1 Elements of Plant Nutrition

At the base of all food webs, plants vastly influence human nutrition. Nutritional deficiencies are subsequently a universal problem: more than 17% of the global population are at risk of zinc (Zn) deficiency (Wessells & Brown, 2012) while almost half of all children under 5 suffer iron (Fe) deficiency. Typically, these nutritional deficiencies are more prevalent in Africa and Asia compared with the Americas and Europe (Benoist, et al., 2008). As well as agricultural production in areas of low mineral phytoavailability (Palmgren, et al., 2008), these deficiencies can be attributed to diets low in vegetables but rich in cereals: although high in fibre, polished cereal grains are inherently low in essential nutrients (Yang, et al., 1998; White & Broadley, 2009). Nutritional quality and crop yield are also impacted by growth on suboptimal or contaminated, toxic soil (Palmgren, et al., 2008). While manganese (Mn) toxicity is a problem on tropical, acidic soils, second only to aluminium toxicity (Adams, 1981), Mn deficiency is a problem on calcareous or alkaline soils. Mn is a commonly reported trace element deficiency that causes growth reductions and yield losses in the calcareous soils of China (Yang, et al., 2007) and marine-sediment-contaminated soils of Scandinavia (Hebbern, et al., 2005; 2009). It is also one of the most prevalent deficiencies for cereals and oil seed rape in the UK (Roques, et al., 2013).

1.1.1 Macronutrients and micronutrients are both essential for plant nutrition

The macronutrients, including nitrogen (N), phosphorus (P) and calcium (Ca), are required at high concentrations within the plant for large scale processes such as photosynthesis and cell signalling (Neuberger & Scott, 1952; Fischer & Hsiao, 1968). Although required at considerably lower concentrations in plant tissue, micronutrients are equally important for the development and function. These include the transition metals, or heavy metals, such as Fe, Zn and manganese (Mn). The functions and typical tissue concentrations of essential macro and micronutrients are summarised in Table 1.1. This summary also includes symptoms observed when these nutrients are present in insufficient or excessive quantities; generally, both extremes have the potential to impact plant growth and, ultimately, crop yield in an agricultural setting. Other mineral elements considered beneficial but not essential to plant nutrition, such as sodium, selenium and cobalt, are not included in this summary (for reviews: Welch & Schumann, 1995; Terry, et al., 2000; Subbarao, et al., 2003). Lead and cadmium can also be taken up by the plant. Although these heavy metals have no physiological function and have the potential to be highly toxic: their high reactivity with sulphydryl groups and displacement of essential cofactors can cause deactivation

Chapter 1

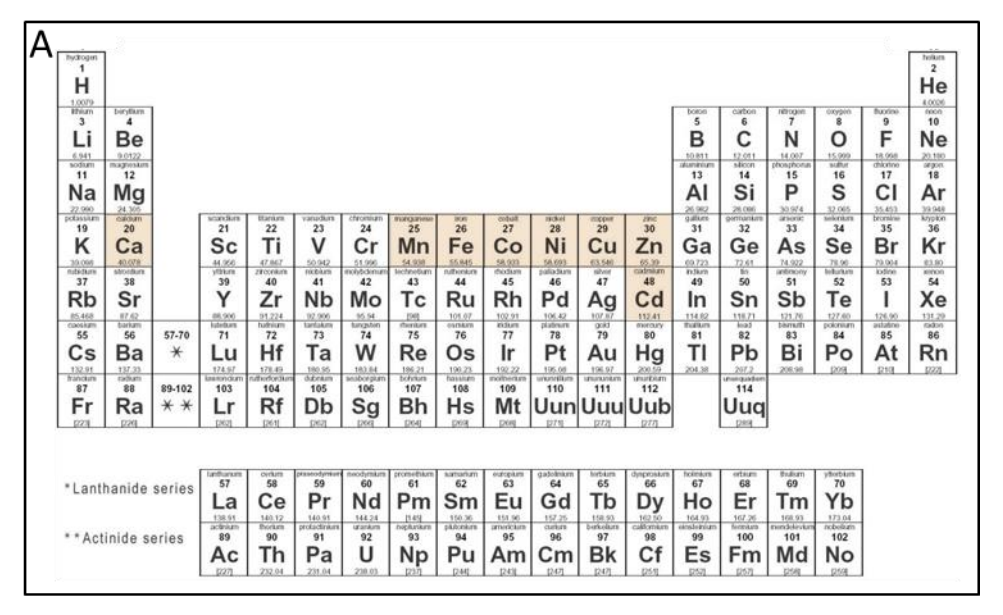
of proteins (Clemens, 2001; Palmgren, et al., 2008). These key metal elements are highlighted in the periodic table in Figure 1.1.

Bioavailability of essential nutrients depends heavily on the environment of the rhizosphere; the root-soil interface. Soil characteristics are influenced by soil compaction and soil particle size and arrangement, all governing nutrient bioavailability and uptake (Barber, 1995). For example, soil compaction can improve Mn uptake, with greater shoot Mn accumulation in barley grown on rolled, compressed soil compared with on untreated soil (Passioura & Leeper, 1963; Pedas et al., 2005). Nutrient bioavailability is also influenced by the presence of organic ligands and sorbents, by forming stable complexes with the nutrient to reduce their availability for uptake (Violante, et al., 2003). The transition metals are heavily influenced by soil pH and redox status, and exist as different, contrastingly bioavailable oxidation states available under different conditions. The effect of pH on transition metal bioavailability is illustrated in Figure 1.1B. Both Fe and Mn are heavily influenced by pH. The oxidative states Mn (II) (Mn²⁺) and Fe (II) (Fe²⁺) are the most readily accumulated and utilised by plants, and are also the most soluble species in soil (Guest, et al., 2002). These states increase in abundance with decreasing pH; as such, Mn toxicity is promoted on acidic soils (Adams, 1981). Conversely, Fe (III) (Fe³⁺), Mn (III) (Mn³⁺) and Mn (IV) (Mn⁴⁺) predominate at higher soil pH (Guest, et al., 2002) but these states are generally less soluble in soil (Lindsay and Schwab, 1982) or cannot be readily accumulated by most plants (Rengel, 2000), promoting deficiencies on alkaline soils. Plants possess a range of mechanisms to promote uptake from soil under poor conditions; these will be described in more detail in section 1.3.

In certain papers the oxidation states are referred to, but this is often not explicitly tested; therefore transition metals in this report will largely be referred to without assigning an oxidative state, with Mn generally referring to Mn^{2+} , although in most cases this is not experimentally confirmed. In the case of Fe, the oxidative state will be listed when authors have experimentally differentiated between Fe²⁺ and Fe³⁺.

1.1.2 Plant development and function is highly influenced by Mn availability

Mn nutrition in plants is of particular interest in this project. While Mn toxicity is a problem on tropical, acidic soils, second only to aluminium toxicity (Adams, 1981), Mn deficiency is a problem on calcareous or alkaline soils. Mn is a commonly reported trace element deficiency that causes growth reductions and yield losses in the calcareous soils of China (Yang, et al., 2007) and marine-sediment-contaminated soils of Scandinavia (Hebbern, et al., 2005; 2009). It is also one of the most prevalent deficiencies for cereals and oil seed rape in the UK (Roques, et al., 2013). To avoid impairment to plant health and function, the tissue concentration of micronutrients must be



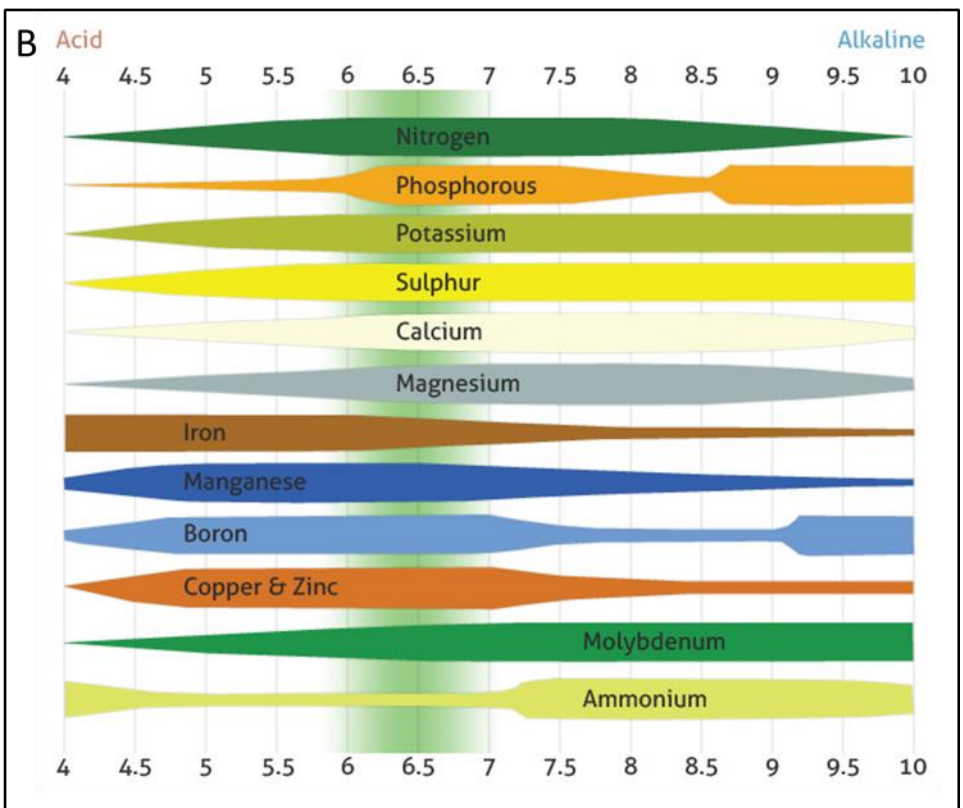


Figure 1.1. Elements in Plant Nutrition

A) Periodic table with key elements highlighted: calcium (Ca), cadmium (Cd) and transition metal nutrients manganese (Mn), iron (Fe), cobalt (Co), nickel (Ni), copper (Cu) and zinc (Zn). B) The effect of soil pH on essential nutrient bioavailability. Wider bars indicate increased availability for uptake (New Wave Agriculture, 2012).

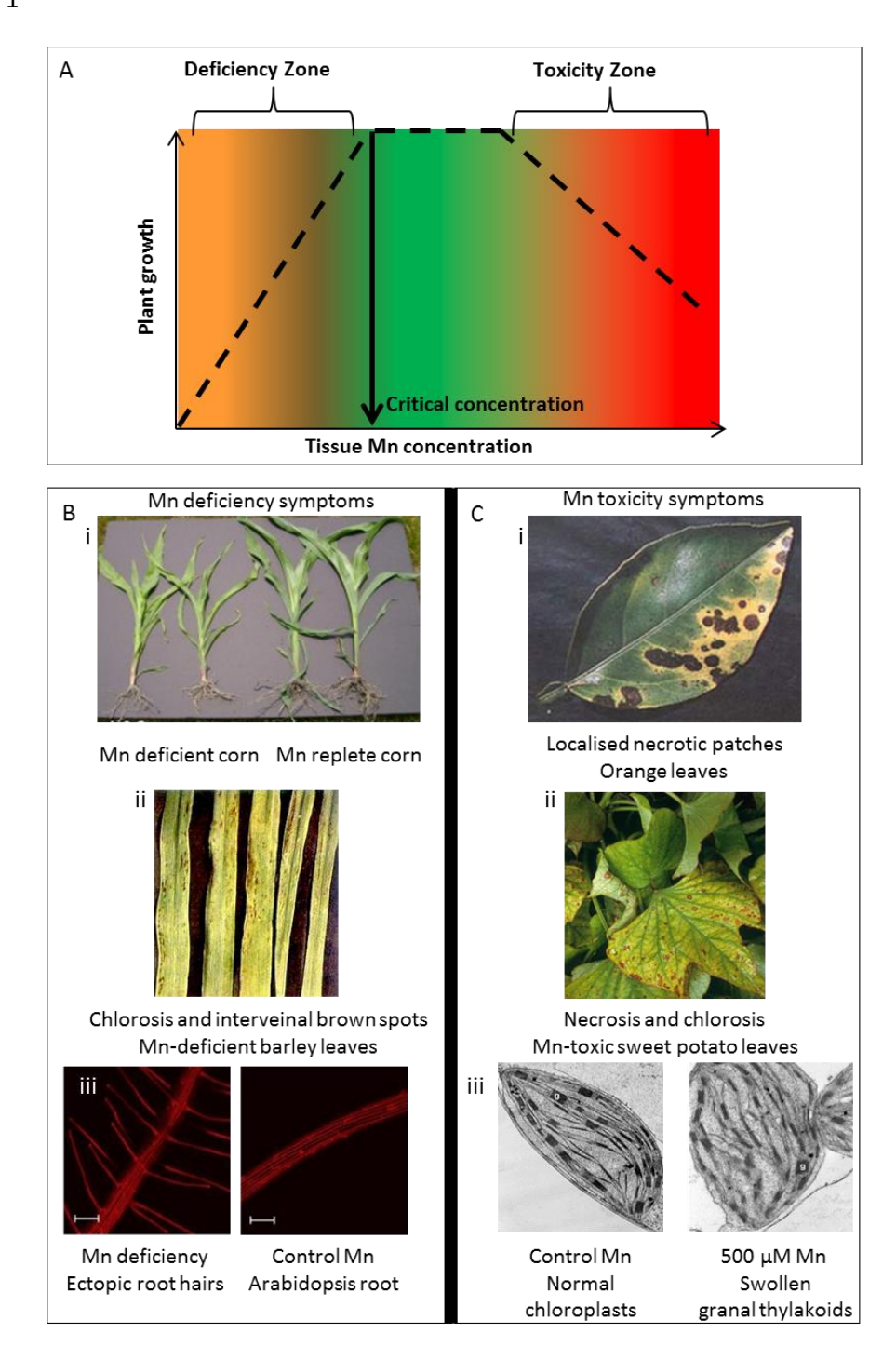


Figure 1.2. Inhibition of plant growth under Mn extremes.

A) Patterns of plant growth potential in relation to Mn tissue concentration within the deficiency zone, above the critical concentration and within the toxicity zone. B) Mn deficiency symptoms: Mn replete corn (right) compared with stunted corn growth on Mn-deficient soils (Sylvester, 2011); Mn-deficient barley leaves exhibiting interveinal chlorosis and brown spots (Taylor, 2010); ectopic root hairs in Arabidosis roots grown under Mn deficiency (left) or control media (14 μ M Mn; right) for 6 days (Yang, et al., 2008). C) Mn toxicity growth symptoms: Chlorosis and localised necrotic patches in orange leaves and sweet potato leaves; swollen granal and stromal thylakoid membranes in chloroplasts of mesophyll cells of maize plants exposed to 500 μ M Mn for 5 days (Doncheva, et al., 2009).

maintained within a particularly narrow range. Figure 1.2A illustrates the impact on plant growth when manganese bioavailability fluctuates. Below the critical concentration, a direct relationship exists between plant yield and tissue concentration. Deficiency symptoms often include stunting (Figure 1.2Bi) and interveinal-chlorosis (yellowing; Figure 1.2Bii) of the leaf which can be attributed to oxidative damage by increased reactive oxygen species (ROS) (Cakmak & Marschner, 1988; Tanaka, et al., 1995; Yu, et al., 1998; Yu & Rengel, 1999). ROS are chemically reactive, natural biproducts of cellular metabolism, capable of damaging DNA and disrupting important enzymes, proteins and lipids by oxidation of cofactors and subunits. While toxic levels of Mn have the potential to contribute to oxidative stress, Mn also plays an important role in detoxification of ROS via Mn-superoxide dismutase (Mn-SOD), a major antioxidative enzymatic system that scavenges superoxide radicals to convert into H₂O₂ (Bowler, et al., 1991). Mn-SOD expression is reduced in Mn-deficient tomato leaves (Shenker, et al., 2004) and photosynthetic algae C. reinhardtii, with cells suffering increased sensitivity to oxidative stress (Allen, et al., 2007). Mn is also a vital cofactor in photosystem II (PSII), a photosynthetic multiprotein complex in the thylakoid membranes of the chloroplast, that is essential for water splitting and oxygen evolution during photosynthesis (Cheniae & Martin, 1968; Ferreira, et al., 2004; Kern & Renger, 2007). 80% of Mn in the chloroplast targets PSII (Terry and Ulrich, 1974). Mn deficiency subsequently lessens photosynthetic capacity; in barley, this is due to a decreased abundance of functional PSII complexes (Husted, et al., 2009). Mn deficiency has also been attributed to altered root hair patterning and development in Arabidopsis to enhance metal uptake from the soil (Yang, et al., 2008; Figure 1.2Biii). Additionally, significant increases in transpiration and decreases in water use efficiency have been reported in barley plants exposed to latent Mn deficiency. This was attributed to a reduction in epicuticular wax content and imperfect stomatal closure, leading to greater transpirational water loss and ion leakage from the leaf (Hebbern, et al., 2009).

Within the adequate zone of Mn nutrition (Figure 1.2), Mn is no longer the limiting factor to plant growth. Above the adequate zone, supraoptimal concentrations also impair yield; Mn toxicity has been attributed to a reduction in biomass and growth in broad bean seedlings (Arya & Roy, 2011), in woody species *Populus cathayaha* (Lei, et al., 2007) and in ryegrass cultivar *Lolium perehne* (De la Luz Mora, et al., 2009). Toxicity-induced yield loss is often accompanied by symptoms such as localised chlorosis and necrosis (Foy, et al., 1969; Foy, et al., 1995); chlorotic zones surrounding necrotic brown spots in older leaves are also typical of Mn oxidative stress, containing localised accumulations of oxidised Mn and Mn compounds (Figure 1.2Ci and ii; Horiguchi, 1987; Horst, 1988). Studies implicate chloroplasts and photosynthesis to be major targets of Mn toxicity, with elevated levels of Mn reported in chloroplasts isolated from toxicity-treated rice (Lidon, et al., 2004). This is associated with a reduction in net photosynthesis and carboxylation efficiency,

Table 1.1. Critical leaf sufficiency and toxicity concentrations of essential mineral elements in non-hypertolerant crop species. Critical concentrations presented as mg g⁻¹ dry mass; sufficiency defined as conc. allowing 90% maximum yield; toxicity defined as conc. above which yield is inhibited by 10%. Example key function of element also summarised. Adapted from (White & Brown, 2010); data from (MacNicol & Beckett, 1985; Brown, et al., 1987; Marschner, 1995; Mengel, et al., 2001)

	Critical leaf c	oncentrations		
	(mg g ⁻¹ dry m	ass)		
Nutrient	Sufficiency	Toxicity	Example of key function	References
Macronutrients				
Nitrogen (N)	15-40	n/a	Key component of all proteins	(Neuberger & Scott, 1952)
			Chlorophyll: 4 N atoms per chlorophyll porphyrin ring	
Potassium (K)	5-40	>50	Maintenance of osmotic control	(Fischer & Hsiao, 1968)
Calcium (Ca)	0.5-10	>100	Cell wall integrity: cross-linking acidic pectin residues	(Tagawa & Bonner, 1957)
			Membrane structure: binds phospholipids for structural integrity	(Jansen, et al., 1960)
			Regulate polarised growth (e.g. root hair cells, pollen tubes)	(Hanson, 1984)
			Calcium signature regulates processes, e.g. stomatal closure, egg activation after	(Allen, et al., 2001)
			fertilisation	(Digonnet, et al., 1997)
Phosphorus (P)	2-5	>10	Component of ATP	
			Component of phospholipids	
Magnesium (Mg)	1.5-3.5	>15	Central ion in chlorophyll porphyrin ring	(Granick, 1961)
Sulphur (S)	1-5		Iron-sulphur proteins, e.g. ferredoxin: photophosphorylation reactions of	(Tagawa, Tsujimoto, &
			photosynthesis, mediates electron transfer chain	Arnon, 1963)
Micronutrients				
Zinc (Zn)	1.5-30x10 ⁻³	100-300x10 ⁻³	Zinc-finger proteins, e.g. transcriptional regulation	(Dietrich, et al., 1997; Isernia, et al., 2003)
			Cu/Zn Superoxide Dismutase (SOD), protects from damage by reactive oxygen species (ROS)	(Kliebenstein, et al., 1998)

Iron (Fe)	50-150x10 ⁻³	>0.5	Cytochromes: electron transfer chain for cyclic phosphorylation for ATP	(Slovacek, Crowther, &
				Hind, 1979)
			FeSOD, protects from damage by ROS	(Kliebenstein, et al., 1998)
Manganese (Mn)	10-20x10 ⁻³	0.2-5.3	Photosynthesis: cofactor in Hill reaction and Photosystem II for water-splitting and	(Eyster, et al.,
			O ₂ evolution	1958)(Cheniae & Martin,
			Mn-SOD – acts on superoxide radical in mitochondria to protect tissues from ROS	1968)
			damage	(Bowler, et al., 1991)
Copper (Cu)	1-5x10 ⁻³	15-30x10 ⁻³	Component of plastocyanin: electron transfer chain for ATP synthesis	(Katoh & Takamiya, 1994)
Boron (B)	5-100x10 ⁻³	0.1-1.0	Borate diester crosslinks with rhamnogalacturonan-II in cell wall: cell wall integrity	(Ishii & Matsunaga, 1996)
Chlorine (CI)	0.1-6.0	4.0-7.0	Maintenance of osmotic control	(Fischer & Hsiao, 1968)
Molybdenum (Mo)	0.1-1.0x10 ⁻³	1	Component of nitrate reductase: nitrogen metabolism	(Nicholas & Nason, 1955)
Nickel (Ni)	0.1x10 ⁻³	20-30x10 ⁻³	Cofactor of urease for urea metabolism	(Dixon, et al., 1975)

considered an early indicator of Mn toxic stress in wheat (Macfie & Taylor, 1992), tobacco (Nable, et al., 1988) and rice (Lidon, et al., 2004). This could be due to ultrastructural changes in the chloroplasts, which feature swollen granal and stromal thylakoids, and are more round in shape, in maize plants treated with elevated Mn (Figure 1.2Ciii; Doncheva, et al., 2009). Possibly owing to its importance in oxygen evolution, however, there appears to be a protective mechanism in place to prevent damage of PSII under Mn toxicity, targeting PSI instead. While there is no effect on the relative abundance of PSII subunits and components, PSI suffers reductions in associated-polypeptide abundance of up to 80%, accompanied by reduced rates of photooxidation and rereduction (Millaleo, et al., 2013).

As soft Lewis metals, the heavy metals have high affinities for electron pair donors such as carboxylic acids and amine groups, thus disturbing protein function when present at high levels (Shriver, 1970; Kraemer, et al., 2007). In addition to the direct toxic effects observed, the transition metals are also capable of displacing other essential cofactors from active sites of important enzymes, altering their geometry and rendering them inactive: for example, Zn is often capable of binding to active Mg sites, and as such is buffered at a concentration up to a million-fold below that of Mg inside most cells (Foster, et al., 2014). An important interaction in Mn homeostasis is the antagonism between Mn and Fe. Chlorosis observed in sunflower leaves (Weinstein and Robbins, 1955) and young rice leaves (Fuhrs, et al., 2010) grown under high Mn conditions has been attributed to secondary induced Fe deficiencies, rather than direct Mn stress. Similarly, the severity of Fe deficiency-induced chlorosis and stunting in Arabidopsis can be exacerbated by elevated Mn conditions (Eroglu, et al., 2016). One proposed reason for this Mn-induced Fe deficiency is direct competition for uptake when Mn is present in high levels; some uptake transporters in the root are permeable to both Mn and Fe (Eide, et al., 1996; Curie, et al., 2000; Vert, et al., 2002; Cailliatte, et al., 2010).

Another important interaction in Mn homeostasis is that between Mn and Ca. Some key functions of Ca as a macronutrient are listed in Table 1.1 and will be discussed further in section 1.3.4. Of particular note here, however, is the role of Ca as a regulator of cellular responses, through controlled Ca oscillations, transients and gradients, tightly coordinated by a range of influx and efflux pathways. Mn and Ca are chemical homologs. Some channels and transporters exist with affinity for both Mn and Ca, with some examples listed in Table 1.4, providing opportunities for Ca/Mn antagonism; however, the ability to transport both metals is not always tested. Application of Ca can alleviate Mn phytotoxicity in peanut plants (Bekker, et al., 1994), tomato (Gures, et al., 1998) and barley (Alam, et al., 2006). Interestingly, Ca can also alleviate Mn-induced Fe deficiency in barley, enabling greater Fe-translocation to the shoot (Alam, et al., 2006). Another

macronutrient, phosphorus, has also been shown to impede Mn uptake and induce Mn deficiency symptoms in barley (Pedas, et al., 2011) although this interaction is less well reported in the literature. Understanding the interactions between different elements, known collectively as the 'ionome' (Lahner, et al., 2003; Salt, 2004) is essential to understand the mechanisms involved in heavy metal homeostasis.

1.1.2.1 Plant species and cultivars differ greatly in their threshold for Mn deficiency and toxicity

During evolution, plants have adapted to widely differing metal availabilities; some plant genotypes and species are now particularly tolerant to extremes of heavy metal availability. The ability to grow uninhibited on low Mn is referred to as Mn-efficient. Different wheat and barley cultivars have been shown to differ in their Mn efficiency (Pedas, et al., 2005; Jiang, 2006). The more efficient barley cultivar featured higher Mn uptake affinity and a 4x greater maximum Mn uptake capacity (V_{max}), and as such did not suffer chlorotic, necrotic leaves under Mn deficiency (Pedas, et al., 2005). Interestingly, the wheat cultivar with greater Mn efficiency is a discontinued genotype, Maris Butler, with greater dry matter and higher photosynthetic yield under Mn deficiency (Jiang, 2006). Although Mn-inefficiency can generally be corrected with application of foliar sprays, investigation of how these Mn-efficient cultivars tolerate Mn deficiency at the cellular and molecular level could provide a long-term, sustainable approach to arable farming on Mn-poor soils.

Plants also vary in their ability to endure toxic Mn conditions. For example, while barley can only accumulate 150 µg g⁻¹ dry weight (DW) Mn before exhibiting Mn toxicity symptoms, rice is a highly Mn-tolerant crop with some species accumulating up to 5000 µg g⁻¹ DW (Vlamis & Williams, 1964). Other species, such as the Australian tree *Gossia bidwillii* are known as hyperaccumulators (Bidwell, et al., 2002). While most species adopt an exlusion strategy, sequestering Mn away from aerial tissue to avoid damage to photosynthetic components, hyperaccumulators are defined as storing 1 % dry weight, or 10000 mg kg⁻¹ Mn in their aerial tissues (Baker and Brooks, 1989; Reeves and Baker, 2000). Interestingly, the Mn hyperaccumulator *Chengiopanax sciadophylloides* correlates foliar accumulation of both Mn and Ca, suggesting an enhanced uptake or root-shoot translocation of both elements and alluding to the Mn/Ca antagonism described in section 1.1.2. However, the pathway or transporter responsible for this is yet to be identified (Mizuno, et al., 2013). The genetic basis of Mn hyperaccumulation is beginning to be elucidated, but will provide further insight into Mn homeostasis when it is determined.

1.2 Manganese nutrition for human health

Manganese is also an essential micronutrient in animals and must similarly be regulated. Symptoms of adverse Mn concentrations are often severe and permanent. Rats fed long-term Mn-deficient diets suffer bone malformation, associated with altered bone calcium and metabolism (Strause, et al., 1986). Similar symptoms are seen in humans on diets of low Mn, suffering bone malformation or osteoporosis and skin lesions. Deficiency is also often accredited to arthritis, schizophrenia and diabetes in humans (Friedman, et al., 1987). The neurological symptoms of epilepsy also often correlate with low blood- or brain-Mn (Carl, et al., 1986; Lee, 2000), with genetically epilepsy-prone rats featuring abnormalities in Mn-dependent enzymes of the brain and liver (Carl, et al., 1993). Reductions in Mn-SOD activity, related to Mn deficiency, have also been linked to increased cancer susceptibility; however, due to the heterogeneity of the Western diet it is difficult to isolate unique instances of Mn deficiency (Borrello, et al., 1993).

Mn toxicity is a more commonly reported problem, although this is more generally observed through occupational (Arschner, et al., 2009) or environmental (Lucchini, et al., 2012) overexposure, rather than through diet, such as long-term exposure to Mn-laden dust by miners or welders. Symptoms of Mn toxicity can include bone deformities (Greger, 1999), cirrhosis and hepatic dysfunction (Butterworth, 2000) and neurotoxicity resulting from abnormal Mn-brain concentrations, and resulting in progressive neuro-deterioration similar to Parkinsonism (Gorrel, et al., 1997; Crossgrove & Zheng, 2004). The genetic basis of Mn homeostasis in humans is only recently beginning to be elucidated. SLC30A10 (for Solute Carrier 30 A10) has recently been identified as playing a role in Mn transport. Mutations in *SLC30A10* cause neurological defects related to Parkinsonism and chronic liver disease due to a defect in Mn efflux from the cytosol, causing cells and neurons to exhibit manganese hypersensitivity (Quadri, et al., 2012; Tuschl, et al., 2012; Levya-Illades, et al., 2014).

1.3 The use of membrane transporters in Mn homeostasis of higher plants

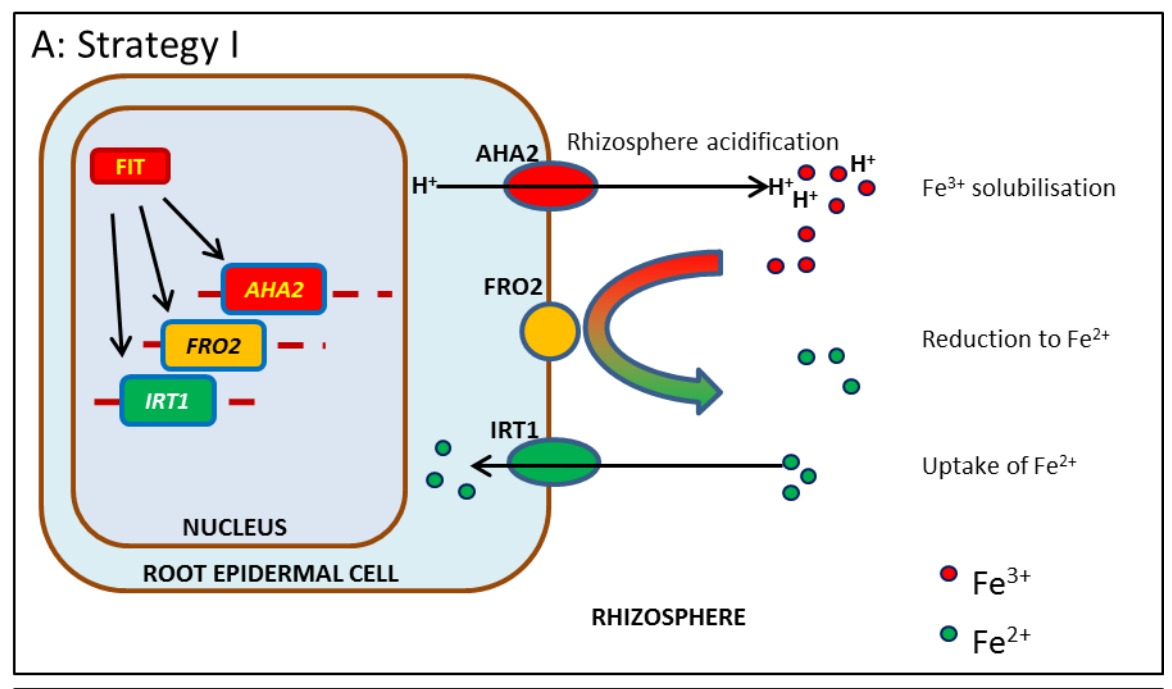
It is essential for plant cells to regulate their transition metal concentrations across particularly narrow adequate ranges to avoid the symptoms of Mn deficiency and toxicity. Cytosolic Mn must be kept extremely low to avoid pools of free, aqueous form ions with potential for toxic effects: values as low as $0.4~\mu M$ have been reported in the maize root tip cell cytoplasm compared with $10~\mu M$ in the vacuole (Quiquampoix, et al., 1993). There is, therefore, a strong electrochemical gradient of Mn into the cytoplasm but the high positive change of Mn²⁺ prevents unassisted diffusion through the bilayer. Facilitative transporters and channels can exploit this gradient to

passively transport Mn, either alone or in parallel with other ions, without additional energy sources; for example, NRAMP1 is involved in Mn uptake (Cailliatte, et al., 2010). Active transporters are also relied upon for continued detoxification, but are energized to move ions against their concentration gradient; for example, members of the P-type ATPases, to be explored further in Section 1.3.4. Many studies that aim to characterise metal transporters take advantage of metal-sensitive yeast mutants for heterologous expression, and the range of T-DNA insertion mutants available in *Arabidopsis thaliana*. These techniques will be described in more detail in subsequent chapters.

1.3.1 Acquisition from the soil: lessons learnt from iron uptake

Relatively little is understood about the mechanisms of Mn acquisition from the soil in higher plants; more is currently understood about the uptake of Fe from the soil and it is possible Mn uptake occurs in similar ways. As described in section 1.1, Fe solubility is very dependent on soil pH; Fe³⁺ becomes 1000-fold more soluble with every unit drop in pH (Mori, 1999). Additionally, Fe²⁺, the predominant oxidative state at lower pH, is more bioavailable than Fe³⁺, which can be reduced to Fe²⁺ prior to uptake. As such, two strategies have evolved in plants to improve uptake of Fe from the soil; these are summarised in Figure 1.3. Strategy I is an acidification- and reduction-based approach activated in non-grasses under Fe deficiency. Active extrusion of protons by H⁺-ATPases acidifies the rhizosphere to improve Fe³⁺ solubility. Acidification occurs mainly by AHA2, a member of the Arabidopsis H⁺-ATPases that is at least partially regulated by bHLH transcription factor FIT (Santi and Schmidt, 2009). AHA7 is another related, FIT-dependent ATPase potentially involved in this process (Colangelo and Guerinot, 2004). Rhizosphere acidification facilitates Fe (III) reduction and solubilisation; FIT is also responsible for upregulating FRO2 (Colangelo and Guerinot, 2004), a membrane-bound reductase that reduces apoplastic Fe³⁺ to Fe²⁺ by transferring electrons from NADH (Robinson, et al., 1999). Fe²⁺ can then be transported into the root. The major transporter for this uptake from the soil is high-affinity Fe²⁺ transporter IRT1 (iron-regulated transporter 1; Eide, et al., 1999; Vert, et al., 2002), also upregulated by FIT under Fe deficiency (Colangelo & Guerinot, 2004).

Strategy II for Fe uptake (Figure 1.3B), generally adopted by grass species such as wheat and rice, is the chelation strategy. Low molecular weight compounds are released into the rhizosphere to chelate Fe³⁺. A key family of these chelators is the mugineic acid (MA) family of phytosiderophores (PS) which have a high Fe³⁺ binding affinity (Mori, 1999). Rice adopts both uptake strategies but secretes relatively few types of PS, while barley secretes large amounts of many types and is therefore more tolerant of Fe deficiency (Bashir, et al., 2006). Arabidopsis has also been shown to secrete bidentate and tridentate chelators, in particular catechol-type coumarins (Schmid, et al.,



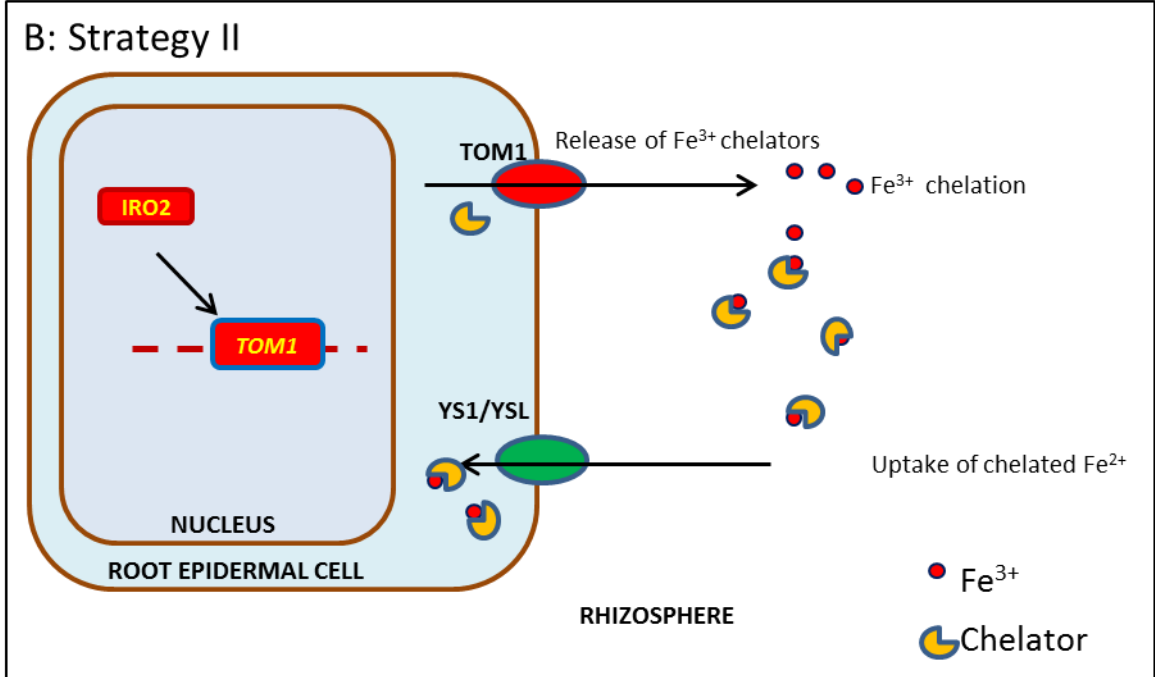


Figure 1.3. Strategies for iron (Fe) uptake from the soil by plants.

A) Strategy I plants, e.g. non-grasses, acidify the rhizosphere by plasma membrane ATPases such as AHA2, to increase the solubility of Fe³⁺. FRO2 reduces Fe³⁺ to Fe²⁺, increasing uptake of Fe²⁺ by influx transporters such as IRT1. *IRT1*, *FRO2* and *AHA2* are upregulated under Fe deficiency by transcription factor *FIT*. B) Strategy II plants, e.g. grasses, release chelators through transporters such as TOM1. These chelate Fe³⁺ in the rhizosphere for uptake of the chelated complex by transporters such as YS1/YSL. Os *TOM1* is positively regulated in rice by Os *IRO2* under Fe deficiency (Ogo, et al., 2007; Ogo, et al., 2011). Adapted from Ivanov (2012) and Krohling, et al., (2016).

2014). Following Fe³⁺ chelation, specific transport systems are utilized for uptake of Fe-chelates. For example, YS1 is a proton-coupled transporter for PS chelates in maize and barley (Schaaf, et al., 2004; Murata, et al., 2006).

In addition to IRT1 and NRAMP1, providing uptake routes from the soil for reduced Fe²⁺ and Mn (Eide, et al., 1996; Curie, et al., 2000; Vert, et al., 2002; Cailliatte, et al., 2010), organic compounds and chelators have been proposed to be released into the soil for Mn chelation (Arrivault, et al., 2006), but are yet to be identified. Both low- and high-affinity Mn uptake systems have been identified in *Hordeum vulgare* (winter barley) although the specific transporters involved remain to be elucidated, including whether they are direct uptake or chelation-based transporters (Pedas, et al., 2005). *S. cerevisiae* possesses a high affinity phosphate-uptake plasma membrane transporter, PHO84, that can also transport Mn bound to phosphate, as MnHPO₄ (Jensen, et al., 2003); the homologous transporters in Arabidopsis and maize, At PHT1;1 and Zm PIP2;5, respectively, are also high affinity phosphate transporters (Bayle, et al., 2011; Loth-Pereda, et al., 2011; Hachez, et al., 2013) but their Mn-transporting abilities are yet to be explored *in planta*.

1.3.2 Cytoplasmic detoxification of Mn

A schematic of various subcellular compartments within a typical plant cell is provided in Figure 1.4. Following transcription and translation, newly synthesised proteins are post-translationally modified in the endoplasmic reticulum (ER). This may include processes such as addition of polysaccharides, cleavage by proteolytic enzymes or formation of multimeric complexes (for review, see Vitale, et al., 1993). Transporters exist at the ER membrane to provide key ions to the lumen for function; for example, At ECA1 pumps Ca into the ER, to support plant growth under conditions of Ca deficiency (Wu, et al., 2002). The endomembrane system of the cell is connected by vesicular traffic. From the ER, proteins are packaged into vesicles and delivered to the cis-face of the Golgi for further processing and modification, before eventual exit at the trans-face (Orci, et al., 1998). Following maturation in the Golgi, proteins generally either target the secretory system to the plasma membrane, or are targeted to other destinations within the cell. To ensure transport to the correct destination, proteins possess particular sequence motifs or signal peptides; more will be discussed regarding these determinants in Chapter 5. As well as this key role in protein sorting and modification, it is possible that the Golgi is also involved in Mn detoxification (Peiter, et al., 2007); this will be discussed further in Section 1.3.3.1 and Chapter 3.

Figure 1.4A summarises some of the key steps involved in Mn detoxification in the plant cell. Chelators also function within the cell to avoid excess accumulation of transition metals within the cytoplasm. Again, more information is currently understood regarding intracellular chelation

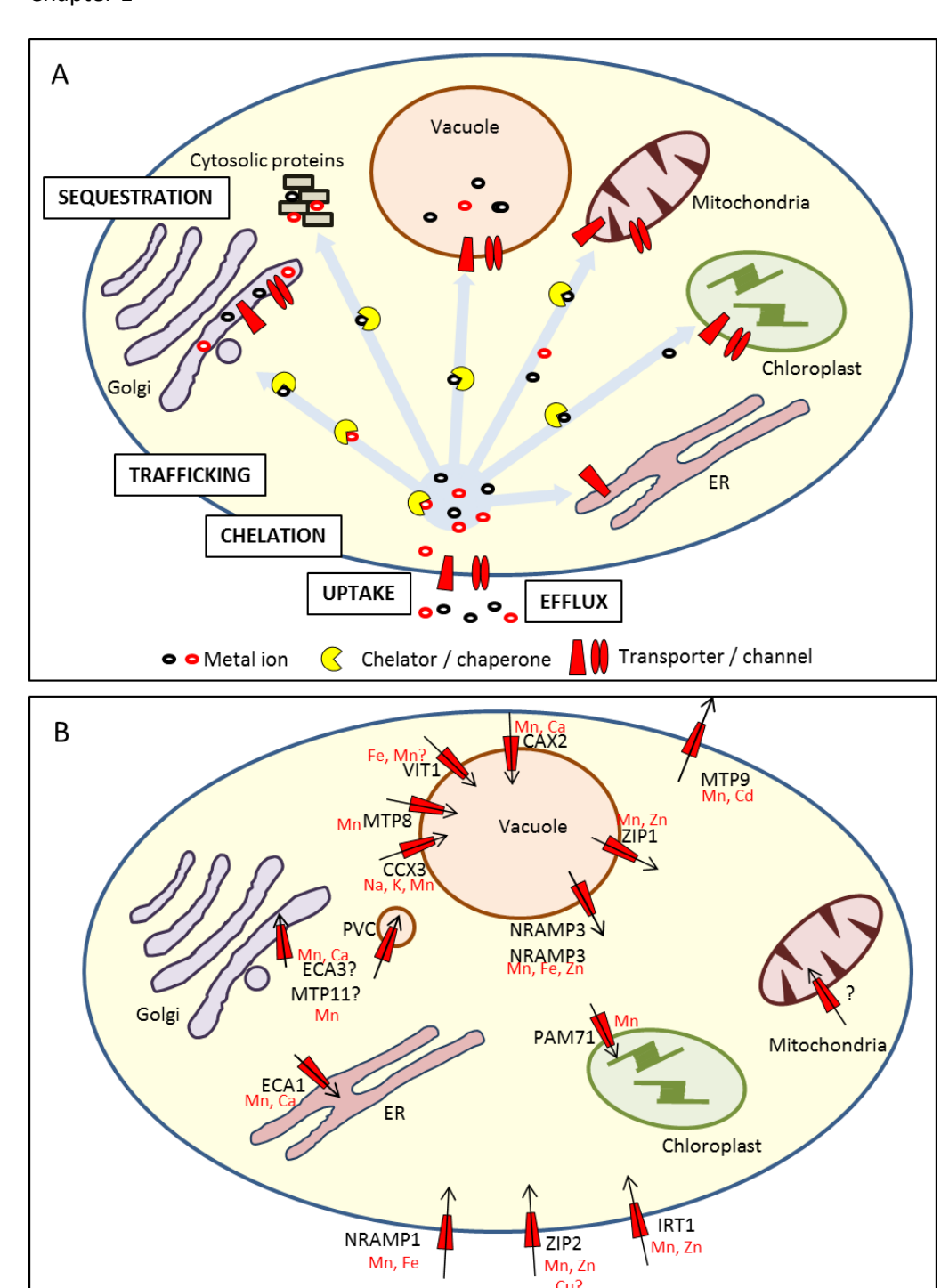


Figure 1.4. Metal homeostasis in a typical plant cell.

A) Hypothetical schematic of cellular mechanisms contributing to heavy metal homeostasis in a typical plant cell. Metals are taken into the cell via transporters (uptake) before being bound by chelators and chaperones (chelation) to buffer free cytosolic metal ions. Ions are delivered specifically to metal-dependent proteins for function (trafficking), or sequestered in subcellular compartments or extruded from the cell (sequestration). Adapted from Clemens, 2001. B) Proposed membrane localisations of transporters and channels involved in Mn transport across plant cell, including any other metals they also transport.?, protein proposed to function here but is as yet undetermined. Based on studies of Arabidopsis and rice proteins (Curie, et al., 2000; Hirschi, et al., 2000; Vert, et al., 2002; Lanquar, et al., 2005; Kim, et al., 2006; Delhaize, et al., 2007; Peiter, et al., 2007; Mills, et al., 2008; Li, et al., 2008; Lanquar, et al., 2010; Ueno, et al., 2015; Eroglu, et al., 2016; Schneider, et al., 2016).

of other transition metals, but metallothioneins are sulfhydryl-rich peptides thought to chelate the majority of transition metals, including Mn (Bell and Vallee, 2009). Relative to *Arabidopsis thaliana*, chelation systems are enhanced in the closely related, Zn-hypertolerant *Arabidopsis halleri*, with greater levels of Zn²⁺ chelation by malate in aerial parts (Sarret, et al., 2002) and greater levels of histidine-zinc complexes in the roots (Verbruggen, et al., 2009).

Another detoxification mechanism is to remove Mn from the cytoplasm, either by efflux (Eide, 2006) or by sequestration within subcellular organelles. The MTP9 proteins from cucumber (Migocka, et al., 2015) and rice (Ueno, et al., 2015) are responsible for Mn efflux from root cells, but this is more likely to aid root-to-shoot translocation than detoxification. The vacuole is also a useful organelle for storing heavy metal ions under conditions of excess, including Mn, Zn, Cd and Cu (for review, see Marty, 1999). Transporters localized at the tonoplast, including VIT1 (Kim, et al., 2006), members of the CAX (cation/proton exchangers) family, CAX2 and CAX5 (Hirshi, et al., 2000; Edmond, et al., 2009), and the very recently characterised At MTP8 (Eroglu, et al., 2016) sequester Mn into the vacuole under conditions of excess. Rather than a 'dumping ground', the vacuole functions as a dynamic storage facility for the cell, the sequestration capacity of which is adjusted according to environmental cues (Peng & Gong, 2014). Chelators are thought to play an important role in this process, both intra-vacuolar chelators (Peng & Gong, 2014) and cytosolic chelators, such as phytochelatin, which forms a stable complex with cytosolic Zn and Cd (Clemens, 2001; Wunschmann, et al., 2007) before sequestration in the vacuole by tonoplast transporters such as At ABCC1 and ABCC2 (Rea, et al., 1998; Park, et al., 2012). More is generally understood about vacuolar detoxification of other metals, such as Zn and Cd, but the role of the vacuole in Mn homeostasis is gradually becoming more understood.

Under low Mn availability, vacuolar Mn is remobilized by NRAMP3 and NRAMP4 to target the chloroplast (Thomine, et al., 2003; Carter, et al., 2004; Lanquar, et al., 2005; Lanquar, et al., 2010). The chaperone involved in the vacuolar-to-chloroplast transit is yet to be identified. However, PAM71 (encoded by PHOTOSYNTHESIS AFFECTED MUTANT 71) has recently been identified as a thylakoid-localised protein that enables Mn uptake into the chloroplast for incorporation into the Mn_3CaO_5 cluster of photosystem II (Schneider, et al., 2016). At PAM71 is related to the putative Ca^{2+}/H^+ exchange transporters, Sc GDT1 and the human TMEM165 (Damaedgd, et al., 2013; 2014).

Figure 1.4B summarises some of the Mn transporters characterized to date, to the level of determining membrane localisation. Compared to other metals and other kingdoms, Mn transport in plants is still relatively understudied. However, it is clear that Mn homeostatic pathways at the cellular level are complex and multifaceted. This project will focus on three specific membrane protein families: the Cation Diffusion Facilitators, the P_{2A}-type ATPases and the

Natural Resistance Associated Macrophage Proteins, to further explore how their members function together in manganese homeostasis of higher plants. Characterisation studies in the past have generally investigated how these proteins function individually; an aim of this work is also to begin to unravel how they work together to coordinate Mn homeostasis, including determining their relative importance under Mn deficiency and toxicity.

1.3.3 Cation Diffusion Facilitators (or Metal Tolerance Proteins) transport divalent metal cations from the cytoplasm

The Cation Diffusion Facilitators (CDFs) are a ubiquitous family of membrane proteins involved in heavy metal homeostasis, although are referred to as Metal Tolerance Proteins (MTPs) in plants. First described in 1995 (Nies and Silver, 1995), a signature sequence to aid identification and functional hypothesis generation was proposed by Paulsen and Saier (1997) but this was later updated by Montanini, et al. (2007). The majority of characterized CDFs are proposed to possess six transmembrane domains (TMDs) (Anton, et al., 1999; Wei and Fu, 2005); the updated signature sequence spans from TMD2 to the start of TMD3, including the connecting cytosolic loop (Montanini, et al., 2007).

Although few CDFs have been structurally characterised, Ec YiiP, a Zn-transporting CDF from *E. coli* was crystallised and shown to form a homodimer with a Y-shaped architectural structure (Lu & Fu, 2007). Three Zn-binding domains were proposed, visualised in Figure 1.5: site A, within the membrane, mediates Zn transport while the cytoplasmic sites B and C are involved in stabilisation of the homodimer and efflux (Wei & Fu, 2005; Lu, et al., 2009; Coudray, et al., 2013). Transmembrane domain 2 (TMD) possesses a HxxxD domain, while TMD5 possesses a DxxxD domain; these are brought together during protein folding to mediate near-tetrahedral binding of Zn²⁺ in binding site A, referred to as DD-HD (Lu, et al., 2009).

All CDFs identified to date possess motifs homologous to these HxxxD/DxxxD domains, but feature amino acid substitutions depending on their proposed substrate. Rather than clustering phylogenetically according to their parental species, the CDFs cluster according to their predicted substrate specificity, falling into three distinct clades: Zn-CDFs, Mn-CDFs and Fe/Zn-CDFs (Montanini, et al., 2007). More recent phylogenetic analysis reveals 18 subgroups, agreeing with the separation of Zn- and Mn-clades, but indicating the presence of additional Zn/Cd, Co/Ni, Fe and Zn/Cd/Fe/Mn clades in place of the general Fe-CDF group, although functional evidence is generally still needed (Cubillas, et al., 2013). Taken together, these findings suggest the importance of conserved regions and sequences in determining transporter function. Further

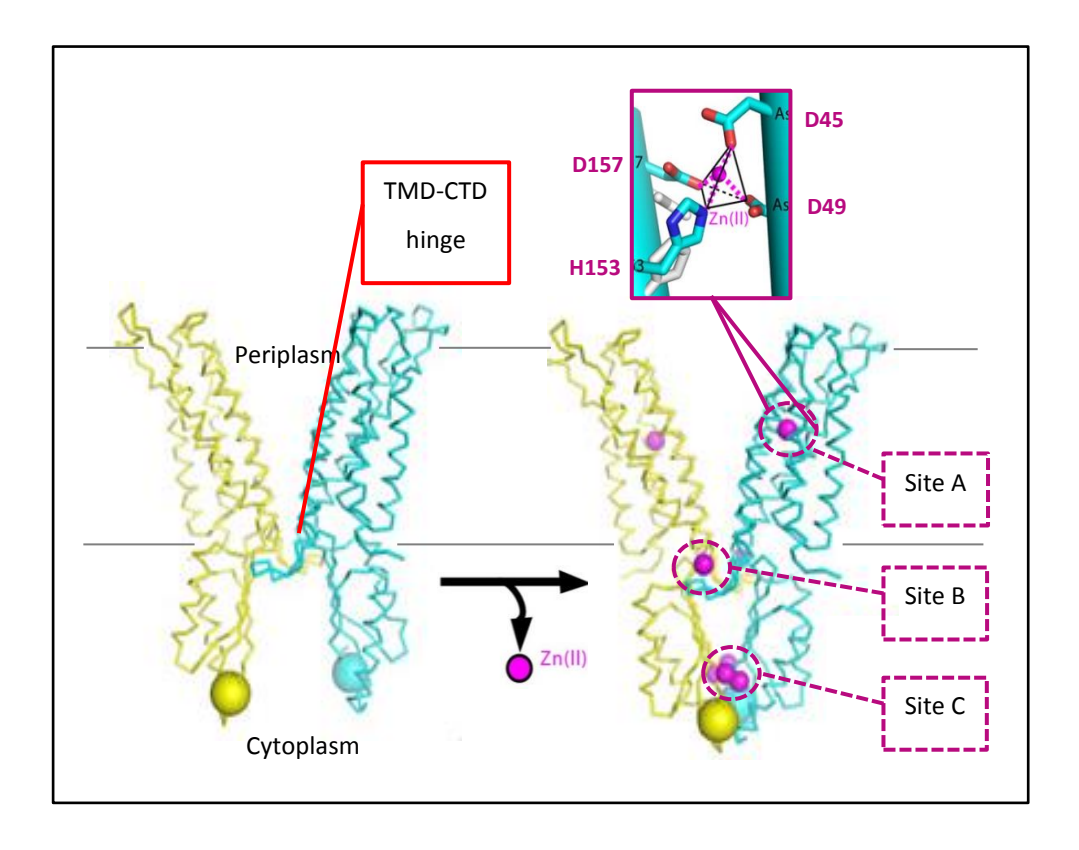


Figure 1.5. Proposed structure of Ec YiiP, the *E. coli* Zn-transporting Cation Diffusion Facilitator.

Zn binding to the 3 active sites (site A, B and C) mediates conformational change as indicated. Site A is coordinated by residues D45 and D49 on transmembrane domain (TMD) 2 and D153 and D157 on TMD5, which fold together to form a DD-HD motif. Adapted from Wei & Fu (2005) and Lu, et al. (2009).

investigation into these motifs and the ion-binding site may provide a useful starting site for understanding transporter specificity; this will be explored further in subsequent chapters.

The plant MTPs cluster further into 7 groups, named after the nomenclature of the 12 Arabidopsis MTP sequences: Zn-MTPs are found in groups 1, 5 and 12; Fe/Zn-MTPs are in groups 6 and 7; Mn-MTPs are found in groups 8 and 9. This phylogenetic tree is shown in Figure 1.6. Sequences from each group are found in each of the plant genomes analysed, including *Arabidopsis thaliana*, *Populus trichocarpa* and *Oryza sativa*, suggesting the emergence of land plants is predated by the expansion of plant MTPs (Gustin, et al., 2011). There are 12 MTPs in Arabidopsis: At MTP1 – MTP12. The first, initially identified as ZAT, or Zinc Transporter of Arabidopsis (Van der Zaal, et al., 1999) and later renamed MTP1, is a Zn transporter: overexpression in Arabidopsis confers Zn hypertolerance (Van der Zaal, et al., 1999) while sensitivity is enhanced when *MTP1* is knocked out (Kobae, et al., 2004) or silenced via RNAi (Desbrosses-Fonrouge, et al., 2005). The homologous transporters in poplar (Blaudez, et al., 2003), barley (Podar, et al., 2012) and rice (Menguer, et al., 2013) have a similar Zn-transporting ability, indicating functional conservation across the MTP family.

Most members of the CDFs characterised so far are proposed to function as antiporters, harnessing the energy from a secondary solute concentration to transport metal cations. The cucumber Cs MTP9 exchanges Mn and Cd for H ⁺; expression of Cs MTP9 in yeast plasma membrane vesicles dissipates a transmembrane pH gradient upon addition of Mn or Cd, in a metal concentration-dependent manner (Migocka, et al., 2015). A similar H⁺/Zn and H⁺/Mn exchange was demonstrated for At MTP1 (Kawachi, et al., 2008) and At MTP11 (Peiter, et al., 2007), respectively, while Zn is exchanged for H⁺ or K⁺ by Bs CzcD, a CDF from the gram-positive bacterium *Bacillus subtillis* (Guffanti, et al., 2002).

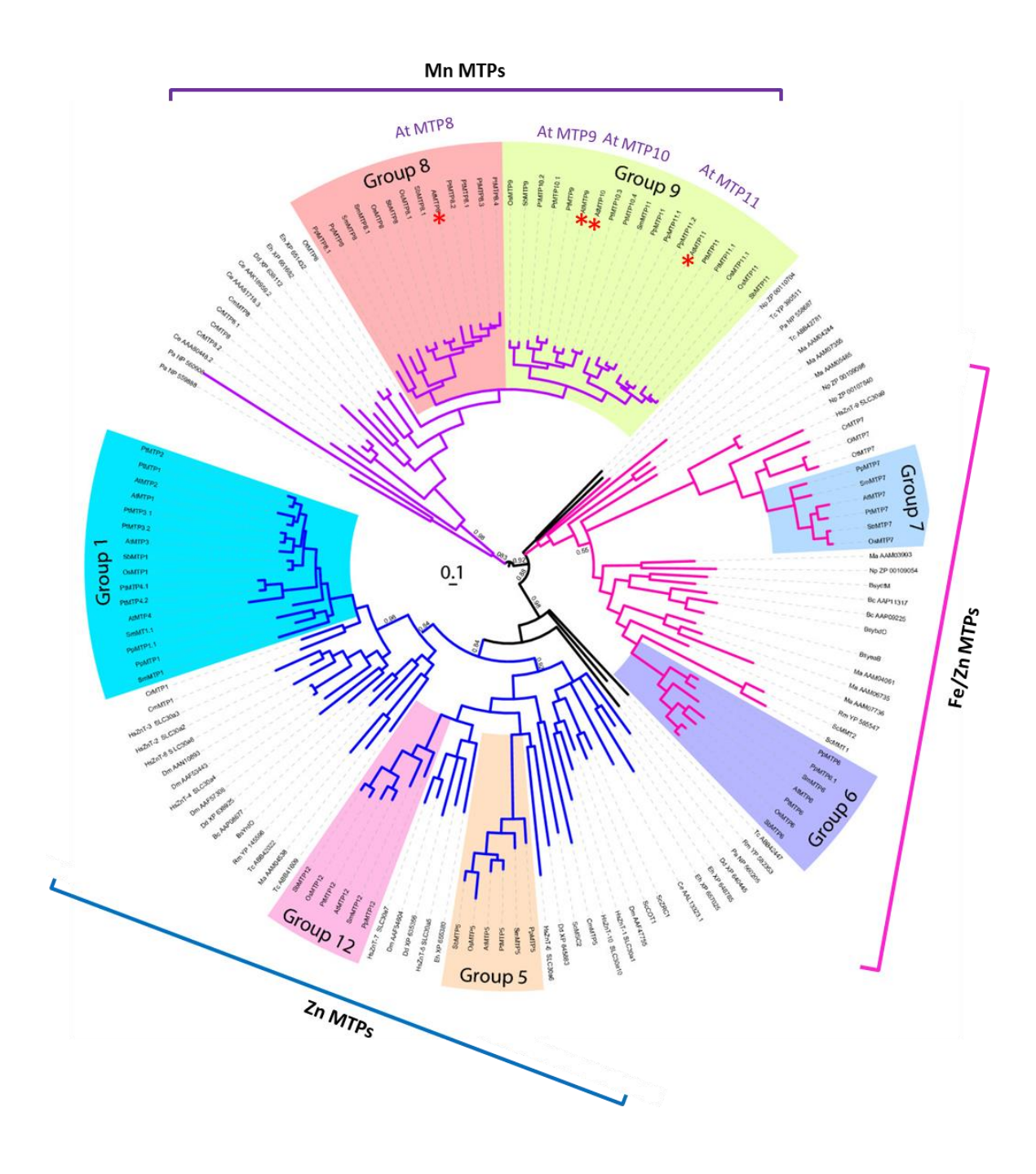


Figure 1.6. Phylogenetic relationship of land plant Metal Tolerance Proteins (MTPs).

Adapted from Gustin, et al. (2011). MTPs divide into three main clades based on their predicted substrate specificity: Mn- (purple), Zn- (blue) and Fe/Zn-transporting MTPs (pink). They divide further into groups based on Arabidopsis MTP nomenclature, e.g. Groups 8 and 9 are Mn-transporting MTPs. At MTP8, MTP9, MTP10 and MTP11 have been marked with '*' in the Mn clade.

1.3.3.1 MTP8 and MTP11 are Mn-transporting proteins

The putative Mn-transporting-MTPs are MTP8, of Group 8, and MTP9, MTP10 and MTP11, of Group 9 (Montanini, et al., 2007; Gustin, et al., 2011); collectively, these proteins will be referred to as the Mn-MTPs, or MTP8-MTP11. Table 1.2 summarises the Mn-MTPs which have been characterised to date, also listing some Zn-transporting examples. The experimental procedures in the majority of these studies include the use of knock out mutants and overexpression studies, fluorescence microscopy to determine subcellular localisation, and heterologous expression in sensitive yeast mutants to determine function; these techniques will be described in more detail in later sections. The first Mn-MTP to be functionally characterised was Sh MTP8, from tropical legume and heavy metal hyperaccumulator Stylosanthes hamata (Delhaize, et al., 2003). In addition to homologous proteins Cs MTP8 from cucumber (Migocka, et al., 2014) and Os MTP8.1 from rice (Chen, et al., 2013), the majority of MTP8 proteins are proposed to alleviate Mn toxicity by sequestering Mn in the vacuole; Hv MTP8 and MTP8.1 from barley are the exception, however, localising to the Golgi in planta (Pedas, et al., 2014). An aim of this thesis was to understand how At MTP8 functions together with other Arabidopsis MTPs to coordinate heavy metal homeostasis. Towards the end of this work, Eroglu, et al. (2016) published information suggesting At MTP8 also functions to detoxify cellular Mn at the tonoplast; this study will be discussed further in Chapter 3.

Although it is clear that At MTP11 also functions to alleviate Mn toxicity, the exact mechanism of this process remains unclear. The discrepancy lies within determining its subcellular localisation; two different endomembrane locations and thus detoxification mechanisms have been proposed for MTP11, as summarised in Figure 1.7 (Delhaize, et al., 2007; Peiter, et al., 2007). Both studies provide relevant evidence for each conclusion, which will be discussed further in Chapter 4; clearly more work is needed to clarify the role of MTP11 in Mn homeostasis. Although the other Arabidopsis Group 9 MTP members have not yet been characterized, MTP9 has been identified in rice (Ueno, et al., 2015) and cucumber (Migocka, et al., 2015); both proteins target the plasma membrane of roots to efflux Mn from root cells in a H⁺-coupling dependent manner. Cs MTP9 also has a transport affinity for Cd (Migocka, et al., 2015).

1.3.4 P_{2A}-type ATPases are calcium pumps with an affinity for manganese

Since very small changes in calcium concentrations can induce significant downstream events, free ion concentrations within the cytoplasm are often kept as low as 100 nM, compared to estimates for the vacuole, which can reach 5 mM Ca (Conn and Gilliham, 2000). Figure 1.8 summarises the range of Ca concentrations across the cytoplasm and organelles of a typical plant cell, highlighting the steep concentration gradient into the cytoplasm (Stael, et al., 2012). Ca-

Table 1.2. Summary of characterised Metal Tolerance Proteins (MTPs) from plants (adapted and updated from Ricachenevsky et al., 2013). '/', not yet determined; 'K/O', knockout mutant. Localisation has generally been determined in up to three ways: a subcellular localisation in yeast, b subcellular localisation in planta, transient expression, c subcellular localisation in planta, stable expression. Transcriptional regulation: ↑, up-regulated; ↓, downregulated. Metal exposure: +/++, severity of elevated metal exposure; -, reduced exposure/deficiency. Proteins divided into 3 clades based on Montanini, et al. (2007) phylogeny: Mn-clade, Zn-clade and Fe/Zn-clade.

MTP	Species	Proposed	Assays used to test transport	Transcriptional regulation	Subcellular	References
		substrate	function and specificity		localisation	
Mn clade						
At MTP8	Arabidopsis	Mn ²⁺	Sensitive yeast mutants: pmr1	个root with ++Mn;	Tonoplast ^a	Eroglu, et al., 2016
	thaliana		mtp8 K/O phenotype	(at 2mM Mn)		
Os MTP8.1	Oryza sativa	Mn ²⁺	Sensitive yeast mutants: pmr1	Mostly shoot exp.	Tonoplast ^b	Chen, et al., 2013
				个shoot with +Mn		
Sh MTP8	Stylosanthes	Mn ²⁺ , Cu ²⁺	INVSc2	/	Tonoplast, ER	Delhaize et al.,
	hamata		Sensitive yeast mutants: pmr1			2003, 2007
			Cnb1			
Hv MTP8	Hordeum	Mn ²⁺	Sensitive yeast mutants: pmr1	↓root with-Mn;	Golgi ^b	Pedas, et al., 2014
	vulgare			↑root, ↓ shoot with +/++Mn		
Hv MTP8.1	Hordeum	Mn ²⁺	Sensitive yeast mutants: pmr1	↑root, ↓shoot with –	Golgi ^b	Pedas, et al., 2014
	vulgare			Mn;	20.8.	. 6445, 664, 2021
	- 3			√root, ↓shoot with		
				+Mn/++Mn		
Cs MTP8	Cucumis	Mn ²⁺	Sensitive yeast mutants: pmr1	Root specific exp.	Tonoplast a, b	Migocka, et al.,
	sativis		K667	-Mn (↓root)		2014
				+Mn (个root)		

Cs MTP9	Cucumis sativis	Mn ²⁺ , Cd ²⁺	Sensitive yeast mutants: pmr1, K667	Root specific exp ↑root with +Cd/+Mn	Plasma membrane ^{a, b}	Migocka, et al., 2015
			Yeast PM vesicles +MTP9 + pH gradient	↓root with -Mn		
Os MTP9	Oryza sativa	Mn ²⁺	Sensitive yeast mutants: pmr1 Proteoliposomes +MTP9 +pH gradient Os mtp9 K/O	Root specific exp No change +/-Mn	Plasma membrane ^b	Ueno, et al., 2015
Bm MTP10	Beta vulgaris spp. maritima	Mn ²⁺	Sensitive yeast mutants: pmr1	•		Erbasol, et al., 2013
At MTP11	Arabidopsis thaliana	Mn ²⁺ , poss Cu ²⁺	INVSc2 Sensitive yeast mutants: pmr1 mtp11 K/O	?	PVC/Trans-golgi	Delhaize, et al., 2007; Peiter et al., 2007
PtMTP11.1	Populus trichocarpa	Mn	Sensitive yeast mutants: pmr1	/	Trans-Golgi	Peiter, et al., 2007
PtMTP11.2	Populus trichocarpa	Mn	Sensitive yeast mutants: pmr1	/	Trans-Golgi	Peiter, et al., 2007
Bm MTP11	Beta vulgaris spp. maritima	Mn, Ni	Sensitive yeast mutants: pmr1, cot1	+ Mn no change	Golgi ^a	Erbasol, et al., 2013
Zinc clade						
At MTP1	Arabidopsis thaliana	Zn ²⁺	Overexpression in Arabidopsis RNAi and T-DNA K/O	Expressed generally stably No change with + Zn	Tonoplast ^b	Van der Zaal, et al., 1999; Kobae, et al., 2004; Desbrosses- Fonrouge, et al.,

Os MTP1	Oryza sativa		zrc1cot1, pmr1, cdf1, ccc1 Os MTP1 expression in Arabidopsis; Os mtp1 K/O with	↑ with + Cd	Tonoplast ^{a, c}	2005; Kawachi, et al., 2008 Yuan, et al., 2012; Menguer, et al., 2013
At MTP5	Arabidopsis	Zn ²⁺	RNAi Sensitive yeast mutants: msc2	/	Form heterodimer to	•
At MTP12	thaliana			No change with +Zn or -Zn	function at the Golgi ^b	2015
Fe/Zn clade						
At MTP6	Arabidopsis thaliana	/	Ionomic profiling of K/O has altered Mg, Mn, Ca, Na, K, Mn, Cd levels; may be important in maintaining ionome	/	/	Baxter, et al., 2006

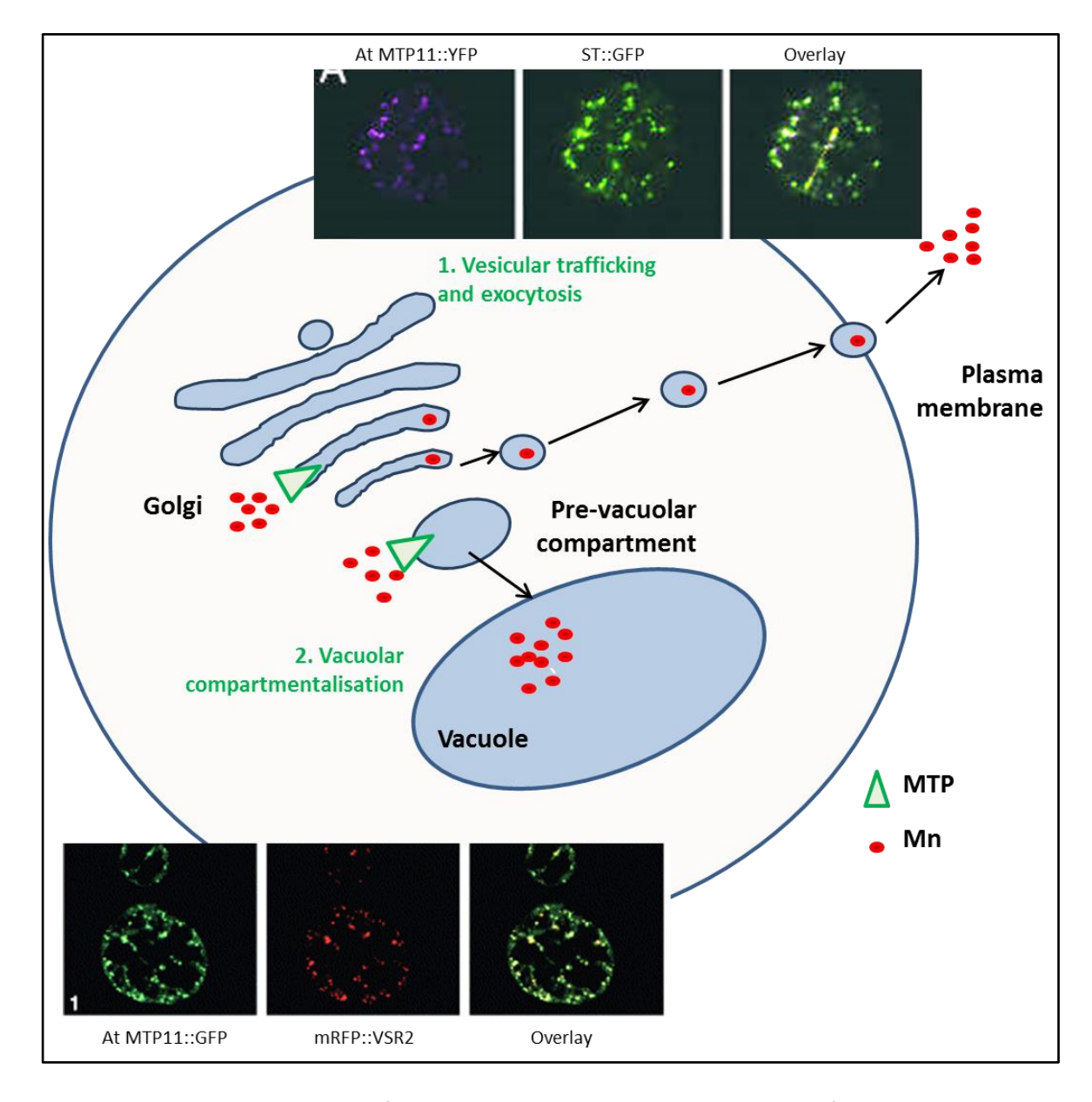


Figure 1.7. Two proposed detoxification mechanisms have been proposed for At MTP11.

1) At MTP11 targets the Golgi; Mn is sequestered into the Golgi and trafficked to the plasma membrane in vesicles for subsequent exocytosis. Confocal microscopy at the top of the figure shows partial overlap of At MTP11 with trans-Golgi marker sialyl transferase, ST::GFP, when transiently expressed in mesophyll protoplasts (Peiter, et al., 2007). 2) At MTP11 targets the pre-vacuolar compartment; Mn is sequestered in the PVC for subsequent compartmentalisation into the vacuole. Confocal microscopy at the bottom of the figure shows overlap of At MTP11 with PVC marker, mRFP::VSR2, when transiently expressed in tobacco protoplasts (Delhaize, et al., 2007).

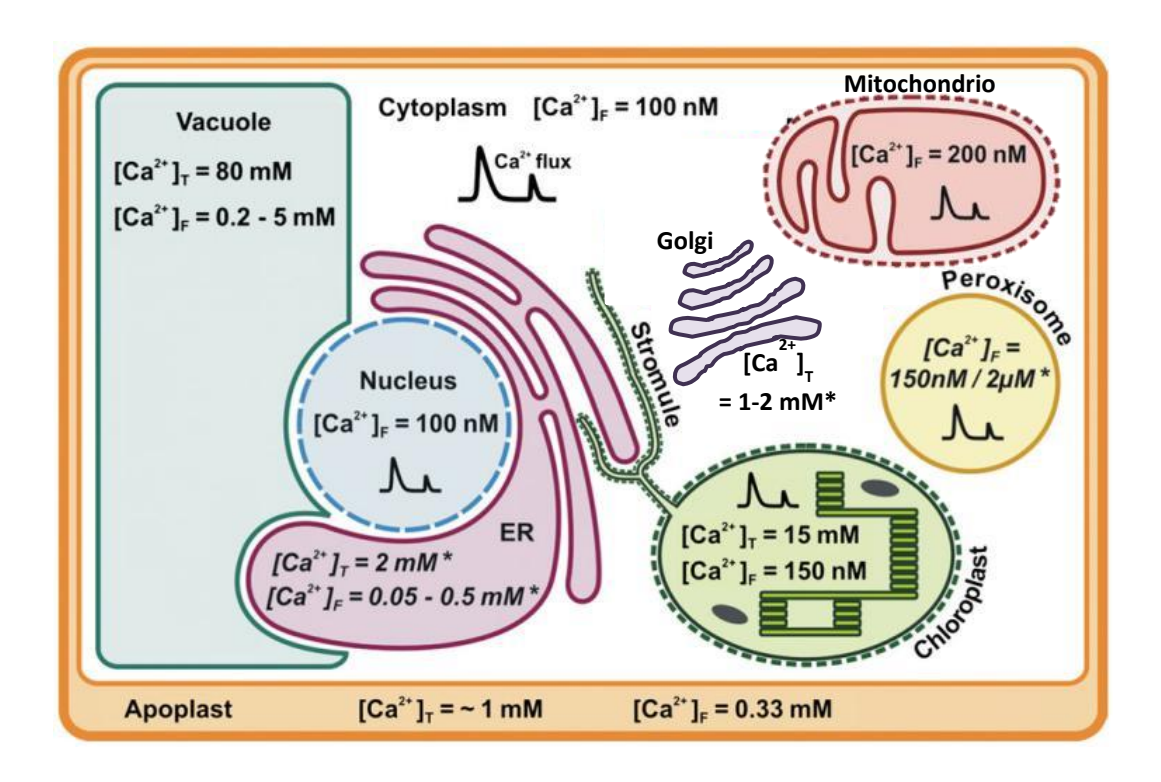


Figure 1.8. Approximate values for Ca concentrations across a typical plant cell.

Values for reported total ($[Ca^{2+}]_T$) and free resting ($[Ca^{2+}]_F$) Ca^{2+} concentrations in the different subcellular organelles of the plant cell (apoplast, cytoplasm, vacuole, nucleus, ER, chloroplast, mitochondrion, golgi and peroxisome). The values are approximate values and probably vary depending on the tissue or plant species, but nevertheless they provide a general impression of Ca^{2+} levels across the cell. For golgi, ER and peroxisomes, no data on Ca^{2+} concentration in plants are available. The given values are taken from the animal field and marked with an (*). Calcium fluxes are illustrated by a double peak-shaped symbol. Adapted from Stael, et al., 2012; golgi information from Chandra, et al., 1991.

permeable channels utilize this gradient to tightly regulate Ca influx; for example, ROS-controlled channels in Arabidopsis root hairs regulate a tip-to-base Ca gradient that ensures polar, directional growth of root hairs (Very and Davies, 1999; Cardenas, 2009). Following influx and the associated signaling event, pumps, such as ACA8 and ACA9 in pollen tube (Schiott, et al., 2004) are often responsible for actively returning Ca concentrations to normal. Table 1.3 provides some examples of a range of different calcium transporters responsible for mediating Ca signalling across the plant.

Table 1.3 also indicates which transporters have been shown to transport Mn in addition to Ca; surprisingly, few studies test the ability to transport both metals. The P_{2A}-type ATPases represent an important subfamily with affinity for both metals (Liang, et al., 1997; Durr, et al., 1998; Mills, et al., 2008; Li, et al., 2008; Barabasz, et al., 2011). A ubiquitous family of membrane proteins, the Ptype ATPases cluster phylogenetically into 5 major clades, according to substrate specificity (Axelsen and Palmgren, 1998; Pedesen, et al., 2012), as summarised in Figure 1.9. Clustering into these clades demonstrates the importance of conserved residues and motifs in determining function and substrate specificity, suggesting the ability to transport new substrates is accompanied by abrupt changes in the rate of sequence evolution. Members of the P-type ATPase family function according to an 'alternating-access' model (Jardetzky, 1966): ATP hydrolysis drives conformational changes between the catalytic 'E1' and modulatory 'E2' states to ensure 'opening' and 'closing' of the enzyme on opposite, alternate sides of the membrane, to pump a substrate up its concentration gradient. This is the Post-Albers mechanism (Albers, 1967; Post, et al., 1969), and is summarized in Figure 1.10, using the rabbit SERCA1a Ca²⁺-ATPase as a model. Originally purified from rabbit while skeletal muscle, the rabbit SERCA1a is the best structurally and functionally characterised P-type ATPase, with more than 20 crystal structures covering almost the full E1/E2 reaction cycle (Toyoshima, et al., 2000; Toyoshima and Nomura, 2002; Toyoshima and Mizutani, 2004; Obara, et al., 2005; Sorensen, et al., 2004; Olesen, et al., 2004; Jensen, et al., 2006). Shifting between E1 and E2 states is facilitated by three cytoplasmic domains. The actuator (A) domain facilitates gating of the ten SERCA1a transmembrane domains (TMDs), enabling binding and release of Ca (Daiko, et al., 2007). ATP binds to the nucleotide-binding (N) domain in the E1 state, stabilised by the binding of cofactor Mg ²⁺ in the phosphorylatory (P) domain, bringing ATP closer to enable nucleophilic attack and phosphoryl transfer to the phosphorylation residue, Asp351 (Sorensen, et al., 2004). This mechanism appears to be conserved for most P-type ATPases (Greie and Altendorf, 2007); the A, N and P domains are labelled in Figure 1.10.

Table 1.3. Examples of different types of putative calcium (Ca) transporters identified in Arabidopsis thaliana. Selectivity of transporters listed, including whether the ability to transport manganese (Mn) was tested or not. Reported physiological function is also listed. Where known, subcellular localization is listed. ?, information as yet unknown.

Name	Family/type of carrier	Selectivity	Was Mn affinity tested?	Subcellular localization	Physiological function	References
At TPC1 (Two-Pore Channel)	Slow voltage gated	Ca ²⁺ , K ⁺ , Ba ²⁺ , Mg ²⁺ , Na ⁺ , Ra ⁺ , Cs ⁺	No	Tonoplast for release (plasma membrane in Os and Nt TPC1)	Guard cell signalling, defense after leafe wounding; cation homeostasis	Furuichi, et al., 2001; Peiter, et al., 2005; Bonaventure, et al., 2007; Ranf, et al., 2008; Islam, et al., 2010
At GLR1.1	Glutamate Receptor Homolog; ligand-gated Ca ²⁺ permeable channel	Na ⁺ , K ⁺	No	Endomembrane system	ABA biosynthesis, ABA signalling, sensing C/N ratio	Chiu, et al., 2002; Kang, et al., 2004; Tapken & Hollmann, 2008;
At GLR1.2	Glutamate Receptor Homolog; ligand-gated Ca ²⁺ permeable channel	?	No	Plasma membrane for influx	Pollen tube growth	Michard, et al., 2011
At CNGC10	Cyclic nucleotide gated channel Calmodulin-binding	K ⁺ , Mg ²⁺	No	Plasma membrane for influx	Ca, K, Mg homeostasis,	Li, et al., 2005; Borsics, et al., 2007; Guo, et al., 2008; Guo,et al., 2010
At CNGC6	Cyclic nucleotide gated channel Heat-activated cAMP binding	Ca ²⁺ , Ba ²⁺ , Na ⁺	No	Plasma membrane for influx	Thermotolerance; induces expression of heat shock proteins for heat shock response Guard cell closure	Gao, et al., 2012; Wang, et al., 2013
At MCA1	Mechanosensitive, component of stretch- activated system	,		Plasma membrane for influx	Mechanosensing at roots	Nakagawa, et al., 2007; Kamano, et al., 2015
ANN1 (Annexin1)	ROS-activated hyperpolarisation activated Ca channel	Ca ²⁺ , K ⁺	No	Plasma membrane for influx	Uptake at roots May function in tip growth	Laohavisit, et al., 2012

At CAX1, CAX2,	Cation Anion	Ca ²⁺ , Mn ²⁺	Yes	Tonoplast for	Maintains low levels Ca in	Hirschi, et al., 2000;
CAX3	exchanger/Cation Antiport			sequestration	apoplast to avoid impairment of	Conn, et al., 2012;
	Exchanger				stomatal movement and cell wall	Connorton, et al., 2012
					rigidity; Ca/Mn homeostasis in	
					developing seed	
At CAX11	Cation Anion	?	No	?	Maintain cytosolic Ca levels,	Wang, et al., 2016
	exchanger/Cation Antiport				signaling in roots under hypoxic	
	Exchanger				conditions	
At ECA3	ER-type Ca-ATPase; P _{2A} -	Ca ²⁺ , Mn ²⁺ ,	Yes	Golgi or other	Alleviate Ca deficiency; functions	Mills, et al., 2008; Li, et
	type ATPase	poss Zn ²⁺		endomembrane	in alleviating either Mn deficiency	al., 2008; Barabasz, et
				compartment	or toxicity	al., 2011
At ACA8	Auto-inhibited Ca-ATPase;	?	No	Plasma membrane for	Maintain cytosolic Ca levels;	Bonza, et al., 2000;
	P _{2B} -type ATPase			efflux	sucrose signaling in early-seedling	Schiott, et al., 2004; dit
	Calmodulin-binding				development; signaling in roots	Frey, et al., 2012;
	G				under hypoxic conditions;	Zhang, et al., 2014;
					immune response	Wang, et al., 2016

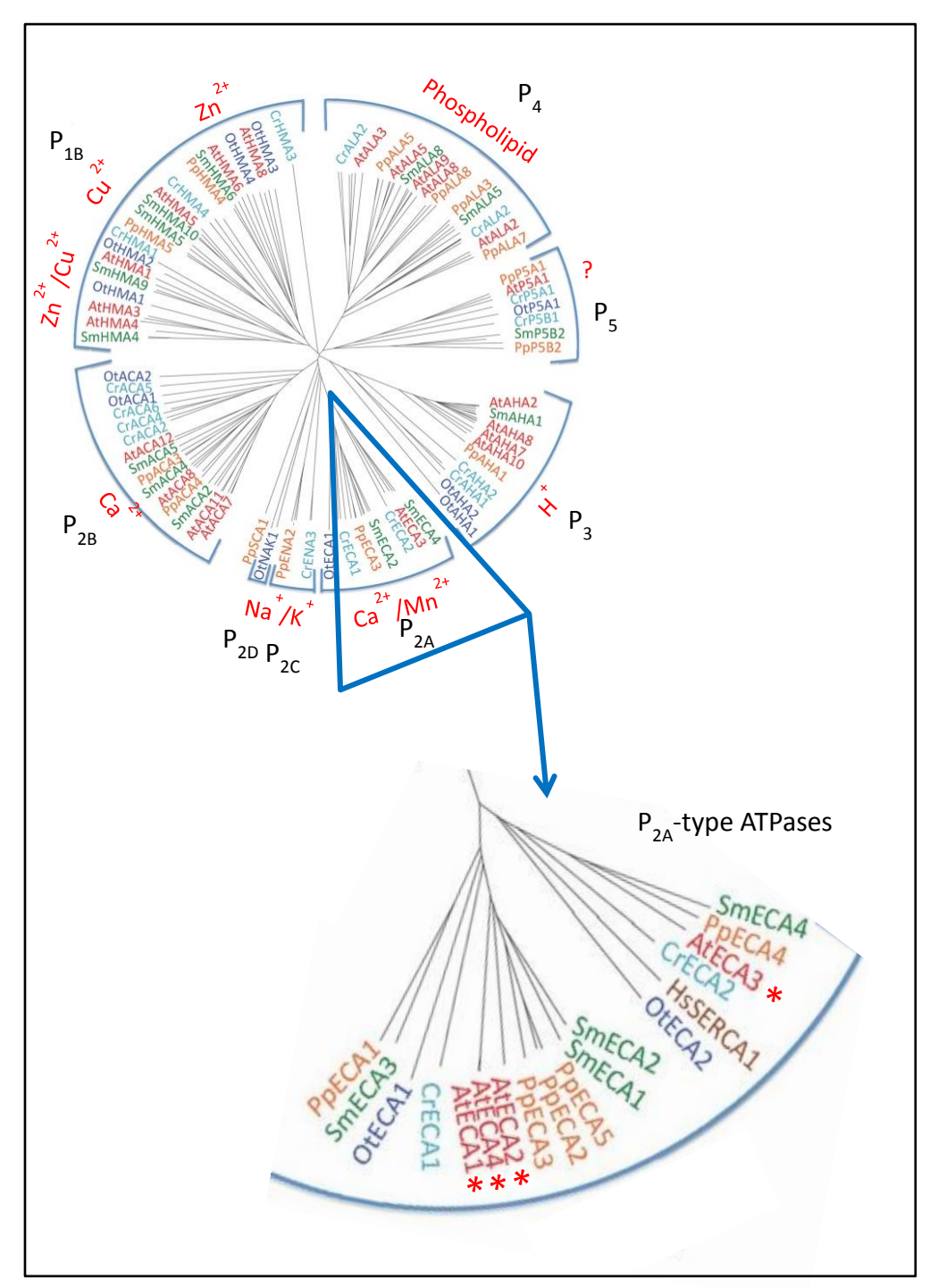


Figure 1.9. Phylogenetic tree of P-type ATPases in plant species.

Black writing, name of clade or subclade. Red writing, proposed substrate of clade; ?, unknown as of yet. Insert, zoom of P_{2A} -type ATPases, the ECAs (ER-type Ca^{2+} -ATPases). Inset shows detail of P_{2A} -type ATPases. *, Arabidopsis ECAs highlighted: At ECA1, 2, 3 and 4. Adapted from Pedersen, et al., 2012.

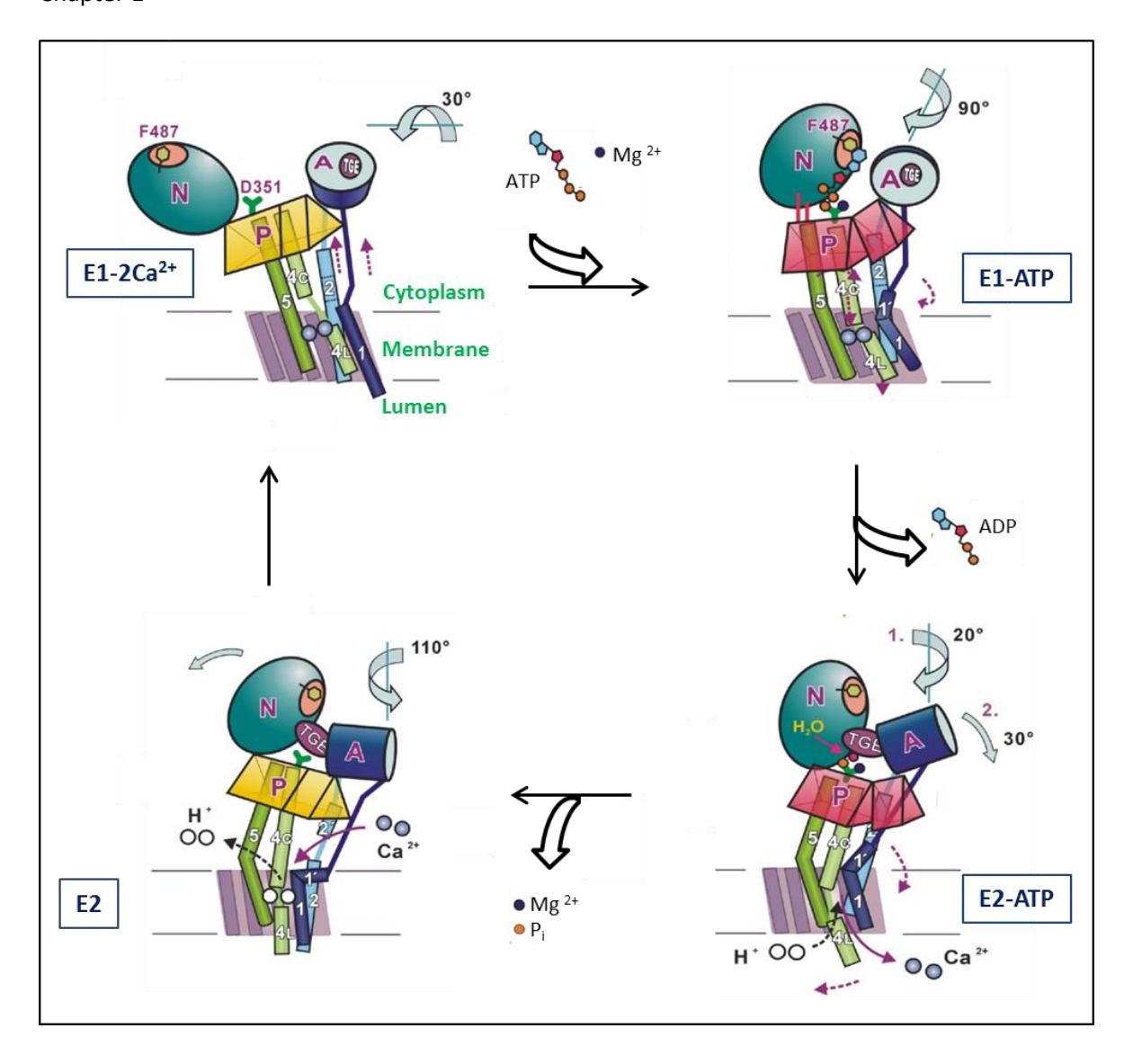


Figure 1.10. Post-Albers mechanism of pumping by P-type ATPases, using the rabbit SERCA1a as an example.

2 Ca²⁺ ions from cell interior ('cytoplasm') bind to a high-affinity site in E1 state, triggering phosphorylation (+ATP) of Asp residue in P domain, enabled by Mg²⁺ cofactor, leading to phosphorylated E1-ATP state. Conformational change results in E2-ATP state, which has reduced affinity for Ca, which is released. H⁺ binds from other side of membrane ('lumen'). Phosphorylated Asp residue is hydrolysed and Mg²⁺ is lost (E2 state), causing a conformational shift that releases H⁺ into the cytoplasm, ready to bind Ca and start a new cycle. Cartoon illustrates architecture of SERCA1a based on 7 crystal structures; 3 cytoplasmic domains (A, N, P) are labelled; α helices of transmembrane domain are labelled 1-5. Adapted from Toyoshima (2009) and Kuhlbrandt (2004).

1.3.4.1 The role of At ECA3 in Mn homeostasis is unclear

The P₂-type ATPases capable of transporting Ca divide into two further clades: P_{2A} and P_{2B} (Axelsen and Palmgren, 1998; Pedesen, et al., 2012). The P_{2B}-type ATPases, or ACAs (Autoinhibited Calcium ATPases), are generally stimulated by calmodulin and show homology to PMCAs, the calmodulin-binding Ca-ATPases of animal membranes (Geisler, et al., 2000). The P_{2A}-type ATPases, or ECAs (originally standing for ER Ca-ATPase), show homology to the SERCAs of the muscle cell ER and generally transport both Mn and Ca (Liang, et al., 1997; Durr, et al., 1998; Mills, et al., 2008; Li, et al., 2008; Barabasz, et al., 2011). Four P_{2A}-type ATPases exist in Arabidopsis: ECA1, 2 and 4 comprise a closely related cluster, separate from the less closely related ECA3 (Axelsen and Palmgren, 2001). Localising to the ER (Liang, et al., 1997; Liang and Sze, 1998), ECA1 was the first Arabidopsis ECA to be characterised. Its expression in sensitive yeast mutants is sufficient to restore tolerance to Mn-toxic and Ca-deficient conditions (Liang, et al., 1997) while the *eca1-1* Arabidopsis mutant is sensitive to these conditions (Wu, et al., 2002). Formation of the ECA1 phosphoenzyme intermediate can be stimulated with Ca, Mn or Zn (Liang, et al., 1997). Taken together, these findings demonstrate the ability of ECA1 to function under both Mn toxicity and Ca deficiency, possibly extending its substrate range to include Zn.

The role of At ECA3 in Mn homeostasis is less clear, with contrasting functions reported. Li, et al. (2008) report a role in alleviating Mn toxicity and Ca deficiency, with the eca3-4 Arabidopsis mutant suffering compromised root growth and shoot expansion on 50 μ M Mn, a condition usually treated as 'basal' Mn levels. Corresponding with this finding, expression of At ECA3 in tobacco improves growth compared to WT on mid-toxic levels of Mn, 100 μ M (Barabasz, et al., 2011). Restoration of Mn-tolerance in Mn-sensitive yeast mutant K616 was also observed, but only under constitutive promoter PMA1 (Li, et al., 2008). Contrastingly, a major role for ECA3 in Mn deficiency was reported by Mills, et al. (2008): both eca3-1 and eca3-1 mutants are chlorotic and stunted under Mn deficiency, but no sensitivity is observed under Mn concentrations up to 500 μ M Mn. Further, while Mills, et al. (2008) expressed ECA3::YFP in tobacco and observed overlap with markers of Golgi compartments, expression in mesophyll protoplasts by Li, et al. (2008) displayed no overlap with Golgi markers, colocalising instead with markers of the endosome/pre-vacuolar compartment (PVC).

It is clear, however, that ECA3 is important for Mn transport: *eca3* mutants are sensitive to low Ca (Li, et al., 2008; Mills, et al., 2008), while expression of ECA3 in tobacco increases tolerance to Ca deficiency (Barabasz, et al., 2011. ECA3 may therefore be important in alleviating Ca deficiency, feasibly by delivering Ca from the cytosol to function in the Golgi (Mills, et al., 2008) or for trafficking from the Golgi to further destinations via endosomes and post-Golgi compartments (Li,

et al., 2008). This project hopes to resolve the role ECA3 plays in Mn homeostasis, and clarify its subcellular localization.

1.3.5 NRAMPs are important transporters of Mn and other divalent metal cations

Another ubiquitous family of membrane transporters involved in divalent metal cation transport, including Mn, is the Natural Resistance Associated Macrophage Proteins (NRAMPs), originally named for their role in metal transport for host defence and immunity. While most members of the CDF family possess relatively tight substrate specificity (Montanini, et al., 2007; Peiter, et al., 2007; Delhaize, et al., 2007; Gustin, et al., 2011; Cubillas, et al., 2013), some members of the NRAMP family show quite a broad substrate specificity. Table 1.4 summarises the specificity of some NRAMP family members and the relevant studies associated with them. Despite the Mn/Ca antagonism alluded to in previous sections, the ability of NRAMP members to transport Ca is not always tested. However, most which are tested for Ca affinity are able to distinguish between divalent metal cations, such as Fe and Mn, and alkaline earth metals such as Ca. For example, Sca DMT, from Staphylococcus capitis, possesses a substrate-binding site capable of coordinating Mn, Fe and Cd, but not Ca; even in ten-fold molar excess, Ca did not interfere with Mn binding (Ehrnstorfer, et al., 2014). Similarly, the human NRAMP2 homolog, DMT1, is able to transport Mn, Fe and Co, but not Ca. As a major transporter involved in human intestinal Fe absorption, the ability to distinguish between micronutrients and Ca is important, with Ca at least 1000-fold more abundant in the duodenum plasma. Correspondingly, the mutation G185R shifts the selectivity of human DMT1 to include Ca, resulting in severe iron deficiency due to Fe/Ca competition in DMT1_{G185R} expressing mice (Su, et al., 1998; Xu, et al., 2004).

Phylogenetically, the NRAMPs fall into two main clades, based on eukaryotic or prokaryotic origin; this is shown in Figure 1.11A. The eukaryotic clade divides into two further groups, with the Arabidopsis NRAMP1 and NRAMP6 in Group 1, and At NRAMP2, 3, 4 and 5 in Group 2 (Thomine, et al., 2000; Pottier, et al., 2015); Figure 1.11B shows the relationship of the Arabidopsis and rice NRAMPs in closer detail (Takahashi, et al., 2011). At NRAMP1, 3 and 4 are included in the cellular diagram of Mn transporters in Figure 1.5; At NRAMP3 and 4 are involved in Mn remobilisation from the vacuole under Mn deficiency (Lanquar, et al., 2005; Lanquar, et al., 2010). Of key interest in this project are At NRAMP1, localized to the plasma membrane of root cells for Mn uptake from the soil under Mn deficiency, with an affinity for Fe²⁺ (Curie, et al., 2000; Cailliatte, et al., 2010) and At NRAMP2. At NRAMP2 remains relatively uncharacterized to date; it is unable to rescue the sensitivity to Fe deficiency of Fe-uptake-defective yeast mutant *fet3*, which may suggest NRAMP2 is unable to transport Fe, if also localised to the plasma membrane (Curie, et al., 2000). Despite contrary nomenclature, Os NRAMP5 is closest relative of At NRAMP1 in rice (Sasaki, et al., 2012),

Table 1.4. Key members of the Natural Resistance Associated Membrane Protein (NRAMP) family that have been characterised to the level of transport specificity and subcellular localisation. Proteins are divided into clades as per phylogenetic relationship of family members (Axelsen and Palmgren, 1998; Pedesen, et al., 2012). The table includes whether or not the ability to transport Ca was tested.

Species	Name/other name	Specificity	Was Ca tested?	Subcellular localization	Related info/function	References
Prokaryotic clad	e					
E. coli	MntH	Fe ²⁺ , Mn ²⁺	No	Plasma membrane	Involved in uptake	Makui, et al., 2000; Kehres and Maguire, 2003; Ikeda, et al., 2005
Staphylococcus capitis	Sca DMT	Fe ²⁺ , Mn ²⁺ , Cd ²⁺ , Zn ²⁺ to a lesser extent	Does not transport Ca	?	?	Ehrnstorfer, et al., 2014
Saccharomyces cerevisiae	SMF1	Mn ²⁺ , Fe ²⁺ , poss Zn ²⁺	No	Plasma membrane for uptake	Both SMF1 and SMF2 are regulated by Mn/Fe status of cell; degraded under replete	Supek, et al., 1996; Portnoy, et al., 2000
	SMF2	Mn ²⁺ , Fe ²⁺ , poss Zn ²⁺	No	Intracellular vesicles (remobilisation of Mn)	conditions	,
Plant subclade						
Arabidopsis thaliana	At NRAMP1	Mn ²⁺ , Fe ²⁺	No	Plasma membrane	Important uptake route into plant	Curie, et al., 2000; Cailliatte, et al., 2010
	At NRAMP3 and At NRAMP4	Mn ²⁺ , Fe ²⁺	No	Tonoplast for remobilisation	Remobilisation from vacuole to target PSII in chloroplast Display functional redundancy	Thomine, et al., 2003; Carter, et al., 2004; Lanquar, et al., 2005; Lanquar, et al., 2010
	At NRAMP6	Cd ²⁺ Mn ²⁺ transport	No	Endomembrane compartment, possibly		Cailliatte, et al., 2009

		inconclusive		acidic vesicular membrane		
Oryza sativa (rice)	Os NRAMP5 (homolog to At NRAMP1)	Mn ²⁺ , Fe ²⁺ ; Cd ²⁺	No	Plasma membrane (uptake)	Mediates transit through root to shoot	Curie, et al., 2000; Sasaki, et al., 2012; Ishimaru, et al., 2012; Ueno, et al., 2015
Nicotiana tabaccum (tobacco)	Ah NRAMP1	Mn ²⁺ , Fe ²⁺	No	Plasma membrane		Sano, et al., 2012
Animal subclac	le					
Human	Slc11A1 (NRAMP1)	Fe ²⁺ , Mn ²⁺ , H ⁺	Does not transport Ca	Disputed: Plasma membrane Or endosome	Antiporter of H ⁺ /cations Involved in immune response	Searle, et al., 1998; Jabado, et al., 2000; Goswami, et al., 2001; Xu, et al., 2004; Nairz, et al., 2009; Fritszche, et al., 2012; Cellier, et al., 2016
	Slc11A2 (NRAMP2/DMT1)	Fe ²⁺ , Mn ²⁺ , Cd ²⁺ , Co ²⁺ , Ni ²⁺ , Zn ²⁺ (not Cu ²⁺)	Ca not transported; Ca is a low affinity non-competitive inhibitor	Different isoforms; Isoform I at plasma membrane; isoform II at recycling endosomes	Symporter of H ⁺ /cations Different isoforms involved in immune response or supplying of Fe/Mn	Gruenheid, et al., 1998; Goswami, et al., 2001; Poon, et al., 2004; Lam- Yuk-Tseung, et al., 2005; Shawki, et al., 2010; Illing, et al., 2012

also targeting the plasma membrane to transport Mn and Fe²⁺ into the plant (Sasaki, et al., 2012; Ishimaru, et al., 2012). Os NRAMP5 and Os MTP9, on opposite sides of root cells, have recently been shown to function together to mediate directional Mn transit through the root to aid root-to-shoot translocation of Mn (Ueno, et al., 2015), highlighting the importance of determining the cooperative role played by proteins to truly understand metal homeostasis. This project aims to begin characterisation of At NRAMP2, determining if and how it functions under Mn deficiency in cooperation with At NRAMP1 (Cailliatte, et al., 2010) and At ECA3 (Mills, et al., 2008).

1.4 Regulation of heavy metal homeostasis

Expression of heavy metal transporters must be tightly regulated for cells to maintain control over their intracellular and subcellular metal concentrations. Although it is known that the regulation of certain genes is affected by Mn status, such as At NRAMP1 which is upregulated under Mn deficiency (Cailliatte, et al., 2010) or At MTP8 which is upregulated under Mn toxicity (Eroglu, et al., 2016), the mechanism behind the regulation is yet to be identified; relatively little is currently understood regarding the regulation of Mn transport in plants. The homologous transporter to NRAMP1 in Salmonella enterica, MntH, is downregulated at the transcriptional level under Mn replete conditions, by transcription factors (TFs) Fur and MntR (Kehres and Maguire, 2002; Ikeda, et al., 2005). Identifying a homolog to either TF in Arabidopsis may be a starting point for elucidating transcriptional control of At NRAMP1. The NRAMP homologs in S. cerevisiae and C. elegans, SMF1 and SMF2, are post-translationally regulated by Mn, degraded in the vacuole under Mn-replete conditions but allowed to target their destination membranes under Mn starvation: SMF1 targets the plasma membrane while SMF2 targets intracellular vesicles. Here they act to transport Mn to final destinations, via uptake from the extracellular environment (SMF1) and possibly mobilisation of the metal from vesicular stores (SMF2) (Portnoy, et al., 2000; Au, et al., 2009).

The importance of histone modification in the transcriptional control of Fe homeostasis is beginning to emerge. To activate aspects of the Fe deficiency response, FIT1 (FER-like Iron deficiency induced Ttranscription factor) must dimerise with members of the Ib subgroup of bHLH TFs, bHLH38, bHLH39, bHLH100 or bHLH101 (Yuan, et al., 2008). This is prevented under Fe replete conditions by At PRMT5 (Protein Arginine Methylase 5; also known as SKB1) which catalyses methylation of chromatin promoter of the *bHLH* TFs, inhibiting their transcription (Fan, et al., 2014; Li, et al., 2016). Correspondingly, a drop in Fe availability results in dissociation of PMRT5 from the *bHLH* chromatin, enabling the subsequently translated TFs to dimerise with FIT1 and upregulate *IRT1* (Vert, et al., 2002), *FRO2* (Colangelo & Guerinot, 2004) and *MTP8* (Eroglu, et

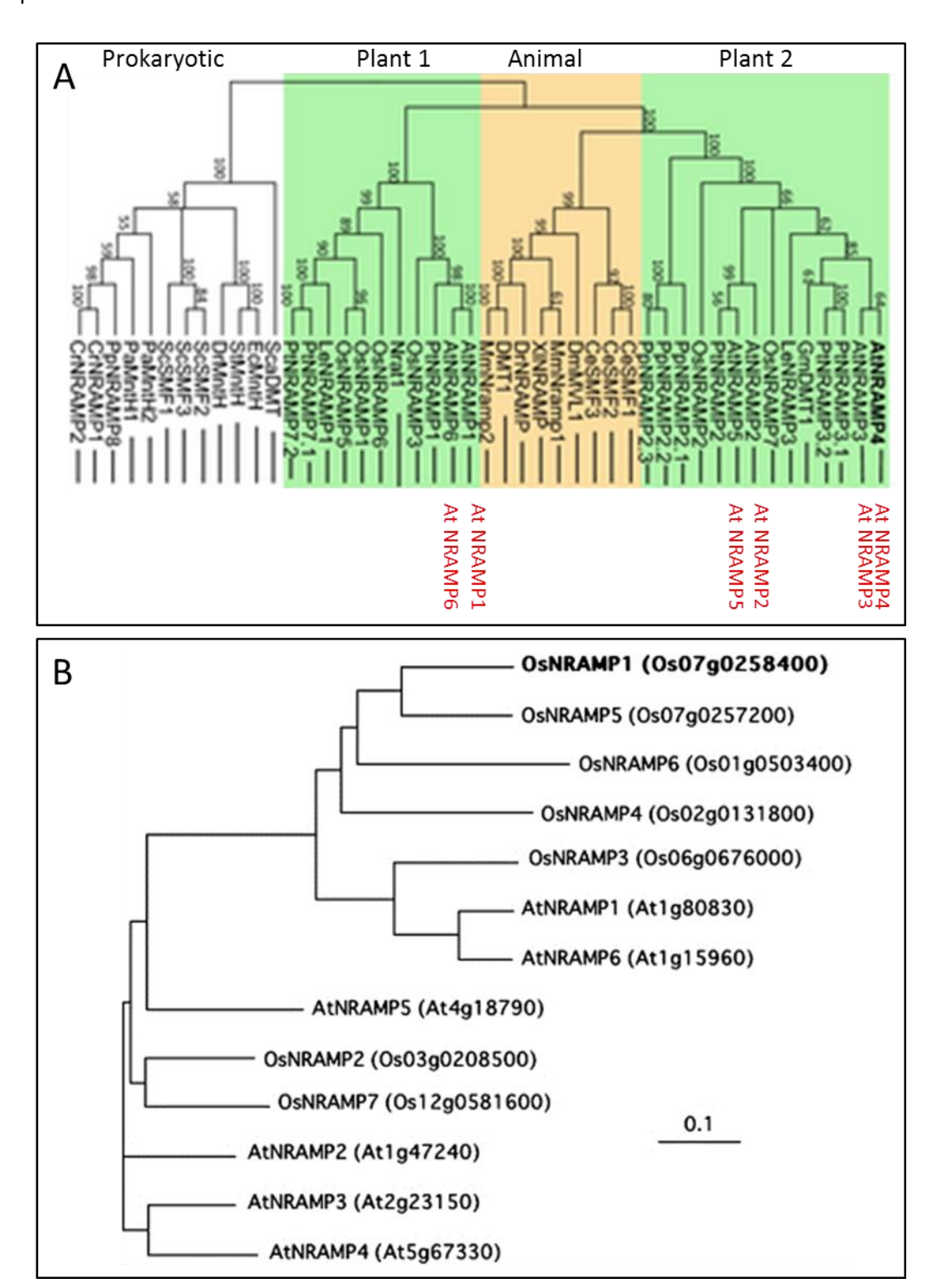


Figure 1.11. Phylogenetic relationship of NRAMP transporters.

A) Phylogenetic tree of natural resistance associated macrophage proteins (NRAMPs), divided into clades based on the evolutionary relationship of their parent species, as labelled. Plants divide further into two clades, Plant 1 and Plant 2. The Arabidopsis NRAMPs have been labelled as reference in red. From Potier, et al. (2015). B) Closer analysis of relationship of Arabidopsis and rice (Os) NRAMPs. From Takahashi, et al. (2011).

al., 2016). This also impacts Mn nutrition, because Mn competes for uptake by IRT1 (Conn0lly, et al., 2003) and is sequestered into the vacuole by MTP8 (Eroglu, et al., 2016) when Fe^{2+} is scarce. The dimerization of FIT1 with the bHLH TFs provides an example of post-translational modification in the Fe response (Yuan, et al., 2008).

Another example of metal homeostasis at the transcriptional level is the role of the bZIP (basic region leucine-zipper) TFs in upregulation of certain ZIP (ZRT-, IRT-like Protein) family members. Under zinc deficiency in Arabidopsis, bZIP19 and bZIP23 bind to a 10 base-pair palindromic region (the ZDRE domain; Zinc Deficiency Response Element) in the promoter of *ZIP4*, upregulating its expression to promote the Zn-deficiency response (Assunçao, et al., 2010).

Histone acetylation has also recently been shown to be involved in Fe homeostasis. Another member of the Fe deficiency response, FRD3, facilitates Fe uptake by effluxing citrate to chelate Fe³⁺ from the soil (Delhaize, 1996; Rogers and Guerinot, 2002; Roschzttardtz, et al., 2011). Acetylation of FRD3 under Fe deficiency, by GCN5 (General Control Non-repressed Protein 5), promotes its transcription, while it is negatively regulated by deacetylation by HDA7 (histone deacetylation 7; Xing, et al., 2015). The *frd3* mutant is allelic to *man1*, a mutant which is characterised by Mn overaccumulation (Delhaize, 1996; Rogers and Guerinot, 2002); it is possible, therefore, that this acetylation of FRD3 is also involved in Mn homeostasis an as-yet-unidentified way, or could simply echo the Fe/Mn antagonism with Mn exploiting routes of Fe uptake when FRD3 is unable to provide citrate for Fe-chelation.

1.5 Potential application of knowledge

Understanding the pathways behind metal homeostasis could be important in biofortification and phytoremediation. According to the 5th report from the United Nations System Standing Committee on Nutrition (SCN) (2004), micronutrient malnutrition affects over half of the world's population. Although progress has been made to control these deficiencies via supplementation, new, sustainable approaches are needed. Cereal grains are inherently low in heavy metal nutrients (Yang, et al., 1998; White & Broadley, 2009). Biofortification aims to enrich cereal grains with particular nutrients, through breeding strategies or genetic modification. This approach targets the rural poor and low-income households, capitalising the need for regular intake of cereal crops as a staple diet, to enhance consumption of essential micronutrients. Similarly, after the initial investment in developing self-fortifying seeds, recurrent costs should be low and, once in place, the system is highly sustainable (Nestel, et al., 2006). Although Mn deficiency is not a pressing concern for human nutrition, dissecting Mn pathways may identify pathways important for shoot-loading of other nutrients too: as alluded to in this report, multiple pathways are

responsible for transport of both Mn and Fe (Vert, et al., 2002; Cailliatte, et al., 2010; Eroglu, et al., 2016), while transporters such as At ZIP2 are involved in root-to-shoot translocation of both Mn and Zn (Milner, et al., 2013).

Improved knowledge of these pathways, in particular those which are altered or enhanced in genotypes differing in their Mn efficiency, could also be used to engineer cultivars that perform better under poor soil conditions. Manganese deficiency in plants is a widespread problem, commonly reported to impact crop yield (Jiang, 2006; Yang, et al., 2007; Hebbern, et al., 2009; Roques, et al., 2013). Correction of nutritional deficiencies in crops with fertiliser is both economically and ecologically unsustainable (Hart, 1997; Cakmak, 2002); a more sustainable approach is needed. As alluded to in an article by Borrill, et al. (2014), determining whether metal uptake and distribution pathways are conserved in different species enables hypothesis generation for these processes in plants where the pathways are less well known, such as wheat. Further characterising genes involved in Mn uptake from soil, such as NRAMP1 (Cailliatte, et al., 2010), and identifying homologous proteins in agriculturally relevant plants, could be a starting point for sustainable strategies to improve crops' abilities for uptake and growth under conditions of deficiency.

Manganese contaminated soil and subsequent toxicity is another prevalent issue (Adams, 1981; Hue, 1988). A similar biotechnological approach for above-ground metal accumulation is phytoremediation; this is the plant-based 'clean-up' of contaminated soils, providing a low-cost, flexible technology (Kraemer, 2007). A basic knowledge of metal pathways in plants is essential in the design of this approach. Identifying agricultural homologs to proteins involved in Mn detoxification, such as members of the Metal Tolerance Proteins (Peiter, et al., 2007; Delhaize, et al., 2007; Chen, et al., 2013; Eroglu, et al., 2016) is an important starting point. Identifying the genetic mechanisms involved in the increased accumulation of Mn in hypertolerant species, such as *Gossia bidwillii* (Bidwell, et al., 2002; Fernando, et al., 2006), and applying this knowledge to plants with greater above-ground tissues, could provide targets for phytoremediation. Similarly, Os NRAMP5 and Os MTP9 are involved in the transport of both Mn and Cd from roots to shoots (Ishimaru, et al., 2012; Ueno, et al., 2015); these could be promising candidate genes for investigating phytoremediation of Mn- or Cd-contaminated soils.

1.6 Overall Aims of the Project

The overall aim of this project is to further elucidate specific pathways involved in manganese homeostasis of higher plants. This will focus primarily on three families of known manganese transporters: the Metal Tolerance Proteins (MTPs), the P_{2A} -type ATPases, and the NRAMPs. The

majority of research will be undertaken using the model plant *Arabidopsis thaliana*, although certain areas will be extended to rice (*Oryza sativa*) and bread wheat (*Triticum aestivum*). The following points summarise the broad aims of this project:

• To further characterise the roles of the Mn-MTPs in Mn homeostasis of Arabidopsis

This will involve isolation and characterisation of single T-DNA insertion mutants for each of *mtp8*, *mtp9*, *mtp10* and *mtp11*. A key aim of this project is to determine the relative involvement of different proteins in Mn homeostasis, and whether they function together. Where possible, double and triple mutants will be generated to explore this.

This project also aims to clone each of MTP8, MTP9, MTP10 and MTP11 for expression in Arabidopsis for overexpression and/or functional complementation studies. Expression in metalsensitive yeast mutants will test the Mn-transporting ability of these proteins, as well as determine their substrate selectivity. Bioinformatic analysis will be performed to determine key residues conserved in different MTP clades; the project aims to determine which residues are important for function and/or specificity by site directedly mutating these residues and comparing their growth differences when compared to non-mutated MTPs in yeast. A key aim is also to determine or confirm the subcellular localisation of these proteins through stable expression of GFP-tagged clones in Arabidopsis, or transient expression in tobacco with relevant organelle markers.

• To further understand the Ca/Mn antagonism

Two calcium regimes will be utilised during this project: low and basal Ca, to determine the growth of potentially Mn-sensitive T-DNA insertion mutants under different Ca availabilities. It is hypothesised that Mn-dependent observations will be exacerbated when Ca is less available. In addition to the agarose plate-based assay routinely used for phenotypic analysis, a hydroponics-based system will be developed to allow exposure to different Mn and Ca conditions at different developmental stages.

• To determine the role of ECA3 in Mn homeostasis

Single and double T-DNA insertion mutants will be used to determine whether ECA3 is involved in Mn homeostasis primarily under Mn deficiency, as proposed by Mills, et al. (2008) or toxicity, as proposed by Li, et al. (2008). Additionally, ECA3 will be transiently expressed in tobacco with relevant subcellular markers to determine clarify its subcellular localisation, in particular in relation to MTP11, another protein which is involved in Mn toxicity (Delhaize, et al., 2007; Peiter, et al., 2007).

To further characterise the roles of the NRAMPs in Mn deficiency

At NRAMP1 has already been implicated in alleviating Mn deficiency (Cailliatte, et al., 2010); this project aims to characterise three insertion mutants with different Mn-dependent growth patterns to further characterise the function of NRAMP1. The role of At NRAMP2 in Mn homeostasis is yet to be determined; this project aims to isolate and characterise single T-DNA insertion mutants for *nramp2* to determine any role in Mn homeostasis. Further, it aims to clone NRAMP2 for expression in tobacco to determine its subcellular localisation, and in yeast to further characterise any transport activity. Double and triple mutants will be made between *eca3*, *nramp1* and *nramp2* to determine the relative involvement of each protein in Mn homeostasis and whether they share any functional redundancy.

• To extend the knowledge learned from Arabidopsis to crop plants

This project aims to perform bioinformatic analyses of the Arabidopsis Mn MTPs, and extend this by performing a phylogenetic analysis to identify homologous transporters in more agriculturally relevant species, such as bread wheat (*Triticum aestivum*), a genome which is being sequenced at present. In collaboration with NIAB (Cambridge, UK) the project aims to downregulate homologous *MTP* genes in *T. aestivum* using RNAi, to determine whether the Mn-transporting function of the Mn-MTPs is conserved between Arabidopsis and wheat.

Two homologs to At MTP11 exist in rice: Os MTP11 and Os MTP11.1 (Chen, et al., 2013). To determine whether the function of MTP11 is conserved in rice, Os MTP11 will be stably expressed in the Mn-sensitive Arabidopsis mutant, *mtp11*, and will be transiently expressed in tobacco to determine its subcellular localisation.

Chapter 2: Materials and Methods

2.1 Plant growth and materials

2.1.1 Growth conditions for soil-grown Arabidopsis thaliana and Triticum aestivum

The Arabidopsis T-DNA insertion mutants used in this project are summarised in Table 2.1. Mutants were isolated from either the Columbia (Col) 8, Col0 or Wassilewskija (Ws) ecotype background. The *mtp11-1* mutant was kindly provided by Dr Jon Pittman. All others were obtained from SIGnAL T-DNA collection (Alonso, et al., 2003; http://signal.salk.edu/). Soil grown plants were sown in 8 cm pots containing soil (one part Levingtons F5 no. 2; one part John Innes no. 2; one part Vermiperl-graded horticultural vermiculite, medium grade; 1:1:1) sterilised by autoclaving at 121 °C for 15 minutes at 1 bar pressure before addition of 0.28 g/L lmidasept insecticide (Fargro). To achieve soil of pH 7.2, soil was limed with 20 g/kg CaCO₃ and 12 g/kg NaHCO₃; pH was determined using 100 mM CaCl₂ (all Sigma Aldrich). Plants were grown in environmentally controlled rooms (23 °C constant; 16 h light, 120 μmol m⁻² s⁻¹, 60% humidity; 18 °C, 8 h dark, 55% humidity cycle). Wheat plants (*Triticum aestivum*; ecotype Fielder) were grown on the same 1:1:1 composition soil in 20 cm diameter pots and grown in a glasshouse.

2.1.2 Generating double mutants in Arabidopsis

To generate double mutants, soil-grown plants were crossed at 5-6 weeks old by emasculating the maternal plant and transferring pollen from paternal anther to maternal stigmata after two days maturation. Crossed siliques were harvested after 15 to 25 days and allowed to dry at room temperature before sowing the F1 generation. F1 plants were confirmed heterozygous and were allowed to self-fertilise and were harvested to obtain the F2 generation. F2 plants were screened for double homozygous plants. The *mtp8-2 mtp10-1*, *eca3-1 nramp1-1*, *nramp1-1 nramp2-1* and *eca3-1 nramp2-1* double mutants were obtained at the F2 generation; *mtp8-2 mtp11-1* was obtained at the F3 generation. The *mtp10-1 mtp11-1* and *eca3-2 mtp11-1* double mutants were provided by Dr. Lorraine E. Williams. The *mtp8-2 mtp10-1 mtp11-1* triple mutant was obtained by crossing *mtp8-2 mtp11-1* homozygous plants with *mtp8-2 mtp10-1 nramp1-1 nramp1-1* homozygous plants with *nramp1-1 nramp2-1* homozygous plants.

Table 2.1. Accession numbers and mutant lines used in the project. The *mtp9* mutant is a FLAG insertion line using the pGBK vector. All other mutants are SALK insertion lines using the pROC2 vector. All mutants were independently isolated in the LEW lab; reference indicates the first description of the mutant.

Accession	Gene	Line	Mutant	T-DNA	WT	Reference
Number			allele	Vector	background	
At3g58060	At MTP8	N568494	mtp8-1	pROC2	Col0	Eroglu, et
		N660626	mtp8-2	pROC2	Col8	al., 2016
At1g79520	At <i>MTP9</i>	FLAG_484F10	mtp9-1	pGKB5	Ws	
At1g16310	At MTP10	N686728	mtp10-1	pROC2	Col8	
		N657894	mtp10-2	pROC2	Col8	
At2g39450	At MTP11	N525571	mtp11-1	pROC2	Col8	Peiter, et
		GABI_366A03	mtp11-3	pAC106	Col0	al., 2007
At1g10130	At ECA3	N545567	eca3-1	pROC2	Col8	Mills, et
		N570619	еса3-2	pROC2	Col8	al., 2008
At1g80830	At NRAMP1	N553236	nramp1-1	pROC2	Col8	Cailliatte, et al., 2010
		N579653	nramp1-2	pROC2	Col8	
		N679062	nramp1-3	pROC2	Col8	
At1g47240	At NRAMP2	WiscDsLoxHs005_04F	nramp2-1	pDsLox	Col8	
		GABI_306A04	nramp2-2	pAC106	Col0	

To confirm zygosity, genomic DNA (gDNA) was extracted from plants using DNAMITE Plant Kit (Microzone Ltd, UK) using 1/3 volumes of manufacturer's instructions. Reverse transcriptase PCR (RT-PCR; see section 2.3.3) using Biomix Taq (Bioline) and primers targeting the gene of interest and the T-DNA vector confirmed the presence of T-DNA and absence of the wild type gene. Primers and PCR conditions are summarised in Table 2.2. Mutants were confirmed twice at the gDNA level before RNA extracted and a cDNA library was synthesised (section 2.3.1). The same primers were used to confirm absence of WT gene at RNA level; amplification of the *ACTIN* gene was used as a control.

2.1.3 Isolating stably transformed Arabidopsis lines

Arabidopsis seedlings were transformed at approx. 6 weeks of age using the floral dip method (Clough & Bent, 1998). At 5 weeks the first shoot bolts were clipped back to the rosette to encourage proliferation of secondary bolts. A positive GV3580 *Agrobacterium* colony (see section 2.2 for details) was inoculated for 16 hours, 30 °C (200 rpm) in 5 mL LB containing 50 μ g/mL rifampicin, 50 μ g/ml carbenicillin and 50 μ g/ml kanamycin. This starter culture was inoculated in 250 mL selective LB and the incubation step repeated. Following incubation, 100 μ M acetosyringone (Sigma Aldrich) was added to the culture and incubation continued for a further 3 hours. Cells were then harvested at 3700 g for 15 minutes and the pellet resuspended in 125 mL 5% sucrose (Sigma Aldrich). Silwett-L77 was added to the suspension at a final concentration of 0.04%. Above-ground parts of the plant were dipped in this solution with gentle agitation for 2 to 3 seconds before securing in a plastic sleeve and leaving in the shade with high humidity. Humidity and light were returned to normal conditions after 24 hours, and plants were grown for 6 to 8 weeks before harvesting T1 seeds.

T1 seeds were screened for positive transformants on ½ MS (1% (w/v) sucrose; 1% (w/v) agar; details section 2.1.4) plates supplemented with 50 μ g ml⁻¹ hygromycin before transplanting to soil and allowed to self-fertilise. Segregation ratio analysis was performed on T2 generation seeds to identify lines with 75% resistance to hygromycin, before transplanting to soil for self-fertilisation. RNA was extracted from T3 lines with 100% resistance to hygromycin; semi-quantitative RT-PCR was performed on resultant cDNA to confirm presence of transgene.

2.1.4 Metal Tolerance Assays in Arabidopsis thaliana

Arabidopsis seeds were sterilised for 20 minutes in 15% hyperchloride (Domestos) before washing with sterile double-distilled 18 M Ω water (SDW). For plate experiments, seeds were sown on

Table 2.2. Primers used to confirm zygosity of single, double and triple *mtp* insertion mutants, and single, double and triple *nramp1*, *nramp2* and *eca3 mutants*. Primers obtained from Integrated DNA Technologies.

Primer	Target	Sequence	Annealing	
			temp	used
			(°C)	
Targeting T-DNA				
LBa1	pROC2	5'-GCGTGGACCGCTTGCTGCAACT	60/62	
FLAG_LB4	pGKB5	5'-CGTGTGCCAGGTGCCCACGGAATAGT	60	
GABI_LB	pAC106	5'-ATATTGACCATCATACTCATTGC	60	
Targeting WT gene of	interest			
MTP8F	МТР8	5'-TGGTTGCGGCCGTTCTTGCTA	60	
MTP82R	MTP8	5'-AGGACGGAATGTTCAGGCTTGTGA	60	
MTP8_topowithstop	MTP8	5'-TCATAAATCGTTGGGGATTGTA	60	
MTP9F	МТР9	5'-AGCGATCGGTTATGGCGGCG	60	
MTP9R	МТР9	5'-CTGGTGGTGCTGAGCGTCCT	60	
MTP10F	MTP10	5'-GATGCGCCGCCGCTTGAATC	62	
MTP10R2	MTP10	5'-GAGACGGCACAACGTTCAAGTATCT	62	
MTP11seq43.F	MTP11	5'-CTGCTCGAGTTTCACGGTAAC	60	
MTP11jkp1.R	MTP11	5'-AATCTGCAATCCAAGTGTTGC	60	
ECA3_10ex_F	ECA3	5'-GCATACACGATTCTATGTTGCAGACAGATGAT	60	
ECA3NR0204	ECA3	5'-GCTCTGCAGATTGGACTACA	60	
NRAMP1b_fwd	NRAMP1	5'-AGGCCCTGGTTTTCTTGTTT	60	
AtNRAMP1R	NRAMP1	5'-GGAACCAACGCAAACGGGAGCT	60	
NRAMP2_promF	NRAMP2	5'-CACCATGGAAAACGACGTCAAAG	60	
NRAMP2_R	NRAMP2	5'-AGCTTCTAACTTCCTCACACCG	60	
NRAMP2_topoF	NRAMP2	5'-TTCAAAATTCAGGTACGTCGAC	60	
Actin2F	ACT2	5'-GGTAACATTGTGCTCAGTGGTGG	60	
Actin2R	ACT2	5'-CTCGGCCTTGGAGATCCACATC	60	

plates generally containing half-strength Murashige & Skoog medium (½ MS; Murashige & Skoog, 1962) containing 1% (w/v) sucrose (VWR Chemicals), 0.8% (w/v) agarose (Melford Laboratories Ltd), with generally 6 plates per condition, and 4 seedlings per genotype per plate. For calcium assays, Ca was adjusted from 100 μM Ca (low Ca) to 1495 μM Ca, provided as CaCl₂ (Sigma Aldrich). For Mn assays, Mn was either omitted from the media or supplied as MnSO₄ (Sigma Aldrich). The pH was adjusted to 5.8 with KOH before autoclaving at 119 °C for 20 minutes at 1 bar pressure. plates were wrapped with Micropore tape (Nu-Care Products Ltd). Seeds were stratified at 4°C for 48 hours before transfer to a controlled-environment cabinet (23°C, 16h light, 120 μmol m⁻² s⁻¹; 18 °C, 8h dark cycle) and incubated vertically. For Fe/pH assays using 'modified Eroglu regime' media, based on Eroglu, et al. (2016), seeds were sown on ½ MS media containing 0.5% (w/v) sucrose and 1% (w/v) agar (Sigma Aldrich). Fe was provided as 28 or 100 μM FeNaEDTA; Mn was supplied at 40 μM MnSO₄. Media was buffered with MES (Sigma Aldrich) and adjusted to pH 5.5 or 6.7 with NaOH. Table 2.3 compares standard ½ MS media and 'modified Eroglu regime' media. Plants were grown for either 21 (standard Ca assays), 23 (Fe/pH assays) or 24 days (low Ca assays).

For hydroponics experiments, seedling holders were prepared by removing the top from a 0.5 mL micro-centrifuge tube (Eppendorf), filling with 400 μ L 0.5% agarose and, when set, removing the bottom to create a hole for the root to grow through. Seeds were sown on the agarose plug before 48 hour stratification as before. Seedling holders were floated in LD45 10mm polyethylene foam (ROS Components) atop 1.5L Modified Hoagland's (MH) solution adjusted to pH 5.6 with KOH. Mn was provided as MnSO₄ and omitted from Mn deficiency assays. The composition of MH media is summarised in Table 2.3. Seedlings were stratified as previously before growth on either control conditions or Mn deficiency from day 0; for the delayed exposure regime, seedlings were grown on control conditions for 29 days before washing 3 times in Mn deficiency media and then growing on Mn deficiency media for the remainder of the experiment. Plants were grown in an environmentally controlled room with short day settings (23 °C constant; 8h light 120 μ mol m⁻² s⁻¹, 16h dark cycle). Growth time is given in the figure legend. Media was changed after the first two weeks of growth and weekly thereafter.

For fresh weight (FW) assays, total and shoot fresh weight were measured using a 5 dp balance. To determine chlorophyll concentrations, shoots were submerged in 90% N,N-dimethylformamide (DMF; Sigma Aldrich) for generally at least 3 weeks before measuring absorbance at 647 and 663 nm (Moran, 1982). To calculate % germination, germinated seeds were counted as at least a 1 mM radical piercing the seed coat. Graphical data is presented as mean value (X) per seedling ±SE. Data was normalised generally with the function log(X) before analysis by 2-way Analysis of Variance (ANOVA) or General Linear Model (GLM) to determine a

Table 2.3. Comparison of nutrient concentrations in basal-strength media used for growing Arabidopsis in plate assays (1/2 MS) or hydroponics assays (Modified Hoaglands solution). Modified Eroglu regime based on Eroglu, et al. (2016). ½ MS, Murashige and Skoog (1962).

	½ MS	½ MS modified	Modified Hoaglands
		Eroglu regime	
Macro elements (mM)		
KNO ₃	9.395	9.395	1.25
CaCl ₂	1.495	1.495	0.5
Ca(NO ₃) ₂ .4H ₂ O	-	-	0.5
MgSO ₄ .H ₂ O	0.75	0.75	0.5
KH ₂ PO ₄	0.625	0.625	0.625
NH ₄ NO ₃	10.305	10.305	-
NaCl	-	-	2
Micro elements (μM)			
CuSO ₄ .5H ₂ 0	0.05	0.05	0.16
ZnSO ₄ .7H ₂ O	14.955	14.955	0.38
MnSO ₄ .7H ₂ O	50	40	1.8
H ₃ BO ₃	50.135	50.135	45
CoCl ₂ .6H ₂ 0	0.055	0.055	0.01
FeNaEDTA	50	28 / 100	42.5
Na ₂ MoO ₄ .2H ₂ 0	0.515	0.515	
(NH ₄) ₆ Mo ₇ O ₂₄ .4H ₂ O	-	-	0.015
KI	2.5	2.5	-
Additional informatio	n		
рН	5.8	5.5/6.7	5.6
MES	-	2.5 / 10 mM	-
Sucrose	1%	0.5%	0
Agarose	0.8%	-	-
Agar	-	1%	-

significant genotype effect, treatment effect or interaction between genotype and treatment. For pH/Fe assays, data was analysed with MANOVA. Significance was taken as p<0.05. Post-hoc testing was performed with Tukey's HSD test; means which do not share a letter at a particular condition are significantly different. All statistical analysis was performed using Minitab v17.

2.1.5 Metal Tolerance Assays in *Triticum aestivum*

Seeds were sterilised and stratified as described previously. Germinated seedlings were positioned in a 38 mm diameter foam plug (Scientific Laboratory Supplies Ltd) and transferred to 1L growth bottles (Fisher Scientific) wrapped in black laboratory tape. Growth bottles contained 1L control Lombnaes solution (Peter & Singh, 2003) pH 6.0, with 80 µM KH₂PO₄ for the first 14 days of growth. Full details of Lombnaes solution are listed in Table 2.4. Plants were grown in an environmentally controlled room (21°C, 16h light, 120 µmol m⁻² s⁻¹; 16 °C, 8h dark cycle) and nutrient solution was changed 3 times per week. After 14 days of growth on control media, plants were transferred to treatment for a further 21 days (with transfer marking day 0); Mn was either omitted from the media or supplied as MnSO₄. Fresh weight values of roots and shoots of three replicate plants were measured using a 5 dp scale.

2.2 Bacterial and yeast growth and materials

The different strains of *Escherichia coli* (hereafter *E. coli*) and *Agrobacterium tumefaciens* (hereafter Agrobacterium) used in this report are summarised in Table 2.5.

2.2.1 Culture of Bacteria

All strains were cultured in Luria-Broth (LB) medium (1% (w/v) tryptone (Melford Laboratories Ltd); 0.5% (w/v) yeast extract; 1% NaCl, pH 7.0) or on LB agar plates (1.5% (w/v) agar). Media and agar were prepared in double distilled water and autoclaved for 20 minutes at 121 °C. Agrobacterium was cultured at 30 °C; *E. coli* was cultured at 37 °C. Innova [™] 4300 Incubator Shaker (New Bruskwick Scientific Ltd., UK) was used to provide agitation to liquid cultures. Plates were incubated in the Classic Incubator (LEEC, UK) at 37 °C or 30 °C.

2.2.2 Preparation of Chemically Competent *E. coli*

E. coli strains were streaked onto non-selective LB plates and incubated at 37 °C overnight. A single, well-isolated colony was inoculated in 5 mL LB medium for 16 hours, 37 °C (250rpm). This starter culture was used to inoculate 250 mL of LB and incubated at 18 – 23 °C (160 rpm) until an

Table 2.4. Concentrations of Lombnaes nutrient solution (Peter & Singh, 2003) used for hydroponically grown wheat seedlings

Macro elements (mM)	
KNO ₃	1
$Ca(NO_3)_2.4H_2O$	2
MgSO ₄ .H ₂ O	0.5
KH_2PO_4	80 (first 14 days) 160 (thereafter)
NaOH	0.9
Micro elements (μM)	
CuCl ₂	2
ZnCl ₂	8
Fe(NO3) ₃	75
MnSO ₄ .7H ₂ O	0.6
H_3BO_3	10
NiCl ₂ .6H ₂ O	0.1
$Na_2MoO_4.2H_2O$	0.1
Chelators (mM)	
MES	1
HEDTA	0.1

Table 2.5. Summar	y of	bacteria	l strains	used ir	n this report.
-------------------	------	----------	-----------	---------	----------------

Bacterial strain		Usage	Source
E. coli DB3.1		Propagation of destination vectors	Homemade chemically
		carrying ccdB gene	competent
E. coli DH5α		Propagation of entry and expression	Homemade chemically
		vectors	competent
E. coli TOP10		Ultra-competent for transformation of	Invitrogen (UK)
		pENTR/D-TOPO entry vectors	
Agrobacterium	GV3850	Stable expression of Arabidopsis	Homemade electro-
C58		T _i plasmid resistance: Carbenicillin	competent
		Chromosome resistance: rifampicin	
Agrobacterium	GV3101	Transient expression in tobacco	Homemade electro-
C58		T _i plasmid resistance: Gentamycin	competent
		Chromosome resistance: rifampicin	

 OD_{600} of 0.5 to 0.8 was obtained (approx. 8 hours). The culture was cooled for 10 minutes on ice before centrifugation to harvest cells at 4000 rpm, 4 °C, for 10 minutes. Cells were washed twice in 20 mL ice-cold transformation buffer (10 mM piperazine-1, 2-bis[2-ethyanesulfonic acid], pH 6.7; 55 mM MnCl₂.4H₂O; 15 mM CaCl₂.2H₂O; 250 mM KCl; all Sigma Aldrich) before final resuspension in up to 1 mL of ice-cold transformation buffer containing 0.075 μ l/mL (v/v) DMSO (Sigma Aldrich). Competent cells were divided into 50 μ l aliquots and immediately snap frozen on liquid nitrogen before storage at -80 °C.

2.2.3 Preparation of Electro-competent Agrobacterium

Untransformed Agrobacterium was grown for 3 days at 30 °C on selective LB agar plates, supplemented with chromosomal and T_i plasmid antibiotics (Table 2.5). A well-isolated colony was picked and inoculated in 5 mL selective LB for 24 hours, 30 °C (225 rpm). This starter culture was used to inoculate 500 mL of selective LB and incubated at 30 °C (225 rpm) until an OD_{550} of 0.5 to 0.8 was obtained (approx. 16 hours). Cells were twice harvested by centrifuging at 4000 g, 10 minutes at 4 °C and resuspended in 50 mL ice-cold SDW, eventually resuspending cells in 5 mL 10% (v/v) ice-cold, sterile glycerol (Sigma Aldrich). Cells were split into 50 μ L aliquots and snap frozen on liquid nitrogen before storage at -80 °C.

2.2.4 Transformation of Competent Bacteria

To transform chemically competent *E. coli*, cells were thawed on ice and 1-3 μ L vector was added before incubating on ice for 30 minutes. Cells were heat-shocked at 42 °C for 30 seconds then returned to ice for two minutes before adding 250 μ L SOC media (2% tryptone, 0.5% yeast extract, 10 mM NaCl, 2.5 mM KCl, 10 mM MgCl₂, 10 mM MgSO₄, and 20 mM glucose(Sigma Aldrich)) and incubating at 37 °C for 1 hour (225 rpm). The culture was spread on a selective LB plate and incubated overnight at 37 °C.

To transform electrocompetent Agrobacterium, cells were thawed on ice and 1-3 μ L vector was added. GV3101 cells were then snap-frozen on liquid nitrogen before incubating at 30 °C for 5 minutes; 1 mL LB or SOC was added to the culture before incubating at 28 °C, 3 hours (180 rpm). GV3580 cells were transferred to clean, chilled 0.2 cm electroporation cuvettes (Bio-Rad Laboratories) and pulsed for 5 ms at 1.8 V (BioRad MicroPulser TM Electroporation Apparatus; Bio-Rad). This was resuspended in 1 mL LB medium before incubation at 30 °C, 225 rpm, for 2 hours. Transformed cells were spread on LB plates with triple selection, for the T_i plasmid, chromosomal and vector antibiotic.

2.2.5 Purification of plasmid DNA from bacterial cells

A single, isolated colony was inoculated in 5 mL LB media containing the appropriate antibiotic, at 37 °C, 16 hours (225 rpm). DNA was extracted using the Qiagen Spin Miniprep kit (Qiagen) according to manufacturers' instructions. DNA was eventually eluted in 20 μ L SDW; yield and purity were quantified by spectrophotometry.

2.2.6 Growth of Saccharomyces cerevisiae

S. cerevisiae strains were typically grown on inverted plates at 30°C for 3 days. Untransformed strains were grown on YPD plates (1% yeast extract, 2% peptone, 2% D-Glucose, 2% agar). Strains transformed with uracil or leucine auxotrophic selection marker were grown on Synthetic Complete (SC) medium containing glucose but without uracil or leucine (0.17% (w/v) yeast nitrogen base extract without amino acids and ammonium sulphate (Difco); 0.5% (w/v) ammonium sulphate (Fisher Scientific); 0.192% amino acids minus uracil or leucine (Sigma Aldrich); 2% (w/v) glucose; 2% (w/v) agar; pH 5.3 with NaOH). The yeast strains used in this report are listed in Table 2.6. Fluorescent strains were a kind gift from Dr. C. W. Gourlay (University of Kent). The Zn-hypersensitive strain was obtained from Dr. U Kramer (Ruhr University, Bochum); other strains were obtained from Euroscarf. Fe-deficiency sensitive *fet3 fet4* was grown on SC glucose pH 4.0, supplemented with 10 μ M FeCl₃. SC galactose was used when inducing expression of the gene of interest, with 2% (w/v) galactose (Sigma Aldrich) in place of glucose.

2.2.7 S. cerevisiae transformation

Yeast strains were transformed using a modified LiOAc/PEG method (Gietz, et al., 1992). Briefly, non-transformed cells were resuspended in 250 μ L PLATE solution (40% (v/v) PEG₄₀₀₀ (Fisher Scientific); 10% (v/v) 1 M LiAc, pH 7.5; 10% (v/v) TE buffer, pH 7.5), 5 μ L single-stranded herring sperm DNA (Invitrogen) and 300-500 ng vector. Cells were incubated at 30 °C for 30 minutes, before incubation at 42 °C for 90 minutes. This was spread on plates containing SC glucose without uracil and grown at 30 °C for 3 days.

Colony PCR was used to confirm the presence of the vector of interest. Around 5 μ L yeast colony was resuspended in 15 μ L SDW. 1 μ L of this resuspension was denatured at 95 °C for 5 minutes; this was used as the template in RT-PCR (see Section 2.3.3).

2.2.8 Metal assays in *S. cerevisiae*

In preparation for the experiment, yeast cultures were inoculated overnight at 30 °C in 5 mL SC glucose without uracil. To induce expression of transgene, cultures washed twice and resuspended in SC galactose without uracil. This was incubated for a further 4 hours before dilution to $OD_{600} = 0.4$. Serial dilutions of 1/10 and 1/100 were also made using SC galactose without uracil. 7 μ L culture was dropped onto 2% agar (w/v) plates containing SC galactose medium without uracil, supplemented with a range of metal concentrations (MnCl₂, ZnSO₄, CoCl₂, FeSO₄; all Sigma Aldrich). Plates were incubated at 30 °C for 5 days.

Table 2.6. Genotypes and growth requirements of *S. cerevisiae* strains used. Where a strain has more than one name, the additional name is listed in brackets.

Strain	Genotype	
WT Strains		
BY4741 (Y00000)	MATa his3-1 leu2-0 met15-0 ura3-0	
DEY1457	MATa ade1-+ can1 his3-1 leu2-0 trp1-0 ura3-0	
DY150	Mat a ade2-1 his3-11 leu2-3,112 trp1-1 ura3-52	
	can1-100(oc)	
Metal-sensitive strains		
pmr1 (Y04534, YGL167c)	BY4741 + pmr1::kanMX4	
zrc1cot1 (CK1)	BY4741 + zrc1::natMX cot1::kanMX4	
ccc1	DY150 + ccc1::HIS3	
fet3 fet4 (DEY1453)	DY1457 + fet3-2::HIS3 fet3-1::LEU2	
Fluorescent strains		
BY4742 Anp1::RFP	MATa his3-1 leu2-0 met15-0 ura3-0 Anp1-RFP- KanMX	
BY4742 Sec13::RFP	MATa his3-1 leu2-0 met15-0 ura3-0 Sec131- RFP-KanMX	
BY4742 Gtr1::GFP	MATa his3-1 leu2-0 met15-0 ura3-0 Gtr1-GFP- KanMX	

2.3 Molecular methods and techniques

2.3.1 Extraction of RNA from Arabidopsis thaliana and Triticum aestivum

Arabidopsis seeds were sterilised as described in Section 2.1.4. Seeds were sown on agar plates containing 1/2 MS, 1% (w/v) sucrose, 1% (w.v) agar. Seeds were stratified at 4°C for 48 hours before transfer to a controlled-environment cabinet (23°C, 16h light, 120 μ mol m⁻² s⁻¹; 18 °C, 8h dark cycle) and incubated horizontally for 14 to 21 days. Approx. 25 seedlings were used per RNA replicate.

Triticum aestivum seeds were sterilised for 15 minutes in 1% hyperchloride solution (Domestos) before washing 5 times with SDW and vernalised for 24 hours at 4 °C on a tilting shaker. Following vernalisation, seeds were positioned on a tray with crease down on half-ply blue roll (Kimwipe), sealed in a clear bag to maintain humidity and left to germinate in the dark at room temperature for 5 days. Approx. 3 seedlings were used per RNA replicate.

Tissue was harvested and immediately snap-frozen on liquid nitrogen; this was then ground to a fine powder using liquid nitrogen and a prechilled, sterile pestle and mortar. $500 - 1000 \, \mu L$ of powdered tissue was homogenised using 1 mL of TRIzol reagent (Life Technologies) and $200 \, \mu L$ chloroform (Sigma Aldrich). RNA was precipitated in $500 \, \mu L$ of isopropanol per $500 \, \mu L$ tissue, before pelleting in 75% ethanol and resuspending in TE buffer. Purity and RNA yield (ng/ μL) were determined by spectrophotometry; quality was determined visually by running 1 mg RNA on a 1% (w/v) agarose electrophoresis gel.

2.3.2 cDNA synthesis

1 μ L of 10 μ M dT₁₈ primer (Sigma Aldrich) was added to 1 mg RNA and made to a total volume of 3.6 μ L using SDW. RNA was denatured at 72 °C for 5 minutes. First-strand cDNA synthesis was carried out using ImPromII RT reverse transcriptase (Promega, UK) according to manufacturer's instructions. All stages were performed using the peqSTAR 96 Universal Gradient PCR machine (peqLAB).

2.3.3 Reverse Transcriptase PCR (RT-PCR) and gel electrophoresis

Reactions were performed in thin-walled PCR tubes (STARLAB Ltd) using the peqSTAR 96 Universal Gradient PCR machine. The Taq polymerase Biomix Red (Bioline) was used in reactions that did not need a proof-reading enzyme, such as confirmatory and colony PCRs, in 10 μ L reactions as summarised in Table 2.7. To perform colony PCR on bacteria, liquid template was

replaced by touching a colony with a sterile pipette tip and mixing with the PCR mix. The typical cycling parameters of Biomix Red are summarised in Table 2.8. Generally, the proof-reading polymerase *Pfu* (Promega) was used to amplify products for cloning or sequencing. The reaction components and cycling parameters for *Pfu* are also summarised in Tables 2.7 and 2.8. Any specific conditions for different PCRs are summarised in tables throughout this chapter. All primers were obtained from Integrated DNA Technologies.

Products of PCR and restriction enzyme digestion were visualised on a 1% (w/v) agarose/TAE (40 mM Tris/acetate, pH 8.0, 1 mM EDTA) gel containing 2.5 μ l/100 ml NANCY-520 dye (Sigma Aldrich) or 5 μ l/100ml Gel Red (Biotium Cambridge Biosciences). In the majority of cases, the entire reaction was loaded into the gel wells; when generating or amiRNA, 4 μ l of a 50 μ l reaction was run on a gel for visualisation before precipitating the DNA from the remaining 46 μ l of reaction with isopropanol. 5 μ l of Hyperladder I (Bioline) molecular weight marker was loaded in a neighbouring well for assessing product size. Gels were run for 1 hour in 1X TAE buffer, at 120 volts using Power Pac 200/2.0 (Bio-Rad). Products were visualized using a UV transilluminator (Syngene).

To purify most amplicons or digested fragments, the band of interest was cut from the gel under UV light using a clean scalpel blade, before purification using Qiaquick Gel Extraction Kit (Qiagen) according to manufacturer's instructions. An isopropanol precipitation method was used to purify products for amiRNA, to achieve a greater DNA concentration prior to restriction digestion: $1/10^{th}$ of the reaction volume of 3M NaAc (pH 5.5; Sigma Aldrich) was added, before mixing with 1.5 reaction volumes of 100% isopropanol (Sigma Aldrich) and centrifuging at 12,000 g for 40 minutes. The pellet washed twice in 1.5 reaction volumes of 70% ethanol before eventually resuspending the pellet in 6 μ L SDW. In both cases, DNA concentration was quantified by spectrophotometry.

2.3.4 Quantitative PCR (qPCR) to Assess Gene Expression

Expression of Ta *MTP8.1* in RNAi-transformed seedlings was assessed using primers 5′-GCATGCCATTGGAGAATCACTC and 5′-TCAAGGCTGGCTGCTAGGAAG. Ta *GADPH* was used as a housekeeper gene using primers 5′-GCTCAAGGGTATCATGGGTTACG and 5′-GCAATTCCAGCCTTAGCATCAAAG. qPCR was performed in a 96-well plate (StarLab) in the StepOnePlus real-time PCR machine, using StepOne v2.2.2 software. Amplification of cDNA was monitored by fluorescence of PrecisionPLUS Master Mix premixed with SYBRGreen (Primer Design, UK). To evaluate gene expression, Ta *MTP8.1* expression was normalized to Ta *GADPH* using an efficiency-calibrated method, using the equation:

Table 2.7. Typical PCR conditions when using Biomix Red Taq (Bioline) or *Pfu* (Promega) as polymerase

	Biomix Red reaction	Pfu reaction
Reagent	Concentration	Concentration
Template DNA	0.1-0.5 μg	0.1-0.5 μg
2X Biomix	1X	-
10X <i>Pfu</i> Buffer	-	1X
10 mM dNTPs	-	200 μΜ
10 μM forward primer	0.2 μΜ	1 μΜ
10 μM reverse primer	0.2 μΜ	1 μΜ
Pfu polymerase	-	1 Unit
Sterile 18M Ω water	Up to 10μl	Up to 25 or 50μl

Table 2.8. Typical PCR parameters when using Biomix Red Taq (Bioline) or *Pfu* (Promega) as polymerase

	Biomix Red reaction	Pfu reaction	
Step	Temperature and Duration		
Initial denaturation	94 °C, 2 minutes	95 °C, 2 minutes	
Denaturation	94 °C, 30 seconds	95 °C, 1 minute	
Annealing	60 °C, 30 seconds	60 °C, 1 minute	
Extension	72 °C, 1 min/1 kb	72 °C, 1.5 min/1 kb	
Repeat cycle	38 cycles	35 cycles	
	(semi-quantitative, 25-30 cycles)		
Final extension	72 °C, 5 minutes	72 °C, 5 minutes	

$$\mathsf{Ratio} = \left(\mathsf{E}_{MTP8.1}^{\quad \Delta \mathsf{Ct}(GADPH\text{-}MTP8.1)}\right) / \left(\mathsf{E}_{GADPH}^{\quad \Delta \mathsf{Ct}(GADPH\text{-}MTP8.1)}\right)$$

Where E is primer efficiency and Ct is the number of PCR cycles at which the fluorescent signal reaches the threshold value (Pfaffl, 2001). Data shows the mean value for two biological replicates, with three technical reps per biological rep.

2.3.5 Generating expression clones and constructs

2.3.5.1 Generating constructs for At MTP8, At MTP9, At MTP11 and At NRAMP2

The cDNA sequences for At MTP8 (At3g58060), MTP9 (At1g79520), MTP11 (At2g39450) and NRAMP2 (At1g47240) are listed on TAIR (Lamesch, et al., 2011). At MTP9 and MTP11 sequences were amplified from WT Columbia 8 cDNA with and without the stop codon, using Pfu and primers which add an N-terminal CACC tag for cloning into the pENTR/D-TOPO vector (Invitrogen; 'TOPO' primers listed Table 2.9). Products were gel-extracted using Qiaquick gel extraction kit (Qiagen). To obtain At MTP8, the full sequence lacking the first 11 bases was amplified using MTP8F2 and MTP8_toponostop; this was gel extracted and used as the template to amplify fulllength At MTP8 with primers MTP8_topoF2 and MTP8_toponostop, adding the remaining 11 bases at the 3' end and the CACC tag. The At NRAMP2 sequence was amplified in two parts which overlapped by 216 bp: NRAMP2_topoF + NRAMP2_R2, and NRAMP2_midF + NRAMP2_topoNS. These were gel extracted and mixed at equimolar concentrations in a Pfu reaction without primers, with 15 cycles: 94 °C, 1 min; 60 °C, 1 min; 72 °C, 3 min, before addition of NRAMP2 topoF and NRAMP2 topoNS primers for a normal Pfu reaction (Table 2.8) with 55 °C annealing temperature. Purified amplicons were cloned into pENTR/D-TOPO vector using TOPOisomerase kit, using manufacturers' instructions at half-strength (Invitrogen). Entry vectors were confirmed correct with at least two independent sequencing reads before recombining with destination vectors using Gateway LR Clonase II TM enzyme (Invitrogen), using manufacturers' instructions at half-strength. The destination vectors used in this project are summarised in Table 2.10. Constructs carrying Os MTP11 and At MTP10 were provided for this project by Dr. Lorraine E. Williams.

2.3.5.2 Generating site-directed mutations for At MTP8 and At MTP11

The site-directed mutants generated in this report are listed in Table 2.11, alongside primers which were RP1-purified and obtained from Sigma Aldrich. Most mutants were generated using QuikChange Lightning Site-Directed Mutagenesis Kit (Agilent), according to manufacturer's instructions. MTP8-D258H was generated in a 2-step RT-PCR reaction. Primers MTP8_topoF + AtM8_D258H_R, and AtM8_D258H_F + MTP8_topoNS were used to amplify fragments from

Chapter 2

pENTR/D-TOPO carrying *MTP8*. Fragments were gel extracted and combined in overlapping PCR, using primers MTP8_topoF + MTP8_topoNS, before cloning into pETNR/D-TOPO, as per protocol for amplification of *NRAMP2* in Section 2.5.3.1.

2.3.5.3 Generating RNAi constructs to downregulate Ta MTP8 and Ta MTP8.1

In collaboration with NIAB (Cambridge, UK), RNAi was designed to downregulate either Ta *MTP8* or *MTP8.1* with limited off-targeting. These sequences are listed below and were amplified from *Triticum aestivum* ecotype Fielder cDNA, using primers that introduce restriction sites at the 3' and 5' side of both products (primers listed Table 2.12). Ta *MTP8* was amplified with *Pfu* at an annealing temperature of 65 °C; Ta *MTP8.1* was amplified with Biomix Red with addition of 1 U *Pfu* using an annealing temperature of 54 °C. 5% glycerol was included in both reactions to overcome secondary structures. Both were purified from a 2% agarose gel.

Ta MTP8.1 RNAi:

ATGGAGGCGAACGGGCGCGGGGACAATGACGCCGCGGGGCGCCGCTCCTGGCGGGCCGGAACTCGGTGGGGTCGAT
GCGCGGGGAATTCGTGTCGCGGCTCCCCAAGAAGGTGCTCGACGCCGTCGACCCGGAGAGGCCGTCCCACGTCGACTTCTCCCGCT
CCAAGGGCCTCCTGGAAGGAGAAAAAAATACTACGAGAAACAATTTGCCACCTTGAGATCCTTTGAGGAAGTTGACTCTATAGAA
GAATCCAATGTAATAAGTGAAGAAGAAGAAGACCTCATGGAGCAAAGGCAGAGTGAATTTGCTATGAAGATATCAAATTATGCAAATGT
TGT

Ta MTP8 RNAi:

CTCTCCATGAAAAGAAGGTGAACATCTACAAGTACCCCATCGGCAAGCTGCGCGTCCAGCCGGTGGGGATCATCGTCTTCGCCGCCA
TCATGGCCACTCTAGGTTTCCAGGTCCTGGTGCAGGCGATCGAGCAGCTGGTGGAGAACGAGCCCGGCGACAAGCTGACCTCGGA
GCAGCTGACATGGCTCTACTCCATCATCATCCTCTCGGCCACCGCCGTCAAGCTC

Ta *MTP8.1*-RNAi was digested alongside pENTR1a (Invitrogen) vector with *XmnI* and *XbaI* (Promega), at 37 °C for 13 hours before enzyme deactivation. This removed the ccdB gene from pENTR1a. Both were treated with Antarctic Phosphatase (New England Biolabs) according to manufacturer's instructions to prevent recirculisation and were run on a 1% agarose gel. The 2244 bp backbone fragment of pENTR1a and 351 bp fragment of Ta *MTP8.1*-RNAi were extracted from the gel and ligated at a 3:1 RNAi:vector molar ratio, using 5 units T4 DNA Ligase and Rapid Ligation Buffer (both Fermentas, Thermoscientific) at room temperature for 2 hours. This was transformed into DH5α and was confirmed to carry the RNAi with two independent sequencing reads (Source Bioscience, UK). This construct was linearised with *DraI* and *BtgI*, while Ta *MTP8*-RNAi was digested with *BsRBI* and *BtgI* (New England Biolabs), before treating with phosphatase and running on a gel. The 2580 bp fragment of the backbone and the 224 bp fragment of the RNAi were gel-extracted and ligated as before to create a concatenated RNAi construct. Ta *MTP8* and Ta *MTP8.1* were confirmed to be amplified from chromosomes 6B and 4B, respectively.

Table 2.9. Primers used to amplify coding sequences from cDNA for cloning into pENTR/D-TOPO vector

Primer	Target gene	Sequence	Optimal annealing temperature
MTP8_topoF2	At <i>MTP8</i>	5'-CACCATGGAAGTCAATTATTGTCC	55
MTP8_F2	At MTP8	5'-TTATTGTCCGGAAACACCGTT	55
MTP8_topowithstop	At MTP8	5'-TCATAAATCGTTGGGGATTGTA	55
MTP8_toponostop	At MTP8	5'-TAAATCGTTGGGGATTGTA	55
MTP9_topoF	At MTP9	5'-CACCATGGCGGCGACGGAGCAT	60
MTP9_topowithstop	At <i>MTP9</i>	5'-TCAAACCTTGCATTTGTGTTCTG	60
MTP9_toponostop	At MTP9	5'-AACCTTGCATTTGTGTTCTG	60
MTP11_topoF	At MTP11	5'-CACCATGGTTGAGCCAGC	60
MTP11_topowithstop	At MTP11	5'-CTAACAGTGGGATCTAGCGTGC	60
MTP11_toponostop	At MTP11	5'-ACAGTGGGATCTAGCGTGC	60
NRAMP2_topoF	At NRAMP2	5'-CACCATGGAAAACGACGTCAAAG	55
NRAMP2_midF	At NRAMP2	5'- GGTCTATGGCGGAACTTGCT	55
NRAMP2_R2	At NRAMP2	5'- AGGACAAACCCATAGTTGCGA	55
NRAMP2_topoNS	At NRAMP2	5'-GCTATTGGAGACGGACACTCTTTT	55

Vector	Expression system	Example construct generated	Reference	•	
pMDC32	Arabidopsis thaliana	P35S::MTP8	(Curtis		&
			Grossnikla	aus, 200	03)
pMDC83	Arabidopsis thaliana	P35S::MTP8::GFP	(Curtis		&
	Nicotiana tabacum		Grossnikla	aus, 200	03)
pEG101	Arabidopsis thaliana	P35S::MTP8::YFP	(Earley, et	al., 20	06)
	Nicotiana tabacum				
pSITE-4NB	Arabidopsis thaliana	P35S::MTP8::mRFP	(Chakraba	irty, et	al.,
	Nicotiana tabacum		2007)		
pAG426galEGFP	Yeast	PGAL::MTP8::EGFP	(Alberti,	et	al.,
		Rescues uracil auxotrophy	2007)		
pAG425galDsRed	Yeast	PGAL::MTP8::DsRed	(Alberti,	et	al.,
		Rescues leucine auxotrophy	2007)		

Table 2.11. Primers used to generate site-directed mutations for at mtp8 and at mtp11.			
Primer	Base	Codon	Sequence
	change	change	
At MTP11 mutation	ns		
ATM11_L130S_F	T389C	L130S	5'-GAGGCAATGATAGCTGAAGAGCCACTAGTGACAGAA
ATM11_L130S_R	T389C	L130S	5'-TTCTGTCACTAGTGGCTCTTCAGCTATCATTGCCTC
ATM11_D427H_F	G739C	D427H	5'-CGTCGAAGAAATGATGTTGAGCATAAGCTTTAACGATCTC
ATM11_D427H_R	G739C	D427H	5'-GAGATCGTTAAAGCTTATGCTCAACATCATTTCTTCGACG
ATM11_D142A_F	A425C	D142A	5'-GATGAAGCCAGAAAGAAGAGAGAGAGAGTCCAATGT
ATM11_D142A_R	A425C	D142A	5'-ACATTGGACTCTCTTCTTGCTCTTCTTCTGGCTTCATC
ATM11_C233H_F	T697C,	C233H	5'-GATCTCGTTAGTGAAGGATCTGTGGTAAAGAACCAGAAGCAGTTTG
	G698A		
ATM11_C233H_R	T697C,	C233H	5'-CAAACTGCTTCTGGTTCTTTACCACAGATCCTTCACTAACGAGATC
	G698A		
ATM11_D138H_F	G412C	D138H	5'-AAGAAGATCAAGAAGAGAGTGCAATGTAGAGGCAATGATAG
ATM11_D138H_R	G412C	D138H	5'-CTATCATTGCCTCTACATTGCACTCTCTTCTTGATCTTCTT
At MTP8 mutations	3		
ATM8_D153A_F	A458C	D153A	5'-CCTCCCGCCATAAGGGCAAGCAATGAGTCGA
ATM8_D153A_R	A458C	D153A	5'-TCGACTCATTGCCCTTATGGCGGGAGG
ATM8_D258H_F	G772C	D258H	5'-CCACATCAAAGTGATGATGCTTTGCATATGCACGGAC
ATM8_D258H_R	G772C	D258H	5'-GTCCGTGCATATGCAAAGCATCATCACTTTGATGTGG
ATM8_I141S_F	T422G	I141S	5'-ATGCTGCAATCGCACTGGATCCACTCTTTACCGTA
ATM8_I141S_R	T422G	I141S	5'-TACGGTAAAGAGTGGATCCAGTGCGATTGCAGCAT
ATM8_D149H_F	G445C	D149H	5'-AAGGTCAAGCAATGAGTGGAGTGTAGATGCTGCAA-3'
ATM8_D149H_R	G445C	D149H	5'-TTGCAGCATCTACACTCCACTCATTGCTTGACCTT-3'

Table 2.12. Primers used to amplify RNAi to target either Ta MTP8.1 or Ta MTP8			
RNAi Target	Primer	Sequence	Restriction site introduced
Ta <i>MTP8.1</i>	TaMTP8.1_Ri1_F	5' CTCATGAACCAATTCCCATGGAGGCGAACGGGC	Xmnl
Ta <i>MTP8.1</i>	TaMTP8.1_Ri1_R	5' CGATGCTCTAGACAACATTTGCATAATTTGATATCT	Xbal
Та <i>МТР8</i>	TaMTP8_Ri5_F	5' GCACTTCCGCTCTCCATGAAGAAGGTGAACA	Dral
Та <i>МТР8</i>	TaMTP8_Ri5_R	5' ATGACTCCATGGAGCTTGACGGCGGTGGC	Btgl

2.3.5.4 Generating amiRNA to downregulate At MTP9

Two artificial microRNA sequences to target At *MTP9* were designed using Weigel world software (Ossowski, et al., 2008). AmiRNA is amplified from pRS300, carrying the precursor for MIR319a, by amplifying different regions with specific vectors to replace MIR319a with the amiRNA of interest. 3 reactions create products A, B and C, which were visualised and extracted from a 1% agarose gel. These products were used as the template for generating the amiRNA hairpin D; each of these PCRs are summarised in Table 2.13. The primers used in these reactions are summarised in Table 2.14 while the components of each PCR are given in Table 2.15. 4 μ L of reaction D was visualised on a 1% agarose gel and DNA was isopropanol-precipitated from the remaining 46 μ L of reaction. 500 ng of reaction D and pENTR1a were digested with Sall and Notl (Promega) at 37 °C for 3 hours, and the DNA precipitated from this using the isopropanol precipitation method. Digested insert and vector were ligated as described for the wheat RNAi. The resultant construct was recombined with pMDC32 before eventual transformation into Arabidopsis.

2.4 Localisation studies

2.4.1 Transient expression in tobacco

For transient expression in tobacco, positive GV3101 *Agrobacterium* colonies were inoculated overnight in LB supplemented with 25 μg/mL rifampicin in methanol, 30 μg/ml gentamycin, and 50 μg/ml kanamycin or spectinomycin and streptomycin. Cultures were washed twice and resuspended to a final OD₆₀₀ of 0.1 to 0.5 in infiltration medium (50 mM MES, pH 5.6; 0.5% (w/v) D-Glucose; 2 mM Na₃PO₄; 60 mg/L acetosyringone in DMSO). For co-expression, transformed colonies were grown separately and mixed at this stage at equal OD₆₀₀. This Agrobacterium suspension was infiltrated into the base of leaves of four- to six-week old glasshouse-grown tobacco plants (*Nicotiana tabacum*, 'Petit Havana', either WT or stably transformed with TGN-marker ST::RFP; plants were kindly provided by Dr. John Runions (Oxford Brookes University)) as described Sparkes, et al. (2006). Infiltrated plants were grown normally for a further 48 hours before observing fluorescence.

2.4.2 Observation of fluorescence

To observe localisation in yeast, in-frame C-terminal fusions of MTP8::GFP, MTP8::DsRed, MTP10::GFP and MTP11::GFP were transformed in the BY4741 WT, or the BY4742 WT stably transformed with Golgi-marker Anp1::RFP, ER-to-Golgi marker Sec13::RFP or tonoplast marker Gtr1::GFP. To induce expression, cultures were grown as Section 2.2.8; MTP8::DsRed was

Table 2.13. Primers and templates involved in 4-PCR strategy to amplify amiRNA from pRS300			
PCR	Forward primer	Reverse primer	Template
Α	amiFA	IV	pRS300
В	III	II	pRS300
С	1	amiFB	pRS300
D	amiFA	amiFB	A + B + C

Table 2.14. Sequences of primers I-IV used to amplify MTP9 amiRNA constructs from pRS300			
amiRNA construct	Primer	Sequence	
amiRNA MTP9 A	amiMTP9_I_A	5' GATACAAGTAGCCTAGTTGACACTCTCTTTTTGTATTCC	
	amiMTP9_II_A	5'GAGTGTCAACTAGGCTACTTGTATCAAAGAGAATCAATGA	
	amiMTP9_III_A	5'GAGTATCAACTAGGCAACTTGTTTCACAGGTCGTGATATG	
	amiMTP9_IV_A	5' GAAACAAGTTGCCTAGTTGATACTCTACATATATATTCCT	
amiRNA MTP9 B	amiMTP9_I_B	5' GATCTATCGTGATATTCAAACCCTCTCTCTTTTGTATTCC	
	amiMTP9_II_B	5' GAGGGTTTGAATATCACGATAGATCAAAGAGAATCAATGA	
	amiMTP9_III_B	5' GAGGATTTGAATATCTCGATAGTTCACAGGTCGTGATATG	
	amiMTP9_IV_B	5' GAACTATCGAGATATTCAAATCCTCTACATATATATCCT	
Both	amiFA	5' CTCCAAGGCGATTAAGTTGGGTAAC	
	amiFB	5' GCGGATAACAATTTCACACAGGAAACAG	

Table 2.15. Components of PCRs to amplify amiRNA from pRS300			
Reagent	Amplifying products	Amplifying hairpin product	
	А, В, С	D	
Template: pRS300	0.5 μg	-	
Template: reaction A	-	0.5 μg	
Template: reaction B	-	0.5 μg	
Template: reaction C	-	0.5 μg	
10X <i>Pfu</i> Buffer	1X	1X	
10 mM dNTPs	200 μΜ	200 μΜ	
10 μM forward primer	1 μΜ	1 μM amiFA	
10 μM reverse primer	1 μΜ	1 μM amiFB	
Pfu polymerase	1.25 Units	1.25 Units	
Sterile 18Ω H2O	Up to 50μl	Up to 50μl	

inoculated in selective media without leucine. Cultures were fixed by resuspending in 100 μ L 4% paraformaldehyde at room temperature for 15 min, before washing twice and resuspending in 100 μ L of a 1 M KH₂PO₄ / 1 M K₂HPO₄ / 2 M sorbitol mix (all Sigma Aldrich). 3 μ L fixed cells were positioned on a microscope slide with cover slip.

To observe localisation in Arabidopsis, stably transformed T3 generation seeds were grown for 7 days on standard ½ MS plates (1% (w/v) agar, 1% (w/v) sucrose); MTP10::GFP was imaged at the T2 generation. Cell wall staining was performed by immersing plants in 19.5 μ M propidium iodide (Invitrogen) before rinsing 3 times with SDW. Whole Arabidopsis seedlings were mounted in approx. 15 μ L SDW on a microscope slide with cover slip. To observe fluorescence in tobacco, 1 cm discs of tobacco leaves were mounted in the same way.

Fluorescence was observed using a Leica SP8 confocal laser scanning microscope. GFP excitation, 488 nm; detection, 500-540 nm. DsRed, RFP and propidium iodide excitation, 561 nm; detection, 565-600 nm. Chlorophyll autofluorescence excitation, 633 nm; detection, 650-700 nm. Untransformed strains and lines, and strains transformed with empty vectors, were used as controls.

2.5 Bioinformatics

Accession numbers and genomic and cDNA sequences for At *MTP8* (At3g58060), At *MTP9* (At1g79520), At *MTP10* (At1g16310), At *MTP11* (At2g39450), At *ECA3* (At1g10130), At *NRAMP1* (At1g80830) and At *NRAMP2* (At1g47240) were obtained from the TAIR database (www.arabidopsis.org). Predictions for gene expression under different conditions were made by searching the Genevestigator database (Hruz, et al., 2008; www.genevestigator.com). These were confirmed by sequencing the amplified and cloned products, where available.

Multiple sequence alignments were performed by Clustal Omega (Sievers, et al., 2011). Percentage similarities and identities were calculated using EMBOSS Matcher (Rice, Longden, & Bleasby, 2000). Transmembrane domains were predicted using AramTmConsens, a consensus transmembrane alpha helix prediction programme which combines output from 18 individual prediction programmes, available on the ARAMEMNON database (Schwacke, et al., 2003). Membrane topologies were visualised using the Protter tool (Omasits, et al., 2013).

For phylogenetic analysis, sequences for protein homologs to At MTP8 – MTP11 were obtained from: *Populus trichocarpa* (poplar) and *Sorghum bicolor* (sorghum), Gustin, et al (2011); *Beta vulgaris* spp. *maritima*, Erbasol, et al (2013); *Oryza sativa* (rice), Chen, et al. (2013); *Hordeum vulgare* (barley), Pedas, et al., 2014; *Cucumbis sativa*, Migocka, et al. (2014). Arabidopsis and rice

Chapter 2

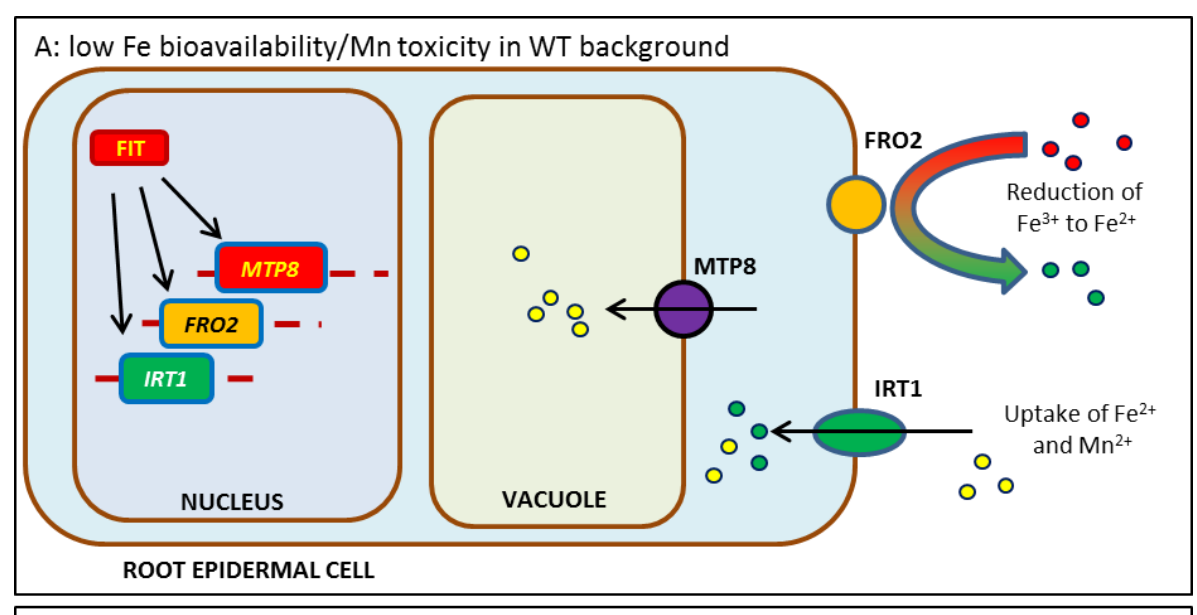
sequences were used to search for homologs in Brassica rapa, Brachypodium distachyon and Zea mays on Phytozome v9.1 (Goodstein, et al., 2012) and in barley on the International Barley Sequencing Consortium database (Schulte, et al., 2009). At the time of writing, the Triticum aestivum (bread wheat) genome is still in the process of being sequenced. To find homologs in wheat, genomic sequences from Arabidopsis, rice, barley and Brachypodium were used to search for potentially homologous regions of contigs on the Wheat Portal of the URGI (Unité de Recherche Génomique Info) database (International Wheat Genome Sequencing Consortium; European Triticeae Genomics Initiative; http://wheat-urgi.versailles.inra.fr). To predict wheat introns and exons, contigs were aligned to homologous cDNA from, where available, Arabidopsis, rice, Brachypodium and, where available, barley; further to this, introns and exons were predicted using the Augustus gene prediction web server was used to predict wheat intron/exon structures, using the organism parameters for Zea mays (Stanke, et al., 2004; Keller, et al., 2011). A phylogenetic tree was reconstructed with Neighbor-Joining method, performed using MEGA (Molecular Evolutionary Genetics Analysis) 7 package (Tamura, et al., 2011) with following parameters: 1000 bootstrap replicates, pairwise deletion, Poisson correction. Accession numbers are listed in the appendix.

Chapter 3: Bioinformatics and Mutant Analysis to Investigate the Metal Tolerance Proteins

3.1 Introduction and Aims

The Metal Tolerance Proteins (MTPs) were introduced in Chapter 1 as playing important roles in heavy metal homeostasis (see Table 1.2 for examples of characterised MTPs). A key aim of this project is to determine how the putative Mn-transporting MTPs in Arabidopsis function together within the plant cell to contribute to Mn homeostasis. Of the 4 members of this group, At MTP8, MTP9, MTP10 and MTP11, only At MTP8 and MTP11 have been characterised to date (Peiter, et al., 2007; Delhaize, et al., 2007; Eroglu, et al., 2016). Although the exact mechanism remains unclear, it is apparent that At MTP11 functions to alleviate Mn toxicity: disruption of *MTP11* with RNAi-mediated silencing (Delhaize, et al., 2007) or T-DNA insertion (Peiter, et al., 2007) confers Mn-sensitivity. This sensitivity can be complemented with expression of both At MTP11 and the poplar Pt MTP11.1, also suggesting a conservation of function between species (Peiter, et al., 2007).

A very recent study by Eroglu, et al. (2016) provided evidence that At MTP8 functions at the tonoplast to sequester Mn into the vacuole; the main purpose of this sequestration was proposed to be to prevent Mn-induced inhibition of the Fe-deficiency response machinery. This is illustrated in Figure 3.1. Under low Fe bioavailability in the WT, At FIT, the bHLH transcription factor, upregulates At *FRO2* and At *IRT1*; this initiates reduction of rhizospheric Fe³⁺ to Fe²⁺ by FRO2, and subsequently uptake of Fe²⁺ by IRT1 (Yi and Guerinot, 1996; Robinson, et al., 1999; Vert, et al., 2002; Figure 1.3). However, Mn can compete with Fe²⁺ for uptake by IRT1 under low Fe availability, increasing the amount of Mn in the cell. Elevated Mn can also inhibit FRO2-reduction of Fe³⁺, diminishing the amount of Fe²⁺ available for uptake by IRT1 and enhancing the symptoms of Fe-deficiency. Thus, FIT also upregulates *MTP8* as part of the Fe-deficiency response, to sequester Mn within the vacuole and prevent inhibition of FRO2. These conclusions are partly based on the chlorotic appearance of *mtp8* mutants under low Fe availability, which is further exacerbated by high pH, in both plate- and soil-grown assays. At MTP8 was implicated as the key player in alleviating the Mn/Fe antagonism in the Fe-deficiency response at the root, although the study did not investigate any contribution made by the other Mn-MTPs.



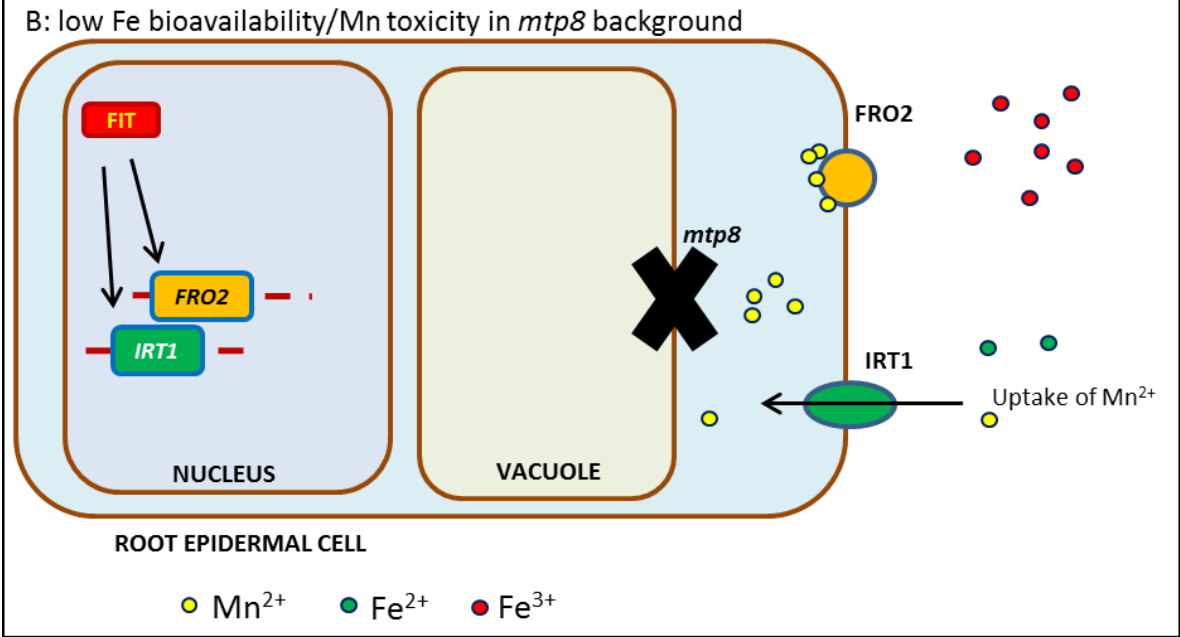


Figure 3.1. The role of At MTP8 in alleviating Mn/Fe antagonism.

A) Under low Fe availability in the wild type (WT) root cell, FIT bHLH transcription factor upregulates At *MTP8*, *FRO2* and *IRT1* (Yi and Guerinot, 1996; Robinson, et al., 1999; Vert, et al., 2002; Eroglu, et al., 2016). This ensures reduction of Fe³⁺ to Fe²⁺ by FRO2, for uptake by IRT1. Mn can also compete for uptake by IRT1, contributing to Mn toxicity within the cell, such as inhibition of FRO2. To avoid this, MTP8 sequesters excess Mn into the vacuole. B) In the *mtp8* background, Mn is not sequestered into the vacuole. As such, Mn inhibits FRO2, preventing reduction of Fe³⁺ to Fe²⁺ for uptake by IRT1 and exacerbating the symptoms of Fe deficiency. Based on findings by Eroglu, et al. (2016).

3.1.1 Bioinformatics

Bioinformatics is an interdisciplinary tool, combining the use of databases, mathematics, statistics and computer science to analyse and understand biological data (Luscombe, et al., 2001). This can aid hypothesis generation when analysing gene expression and protein function; the use of bioinformatics has also aided genome annotation, enabling identification of homologous genes in different organisms. Additionally, an understanding of temporospatial and developmental regulation of gene expression is also important for determining protein function. Both Cs MTP9 from cucumber (Migocka, et al., 2014) and Os MTP9 from rice (Ueno, et al., 2015) are expressed specifically in the roots, with expression upregulated under Mn toxicity. Alongside other key findings results, these results indicate Cs MTP9 and Os MTP9 efflux Mn at the plasma membrane of root cells to aid root-to-shoot translocation of Mn (Migocka, et al., 2014; Ueno, et al., 2015). Genevestigator is a useful database for initial hypothesis generation, utilising data from microarray and RNAseq to analyse expression with regards to developmental stage, tissue specificity and different experimental conditions (Hruz, et al., 2008). This database will be used to investigate the expression pattern of the Mn-MTPs from Arabidopsis.

Although Arabidopsis is a very useful model organism for improving our understanding of how different proteins function, the knowledge obtained from working with this plant must be applied to more agriculturally relevant species, if we are to tackle issues such as food security. This requires identification of protein homologs in species such as cereal crops. The Basic Local Alignment Search Tool (BLAST) algorithm searches databases with a query sequence, typically a coding gene sequence or a primary protein sequence, to identify similar sequences in specific libraries. Libraries are found in sequence databases including NCBI (Geer, et al., 2010) and UniProt (The UniProt Consortium, 2014). Annotated genetic information is available from fully sequenced genomes, such as Oryza sativa (rice) and Brachypodium distachyon, and often individual sequences can be obtained from non-sequenced genomes that have been confirmed experimentally. Hordeum vulgare (barley) and Triticum aestivum (bread wheat) are in the process of having their genomes fully annotated. Throughout the course of this project, annotation of the Triticum aestivum genome has dramatically increased, through efforts of the International Wheat Genome Sequencing Consortium. Sequences from wheat and barley are typically available from databases as genomic contiguous sequences (contigs). To identify homologs in barley and wheat, any contigs returned as significantly similar to the query sequence can be aligned to known coding sequences to predict intron/exon boundaries. In phylogenetic analyses, the MTPs have been seen to cluster according to proposed substrate specificity, with the putative Mn-MTPs dividing further into two subclades, Group 8 and 9 (Montanini, et al., 2007; Gustin, et al., 2011). This study aims to identify homologous Group 8 and 9 MTPs in crop species and perform a phylogenetic analysis to

Chapter 3

make predictions about their putative Mn-transporting abilities. Key motifs may support designation of proteins as Mn MTPs, including the broad CDF signature sequence that spans TMD2 to the start of TMD3. Additionally, while the majority of Zn-MTPs characterised to date possess a HxxxD motif on TMD5, and sometimes TMD2, the majority of Mn-MTPs possess DxxxD domains in their place (Montanini, et al., 2007; Gustin, et al., 2011). The structural relevance of these domains will be explored in greater detail in Chapter 5.

3.1.2 Use of mutants as a tool for investigating transporter function

Bioinformatics and expression analyses are useful tools for generating functional hypotheses where experimental data is unavailable. However, gene knockout and knockdown studies provide the opportunity to directly observe phenotypic effects when a protein is non-functional, thus providing information on a protein's physiological role. Since Arabidopsis has small introns and little intergenic material, it is possible to dramatically disrupt translation and expression of a gene, by inserting foreign elements such as T-DNA into the gene of interest, including in the coding sequence or promoter sequence. T-DNA can also act as a marker for identifying the point of insertion. It should be noted, however, that T-DNA insertion does not always result in a complete knockout; insertion at a particular position may still allow translation of part of the sequence, resulting in a functional or semi-functional truncated protein, or in a reduction of expression rather than a complete knockout (knock-down; Krysan, et al., 1999). Some of the possible outcomes of T-DNA insertion are summarised in Figure 3.2A.

The majority of T-DNA insertion mutants used in this project will be identified using the Arabidopsis genome mapping tool, T-DNA Express (Alonso, et al., 2003) and obtained through The European Arabidopsis Stock Centre (NASC). An aim of this project is to isolate and characterise single insertion for each of the putative Arabidopsis Mn-MTPs, At MTP8, MTP9, MTP10 and MTP11, and then generate combinations of double mutants for functional analysis. Single mutants have previously been reported for MTP11, mtp11-1 and mtp11-3, displaying sensitivity to elevated Mn (Peiter, et al., 2007). As described at the start of this chapter, the Mn-sensitivity of mtp8-1 and mtp8-2 insertion mutants was reported towards the end of this thesis work, with more focus paid to the chlorotic phenotype observed under low Fe availability, induced by high pH (Eroglu, et al., 2016). Although MTP8 was implicated as the key player in alleviating Mn/Fe antagonism, the other Mn-MTPs were not investigated; the single and double mutants isolated here will be used to explore whether any of the other Mn-MTPs play a role in this process.

3.1.3 Ethyl methanesulfonate mutagenesis and forward genetics

Another method of mutagenesis is ethyl methanesulfonate (EMS) mutagenesis. This is an alkylating agent that chemically modifies nucleotides, typically by alkylation of guanine to O-6-ethylguanine, preventing pairing with cytosine but enabling pairing with thymine. Following subsequent rounds of DNA replication, the original G/C pair can be replaced with A/T, which in turn can result in changes to the protein sequence (Greene, et al., 2003). The mutagenesis is random and can occur multiple times in the genome, typically between 10⁻⁷ and 10⁻⁸ events per base pair per generation (Kovalchuk, et al., 2000). After identification of a mutation, the EMS plant should be backcrossed with a wild type several times to eliminate other unidentified background mutations.

The Purdue Ionomics Information Management System (PiiMS) provides information regarding shoot concentrations of a range of metals, including Mn, in various Arabidopsis lines and mutants (Baxter, et al., 2007). Searching the PiiMS database identified 954-12, an Arabidopsis EMS mutant, as having enhanced Mn accumulation in shoot tissues. This is shown in Figure 3.2B; 954-12 shows around a 55 % median percentage increase in shoot Mn accumulation compared to the wild type (WT; Baxter, et al., 2007). Certain *mtp* insertion mutants have been shown to have altered Mn accumulation in different parts of the plant, suggesting disruption of particular transporters affects Mn distribution. For example, both the Arabidopsis *mtp11* (Peiter, et al., 2007) and rice *mtp9* (Ueno, et al., 2015) mutants accumulate more Mn in roots than in shoots, while *mtp8-2* features increased root-to-shoot translocation of Mn (Eroglu, et al., 2016). It is possible that the 954-12 EMS mutant has a mutation in one of the Mn-MTPs or another part of the Mn homeostatic machinery; this will be explored further in this chapter.

3.1.4 Artificial microRNA (amiRNA) as a tool for downregulation

At MTP9 and MTP10 are both found on chromosome 1 and cluster most closely in phylogenetic analysis of the Arabidopsis Mn-MTPs (Montanini, et al., 2007; Gustin, et al., 2011). It is hypothesised, therefore, that these transporters share a functional redundancy and that neither mtp9 nor mtp10 will display a metal-dependent phenotype individually. To evaluate this hypothesis, ideally a double knockout for mtp9 mtp10 would be generated and its phenotype explored as with the other double mutants. However, at the start of this project, there were no insertion mutants in the coding region of MTP9 or MTP10 available in the same wild type background: Arabidopsis exists as different ecotypes, or species variants, based on their geographic distribution, which possess polymorphic differences that can result in

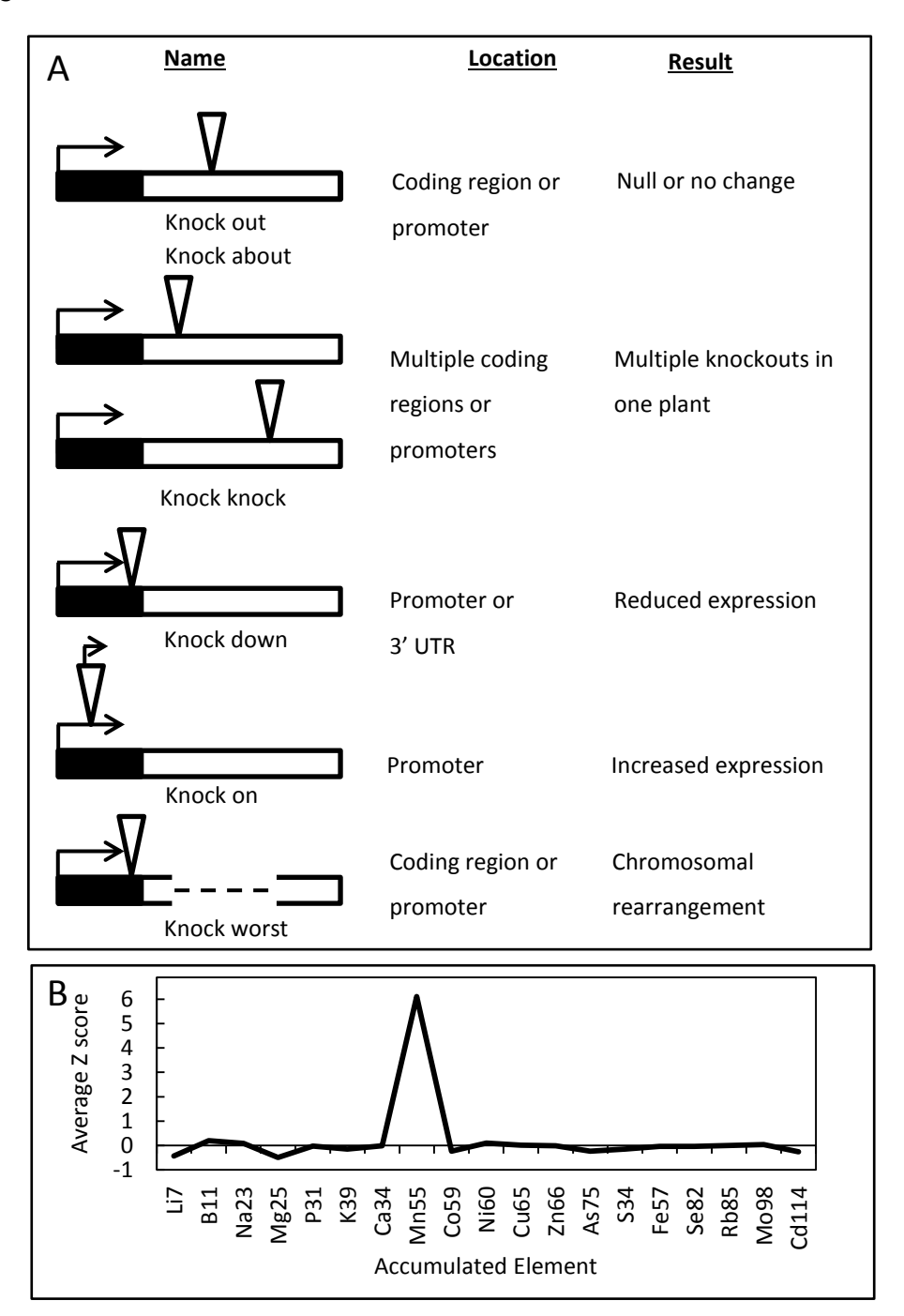


Figure 3.2 Impacts of different types of mutants.

A) Potential changes in expression as a result of T-DNA inserted into an Arabidopsis chromosome, with corresponding nomenclature, or 'knockology'. White box = coding region; black box with an arrow = promoter; triangle = T-DNA insert. KOs knockouts; UTR, untranslated region. Adapted from Krysan et al. (1999). B) Ethyl methanesulfonate (EMS) mutant 954-12 features enhanced Mn accumulation in shoots compared to wild type (WT) Arabidopsis when grown on soil. This information was obtained from the PiiMS database (Baxter, et al., 2007) but the mutant was identified by the LEW lab. Ionomic data shows average z-scores (number of SDs away from mean of WT analysed at same time) where n = 12.

molecular and phenotypic differences. These variations should therefore be considered when generating double mutants from different wild type backgrounds (Passardi, et al., 2007). Additionally, when genes are positioned closely on the chromosome, it can be difficult to isolate double homozygous mutants due to spontaneous crossing-over events during meiosis. However, Boutigny, et al. (2014) successfully obtained a double mutant of *paa1.1* (At4g33525; Lansberg ecotype) and *hma1* (At3g37270; Ws ecotype), positioned around 1.4 Mbp apart at the 5' end of chromosome 4. Instead of the normal 1/16 ratio of double homozygous at the F2 generation, 2 plants from 140 F2 generation plants were identified as hom/het, and eventually 7 out 56 F3 generation plants were identified as double homozygous mutants (Boutigny, et al., 2014). Based on this success, an aim developed later in the proceedings of this project, is to isolate *mtp9-1 mtp10-1*.

Another option for developing a functional double knockdown, however, is the use of artificial microRNA (amiRNA). Two types of small RNAs exist naturally, playing important roles in regulating gene expression in plants and animals: microRNA (miRNA) and small interfering RNA (siRNA). In plants, miRNAs are transcribed from primary miRNAs by RNA polymerase II (Lee, et al., 2004; Xie, et al., 2005), generally from imperfect inverted repeats in the genome, to form fold-back precursors or hairpins. The hairpin is processed by DICER-LIKE1 (DCL1) and split to release a single sense strand miRNA, and an anti-sense strand which is degraded (Park, et al., 2002; Reinhart, et al., 2002; Kurihara & Watanabe, 2004). This miRNA forms the specificity component of the RNA-induced silencing complex (RISC) to recognise complementary motifs in the target sequence for downregulation, summarised in Figure 3.3C.

A web-based tool, WeigelWorld, exploits the natural parameters of miRNA to design amiRNA, targeting the endogenous RNAs of Arabidopsis (Ossowski, et al., 2005; 2009; available www.weigelworld.org). This is based on a series of amiRNAs in Arabidopsis (Schwab, et al., 2006), rice (Warthmann, et al., 2008); *Physicomitrella patens* (Khraiwesh, et al., 2008) and *Chlamydomonas reinhardtii* (Molnar, et al., 2009) that successfully silenced single or multiple targets with limited off-target effects. Compared to animal miRNAs, which have up to hundreds of targets (Farh, et al., 2005; Lim, et al., 2005), plant miRNAs target a small number of genes with high but not perfect miRNA-target sequence complementarity (Llave, et al., 2002). Key design parameters for amiRNA are based on these sequence mismatches, but must be complementary at positions 10 and 11, the presumptive site of endonucleolytic cleavage by RISC (Schwab, et al., 2006). The principle of amiRNA generation is shown in Figure 3.3. This chapter aims to use the WeigelWorld amiRNA system to achieve a functional knockdown of *MTP9* in the *mtp10* knockout background.

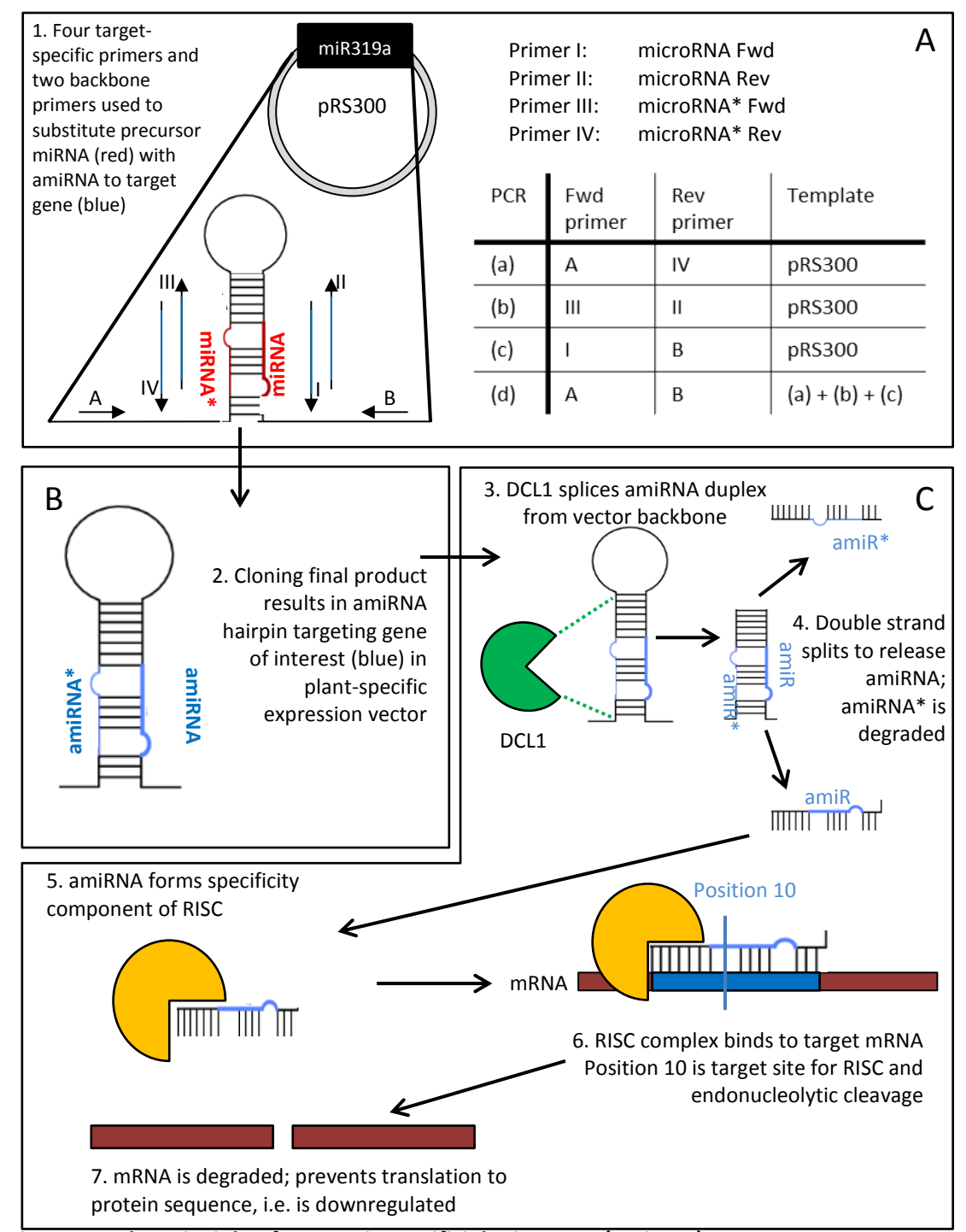


Figure 3.3 The principle of generating artificial microRNA (amiRNA) constructs

A) pRS300 vector carries natural miRNA hairpin, miR319a (red); multiple PCRs with backbone primers (A + B) and gene-specific primers (I-IV) replace miR319a with amiRNA to target gene of interest (blue). '*' marks anti-sense strand, which is later degraded. B) amiRNA is digested and ligated into entry vector (pENTR1a) and subcloned into plant-specific expression vector for transformation into Arabidopsis. C) Summary of downregulation by amiRNA within the plant. DCL1, Dicer-Like 1; RISC, RNA-induced silencing complex. Hump in amiRNA marks mismatching to target gene at position 21; mismatching ensures correct orientation within RISC. amiRNA strategy, Schwab, et al. (2006). Downregulation summary, (Park, et al., 2002; Reinhart, et al., 2002; Llave, et al., 2002; Kurihara & Watanabe, 2004).

3.1.5 Downregulating wheat genes with RNAi

The second type of small RNAs, siRNAs, are formed when endogenous, double-stranded RNAs are cleaved by the Dicer RNase; this releases double stranded intermediates, usually 21 nucleotides in length, with a 3' overhang. This overhang ensures correct orientation in RISC and guides the complex to fully complementary target mRNA for cleavage and degradation (Elbashir, et al., 2001; Martinez, et al., 2002). This is the principle of RNA interference (RNAi), a pathway which, like amiRNA, is often exploited artificially as a reverse genetics tool. RNAi has been used to downregulate *MTP* genes for functional analysis; a Mn-dependent phenotype is observed in the RNAi-silenced lines At *mtp11* (Delhaize, et al., 2007) and the rice Os *mtp8.1* (Chen, et al., 2013).

The majority of mutant analyses performed in this chapter will use the model organism Arabidopsis. As described in Chapter 1, however, a further aim of this project is to expand this analysis into more agriculturally relevant species; this chapter aims to perform a phylogenetic analysis to identify Mn-MTPs in cereal crops, in particular wheat. Generally speaking, higher plants divide phylogenetically into monocots (with one cotyledon, such as the cereal plants wheat and barley) and dicots (with two cotyledons, including flowering plants such as Arabidopsis); the evolutionary monocot-dicot divergence has been estimated at around 200 million years ago (Wolfe, et al., 1989). A key evolutionary difference between Mn-MTPs identified so far is the presence of both MTP8 and MTP8.1 in certain monocots (Chen, et al., 2013; Pedas, et al., 2014) but only At MTP8 in Arabidopsis. It is therefore hypothesised that wheat will also possess both MTP8 and MTP8.1. However, while Arabidopsis has a diploid genome, wheat has a hexaploid genome due to two separate hybridisation events during the evolution and domestication of bread wheat, Triticum aestivum. This has resulted in a hybrid species possessing 6 complete genomes, each of 7 chromosomes: genomes AA, BB and DD, donated from tetraploid and diploid Although the ancestral genomes are related, they have various polymorphic similarities and differences throughout, generally resulting in slightly different protein sequences; homologous sequences on each genome are referred to as homeologues (Feldmen, 2001; Tanno and Willcox, 2006; Matsuoka, et al., 2011).

An aim of this chapter is to begin to identify homologous sequences to each of the Mn-MTPs in wheat, including whether they possess the CDF signature sequence and the DxxxD domains. The main focus, however, will be on beginning to characterise Ta *MTP8* and *MTP8.1*. Following identification, an RNAi approach will be attempted, in collaboration with NIAB (Cambridge, UK), to downregulate these homeologues simultaneously. Disruption of Os *MTP8.1* results in a Mn-sensitive phenotype compared to the WT (Chen, et al., 2013); it is hypothesised that if Ta *MTP8*

Chapter 3

and *MTP8.1* are successfully downregulated, the mutant plants will show an increased level of sensitivity to excess Mn.

3.1.6 Chapter aims

The work to be carried out in this chapter falls under three overall aims:

- 1. Perform bioinformatics analysis of Arabidopsis Mn MTPs
 - Search databases for information on differential expression of the Arabidopsis Mn-MTPs, to form hypotheses regarding developmental and temporospatial functions

2. Phylogenetic analysis of MTPs

- Identify homologous proteins to the Mn MTPs in more agriculturally relevant crop species such as wheat, sorghum, maize and barley; this will include the identification of different homeologues from bread wheat (*Triticum aestivum*)
- Generate an updated phylogenetic tree, including the newly identified MTPs

3. Mutant analysis

- o Isolate and confirm single and double mutants for Mn MTPs
- Characterise these single and double mutants, to determine any Mn- or other
 metal-dependent phenotype, or any additive phenotype which might suggest
 redundancy of function between proteins, or that they function at different parts
 of the cell or plant. Directly compare these mutants to determine the relative
 importance of these transporters in Mn homeostasis.
- Eroglu et al. (2016) describe MTP8 as the key player in alleviating Mn antagonism in Fe nutrition, yet did not test the other Arabidopsis Mn-MTPs under the same conditions; test the isolated single and double mutants to determine whether MTP9, 10 and 11 also play a role in this process
- Generate amiRNA clones to downregulate MTP9 in the mtp10 knockout background
- After identification of MTP8 homologues in wheat and individual homeologues, design RNAi sequences to target specifically MTP8 and MTP8.1. Generate RNAi construct to target all homeologues simultaneously. The construct will be transformed into wheat (by NIAB) and changes in levels of expression will be quantified by qPCR.

3.2 Results

3.2.1 Bioinformatic analysis of At MTP8 – MTP11

Table 3.1 compares the protein sizes for At MTP8 – 11. The corresponding % similarity and identity of these amino acid sequences are shown in Table 3.2. Of these transporters, MTP8 shares the lowest % identity and similarity with MTP9-11; this transporter clusters separately in group 8 (Gustin, et al., 2011), as confirmed later in Figure 3.6. MTP9 – 11 share higher % identity and similarity, clustering together in group 9. At MTP9 and At MTP10 share the highest % identity and similarity, both found on chromosome 1. Two gene models are listed on the Arabidopsis Information Resource (TAIR) for MTP9 (locus At1g79520), differing in 36 bases in exon 6, which are either part of intron 5 (model At1g79520.1) or part of the coding sequence in exon 6 (At1g79520.2). Chapter 5 amplifies and confirms the coding sequence for each Arabidopsis Mn MTP to be identical to that proposed by TAIR. The coding sequence amplified for *MTP9* included the discrepant 36 bases, corresponding to At1g79520.2. The intron/exon structures for each of the Mn-MTPs are presented in Figure 3.2. MTP9 - 11 are all predicted to possess 6 exons, with a large 2nd intron, while MTP8 possesses 7 exons.

3.2.2 Using Genevestigator for expression analysis of At MTP8-11

The Genevestigator Affymetrix database (Hruz et al, 2008) provides information about gene expression under different conditions, including tissue specificity, developmental stage and perturbations to the growth environment. Figure 3.5A illustrates the absolute expression levels of At MTP8-11 across ten stages of Arabidopsis development, as predicted from the signal intensity on a 22k array; medium expression level is defined as the interquartile range, with high and low expression either side of this range. Of the Arabidopsis Mn-MTPs, MTP11 is consistently expressed at the highest level throughout development, spanning the divide between medium and high expression at the seedling and young rosette stage, but dropping to low expression during senescence.

Contrastingly, *MTP8* is consistently expressed at the lowest levels, except in the germinating seed and during senescence. Examination of the tissue specificity of *MTP8* expression indicates this gene is consistently expressed at very low levels under basal conditions, with the exception of primary root elongation zone and the inflorescence, and the seed, where expression reaches medium levels. The top 10 conditions to cause an upregulation of *MTP8* are presented in Table 3.3. Aside from two cases related to germination, the majority of conditions to cause an upregulation of *MTP8* are related to Fe deficiency, with fluctuations localised to the root.

Table 3.1 Analysis of At Mn-MTP protein sequences.

Accession numbers: At MTP8, At3g58060; At MTP9, At1g79520; At MTP10, At1g16310; At MTP11. At2g39450. Protein length measured in number of amino acids.

	Protein length	MW (kDa)	
MTP8	411	46.2	
МТР9	414	46.9	
MTP10	428	49.1	
MTP11	394	44.6	

Table 3.2 At Mn-MTP protein sequence similarity and identity.

Sequence % similarity (unshaded cells) and % identity (shaded cells) between At MTP8 – AtMTP11. Calculated using EMBOSS program Matcher (Rice, et al., 2000).

	MTP8	MTP9	MTP10	MTP11
MTP8	-	44.5	44.6	44.2
МТР9	58.6	-	77.5	54.7
MTP10	58.8	83.6	-	51.4
MTP11	60.9	69.7	65.9	-

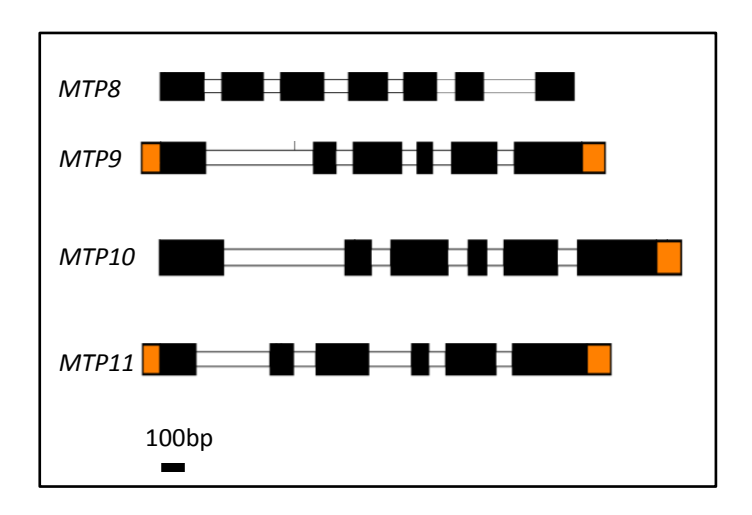


Figure 3.4. Intron/exon structure of At MTP8 - MTP11.

Black box, exon; white box, intron; orange box, 5' and 3' untranslated regions; sequences originally obtained from TAIR, intron/exon junctions confirmed with sequencing. Black bar, 100bp scale.

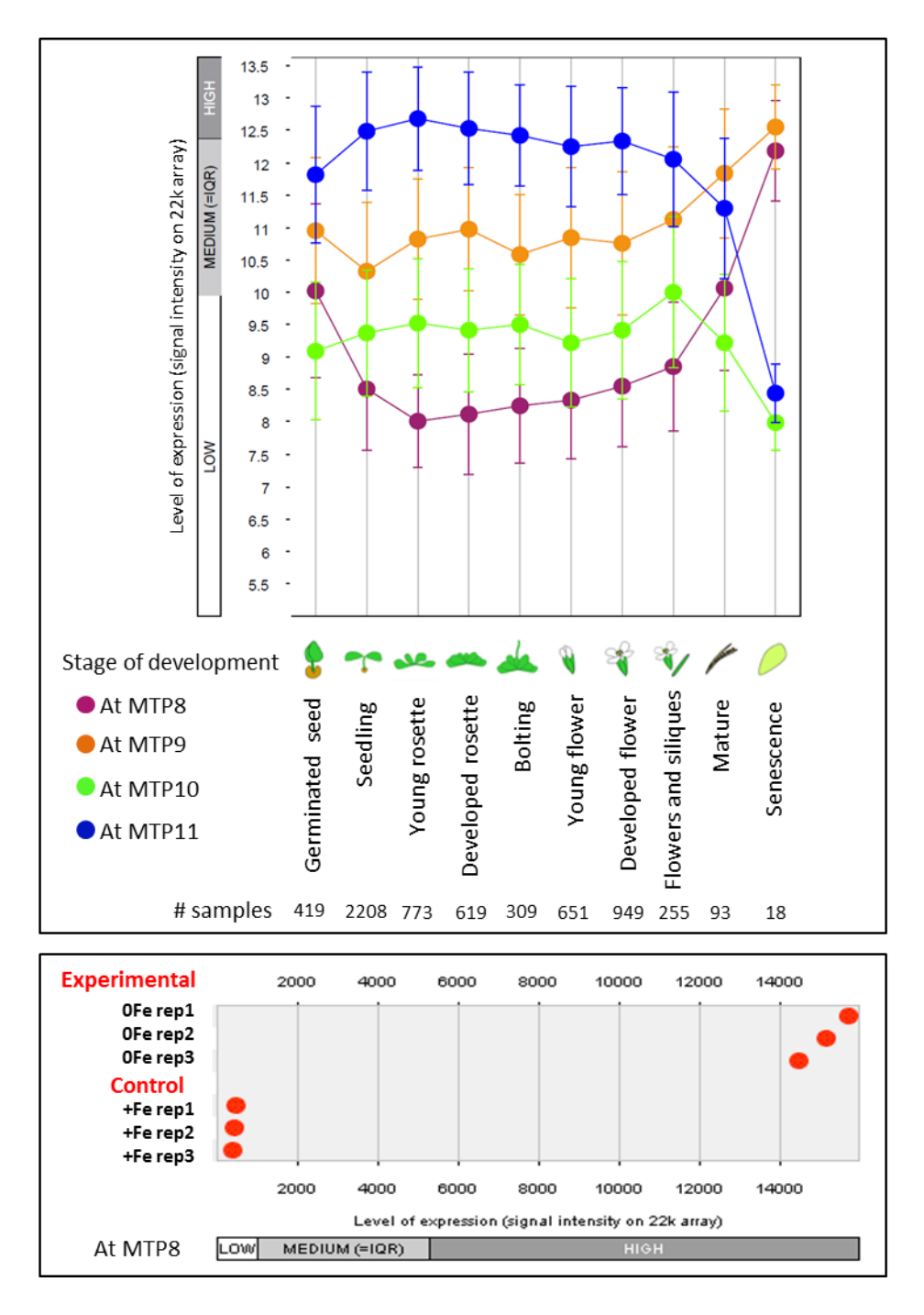


Figure 3.5 Expression patterns of Arabidopsis Mn-MTPs obtained from Genevestigator.

A) Average absolute expression levels of At MTP8, At MTP9, At MTP10 and At MTP11 in Arabidopsis across a range of developmental stages. B) Absolute expression levels of At MTP8 in Columbia wild type roots under control and Fe deficiency conditions (experimental). 10 day old seedlings were transferred from control plates to either new control media ('control') or media lacking FeEDTA ('experimental'). Level of expression is calculated from signal intensity on a 22k affymetrix array; medium expression is defined as the interquartile range. Created with Genevestigator (Hruz, et al., 2008).

Table 3.3. Top 10 conditions that cause an upregulation in expression of At MTP8

Level of expression calculated from signal intensity on a 22k affymetrix array; fold change in expression determined by comparing intensity to untreated control, e.g. not exposed to Fe deficiency. Data obtained from Genevestigator (Hruz, et al., 2008)

	Condition	Genetic background	Devt stage	Anatomy	Fold change in upregulation
1	Fe deficiency	Col0	Seedling	Root maturation zone	38.4
2	Fe deficiency	Col0	Seedling	Whole root	34.83
3	Fe deficiency	Col0 overexpressing Cs UBC13	Seedling	Whole root	28.68
4	Fe deficiency	ubc13 T-DNA insertion mutant	Seedling	Whole root	27.99
5	Stratification (48h)	Col0	Germinated seed	Seed	22.06
6	Germination (1h)	Col0	Germinated seed	Seed	16.19
7	Fe deficiency	Col0	Seedling	Whole root	16.07
8	Fe deficiency	Col0	Seedling	Whole root	9.58
9	Fe deficiency	Col0	Seedling	Whole root	8.83
10	Fe deficiency	pye-1 T-DNA insertion mutant	Seedling	Whole root	7.96

One example of these is visualised in Figure 3.5B. Generally these changes are observed in the WT background, although upregulation is also observed in mutant lines related to UBC13 and PYE. A ubiquitin-conjugating enzyme and a bHLH transcription factor, respectively, both proteins are involved in the Fe response (Li and Schmidt, 2010; Long, et al., 2010). Fe deficiency had no impact on expression of the other Mn-MTPs (data not shown).

Despite the expression of MTP10 falling mostly under 'low' levels and MTP9 mostly under 'medium' levels between the germinated seed and flowers/siliques stages of development, the error bars for average expression levels considerably overlap. From the mature silique stage of development, however, expression of these genes begins to diverge, with expression of MTP9 reaching 'high' in seeds, and expression of MTP10 dropping further into low (Figure 3.4A). This correlates with the anatomical expression of MTP9 and MTP10; highest levels of MTP9 expression are seen in the senescent leaf and in reproductive parts of the plant, including the endosperm, stamen, sepal and pollen, with expression upregulated in during pollen tube growth. MTP9 was expressed at lower levels in the root, including the elongation zone, root epidermis and lateral root. Contrastingly, MTP10 expression is lowest in the reproductive parts of the plant but is expressed at high levels in protoplasts isolated from the root xylem and phloem pericycle, and the root vascular tissue. It should be noted that there is no perturbation information available for changes in Mn expression. A perturbation that may be of interest is the change in expression post infection with soil-born pathogen Phytophthora parasitica. Compared to non-infected samples, MTP9, and to a lesser extent MTP10 and MTP11, are downregulated in roots after infection with soil-born pathogen; MTP8 expression remains unchanged (data not shown).

3.2.2.1 Identifying homologous Mn-MTPs in cereal plants

A key aim of this chapter is to identify homologous MTPs in more agriculturally relevant crop species. All potentially homologous proteins identified in this chapter are included in the neighbour-joining phylogenetic tree of Figure 3.6, using 1000 bootstrap replicates. Thus, the proposed nomenclature in Table 3.4 is based on the clustering pattern of this tree. Included in the analysis were At MTP8 – MTP11 and the homologous Group 8 and Group 9 proteins previously identified in *Oryza sativa, Populus trichocarpa, Sorghum bicolor, Hordeum vulgare, Cucumis sativis* (cucumber) and *Beta vulgaris* spp. maritima (Peiter, et al., 2007; Gustin et al, 2011; Erbasol et al, 2013; Chen, et al., 2013; Pedas, et al., 2014; Migocka, et al., 2014). Members of the other MTP clades, Zn-transporting At MTP1 of Group 1 and At MTP6 and MTP7 of Groups 6 and 7, were included as controls for any falsely-identified non-Group 8 or 9 MTPs (Van der Zaal, et al., 1999; Kobae, et al., 2004; Desbrosses-Fonrouge, et al., 2005). A search for any additional Group 8 or 9 proteins in rice, *Oryza sativa*, was carried out on the Rice Genome Annotation Project (RGAP;

Chapter 3

Kawahara, et al., 2013) but no new Mn-MTPs were identified; this confirms the finding that rice possesses 2 Group 8 members, Os MTP8 and MTP8.1, and 3 Group 9 members, Os MTP9, MTP11 and MTP11.1 (Chen, et al., 2013). No Os MTP10 has previously been identified, nor was it found in this analysis. Using formerly identified Mn-MTPs to search on RGAP, UniProt (The UniProt Consortium, 2014) and Phytozome v9.1 (Goodstein, et al., 2012), potential homologs were identified from both Groups 8 and 9 in *Brassica rapa*, *Sorghum bicolor*, *Brachypodium distachyon* and *Zea mays*; these are listed in Table 3.4. While one copy of Br MTP9 was identified in *Brassica rapa*, clustering closely with At MTP9, two potential Br MTP10 and three potential Br MTP8 proteins were identified. These proteins share upwards of 90% identity and it is possible they represent recent duplications within the *Brassica rapa* genome. Searching the International Barley Sequencing Consortium database (Schulte, et al., 2009) identified HvAK372762.1, which is proposed to be named Hv MTP11; no further Group 9 or Group 8 members were identified, in addition to those previously identified (Hv MTP8 and Hv MTP8.1; Pedas, et al., 2014) although it should be noted that the *Hordeum vulgare* genome is still in the process of being fully sequenced.

The Triticum aestivum (bread wheat) genome is also in the process of being sequenced; genomic sequence information is mostly available as contiguous sequences (contigs) of chromosome arm survey sequences, with intron/exon boundaries not yet fully predicted for the majority of the genome. ESTs/cDNA sequences are available in some regions of the genome but did not cover the regions proposed here to carry the Mn-MTPs. Genomic sequence information for homologous proteins in Oryza sativa, Brachypodium distachyon and, where available, Hordeum vulgare was used in the ViroBLAST search tool on each of the chromosomes, available on the WheatPortal of the URGI database (Unité de Recherche Génomique Info; Deng, et al., 2007), to search for putative wheat Mn-MTPs. Returned contigs did not always span the whole region of interest (i.e. did not cover the full gene), but rather covered portions of the gene at the 5' or 3' end. If more than one contig was returned in the output, they were aligned and combined to attempt to cover the whole region of interest. Intron/exon boundaries were predicted based on coding sequence information for Mn-MTPs from Oryza sativa, Brachypodium distachyon and Hordeum vulgare; the prediction programme Augustus (Stanke, et al., 2008) was also utilised to help predict intron/exon boundaries, although this tended to predict 'too short' proteins that did not always carry the full CDF signature sequence. Table 3.5 lists the predicted Mn-MTPs from Triticum aestivum and these were included in the phylogenetic analysis of Figure 3.6. Proteins are listed as 'complete' if they align well with the homologous protein in Oryza sativa, Brachypodium distachyon and Hordeum vulgare, and carry both the CDF signature sequence and the 2 DxxxD motifs characteristic of Mn-MTPs in plants (Montanini, et al., 2007; Gustin, et al., 2011). At least one full homologous protein sequence was identified for Ta MTP8, MTP8.1, MTP9, MTP11 and MTP11.1; partial or complete

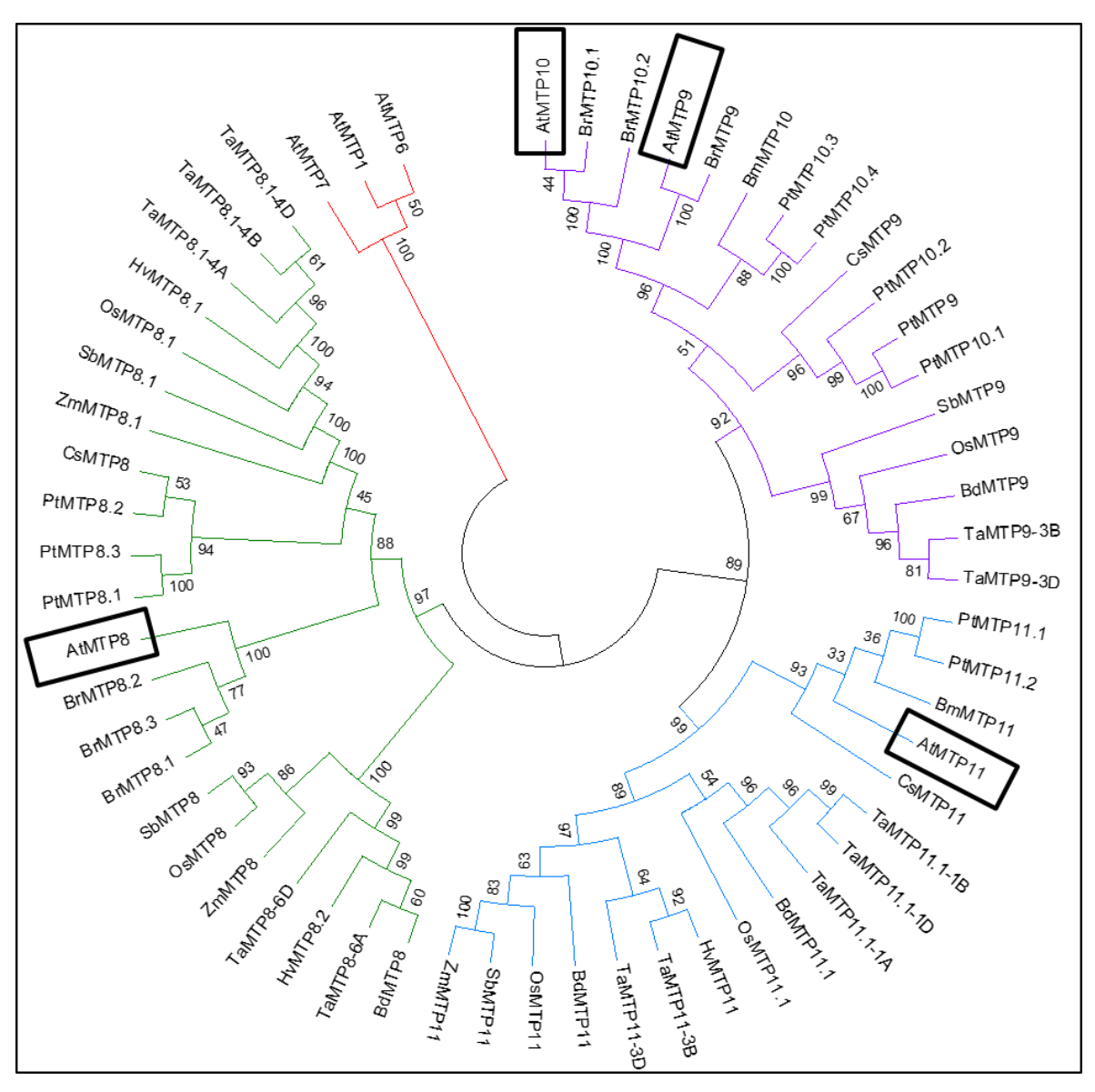


Figure 3.6. Evolutionary relationship of putative Mn-MTPs from different plant species shows clustering into 3 main sub-clades.

Green, group 8 MTP8 and MTP8.1; blue, group 9 MTP11 and MTP11.1; purple group 9 MTP9 and MTP10. Red, At MTP1, MTP6 and MTP7 included as controls for other MTP sub groups. Evolutionary relationships inferred using the Neighbour-Joining method; bootstrap consensus inferred from 1000 replicates and is taken to represent the evolutionary history of the proteins analysed. The evolutionary distances were computed using the Poisson correction method and are in the units of the number of amino acid substitutions per site. The analysis involved 59 amino acid sequences. All ambiguous positions were removed for each sequence pair. Evolutionary analyses were conducted in MEGA7 phylogenetic analysis package (Tamura, et al., 2007; Migeon, et al., 2010). At MTP8, MTP9, MTP10 and MTP11 are highlighted in boxes for reference. Protein sequences obtained from: *Arabidopsis thaliana* ('At'), Brassica rapa ('Br'), *Beta vulgaris* spp. maritima ('Bm'), *Populus trichocarpa* ('Pt'), *Sorghum bicolor* ('Sb'), *Brachypodium distachyon* ('Bd'), *Triticum aestivum* ('Ta'), *Cucumbis sativis* ('Cs'), *Oryza sativa* ('Os'), *Zea mays* ('Zm'), *Hordeum vulgare* ('Hv').

Table 3.4.

Homologous Mn MTPs identified in different cereal species after phylogenetic searching with rice and Arabidopsis genomic sequences for MTP8, MTP9, MTP10 and MTP11.

Proposed names are based on phylogenetic tree in Figure 3.6. Obtained from databases: Phytozome v9.1 (Goodstein, et al., 2012), UniProt (The UniProt Consortium, 2014) and IBSC, international barley consortium database (IBSC; Schulte, et al., 2009).

Brachypodium Bd MTP8		obtained
Brachypodium Bd MTP8		obtailea
	Bradi3g57420	Phytozome9.1
distachyon Bd MTP9	Bradi2g02050	Phytozome9.1
Bd MTP1:	1 Bradi2g23070	Phytozome9.1
Bd MTP1:	Bradi2g54410	Phytozome9.1
Zea mays Zm MTP8	ZmGRMZM5G86	2882_T02 Phytozome9.1
(maize) Zm MTP8	.1 ZmGRMZM2G11	8497_T02 Phytozome9.1
Zm MTP1	1 ZmGRMZM2G01	4454_T01 Phytozome9.1
Sorghum bicolor Sb MTP8	Sb04g034705	Phytozome9.1
(sorghum) Sb MTP8.	1 Sb01g041820	Phytozome9.1
Sb MTP9	Sb03g007250	Phytozome9.1
Sb MTP11	Sb03g039220	Phytozome9.1
Brassica rapa FPsc Br MTP8.	1? Bra007377	Phytozome9.1
(turnip mustard) Br MTP8.	2? Bra014588	Phytozome9.1
Br MTP8.	3? Bra003316	Phytozome9.1
Br MTP9	Bra035123	Phytozome9.1
Br MTP10	.1? Bra026067	Phytozome9.1
Br MTP10	.2? Bra026723	Phytozome9.1
Hordeum vulgare Hv MTP8.	1 MLOC_65324.1	UniProt, IBSC
(barley) Hv MTP8.	2 MLOC_55775.1	UniProt, IBSC
Hv MTP1:	HvAK372762.1	IBSC

Table 3.5. Identification of Mn-MTP homeologues in Triticum aestivum (bread wheat).

Sequences obtained from International Wheat Genome Sequencing Consortium chromosomearm survey sequences ('chr. arm sequence'), identified by ViralBLAST tool on URGI database (Unité de Recherche Génomique Info; Deng, et al., 2007). Completion status indicates whether predicted protein sequence is considered to be the full, in-frame sequence with both the CDDF signature sequence and both Mn-MTP DxxxD motifs (Montanini, et al, 2007; Gustin, et al., 2011). Number of amino acids refers to portion of completed protein assumed correct, e.g. '134...' indicates the first 134 codons are proposed correct before an early stop codon or the sequence becomes out of frame. '?', # amino acids cannot be predicted.

Wheat	Chromosome	Chr. arm sequence	Completion status	# amino
homologue	& genome			acids
Та МТР8	6A	6AL_5795943 +	Nearly COMPLETE but possibly	370
		6AL_5818856 +	premature termination codon	
		6AL_5766608		
	6B	6BL_4395039 +	No information available	?
		6BL+4292057		
	6D	6DL_3125108	Incomplete; 3' end is in frame	317
Ta MTP8.1	4A	4AS_5965838	COMPLETE	402
	4B	4BL_7037499 +	COMPLETE	310
		4BL_6931319		
	4D	4DL_14402153	COMPLETE	401
Та МТР9	3A	3AS_3289379	Incomplete; have some of 5'	Out of
			end	frame
	3B	3B_10724521 +	COMPLETE	393
		3BF060500410CF_t1		
	3D	3DS_948407	Incomplete; some of 5' end	134
Ta MTP11	3A	3AL_4259891 +	Incomplete; all out of frame	?
		3AL_4258676		
	3B	3B_10636290 +	COMPLETE	404
		3BF117500050CFD_t1		
	3D	3DL_6937261	Incomplete; have most of 5'	291
			end	
Ta MTP11.1	1A	1AL_3967773	COMPLETE	398
	1B	1BL_3832922	Incomplete; have most of 5'	281
			end	
	1D	1DL_2287002	Incomplete; have most of 5'	209
			end	

Α	133
BrMTP8.3	ATLKSGSIAIAASTLDSLLDLMAGGILWFTHLSMKNINIYKYPIGKLRVQPVGIIIFAAVMATLGFQVLLVAAEQLIANE
AtMTP8	ATVKSGSIAIAASTL <mark>DSLLD</mark> LMAGGILWFTHLSMKNVNIYKYPIGKLRVQPVGIIIFAAVMATLGFQVLLVAAEQLISNE
BrMTP8.1	ATIKSGSIAVAASTL <mark>DSLLD</mark> LMAGGILWFTHLSMKNINIYKYPIGKLRVQPVGIIIFAAVMATLGFQVLLEATEQLIKNE
BrMTP8.2	ATIKSGSIAIAASTLDSLLDLMAGGILWFTHISMKNINIYKYPIGKLRVQPVGIIIFAAVMATLGFQVLLVAAEKLITNE
BdMTP8	ATVKTGSMAIAASTLDSLLDLMAGGILWFTHLSMKKVNIYKYPIGKLRVQPVGIIVFAAIMATLGFQVLVQAIEQLVENF
HvMTP8.2	ATIRTGSMAIAASTLDSLLDLMAGGILWFTHLSMKKVNIYKYPIGKLRVQPVGIIVFAAIMATLGFQVLVQAIEQLVENE
TaMTP8-6A	ATIRTGSMAIAASTLDSLLDLMAGGILWFTHLSMKKVNIYKYPIGKLRVQPVGIIVFAAIMATLGFQVLVQAIEQLVENE
OsMTP8	ATIKTGSMAIAASTLDSLLDFLAGGILYFTHLTMKSVNIYKYPIGKLRVQPVGIIVFAAIMATLGFQVLIQAIEQLVENK
TaMTP8-6D	ATIRTGSMAIAASTLDSLLDLMAGGILWFTHLSMKKVNIYKYPIGKLRVQPVGIIVFAAIMATLGFQVLVQAIEQLVENE
SbMTP8	ATIRTGSMAIAASTLDSLLDFMAGGILWFTHLSMKRVNIYKYPIGKLRVQPVGIIVFAAIMATLGFQVLVQAVEQLVENF
ZmMTP8	ATIRTGSMAIAASTLDSLLDFMAGGILWFTHLSMKRVNIYKYPIGKLRVQPVGIIVFAAIMATLGFQVLVQAVEQLVENK
PtMTP8.1	ATIRTGSIAIAASTLDSLLDLMAGGILWFTHISMKNINIYKYPIGKLRMQPVGIIIFAAVMATLGFQILVLAAEELIEDE
PtMTP8.3	ATIRTGSIAIAASTL <mark>DSLLD</mark> LLAGGILWFTHISMKNINIYKYPIGKLRVQPVGIIIFAAVMATLGFQILIQALEELIVNE
CsMTP8	ATVRSGSIAIAASTLDSLLDLMAGGILWFTHLYMKQVNIYKYPIGKLRVQPVGIIVFAAVMATLGFQVLLQAVEQLIQDF
PtMTP8.2	ATIKTGSLAIAASTL <mark>DSLLD</mark> LMAGGILWFTHLSMKKINIYKYPIGKLRVQPVGIVIFAAIMATLGFQILTKAVEQLIQHK
TaMTP8.1-4B	ATVKSGSIAIAASTL <mark>DSLLD</mark> LMAGGILWFTHLSMKSINVYKYPIGKLRVQPVGIIIFAAVMATLGFQVFLQAVEKLVVNV
HvMTP8.1	ATVKSGSIAIAASTL <mark>DSLLD</mark> LMAGGILWFTHLSMKSINVYKYPIGKLRVQPVGIIIFAAVMATLGFQVFLQAVEKLVVNV
TaMTP8.1-4A	${\tt ATVKSGSIAIAASTL} \underline{{\tt DSLLD}} {\tt LMAGGILWFTHLSMKSINVYKYPIGKLRVQPVGIIIFAAVMATLGFQVFLQAVEKLVVNVNCMMMMMMMMMMMMMMMMMMMMMMMMMMMMMMMMM$
TaMTP8.1-4D	${\tt ATVKSGSIAIAASTL} \underline{{\tt DSLLD}} {\tt LMAGGILWFTHLSMKSINVYKYPIGKLRVQPVGIIIFAAVMATLGFQVFLQAVEKLVVNNNNNNNNNNNNNNNNNNNNNNNNNNNNNNNNNN$
OsMTP8.1	${\tt ATIKSGSIAIAASTL} \underline{{\tt DSLLD}} {\tt LMAGGILWFTHLSMKSINVYKYPIGKLRVQPVGIIIFAAVMATLGFQVFVQAVEKLIVNE}$
SbMTP8.1	ATIKSGSIAIAASTL <mark>DSLLD</mark> LMAGGILWFTHLSMKSINVYKYPIGKLRVQPVGIIIFAAVMATLGFQVFIQAVEKLIVNE
ZmMTP8.1	${\tt ATIKSGSIAIAASTL} \underline{{\tt DSLLD}} {\tt LMAGGILWFTHLSMKSINVYKYPIGKLRVQPVGIIIFAAVMATLGFQVFIQAVEKLVVNECTORS and {\tt DSLLD} {\tt DSLL$
	:::*******************************
<u></u> В	251 287
BrMTP8.3	VRAYAKDHHEDVVTNVI.GLTSAVI.GNAFYWWTDPAG
AtMTP8	VRAYAKDHHEDVYTNVLGLIVAAVLANAFYWWLDPTG

В	251	287
BrMTP8.3	VRAYAKDHHFDVVTNVLGLISAVLGNAFYWW	IDPAG
AtMTP8	VRAYAK <mark>DHHFD</mark> VVTNVLGLVAAVLANAFYWW	LDPTG
BrMTP8.1	VRAYAK <mark>DHYFD</mark> VVTNVLGLVAAVLGNAFYWW	IDPAG
BrMTP8.2	VRAYAK <mark>DHYFD</mark> VVTNVLGLVAAVLGNAYYWW	IDPSG
BdMTP8	VRAYAK <mark>DHYFD</mark> VITNVVGLVAAVLGDKFFWW	IDPAG
HvMTP8.2	VRAYAK <mark>DHYFD</mark> VITNVVGLVAAVLGDRFLWW	IDPAG
TaMTP8-6A	VRAYAK <mark>DHYFD</mark> VITNVVGLVAAVLGDRFLWW	IDPAG
OsMTP8	VQAYAK <u>DHYFD</u> VVTNVVGLVAAVLGDKFFWW	IDPVG
TaMTP8-6D	VRAYAK <mark>DHYFD</mark> VITNVVGLVAAVLGDRFLWW	IDPAG
SbMTP8	VRAYAK <u>DHYFD</u> VITNVVGLVAAVLGDKFLWW	IDPVG
ZmMTP8	VRAYAK <u>DHYFD</u> VITNVVGLVAAVLGDKFLWW	IDPAG
PtMTP8.1	VRAYAK <u>DHYFD</u> VVTNVVGLVAAVLGDKYYWW	IDPAG
PtMTP8.3	VRAYAK <u>DHYFD</u> VVTNVVGLVAAVLGDKYYWW	IDPTG
CsMTP8	VRAYAK <u>DHYFD</u> VVTNVVGLVAAILGDKIFWW	IDPVG
PtMTP8.2	VRAYAK <u>DHYFD</u> VVTNIVGLIAAVLGNKFYWW	MDPTG
TaMTP8.1-4B	VRAYAK <u>DHYFD</u> VVTNVVGLAAAVLGDMFYWW	IDPVG
HvMTP8.1	VRAYAK <u>DHYFD</u> VVTNVVGLAAAVLGDMFYWW	IDPVG
TaMTP8.1-4A	VRAYAK <u>DHYFD</u> VVTNVVGLAAAVLGDMFYWW	IDPVG
TaMTP8.1-4D	VRAYAK <u>DHYFD</u> VVTNVVGLAAAVLGDMFYWW	IDPVG
OsMTP8.1	VRAYAK <u>DHYFD</u> VVTNVVGLAAAVLGDMFYWW	IDPVG
SbMTP8.1	VRAYAK <u>DHYFD</u> VVTNVVGLAAAVLGDRFYWW	IDPIG
ZmMTP8.1	VRAYAK <u>DHYFD</u> VVTNVVGLAAAVLGDRFYWW	IDPIG
	*:*************	:** *

Figure 3.7 Conservation of CDF signature sequence and DxxxD motifs in putative Mn-MTPs.

Alignment of putative Mn-MTPs from a range of plant species, performed using Clustal Omega. A) Red, CDF signature sequence proposed by Montanini, et al. (2007). Dark red underlined, DxxxD motifs typically found on transmembrane domains two (A) and five (B). Green numbers mark position in amino acid sequence of At MTP8. (*), positions with a single, fully conserved value. (:), conservation between amino acids of strongly similar properties. (.), conservation between amino acids of weakly similar properties.

homeologues on each chromosome were able to be predicted for most, although not all proteins. This is presumed due to incomplete sequencing on that particular chromosome but could also be that this homeologue does not exist in that particular *Triticum aestivum* genome. As with rice, no homologous protein to At MTP10 was identified in wheat.

Some key details regarding the phylogenetic tree in Figure 3.6 are the differences between monocots and dicots. The dicots, such as Arabidopsis and *Brassica rapa*, have a single clade of MTP8s, although it appears *Brassica rapa* has more than one potential duplicate within this clade. In addition to the MTP8 clade, the monocots, including barley, rice, sorghum and wheat, possess a second clade, carrying MTP8.1 proteins. The same is true for MTP11; while the dicots possess only one MTP11, most monocots possess a second MTP11.1 clade, although no MTP11.1 was identified for barley. Additionally, while Arabidopsis and *Brassica rapa* possess both MTP9 and MTP10 proteins, only MTP9 has been identified in most monocot species. These differences appear to have evolved since the monocot/dicot split; this is particularly interesting for At MTP9 and MTP10, which are hypothesised to share a functional redundancy due to a duplication event. All homologous putative Mn-MTPs identified in this analysis possess both the CDF signature sequence and the DxxxD domains; this is shown for MTP8 and MTP8.1 proteins in the alignment of Figure 3.7.

3.2.3 Isolating T-DNA insertion mutants for At MTP8-11

The T-DNA insertion sites for *mtp11-1* and *mtp11-3* were previously confirmed to be in the second exon (Peiter, et al., 2007). Here, the insertion sites were confirmed for *mtp9-1*, in the first intron, *mtp10-1*, in the second exon, and *mtp10-2*, which falls in the 3' UTR, 50 bases after the stop codon. Although *mtp10-2* was initially included in phenotypic analysis, this was discontinued after confirming its insertion after the stop codon; insertions in the 3' untranslated region (UTR) are less likely to have affect transcript or protein expression than those in exons (Wang, 2008). Towards the end of this thesis work, *mtp8-1* and *mtp8-2* were shown to feature insertions in the first and sixth exons, respectively (Eroglu, et al., 2016); these mutants were independently isolated in this study and their insertion positions were confirmed in this analysis. The insertion sites for each *mtp* mutant are presented in Figure 3.8. Homozygous mutants were isolated and confirmed by PCR at the genomic level before confirmation at the RNA level, using cDNA as a template. Further to isolating single mutants, double mutants were generated for *mtp8-2 mtp10-1*, isolated at the F2 generation, and *mtp8-2 mtp11-1*, isolated at the F3 generation. Figure 3.9 shows confirmation of these mutants at the mRNA level. Another double mutant, *mtp10-1 mtp11-1*, was provided for comparison. Further, a triple mutant was generated and provided for

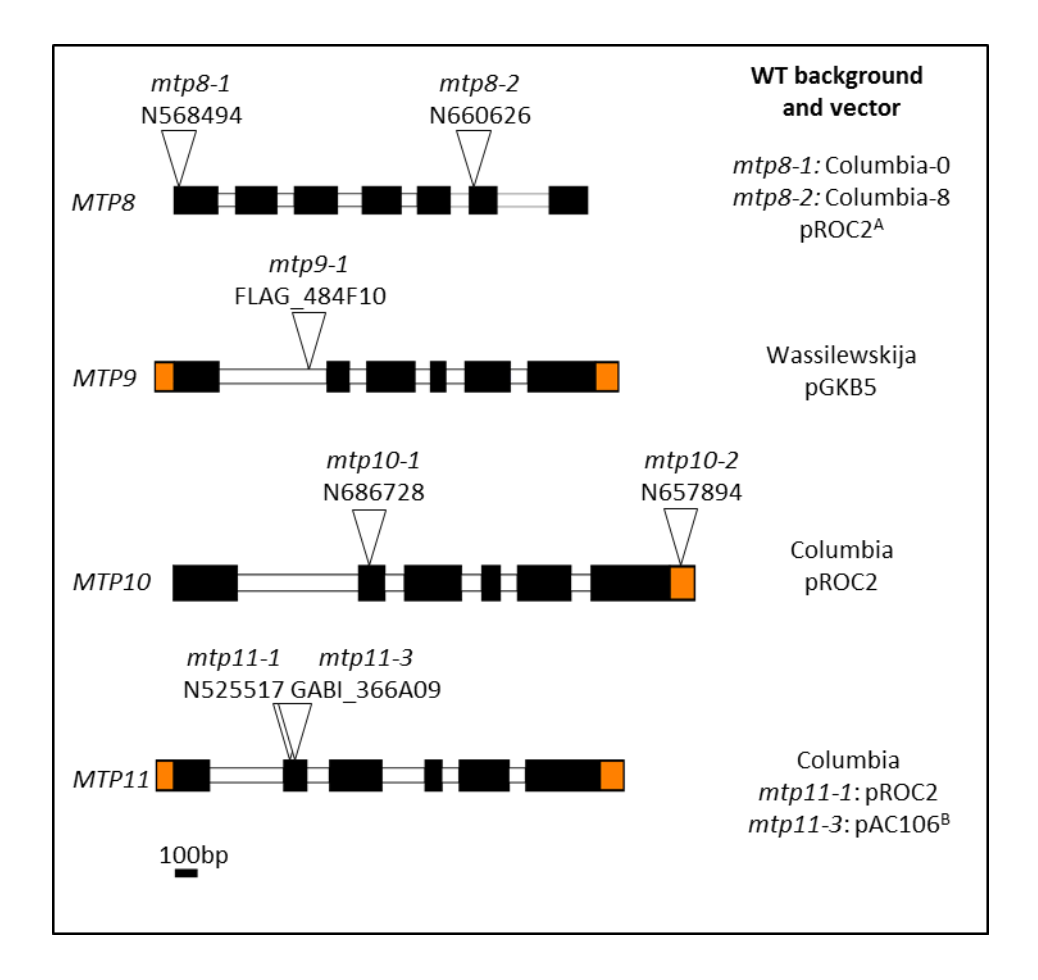


Figure 3.8. Insertion sites for T-DNA mutants for At MTP8 – MTP11, confirmed by sequencing.

Positions are labelled on genomic schematic for each gene. Black box, exon; white box, intron; orange box, 5' and 3' untranslated regions, obtained from TAIR. Arrow, insertion site for *mtp* mutant confirmed by sequencing. Information on right lists the wild type (WT) background and inserted T-DNA vector for each mutant. A Described Eroglu, et al. (2016). B Described Peiter, et al. (2007). All mutants were isolated independently as part of this thesis work.

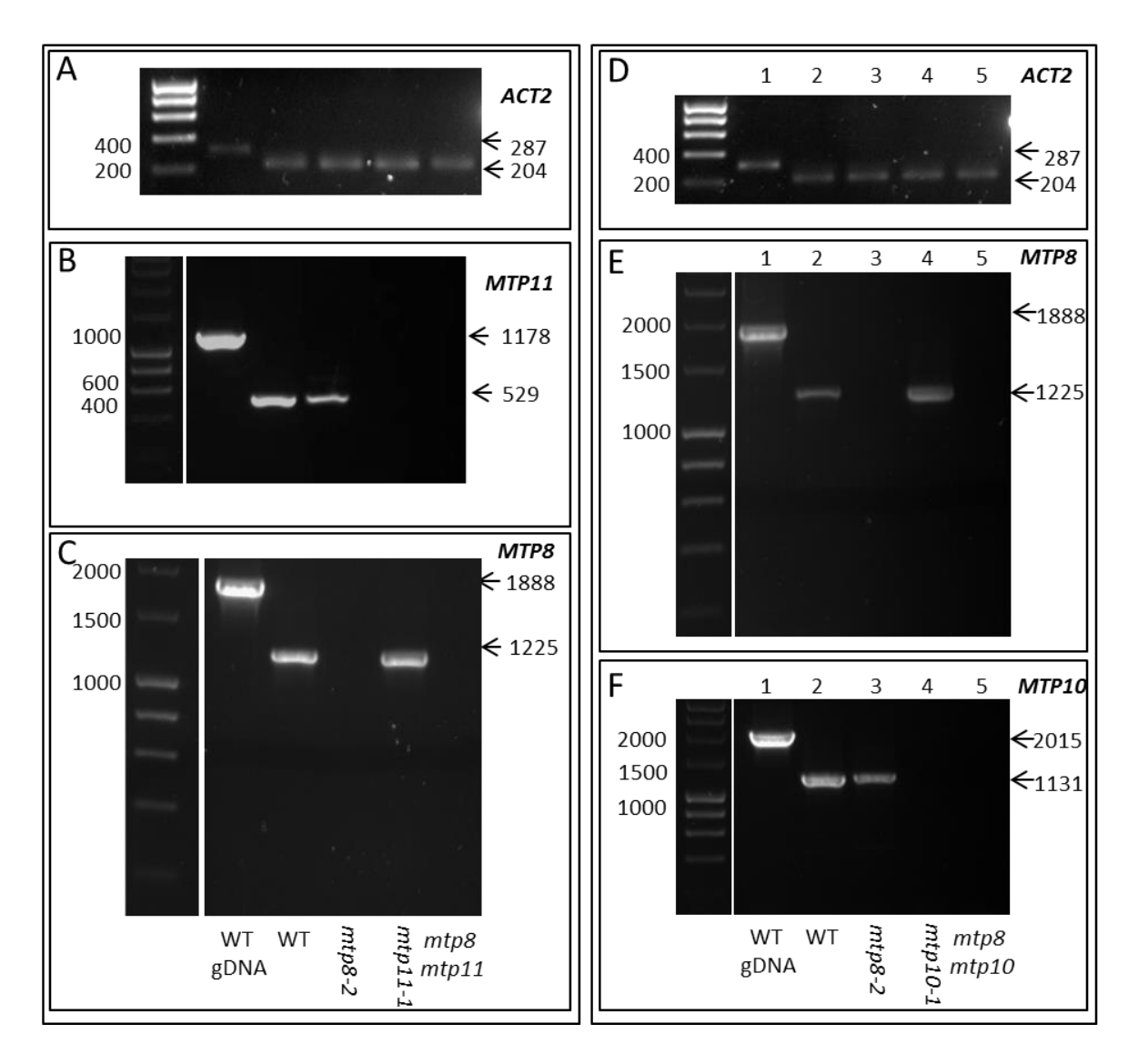


Figure 3.9. Confirmation of mtp8-2 mtp11-1 and mtp8-2 mtp10-1 double mutants at RNA level.

A-C) Confirmation of *mtp8-2 mtp11-1*; D-F) confirmation of *mtp8-2 mtp10-1*. A + D) *ACTIN2* primers amplify products of 287 bp from gDNA and 204 bp from cDNA indicating all cDNA samples are of good quality with no genomic contamination. C + E) *MTP8* primers amplify products of 1888 bp from gDNA and 1225 bp from cDNA; no product can be amplified from *mtp8*, *mtp8 mtp11* or *mtp8 mtp10* cDNA indicating no transcript is produced. B) *MTP11* primers amplify products of 1178 bp from gDNA and 529 bp from cDNA; no product can be amplified from *mtp11* or *mtp8 mtp11* cDNA indicating no transcript is produced. F) *MTP10* primers amplify products of 2015 bp from gDNA and 1131 bp from cDNA; no product can be amplified from *mtp10* or *mtp8 mtp10* cDNA indicating no transcript is produced. Sizes of molecular weight marker on left; predicted sizes of amplified fragments listed on right.

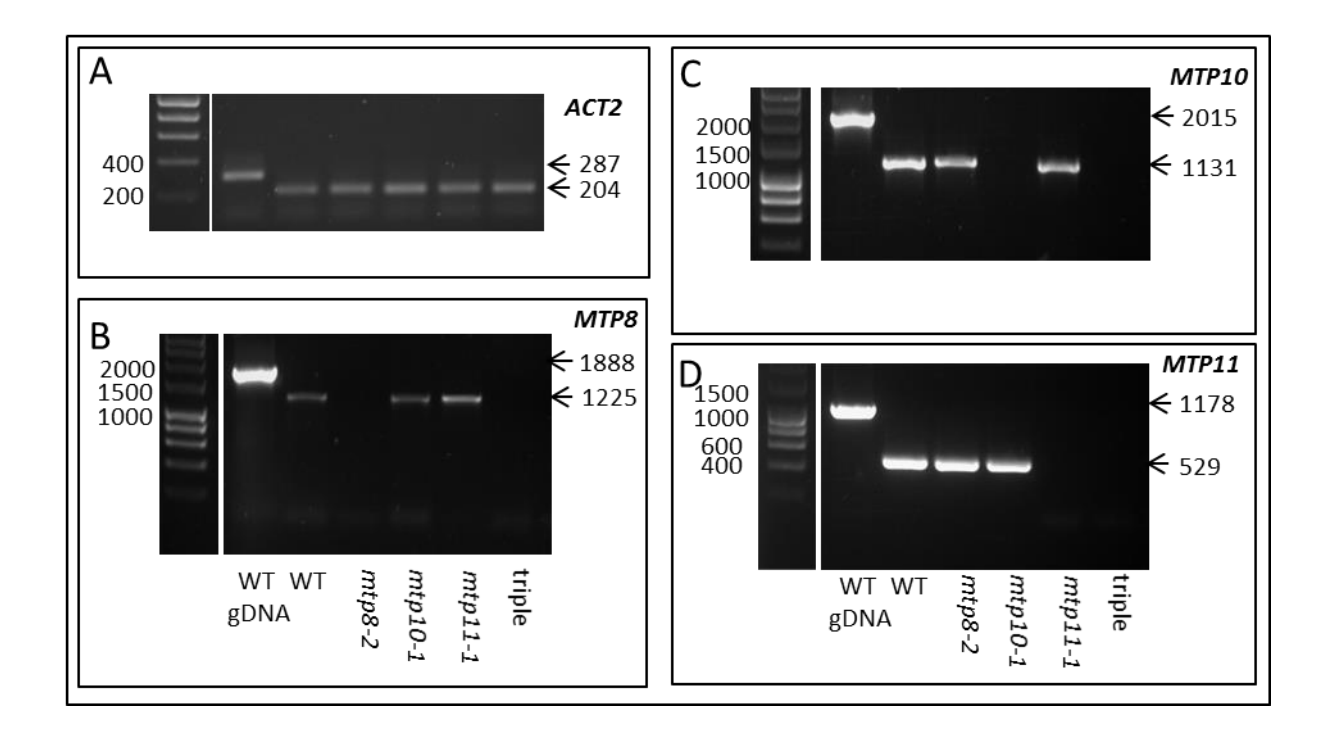


Figure 3.10. Confirmation of *mtp8-2 mtp10-1 mtp11-1* triple mutant at RNA level.

Templates used in PCR: Columbia wild type (WT) gDNA, WT cDNA, cDNA from *mtp8-2*, *mtp10-1* and *mtp11-1* cDNA, and cDNA from *mtp8-2 mtp10-1 mtp11-1* triple mutant (triple). A) *ACTIN2* primers amplify products of 287 bp from gDNA and 204 bp from cDNA indicating all cDNA samples are of good quality with no genomic contamination. B) *MTP8* primers amplify products of 1888 bp from gDNA and 1225 bp from cDNA; no product can be amplified from *mtp8* or triple mutant cDNA indicating no transcript is produced. C) *MTP10* primers amplify products of 2015 bp from gDNA and 1131 bp from cDNA; no product can be amplified from *mtp10* or triple mutant cDNA indicating no transcript is produced. D) *MTP11* primers amplify products of 1178 bp from gDNA and 529 bp from cDNA; no product can be amplified from *mtp11* or triple mutant cDNA indicating no transcript is produced. Sizes of molecular weight marker on left; predicted sizes of amplified fragments listed on right.

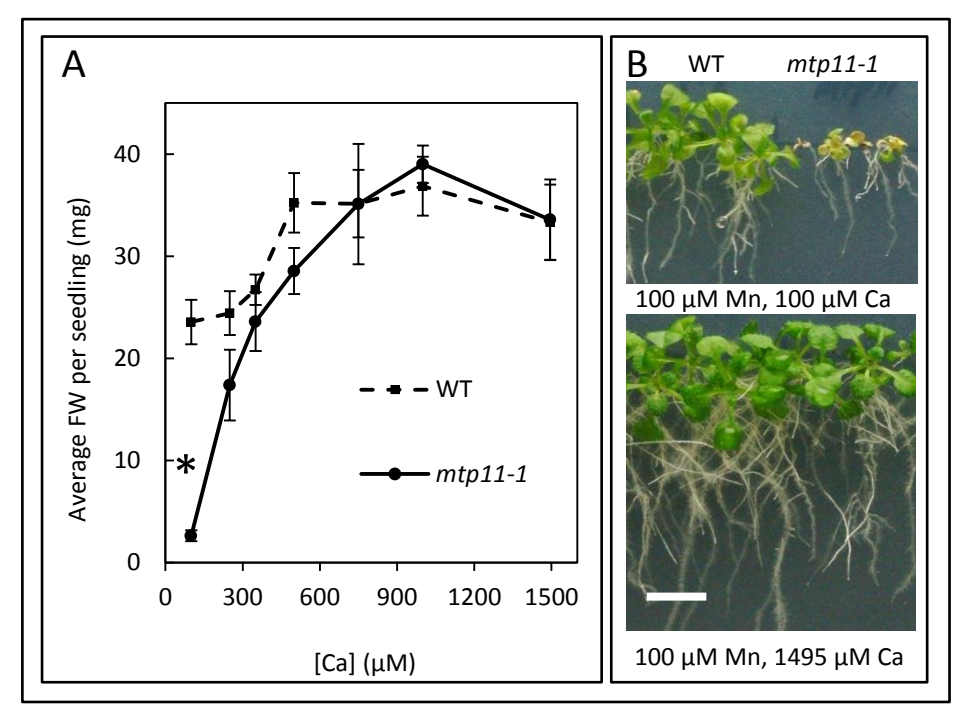
this project by crossing *mtp8-2 mtp11-1* with *mtp8-2 mtp10-1*; Figure 3.10 shows confirmation of the *mtp8-2 mtp10-1 mtp11-1* triple mutant at the RNA level, performed as part of this thesis.

3.2.4 MTP8 and MTP11 are essential for alleviating Mn toxicity in Arabidopsis

Having isolated double and triple mutants, the next step was to determine whether they exhibit different sensitivities to Mn extremes. The concentrations of Mn and Ca in basal ½ MS are 50 μ M Mn and 1.495 mM Ca. Mn-sensitivity above 500 μ M Mn has previously been demonstrated for *mtp11-1* and *mtp11-3*, when grown on ½ MS media containing Ca supplied at basal levels (Delhaize, et al., 2007). To determine if there was any antagonism between Mn and Ca that would affect the Mn-dependent phenotype of *mtp11-1*, it was compared to WT growth on 100 μ M Mn, across a range of Ca concentrations, from 1495 μ M Ca to 100 μ M Ca. As shown in Figure 3.11A, 100 μ M Mn is not inhibitory to either genotype upwards of 750 μ M Ca, but both genotypes begin to show reduced fresh weight (FW) values below 350 μ M Ca. The *mtp11-1* mutant is significantly stunted compared to WT at 100 μ M Ca; therefore, when comparing Ca conditions throughout this chapter, 'low Ca' and 'basal Ca' will be taken as 100 μ M and 1495 μ M Ca, respectively. As confirmed in Figure 3.11C, *mtp11-3* is also sensitive to elevated Mn under low Ca conditions.

Of the two mtp8 insertion mutants independently isolated in this project, the majority of experiments in this chapter will utilise mtp8-2. Eroglu, et al. (2016) reported a Mn-sensitive phenotype for mtp8-2 on basal Ca, above 1 mM Mn. Here, the mtp8-2 phenotype is shown to be sensitive compared to the WT at 600 and 750 μ M Mn under basal Ca conditions (Figure 3.12 A+B). The low Ca regime also appears to impact the growth of both mtp8 mutants, initiating Mn sensitivity at lower Mn concentrations: both mtp8-1 and mtp8-2 are significantly stunted compared to WT at 200 μ M Mn (Figure 3.12C+D).

An aim of this project was to directly compare the Mn-dependent phenotypes of the mtp mutants, to determine the relative importance of the Mn-MTPs in Mn homeostasis. As such, mtp8-2 and mtp11-1 were compared on ½ MS agarose plates, supplemented with varying Mn concentrations. Similar growth is observed between all genotypes on the control 50 μ M Mn plates, under both basal and low Ca regimes. Under low Ca, mtp11-1 becomes sensitive at lower concentrations of Mn than mtp8-2, with stunted FW at 100 μ M Mn, while mtp8-2 shows an intermediate phenotype, becoming sensitive compared to WT at 200 μ M Mn. The same pattern is seen under basal Ca, with significant inhibition of mtp11-1 at 350 μ M Mn, while the intermediate stunting of mtp8-2 comes into effect at 600 μ M Mn. This is shown in a representative experiment in Figure 3.13.



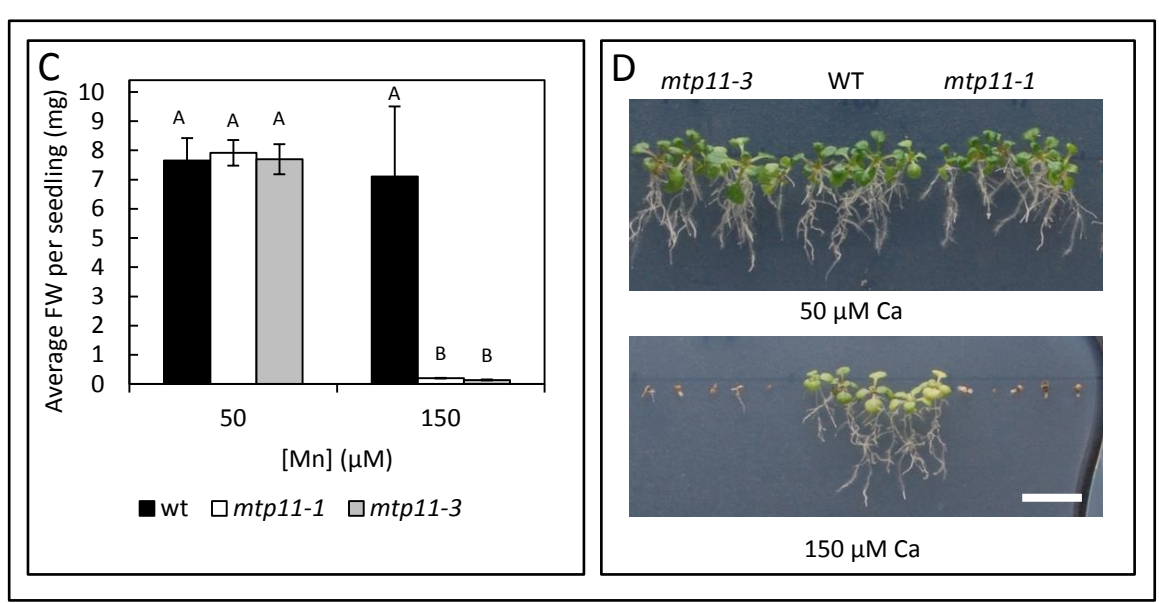


Figure 3.11. The Mn-dependent phenotype of *mtp11* can be induced at lower Mn concentrations when there is less Ca available in the growth media.

Growth of mtp11-1, mtp11-3 and wild type (WT; Columbia 8) when grown for A-B) 21 days across a range of CaCl₂ concentrations with Mn supplied at 100 μ M Mn and C-D) 24 days at under low Ca conditions (100 μ M Ca) with a range of Mn concentrations. A + C) Fresh weight per seedling (FW; mg); data shows mean FW \pm SE for 4 to 6 plates per condition, with 4 seedlings per genotype per plate. A) According to GLM, there is a significant effect of genotype (F_(1,67) = 45.02; p<0.001), [Ca] (F_(6,62) = 44.26; p<0.001) and interaction between genotype and [Ca] (F_(6,62) = 24.14, p<0.001) on FW. C) There is a significant effect of genotype (F_{2,10}= 57.96, p<0.001), [Mn] (F_{1,11}= 150.25, p<0.005) and interaction of genotype and [Mn] (F_{2,10}= 82.30, p<0.001) on fresh weight. A) *, significantly smaller than WT; C) means not sharing a letter at a particular condition are significantly different, as determined by Tukey post hoc test. B and C) Representative images showing growth at different conditions. Data for A was provided by Dr. L.E. Williams and the analysis was carried out as part of this thesis.

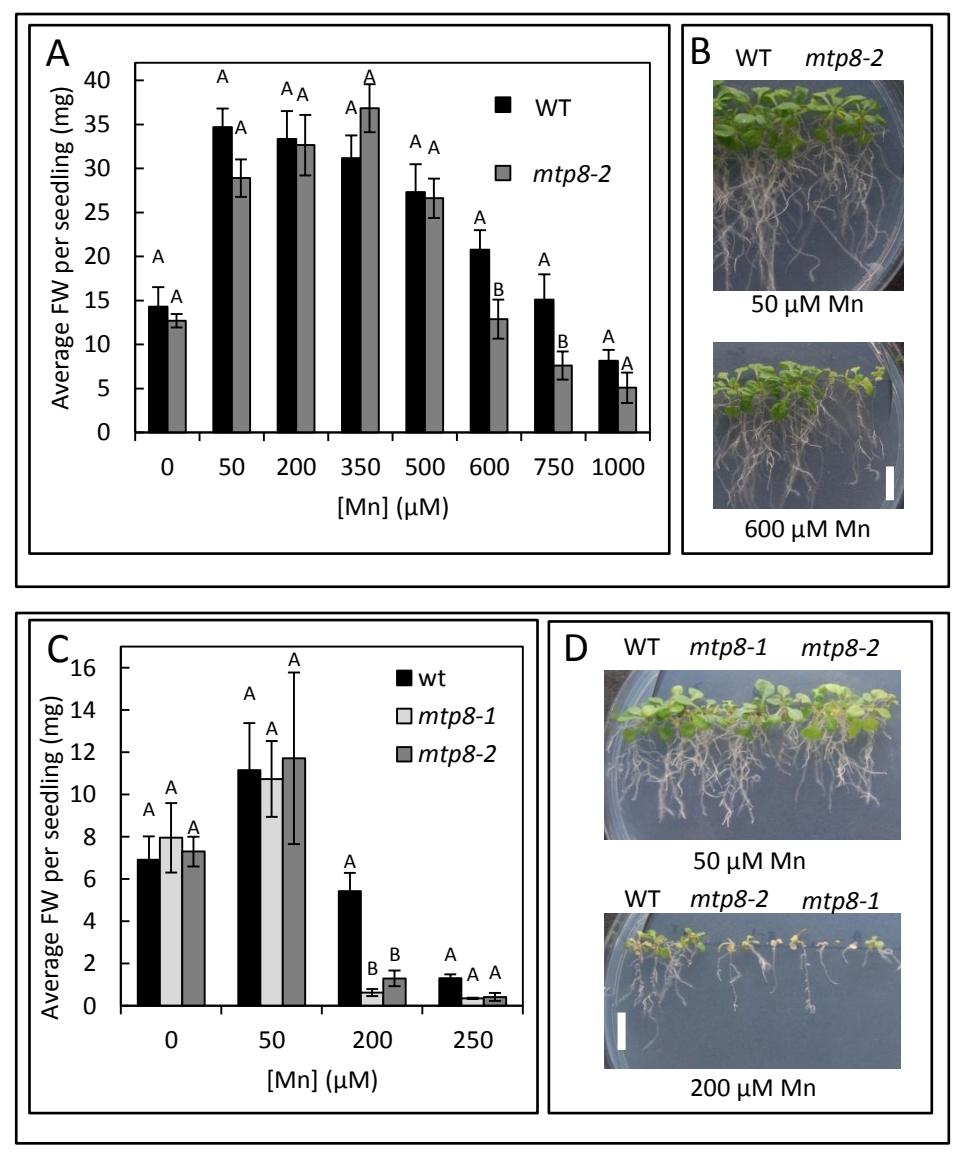


Figure 3.12. The mtp8 mutants are sensitive to elevated Mn under different Ca regimes.

Comparison of WT (Columbia 8) and mtp8-2, and mtp8-1 (in C, D), when grown on ½ MS containing A-B) 1495 μ M Ca (basal Ca) for 21 days and C-D) 100 μ M Ca (low Ca) for 24 days, across a range of Mn concentrations supplied as MnSO₄. A + C) Results show mean fresh weight (FW; mg) per seedling calculated for 4 to 6 plates (\pm SE) with four seedlings per genotype, per plate; results are representative of 2 independent experiments. A) As determined by 2-way ANOVA, there is a significant effect of genotype (F_{1,37} = 32.09., p<0.005), [Mn] (F_{7,31}= 43.59, p<0.001) and interaction of genotype and [Mn] (F_{7,31}= 3.529, p=0.0051) on fresh weight. C) There is a significant effect of genotype (F_{2,20}= 7.674., p<0.001), [Mn] (F_{3,19}= 102.3, p<0.005) and interaction of genotype and [Mn] (F_{6,16}= 13.64, p<0.001) on fresh weight. Means which do not share a letter at a particular concentration are significantly different, according to Tukey's post-hoc test. B + D) Image displaying plant growth on different Mn concentrations. White bar = 1 cm

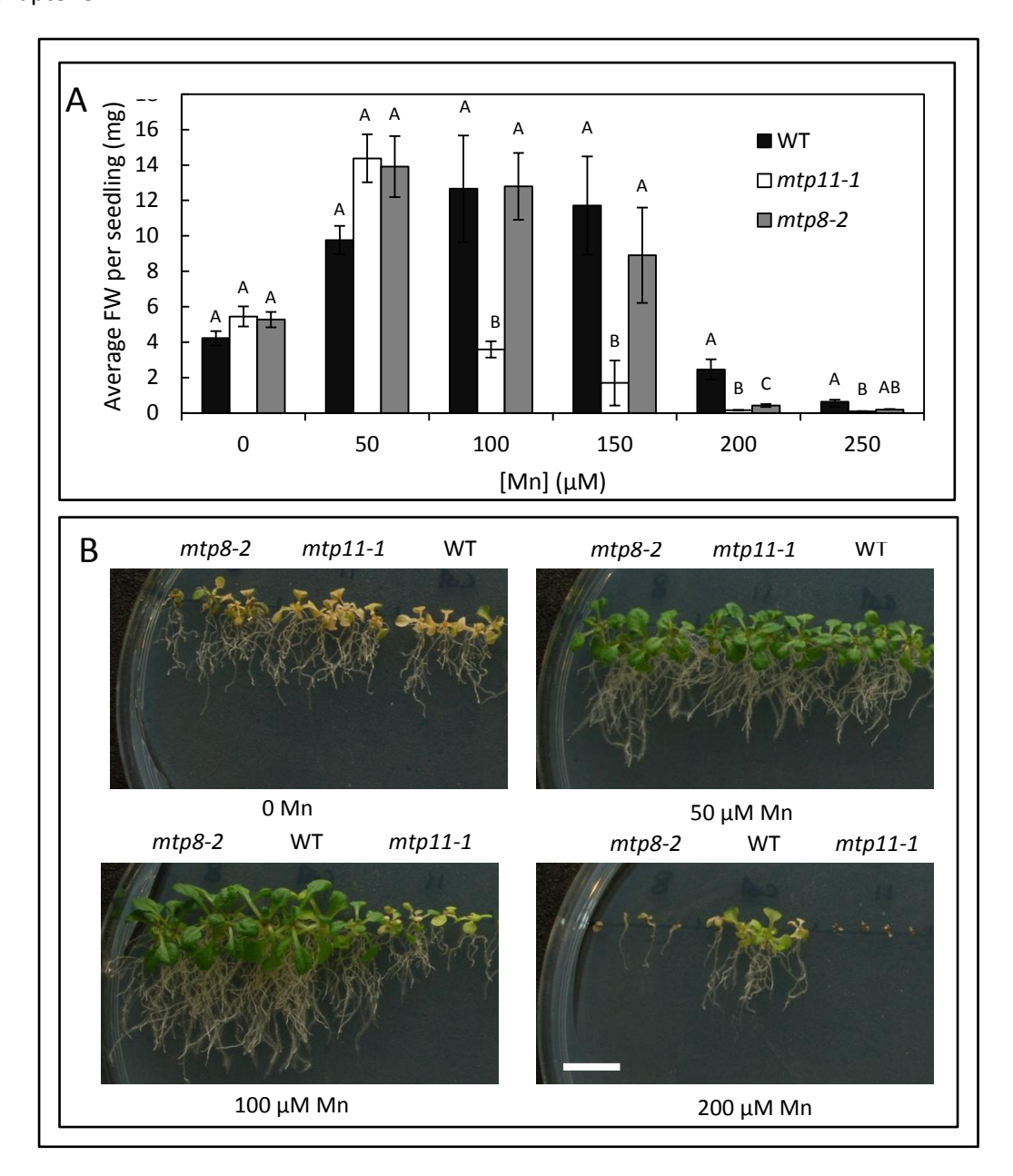


Figure 3.13. Insertion mutants for *mtp8-2* and *mtp11-1* display sensitive phenotypes to Mn under the low Ca regime.

Fresh weight per seedling of mtp8-2 and mtp11-1 mutants after 24 days growth on ½ MS containing 100 μ M Ca and a range of Mn concentrations supplied as MnSO₄. Results represent one of four independent experiments. A) Data shows mean fresh weight (FW) (mg) per seedling calculated for 6 plates (\pm SE), with four seedlings per plant line, per plate. As determined by 2-way ANOVA, there is a significant effect of genotype ($F_{2, 85}$ = 44.17, P<0.001), [Mn] ($F_{3, 84}$ = 126.39, p<0.001) and interaction of genotype and [Mn] ($F_{6, 81}$ = 9.39, p<0.001) on fresh weight; means not sharing a letter are significantly different according to Tukey post-hoc test. B) Image displaying plant growth on 0, 50, 100 and 200 μ M Mn. White bar = 1 cm

As illustrated in Figures 3.16 and 3.17, *mtp10-1* does not display a Mn-dependent phenotype under either Ca regime.

The double mutants generated in this project provide further opportunity for determining the relative importance of Mn-MTPs. Of the 3 double mutants isolated, mtp8-2 mtp11-1 displays the most striking additive phenotype; this is shown under low Ca in Figure 3.14 and basal Ca in Figure 3.15. Interestingly, mtp8-2 mtp11-1 performs better than the other genotypes under Mn deficiency, but becomes hypersensitive to Mn at much lower concentrations than both mtp8-2 and mtp11-1; under low Ca, this is apparent at 50 μM Mn, the concentration generally treated as basal Mn. Germination is also impaired by excess Mn under low Ca; mtp8-2 mtp11-1 features significantly inhibited germination above 125 μM Mn (Figure 3.13B). Inhibition of germination is not observed under basal Ca, tested up to 1 mM Mn (data not shown). Meanwhile, mtp10-1 mtp11-1 gives consistently smaller FW values than mtp11-1 under elevated Mn, under both basal and low Ca, but this difference is not significant (Figure 3.16). The mtp8-2 mtp10-1 double mutant also does not display an additive sensitivity to elevated Mn compared to mtp8-2 (Figure 3.17). However, the triple mutant mtp8-2 mtp10-1 mtp11-1 displays a highly sensitive additive phenotype under both Ca regimes (Figures 3.18 and 3.19), significantly stunted compared to mtp8-2 mtp11-1 at just 10 μM Mn under low Ca. Germination is also further impaired by elevated Mn under low Ca (Figure 3.18B) but remains unaffected by basal Ca (data not shown).

Single mutants mtp8-2, mtp10-1 and mtp11-1 were grown under Fe and Zn deficiency and toxicity, to investigate the metal specificity of these transporters. Basal conditions are treated as 15 μ M Zn or 50 μ M Fe, while Mn and Ca were kept at standard basal conditions. Figure 3.20 demonstrates that neither mtp8-2, mtp10-1 nor mtp11-1 shows a Fe- or Zn-dependent phenotype, under deficiency or toxicity conditions.

Despite not showing sensitivity to Fe deficiency under these conditions, mtp8-1 and mtp8-2 have recently been reported to show stunting and chlorosis under Fe deficiency induced by high pH, implicating MTP8 as a key player in alleviating Mn/Fe antagonism (Eroglu, et al., 2016). Some key differences between the standard media used in this project and that used by Eroglu, et al. (2016) include the use of 0.5 % sucrose and 1% agar instead of 1 % sucrose and 0.8 % agarose used here; further, Eroglu, et al. (2016) employ basal concentrations of 40 μ M Mn and 100 μ M, Fe instead of 50 μ M Mn and 50 μ M Fe used in this study. The experimental set up was repeated here, referred to as the 'modified Eroglu regime', as not all conditions were listed in the original study; media was buffered to pH 5.5 and 6.7, with Fe concentrations supplied as 28 and 100 μ M FeNaEDTA. Figure 3.21 confirms the sensitivity of both mtp8-1 and mtp8-2 under low Fe in combination with high pH ('Fe 28/pH 6.7'). The mtp8-1 mutant consistently outperformed mtp8-2 and the WT on

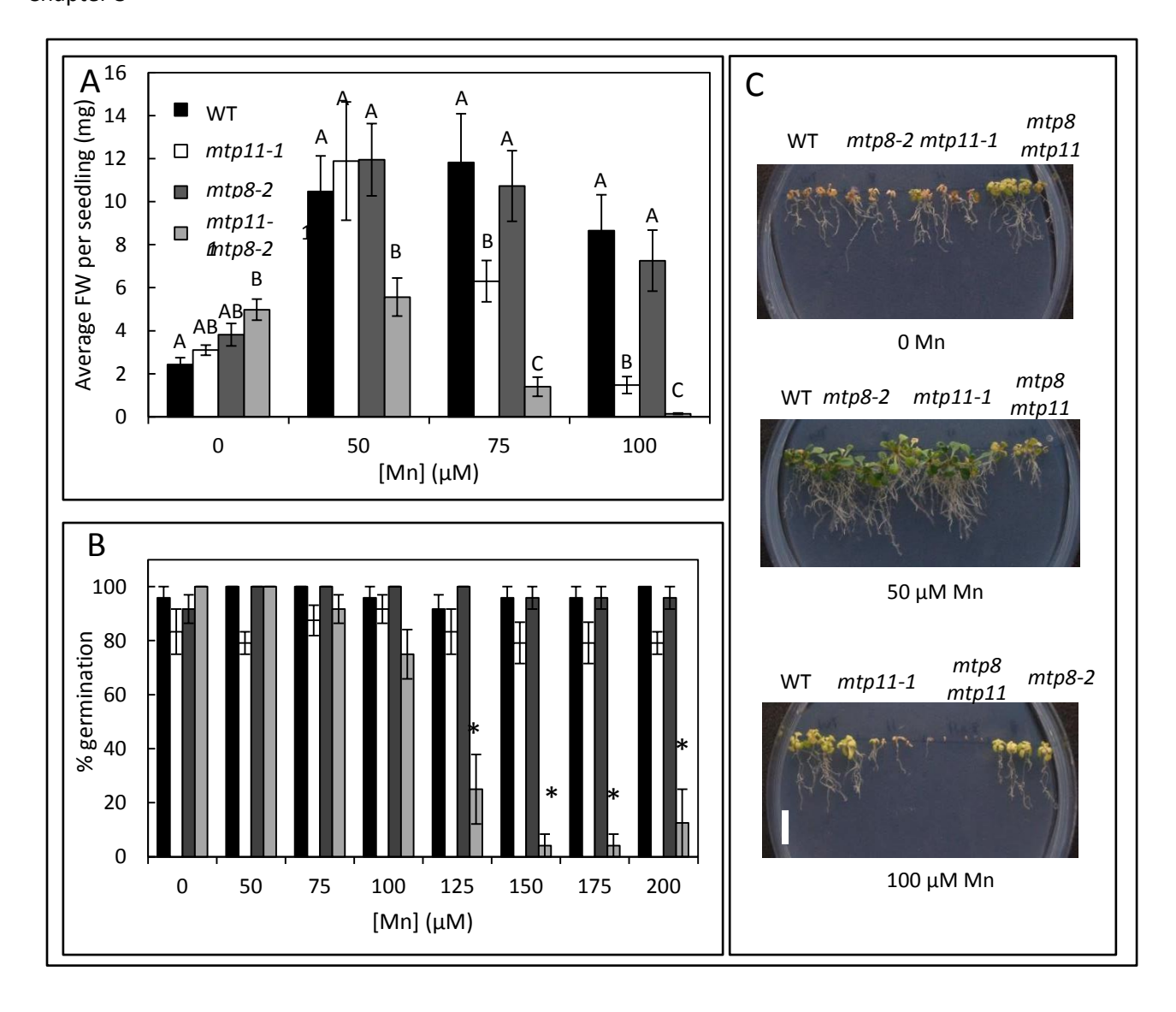
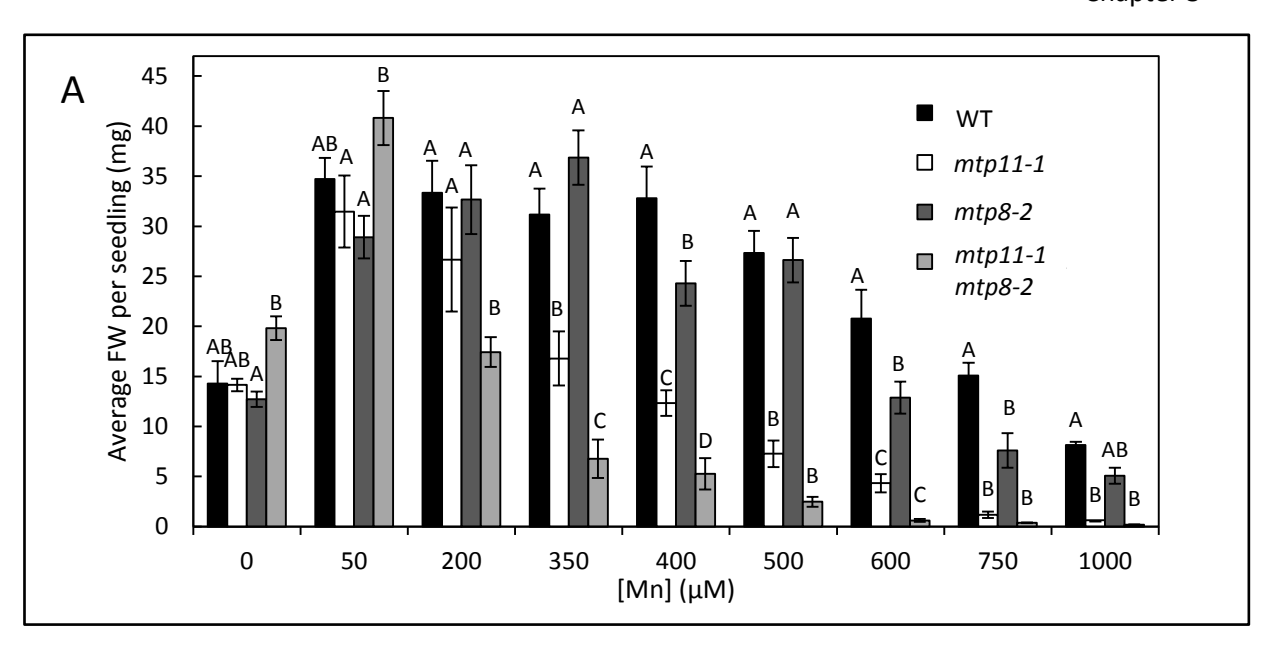


Figure 3.14. The *mtp8 mtp11* double mutant displays an additive Mn-dependent phenotype under the low Ca regime.

Fresh weight per seedling of mtp8-2, mtp11-1 and mtp8-2 mtp11-1 mutants after 24 days growth on ½ MS containing 100 μ M Ca and a range of Mn concentrations supplied as MnSO₄. Results represent one of 3 independent experiments. A) Data shows mean fresh weight (FW) (mg) per seedling calculated for 6 plates (\pm SE), with four seedlings per plant line, per plate. As determined by GLM, there is a significant effect of genotype (F_{3, 77} = 51.0, P<0.0001), [Mn] (F_{3, 77} = 11.68, p<0.0001) and interaction of genotype and [Mn] (F_{9, 71} = 16.62, p<0.0001) on fresh weight; means not sharing a letter at each individual concentration are significantly different according to Tukey post-hoc test. B) Data shows % successful germination per genotype calculated for 6 plates \pm SE. As determined by GLM, there is a significant effect of genotype (F_{3, 157} = 118.62, P<0.0001), [Mn] (F_{7, 157} = 18.69, p<0.0001) and interaction of genotype and [Mn] (F_{21, 139} = 14.96, p<0.0001) on fresh weight; means not sharing a letter at each individual concentration are significantly different according to Tukey post-hoc test. C) Image displaying plant growth on 0, 50 and 100 μ M Mn. White bar = 1 cm



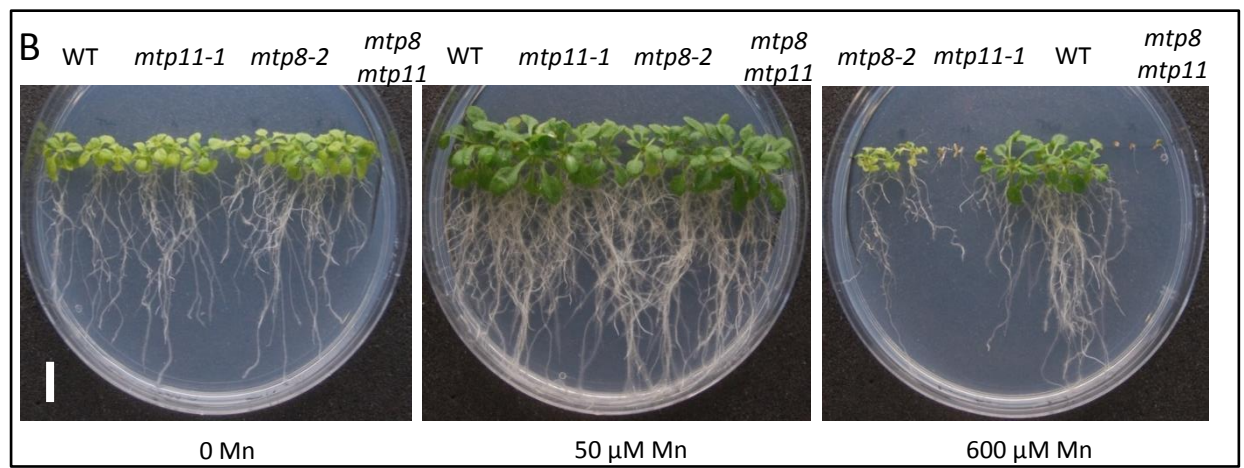
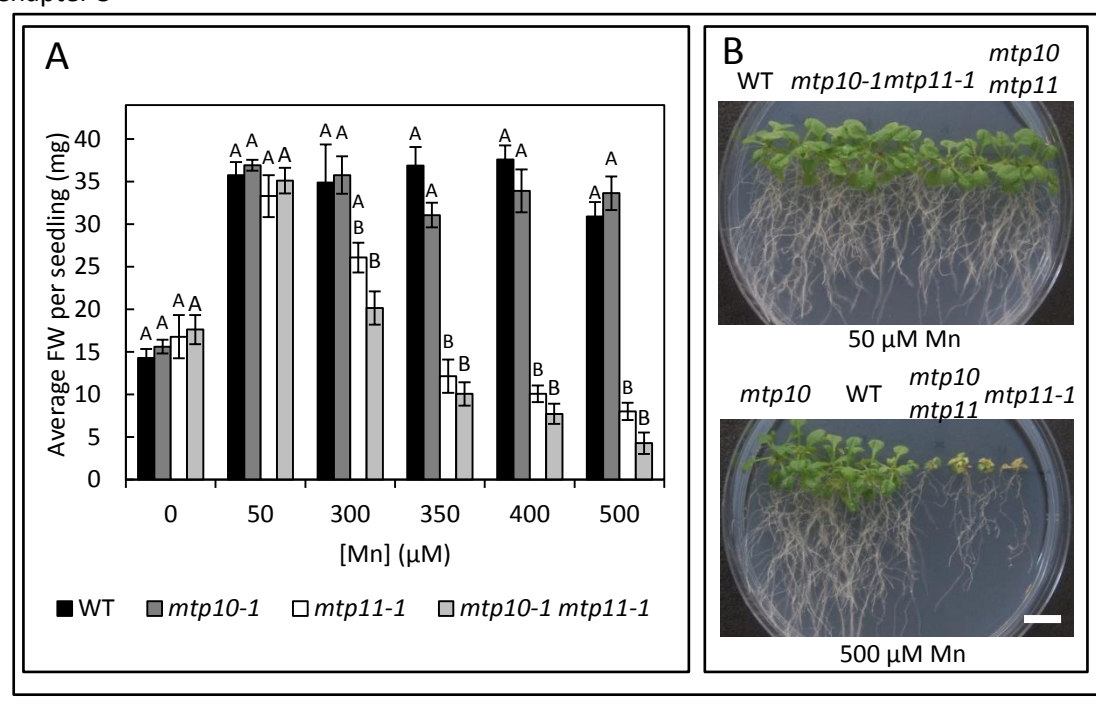


Figure 3.15. The *mtp8 mtp11* double mutant displays an additive Mn-dependent phenotype under the basal Ca regime.

Fresh weight per seedling of mtp8-2, mtp11-1 and mtp8-2 mtp11-1 mutants after 21 days growth on ½ MS containing 1.495 mM Ca and a range of Mn concentrations supplied as MnSO₄. Results represent one of 3 independent experiments. A) Data shows mean fresh weight (FW) (mg) per seedling calculated for 6 plates (\pm SE), with four seedlings per plant line, per plate. As determined by GLM, there is a significant effect of genotype (F_{3, 129} = 108.0, P<0.0001), [Mn] (F_{8,43} = 77.91, p<0.0001) and interaction of genotype and [Mn] (F_{24, 129} = 12.72, p<0.0001) on fresh weight; means not sharing a letter at each individual concentration are significantly different according to Tukey post-hoc test. B) Image displaying plant growth on 50 μ M and 250 μ M Mn. White bar = 1 cm



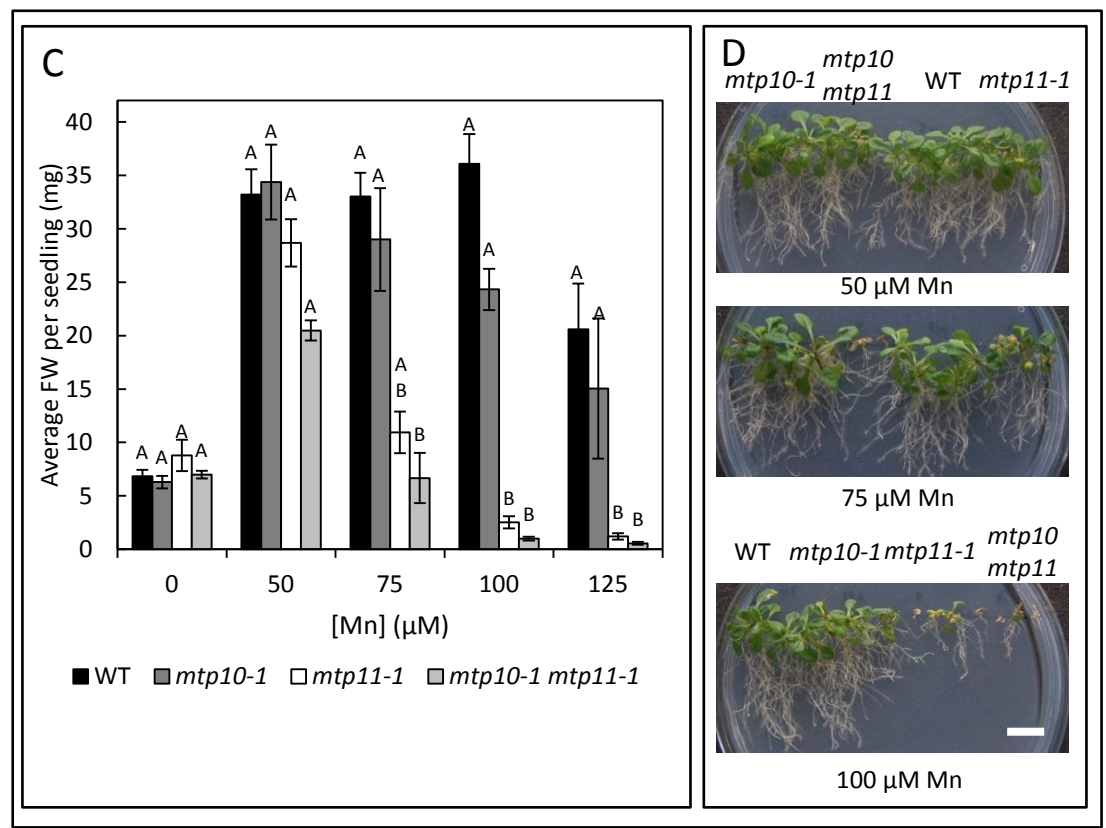


Figure 3.16. Growth pattern of the mtp10 mtp11 double mutant at elevated Mn.

Comparison of mtp10-1, mtp11-1 and mtp10-1 mtp11-1 mutants after growth on ½ MS containing A-B) 1495 μ M and C-D) 100 μ M Ca, supplemented with a range of Mn concentrations supplied as MnSO₄. A + C) Mean fresh weight (FW; mg) per seedling calculated for 6 plates (\pm SE), with 6 seedlings per genotype, per plate. A) As determined by 2-way ANOVA there is a significant effect of [Mn] (F_{5, 108} = 54.41; p<0.001), genotype (F_{3, 108} = 111.83; p<0.001) and interaction between [Mn] and genotype (F_{15, 131} = 14.72; p<0.001) on fresh weight. C) There is a significant effect of [Mn] (F_{4, 80} = 73.18; p<0.001), genotype (F_{3, 80} = 107.27; p<0.001) and interaction between [Mn] and genotype (F_{12, 99} = 19.13; p<0.001). Means not sharing a letter at a particular concentration are significantly different, according to Tukey's post-hoc test. B + D) Images displaying plant growth on a range of Mn concentrations. White bar = 1 cm.

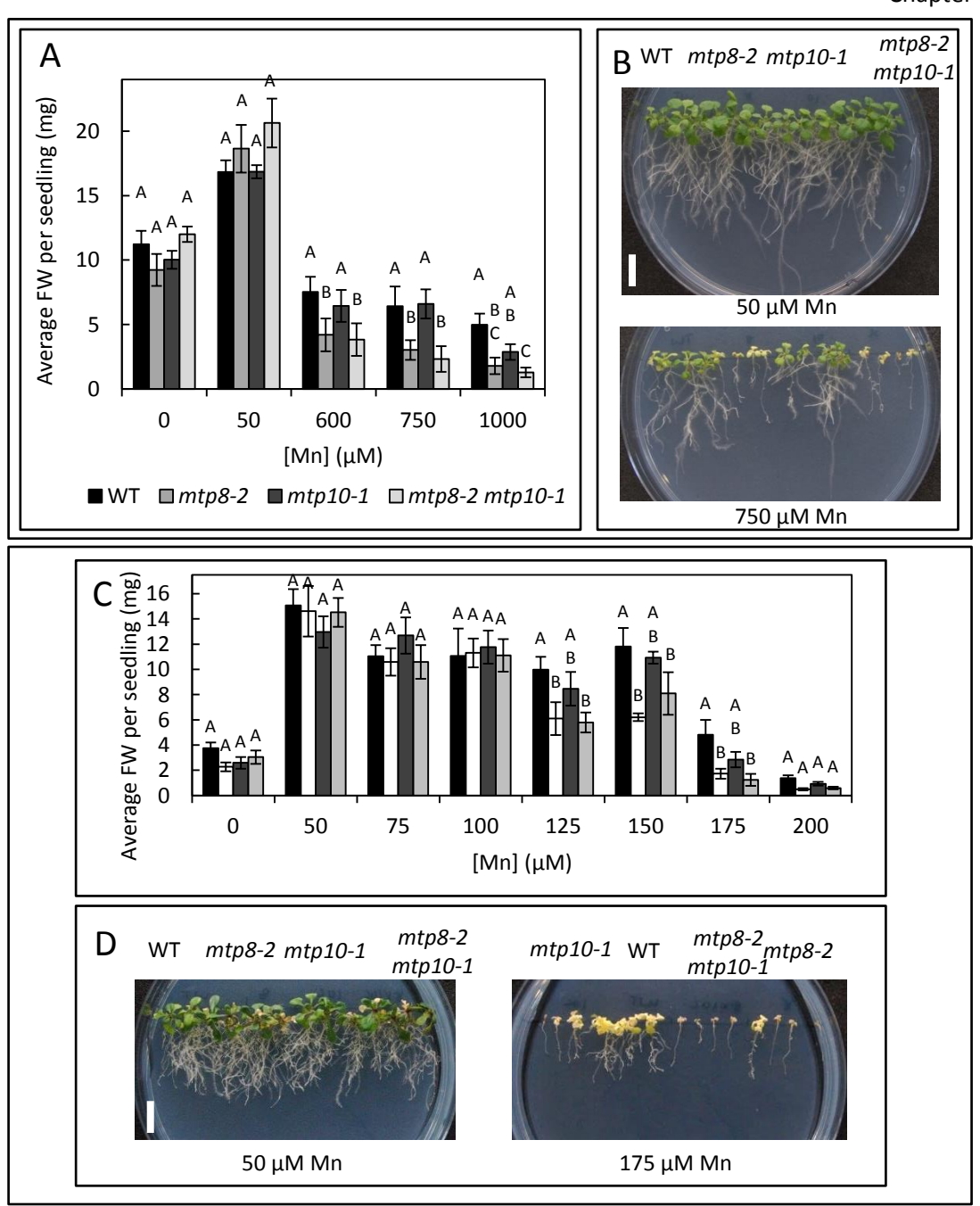


Figure 3.17. The mtp8-2 mtp10-1 double mutant does not display an additive phenotype on elevated Mn.

Comparison of mtp8-2, mtp10-1 and mtp8-2 mtp10-1 mutants after growth on ½ MS containing A-B) 1495 μ M and C-D) 100 μ M Ca, supplemented with a range of Mn concentrations supplied as MnSO₄. A + C) Mean fresh weight (FW; mg) per seedling calculated for 6 plates (\pm SE), with 6 seedlings per genotype, per plate. A) As determined by 2-way ANOVA there is a significant effect of [Mn] (F₄, 92 = 221.13; p<0.001), genotype (F₃, 92 = 32.31; p<0.001) and interaction between [Mn] and genotype (F₁₂, 111 = 8.86; p<0.001) on fresh weight. C) There is a significant effect of [Mn] (F₇, 160 = 120.75; p<0.001), genotype (F₃, 160 = 12.67; p<0.001) and interaction between [Mn] and genotype (F₂₁, 191 = 1.97; p<0.001). Means not sharing a letter at a particular concentration are significantly different, according to Tukey's post-hoc test. B + D) Images displaying plant growth on a range of Mn concentrations. White bar = 1 cm.

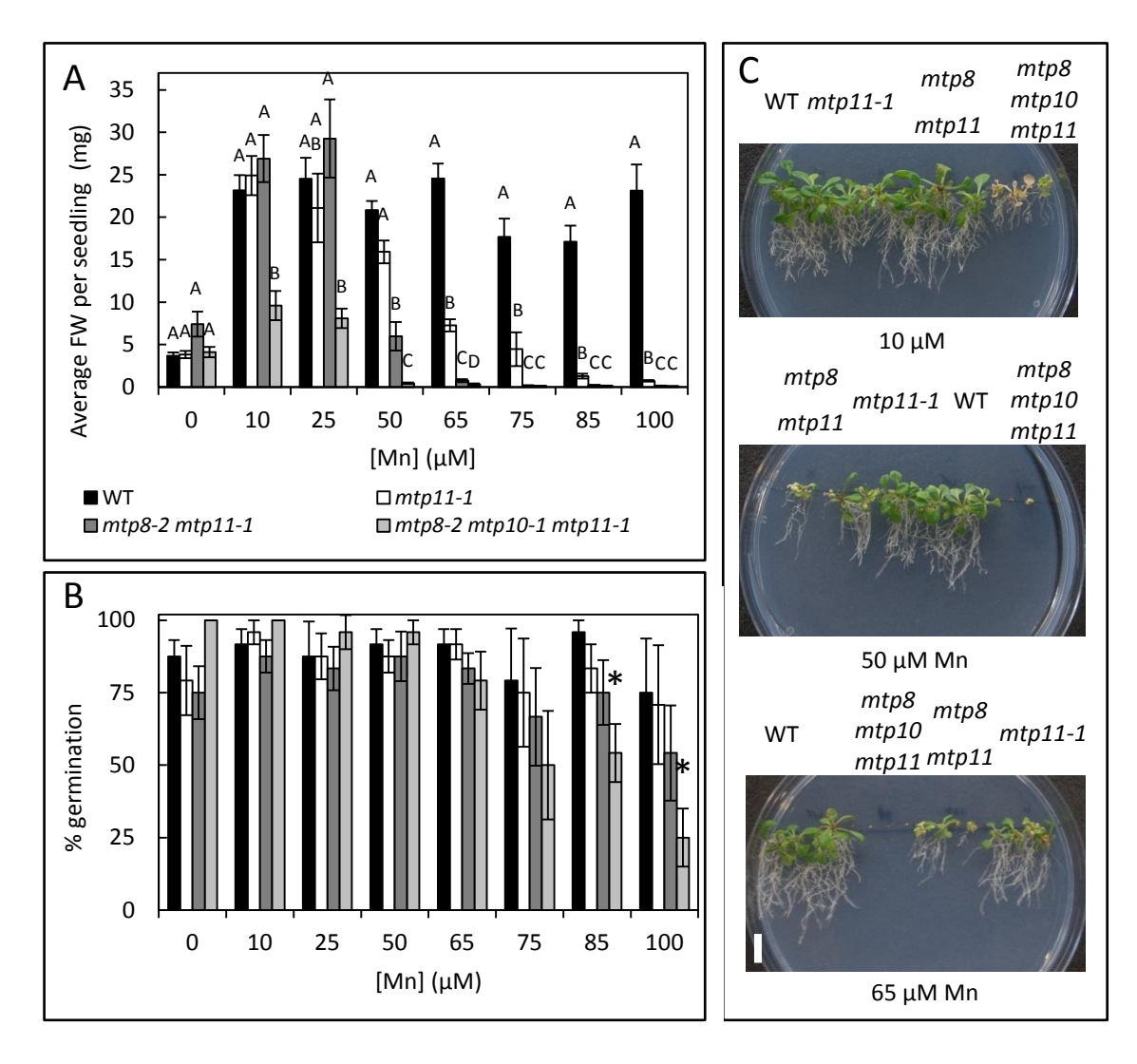


Figure 3.18. The *mtp8 mtp10 mtp11* triple mutant displays a strong additive Mn-dependent phenotype under the low Ca regime.

Comparison of mtp8-2, mtp11-1 and mtp8-2 mtp11-1 mutants after 24 days growth on ½ MS containing 100 μ M Ca and a range of Mn concentrations supplied as MnSO₄. Results represent one of 2 independent experiments. A) Data shows mean fresh weight (FW) (mg) per seedling calculated for 6 plates (\pm SE), with four seedlings per plant line, per plate. As determined by GLM, there is a significant effect of genotype (F₃, \pm 151 = 293.21, P<0.0001), [Mn] (F₇, \pm 151 = 106.88, p<0.0001) and interaction of genotype and [Mn] (F₂₁, \pm 182 = 31.84, p<0.0001) on fresh weight; means not sharing a letter at each individual concentration are significantly different according to Tukey post-hoc test. B) % germination per seedling; there is a significant effect of genotype and [Mn] on germination rates (F₂₁, \pm 183 = 2.50, p<0.001). *, significantly different to WT germination rate. C) Image displaying plant growth on 10, 50 and 65 \pm 1 MMn. White bar = 1 cm.

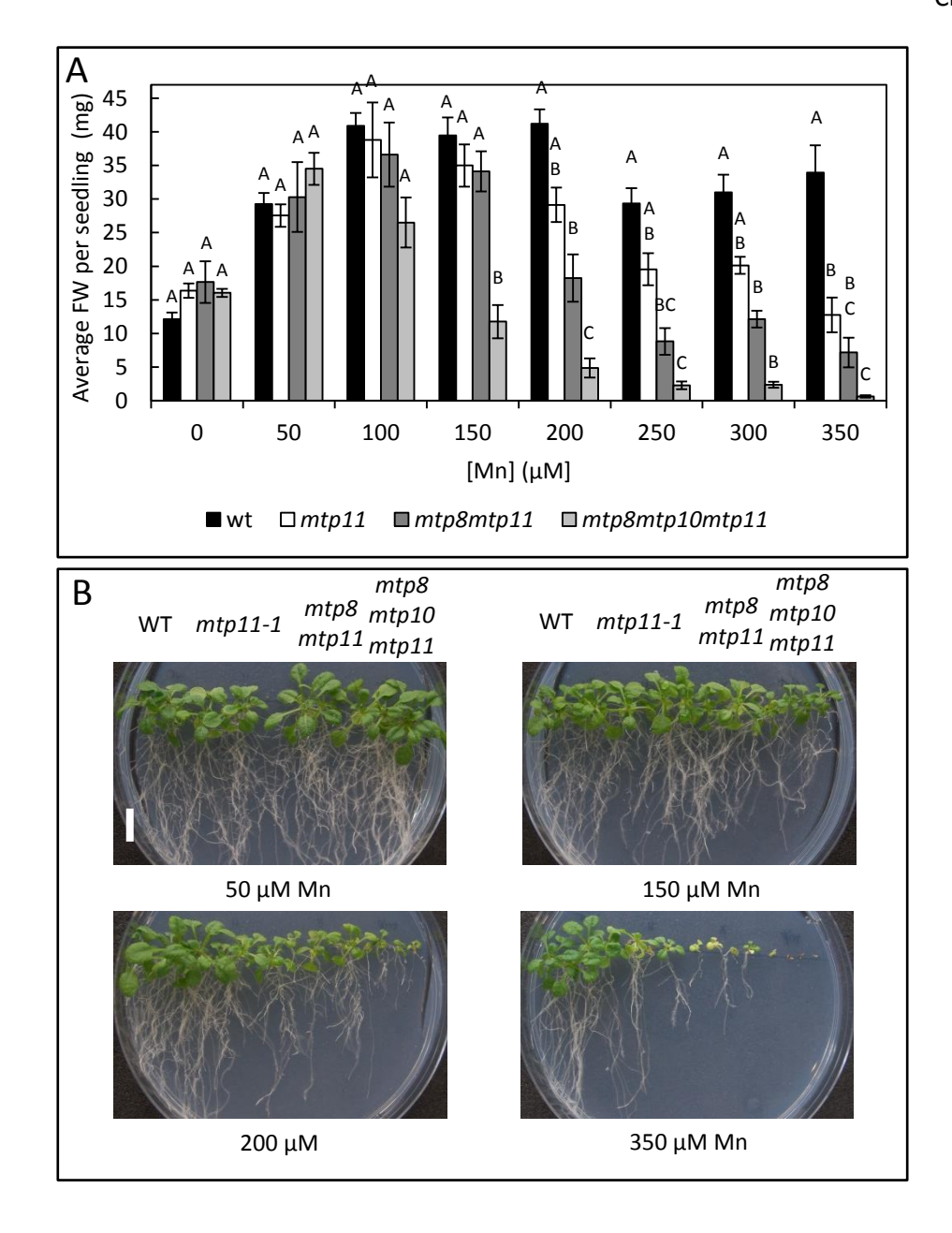


Figure 3.19. The *mtp8 mtp10 mtp11* triple mutant displays an additive Mn-dependent phenotype under the basal Ca regime.

Comparison of mtp8-2, mtp11-1 and mtp8-2 mtp11-1 mutants after 21 days growth on ½ MS containing 1495 μ M Ca and a range of Mn concentrations supplied as MnSO₄. A) Data shows mean fresh weight (FW) (mg) per seedling calculated for 6 plates (\pm SE), with four seedlings per plant line, per plate. As determined by GLM, there is a significant effect of genotype ($F_{3, 160} = 163.91$, P<0.001), [Mn] ($F_{7, 160} = 61.13$, p<0.001) and interaction of genotype and [Mn] ($F_{21, 191} = 18.43$, p<0.001) on fresh weight; means not sharing a letter at each individual concentration are significantly different according to Tukey post-hoc test. B) Image displaying plant growth on 50, 150, 200 and 350 μ M Mn. White bar = 1 cm.

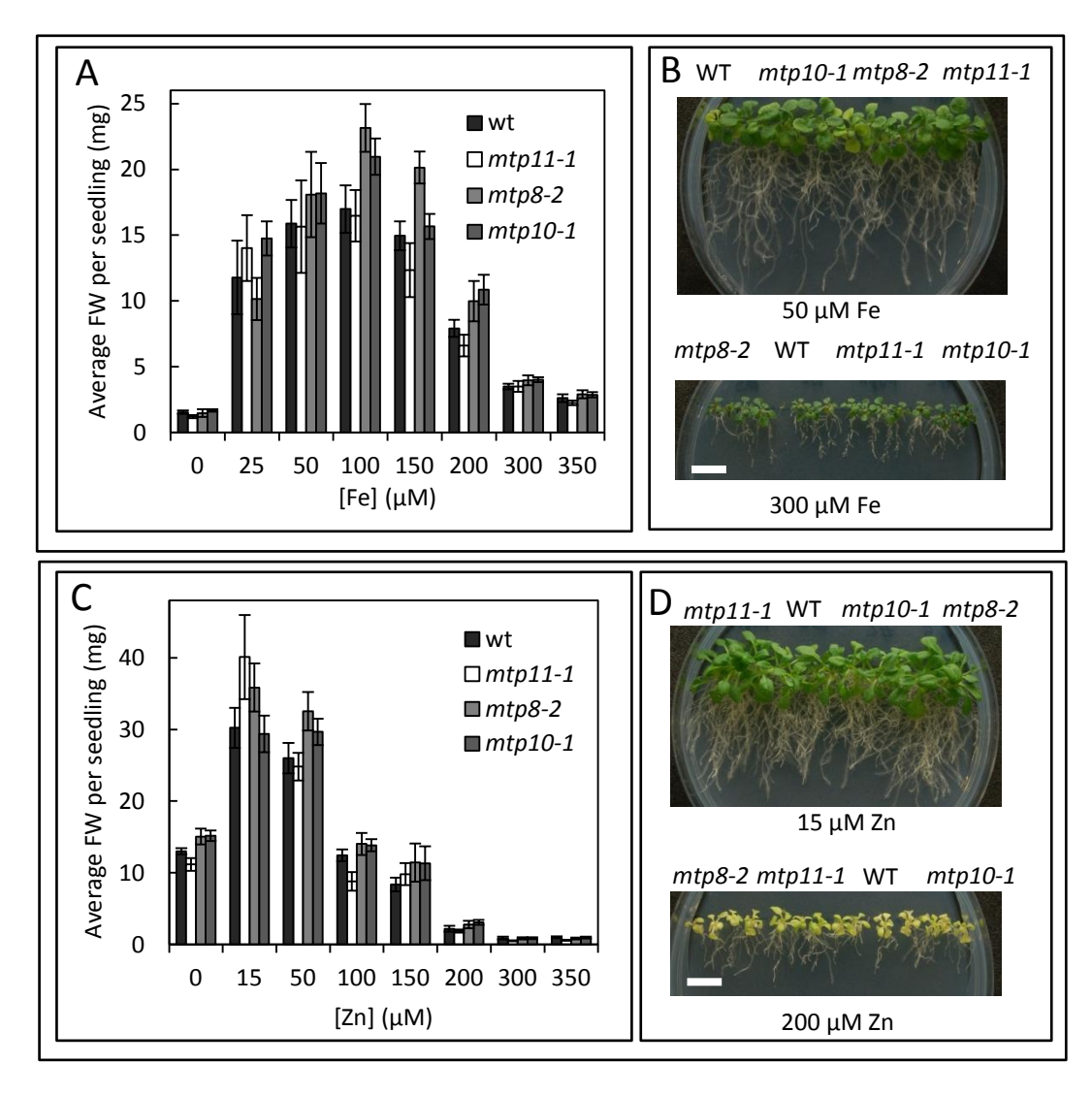


Figure 3.20. Single mutants *mtp8-2*, *mtp11-1* and *mtp10-1* do not display sensitive phenotypes under Fe or Zn extremes.

Fresh weight per seedling of mtp8-2, mtp11-1 and mtp10-2 mutants after 21 days growth on ½ MS supplemented with a range of Fe (A-B) and Zn (C-D) concentrations, supplied as FeNaEDTA and ZnSO₄, respectively. Basal concentrations are 15 μ M Zn and 50 μ M Fe. A+C) Data shows mean fresh weight (FW) (mg) per seedling calculated for 6 plates (\pm SE), with four seedlings per plant line, per plate. A) As determined by 2-way ANOVA, there is a significant effect of genotype (F_{3, 160}= 63.75, P<0.05) and [Fe] (F_{21, 191}= 17.52, p=0.224) on FW. C) There is a significant effect of interaction between genotype and [Zn] (F_{21, 191}= 0.98, p=0.5). According to Tukey post hoc test, there are no significant differences between genotypes at any single concentration. B+D) Images displaying plant growth under basal and toxic conditions. White bar = 1 cm. Data for these experiments was provided by Dr. L.E. Williams and the analysis was carried out as part of this thesis.

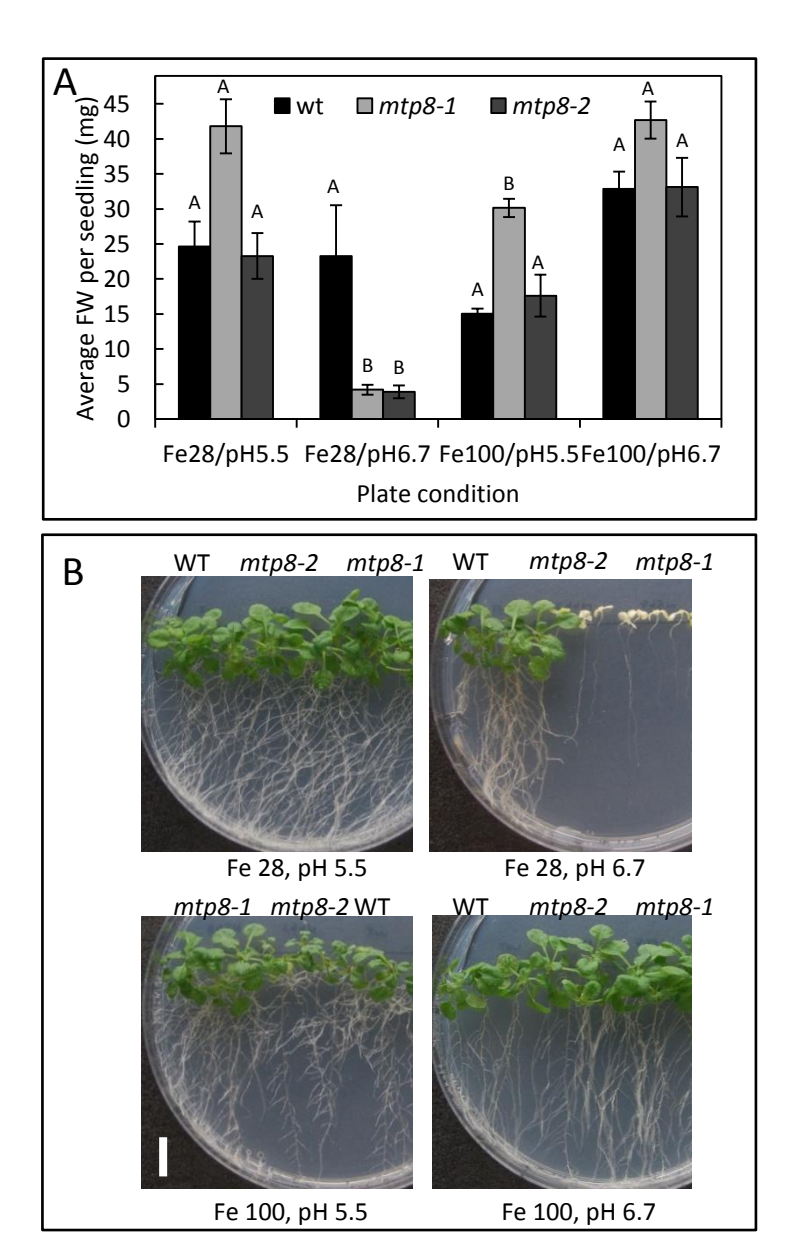


Figure 3.21. mtp8-1 and mtp8-2 are sensitive to Fe deficiency under higher pH.

Fresh weight per seedling of mtp8-1, mtp8-2 and WT after 23 days growth on ½ MS (adapted Eroglu regime) supplemented with either 28 μ M or 100 μ M Fe (Fe28 and Fe100, respectively) supplied as FeNaEDTA, and buffered to pH 5.5 or 6.7 with NaOH. A) Data shows mean fresh weight (FW) (mg) per seedling calculated for 6 plates (\pm SE), with four seedlings per plant line, per plate. As determined by MANOVA, there is an interaction effect of genotype, Fe and pH on FW (F_{3, 68} = 3.69, p<0.01). Genotypes not sharing a letter at one individual plate condition are significantly different from each other at that condition, according to Tukey post hoc test. B) (chlorophyll). C) Image displaying plant growth under all conditions. White bar = 1 cm

the other tested conditions, significantly so under Fe100/pH5.5. This could be because the true WT background for *mtp8-1* is Col0, not Col8; however, the inhibition under Fe28/pH6.7 is clear.

MTP8 was claimed to be the 'key player' in alleviating Mn/Fe antagonism (Eroglu, et al., 2016), yet the other Mn-MTPs have not been investigated directly. To determine whether they also play a role in this process, *mtp11-1*, *mtp10-1*, *mtp8-2 mtp11-1* and *mtp8-1 mtp10-1* were grown alongside *mtp8-2* under the same conditions. As shown in Figures3.22 and 3.23, *mtp8-2* consistently displays stunting and chlorosis under Fe28/pH6.7 but the same phenotype is not observed for *mtp11-1*or *mtp10-1*. Similarly, the double mutants *mtp8-2 mtp11-1* and *mtp8-2 mtp10-1*, and triple mutant *mtp8-2 mtp10-1 mtp11-1*, display stunting similar to *mtp8-2*, but do not demonstrate an additive phenotype (Figure 3.22, 3.23 and 3.24, respectively). Interestingly, *mtp8-2 mtp10-1* consistently outperformed the other genotypes on all other tested conditions (Figures 3.23 and 3.24).

As well as on plates, Eroglu, et al. (2016) also observed a clear stunted, chlorotic phenotype for mtp8-1 when grown under alkaline soil conditions when watered with 160 μM Mn; the result without addition of Mn was not shown. The basal soil used in the original experiment (Eroglu, et al., 2016) was at a pH of 5.6, and limed to pH 7.2 using 20 g kg⁻¹ CaCO₃ and 12 g kg⁻¹ NaHCO₃. The normal soil used for plant growth throughout this project is slightly less acidic, at pH 6.0, and resulted in a pH of 8.0 when limed with the same reagent concentrations as the Eroglu soil regime; this resulted in very poor germination when tested. To achieve pH 7.2, 1/5-strength concentrations of liming agents were used instead: 4 g kg⁻¹ CaCO₃ and 2.4 g kg⁻¹ NaHCO₃. Each of the mtp single mutants and double mutants isolated in this chapter were tested on pH 6.0 and 7.2, watered as normal for 13 days, before either watering with 160 µM MnCl₂ or continuing with watering for 7 days. All genotypes appeared stunted at higher pH compared to basal soil; mtp8-1, mtp8-2, mtp8-2 mtp11-1 and mtp8-2 mtp10-1 and mtp8 mtp10 mtp11 appeared stunted and chlorotic compared to the WT at higher pH, regardless of Mn addition; the double mutants were not additive. The same phenotype was observed with and without addition of Mn. As with growth on plates, neither mtp9-1, mtp10-1 nor mtp11-1 were stunted or chlorotic compared to the WT with high pH. These findings are shown photographically in Figure 3.25 and 3.26.

3.2.5 954-12 is an EMS mutant with a similar phenotype to *mtp8* insertion mutants

As highlighted in Section 3.1, 954-12 is an EMS mutant that accumulates more Mn in its shoots than the WT. To determine whether it shows a Mn-dependent phenotype, 954-12 was grown on low Ca $\frac{1}{2}$ MS, supplemented with a range of Mn concentrations. As shown in Figure 3.27, it displays a very similar phenotype to mtp8-2, becoming sensitive compared to WT at 200 μ M Mn.

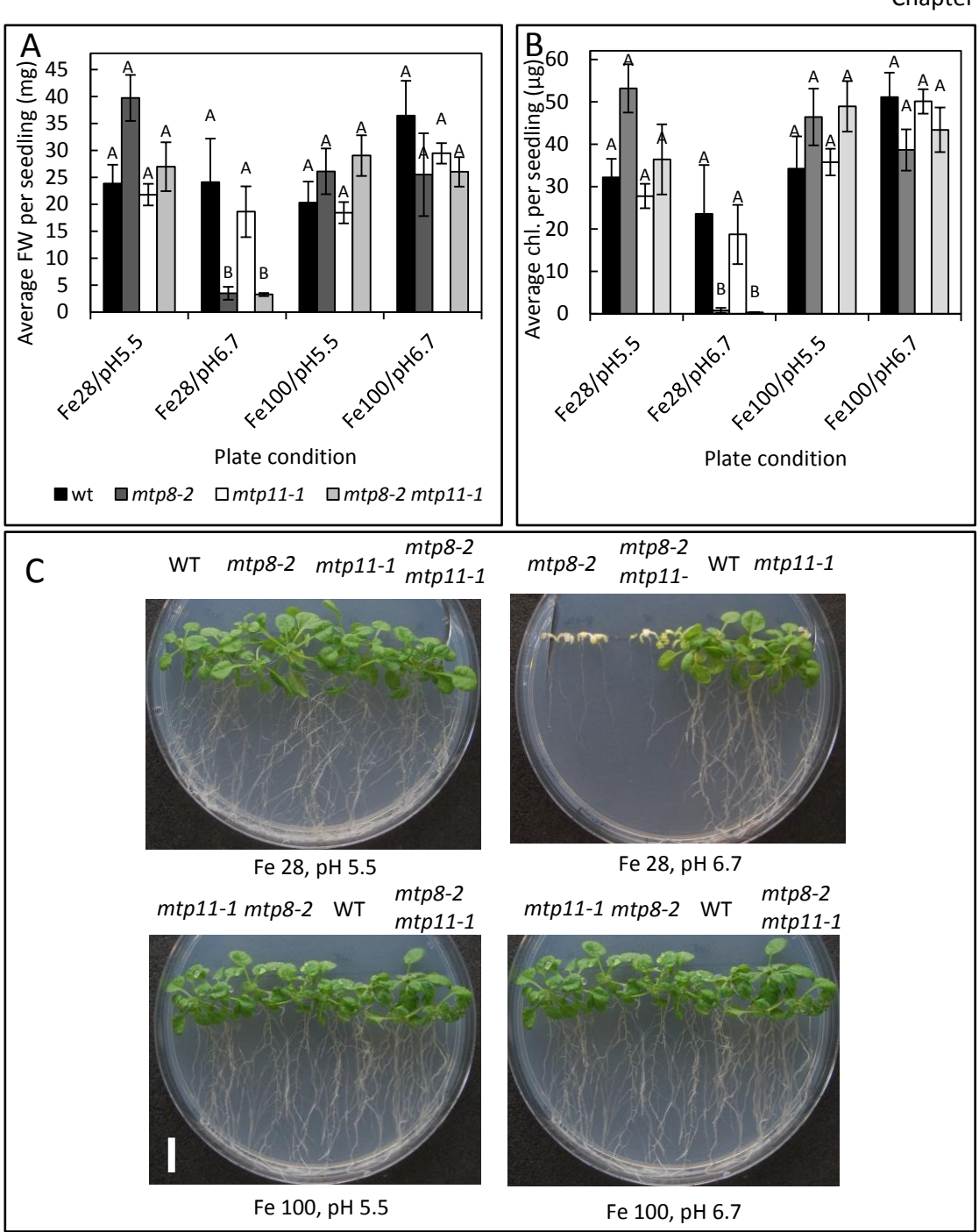


Figure 3.22. Stunted and chlorotic phenotype of mtp8-2 and mtp8-2 mtp11-1 under low Fe, high pH.

A)Fresh weight per seedling of mtp8-2, mtp11-1, mtp8-2 mtp11-1 and WT after 23 days growth on ½ MS (adapted Eroglu regime) supplemented with either 28 μ M or 100 μ M Fe (Fe28 and Fe100, respectively) supplied as FeNaEDTA, and buffered to pH 5.5 or 6.7 with NaOH. A) Data shows mean fresh weight (FW) (mg) per seedling calculated for 6 plates (\pm SE), with four seedlings per plant line, per plate. As determined by MANOVA, there is a interaction effect of genotype, Fe and pH on FW (F_{3,87} = 3.46, p<0.05). *, significantly different to WT at that condition, as determined by Tukey post hoc test. B) Total chlorophyll per seedling (μ g) at time of harvest, determined by DMF chlorophyll method. As determined by MANOVA, there is a interaction effect of genotype, Fe and pH on total chlorophyll production (F_{3,87} = 6.28, p<0.005).). Means not sharing a letter at a particular concentration are significantly different, as determined by Tukey post hoc test. C) Image displaying plant growth under all conditions. White bar = 1 cm.

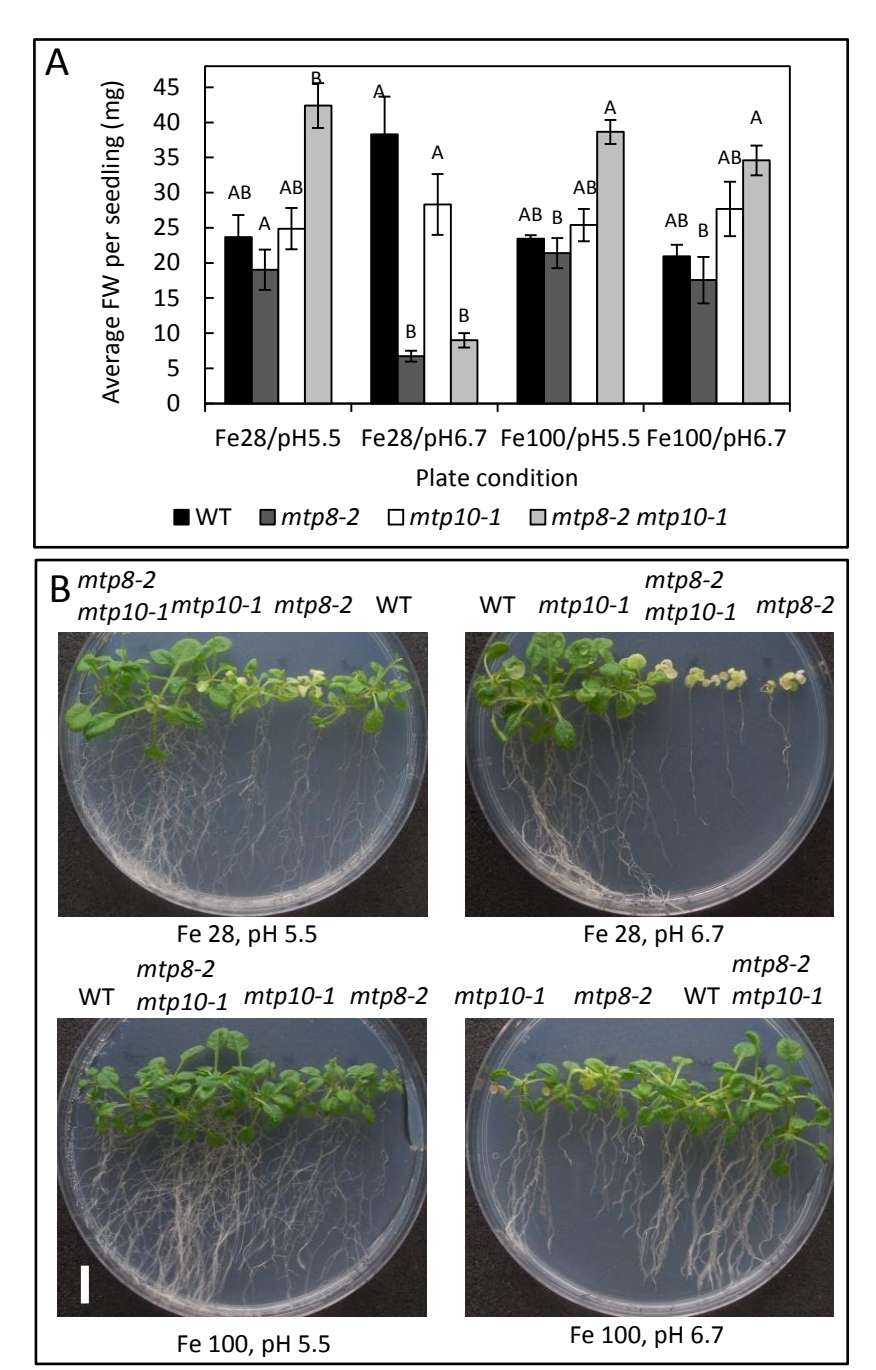


Figure 3.23. Stunted and chlorotic phenotype of *mtp8-2* and *mtp8-2* mtp10-1 under low Fe, high pH.

A)Fresh weight per seedling of mtp8-2, mtp10-1, mtp8-2 mtp10-1 and WT after 23 days growth on ½ MS (adapted Eroglu regime) supplemented with either 28 μ M or 100 μ M Fe (Fe28 and Fe100, respectively) supplied as FeNaEDTA, and buffered to pH 5.5 or 6.7 with NaOH. A) Data shows mean fresh weight (FW) (mg) per seedling calculated for 5 or 6 plates (\pm SE), with four seedlings per plant line, per plate. As determined by MANOVA, there is a interaction effect of genotype, Fe and pH on FW (F_{3, 87} = 13.55, p<0.001). Means not sharing a letter at a particular condition are significantly different, according to Tukey's post hoc test. B) Image displaying plant growth under all conditions. White bar = 1 cm.

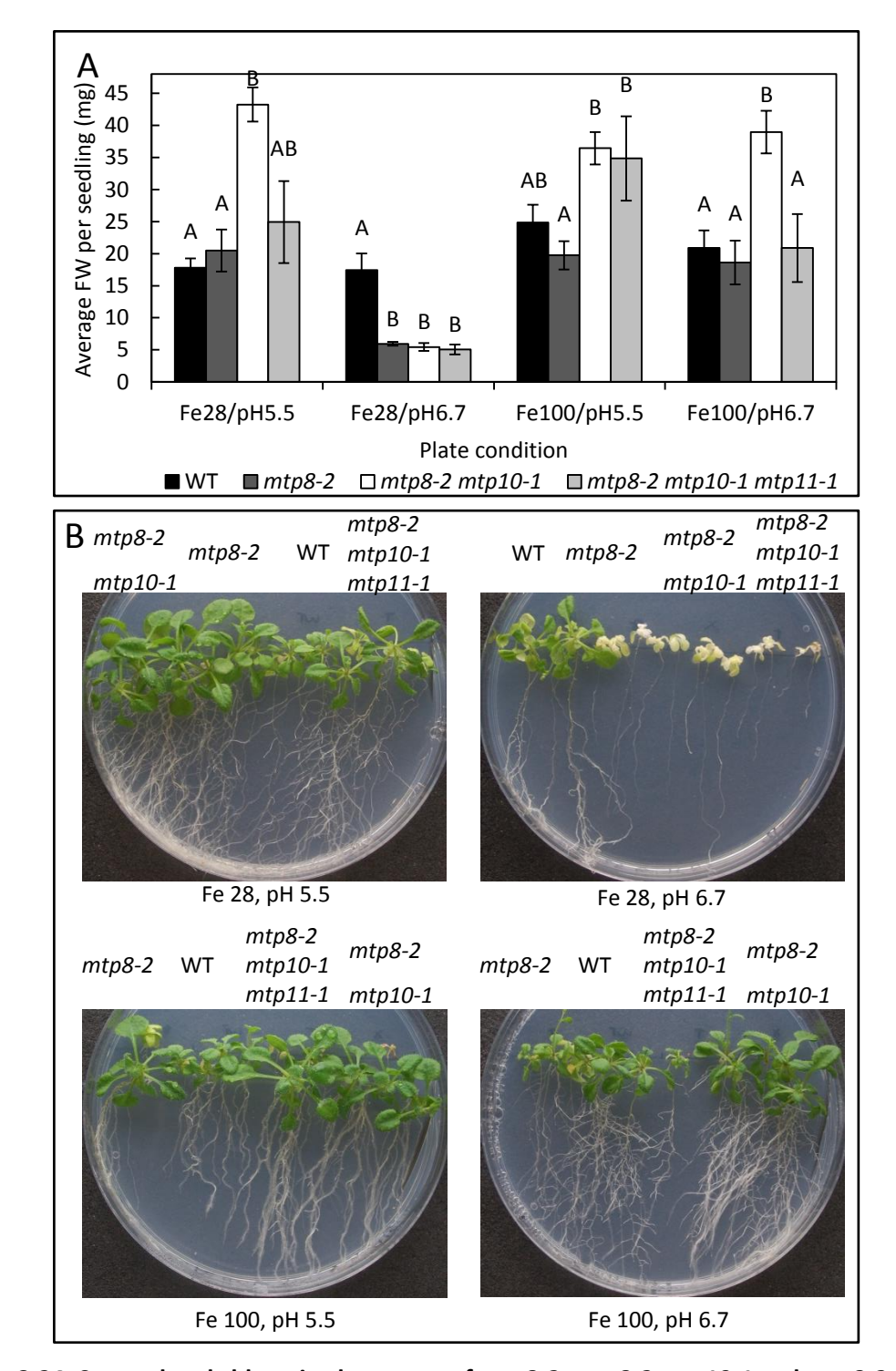


Figure 3.24. Stunted and chlorotic phenotype of *mtp8-2, mtp8-2 mtp10-1* and *mtp8-2 mtp10-1* mtp11-1 mutants under low Fe, high pH.

A)Fresh weight per seedling of mtp8-2, mtp8-2 mtp10-1, mtp8-2 mtp10-1 mtp11-1 and WT after 23 days growth on ½ MS (adapted Eroglu regime) supplemented with either 28 μ M or 100 μ M Fe (Fe28 and Fe100, respectively) supplied as FeNaEDTA, and buffered to pH 5.5 or 6.7 with NaOH. A) Data shows mean fresh weight (FW) (mg) per seedling calculated for 5 or 6 plates (\pm SE), with four seedlings per plant line, per plate. As determined by MANOVA, there is a interaction effect of genotype, Fe and pH on FW (F₃, \pm 91 = 8.42, p<0.001). Means not sharing a letter at a particular condition are significantly different, according to Tukey's post hoc test. B) Image displaying plant growth under all conditions. White bar = 1 cm

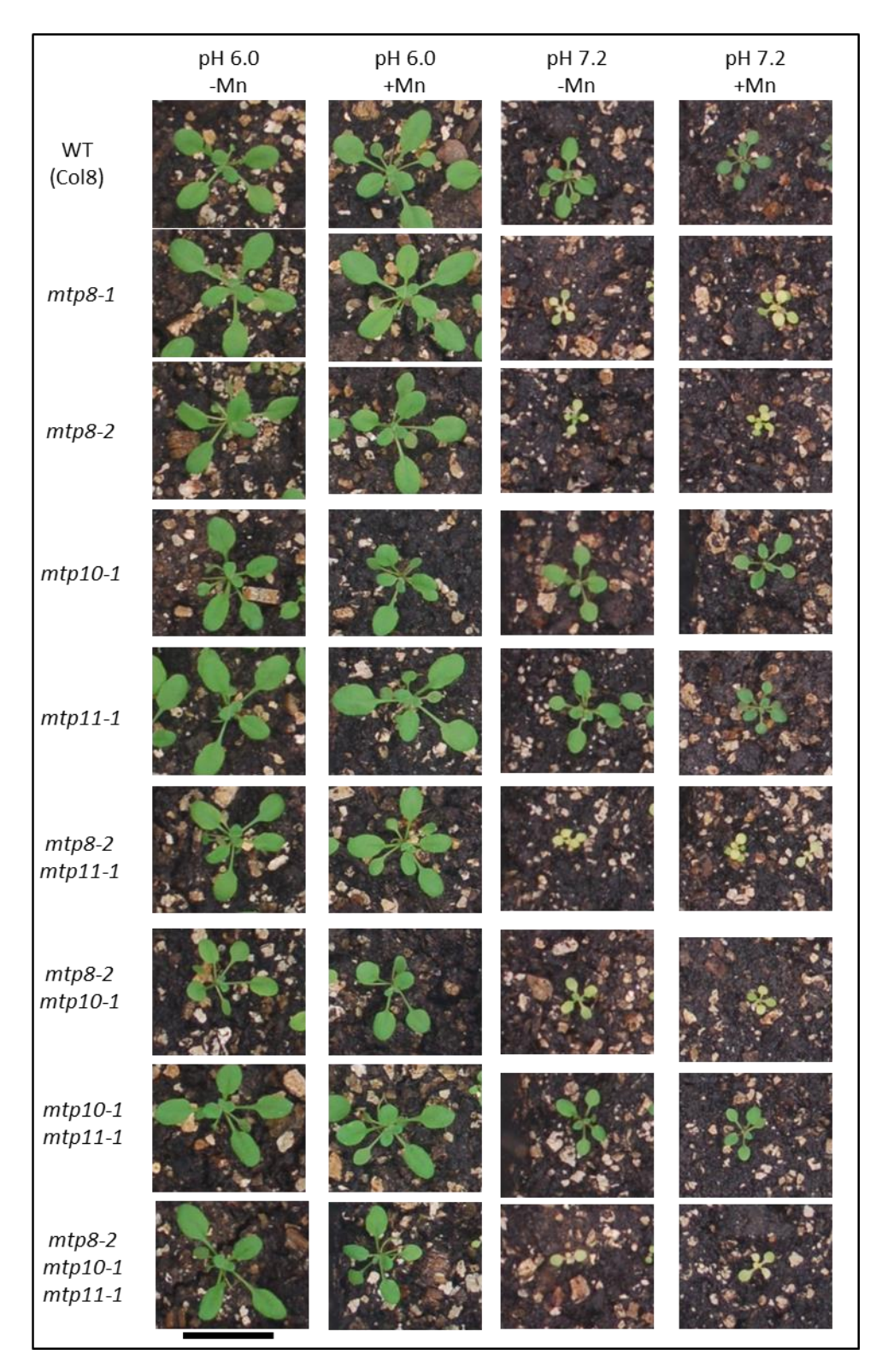


Figure 3.25. Chlorotic phenotype of *mtp8* mutants on soil limed to pH 7.2.

Growth of different mtp single, double and triple mutants on non-limed (pH 6.0) and limed (pH 7.2) potting soil, watered as normal for 13 days before either continuing normal watering regime (-Mn) or watering with 160 μ M MnCl₂ (+Mn) for a further 6 days. Plants photographed after 19 days growth. Photos are representative of 24 plants per genotype on each condition. Black bar, 2 cm.

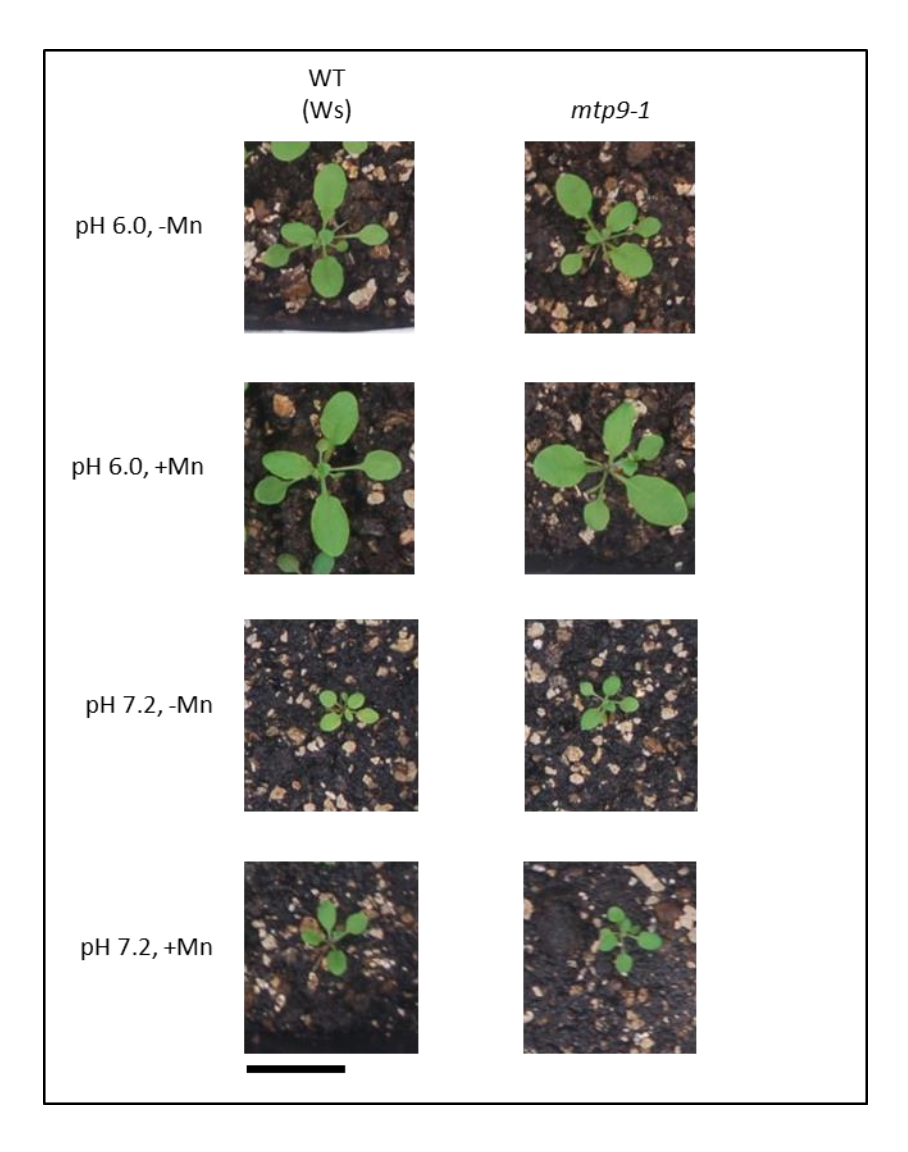


Figure 3.26. The mtp9-1 single mutant does not display a chlorotic phenotype on limed soil.

Growth of mtp9-1 insertion mutant with WT Wassilewskija (Ws) on non-limed (pH 6.0) and limed (pH 7.2) potting soil, watered as normal for 13 days before either continuing normal watering regime (-Mn) or watering with 160 μ M MnCl₂ (+Mn) for a further 6 days. Plants photographed after 19 days growth. Photos are representative of 32 plants on each condition. Black bar, 2 cm.

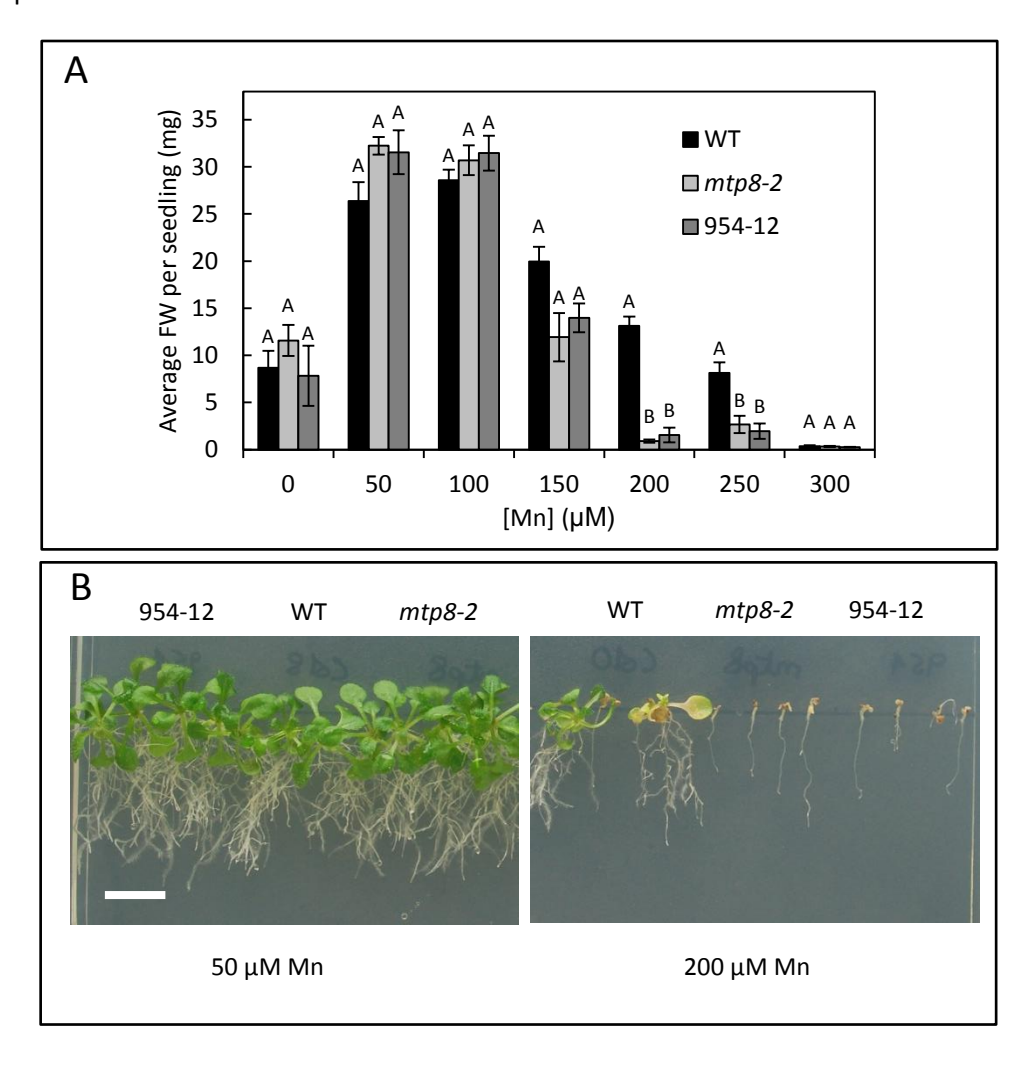


Figure 3.27. The 954-12 EMS mutant displays a similar Mn-sensitivity to mtp8-2

Fresh weight per seedling of mtp8-2 and 954-12 mutants and Columbia 0 wild type (WT) after 21 days growth on ½ MS supplemented with a range of Mn concentrations supplied as MnSO₄. A) Data shows mean fresh weight (FW) (mg) per seedling calculated for 4 plates (\pm SE), with four seedlings per plant line, per plate. As determined by GLM, there is a significant effect of genotype (F_{2, 57}= 16.55, P<0.001), [Mn] (F_{6, 57} = 131.33, p<0.001) and interaction between genotype and [Mn] (F_{12, 77}= 6.89, P<0.001) on FW. Means not sharing a letter at a particular concentration are significantly different, according to Tukey post hoc test. B) Image displaying plant growth on 50 μ M and 200 μ M Mn. White bar = 1 cm. Data for this experiment was provided by Dr. L.E. Williams and the analysis was carried out as part of this thesis.

In addition to the Mn-dependent phenotype, 954-12 also behaves similarly to *mtp8-2* under the modified Eroglu regime: 954-12 shows stunting and chlorosis under the Fe28/pH6.7 plate condition (Figure 3.28) and on both pH 7.2 soil conditions, with and without addition of Mn (Figure 3.29). Further, similarly to *mtp8-2*, 954-12 is not sensitive to Zn extremes (data not shown). It was therefore hypothesised that 954-12 carries a defect in MTP8, a protein with a similar function to MTP8, or a protein involved in the regulation of MTP8. To investigate further, 954-12 plants were crossed with pollen from *mtp8-2*, or backcrossed with the Col0 wild type. Based on Mendelian ratios, it was hypothesised that, all 954-12 *mtp8-2* crossed seedlings would display a similar Mn-dependent phenotype to *mtp8-2* when the F1 generation of these crosses were grown on excess Mn, if 954-12 did indeed carry a defect in MTP8 or similar machinery. Meanwhile this would be seen in 1 in 4 954-12 Col0 seedlings. The results are shown photographically in Figure 3.30, with two high-Mn plates shown as representative examples. While the ¼ ratio of 954-12 crossed with WT is clear, the phenotype of 954-12 crossed with *mtp8-2* is more sporadic.

Full length *MTP8* was amplified using a proof reading polymerase from 954-12 genomic DNA and cDNA, and compared to the same product from the Col0 WT background. Initially this indicated there was a guanine to adenine base substitution mutation at position G1358A of genomic DNA, corresponding to G934A of the coding sequence, which would result in a codon substitution of glycine to arginine at G312R of the translated protein sequence. As shown in Chapter 5, this corresponds with a conserved residue in the Arabidopsis MTPs; arginine is present in Zn transporting At MTP1 at this position, but is conserved as glycine in the Mn MTPs at this position. This mutation was present in 2 independent amplification and sequencing reactions. However, repeated rounds of this amplification failed to identify this mutation again; generally no mutation was present in the sequencing report. Currently, the conclusion is that there is no mutation in the coding sequence for *MTP8*, because the mutation has not been found in subsequent repeats.

3.2.6 Exploring the possibility that MTP9 and MTP10 share a functional redundancy

As shown Figures 3.16 and 3.17, *mtp10-1* does not display a Mn-sensitive phenotype compared to WT. Similarly, *mtp9-1* is not sensitive to elevated Mn compared to Ws WT, under either basal or low Ca regimes (Figure 3.31).

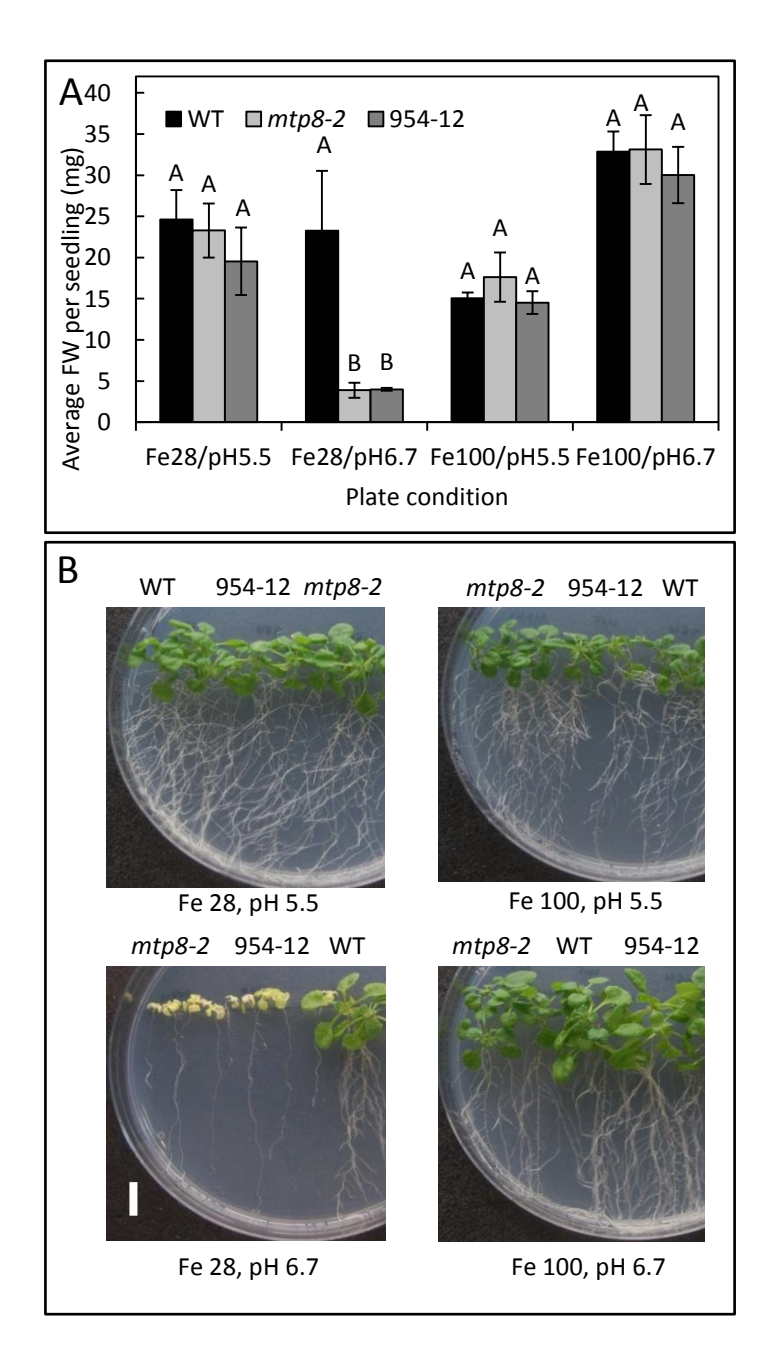


Figure 3.28. EMS mutant 954-12 displays similar phenotype to mtp8-2 under low Fe, high pH.

Fresh weight per seedling of mtp8-2, 954-12 and WT after 23 days growth on ½ MS (Eroglu regime) supplemented with either 28 μ M or 100 μ M Fe (Fe28 and Fe100, respectively) supplied as FeNaEDTA, and buffered to pH 5.5 or 6.7 with NaOH. A) Data shows mean fresh weight (FW) (mg) per seedling calculated for 6 plates (\pm SE), with four seedlings per plant line, per plate. As determined by MANOVA, there is a interaction effect of genotype, Fe and pH on FW (F_{3, 68} = 3.69, p<0.01). Means which do not share a letter are significantly different according to Tukey's post hoc test. B) Image displaying plant growth on Fe100, pH 5.5 and Fe28, pH 6.7. White bar = 1 cm.

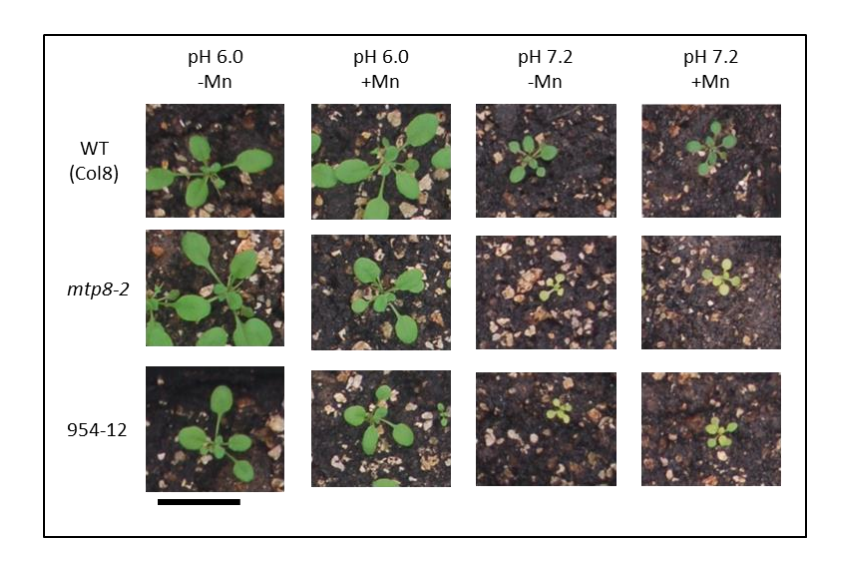


Figure 3.29. Chlorotic phenotype of *mtp8-2* insertion mutant and 954-12 EMS mutant on soil limed to pH 7.2.

Growth of mtp8-2, 954-12 and WT on non-limed (pH 6.0) and limed (pH 7.2) potting soil, watered as normal for 13 days before either continuing normal watering regime (-Mn) or watering with 160 μ M MnCl₂ (+Mn) for a further 6 days. Plants photographed after 19 days growth. Photos are representative of 24 plants per genotype on each condition. Black bar, 2 cm.

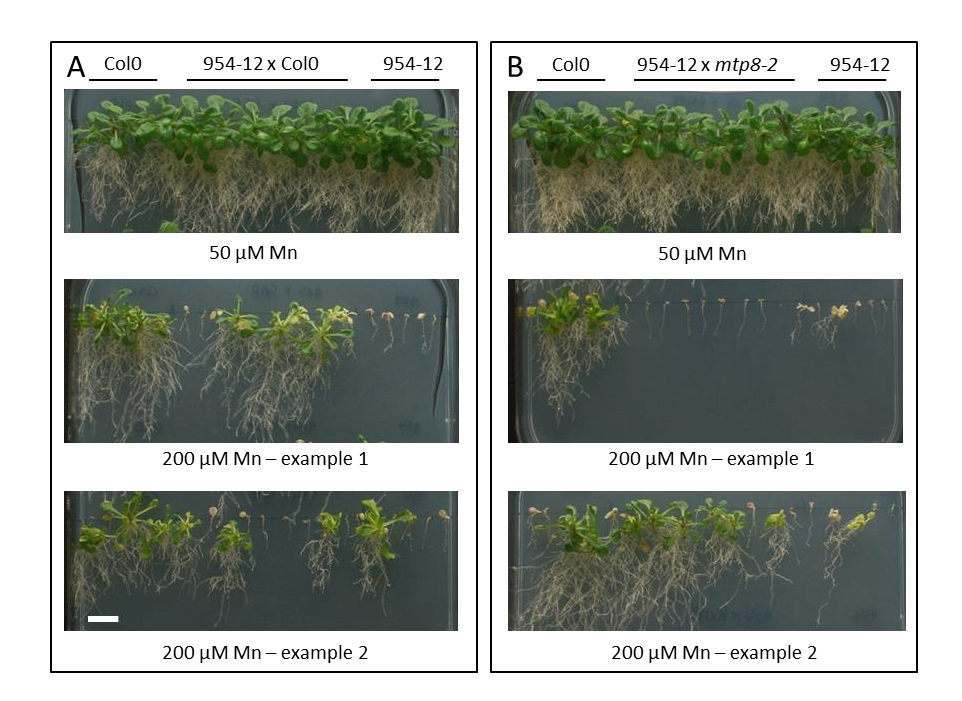


Figure 3.30. Mn-dependent phenotype of F2 generation 954-12 Col0 WT and 954-12 *mtp8-2* crosses.

Growth of Col0, 954-12 and F2 generation crosses of 954-12 crossed with pollen from either Col0 WT or mtp8-2, grown for 24 days on ½ MS containing 100 μ M CaCl₂ and either 50 or 200 μ M MnSO₄. Two examples of growth on 200 μ M MnSO₄ are provided. White bar, 1 cm.

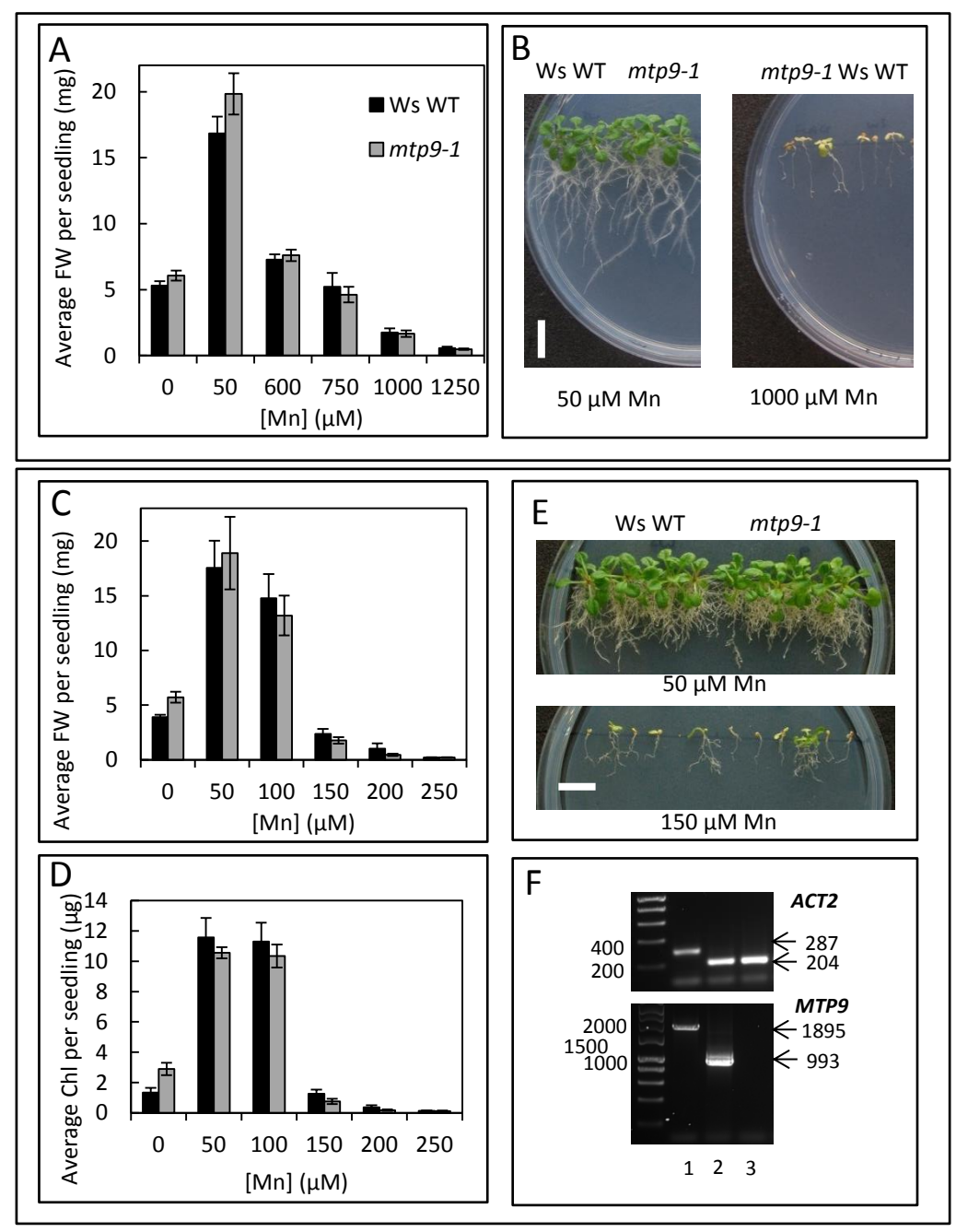


Figure 3.31. The insertion mutant mtp9-1 is not sensitive to Mn.

Comparison of wild type (Ws WT) and mtp9-1 mutant after growth on ½ MS containing (A-B) 1495 μ M Ca for 21 days or (D-E) 100 μ M Ca for 24 days, with a range of Mn concentrations supplied as MnSO₄. A + D) Mean fresh weight (FW; mg) per seedling calculated for 6 plates (\pm SE) with 4 or 6 seedlings per genotype, per plate. A) As determined by 2-way ANOVA, there is a significant effect of Mn (F_{5,60} = 153.66., p<0.001) but not of genotype (F_{1,60} = 1.72, p=0.2) or interaction of genotype and [Mn] (F_{5,71} = 1.56, p=0.19) on fresh weight. C) There is a significant effect of Mn (F_{5,60} = 53.0., p<0.001) but not of genotype (F_{1,60} = 0.01, p=0.93) or interaction of genotype and [Mn] (F_{5,71} = 0.38, p=0.86) on fresh weight. D) Total chlorophyll (μ g) per seedling under low Ca. There is a significant effect of Mn (F_{5,60} = 154.24., p<0.001) but not of genotype (F_{1,60} = 0.29, p=0.59) or interaction of genotype and [Mn] (F_{5,71} = 1.24, p=0.3) on chlorophyll per seedling. There is no significant difference between the genotypes at any given concentration, according to Tukey's post hoc test. C + E) Image displaying representative plant growth. White bar = 1 cm. F) Confirmation of mtp9-1 single mutant at RNA level; templates 1, WT gDNA; 2, WT cDNA; 3, mtp9-1 cDNA. Amplification of ACTIN2 housekeeper and MTP9 indicates mtp9-1 is a knockout at RNA level.

MTP9 and MTP10 are both found on chromosome 1, separated by approximately 217 kbp. Based on this information, and the lack of significant Mn-dependent phenotype for mtp9-1, mtp10-1 and mtp10-2, it was hypothesised that these proteins share a functional redundancy. Efforts are underway to generate a double mutant for mtp9-1 mtp10-1 (Williams, et al., unpublished data) but it has not been possible to isolate this double mutant within the time-frame of this thesis; additionally, it is possible that background polymorphisms in the Ws background of mtp9-1 and the Col8 background of mtp10-1 may interfere with determining the true phenotype of this mutant. Artificial microRNA (amiRNA) has therefore been designed to knockdown MTP9 in the mtp10-1 background. Using the Weigel World amiRNA design software, amiRNA was designed that fits the selection criteria for efficient silencing, as described in the introduction (Schwab, et al., 2006). The possibility of designing amiRNA to target MTP9 and MTP10 simultaneously was explored but non-specific targeting of the other MTPs was predicted for these constructs. Since knockdowns exhibit a 75% success rate, two different amiRNA constructs were designed to target MTP9: MTP9-A and MTP9-B. The subsequent amiRNA sequences are listed in Table 3.6, with relative positions on MTP9 illustrated in Figure 3.32A.

Figure 3.3 in the introduction illustrates the process of amiRNA, working on the principle of overlapping PCRs to replace the Arabidopsis precursor miRNA MIR319a from the pRS300 vector with amiRNA to target *MTP9*. Following 3 replacement PCRs and a final overlapping PCR with primers to the vector backbone, the resultant product was successfully digested and ligated into pENTR1a; this was confirmed with sequencing, with the diagnostic digest of the *MTP9*-A construct is shown in Figure 3.32B. The plant expression clone in the pMDC32 backbone, P35S::amiRNA-*MTP9*-A, was generated by LR cloning, again confirmed by sequencing and diagnostic digestion (Figure 3.32C). Constructs were transformed into WT, *mtp10-1* and *mtp8-2 mtp10-1* with the aim of downregulating *MTP9*. Due to time constraints it was not possible to characterise these transformed lines within the scope of this thesis; the next step would be to determine the level of downregulation of *MTP9* with qPCR and perform Mn assays to determine any phenotype.

3.2.7 Generating an RNAi knockdown mutant for Ta MTP8 and MTP8.1

When designing RNAi for downregulating *MTP8* and *MTP8.1* in wheat, it was decided to attempt to knock down both genes simultaneously, in case there was any functional redundancy of the copies that could interfere with an observable phenotype. Further, it was decided to generate a concatemer construct that would target *MTP8* and *MTP8.1* independently, but in the same expression construct, rather than one RNAi sequence to target both, since there was concern that other wheat MTPs would also be targeted due to areas of sequence similarity. The cloning strategy is summarised in Figure 3.33.

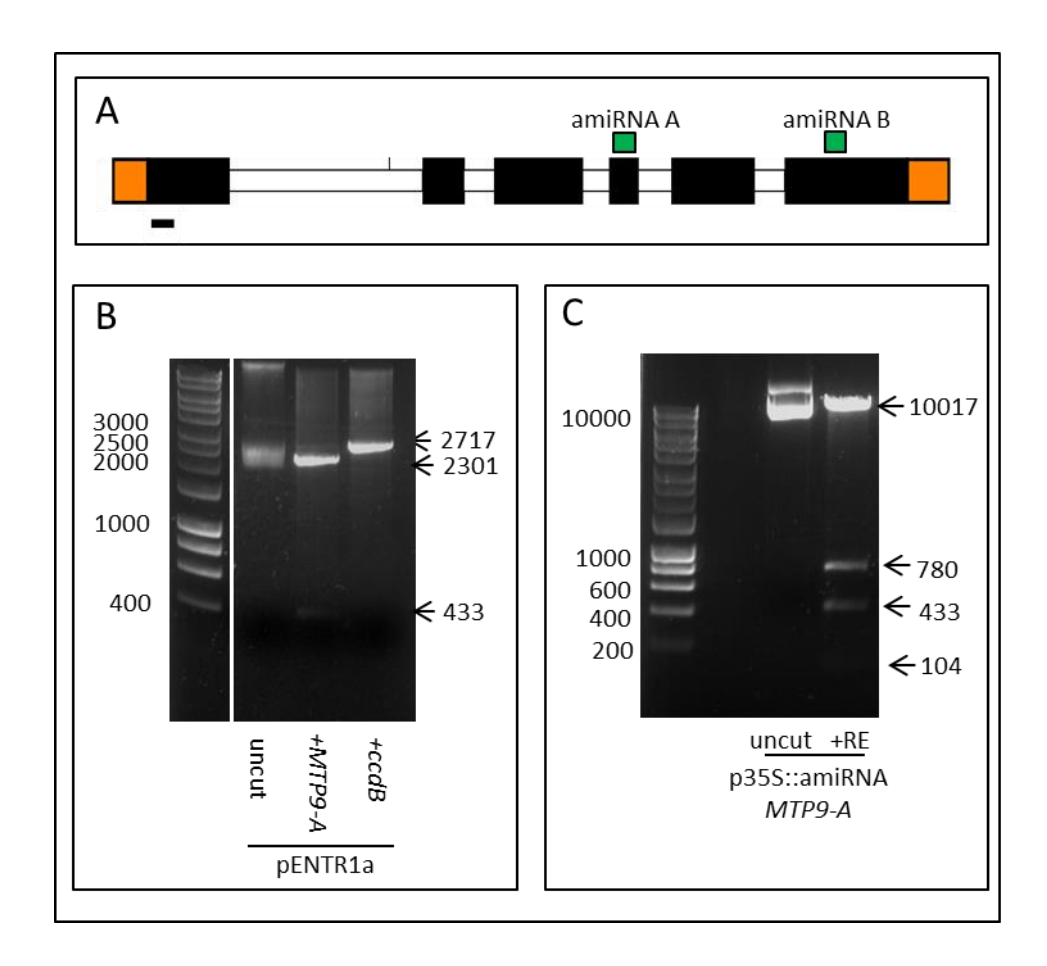


Figure 3.32. Generation of amiRNA constructs to target At MTP9.

A) Genomic schematic for *MTP9* indicating complementary sites of amiRNA constructs *MTP9*-A and *MTP9*-B (green squares). Black box, exon; white box, intron; orange box, 5' and 3' untranslated region; black bar, 100 bp scale. B) Diagnostic digestion analysis of amiRNA *MTP9*-A cloned into pENTR1a, alongside pENTR1a with ccdB and uncut vector as controls. Cut with *BamHI* and *HindIII*, pENTR1a + *MTP9*-A gives fragments of 2301 and 433 bp; pENTR1a + ccdB gives one fragment of 2717 bp, as labelled. C) Digestion analysis of *MTP9*-A in pMDC32: p35S::amiRNA *MTP9*-A. Digestion with *BamHI* and *HindIII* gives fragments of 10017, 780, 433 and 104 bp, as labelled. Uncut vector included as a control. Molecular weight markers labelled on left of gels.

Table 3.6. Artificial microRNA sequences designed to downregulate *MTP9*; designed using WeigelWorld software (Ossowski, et al., 2005; 2009; available www.weigelworld.org)

Construct	Sequence	Targeted region of gene
Α	TACAAGTAGCCTAGTTGACAC	774 bp cDNA
		3 rd exon
В	TCTATCGTGATATTCAAACCC	1338 bp cDNA
		6 th exon
	Α	A TACAAGTAGCCTAGTTGACAC

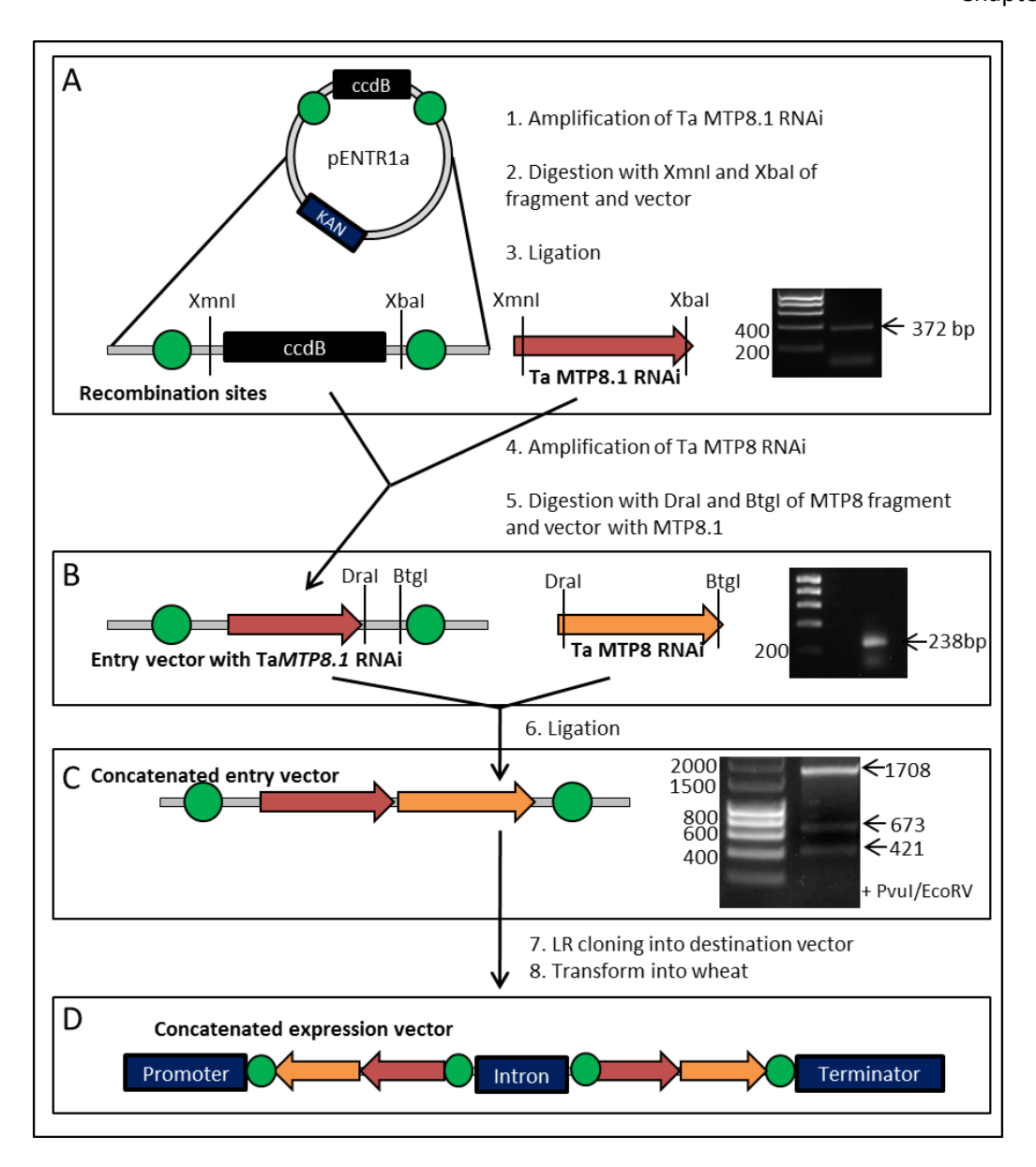


Figure 3.33. Cloning strategy to generate concatenated RNAi hairpin targeting Ta MTP8 and MTP8.1 in wheat.

A) pENTR1a vector digested with *XmnI* and *XbaI* to linearise and remove suicide gene *ccdB*. Ta *MTP8.1* RNAi fragment (red arrow) amplified from wild type (WT; Fielder) cDNA with primers that introduce *XmnI* and *XbaI* sticky ends when digested; gel shows successful amplification of this 372bp product (molecular weight marker labelled on left of gel). B) Ligation of digested samples generates 'entry vector with Ta MTP8.1 RNAi'; this is digested with *DraI* and *BtgI* to linearise. Ta *MTP8* RNAi fragment (orange arrow) amplified with primers that introduce *DraI* and *BtgI* sticky ends when digested; gel shows successful amplification of this 238bp product (200 bp molecular weight marker labelled on left of gel). C) Ligation of digested samples in B generates concatenated entry vector; diagnostic digest of this construct with PvuI and EcoRV results in correctly sized fragments of 1708, 673 and 421 bp, as labelled in gel; molecular weight markers labelled on left of gel. D) Concatenated entry vector is flanked by recombination sites (green circles); LR cloning of entry vector with pAct-IR-2 destination vector at these recombination sites results in concatenated RNAi hairpin, separated by intron under control of constitutive promoter.

The predicted coding sequences for Ta MTP8 – 11 have regions of similarity so it was important to design RNAi that would be specific to MTP8 and MTP8.1, while avoiding non-specific targeting. Within the cell, siRNA is cleaved into smaller polymers typically of 18-21 bases; when designing RNAi, potential sequences were rejected if they shared regions of high percentage identity of more than 12 bases with off-target MTPs. Sequences of 344 bases and 224 bases were eventually chosen for targeting Ta MTP8.1 and Ta MTP8, respectively. These are listed in the Materials and Methods, Chapter 2. Primers were designed to introduce restriction enzyme sites either side of the amplicons. The Ta MTP8.1 primers had quite strong secondary structures predicted but successfully amplified the fragment from wheat shoot cDNA, of the Fielder ecotype, after addition of 5% glycerol in the PCR mix (Figure 3.33A). This was sequenced after digestion and ligation into pENTR1a and was confirmed identical to the predicted sequence for Ta MTP8.1 on chromosome 4B. RNAi for Ta MTP8 was also successfully amplified (Figure 3.33B), before digestion/ligation cloning to generate the concatenated construct. The wheat genome is not yet sufficiently complete to cover each MTP8 sequence; as such, the Ta MTP8 RNAi was designed to target chromosome 6A, the only near-complete MTP8 sequence available at the time. The amplified product differs by 3 bases to the original prediction, but these changes did not affect the corresponding protein sequence. Therefore it is hypothesised that RNAi for Ta MTP8 was instead amplified from chromosome 6B or 6D. Figure 3.33C shows positive diagnostic digestion of the concatenated construct.

The concatemer was then sent for processing at NIAB, the collaborator of this project. Recombination of the concatemer with an expression vector for wheat transformation generated a concatemer hairpin under control of a constitutive promoter, which was transformed into wheat calluses. Tissue was collected at the T_0 stage and approximate copy number determined by PCR (performed at NIAB, data not shown). More tissue was collected from positive transformants as part of this thesis; RNA was extracted from samples with a copy numbers ranging from 1 to 4, and the corresponding WT control grown alongside transformed samples (con1 and con2; 0 copy numbers). Amplification of GADPH from the corresponding cDNA in Figure 3.33A indicates there is no genomic contamination. Primers for qPCR were successfully designed to target the 3' end of Ta MTP8.1; due to similarity at the 3' end with other Mn-MTPs, primers for Ta MTP8 were targeted more towards the middle of the gene. Figure 3.34A shows semi-quantitative PCR for Ta MTP8.1 and MTP8, using 25 and 28 cycles, respectively. Based on the signal intensity of these gels, it appears there may be a slight downregulation of both Ta MTP8 and MTP8.1 compared to the WT control. Quantitative real-time PCR (qPCR) was performed on these samples to determine the level of downregulation of Ta MTP8.1, with expression normalised to that of GADPH using a primer-efficiency calibrated method. Primers gave good efficiencies within the 90-100% range. As

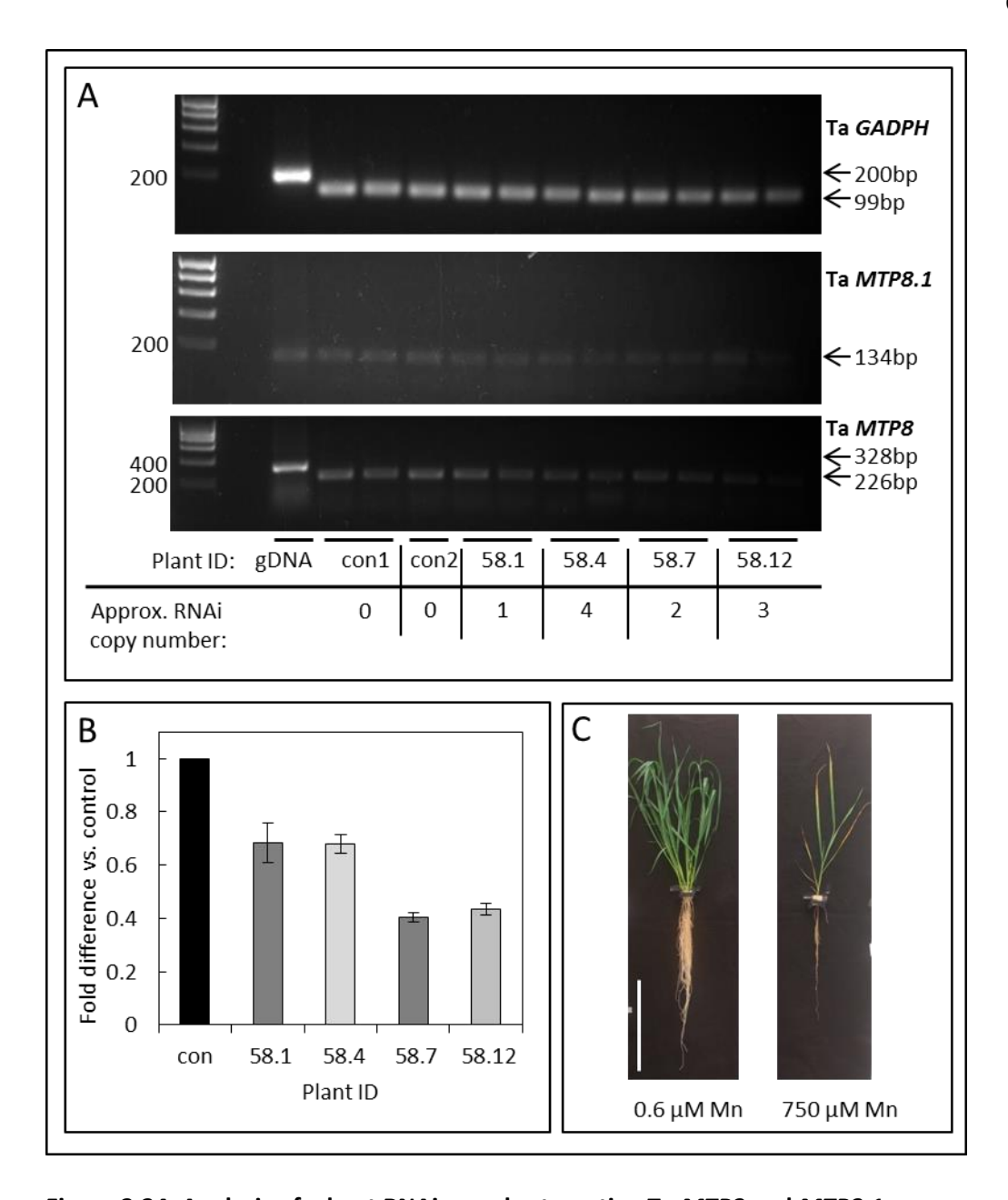


Figure 3.34. Analysis of wheat RNAi samples targeting Ta MTP8 and MTP8.1.

A) Semi-quantitative PCR to determine approximate changes in expression levels of housekeeping gene Ta GADPH (30 cycles), Ta MTP8.1 (25 cycles) and Ta MTP8 (28 cycles). Wild type genomic DNA (gDNA) used as control for gDNA contamination in experimental samples; con1 and con2, untransformed Fielder wheat grown at same time as transformed samples; 58.1, .4, .7 and .12, T_0 generation wheat seedlings transformed with RNAi construct targeting Ta MTP8 and MTP8.1. Molecular weight marker sizes listed on left of gels; predicted amplicon sizes listed on right. T_0 lines differ in approx. copy number of concatenated construct as listed below gels; this information was provided by NIAB. B) Quantitative PCR to determine expression levels of Ta MTP8.1 in transformed lines. Fold difference represents expression of Ta MTP8.1 normalised to GADPH using primer-efficiency calibrated method. Results are mean fold difference \pm SE of 2 biological reps with 3 technical reps. C) Preliminary hydroponics experiment growing Fielder WT wheat under control Mn (0.6 μ M MnCl₂) and toxic levels of Mn (750 μ M Mn) for 21 days. White scale bar = 30 cm.

shown in Figure 3.34B, samples 58.1 and 58.4, and samples 58.7 and 58.12, appear to downregulate Ta *MTP8.1* by around 30% and 60%, respectively. It should be noted that the error bars are based on 2 biological replicates, with 3 technical replicates each, rather than the ideal 3 biological replicates; the T₀ plants were too small at the time of collection to obtain sufficient tissue for 3 replicates. Ta *MTP8* primers gave a small amount of primer dimer which is not suitable for qPCR; quantitatively determining the levels of Ta *MTP8* expression may need to wait until more sequence information is available, to design better suited primers specific to Ta *MTP8*.

The next step in this process is to determine whether downregulation of Ta *MTP8.1*, and potentially Ta *MTP8*, has any effect on the Mn-sensitivity of wheat. A hydroponics assay was tested to determine at which Mn concentration yields a Mn-toxicity effect. As shown in Figure 3.34C, exposure to 750 μ M Mn for 21 days induces stunting in WT plants, with shorter roots, fewer leaves and brown patches on the leaves, while the control plants exposed to 0.6 μ M Mn remain healthy. Based on these observations, it is suggested that the RNAi plants should be tested under control, 500 μ M and 750 μ M Mn, to determine at which concentration *MTP8* and *MTP8.1* knockdown plants become sensitive relative to the WT.

3.3 Discussion

3.3.1 Identifying homologous proteins in more agriculturally relevant species

The phylogenetic tree in Figure 3.6 agrees with conclusions made by Gustin, et al. (2011) that MTP8 transporters cluster in Group 8, separately to those of Group 9 (MTP9, 10 and 11). This is echoed in Table 3.2; At MTP8 shares the lowest % similarity and identity with the other transporters. In addition to confirming proteins previously included in other analyses (Montanini, et al., 2007; Gustin, et al., 2011; Migocka, et al., 2014), BLAST searching on different genome databases has identified potentially homologous proteins in *Brassica rapa, Brachypodium distachyon, Zea mays* (maize), *Hordeum vulgare* (barley) and *Triticum aestivum* (wheat). Similarly, when aligning the newly identified sequences, each translated amino acid sequence contains the CDF signature sequence and the DxxxD domains, indicating these proteins are indeed CDF members, and at least possess sequence regions thought to be important for Mn transport.

Contrasting the single copy of each of At MTP8 – 11 found in the Arabidopsis genome, it appears the monocot species often have additional potential orthologs or paralogs clustering separately at the sub-group level. Like *Oryza sativa* and *Hordeum vulgare* (Chen, et al., 2013; Pedas, et al., 2014) MTP8.1 was found in addition to MTP8 in *Zea mays, Sorghum bicolor* and *Triticum aestivum* while only MTP8 is found in Arabidopsis. Interestingly, while the Os MTP8.1 is more restricted to shoot

expression, Os MTP8 and At MTP8 are more restricted to root expression (Chen, et al., 2013; Eroglu, et al., 2016; Genevestigator results of this chapter). As proposed by Eroglu, et al. (2016) it is possible the two Group 8 proteins in monocots have evolved different tissue specificity to increase the capacity of the whole plant to compartmentalise Mn in the vacuole, enabling tolerance to excess Mn. Comparatively, only one MTP11 protein has been identified in Hordeum vulgare, Sorghum bicolor and Zea mays, while two were found in Oryza sativa, Brachypodium distachyon and Triticum aestivum. Perhaps the additional MTP11 could be one explanation for the increased Mn tolerance and accumulation in rice compared to, for example, barley (Vlamis and Williams, 1964). The Mn accumulation in Brachypodium distachyon is currently unknown but this organism is emerging as a model for comparative and functional genomics in grass species, with BAC End Sequences (BES) sharing 82.4% homologous proteins with the rice genome (Huo, et al., 2009). It could be that a similar mechanism therefore exists for Mn tolerance in Brachypodium. The Western Regional Research Centre (WRRC) Brachypodium T-DNA insertional mutant collection (Bragg, et al., 2012) has recently been updated; searching the database shows there is an insertion mutant currently available for Bd MTP11. It would be interesting to obtain a homozygous mutant for this line and investigate any potential Mn sensitivity.

While copies of both *MTP9* and *MTP10* are found in the dicots included in this analysis (e.g. Arabidopsis, poplar and *Brassica rapa*), only *MTP9* appeared to be found in the genome of the monocots; no *MTP10* was identified in these species. This favours the hypothesis that At MTP9 and MTP10 share a functional redundancy, perhaps evolving through a genome duplication event after the monocot/dicot split. This hypothesis is also furthered by the lack of Mn-dependent phenotype observed in both *mtp9-1* and *mtp10-1* single mutants; the additive effect of MTP10 in the triple mutant will be discussed in the next section. MTP9 proteins characterised so far are proposed to be involved in Mn efflux at the plasma membrane for root-to-shoot Mn translocation (Migocka, et al., 2015; Ueno, et al., 2015); similarly, the only characterised MTP10 protein, Bm MTP10, is proposed to aid Mn efflux by sequestering in the Golgi for vesicular trafficking to the plasma membrane (Erbasol, et al., 2013). More work is clearly needed to explore this functional redundancy hypothesis further; characterising the plants transformed with amiRNA to downregulate *MTP9* in this chapter would be a useful starting point, while Chapter 4 aims to determine the subcellular localisation of these proteins in Arabidopsis.

This analysis also successfully identified putative Mn-MTPs in wheat, beginning to downregulate Ta MTP8 and MTP8.1 by RNAi as a first step in characterising these proteins. These lines appear to have successfully downregulated Ta MTP8.1; quantitatively assessing Ta MTP8 expression is dependent on new, quality sequence information being released to enable the design of specific primers with no secondary structures or off-targeting. Future work should expose transformed

lines to Mn deficiency and toxicity to determine whether downregulation of *MTP8.1*, and potentially *MTP8*, has any effect on wheat tolerance to Mn. Additionally it would be interesting to see whether Ta *MTP8* and *MTP8.1* show any upregulation under low Fe bioavailable conditions. If so, it is possible the RNAi-transformed lines may also show sensitivity these conditions, which may suggest Ta MTP8 and MTP8.1 play a similar role to At MTP8 in alleviating Fe/Mn antagonism (Eroglu, et al., 2016).

3.3.2 Predicted expression patterns of At MTP8 – 11

Figure 3.5 illustrates the developmental expression pattern of At MTP8 – 11, as predicted by Genevestigator. Until silique maturation and senescence, At *MTP11* is consistently expressed at the highest levels of the MTPs, while At *MTP8* is consistently expressed at lowest levels, a finding also reported by Delhaize, et al. (2007). Correspondingly, under basal conditions, *MTP8* expression remains low in all parts of the plant except the root elongation zone.

The root-specific expression of Os MTP9 is unaffected by Mn concentration (Ueno, et al., 2015), while Cs MTP9 is upregulated by Mn toxicity (Migocka, et al., 2015); interestingly, data from Genevestigator suggests At MTP9 expression is generally quite low in roots, although it is possible a different expression pattern would be observed under Mn perturbations. Additionally, At MTP9 expression increases during senescence. If elevated Mn conditions indeed induce At MTP9 expression in the roots, it is possible the root-to-shoot translocation mechanism of Cs MTP9 and Os MTP9 is conserved in Arabidopsis; upregulation during senescence may therefore promote vascular transport to the shoot for Mn seed loading. Additionally, At MTP9 is downregulated more than 3-fold in roots after infection with *Phytophthora parasitica*, a pathogen that attacks the roots (Hansen, 1990). This could be interesting; Segond, et al. (2009) report a 'significant' upregulation of At NRAMP3 in leaves in response to bacterial infection. It was shown that At NRAMP3 is involved in defence against this bacterium by remobilising Fe from the vacuole to trigger ROS production and inhibit pathogen growth; the ability of Mn to inhibit pathogen growth via NRAMP3 was not explored in this study, but At NRAMP3 is also an important Mn transporter in the leaf (Languar, et al., 2010). If At MTP9 also functions as an efflux transporter at the plasma membrane, downregulation during infection may increase Mn levels within the root cell cytoplasm, thus increasing ROS production to target invasive pathogens. It may be interesting to explore this further.

Contrastingly to *MTP9*, expression of *MTP10* and *MTP11* decreases during senescence. This may support a hypothesis that At MTP10 and At MTP11 are expressed at an intracellular membrane for subcellular compartmentalisation, such as the PVC localisation proposed for MTP11 by

Delhaize, et al. (2007): with downregulation, less Mn would be sequestered in internal organelles so more could be remobilised from senescing organs to the developing seed. Subcellular localisation will be investigated in further detail in Chapters 4 and 5. The data obtained from Genevestigator is a useful starting point for hypothesis generation. Quantitative PCR is needed to confirm these findings experimentally. Additionally, promoter analysis is necessary to determine true tissue specificity of At MTP8 – MTP11. This will be especially important for assigning the true function of these proteins.

3.3.3 At MTP8 and At MTP11 are essential for manganese homeostasis

The Mn-dependent phenotypes of mtp11-1, mtp11-3 and mtp8-2 suggest Mn homeostasis is significantly impaired when these transporters are non-functional. That mtp11 mutants are more detrimentally affected by Mn toxicity may suggest At MTP11 plays a more important contribution to alleviating Mn toxicity than At MTP8. Further, the double mutant mtp8-2 mtp11-1 displays an additive phenotype under Mn toxicity, which may imply a level of compensatory function between MTP8 and MTP11. At MTP11 expression is quite broad across different tissues (Peiter, et al., 2007), with Genevestigator suggesting it remains at medium-to-high expression levels across the plant; meanwhile, MTP8 is been reportedly expressed at higher levels in the root, with significant upregulation here under Mn toxicity (Eroglu, et al., 2016). At MTP11 has been implicated to be expressed at either the PVC or the Golgi (Delhaize, et al., 2007; Peiter, et al., 2007); contrastingly At MTP8 localises to the tonoplast when expressed in mesophyll protoplasts (Eroglu, et al., 2016). Subcellular localisation will be explored in more detail in Chapter 4, but based on the additive phenotype of mtp8-2 mtp11-1, localisation to different subcellular compartments seems logical. If both a vacuolar sequestration route and an exocytosis route via the Golgi are lost, the elevated level of Mn within the cytoplasm under Mn toxicity conditions would put extra stress on the cell, inducing symptoms of Mn toxicity. Contrastingly, mtp8-2 mtp11-1 performs better than the WT under Mn deficiency. This is also logical; under Mn deficiency, residual environmental Mn would be acquired by plasma membrane transporters such as NRAMP1 (Cailliatte, et al., 2010) while maternal stores in the seed vacuole would be remobilised to the cytoplasm by NRAMP3 and NRAMP4 (Languar, et al., 2005; 2010). In the WT, MTP11 and MTP8 may function to sequester this residual Mn into subcellular stores; in the double mutant however, free ions would remain unsequestered and available for use elsewhere in the cell or plant.

Additionally, the further additive phenotype of the *mtp8 mtp10 mtp11* triple mutant demonstrates losing MTP10 in addition to MTP8 and MTP11 is detrimental to plant growth. This also highlights the importance of generating double and triple mutants to investigate gene

function: the role of MTP10 in Mn homeostasis was not so clear from *mtp10-1* or the double mutant functional studies. Further to the hypothesis that MTP11 provides a greater contribution to Mn homeostasis than MTP8, it is possible that MTP10 provides a 'back up' mechanism to avoid Mn toxicity when MTP11 is non-functional. This will be explored in later chapters, determining subcellular localisation and transport ability of these proteins when expressed in yeast.

3.3.4 Mn toxicity is exacerbated by lower Ca availability

The low and basal Ca regimes introduced in this chapter clearly demonstrate that Mn toxicity is exacerbated by lower Ca availability: the Mn-dependent phenotypes of *mtp11*, *mtp8* and corresponding double and triple mutants are observed at lower Mn concentrations under low Ca conditions, than under basal Ca conditions; elevated Mn also inhibits germination in some mutant lines under low Ca, but not under basal Ca. The Mn/Ca antagonism is more apparent in the mutants than in the WT. Examples of Ca alleviating Mn toxicity have previously been reported in the literature, with examples listed in Chapter 1. Recently, Mn toxicity has been shown to inhibit accumulation of Ca and Fe in wheat calli (Siewprawska, et al., 2016).

Although the mechanism behind Mn/Ca antagonism is rarely explored in detail, the use of these mutants suggests a competitive pathway or site exists for this antagonism. Table 1.4 indicates that some Ca transporters have affinity for Mn, for example members of the CAX and ECA families (Wu, et al., 2002; Kamiya and Maeshima, 2004; Mills, et al., 2008; Li, et al., 2008), but also that Mn transport ability is not always investigated during characterisation of transporters. Root-to-shoot translocation of Mn is inhibited in barley plants exposed to high Ca (Alam, et al., 2006). Therefore it is possible that, under low Ca availability, Mn competes for a pathway to enter root cells and cause cytoplasmic toxicity, or for loading to the shoot to cause toxicity in the aerial tissues. Alternatively, Ca and Mn could compete for targets within the cell that, under basal conditions, would alleviate the toxic effect of Mn. There is little information available regarding Mn/Ca displacement, but there are examples of other elements competing with Ca for active sites in proteins. For example, lanthanides can compete with Ca in the water splitting/oxygen evolving complex of photosystem II, Mn₄CaO₅ (Ghanotakis, et al., 1985); Ca can be replaced by other metals in this protein and retain the core structure, but Ca is essential for proper function due to its role in organising the surrounding water network (Lohmiller, et al., 2015).

Regardless of whether Mn outcompetes Ca for routes into the cytoplasm or for subcellular targets, the use of mutants in this chapter indicates that the subsequent Mn toxicity is exacerbated when routes for Mn detoxification are lost.

3.3.5 MTP8 is the key Arabidopsis Mn-MTP involved in alleviating Mn/Fe antagonism

It was recently claimed by Eroglu, et al. (2016) that MTP8 plays a key role in alleviating Mn/Fe antagonism, upregulated under Fe deficiency to sequester excess Mn in the vacuole. Corresponding with this report, mtp8-1 and mtp8-2 are sensitive to pH-induced Fe deficiency. This was the case in both plate- and soil-grown assays, although the chlorosis on soil was seemingly pH-dependent and independent of Mn supply; watering limed soil with 160 μM Mn had no effect on chlorosis or stunting in this work. Additionally, of the top ten perturbations identified by Genevestigator to upregulate MTP8, almost all correspond with Fe deficiency. Interestingly, upregulation of MTP8 also corresponded with alterations in expression of UBC13, a ubiquitin conjugase enzyme important for root hair formation under conditions of low Fe availability (Li and Schmidt, 2010). Similarly, expression is increased in the pye-1 mutant; PYE (POPEYE) is a root pericycle-specific bHLH transcription factor that positively regulates members of the Fe deficiency response to ensure continued growth under low Fe conditions (Long, et al., 2010). Alongside other components of the Fe-deficiency response, IRT1 and FRO2, MTP8 is positively regulated by bHLH FIT1 under Fe deficiency (Eroglu, et al., 2016). Taken together, these findings suggest MTP8 is not directly regulated by PYE, but the hypersensitive Fe-deficiency phenotype of pye-1 mutants may indirectly continue to upregulate MTP8, as components of the Fe response downstream of PYE may not be activated.

Although MTP8 was described as the key player in alleviating Mn/Fe antagonism, none of the other Mn-MTPs were investigated. Here it is shown that MTP9, MTP10 and MTP11 do not appear involved in this process; no chlorosis or inhibition is seen in the single mutant lines relative to the WT, nor is any additive phenotype observed in the double and triple mutants tested. However, the EMS mutant 954-12 does appear to suffer a defect in a component of this process, displaying a very similar phenotype to mtp8-2 under both pH-induced Fe deficiency, and Mn toxicity conditions. Additionally, 954-12 features enhanced Mn accumulation in the aerial tissues, correlating with reports of enhanced root-to-shoot translocation of Mn in mtp8-2 (Eroglu, et al., 2016). It was originally hypothesised that 954-12 may suffer a mutation in the MTP8 coding sequence, although it was eventually concluded this was not the case as the sequencing result could not be repeated. Instead it might be possible that 954-12 features a mutation in the MTP8 promoter resulting in a knockdown; although efforts have been made to amplify regions of this promoter, so far it has not been possible with a proof-reading polymerase. Alternatively, 954-12 could feature a defect in one of the components of the MTP8 regulatory response, such as FIT. It would be interesting to see whether there is a mutation in FIT in 954-12, and if so, to compare the phenotype of a non-lethal fit allele to mtp8-2 under different conditions. Future work with this

mutant may involve next generation sequencing (NGS) to identify any background polymorphic differences between 954-12 and the WT, which may contribute to its phenotype.

Chapter 4: Functional analysis of MTPs using transgenic plants

4.1 Introduction and aims

4.1.1 Transgenic plants as a tool for overexpression and complementation studies

Cloning a gene of interest into a plant-specific vector, under control of a constitutive promoter such as the Cauliflower Mosaic Virus (CaMV) 35S promoter, confers strong expression of the gene to all transformed cells (Covey, et al., 1981). This technique has previously been used to investigate the function of certain MTPs. For example, At MTP1 is a vacuolar zinc transporter, resulting in a Zn-hypersensitive phenotype in the *mtp1-1* knockout mutant (Kobae, et al., 2004); correspondingly, overexpression of this transporter in WT plants leads to enhanced Zn tolerance and Zn accumulation in roots (van der Zaal, et al., 1999). Similarly, when At MTP11 is overexpressed, transgenic plants are hypertolerant to Mn toxicity compared to the WT, but show increased sensitivity to Mn deficiency (Peiter, et al., 2007). Overexpression of At MTP8 leads to increased Mn accumulation in roots (Eroglu, et al., 2016); however, no phenotype of plants overexpressing At MTP8 has yet been reported. Here, At MTP8- and At MTP11-overexpressing plants will be generated and their phenotypes investigated, under both the basal and low Ca regimes introduced in Chapter 3.

Complementation studies can also be carried out to test whether a particular mutant phenotype can be rescued by a closely related gene. For example, the Zn-hypersensitive phenotype of *mtp1-1* can be rescued with expression of either the native At MTP1 (Kobae, et al., 2004) or with Os MTP1, a homologous protein in rice (*Oryza sativa*; Menguer, et al., 2013). Similarly, two related genes from poplar, Pt MTP11.1 and MTP11.2, are able to complement the Mn-sensitivity of *mtp11-1* (Peiter, et al., 2007). An ability to rescue a phenotype may suggest a conservation of function, either directly or compensatorily. Os MTP11 clusters phylogenetically with At MTP11 (Figure 3.7). In this chapter, Os MTP11 will be expressed in *mtp11-3* to determine whether any functional complementation is observed. It is also important to complement a mutant with its native protein to demonstrate any mutant phenotype is due to the knocked out protein, rather than other unidentified mutations; *MTP8* will be expressed in *mtp8-2* to confirm this.

The process of generating transgenic plants requires cloning of genes into expression vectors, which allows flanking of the genes with specific promoters such as 35S, or fluorescent protein tags

Chapter 4

such as GFP. In the past, cloning technology predominantly relied on restriction digestion and ligation; this is often hampered by inappropriately positioned restriction sites, particularly when cloning large DNA fragments. Different cloning technologies now exist, such as Gateway Cloning: after cloning of a gene of interest into an entry vector, it can be recombined with specific destination vectors to produce expression clones. This technology will be utilised in this Chapter to generate plant-specific expression clones for At MTP8, 9 and 11. In addition to Os MTP11, these clones will be transformed into Arabidopsis for overexpression and complementation studies, mediated by the *Agrobacterium tumefaciens* binary vector system.

4.1.2 Determination of subcellular localisation to investigate protein function

Table 1.2 demonstrates which plant Mn-MTPs have been characterised to the degree of subcellular localisation. There is a discrepancy regarding the cellular localisation of At MTP11, with targeting to the prevacuolar compartment (PVC) (Delhaize, et al., 2007) or to the Golgi (Peiter, et al., 2007) both suggested. Both conclusions are based on valid colocalisation studies. Peiter, et al. (2007) reported colocalisation of MTP11 with trans-Golgi marker sialyl transferase (ST), which was disrupted with treatment of Golgi destabilising agent Brefeldin A, when expressed in mesophyll protoplasts. Contrastingly, Delhaize, et al. (2007) observed no colocalisation with cis-Golgi marker Manl when expressed in tobacco protoplasts, instead reporting localisation with PVC marker, VSR2. These differences have led to distinctly different detoxification mechanisms proposed by each study (Figure 1.7). No subcellular localisation has yet been assigned to Os MTP11; however, if this protein can functionally complement *mtp11-1* under Mn toxicity, it is possible these proteins share the same subcellular localisation.

At MTP8 has recently been shown to target the tonoplast when transiently expressed in mesophyll protoplasts (Eroglu, et al., 2016). Other Group 8 MTPs from *Stylosanthes hamata* (Delhaize, et al., 2003), rice (Chen, et al., 2013) and cucumber (Migocka, et al., 2015) also target the tonoplast, while the barley MTP8.1 and MTP8.2 target the Golgi (Pedas, et al., 2014). This project aims to confirm the subcellular localisation of MTP8. Further, no information is available for the subcellular localisation of At MTP10, although the related protein from *Beta vulgaris* spp. *maritima*, Bm MTP10, targets the Golgi in yeast (Erbasol, et al., 2013). Localisation of both At MTP8 and At MTP11 has only been explored when expressed in protoplasts. This chapter aims to determine the subcellular localisation of each of the Arabidopsis Mn-MTPs and Os MTP11 when stably expressed in Arabidopsis and when transiently expressed in tobacco. Expression in tobacco is a useful tool, enabling co-expression with subcellular markers with relative ease.

GFP is a bulky protein that, when tagged to a putative membrane protein, can sit at the membrane face and potentially interfere with or disrupt regions of the protein that are important for function. For example, the poplar Ptd MTP1, a member of the Zn-MTP clade, forms functional oligomers, possibly stabilised by disulphide bridges (Blaudez, et al., 2003). Fluorescent protein tagging has the potential to destabilise this structure and impair transporter function so it is important to compare both a tagged and non-tagged control. Therefore, the full-length coding sequences for At MTP8, MTP9, MTP10 and MTP11 will be amplified with and without the stop codon; the subsequent phenotypes of these transgenic plants will be compared to ensure the GFP tag does not interfere with the function of the gene when expressed *in planta*.

4.1.3 Chapter Aims

The key aims of this chapter will utilise cloned coding sequences to investigate protein function:

- 1. To clone At *MTP8*, *MTP9* and *MTP11* into various expression vectors for functional analysis
- To generate stable Arabidopsis lines expressing some of these genes, and additionally Os MTP11
- To determine whether overexpression of At MTP8 and MTP11, and expression of Os MTP11, in wild type Arabidopsis enhances Mn tolerance
- 4. To determine whether MTP11 function is conserved between Arabidopsis and rice, by expressing Os *MTP11* in *mtp11-3*
- To determine the subcellular localisation of At MTP8, MTP10, MTP11 and Os MTP11.
 This will be achieved using stably transformed in Arabidopsis seedlings and transient expression in tobacco epithelial cells.

4.2 Results

4.2.1 Cloning of Arabidopsis group 8/9 MTPs

As a first step to functionally characterising the Arabidopsis group 8/9 MTPs, the cDNAs for MTP8, 9 and 11 were cloned. The TOPO cloning method used here requires amplification of the target sequence with a CACC sequence tag at the 5' end, ensuring correct orientation of the sequence in the entry vector. However, amplification of *MTP8* was initially unsuccessful, and was amplified in two parts, as summarised in Figure 4.1A (see Materials and Methods for details). It was, however, possible to amplify the 5' end of *MTP8* with Taq polymerase, indicating this part of the sequence was present. Following successful amplification, the full-length sequence of *MTP8* was cloned into

Chapter 4

pENTR/D-TOPO vector; the positive restriction digest for this construct is shown in Figure 4.1B. Amplification of *MTP9* and *MTP11* were both achieved in one step, as summarised in Figure 4.2A and C; Figure 4.2B and D show the positive restriction digests for the *MTP9* and *MTP11* entry clones, respectively. All entry clones were confirmed by at least two independent sequencing reads. As alluded to in Chapter 3, the coding sequence for *MTP8* was identical to information provided from the Arabidopsis Information Resource (TAIR), while *MTP9* matched model *MTP9.2* on TAIR; the *MTP11* sequence was identical to that previously published (Delhaize, et al., 2007). These constructs carrying the full-length coding sequences were used as the template for amplifying the coding sequence without the stop codon (not shown). Despite multiple attempts to clone *MTP9*, the sequenced repeatedly entered pENTR/D-TOPO in the wrong orientation; therefore, although the coding sequence was confirmed, *MTP9* could not be recombined with destination vectors, as the resultant inverted protein sequence would be incorrect.

Plant-specific expression clones were generated for MTP8 and MTP11; constructs with a stop codon were recombined with vector pMDC32 (Curtis & Grossniklaus, 2003) with diagnostic digests for P35S::MTP8 and P35S::MTP11 provided in Figures 4.1C and 4.2E, respectively. The nonstop version was recombined with pMDC83 (Curtis & Grossniklaus, 2003), pEG101 (Earley, et al, 2006) and pSITE-4NB (Chakrabarty, et al., 2007), providing a 35S promoter and a C-terminal GFP, YFP or mRFP tag, respectively. At MTP10 and Os MTP11 expression clones were generated in the same way (results not shown). Constructs were transformed into WT seedlings for overexpression, and various mtp insertion mutants for functional complementation analysis. Homozygous transformed lines were generated and isolated at the T3 generation, after three rounds of selection on the selectable herbicide marker; Figure 4.3 shows isolation of the MTP8 overexpressor, P35S::MTP8 in Col8 WT as an example. Multiple independent (i.e. non-sister) transformed lines were generated for each construct in different backgrounds, although this was difficult for lines transformed into the mtp8-2 background, due to high levels of silencing. Figures 4.4 and 4.5 show confirmation at the RNA level, for plants transformed with At MTP8, At MTP11 and Os MTP11. The semi-quantitative PCR of Figure 4.4A suggests MTP8 is expressed at higher levels in the three overexpressing lines than in the WT control.

4.2.2 Phenotypic analysis of stably transformed Arabidopsis lines

4.2.2.1 MTP8 overexpression confers Mn hypertolerance

MTP8 confers considerable hypertolerance to Mn when overexpressed in WT Arabidopsis; while WT becomes detrimentally affected by Mn toxicity at moderate Mn concentrations, two

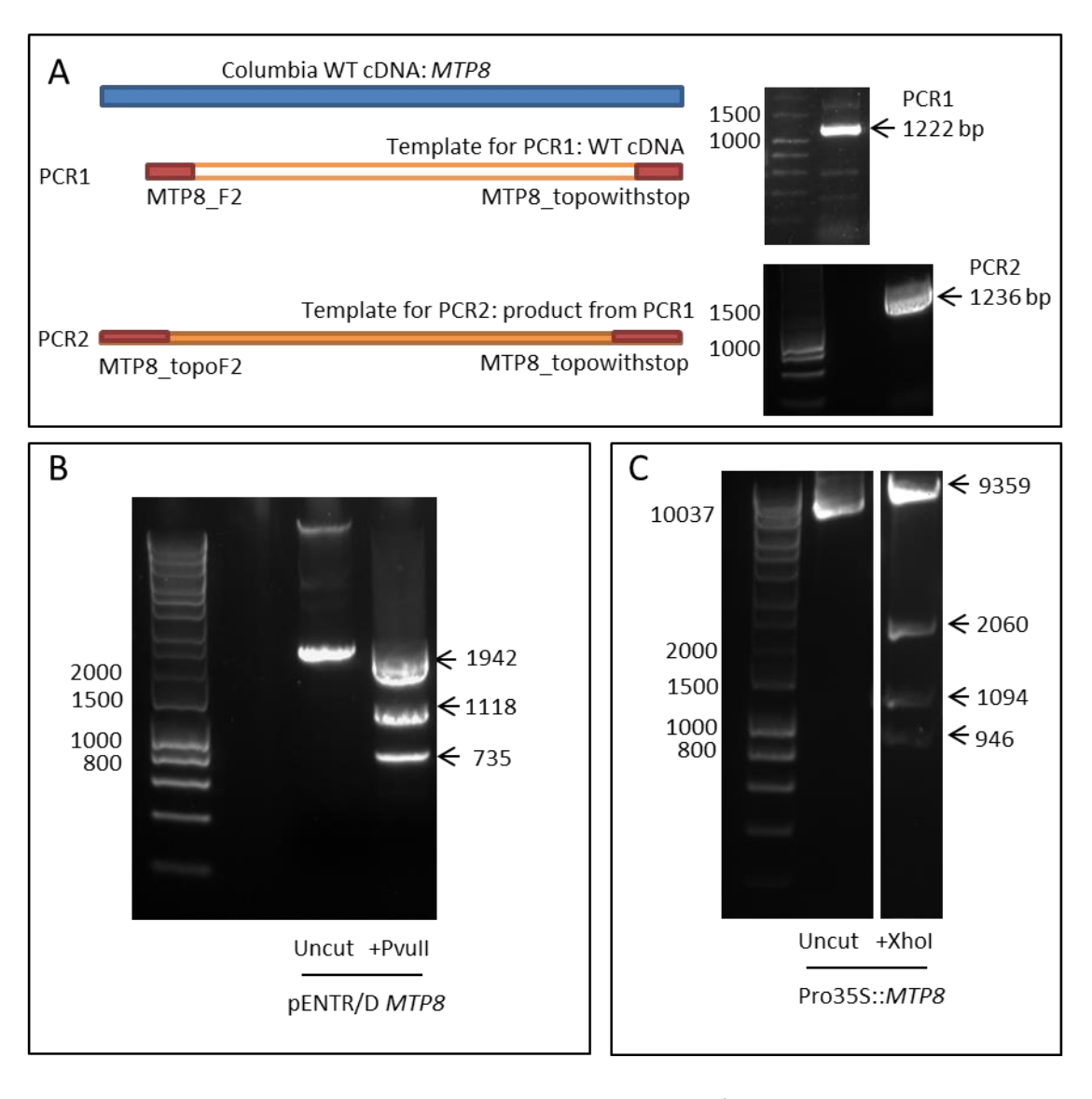


Figure 4.1. Cloning process to generate p35S::At MTP8 construct for plant expression.

A) Amplification strategy for *MTP8* from Columbia wild type (WT) cDNA. cDNA used as template for PCR 1, which amplifies full-length *MTP8* minus the first 11 bases at the N-terminus. PCR 1 is gel extracted and used as template for PCR 2, which adds remaining 11 bases at N-terminus plus CACC tag necessary for TOPO-isomerase cloning. B) Digestion analysis of pENTR/D-TOPO vector with *MTP8* using *Pvull* to give predicted fragment sizes of 1942, 1118, 735 base pairs (bp). Uncut vector run alongside on gel as a control. C) pENTR/D *MTP8* was recombined with pMDC32 destination vector to generate P35S::At *MTP8* construct. Digestion analysis of P35S::At *MTP8* construct with *Xhol* to give predicted fragment sizes of 9359, 2060, 1094 and 946 bp. Uncut vector run alongside on gel as a control. Predicted sizes are indicated on right of gel; molecular marker sizes are labelled on left.

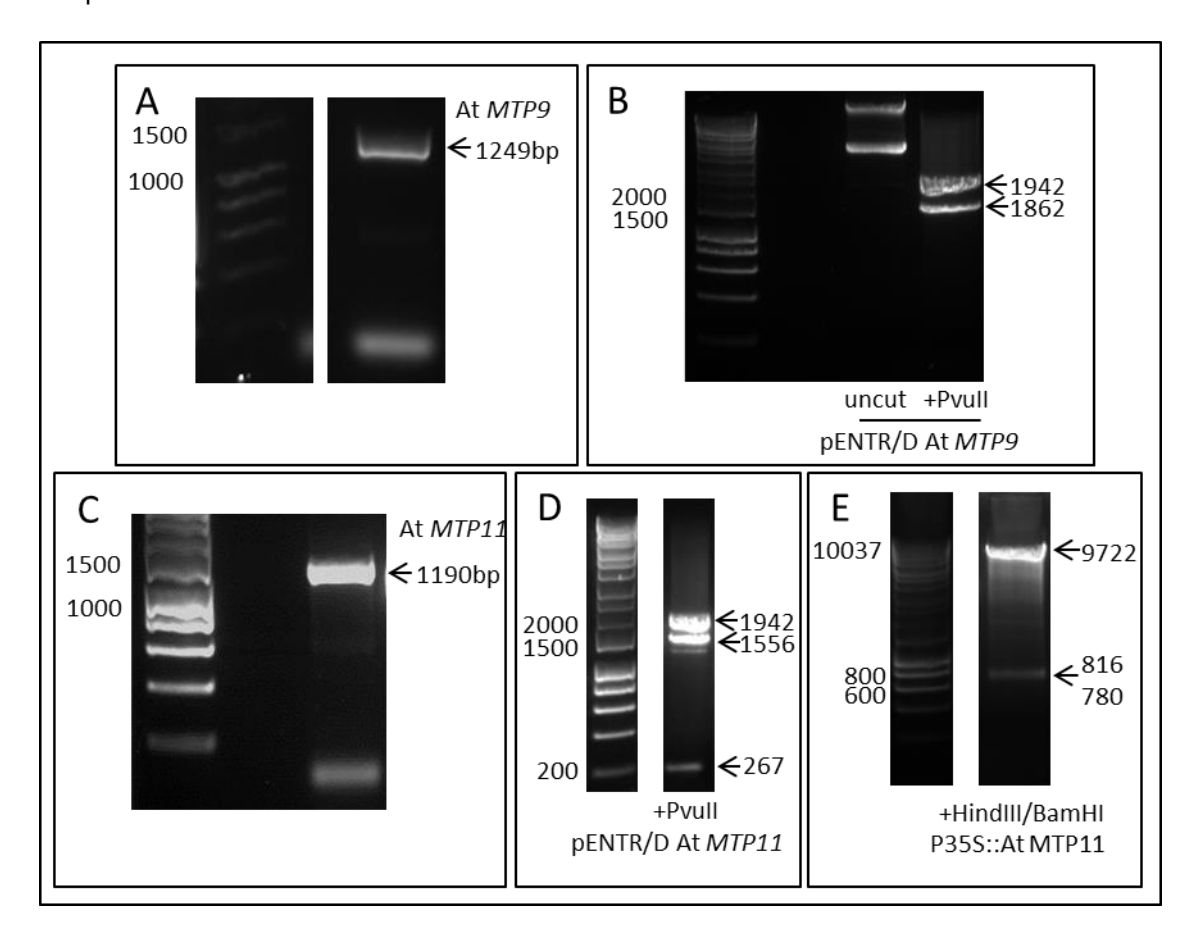


Figure 4.2. Cloning steps for At MTP9 and MTP11.

Amplification of full-length A) *MTP9* and C) *MTP11* coding sequences from Columbia-8 wild type cDNA, with CACC N-terminal tag for TOPO-isomerase cloning. These products were cloned into pENTR/D-TOPO vector. Digestion analysis of B) pENTR/D *MTP9* and D) pENTR/D *MTP11* with *Pvull* to give fragments of 1942 and 1862 (B) or 1942, 1556, 267 base pairs (bp) (D). *MTP9* was cloned in the wrong orientation and was not used for LR recombination. pENTR/D *MTP11* was recombined with pMDC32 to generate P35S::At *MTP11* construct. E) Digestion analysis of P35S::At *MTP11* with HindIII and BamHI to give fragments of 9722, 816 and 780 bp. A-E) Predicted sizes are indicated on right; molecular marker sizes are labelled on left of gel.

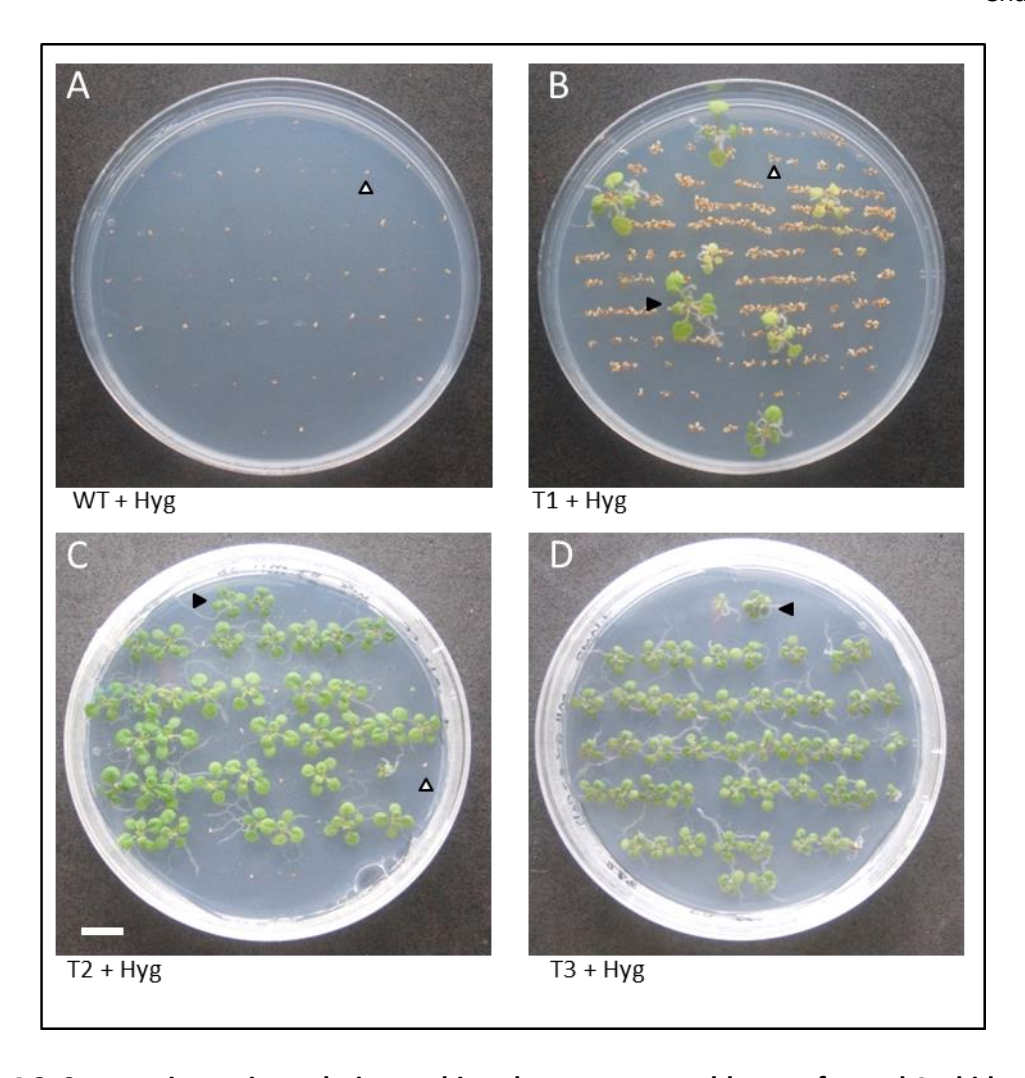
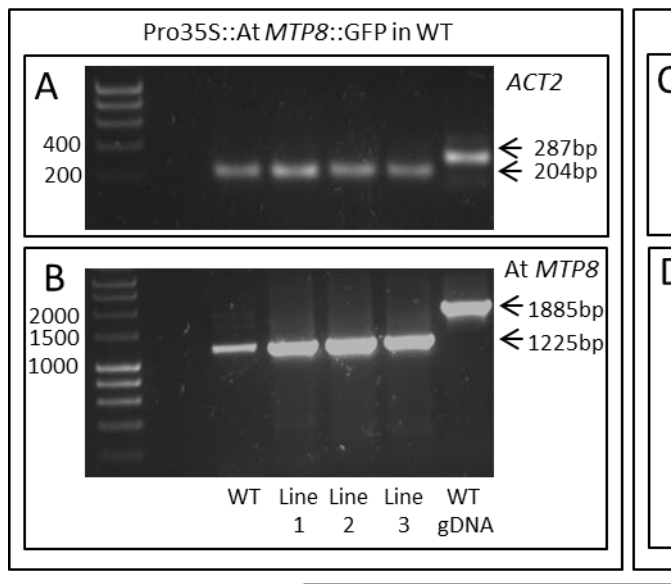
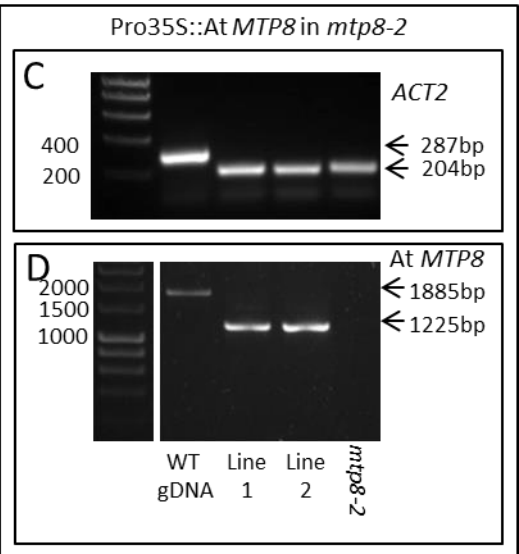


Figure 4.3. Segregation ratio analysis to achieve homozygous stably transformed Arabidopsis seedlings at T3 generation, using p35S::At MTP8 in Columbia-8 wild type as an example.

WT Arabidopsis transformed with p35S::At MTP8 constructs are tolerant to hygromycin, but wild type (WT) plants are sensitive and do not survive (A). B) T1 generation seeds are screened for resistance; resistant seedlings are transplanted to soil and allowed to self-fertilise. C) The progeny, T2, should be 75% resistant if there is only one insertion in the genome; in this example, 13/50 seedlings were not resistant to hygromycin, giving a segregation ratio of 74 %. Resistant seedlings were transplanted to soil and allowed to self-fertilise. D) T3 progeny were screened for 100% resistance to hygromycin; this example shows 100% resistance, indicating it is homozygous for the insert. White arrow, non-transformed seedling is sensitive to hygromycin and dies during selection. Black arrow, transformed seedling grows successfully on hygromycin.





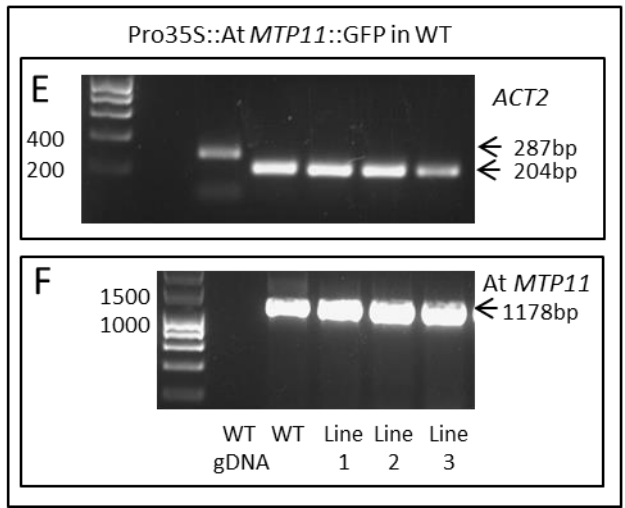
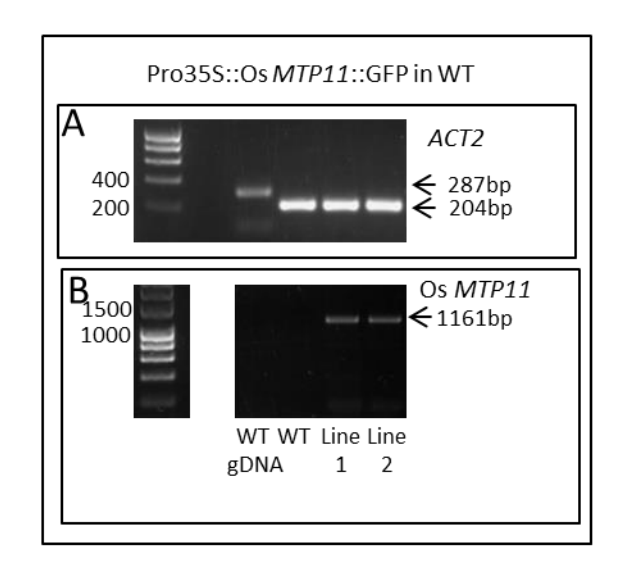


Figure 4.4. Confirmation of transgenic Arabidopsis lines transformed with At MTP8 and At MTP11.

Confirmation at the RNA level of 2-3 independent homozygous transformed plants for each transgenic line, A-B) P35S::At*MTP8*::GFP in WT, C-D) P35S::At*MTP8* in *mtp8-2* and E-F) P35S::At*MTP11*::GFP in WT, compared to wild type (WT) or *mtp8-2* cDNA and WT gDNA. A, C, E) *Actin2* primers amplify products of 287 base pairs (bp) from gDNA and 204 bp from cDNA, indicating cDNA is of good quality with no gDNA contamination. B+D) At *MTP8* primers amplify products of 1885 bp from gDNA and 1225 from cDNA; 30 cycles were used for semi-quantitative PCR. F) At *MTP11* primers amplify product of 1178 bp from cDNA; 30 cycles were used for semi-quantitative PCR.



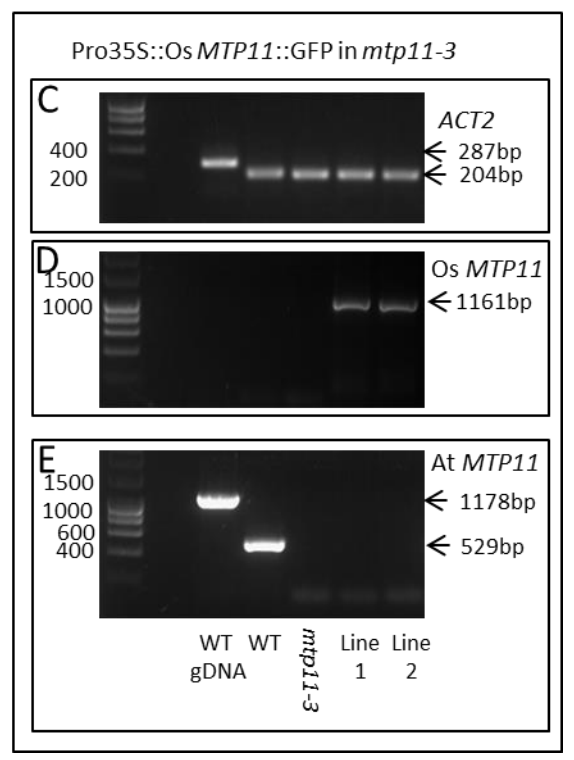


Figure 4.5 Confirmation of transgenic Arabidopsis lines transformed with Os MTP11::GFP.

Confirmation at the RNA level of 2-3 independent homozygous transformed plants for each transgenic line, P35S::OsMTP11::GFP A-B) in WT and C-D) in *mtp11-3*, compared to wild type (WT) cDNA and gDNA. A, C) *Actin2* primers amplify products of 287 base pairs (bp) from gDNA and 204 bp from cDNA, indicating cDNA is of good quality with no gDNA contamination. B+D) Os *MTP11* primers amplify products of 1161 bp from transformed cDNA; no product is amplified from non-transformed lines. F) At *MTP11* primers amplify product of 1178 bp from gDNA and 529 bp from cDNA; no product is amplified from lines in the *mtp11-3* mutant background.

Chapter 4

overexpressing lines remain unaffected until relatively high levels of Mn, under both Ca regimes (Figure 4.6). Overexpressing Line 3 showed low levels of silencing when grown on hygromycin; correspondingly, although still consistently larger than WT at all concentrations tested, this line only confers an intermediate level of hypertolerance to elevated Mn, that is only statistically significant under basal Ca (Figure 4.6A and C). Tagging At *MTP8* with GFP still confers hypertolerance relative to the WT under basal Ca conditions, but this does not appear to be to the same extent as the non-tagged version (Figure 4.7). Growth of tagged and non-tagged constructs on the same plates is needed, however, to directly compare the effect of tagging on function.

As confirmed in Chapter 3, both *mtp8* insertion mutants are sensitive to the pH-induced Fe deficiency generated by the modified Eroglu regime growth media (Eroglu, et al., 2016). Correspondingly, overexpression of *MTP8* also confers hypertolerance to these conditions: two overexpressing lines grow considerably better than WT under conditions of low Fe availability (Figure 4.8).

4.2.2.2 MTP8 expression rescues the Mn-sensitivity of mtp8-2

In addition to conferring hypertolerance to WT, expression of At *MTP8* restores Mn-tolerance in *mtp8-2*, comparative to that WT, under both Ca regimes (Figure 4.9). This suggests the Mn-sensitive phenotype is due to the absence of *MTP8*, rather than a background mutation. It was not possible to isolate *mtp8-2* expressing the tagged version of *MTP8*, due to high levels of silencing in this line.

4.2.2.3 Expression of Os MTP11 complements the Mn-dependent phenotype of mtp11-3

To investigate whether the Arabidopsis and rice MTP11 are functional homologs, or share a similar function across different species, P35S::OsMTP11 was expressed in *mtp11-3*. As shown in Figure 4.10, two independent lines were able to restore Mn tolerance of *mtp11-3*, comparative to WT, under both Ca regimes. The C-terminal GFP tag did not appear to influence function; the same result was observed when transformed with P35S::OsMTP11::GFP (Figure 4.11).

4.2.2.4 Mn hypertolerance is not conferred by overexpression of At MTP11 or Os MTP11

Overexpression of At *MTP11* has previously been shown to enhance Mn tolerance (Peiter, et al., 2007). However, none of the WT lines expressing At MTP11 isolated and tested here conferred significant levels of Mn hypertolerance compared to WT under low Ca; although 1 line gave consistently larger FW values, this was not significant (Figure 4.12). Similarly, expression of

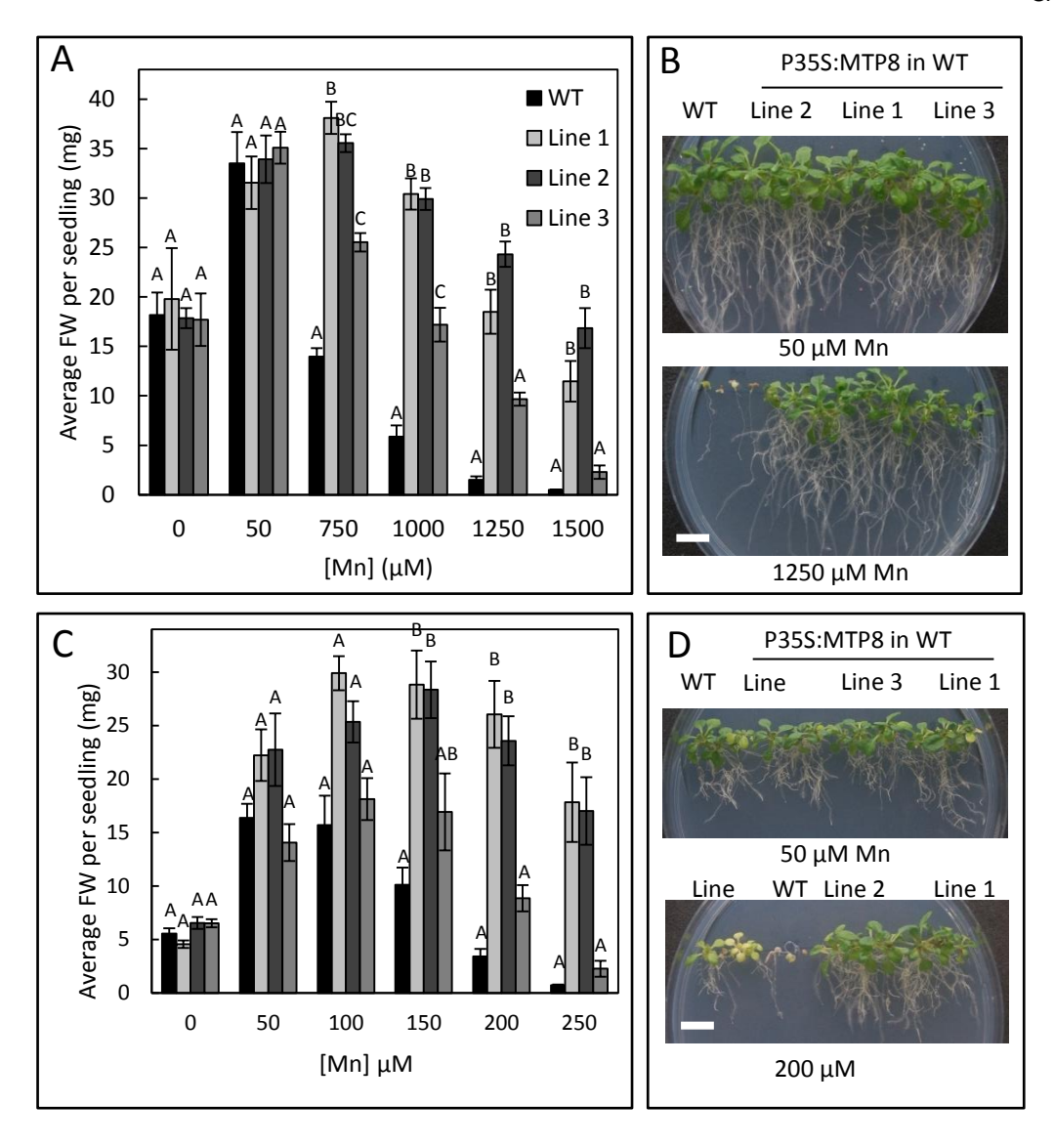


Figure 4.6. Overexpression of MTP8 confers hypertolerance in WT Arabidopsis.

Comparison of Col8 wild type (WT) and three independent Col8 lines expressing P35S::MTP8 after growth on ½ MS supplemented with a range of MnSO₄ concentrations for either A-B) 21 days supplied with 1.495 mM Ca or C-D) 24 days supplied with 100 μ M Ca. A+C) Data shows mean fresh weight (FW; mg) per seedling calculated for 5 or 6 plates (\pm SE) with four seedlings per genotype, per plate. A) As determined by 2-way ANOVA, there is a significant effect of genotype (F_{3, 120}= 70.64, p<0.001), [Mn] (F_{5, 120}= 97.21, p<0.001) and interaction of genotype and [Mn] (F_{15, 143} = 8.82, p<0.001) on FW. C) There is a significant effect of genotype (F_{3, 120}= 54.16, p<0.001), [Mn] (F_{5, 120}= 36.78, p<0.001) and interaction of genotype and [Mn] (F_{15, 143}= 4.00, p<0.001) on FW. Means not sharing a letter at a particular concentration are significantly different, according to Tukey post hoc test. B+D) Image displaying plant growth at different Mn concentrations. White bar = 1 cm.

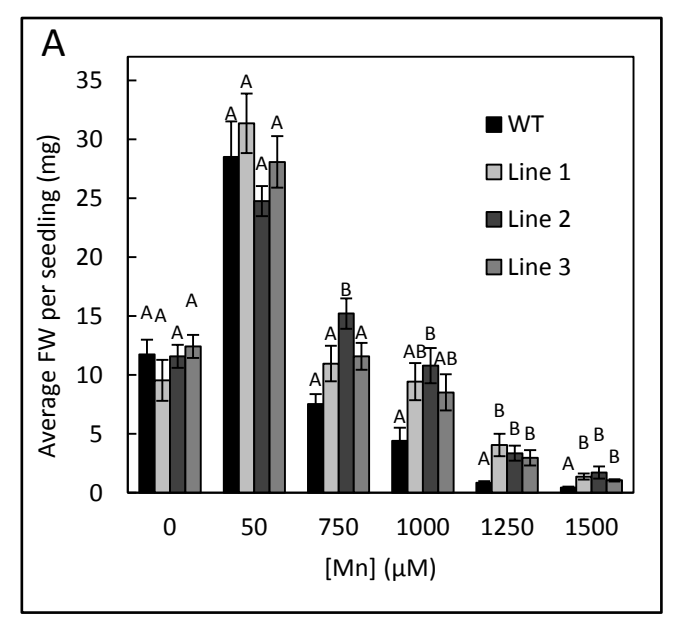
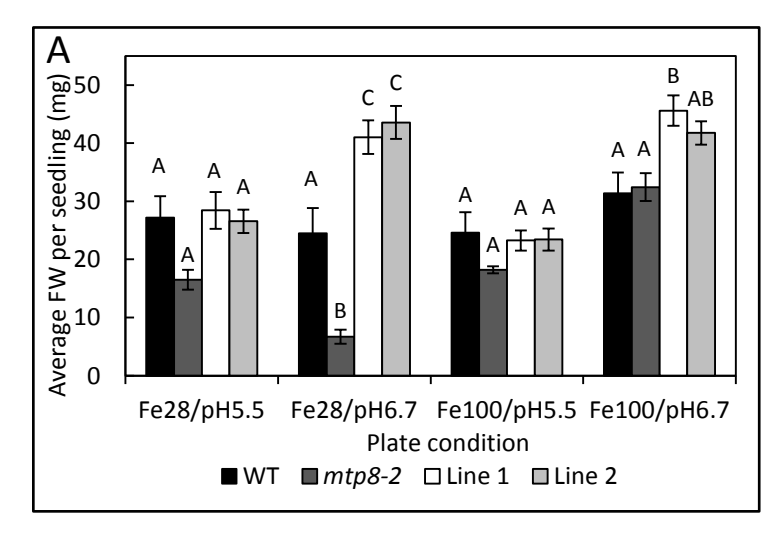




Figure 4.7. Overexpression of MTP8::GFP confers hypertolerance in WT Arabidopsis.

Comparison of Col8 wild type (WT) and three independent Col8 lines expressing P35S:MTP8:GFP after 21 days growth on ½ MS containing 1495 μ M Ca, supplemented with a range of Mn concentrations supplied as MnSO₄. A) Data shows mean FW (mg) per seedling calculated for 5 or 6 plates (\pm SE) with four seedlings per genotype, per plate. As determined by 2-way ANOVA, there is a significant effect of genotype ($F_{3, 112}$ = 25.46, p<0.001), [Mn] ($F_{5, 112}$ = 263.96, p<0.001) and interaction of genotype and [Mn] ($F_{15, 135}$ = 4.22, p<0.001) on FW. Means not sharing a letter at a particular concentration are significantly different, according to Tukey post hoc test. B) Image displaying plant growth on 50 and 1250 μ M Mn. White bar = 1 cm.



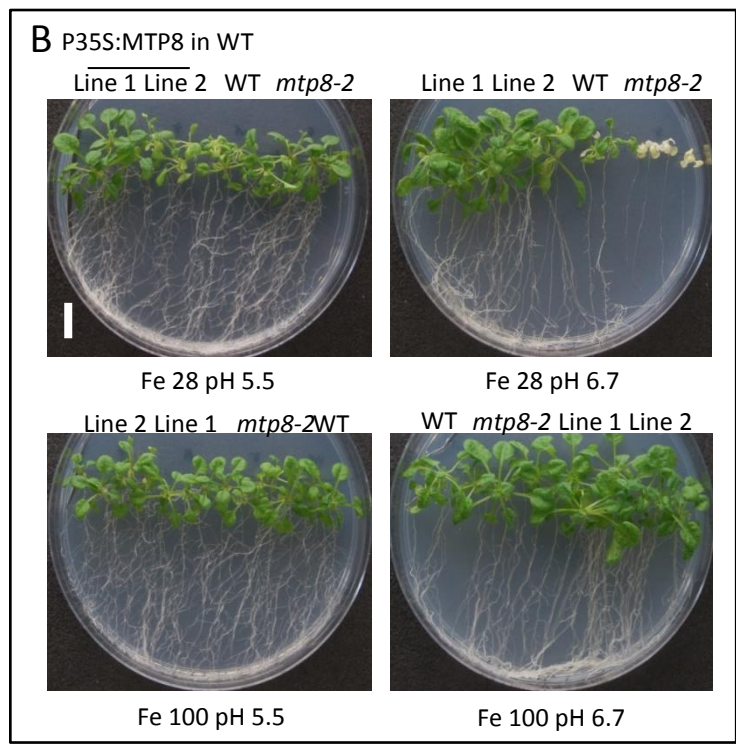


Figure 4.8. Overexpression of At MTP8 confers hypertolerance to low Fe induced by high pH conditions.

Comparison of wild type (WT), mtp8-2 and 2 WT lines overexpressing MTP8 after 23 days growth on ½ MS (modified Eroglu regime) supplemented with either 28 μ M or 100 μ M Fe (Fe 28 and Fe 100, respectively) supplied as FeNaEDTA, and buffered to pH 5.5 or 6.7 with NaOH. A) Data shows mean fresh weight (FW) (mg) per seedling calculated for 6 plates (\pm SE), with four seedlings per genotype, per plate. As determined by MANOVA, there is an interaction effect of genotype, Fe and pH on FW (F_{3, 95} = 3.42, p<0.05). Means which do not share a letter at a particular condition are significantly different, according to Tukey post hoc test. B) Image displaying plant growth across different conditions. White bar = 1 cm

Chapter 4

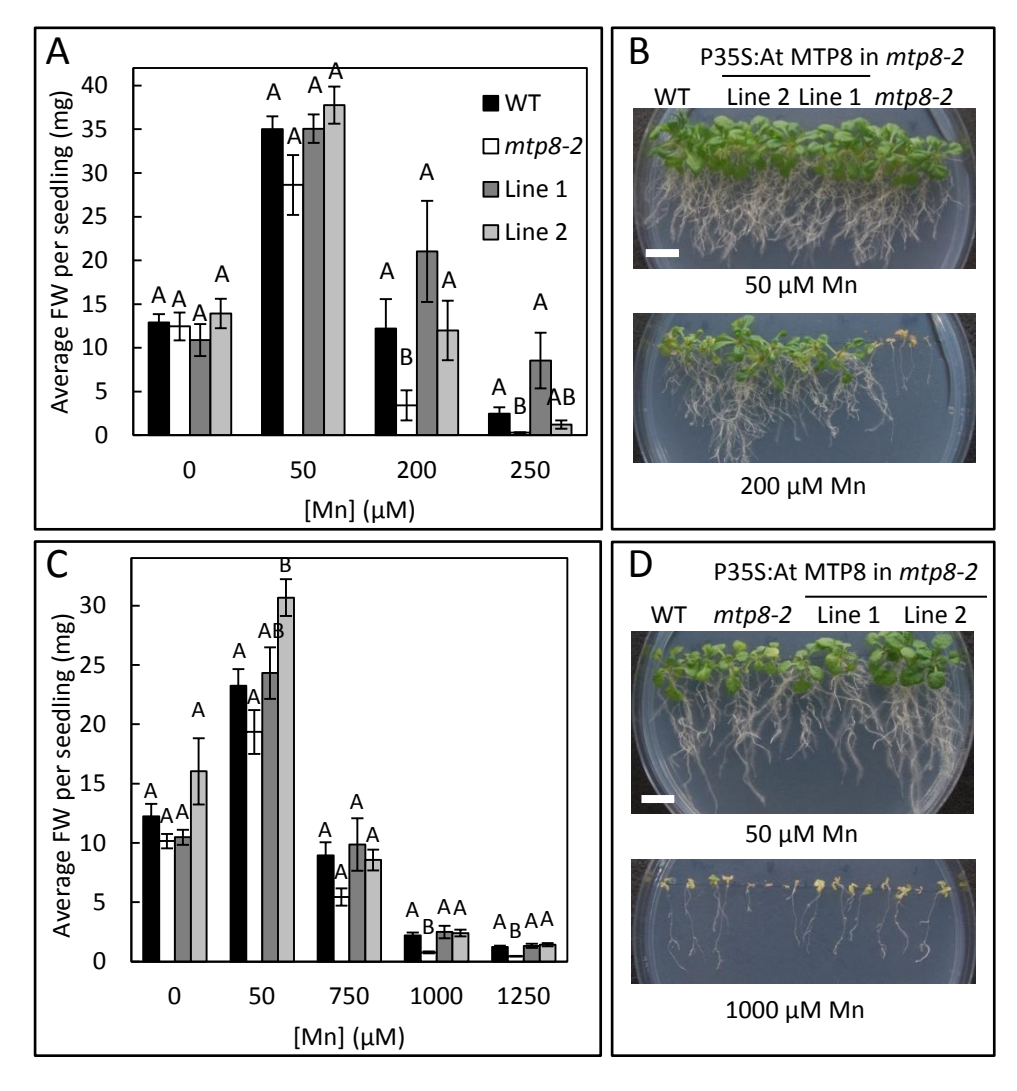


Figure 4.9. Expression of At MTP8 complements the Mn-sensitivity of mtp8-2.

Comparison of Columbia8 wild type (WT), mtp8-2 T-DNA insertion mutant and 2 independent mtp8-2 lines expressing At MTP8 when grown on ½ MS supplemented with a range of MnSO₄ concentrations for either A-B) 24 days, supplied with 100 μ M Ca, or C-D) 21 days, supplied with 1495 μ M Ca. A+C) Data shows mean FW (mg) per seedling calculated for 6 plates (\pm SE) with four seedlings per genotype, per plate. A) As determined by GLM, there is a significant effect of [Mn] (F_{3,80} = 109.69, p<0.001), genotype (F _{3,80} = 18.55, p<0.001) and interaction between [Mn] and genotype (F_{9,95} = 6.14; p<0.001) on FW. C) There is a significant effect of [Mn] (F_{4,88} = 268.65, p<0.001), genotype (F _{3,88} = 31.32, p<0.001) and interaction between [Mn] and genotype (F_{12,107} = 3.68; p<0.001) on FW. Means not sharing a letter at a particular concentration are significantly different, according to Tukey post hoc test. B+D) Image displaying plant growth across different Mn conditions. White bar = 1 cm.

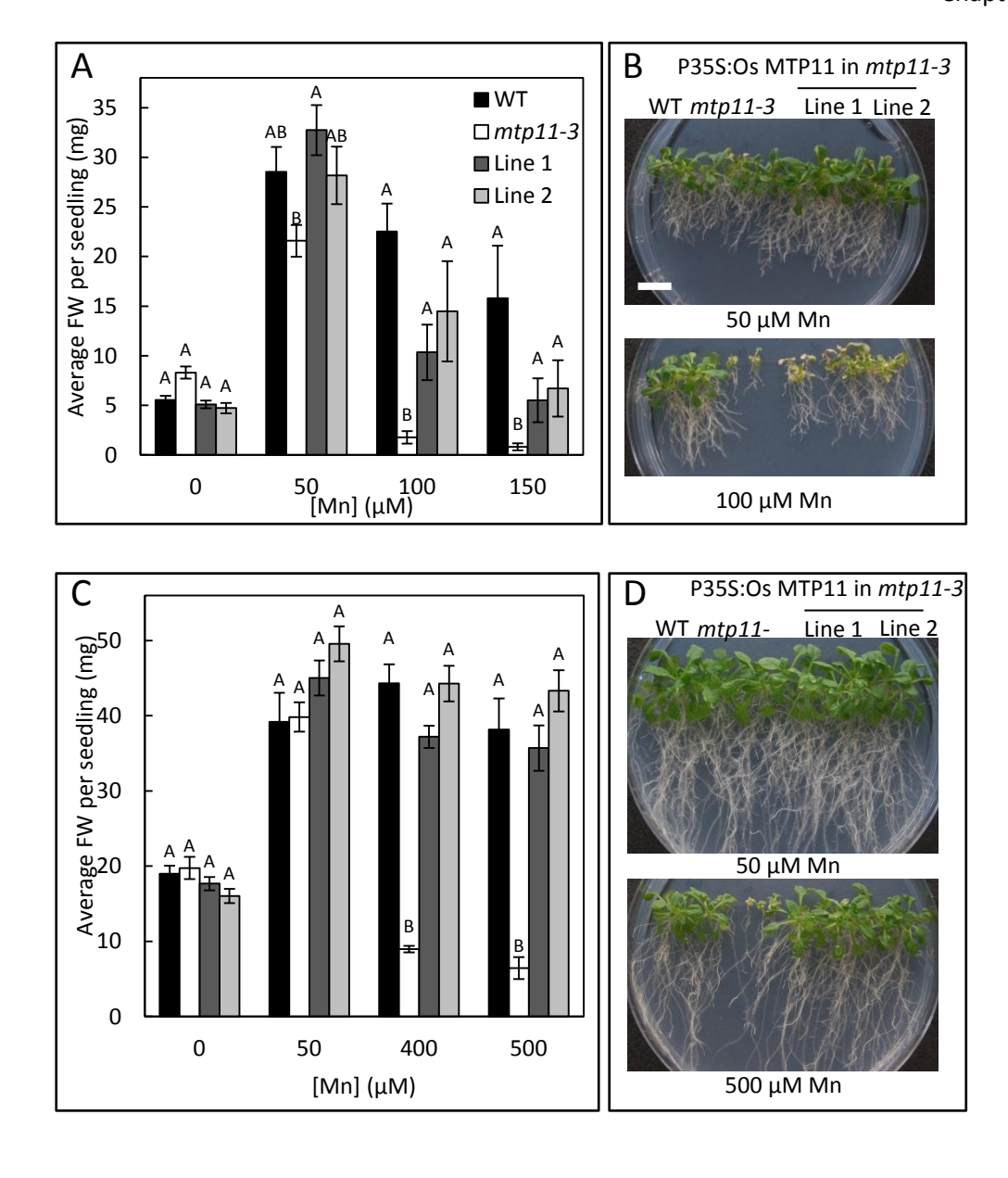


Figure 4.10. Expression of Os MTP11 rescues the Mn-sensitivity of mtp11-3.

Comparison of Columbia 0 wild type (WT), mtp11-3 and 2 independent mtp11-3 lines expressing Os MTP11 when grown on ½ MS supplied with a range of MnSO₄ concentrations for A-B) 24 days, supplied with 100 μ M Ca or C-D) 21 days, supplied with 1495 μ M Ca. A+C) Data shows mean fresh weight (FW; mg) per seedling calculated for 5 or 6 plates (\pm SE) with four seedlings per genotype, per plate. A) As determined by GLM, there is a significant effect of genotype (F_{3, 76} = 60.35, p<0.001), [Mn] (F_{3, 76} = 90.68, p<0.001) and interaction of genotype and [Mn] (F_{9, 91} = 18.78, p<0.001) on FW. C) There is a significant effect of genotype (F_{3, 76} = 11.34, p<0.001), [Mn] (F_{4, 76} = 60.18, p<0.001) and interaction of genotype and [Mn] (F_{9, 91} = 3.74, p<0.001) on FW. Means not sharing a letter at a particular concentration are significantly different, according to Tukey post hoc test. B+D) Image displaying plant growth across different Mn concentrations. White bar = 1 cm.

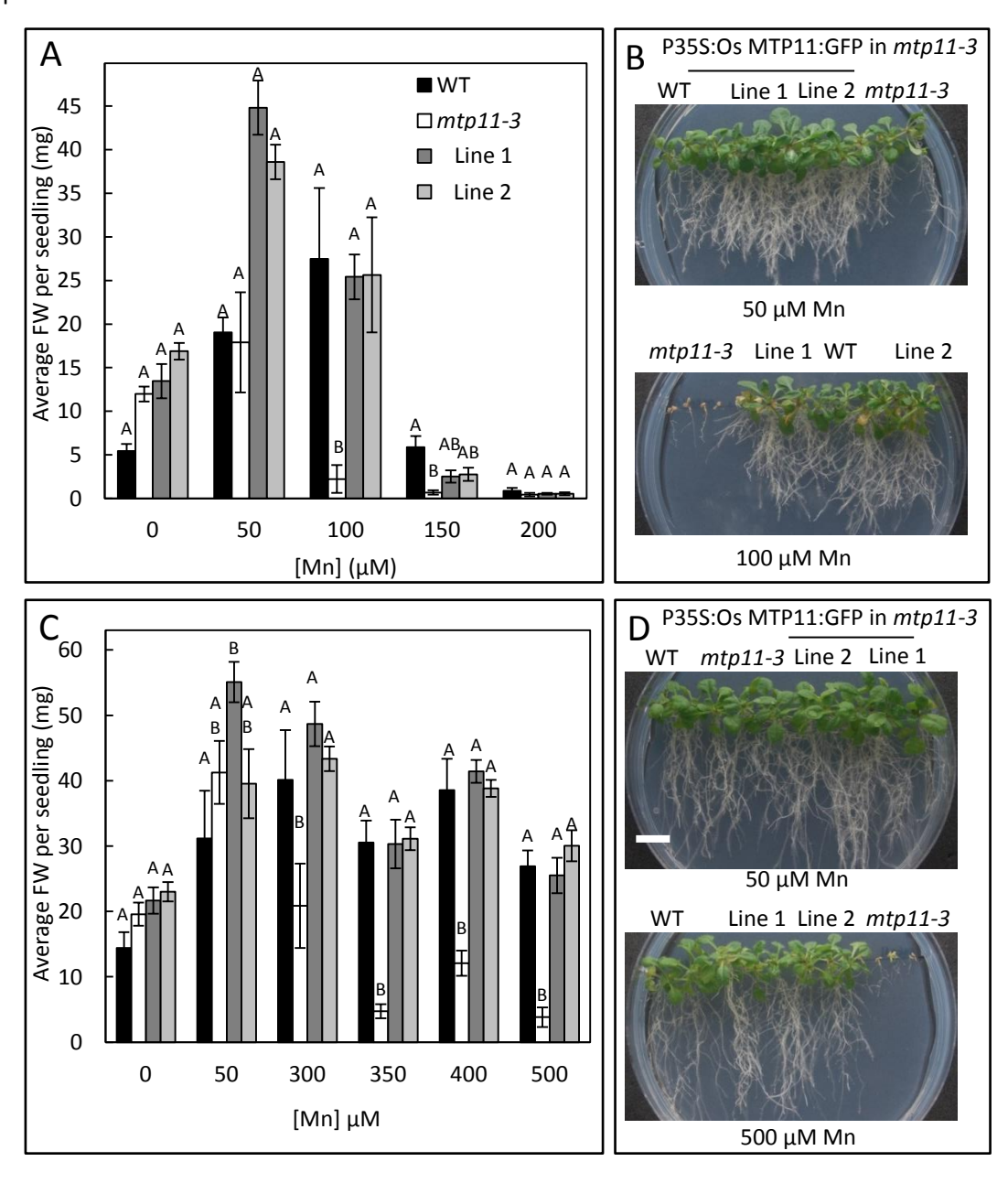


Figure 4.11. Expression of Os MTP11::GFP rescues the Mn-sensitivity of mtp11-3.

Comparison of Columbia 0 wild type (WT), mtp11-3 and 2 independent mtp11-3 lines expressing Os MTP11::GFP when grown on ½ MS supplied with a range of MnSO₄ concentrations for A-B) 24 days, supplied with 100 μ M Ca or C-D) 21 days, supplied with 1495 μ M Ca. A+C) Data shows mean fresh weight (FW; mg) per seedling calculated for 5 or 6 plates (\pm SE) with four seedlings per genotype, per plate. A) As determined by GLM, there is a significant effect of genotype (F_{3, 87} = 21.67, p<0.001), [Mn] (F_{4, 87} = 141.36, p<0.001) and interaction of genotype and [Mn] (F_{12, 106} = 7.15, p<0.001) on FW. C) There is a significant effect of genotype (F_{3, 116} = 33.31, p<0.001), [Mn] (F_{5, 116} = 24.11, p<0.001) and interaction of genotype and [Mn] (F_{15, 139} = 4.15, p<0.001) on FW. Means not sharing a letter at a particular concentration are significantly different, according to Tukey post hoc test. B+D) Image displaying plant growth on different Mn concentrations. White bar = 1 cm.

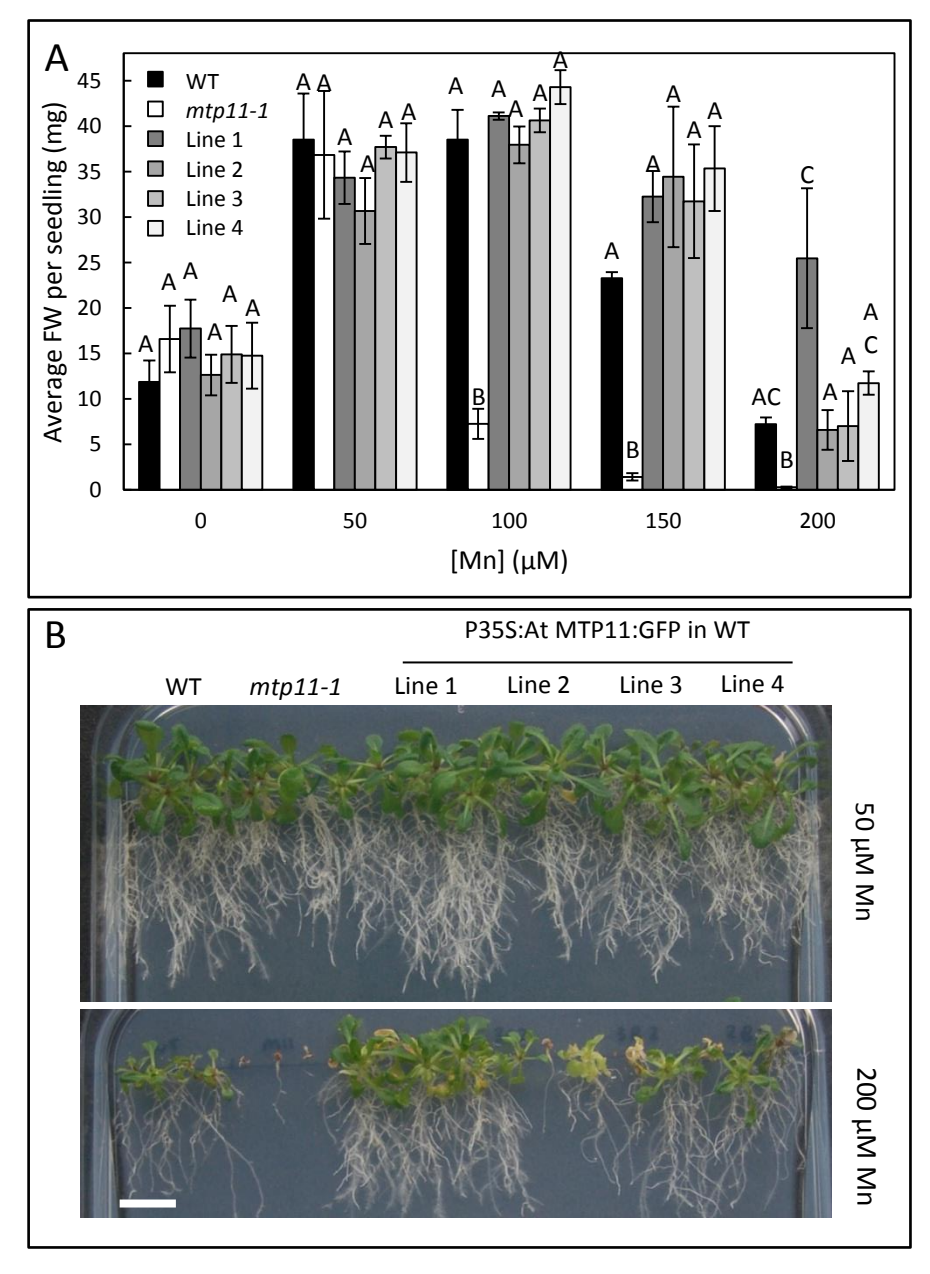


Figure 4.12. Over-expression of At MTP11 in Columbia-0 WT does not enhance Mn tolerance under low Ca regime.

Comparison of Col0 wild type (WT), mtp11-1 and 4 independent Col0 lines expressing P35S::At MTP11::GFP after 24 days growth on ½ MS containing 100 μ M Ca, supplemented with a range of Mn supplied as MnSO₄. A) Data shows mean fresh weight (FW; mg) per seedling calculated for 3 or 4 plates (\pm SE) with four seedlings per genotype, per plate. As determined by GLM, there is a significant effect of genotype (F_{5, 66} = 67.28, p<0.001) and [Mn] (F_{4, 66} = 79.04, p<0.001) and interaction effect between genotype and [Mn] (F_{20, 95} = 14.31, p<0.001) on FW. Means not sharing a letter at a particular concentration are significantly different, according to Tukey post hoc test. B) Image displaying plant growth on 50 and 200 μ M Mn. White bar = 1 cm.

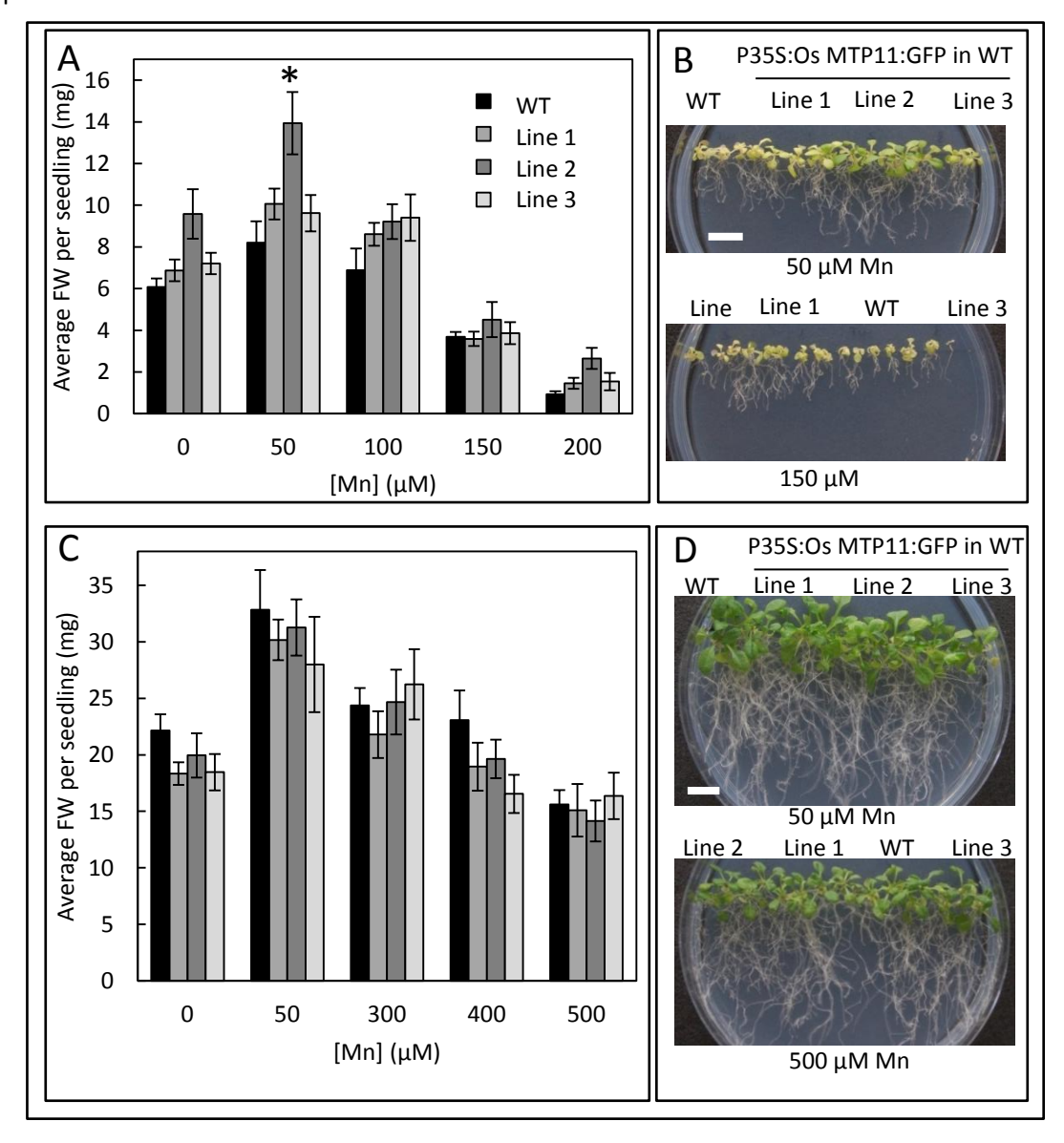


Figure 4.13. Over-expression of Os MTP11 in Columbia-0 WT does not enhance Mn tolerance.

Comparison of Columbia 0 wild type (WT) and three independent Col0 lines expressing P35S::OsMTP11::GFP after growth on ½ MS supplemented with a range of MnSO₄ concentrations, for either A-B) 24 days supplied with 100 μ M Mn or C-D) 21 days supplied with 1495 μ M Mn. A+C) Data shows mean FW (mg) per seedling calculated for 6 plates (\pm SE) with four seedlings per genotype, per plate. A) As determined by GLM, there is a significant effect of genotype (F_{3, 100} = 11.75, p<0.001) and [Mn] (F_{4, 100} = 86.93, p<0.001) on FW, but no significant interaction between genotype and [Mn] (F_{12, 119} = 1.46, p=0.152) on FW. C) There is a significant effect of [Mn] on FW (F_{4, 96} = 25.13, p<0.001) but no significant effect of genotype (F_{4, 96} = 1.38, p=0.253) or interaction effect between genotype and [Mn] (F_{12, 115} = 0.52, p=0.894) on FW. *, significantly different to WT, according to Tukey post hoc test. B+D) Image displaying plant growth under different conditions. White bar = 1 cm.

Os MTP11 in WT does not confer hypertolerance to Mn under either Ca regime (Figure 4.13). It is noted that the FW values for the experiment in Figure 4.13A are particularly low at 50 μ M Mn; it is possible this experiment was exposed to higher than normal light conditions and should thus be repeated to draw true conclusions for this construct.

4.2.3 Determining subcellular localisation with stable and transient expression in Arabidopsis and tobacco

4.2.3.1 At MTP8 is a tonoplast localised protein in planta

Stable expression of P35S::MTP8::GFP in Arabidopsis indicates At MTP8 targets the tonoplast (Figure 4.14). As it can be difficult to differentiate between plasma membrane and tonoplast signals, efforts were made to distinguish the true localisation of At MTP8. Staining of the root tip cell wall with propodium iodide indicates At MTP8 expression is clearly enclosed within the cell, rather than running around the cell perimeter. Additionally it is possible to see multiple vacuoles in the developing vacuolated cells of the root tip (Figure 4.14A-C). The tonoplast localisation is also apparent in shoots: Figure 4.14D shows At MTP8 expression is distinctly enclosed within adjacent epithelial cells, with vacuole-like invaginations in guard cells. This is demonstrated in the 3D guard cell images of Figures 4.14E and F: At MTP8 expression clearly does not enclose the chloroplasts in the way the plasma membrane would, and additionally shows the formation of transvacuolar strands (TVSs), as indicated. Figure 4.15 demonstrates At MTP8 signal forming multiple TVSs in a series of time-lapse images, when expressed transiently in tobacco.

A benefit of expression in tobacco is the use of co-expressed organelle markers with relative ease. As shown in Figure 4.16A-C, At MTP8 expression is distinct from that of TGN-marker ST, the punctate signal of which is generally not enclosed within the membrane of At MTP8. Additionally, co-expression with plasma membrane marker LT16b suggests the At MTP8 tonoplast signal is enclosed within the plasma membrane, rather than displaying colocalisation.

Taken together, these findings indicate At MTP8 targets the vacuolar tonoplast in planta.

4.2.3.2 At MTP10, At MTP11 and Os MTP11 localise to the Golgi

The expression pattern of At MTP10, At MTP11 and Os MTP11 are very different to At MTP8, with punctate fluorescence observed when stably expressed in Arabidopsis. This punctate localisation has been shown for expression in both the root tip and the shoots; this is shown to be clearly distinct from chloroplast autofluorescence in the shoots, where possible (Figures 4.17A-C, 4.19 and 4.20). Punctate expression can suggest targeting to the ER, PVC or different parts of the

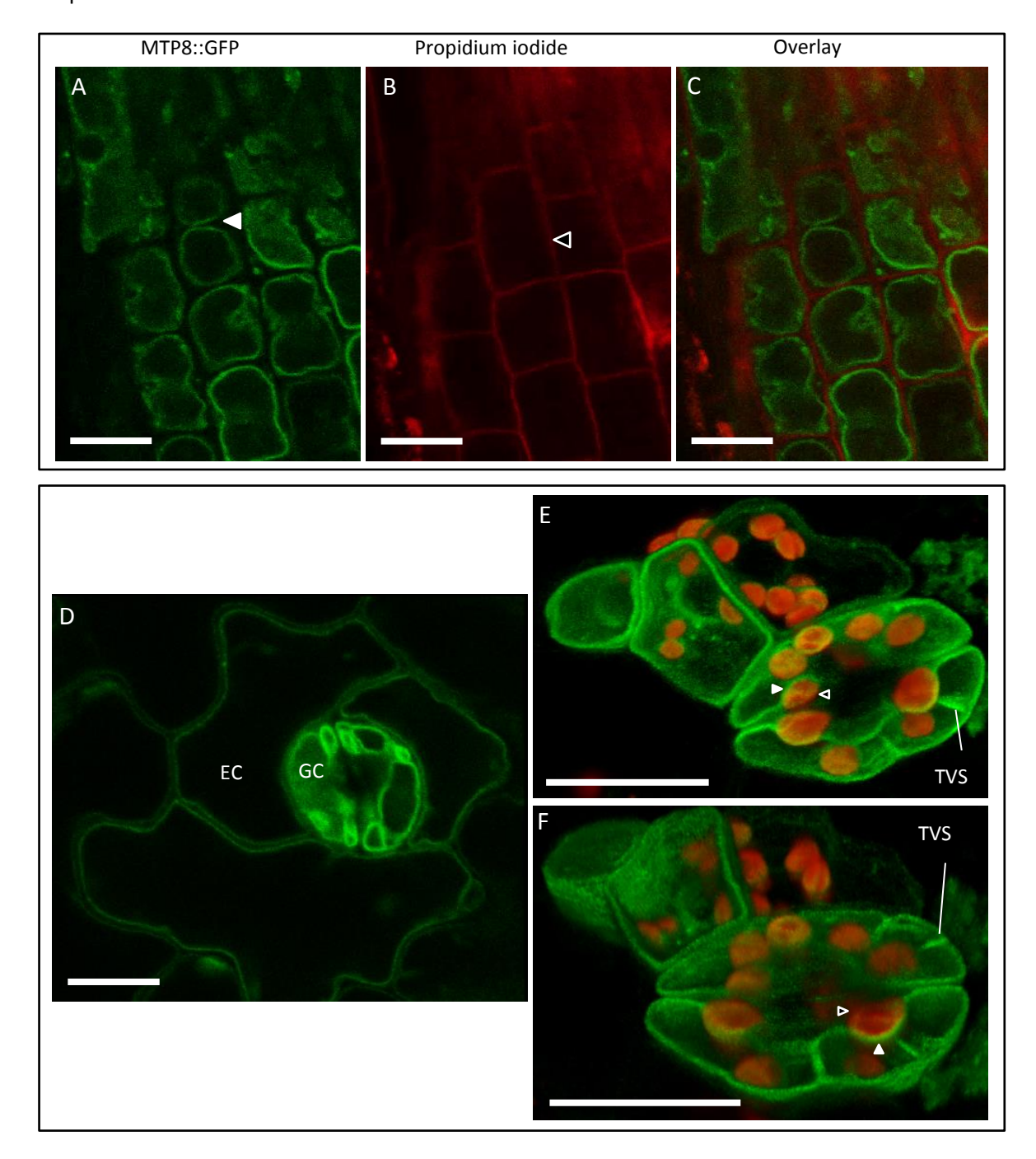


Figure 4.14. At MTP8 localises to the tonoplast in stably transformed Arabidopsis.

Stable expression of P35S::MTP8::GFP in 7 day old WT Arabidopsis seedlings. A) MTP8::GFP and B) cell walls stained with propidium iodide in root elongation zone cells; C) merged image of A and B. Filled arrow, double vacuole in root cell; unfilled arrow, stained cell wall. D) MTP8::GFP in cotyledon epidermal cells and guard cells. GC, guard cell; EC, epidermal cell. E+F) Merged 3D Z-stack of guard cell with chloroplast autofluorescence (red signal; filled arrow) and MTP8::GFP (green; unfilled arrow) showing MTP8 signal does not enclose the chloroplast and is reminiscent of tonoplast localisation. TVS, transvacuolar strand. White scale bar = $10 \mu M$.

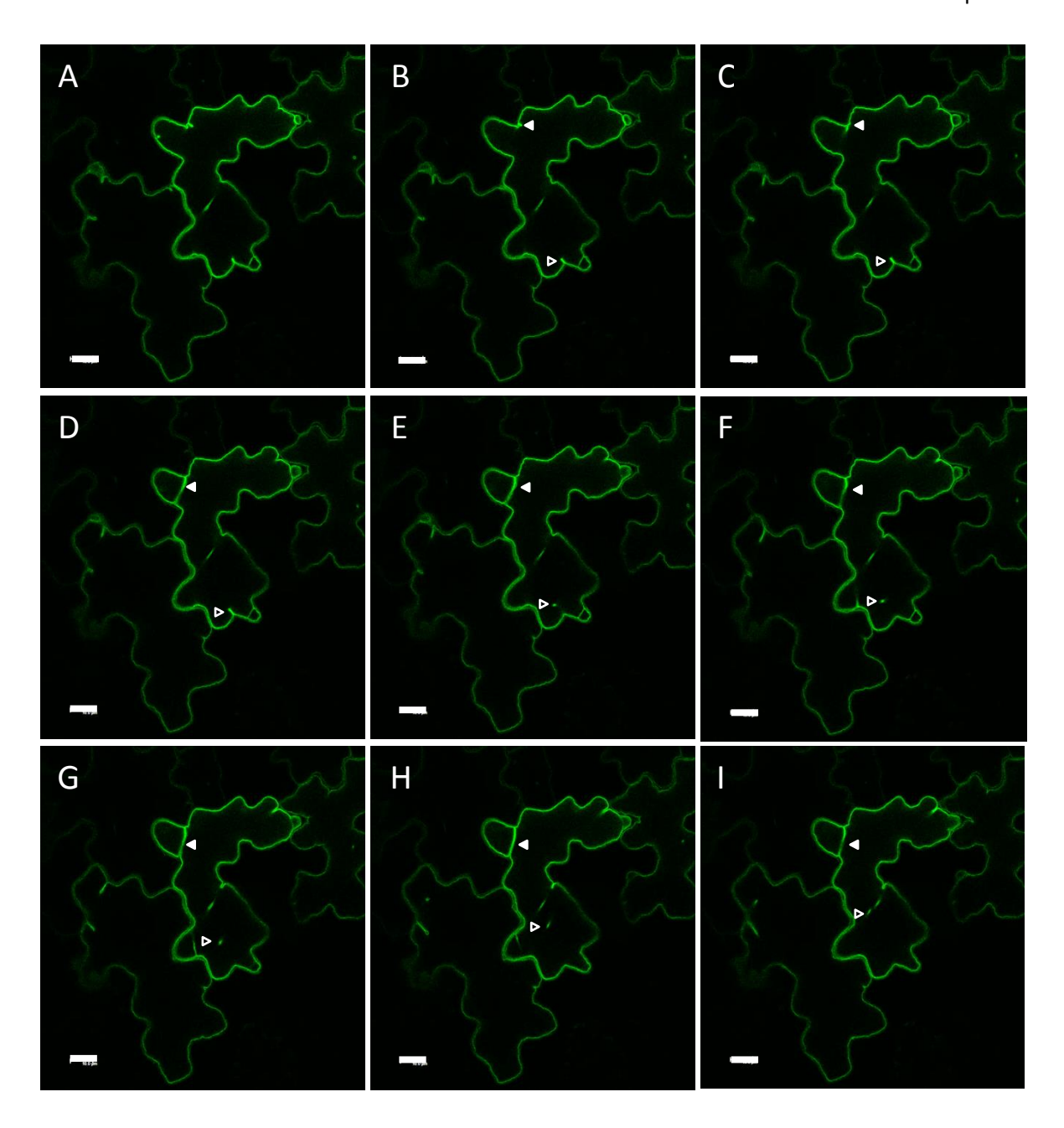


Figure 4.15. Time-lapse of MTP8::GFP forming trans-vacuolar strands in tobacco cells.

A-I) Transient expression of P35S::MTP8::GFP in tobacco epithelial cells. Time lapse of MTP8::GFP producing transvacuolar strands (TVS) and invaginations. Filled arrow, formation of TVS #1; unfilled arrow, formation of TVS #2 and movement across cell. Intervals between images, 2.8 seconds. White scale bar = $10 \mu M$.

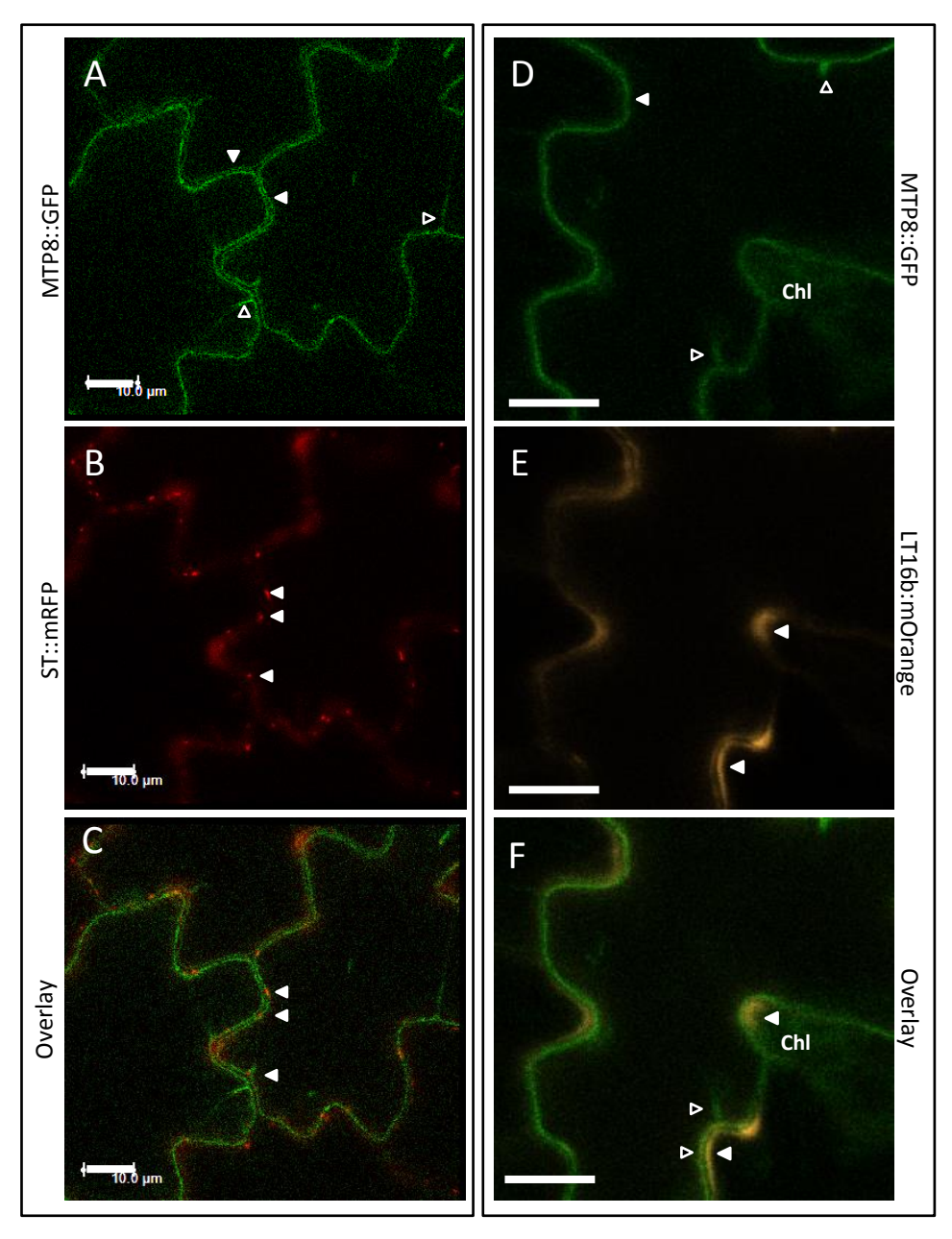


Figure 4.16. Co-expression of At MTP8 with ST::RFP and LT16b::mOrange2 in tobacco.

Transient expression of P35S::MTP8::GFP in tobacco epithelial cells. A) and D) Tonoplast-like signal of MTP8::GFP (green signal; filled arrow, tonoplast; empty arrow, formation of transvacuolar strands; chl, chlorophyll autofluorescence). B) Punctate signal of Golgi marker ST::RFP (red signal; filled arrow, examples of punctate signal); C) merge of A and B (filled arrow, chloroplast autofluorescence is not enclosed by MTP8 signal). D) Plasma membrane marker LTI6b::mOrange2 (filled arrow, example of plasma membrane) F) merge of D and E (filled arrow, plasma membrane; unfilled arrow, tonoplast). White scale bar = $10 \mu M$.

Golgi, the latter two of which have been suggested for At MTP11 (Delhaize, et al., 2007; Peiter, et al., 2007). Targeting to the ER was ruled out as the 'web-like' pattern of expression reminiscent of ER was not observed for either protein. Each protein is shown to move around the cell similarly to the Golgi in a series of time-lapse images, but this could also be indicative of the PVC (Figure 4.18D-F; Figure 4.19 G-I, Figure 4.20D-F).

Each protein was transiently co-expressed in tobacco with TGN marker, ST:RFP. While MTP10 (Figure 4.19D-I) and Os MTP11 (Figure 4.20G-I) both show areas of clear overlap with ST, indicated by the combined yellow signal in the overlay images, At MTP11 did not show full overlap with ST. Instead, the punctate signal of At MTP11 was generally adjacent to ST and moved around the cell at the same rate (Figure 4.18A-F). To investigate further, At MTP11 was tagged with mRFP and co-expressed with markers of the cis-Golgi and PVC (ManI::GFP and VSR2::GFP; Shen, et al., 2013). Unfortunately no signal was detected for the PVC marker when expressed in tobacco. However, strong levels of overlap are observed for At MTP11::mRFP with ManI::GFP (Figure 18H-J). Taken together, these findings suggest At MTP10 and Os MTP11 target the trans-Golgi, while At MTP11 targets the cis-Golgi.

4.3 Discussion

4.3.1 Overexpression of At MTP8 confers marked tolerance to Mn via vacuolar sequestration

Overexpression of At MTP8 enhances Mn tolerance, enabling uninhibited growth at higher Mn concentrations than WT Arabidopsis. Tolerance is also enhanced under conditions of low Fe availability induced by high pH. Additionally, both stable expression in Arabidopsis and transient expression in tobacco carried out for this thesis work provides strong evidence that At MTP8 targets the tonoplast; this supports previous reports concluded from protoplast studies (Eroglu, et al., 2016). Taken together, these findings imply At MTP8 functions to alleviate Mn toxicity, by sequestering excess Mn into the vacuole. While expression of At MTP8 (Eroglu, et al., 2016) and related protein Cs MTP8 (Migocka, et al., 2014) are restricted mostly to the root under normal conditions, this study placed *MTP8* under control of 35S, a constitutive promoter that induces expression across the whole plant. As demonstrated by semi-quantitative PCR, At *MTP8* is expressed at higher levels in overexpressing lines than in the WT. It is likely that the WT becomes sensitive to Mn earlier than the transgenic lines because Mn detoxification mechanisms such as At MTP8 sequestration in the root are saturated, enabling excess Mn to become toxic in the root and

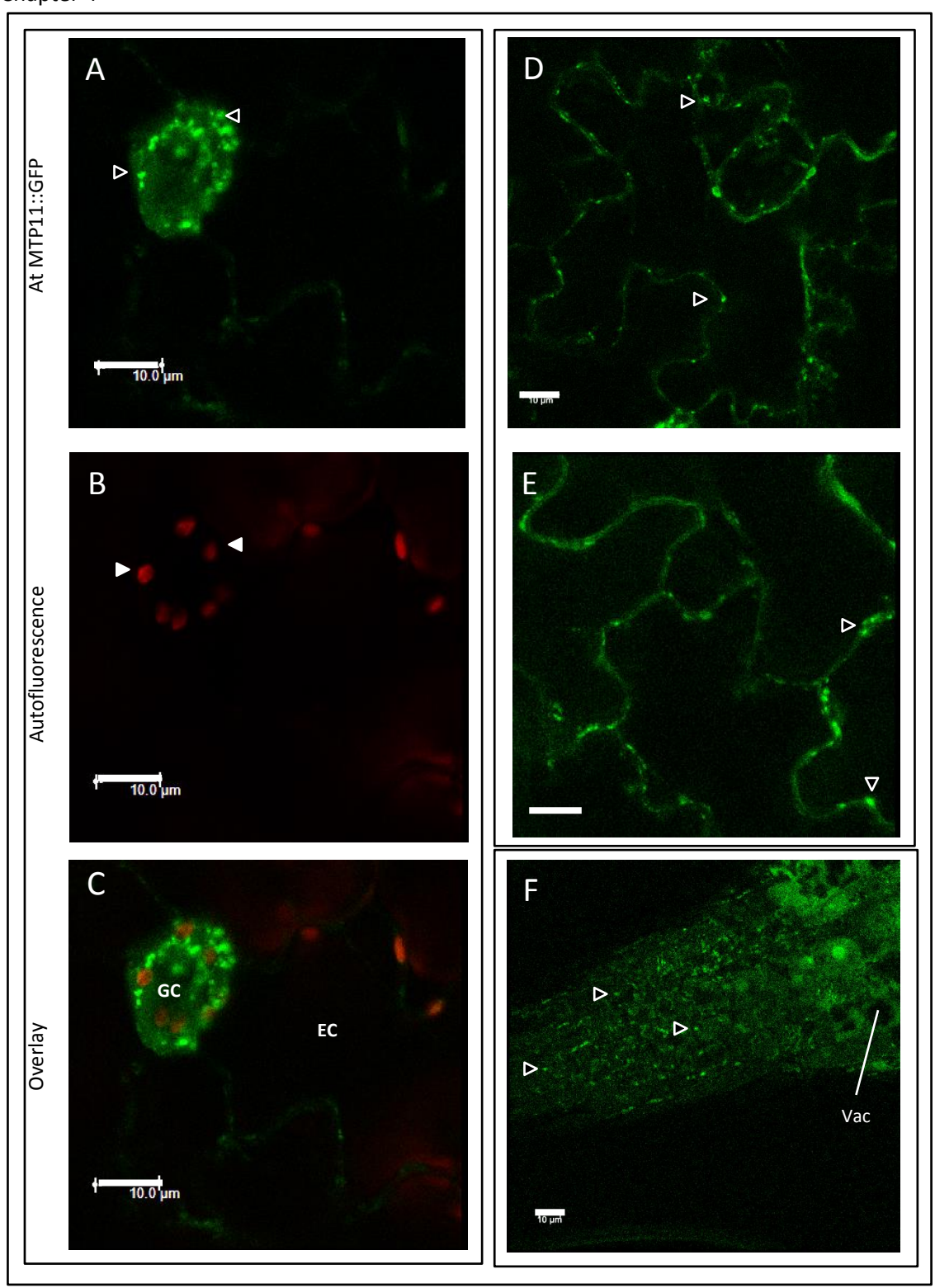


Figure 4.17. Punctate expression of At MTP11 in Arabidopsis.

Stable expression of P35S::AtMTP11::GFP in 7 days old Arabidopsis WT seedlings. A) MTP11::GFP displaying punctate expression (unfilled arrow) and B) chloroplast autofluorescence (filled arrow) in 7-day old Arabidopsis guard cells (GC) and neighbouring epithelial cells (EC); C) merged image of A and B. D-F) MTP11::GFP expression in Arabidopsis cotyledon epithelial cells (D-E) and root tip cells (F). Signal is distinct from developing vacuoles in root tips ('Vac'). Unfilled arrow, labelled examples of punctate expression of AtMTP11::GFP. White scale bar = $10 \mu M$.

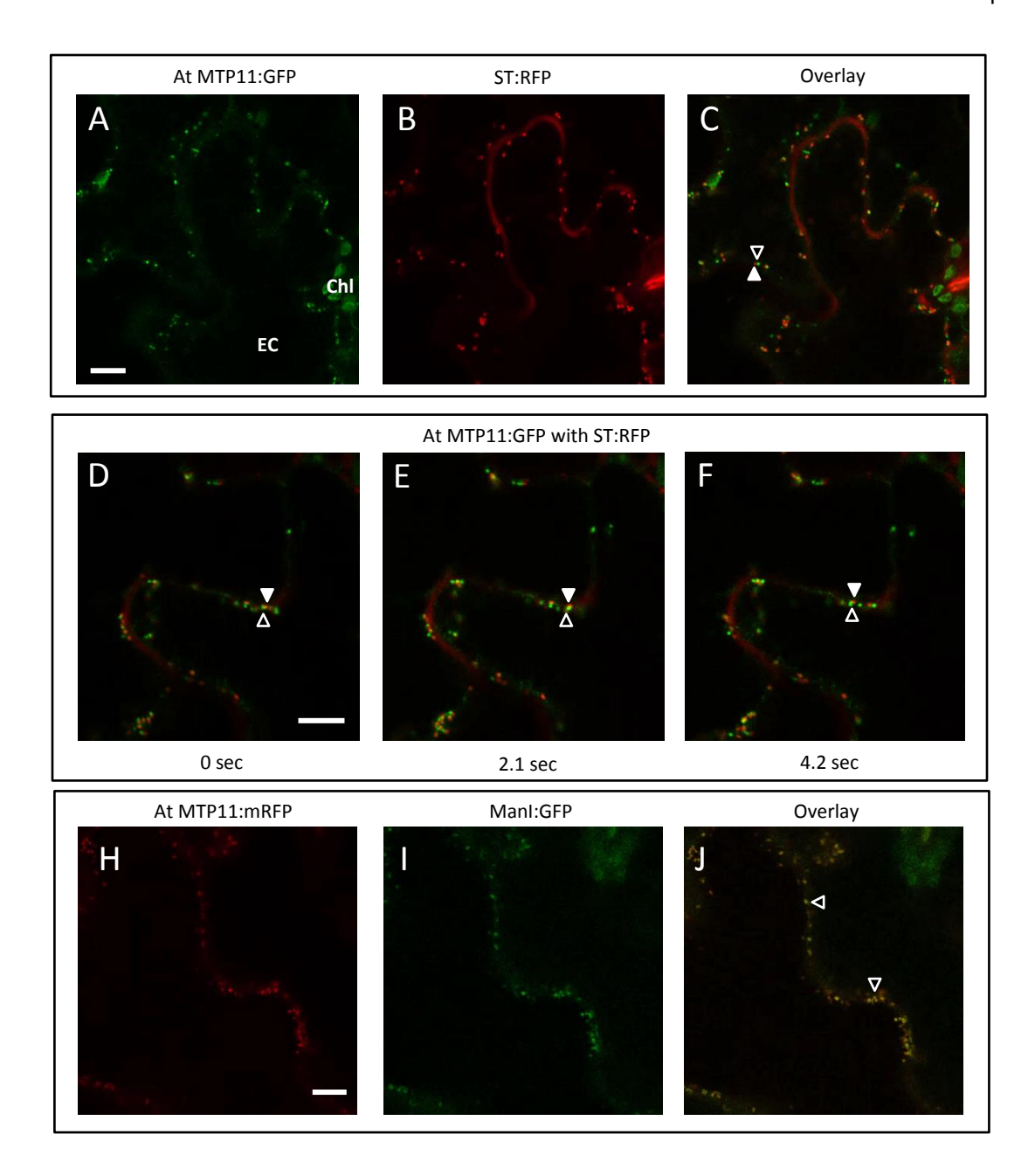


Figure 4.18. At MTP11 targets the cis-Golgi when transiently expressed in tobacco.

Transient expression of P35S::AtMTP11::GFP and P35S::AtMTP11::mRFP in tobacco epithelial cells. A-C) Partial overlap of MTP11:GFP (A, green signal; unfilled arrows) with TGN-marker sialyl transferase:RFP (B, ST:RFP; red signal, unfilled arrows); overlapping signal is yellow (C). EC, epithelial cell; chl, chlorophyll autofluorescence. D-F) MTP11:GFP (unfilled arrow) moves at same rate as ST:RFP (filled arrow) but does not fully overlap; timelapse video, 2.1 second intervals. Arrows track movement of specific Golgi signal around cell. H-J) Overlap of MTP11:mRFP (H, red signal) with cis-Golgi marker Manl:GFP (I, green signal); overlapping signal is yellow (J). White scale bar = 10 μm.

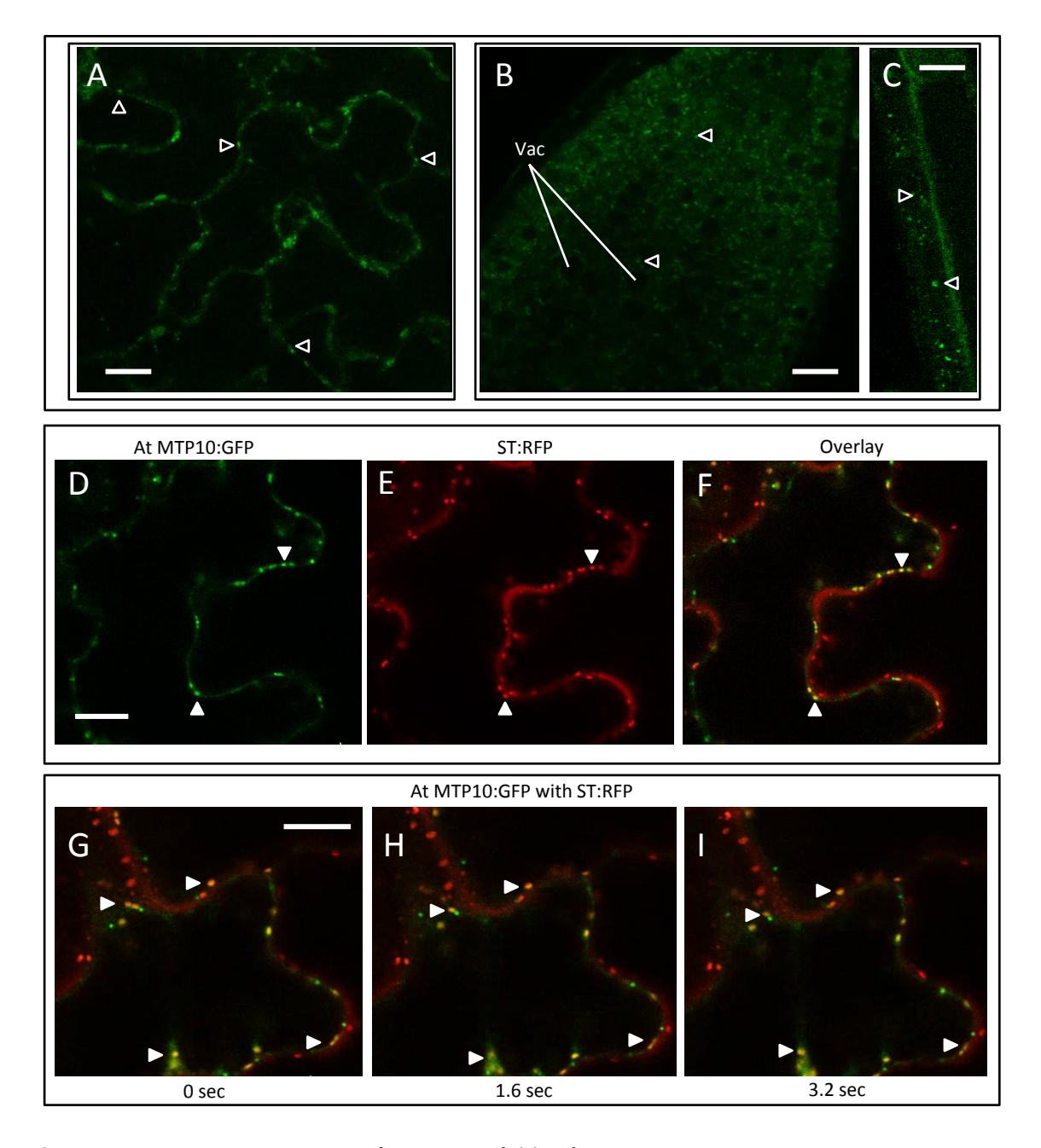


Figure 4.19. MTP10::GFP targets the trans-Golgi in planta.

A-C) Stable expression of P35S::AtMTP10::GFP in Columbia 8 wild type Arabidopsis, 7 days old; punctate expression of MTP10 in epithelial cells (G), root tip cells (H) and mid-root cell (I) marked with unfilled arrow; H) punctate signal is clearly distinct from developing vacuoles in root tip cells, marked 'Vac'. D-I) Transient expression of P35S::AtMTP10::GFP in tobacco epithelial cells. Punctate expression of D) MTP10::GFP and E) TGN marker ST::RFP; F) overlap of D and E, areas of overlap are yellow. Filled arrow, example of areas of overlap. G-I) Timelapse of MTP10::GFP (green) coexpressed with ST::RFP (red); overlap is yellow. Filled arrow, example of area of overlap tracked around the cell. Intervals between images, 1.6 seconds. G-I) White scale bar = $10 \mu M$.

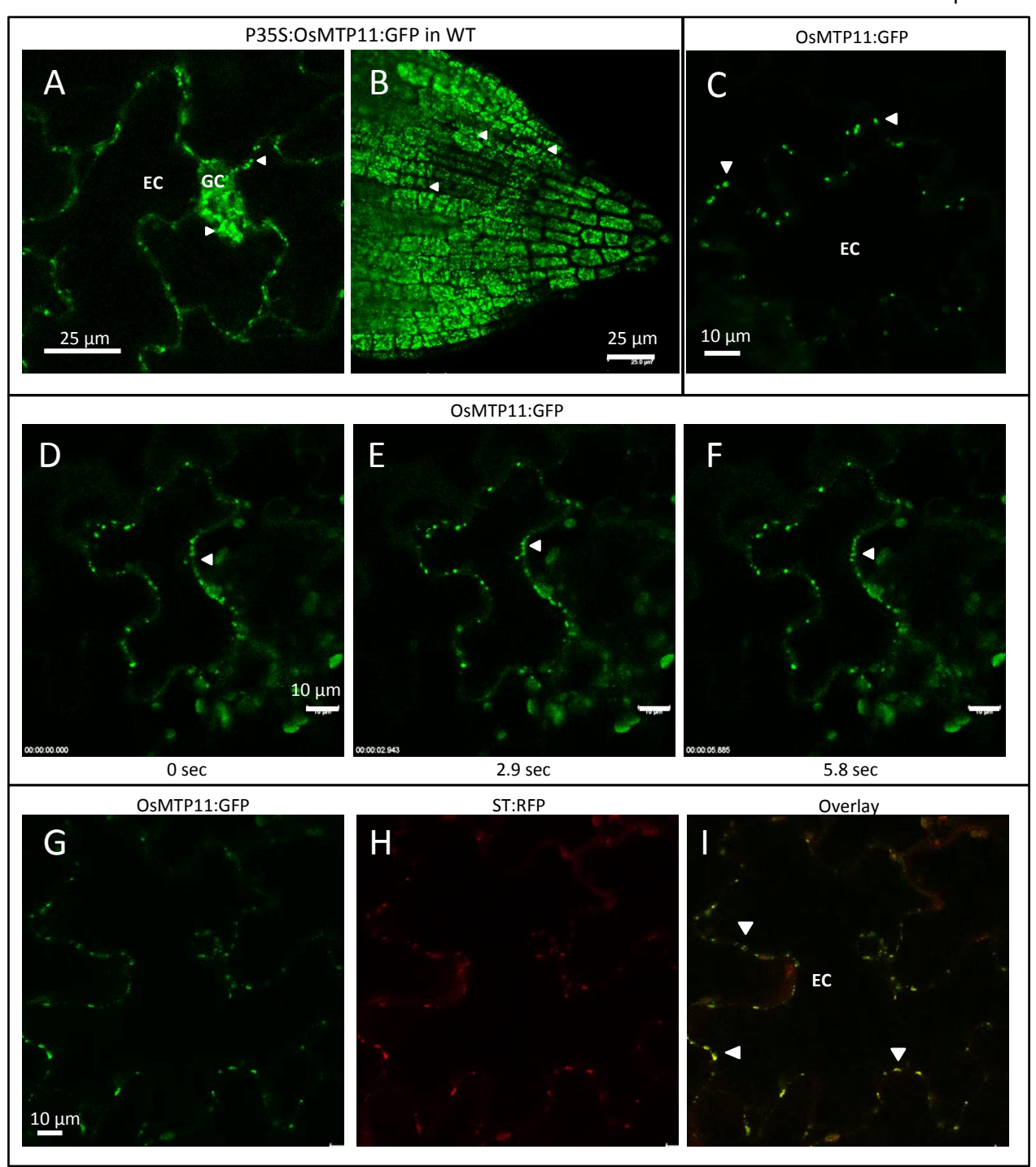


Figure 4.20. Os MTP11 targets the trans-Golgi when expressed in Arabidopsis and tobacco.

A+B) P35S:OsMTP11:GFP stably expressed in 7 day old Columbia-o WT Arabidopsis seedlings. Punctate Os MTP11:GFP expression in A) guard cells (GC) and neighbouring epithelial cells (EC) of cotyledons and B) root tip. D-I) P35S:OsMTP11:GFP transiently expressed in tobacco epithelial cells. C) Punctate expression of OsMTP11:GFP in tobacco epithelial cells. D-F) Time-lapse of Os MTP11:GFP movement around tobacco epithelial cells, 2.9 second intervals. Arrows track punctate movement around cell. G-I) Overlap of Os MTP11:GFP signal (G; green signal) with TGN-marker sialyl transferase:RFP (ST:RFP; H; red signal); overlap is yellow (I). Filled arrows, examples of OsMTP11::GFP punctate signal. White scale bar, as labelled.

Chapter 4

translocate to the shoot, as it is not sufficiently sequestered into the root vacuole. In addition to enhanced vacuolar sequestration by At MTP8 in the root, the constitutive expression in overexpressing lines may result in new sequestration into the shoot vacuoles by At MTP8, conferring greater tolerance to Mn across the whole plant. Enhanced levels of sequestration in the root would also alleviate Mn/Fe antagonism, preventing Mn-inhibition of the Fe deficiency machinery such as At FRO2 (Eroglu, et al., 2016), providing greater tolerance to the conditions of pH-induced, low Fe bioavailability.

4.3.2 At MTP11 and At MTP10 localise to different parts of the Golgi

This thesis favours findings that At MTP11 targets a 'Golgi-like compartment', originally proposed by Peiter, et al., (2007). At MTP11 shows significant overlap with cis-Golgi marker, Manl. Further, although not completely overlapping, the punctate signal of At MTP11 generally sits adjacent to TGN marker ST, moving around the cell at the same rate. Although colocalisation with a PVC marker could not be investigated due to poor expression in tobacco, this suggests At MTP11 targets the cis-Golgi. This could be explored further by exposing cells to monensin, which dramatically reduces protein secretion and results in swelling of the trans-Golgi, followed by cisternae of the medial-Golgi and finally of the cis-Golgi (Zhang, 1993; Madison & Nebenfuhr, 2011). It might be informative to track any time-dependent changes in expression of At MTP11 following addition of this reagent, compared to that of Golgi markers, to truly determine at which part of the Golgi MTP11 functions.

Overexpression of At MTP11 does not confer hypertolerance to Mn; this may be because At MTP11 is already expressed at relatively high levels under normal conditions, with expression levels relatively unaffected by Mn exposure (Delhaize, et al., 2007). Alternatively, it may suggest a feedback mechanism or post-translational modification exists to control expression of At MTP11, preventing high levels of expression and thus preventing conference of hypertolerance. It should be noted that this contradicts the hypertolerance observed in At MTP11-overexpressing lines by Peiter, et al. (2007).

At MTP10 shows strong levels of overlap with ST, suggesting targeting to the TGN. The punctate expression in Arabidopsis was observed at the T2 generation and more work is required to isolate homozygous lines expressing MTP10 at the T3 generation. However, following this isolation it would be interesting to determine whether At MTP10 overexpression confers Mn hypertolerance, like At MTP8, or has no significant effect, like At MTP11. This outcome might imply differences in the relative importance of sequestering Mn into the Golgi compared to the vacuole, in relation to providing Mn tolerance.

4.3.3 Os MTP11 restores the Mn-dependent phenotype of Arabidopsis mtp11-3

Expression of Os MTP11 in *mtp11-3* can complement the Mn sensitivity of *mtp11-3*, while its expression in WT also does not confer Mn hypertolerance. Functional complementation can suggest both proteins carry out a similar function, targeting the same membrane, or alternatively provide compensatory complementation mechanisms through a different mode of function. Interestingly, while At MTP11 targets the cis-Golgi, Os MTP11 appears to target the trans-Golgi. Therefore it appears a Golgi-based Mn-detoxification mechanism has been conserved between species, but they may target distinct regions of the Golgi within the cell. An additional MTP11 protein exists in rice, Os MTP11.1 (Figure 3.6); it would be interesting to determine which Golgi-based localisation is conserved in Os MTP11.1, or whether it targets a different membrane altogether.

Functional studies with At MTP1 and Os MTP1 have previously demonstrated the Zn-transporting ability of Zn-MTPs can be conserved between rice and Arabidopsis (Menguer, et al., 2013). The findings of this chapter contribute to evidence that the role of the Mn-MTPs are also conserved between these species, with Os MTP11 and Os MTP8.1 (Chen, et al., 2013) both playing potentially important roles in Mn homeostasis in rice. Mn deficiency can be problematic in rice paddy areas of China, where leaching, unfavourable soil texture and high pH contribute to low Mn availability (Lu, et al., 2004). Investigating the links between proteins in Arabidopsis and rice may be an important starting point for treating Mn-related problems in rice farming, which may ultimately lead to an increase in agricultural yield.

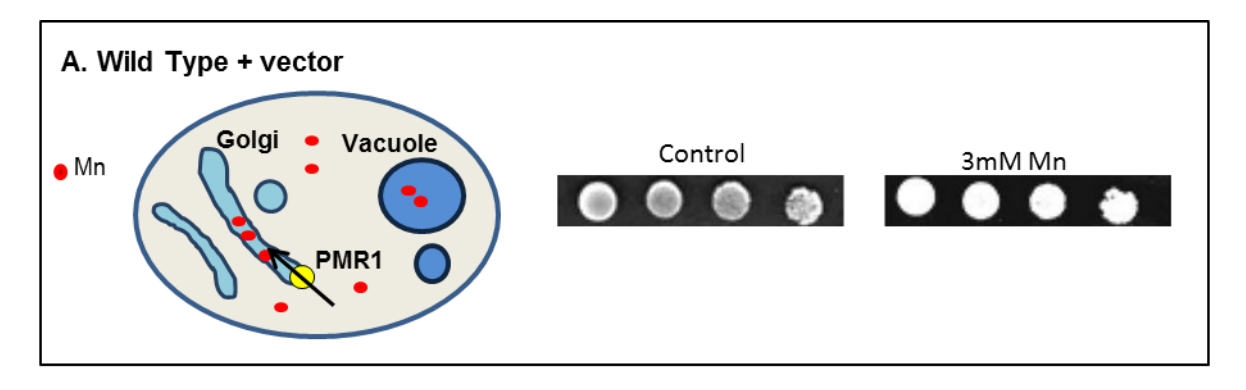
Chapter 5: Functional analysis of MTPs using heterologous expression in yeast

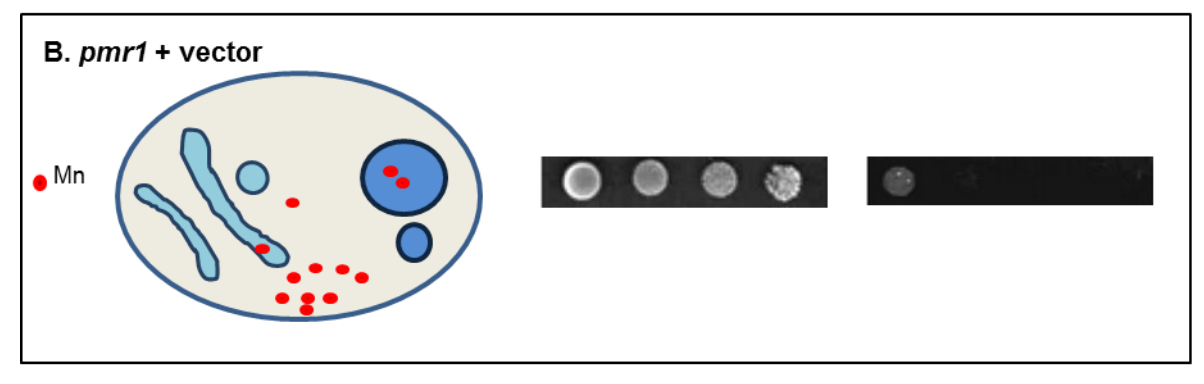
5.1 Introduction and Aims

5.1.1 Using yeast mutants to investigate MTP transport ability

Due to the intricate nature of plant metabolism and the potential for silencing transgenes, less sophisticated organisms are often used for heterologous functional protein analysis. *Saccharomyces cerevisiae* is widely used for its rapid growth, simple culturing conditions and conservation of basic cellular machinery of higher eukaryotes (Ton & Rao, 2004). Various yeast mutants exist that are defective in a particular metal-transport system, subsequently suffering a sensitive phenotype when grown on a media under toxic or deficient levels of that metal. If expression of a heterologous protein is capable of restoring tolerance of the sensitive mutant under these conditions, relative to the wild type, this generally suggests the protein is able to transport that particular substrate. Alternatively, a rescued phenotype does not always directly correlate with transport and could instead be associated with other aspects of metal homeostasis, such as binding: expression of the At HMA4 C-terminal in yeast alleviates Cd and Zn sensitivity, but not does possess transmembrane domains (TMDs) and is instead proposed to confer metal tolerance by acting as a metal-binding peptide (Mills, et al., 2010).

The yeast tolerance assay is often used when investigating the MTPs; At MTP11 is shown as an example in Figure 5.1. PMR1 is a Ca/Mn-ATPase that targets a Golgi-like compartment, physiologically supplying Ca and Mn to the Golgi while aiding Mn detoxification from the cytosol (Antebi & Fink, 1992; Durr, et al., 1998). While the WT is able to grow at elevated Mn concentrations (Figure 5.1 A), the *pmr1*Δ mutant is sensitive to excess Mn (Figure 5.1B; Lapinskas, et al., 1995; Durr, et al., 1998). Expression of both At MTP11 and MTP8 can rescue the Mnsensitive phenotype of *pmr1* (Figure 5.1C shows At MTP11), suggesting they act as transporters to detoxify Mn from the cytoplasm. Their expression did not rescue the copper-, zinc-, cadmium- or cobalt-sensitive phenotypes of other mutants, indicating the Mn-transporting ability is specific (Peiter, et al., 2007; Eroglu, et al., 2016). The transport kinetics of homologous MTP8 proteins from barley (Pedas, et al., 2014), rice (Chen, et al., 2013) and cucumber (Migocka, et al., 2014) are also quite specific for Mn. However, the Fe-transporting abilities have not been reported for any of these proteins, which would be important to investigate since MTP8 has also been implicated to play a role in alleviating Fe deficiency (Eroglu, et al., 2016). This Chapter aims to confirm the





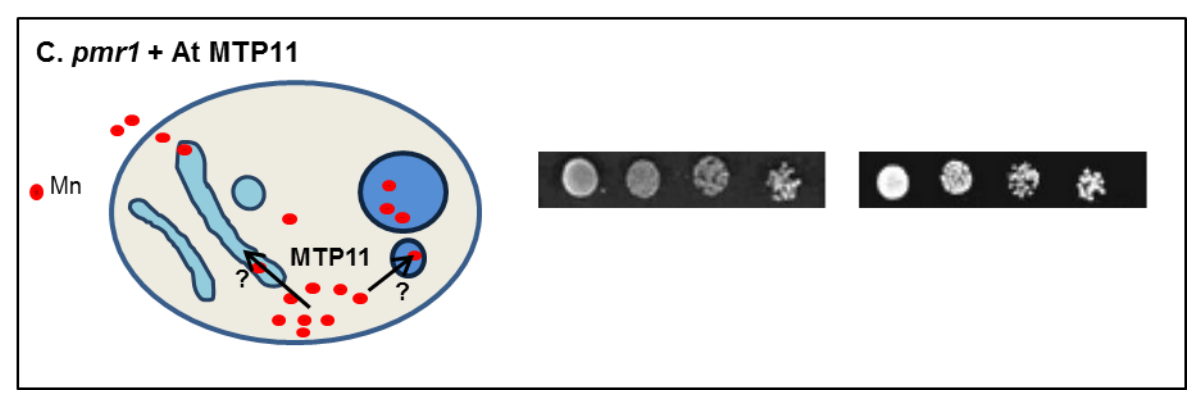


Figure 5.1. Schematic illustrating use of yeast transport mutants for investigating protein function.

A) Wild type yeast carrying 'empty' expression vector grows well on control plate, and plate supplemented with 3 mM MnCl₂. B) The *pmr1* mutant is defective in Golgi Mn/Ca transporter and is sensitive to higher levels of Mn. C) This phenotype can be rescued when *pmr1* is transformed with At MTP11, enabling growth on 3 mM Mn. At MTP11 is proposed to alleviate Mn toxicity either at the pre-vacuolar compartment (PVC) for subsequent sequestration in the vacuole (Delhaize, et al., 2007) or at the Golgi, for subsequent vesicular trafficking to the plasma membrane for exocytosis from the cell (Peiter, et al., 2007). Yeast blots adapted from Peiter, et al. (2007).

Mn-transporting abilities of At MTP11 and MTP8, as well as determining their true specificity and any ability to transport iron. At MTP10 will also be investigated in this respect, using clones provided for this project by Dr. Lorraine E. Williams (unpublished data). At MTP11 is the only Arabidopsis Group 9 MTP to have been investigated so far. However, the cucumber Cs MTP9 (Migocka, et al., 2014) and the *Beta vulgaris* spp. *maritima* Bm MTP10 (Erbasol, et al., 2013), which cluster most closely with At MTP9 and MTP10 (Figure 3.6), are also able to restore Mn tolerance when expressed in yeast.

The expression vectors to be used for this purpose, pAG426GAL-EGFP and pAG425GAL-DsRed, provide C-terminal GFP and DsRed tags, respectively (Alberti, et al., 2007). The use of these vectors will allow fluorescence studies to determine subcellular localisation of At MTP8, MTP10 and MTP11 in a simple eukaryotic cell.

5.1.2 Site-directed mutagenesis to determine functionally important residues

As alluded to in the General Introduction, crystallography studies indicate Ec YiiP has three Zn-binding sites. Site A, in the membrane-bound portion of the protein, is coordinated by DxxxD and HxxxD motifs on TMDs 2 and 5; when folded, these residues coordinate a tetrahedral binding site, referred to as the DD-HD domain (Wei & Fu, 2005; Lu, et al., 2009; Coudray, et al., 2013). These motifs are conserved in all CDFs characterised to date; where tested, the motifs have been shown to be important for transporter specificity, although the exact residues are not tightly conserved. For example, all plant Mn-MTPs identified so far possess two DxxxD domains, which are hypothesised for form a DD-DD coordination site at site A (Montanini, et al., 2007; Chapter 4); both motifs are substituted for HxxxD motifs in all plant Zn-MTPs, forming a HD-HD coordination site (Montanini, et al., 2007). Meanwhile, SLC30A10, the only human Mn-CDF, and Sp MntE, the Mn-CDF from *Streptococcus pneumoniae*, possess ND-HD and ND-DD coordination sites, respectively (Martin & Giedroc, 2016; Nishito, et al., 2016; Zogzas, et al., 2016).

Site-directed mutagenesis studies have been a useful tool to investigate the functional importance of these domains in the Zn-transporting MTP1 from a range of plant species. Substituting HD-HD for DD-HD abolishes Zn-transport in At MTP1 (Kawachi, et al., 2008), Ptd MTP1 (Blaudez, et al., 2003) and Os MTP1, but enhances the ability of Os MTP1 to transport Fe (Menguer, et al., 2013). Substitution of HD-HD for HA-HD also abolishes Zn transport in these proteins, and in related protein from yeast Sc ZRC1, but does not enhance the transport kinetics of any other metal (Kawachi, et al., 2008; Lin, et al., 2008; Menguer, et al., 2013). Substitutions that entirely abolish transport imply the residue is important for protein function, but this may simply be by maintaining the correct tertiary structure; they tell little about the role of a residue

Chapter 5

with regards to substrate affinity compared to mutations which cause an alteration or shift in substrate specificity. This chapter aims to identify residues conserved within the Mn-MTPs that are potentially important for function, and begin to determine their relative importance in maintaining the specificity of At MTP8 and MTP11. This will be investigated by generating site-directed mutants and testing them in the yeast metal tolerance assay. Of particular interest are the roles played by the DxxxD domains. Bioinformatic analysis will also be used to predict the secondary and tertiary structures of At MTP8 and MTP11, to further predict the roles played by these residues in transporter function.

As described in the general introduction, following protein modification in the ER and Golgi, proteins are packaged into vesicles for transit to the plasma membrane, or to other destinations within the cell. Proteins which are destined to target the vacuole often follow a vesicular pathway from the trans-Golgi to the pre-vacuolar compartment (PVC). Certain motifs exist in protein sequences that may enable targeting to particular subcellular organelles; identifying these sequences may aid hypothesis generation regarding subcellular destinations. Although similarities exist between kingdoms, differences between plant and yeast signals and subsequent recognition in secretory systems mean plant proteins may mislocalise when expressed in yeast, and vice versa (Bassham & Raikhel, 2000). Of interest in the plant system to direct targeting to the tonoplast are the dileucine motifs, and diacidic motifs. The dileucine motif generally follows the consensus sequence DXXXL or [DE]XXXL[LI], where X can be any amino acid while any of the amino acids between the brackets is possible (Bonifacino, et al., 2003; Baulke, et al., 2009). This motif is likely recognised by the Adaptor Protein (AP) complexes (Zwiewka, et al., 2011; Wang, et al., 2014) to ensure tonoplast-targeting in Arabidopsis; its mutation or deletion in Ca²⁺ tonoplast channel At TPC1 causes mislocalisation to the plasma membrane (Larisch, et al., 2012). The diacidic motif, DXE, is also important for the export of some membrane proteins from the ER and Golgi to the tonoplast, such as At TPK1 (a tandem pore potassium channel; Dunkel, et al., 2008). This motif is likely recognised by Sec24, a component of the COPII coat thought to recruit membrane proteins into vesicles, for transit to their final destination (Mossessava, et al., 2003; Sieben, et al., 2008).

A motif that may be important for correct targeting of Golgi-localised membrane proteins is the tyrosine-based motif: YXXØ, where Ø is a bulky, hydrophobic amino acid such as F, Y or W (Bonifacino, et al., 2003; Baulke, et al., 2009). This sequence is essential for correct targeting of At BP80, a vacuolar sorting receptor, to the trans-Golgi network; its mutation or deletion causes mistargeting of BP80 to the plasma membrane (Sanderfoot, et al., 1998; Happel, et al., 2004; da Silva, et al., 2006). It may therefore be residues such as these which prevent targeting of cargo vesicle to the plasma membrane, in favour of other organelles. Other signal sequences are predicted to enable targeting to other organelles, such as the KDEL motif, which causes proteins

to be retained in, or retrieved back to, the ER (Munro & Pelham, 1987). However, it should be noted that the presence of KDEL does not always result in ER-localisation, and may result in a false positive prediction (Wrzeszczynksi & Rost, 2003. Therefore, reliance on this method when predicting subcellular localisation should aid hypothesis generation, but should not replace experimental evidence.

Thus, in addition to using bioinformatics to predict the TMDs of MTPs, their sequences will also be analysed to identify any potential motifs that may influence their subcellular targeting.

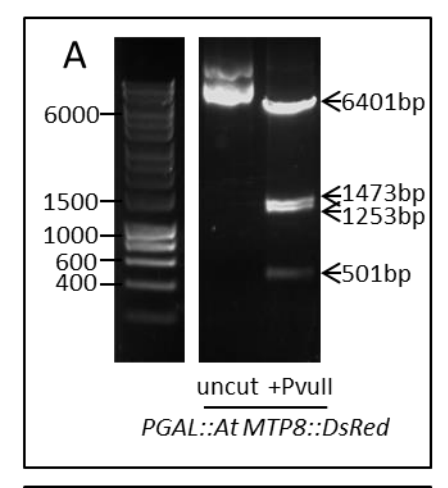
5.1.3 Aims

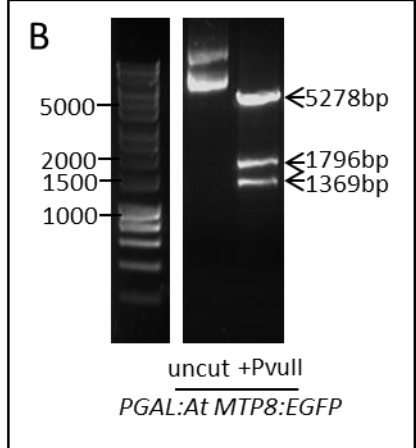
- 1. To generate yeast-specific destination vectors for At MTP8 and MTP11
- To express At MTP8, MTP10 and MTP11 in metal-sensitive yeast mutants to determine their possible transport ability and specificity
- 3. To determine subcellular localisation of At MTP8, MTP10 and MTP11 in yeast
- 4. To use bioinformatics databases to perform sequence analysis on At MTPs, predicting transmembrane domains and any signal peptides or motifs
- To identify conserved or non-conserved residues in At MTP8 and MTP11 which may be important for function, and determine where they lie in relation to protein structure
- To generate site-directed mutants and determine the effect of these mutations on the transport function and specificity of At MTP8 and MTP11

5.2 Results

5.2.1 Generating yeast expression clones for At MTP8 and MTP11

To express At MTP8 and MTP11 in yeast, the entry vectors generated in Chapter 4 were cloned into yeast-specific expression vectors. Figure 5.2A and B shows this process, using MTP8 as an example: cloning *MTP8* without a stop codon has successfully generated *PGAL::MTP8::GFP* and *PGAL::MTP8::DsRed*. Clones with the stop codon were also generated, to compare the effect of GFP-tagging on protein function (confirmation gels not shown). Clones were transformed into metal-sensitive yeast mutants: Mn-sensitive *pmr1* (Lapinskas, et al., 1995; Durr, et al., 1998), Zn-and Co-sensitive *zrc1 cot1* (Conklin, et al., 1992; MacDiarmid, et al., 2000); Fe-sensitive *ccc1* (Li, et al., 2001; Lin, et al., 2008) and Fe-deficient *fet3 fet4* (Eide, et al., 1996; Li & Kaplan, 1998). PCR was performed on yeast colonies to confirm successful transformation; *PGAL::MTP8::GFP* in *pmr1* is shown as an example in Figure 5.2C.





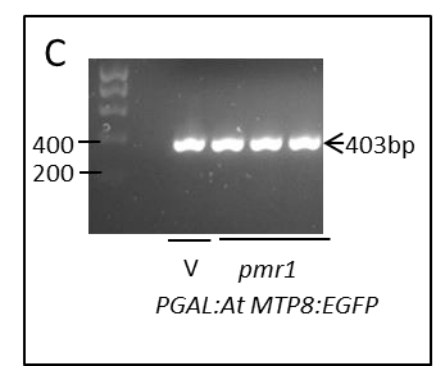


Figure 5.2. Generation of yeast expression vectors for MTP8.

Digestion analysis with *Pvull* of A) PGAL:At MTP8:DsRed and B) PGAL:At MTP8:EGFP. Uncut vector run alongside on gel as a control. Predicted fragment sizes in base pairs (bp) are labelled at right of gel; molecular marker sizes are labelled on left of gel. C) Yeast colony PCR to show successful transformation of PGAL:At MTP8:EGFP in three colonies of *pmr1*, using primers MTP8F + MTP82R to produce a product of 403 bp. V, PCR on vector control. *pmr1*, PCR on colonies.

5.2.2 At MTP8, MTP10 and MTP11 function as Mn transporters when expressed in yeast

Expression of At MTP8, MTP10 or MTP11 in *pmr1* confers Mn-hypertolerance relative to that of the WT; this is shown in Figure 5.3. This confirms the findings by Peiter, et al. (2007) and Eroglu, et al. (2016), suggesting that MTP8 and MTP11 can transport Mn and also indicates that MTP10 is capable of Mn transport. Previous studies have only tested up to 3 mM and 6 mM for MTP11 and MTP8, respectively; here, all colonies were tested up to 20 mM Mn. MTP8 and non-tagged MTP10 were able to restore WT-like tolerance to Mn up to 20 mM; MTP11 confers tolerance up to 5mM Mn, and allows slightly impeded growth above this concentration. Also interesting to note is that tagging MTP10 with GFP interferes with transporter function: the non-tagged version of MTP10 is unable to confer WT-like tolerance above 1mM Mn.

Eroglu, et al. (2016) claim that MTP8 is involved in Fe and Mn homeostasis but did not test its ability to transport Fe. Here it was expressed in *ccc1* and Fe-tolerance was not restored (Figure 5.4A). Instead, a slight impairment is routinely seen at low levels of Fe, suggesting colonies grow less well when expressing MTP8 compared to transformation with an empty vector. MTP10 does not confer Fe-tolerance to *ccc1*. Comparatively, expression of non-tagged MTP11 confers tolerance to Fe up to 6 mM, at which point the WT strain also fails to grow. The Fe-transporting abilities of MTP11 have not been previously tested; it appears, therefore that MTP11 is able to transport Fe (Figure 5.4A). MTP11 expression confers a very slight tolerance to Zn in *zrc1 cot1*; MTP8 does not confer tolerance, and it is difficult to conclude this for MTP10 due to poor growth under control conditions (Figure 5.4B). The mutant *fet3 fet4* is sensitive to Fe deficiency, a phenotype enhanced by high pH. Tolerance to these conditions was not conferred with expression of MTP8, MTP10 or MTP11 (Figure 5.5).

5.2.3 At MTP8, MTP10 and MTP11 target Golgi-like compartments in yeast

When expressed in WT yeast, GFP-tagged MTP8, MTP10 and MTP11 all display punctate, intracellular expression, as observed by confocal fluorescent microscopy (Figure 5.6D-L). This is different from the cytoplasmic expression of the empty vector, shown in Figure 5.6A-C. To determine which membrane these proteins are targeting, *PGAL::MTP11::GFP*, *PGAL::MTP8::GFP* and *PGAL::MTP8::DsRed* were co-expressed with organelle markers, as shown in Figures 5.7 and 5.8. MTP8 shows strong colocalisation with early-Golgi-marker Anp1:RFP (Figures 5.6A-F); this is particularly apparent in the 3D stack in Figures 5.7A-C. Further, the punctate spots of MTP8 do not seem to overlap with ER- and Golgi-marker, Sec13:RFP (Figure 5.7G-I) or tonoplast marker Gtr1:GFP (Figure 5.7J-L). MTP11 also shows areas of overlap with Anp1:RFP, although this overlap is not complete (Figure 5.8A-C); MTP11 does not overlap with Sec13:RFP (Figure 5.8D-F).

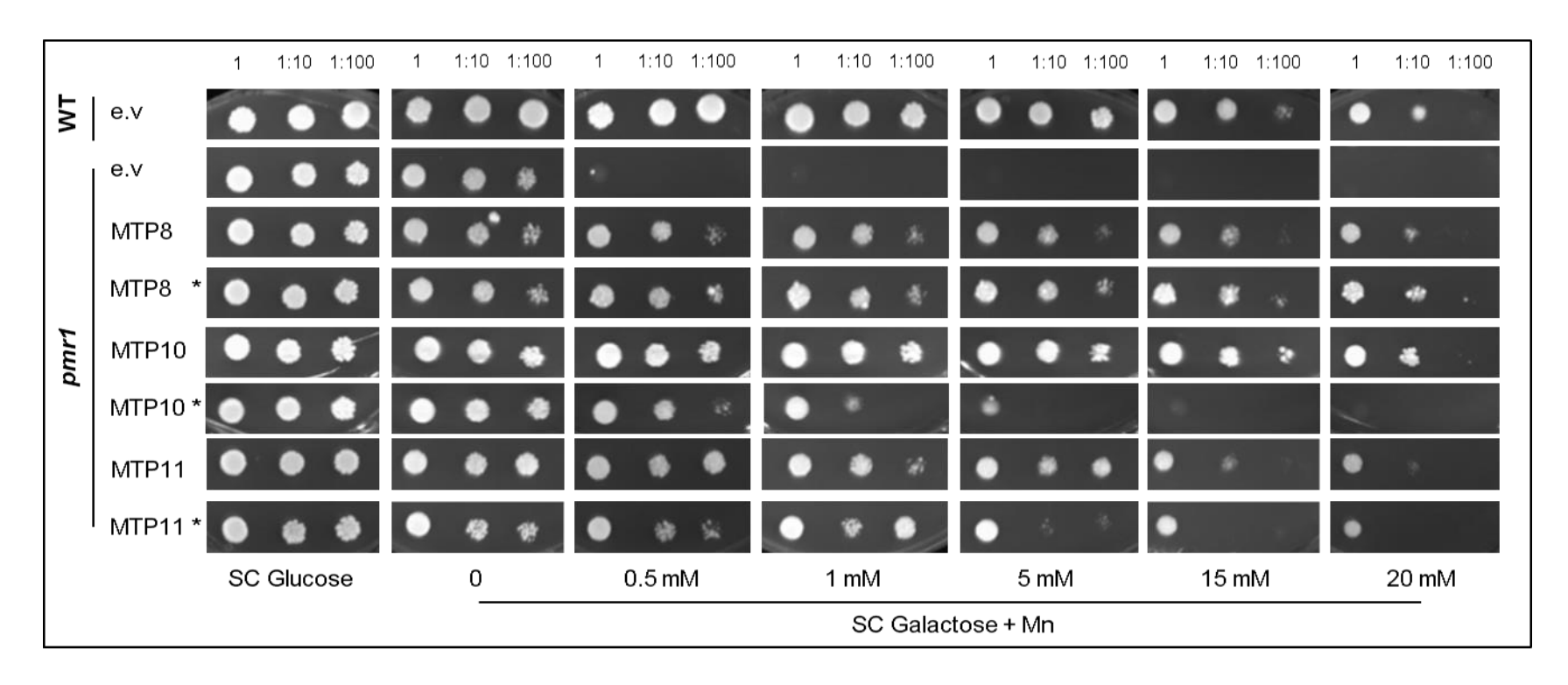
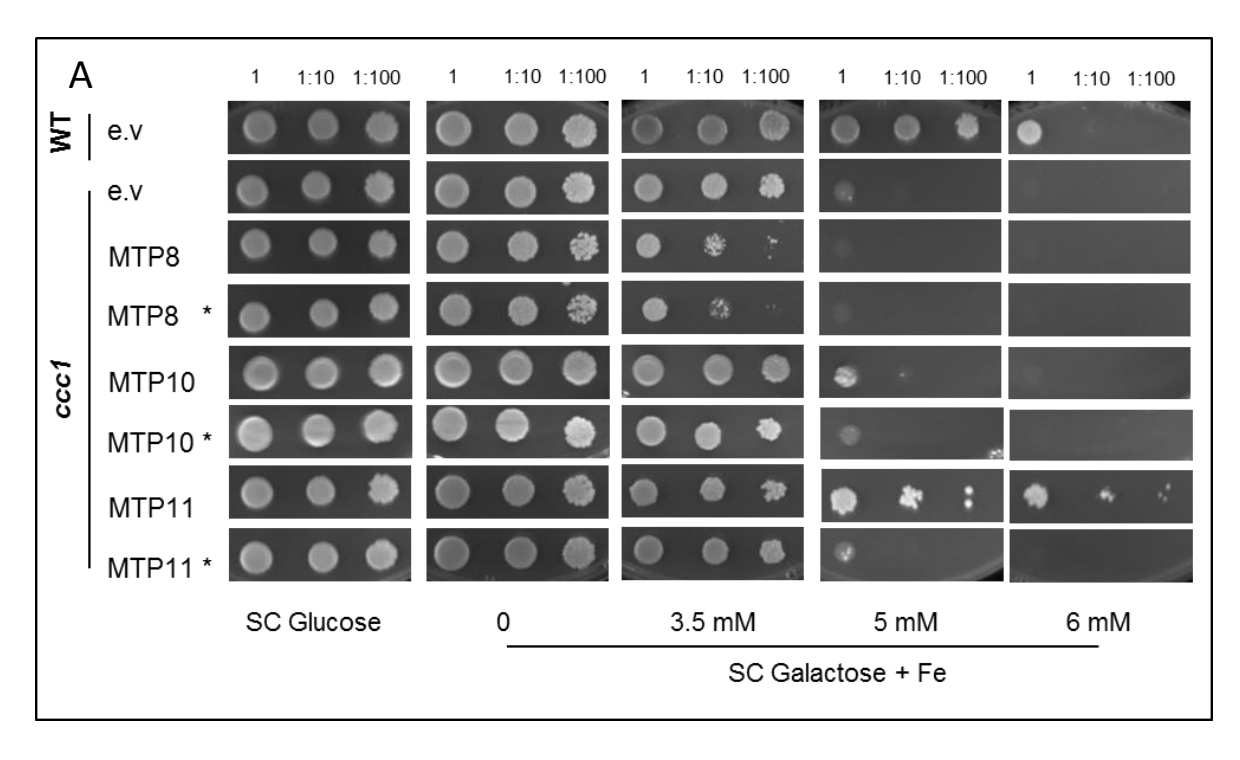


Figure 5.3. Functional analysis of At MTP8, MTP10 and MTP11 in the Mn-sensitive Saccharomyces cerevisiae mutant pmr1.

BY4741 wild type (WT) was transformed with pAG426GAL-EGFP empty vector (e.v.); pmr1 was transformed with pAG426GAL-EGFP vector either empty or expressing At MTP8, MTP10 or MTP11 with or without stop codon (*). The latter generates a PGAL::MTP::EGFP fusion protein. Numbers represent serial dilutions of yeast cells in liquid SC galactose without uracil: 1, undiluted OD $_{600} = 0.5$, 1:10 and 1:100, dropped onto SC glucose or SC galactose without uracil, supplemented with a range of Mn concentrations, supplied as MnCl₂. Plates were incubated for 5 days at 30 °C. Photos are representative of at least 3 experiments per construct.



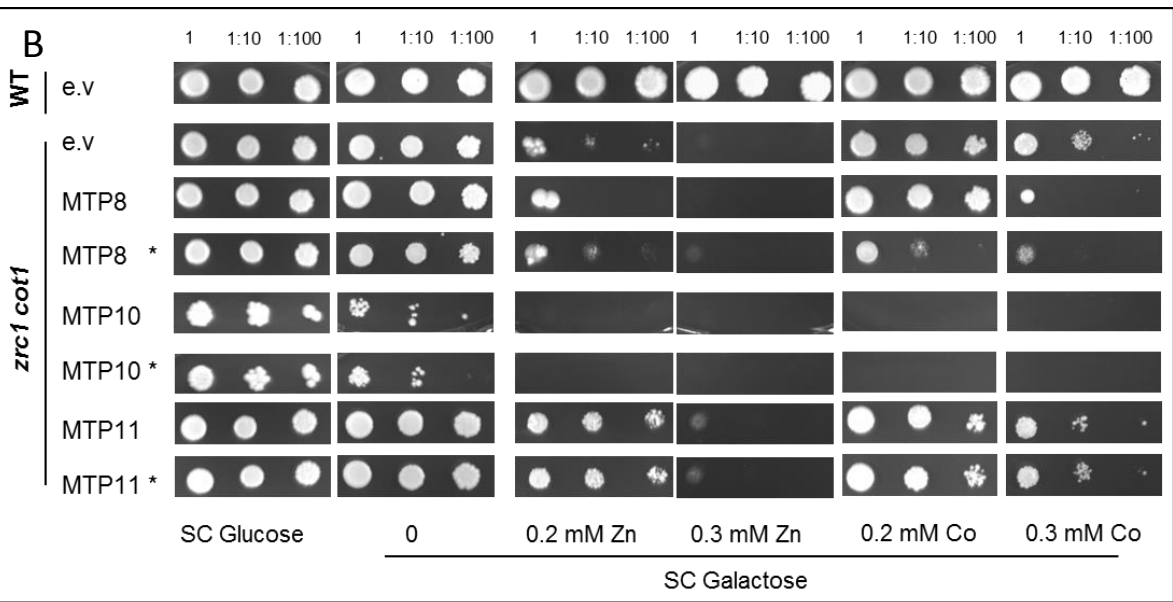


Figure 5.4. Functional analysis of At MTP8, MTP10 and MTP11 in the Fe-sensitive mutant *ccc1*, and Zn- and Co-sensitive mutant *zrc1* cot1.

Wild type (WT; A, DY150; B, BY4741) was transformed with pAG426GAL-EGFP empty vector (e.v.); ccc1 (A) and ccc1 (B) was transformed with ccc1 with ccc1 (B) was transformed with ccc1 with or without stop codon (*). The latter generates a ccc1 ccc1 fusion protein. Numbers represent serial dilutions of yeast cells in liquid SC galactose without uracil: 1, undiluted OD ccc1 cc

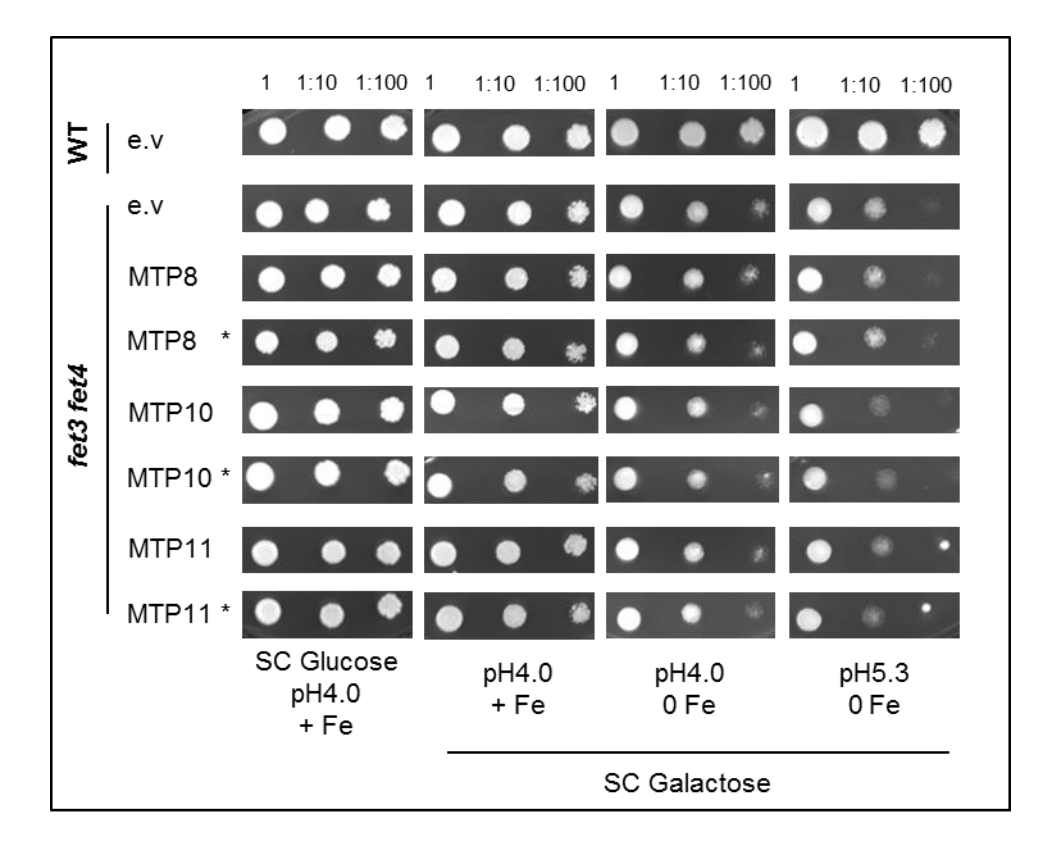


Figure 5.5. Functional analysis of At MTP8, MTP10 and MTP11 in the Fe deficiency-sensitive Saccharomyces cerevisiae mutant fet3 fet4.

DY1457 wild type (WT) was transformed with pAG426GAL-EGFP empty vector (e.v.); zrc1 cot1 was transformed with pAG426GAL-EGFP vector either empty or expressing At MTP8, MTP10 or MTP11 with or without stop codon (*). The latter generates a PGAL::MTP::EGFP fusion protein. Numbers represent serial dilutions of yeast cells in liquid SC galactose without uracil: 1, undiluted OD $_{600}$ = 0.5, 1:10 and 1:100 dropped onto control plates SC glucose without uracil or SC galactose without uracil (pH 4.0, with 10 μ M FeCl₃), or experimental plates SC galactose without uracil, either pH 4.0 or pH 5.3, without addition of Fe. Plates were incubated for 5 days at 30 °C.

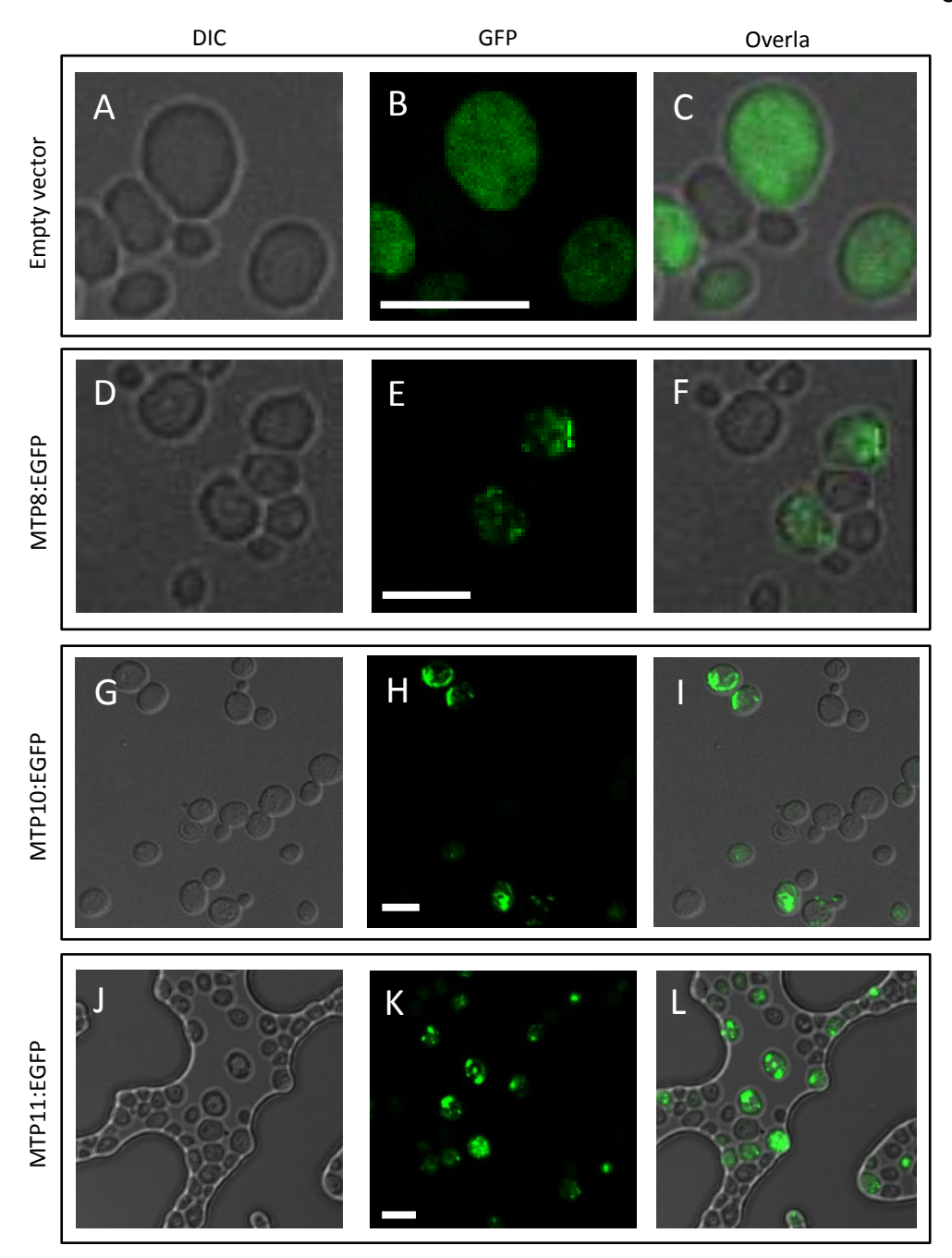


Figure 5.6. At MTP8, MTP10 and MTP11 are all expressed at intracellular membranes in yeast.

A-C) Empty *pAG426GAL-EGFP* vector displays cytoplasmic expression when expressed in BY4741 wild type yeast. Overlay of DIC image with GFP fluorescence. B-J) punctate expression of *PGAL::MTP8::EGFP* (B-D), *PGAL::MTP10::EGFP* (E-G) and *PGAL::MTP11::EGFP* (H-J) in WT yeast cells. A, D, G, J, DIC images of cells; B, E, H, K, fluorescence of GFP-protein fusion excited at 488 nm; C, F, I, L, overlay of DIC and fluorescence.

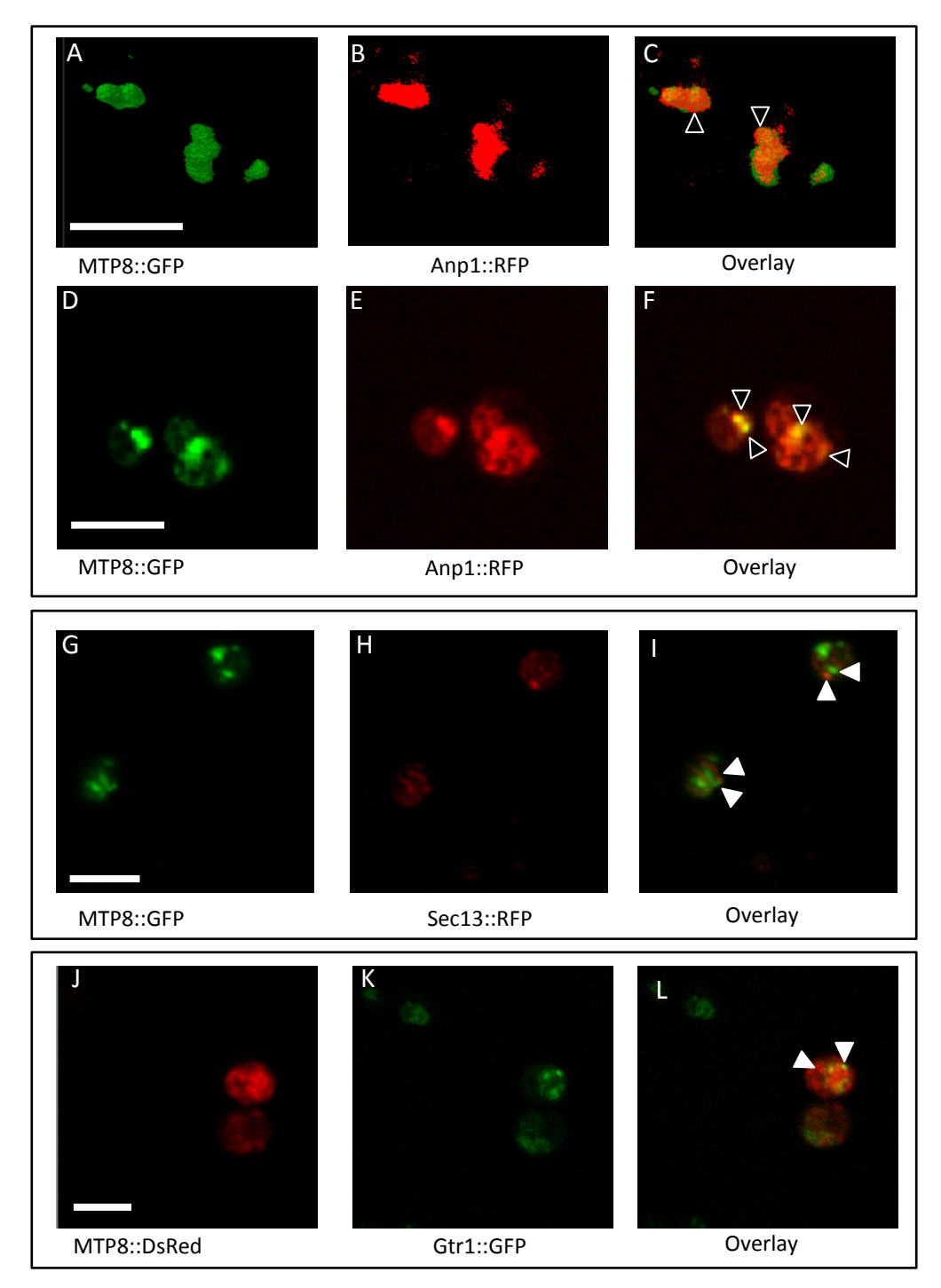


Figure 5.7. At MTP8 expression overlaps with that of Golgi marker when expressed in yeast.

A-I) *PGAL::MTP8::EGFP* expressed in BY4742 stably transformed with A-F) early Golgi marker Anp1::RFP and G-I) ER- and Golgi-marker Sec13::RFP. A-C, 3D Z stack. J-L) *PGAL::MTP8:: DsRed* expressed in BY4742 stably transformed with tonoplast marker Gtr1::GFP. A, D, G, J, fluorescent signal of MTP8; B, E, H, K, fluorescent signal of organelle marker; C, F, I, L, overlay. A-C)16 x 5.02 μ M slices in Z-axis combined into Z-stack. Unfilled arrow, areas of co-expression that overlap. Filled arrow, areas of coexpression that do not overlap. White scale bar = 5 μ M.

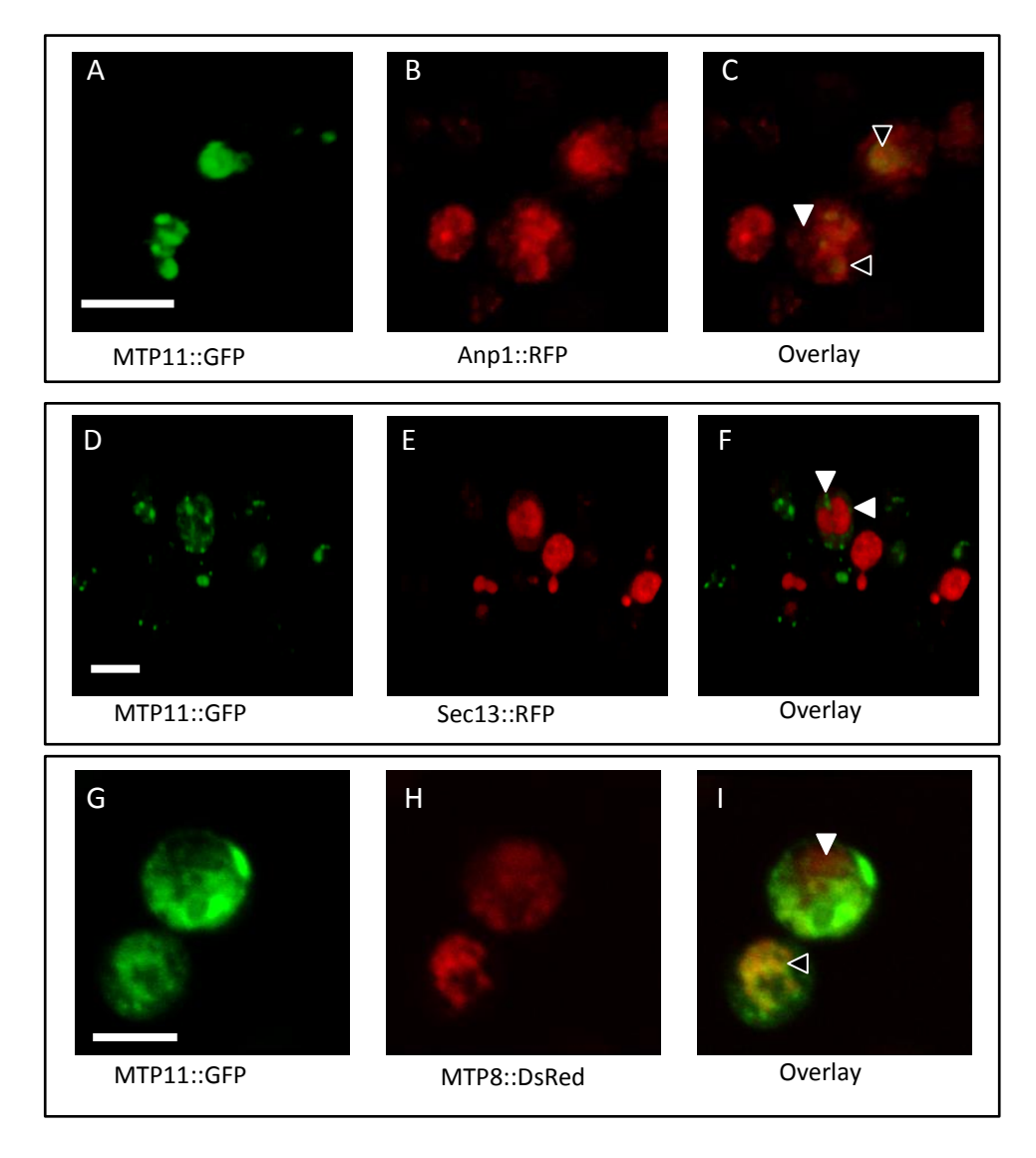


Figure 5.8. At MTP11 expression overlap with that of Golgi marker when expressed in yeast.

Expression of PGAL::MTP11::EGFP in BY4742 stably transformed with A-C) early Golgi marker Anp1::RFP, D-F) ER- and Golgi-marker Sec13::RFP. And G-I) PGAL::MTP8::DsRed. A, D, G, fluorescent signal of MTP11; B, E, H, fluorescent signal of co-expressed protein; C, F, I, overlay. Unfilled arrow, areas of co-expression that overlap. Filled arrow, areas of coexpression that do not overlap. White scale bar = 5 μ M.

Chapter 5

MTP8:DsRed and MTP11:GFP were co-expressed in Figure 5.8G-I; these proteins show areas of overlap, although there are some areas which do not overlap fully. It appears, therefore, that when expressed in yeast, MTP8 and MTP11 target the Golgi, but possibly to different compartments.

While MTP11 also appears to target the Golgi when expressed in plants, At MTP8 targets the tonoplast when expressed in Arabidopsis and tobacco (Chapter 4). Bioinformatics tools were used to predict the likelihood of At MTP8 – 11 targeting the chloroplast, mitochondrion, nucleus, Golgi or secretory system, based on signal peptides and sequence motifs. Predictions for the tonoplast or plasma membrane were not available using these tools. As shown in Figure 5.9A, At MTP10 and At MTP11 both exceed the threshold of 20 and are thus predicted to target the Golgi; a cleavable signal peptide is also predicted at the first 15 residues of At MTP10, using programme SOSUIsignal (Gomi, et al., 2004), but not when using a different programme, SignalP (Petersen, et al., 2011). At MTP8 also has a relatively high score of 18.22 for Golgi-targeting, compared to a score of 0 for At MTP9. At MTP10 is the only protein to exceed the prediction threshold for targeting the secretory pathway. Sequence analysis suggests At MTP8 does not possess a dileucine motif, but does possess a diacidic motif: DHE and DPE in the N-terminus, potentially favouring tonoplast-targeting in plants. YXXØ motifs, which may favour Golgi-targeting, are found in both At MTP10 and At MTP11 (Figure 5.10). Neither of these motifs was found in At MTP9.

5.2.4 Identifying potentially important residues for Mn-MTP function

An aim of this chapter is to identify amino acid residues which may play an important role in function and specificity of At MTP8 and At MTP11. Multiple bioinformatics programmes exist for the prediction of membrane topology. At MTP8 (originally At MTPc3) was predicted by Maser et al (2001) to have four transmembrane domains (TMDs). The consensus output programme AramTmConsens, available on the ARAMEMNON database (Schwake, et al., 2003), integrates predictions from 18 membrane topology prediction programmes; 6 TMDs are predicted for each of At MTP8, MTP9, MTP10 and MTP11 when analysed in this respect, as shown in Figure 5.9B. Although 3 out of 18 programmes predict a 7th TMD for At MTP10 at the 5' end, the consensus score is very low (0.19), below the threshold value of 0.42 to be counted as a TMD by AramTmConsens, and it is concluded each of At MTP8 – 11 likely possess 6 TMDs.

These predicted TMDs are highlighted in the alignment of At MTP8-11, in Figure 5.10. This alignment suggests At MTP10 possesses an extension at the 5' end of 25-30 amino acids, which corresponds with the signal peptide predicted by SOSUIsignal. Each protein is labelled with the CDF signature sequence stretching from TMD 2 to TMD 3 and the DxxxD domains of TMD 2 and 5

Α	Chloroplast	Mitochondrion	Secretory pathway	Nucleus	Golgi
МТР8	1.9	-1.4	2.3	-1.4	18.22
МТР9	3.7	-1.0	2.1	-0.5	0
MTP10	3.3	2.3	11.9	-1.9	21.92
MTP11	0.1	-1.6	2.5	1.7	20.27

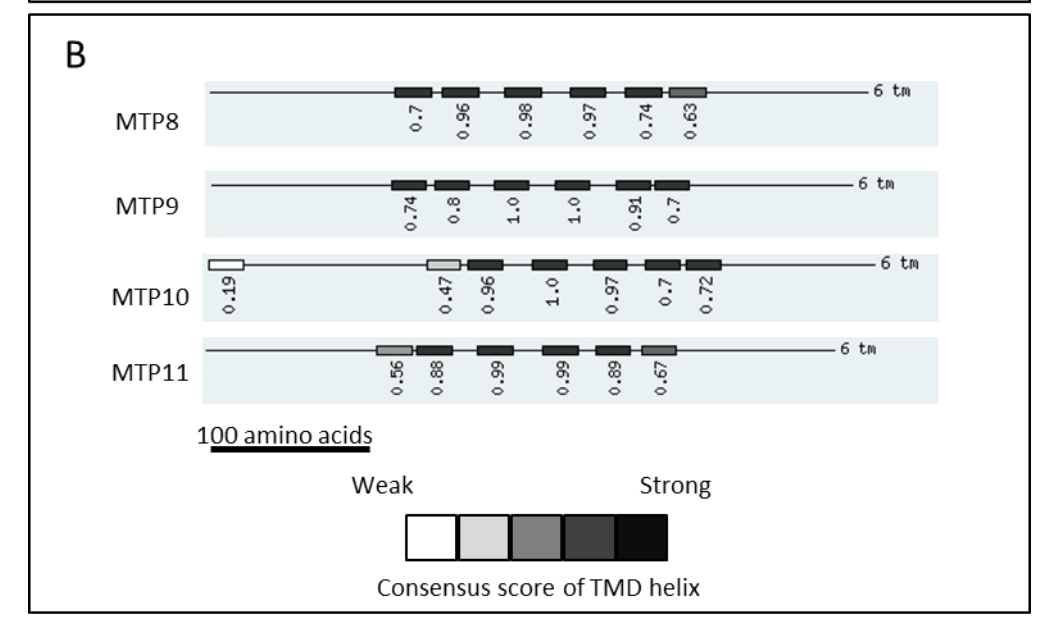


Figure 5.9. Output of consensus prediction programmes available at ARAMEMNON database.

A) Prediction values for At MTP8-11 to target different subcellular organelles. Chloroplast, mitochondrion, secretory pathway and nucleus: output of AramLocCon (Schwake, et al., 2007), a consensus programme that combines up to 20 individual algorithms predicting subcellular localisation based on signal peptides and specific protein motifs. Golgi: output of Golgi Predictor (Yuan and Teasdale, 2002). Increasingly positive or negative values, increasingly likely or unlikely, respectively, to target that organelle. Values above threshold for strong prediction highlighted in pink (AramLocCon threshold >10; Golgi Predictor threshold >20).

B) 6 transmembrane domains (TMDs) are predicted for At MTP8, MTP9, MTP10 and MTP11, based on consensus of 18 TMD prediction programmes, evaluated using AramTmConsens tool (Schwake, et al., 2003). Positions of predicted TMDs marked on primary sequence, labelled with consensus score; threshold for TMD is consensus score of 0.42. Scale bar, 100 amino acids. Shaded boxes, weak to strong consensus score of each predicted TMD.

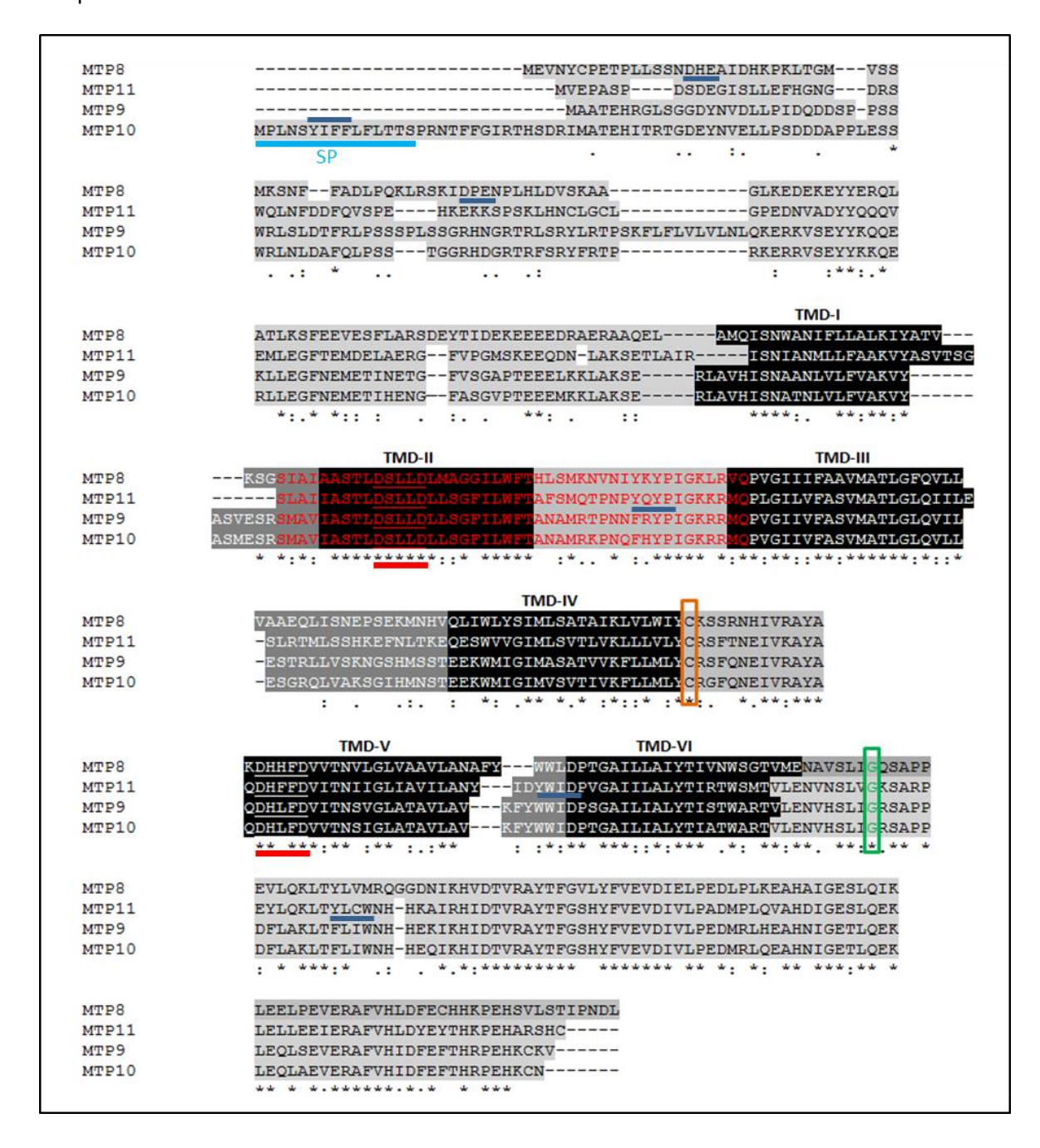


Figure 5.10. Multiple sequence alignment of At MTP8, At MTP9, At MTP10 and At MTP11.

Adapted from that generated by ClustalOmega (Seivers, et al., 2011). (*), fully conserved residues between sequences; (:), conservation of residues with strongly similar properties; (.), conservation of residues with weakly similar properties. Transmembrane domains (TMDs; highlighted in black) predicted by AramTmConsens (ARAMEMNON; Schwacke, et al., 2003). CDF signature sequence marked by red letters. Other regions predicted by Montanini, et al. (2007) to be important for function have also been highlighted: DxxxD domain of TMD 2 and TMD 5, underlined in red; conserved cysteine after TMD 4, orange box. SP, signal peptide predicted by SOSUIsignal (Gomi, et al., 2004). Conserved glycine potentially mutated in 954-12 EMS mutant, green. Putative diacidic motifs (DXE) in At MTP8 and tyrosine-based motifs (YXXØ) in At MTP10 and MTP11 sequences underlined with dark blue.

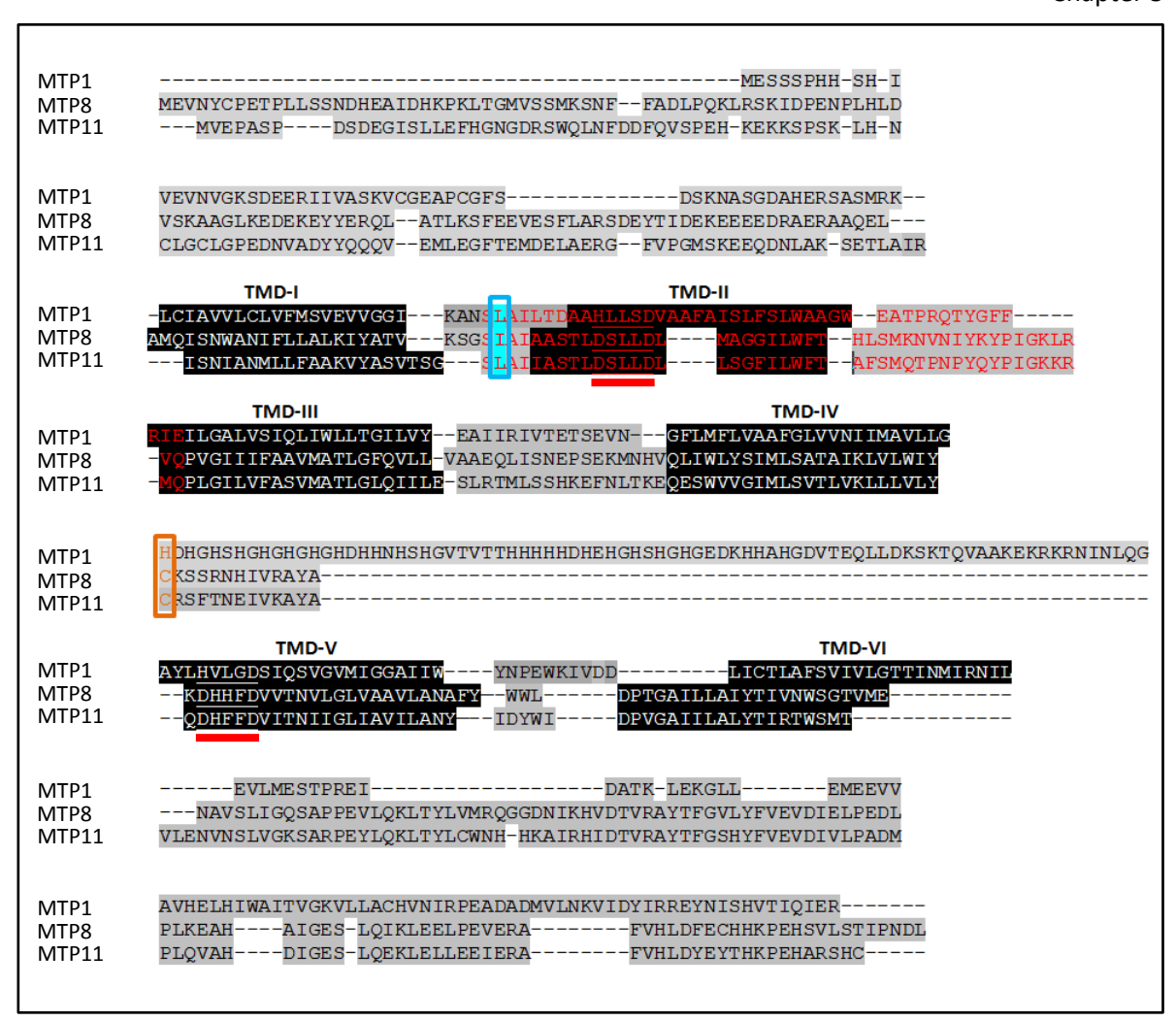


Figure 5.11. Multiple sequence alignment of At MTP8, At MTP11 and At MTP1.

Adapted from that generated by ClustalOmega (Seivers, et al., 2011). Transmembrane domains (TMDs; highlighted in black) predicted by AramTmConsens (ARAMEMNON; Schwacke, et al., 2003). CDF signature sequence marked by red letters. Other regions predicted by Montanini, et al. (2007) to be important for function have also been highlighted: Underlined in red, DxxxD/HxxxD domains of TMD 2 and TMD 5; orange box, conserved cysteine/histidine after TMD 4; blue box, homologous residue to L82 in Os MTP1, shown to be importantfor transporter function (Menguer, et al., 2013).

Chapter 5

(Montanini, et al., 2007). There are many residues throughout the sequences conserved between these proteins; this includes the glycine (G) at residue 312 of At MTP8, which is conserved throughout the Mn-MTPs and was originally hypothesised to be mutated in Mn-sensitive EMS, mutant 954-12 (Chapter 3). A conserved cysteine (C) was highlighted by Montanini, et al. (2007) to be conserved in Mn-MTPs; this is also highlighted in Figure 5.10. Comparatively, this C is substituted for a histidine (H) in the alignment of At MTP8, At MTP11 and Zn-transporting At MTP1, in Figure 5.11. Other key differences include the H-rich loop between TMD 4 and TMD 5 of MTP1, which is absent from MTP8 and MTP11. It is also confirmed that the DxxxD domains of TMD 2 and TMD 5 are substituted for HxxxD domains in At MTP1. A key similarity that has been highlighted in Figure 5.11 is the conserved leucine (L) or isoleucine (I) at position L82 for At MTP1, L130 for At MTP11 or I141 for At MTP8.

Based on these alignments, 5 residues were chosen to mutate in both At MTP8 and At MTP11. These are listed in Figures 5.12 and 5.13 and are labelled with their position on the predicted membrane topology of each protein. At MTP9 and MTP10 were not mutated but their topologies are included in Figure 5.14 for comparison. The diagrams here, generated by Protter (Omasits, et al., 2014), visualise the 6 TMDs predicted by AramTmConsens; again, this highlights the absence of a large, histidine-rich loop between TMD 4 and TMD 5. The chosen mutations include substituting the conserved C of Mn-MTPs immediately after TMD 4 to the conserved H of Zn-MTPs (C233H and C244H for MTP11 and MTP8, respectively). Additionally the conserved leucine (L130S of MTP11) and isoleucine (I141S of MTP8) in the loop between TMD 1 and 2 has been chosen; this falls at the start of the signature sequence and is homologous to L82 of Os MTP1 (Menguer, et al., 2013) and L33 of Sc ZRC1 (Lin, et al., 2008), which have been shown to important for transporter function and specificity. Also of particular interest are the Mn-MTP-conserved DxxxD domains on TMDs 2 and 5. The mutations D149H and D258H of MTP8, and D138H and D247H of MTP11, will substitute these motifs for the Zn-MTP-conserved HxxxD domains, hypothetically substituting the DD-DD coordination at site A for HD-DD and DD-HD, respectively. D153A and D142A, of MTP8 and MTP11, respectively, will substitute this site for DA-DD; the equivalent mutation in Sc ZRC1 (Lin, et al., 2008) and At MTP1 (Kawachi, et al., 2012) abolishes transporter function.

5.2.5 Generating site-directed mutants for At MTP8 and At MTP11 and assessing their effect on function and specificity

The majority of site-directed mutants were generated using a kit to mutate the entry vector; MTP11-D142A is shown as an example of this process in Figure 5.15D and E. It was not possible to

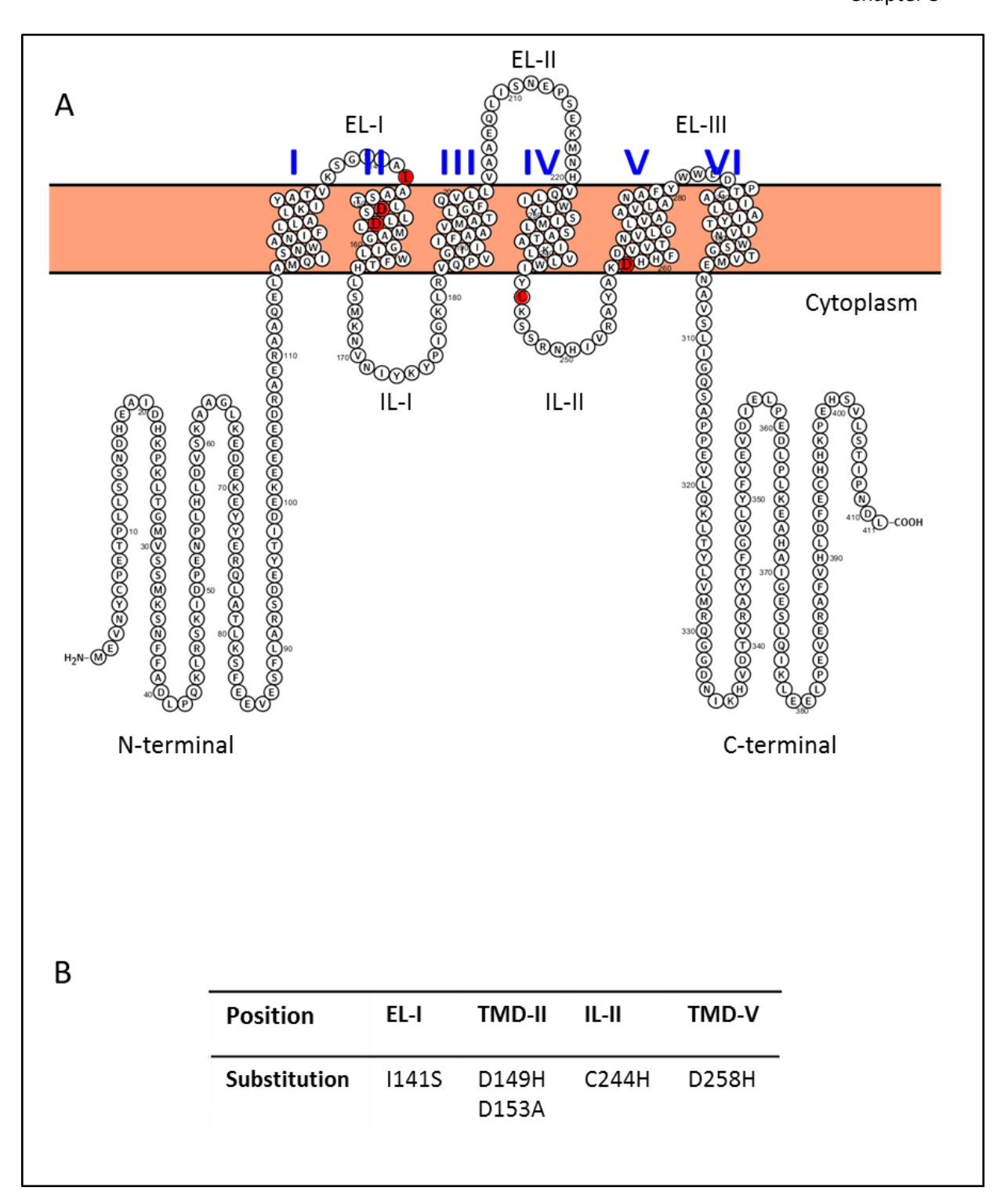


Figure 5.12. Hypothetical membrane topology of At MTP8.

A) Based on predictions by AramTmConsens (Schwacke, et al., 2003). Red residues are those chosen for At MTP8 site-directed mutagenesis. EL, extracytosolic loop; IL, intracytosolic loop. Visualised with Protter (Omasits, et al., 2014). B) Substitutions for site-directed mutagenesis of At MTP8, listed with positions in secondary membrane structure.

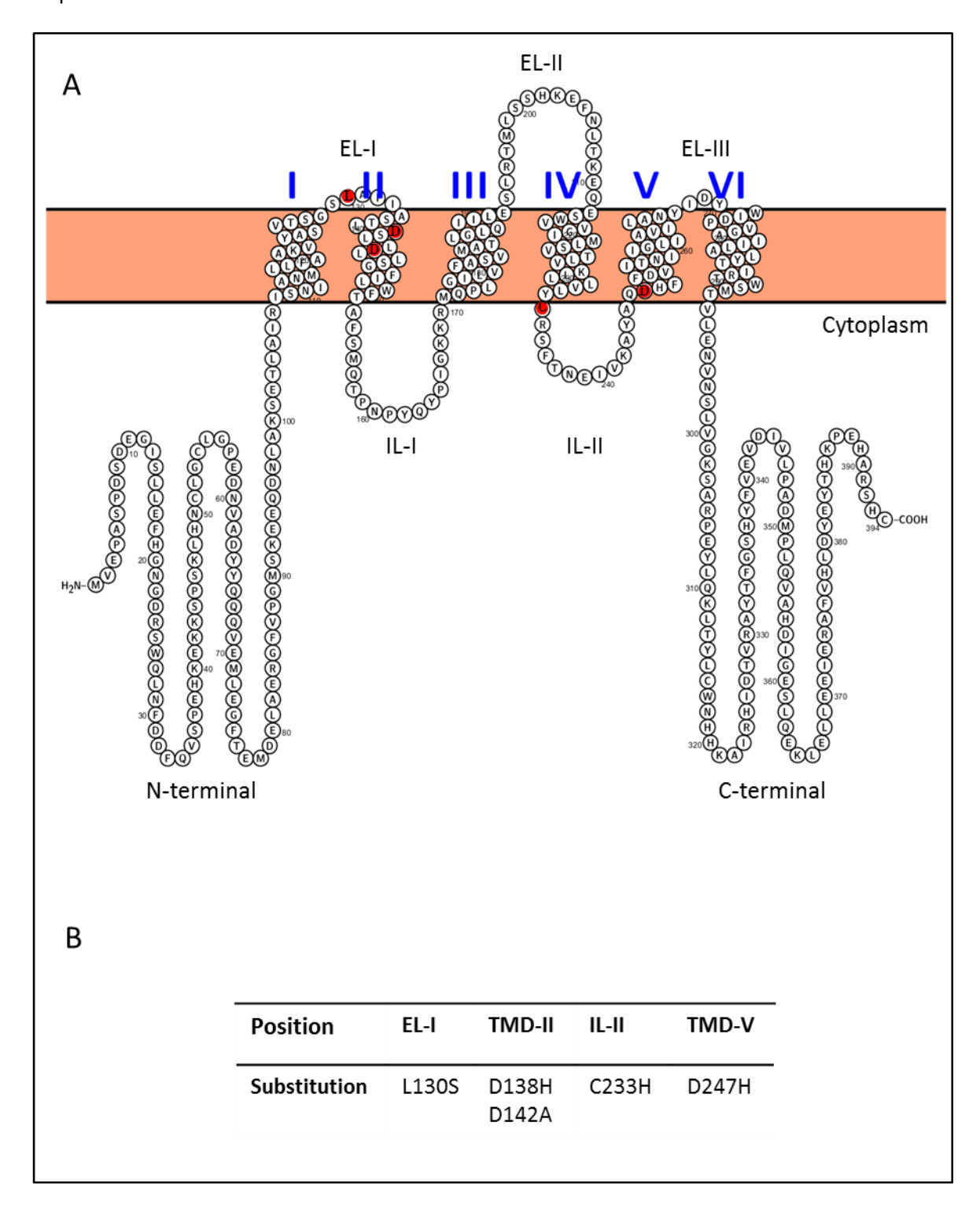


Figure 5.13. Hypothetical membrane topology of At MTP11.

A) Based on predictions by AramTmConsens (Schwacke, et al., 2003). Red residues are those chosen for At MTP11 site-directed mutagenesis. EL, extracytosolic loop; IL, intracytosolic loop. Visualised with Protter (Omasits, et al., 2014). B) Substitutions for site-directed mutagenesis of At MTP11, listed with positions in secondary membrane structure.

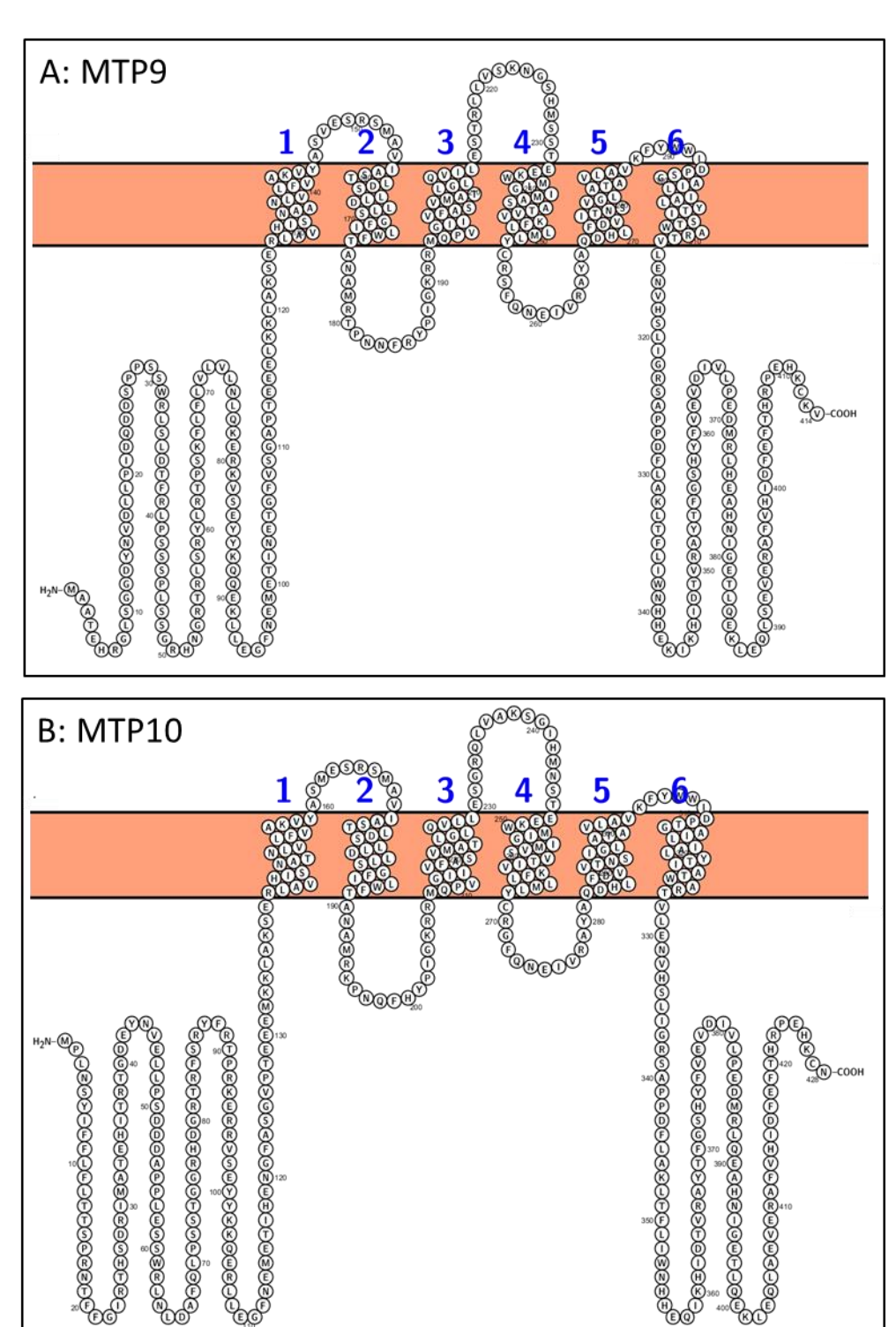


Figure 5.14. Hypothetical membrane topology of A) At MTP9 and B) At MT10.

Based on predictions by AramTmConsens (Schwacke, et al., 2003). Visualised with Protter (Omasits, et al., 2014).

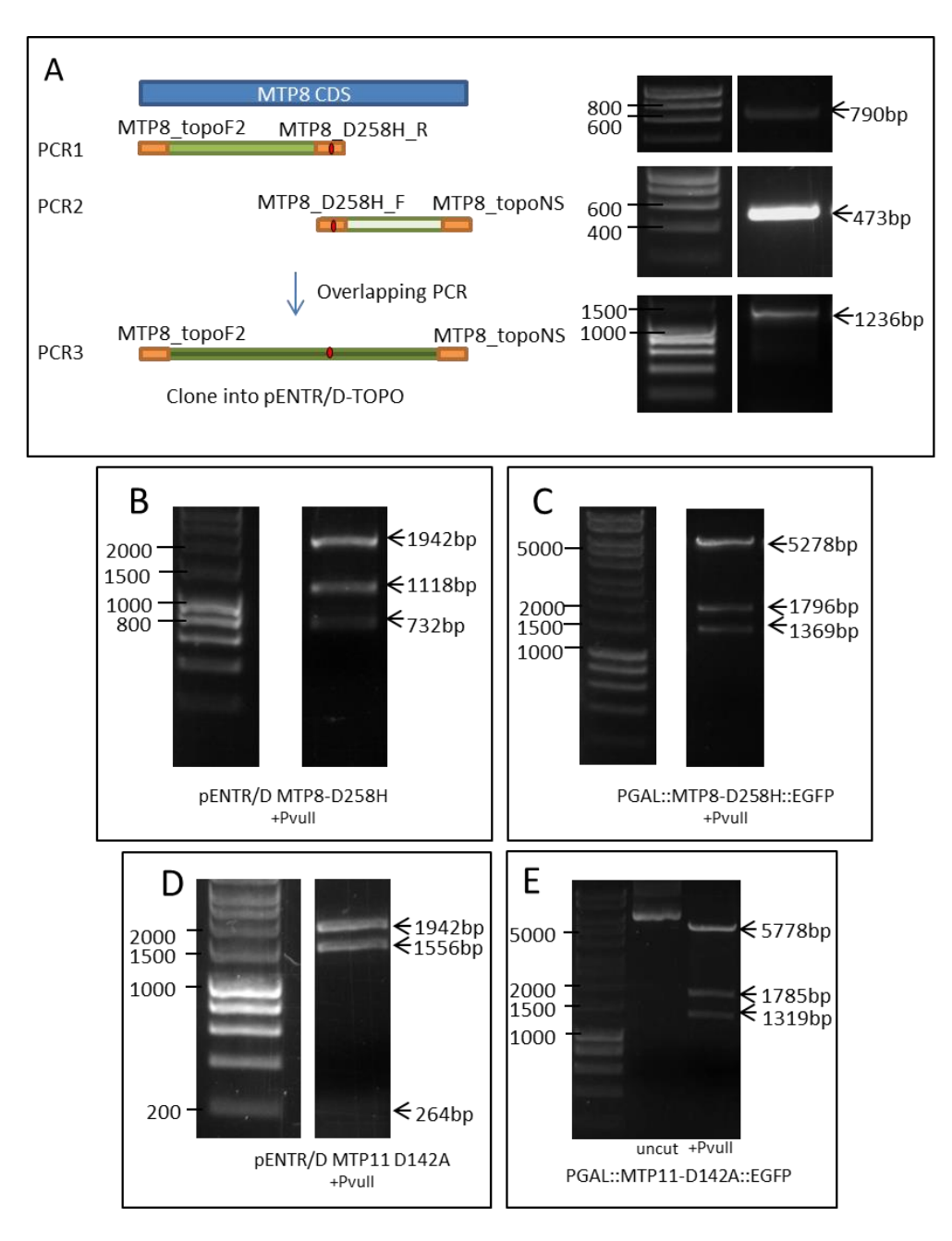


Figure 5.15. Generation of At MTP8 and At MTP11 site-directed mutants.

A) Cloning strategy to generate MTP8 mutant D258H. Two independent PCRs (1 and 2) amplify from MTP8 coding sequence (CDS), using primers that overlap and introduce D258H mutation. These are gel extracted and combined in overlapping PCR (3) to amplify full length MTP8 with D258H mutation. Successful amplification shown on right. B and C) Restriction digestion analysis of entry clone (B; pENTR/D MTP8-D258H) and yeast expression clone (C; PGAL::MTP8-D258H::EGFP) using *Pvull*. D and E) Normal process to generate site-directed mutants with QuickChange Lightning kit (Agilent) using MTP11-D142A as an example. Restriction digestion analysis of D) pENTR/D MTP11-D142A and E) PGAL::MTP11-D142A::EGFP with *Pvull*. All other mutants were generated in this way. A-E) Molecular weight marker sizes on left of gel; predicted fragment sizes on right of gel. All mutations confirmed with two independent sequencing reads.

generate MTP8-D258H using this kit, without resulting in sequence duplication or splicing from the MTP8 coding sequence. Instead, an overlapping PCR strategy was designed and employed (Figure 5.15A); positive clones were generated this way, as shown in Figure 5.15B and C. In all cases, mutations were generated in the GFP-tagged construct. All mutations were confirmed with at least two independent sequencing reads. Unfortunately, it was not possible to make the MTP8-C244H mutant either with the kit or the overlapping PCR method. Mutants were transformed into the Mn-, Zn-, Co- and Fe-sensitive yeast strains used previously.

Figures 5.16 and 5.17 show the effect of these mutations on the ability of At MTP8 and MTP11 to complement the Mn-sensitive *pmr1*. MTP8-I141S and MTP11-L130S are the only mutants to rescue Mn-sensitivity to the same level as the non-mutated version. All mutations relating to the DxxxD domains severely abolished Mn transport in both MTP8 and MTP11 and were unable to complement the Mn-sensitive phenotype of *pmr1*. It is noted that MTP8 mutations D149H, D153A and D258H failed to grow as well as the non-mutated version on galactose before addition of Mn; however, their growth is clearly further inhibited when the media is supplemented with Mn.

Each of the MTP8 mutants I141S, D149H and D258H displayed a very slight increase in tolerance to low levels of Zn compared to the non-mutated versions (Figure 5.18A). None of the mutations affected the Zn- or Co-transporting ability of MTP11 (Figure 5.18B). Both MTP8-D149H and MTP8-D258H, which would result in HD-DD and DD-HD, respectively, slightly increase the sensitivity of *ccc1* to Fe compared to the non-mutated version (Figure 5.19A); the equivalent mutations in MTP11 had no effect on sensitivity. MTP11-L130S is the only mutation to affect MTP11 Fesensitivity, with a slight enhancement of Fe-tolerance (Figure 5.19B).

The effect of these mutations on transporter function is summarised in Table 5.1. Unfortunately it was not possible to conclude the impact of some of the mutations as they repeatedly failed to grow on control conditions, galactose without addition of metal. Fluorescent microscopy was used to confirm that these mutations did not affect the subcellular localisation of MTP8 or MTP11 in yeast (not shown).

5.2.6 Modelling the potential tertiary structure of At MTP8

Ec YiiP is one of the few CDFs to be crystallised to date. The model of Ec YiiP Zn-transport is summarised in Figure 5.20A, which is coordinated by 3 Zn-binding sites, A, B and C. Ec YiiP forms a homodimer, stabilised by a key cysteine residue, C287 (Lu, et al., 2009); this is conserved in At MTP8 at C395, as highlighted in the alignment between Ec YiiP and At MTP8 in Figure 5.20B. Other key residues which are conserved include H261, H283 and D285, which facilitate a network of hydrogen-bonds to stabilise Zn-binding at site C (Lu, et al., 2009); as highlighted, these are

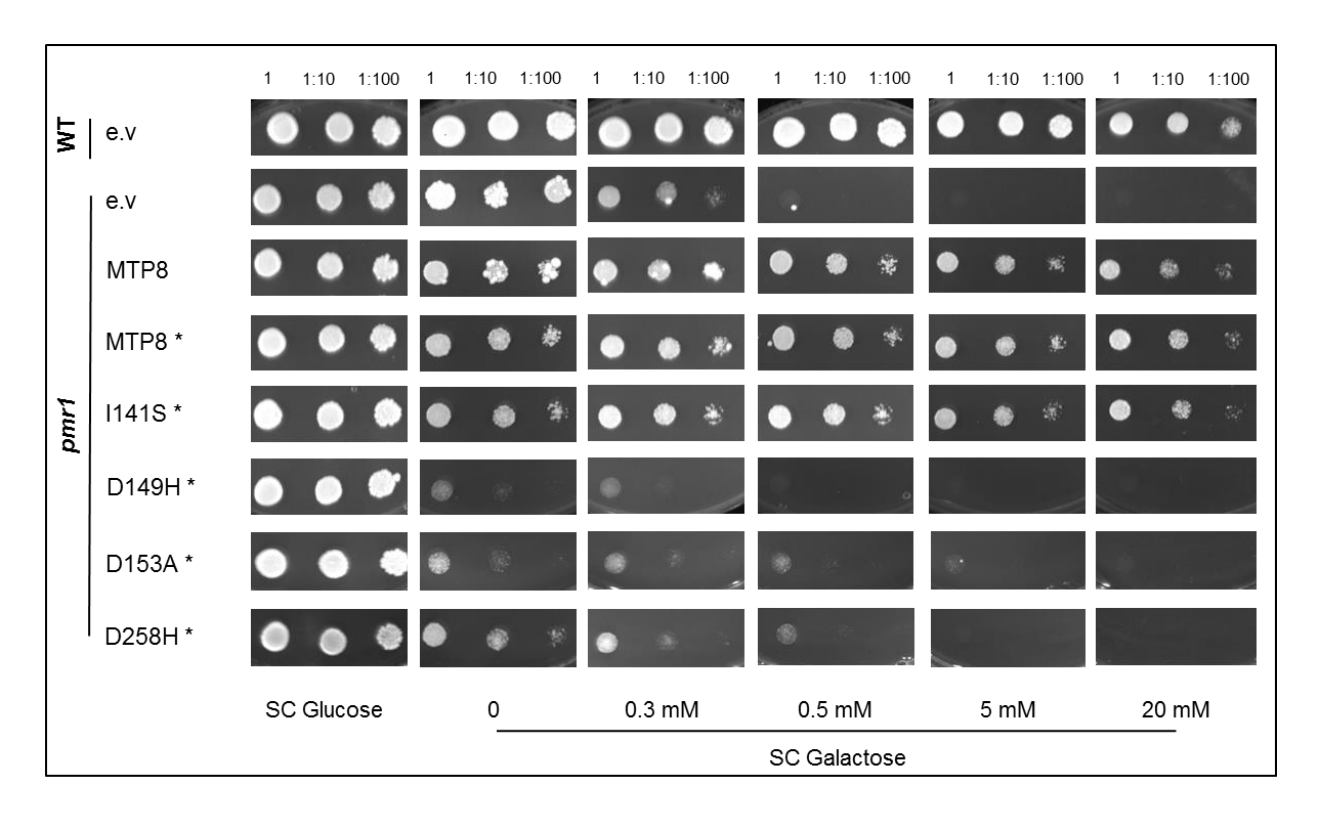


Figure 5.16. Functional analysis of At MTP8 and site-directed mutants in the Mn-sensitive Saccharomyces cerevisiae mutant pmr1.

BY4741 wild type (WT) was transformed with pAG426-EGFP empty vector (e.v.); pmr1 was transformed with pAG426-EGFP vector either empty or expressing At MTP8 with or without stop codon (*) or a range of At MTP8 * site-directed mutants. At MTP8 without stop codon generates a PGAL::MTP8::EGFP fusion protein. Numbers represent serial dilutions of yeast cells in liquid SC galactose without uracil: 1, undiluted OD $_{600}$ = 0.5, 1:10 and 1:100, dropped onto SC glucose or SC galactose without uracil supplemented with a range of Mn concentrations supplied, supplied as MnCl₂. Plates were incubated for 5 days at 30 °C.

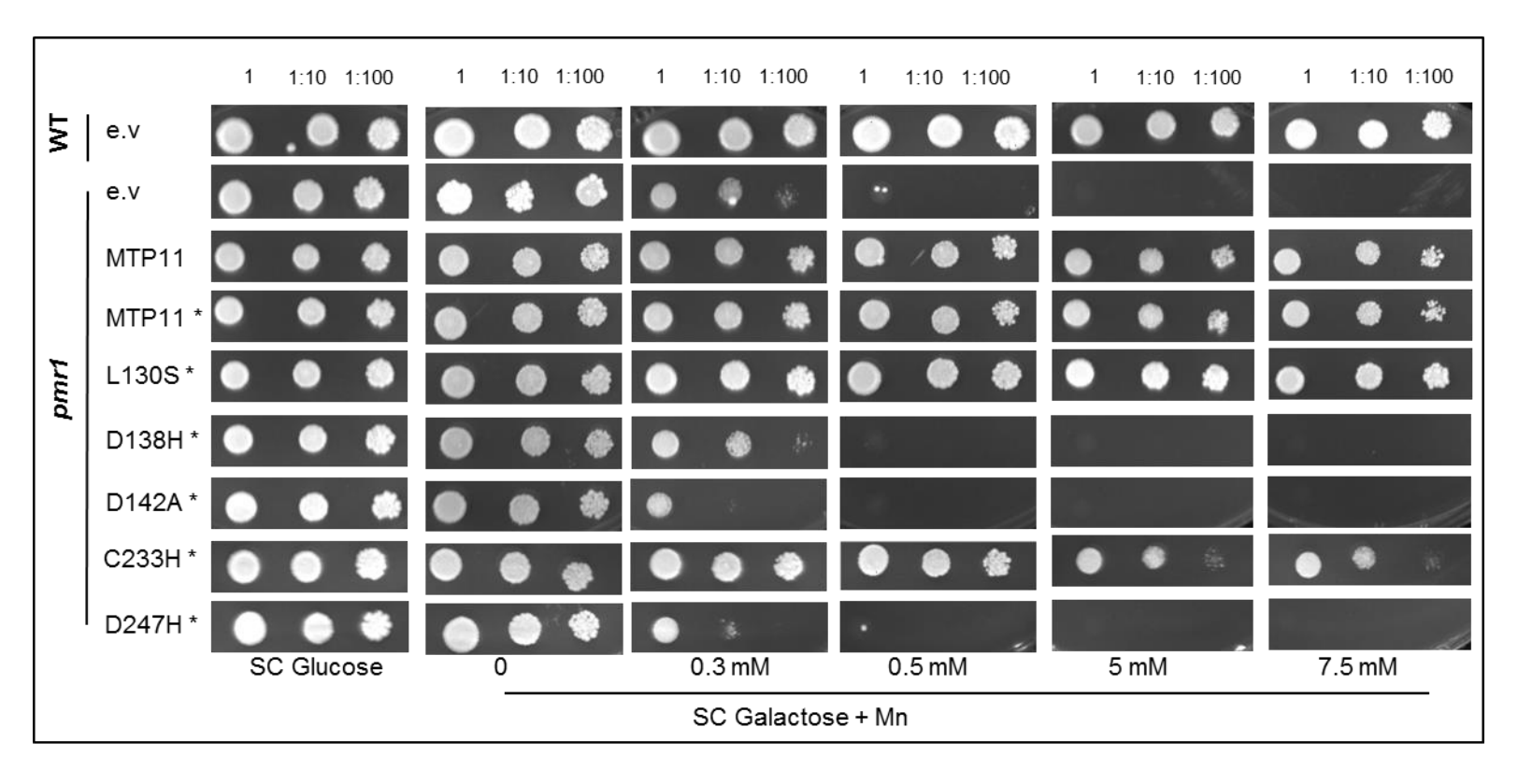


Figure 5.17. Functional analysis of At MTP11 and site-directed mutants in the Mn-sensitive Saccharomyces cerevisiae mutant pmr1.

BY4741 wild type (WT) was transformed with *pAG426GAL-EGFP* empty vector (e.v.); *pmr1* was transformed with *pAG426GAL-EGFP* vector either empty or expressing At MTP11 with or without stop codon (*) or a range of At MTP11 * site-directed mutants. At MTP11 without stop codon generates a PGAL::MTP11::EGFP fusion protein. Numbers represent serial dilutions of yeast cells in liquid SC galactose without uracil: undiluted (1) OD ₆₀₀ = 0.5, 1:10 and 1:100, dropped onto SC glucose or SC galactose without uracil supplemented with a range of Mn concentrations, supplied as MnCl₂. Plates were incubated for 5 days at 30 °C.

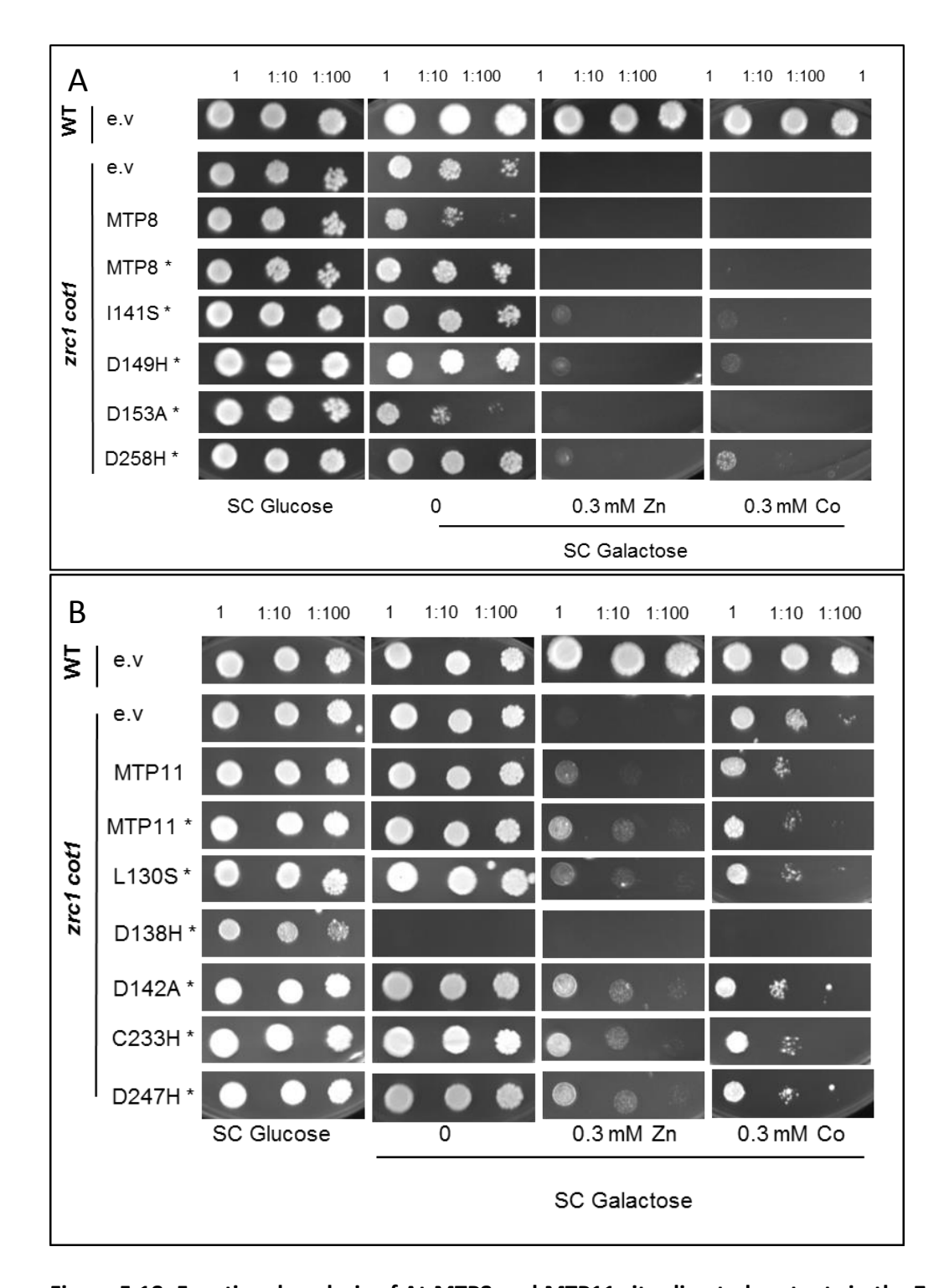
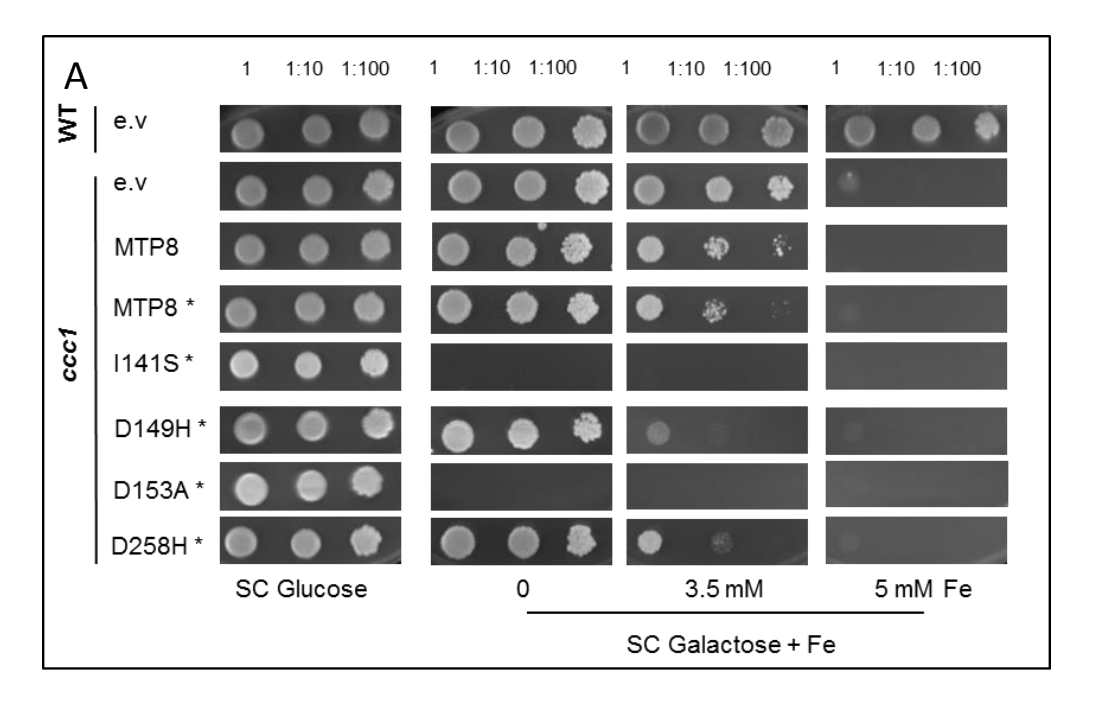


Figure 5.18. Functional analysis of At MTP8 and MTP11 site-directed mutants in the Zn- and Cosensitive *Saccharomyces cerevisiae* mutant *zrc1 cot1*.

BY4741 wild type (WT) was transformed with pAG426GAL-EGFP empty vector (e.v.); zrc1 cot1 was transformed with pAG426GAL-EGFP vector either empty or expressing A) At MTP8 or B) At MTP11 with or without stop codon (*) or a range of * site-directed mutants. At MTP8 without stop codon generates a PGAL::MTP8::EGFP fusion protein. Numbers represent serial dilutions of yeast cells in liquid SC galactose without uracil: undiluted (1) OD $_{600}$ = 0.5, 1:10 and 1:100, dropped onto SC glucose or SC galactose without uracil supplemented with 0.3 mM Zn or Co, supplied as ZnSO₄ and CoCl₂. Plates were incubated for 5 days at 30 °C.



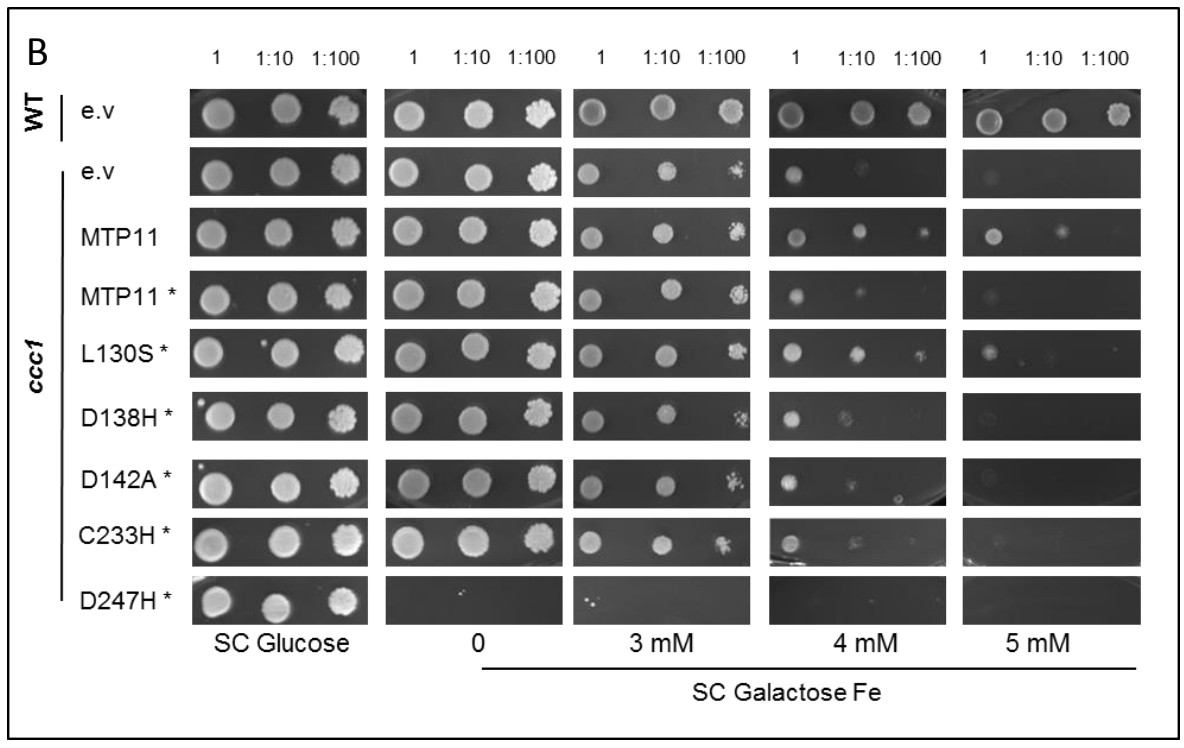


Figure 5.19. Functional analysis of At MTP8 and At MTP11 site-directed mutants in the Fesensitive *Saccharomyces cerevisiae* mutant *ccc1*.

DY150 wild type (WT) was transformed with pAG426GAL-EGFP empty vector (e.v.); ccc1 was transformed with pAG426GAL-EGFP vector either empty or expressing A) At MTP8 or B) At MTP11 with or without stop codon (*) or a range of * site-directed mutants. At MTP8 without stop codon generates a PGAL::MTP8::EGFP fusion protein. Numbers represent serial dilutions of yeast cells in liquid SC galactose without uracil: undiluted (1) OD $_{600} = 0.5$, 1:10 and 1:100, dropped onto SC glucose or SC galactose without uracil supplemented with a range of Fe concentrations, supplied as FeSO₄. Plates were incubated for 5 days at 30 °C.

Table 5.1. Impact of different mutations on metal transport ability of At MTP8 and At MTP11 when expressed in metal-sensitive yeast mutants.

x, reduction in tolerance; +, improvement in tolerance: number of symbols represents severity of change, from (x) very slight to (xxxx) severe; -, no change; ?, undetermined due to no growth on control plate; *, poor growth on control plate but could still observe a change with exposure to treatment.

	Mn	Zn	Со	Fe				
Mutation	Mutation in At MTP8							
I141S	-	+	+	?				
D149H	xxxx*	+	+	x				
D153A	xxxx*	-	-	?				
D258H	xxxx	+	+	-				
Mutation	Mutation in At MTP11							
L130S	-	-	-	+				
D138H	xxx	?	?	-				
D142A	XXXX	-	-	-				
D247H	xxx	-	-	?				
C233H	x	-	-	-				

conserved as H368, H390 and D392, respectively, in At MTP8. Contrastingly, H232 and H248 of Ec YiiP, which bind Zn at site C, are substituted for aspartate at D339 and D355, respectively. The hinge between the TMD portion and cytoplasmic domain (CTD) portion of Ec YiiP, the 'TMD-CTD hinge', is also labelled on Figure 5.20B.

Using Ec YiiP as a homology model template, the tertiary structures of At MTP8 and MTP11 were predicted and visualised using Swissmodel and PyMol (Biasini, et al., 2014); this is shown in Figure 5.21, alongside Ec YiiP. There are two clear protein domains; it is proposed these are the membrane-bound domain and the cytoplasmic domain, as labelled. Highlighted in red are the two DxxxD motifs; the inset shows a zoom of this area, forming the DD-DD site in At MTP8 and MTP11, or DD-HD in Ec YiiP. The aspartate and histidine residues of these domains are labelled. It is hypothesised, therefore, that these residues in At MTP8 and MTP11 form a DD-DD-coordinated Mn-binding pore, similarly to the DD-HD Zn-binding site A in Ec YiiP.

5.3 Discussion

5.3.1 At MTP8, At MTP10 and At MTP11 target the Golgi when expressed in yeast

Each of At MTP8, MTP10 and MTP11 appear punctate when expressed in yeast, indicating targeting to an intracellular membrane. Additionally MTP10 is predicted to possess a cleavable Nterminal signal peptide. The use of subcellular markers suggests MTP8 and MTP11 target the Golgi, correlating with that for MTP11 in planta. However, MTP8 targets the tonoplast when expressed in Arabidopsis and tobacco (Chapter 4). Other examples of proteins mislocalising when expressed in yeast include Sh MTP8, which also localises to the vacuole in planta but to the ER in yeast (Delhaize, et al., 2003), and the plasma membrane H⁺-ATPases AHA1 and AHA2 which are retained in the Golgi and ER, the protein secretory system, in yeast (Villalba, et al., 1992; Jahn, et al., 2001). In the case of AHA1, the protein was still fully functional (Villalba, et al., 1992) as appears to be the case for MTP8, which can confer Mn tolerance to at least 20 mM Mn. Different hypotheses have been proposed for assumed incorrect targeting in different systems. For example, correct folding of monomers and assembly into oligomers is often a prerequisite for protein export from the secretory system (Lodish, et al., 1988). Alternatively, it is possible another endogenous plant protein is required for correct localisation. For example, At MTP5 and MTP12 must form a functional heterodimer in the Golgi to restore Zn-tolerance in zrc1 cot1 (Fujiwara, et al., 2015); a similar interaction is maybe needed for MTP8 to target the tonoplast. However, it is also possible that the MTP8 coding sequence contains a motif that either does not permit exiting from the secretory system to target other membranes when expressed in yeast, or motifs which dictate targeting specifically to the Golgi. Sequence analysis of the MTPs predicted targeting of

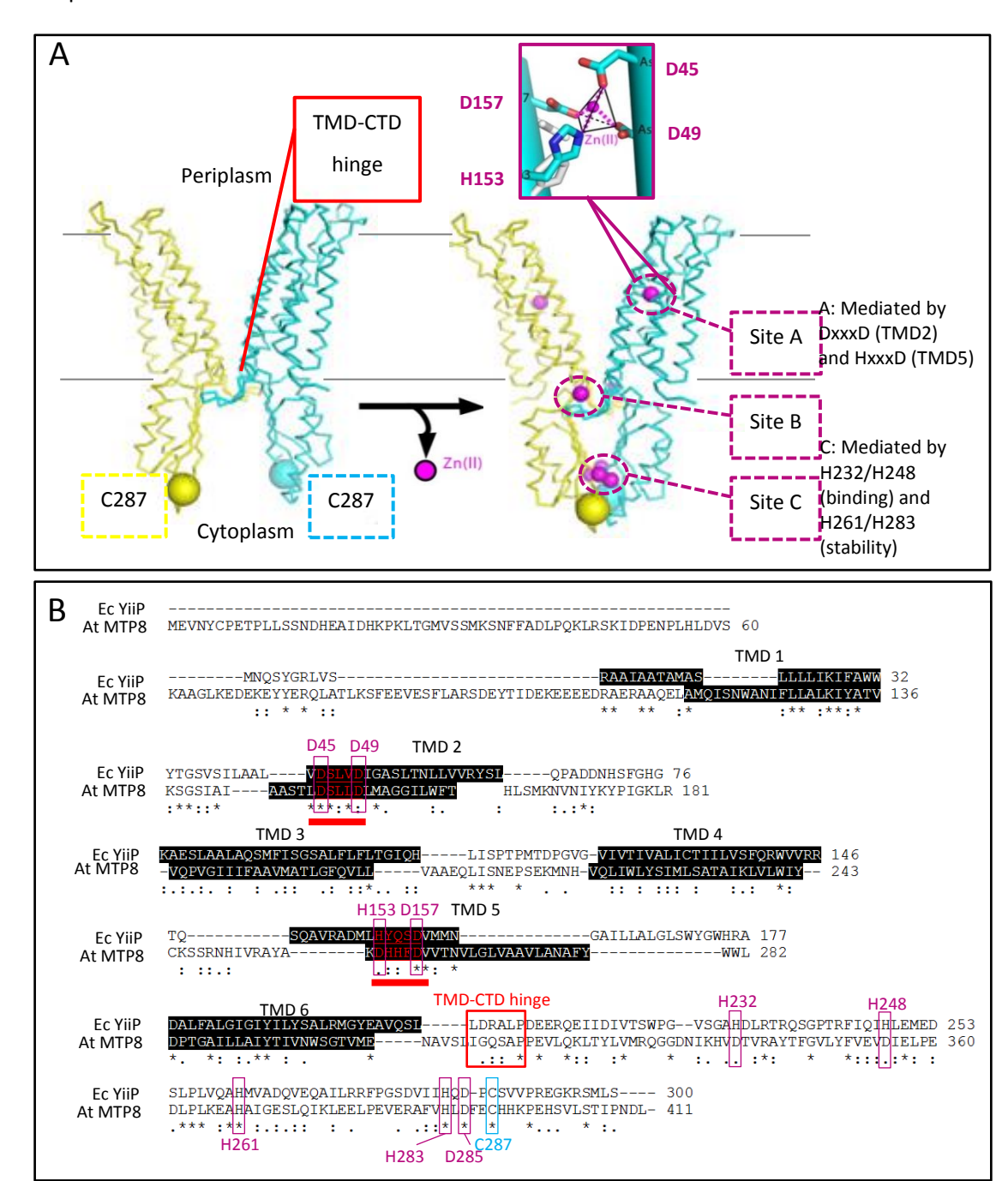


Figure 5.20. Comparison of Ec YiiP with At MTP8.

A) YiiP structure within the transmembrane domain (TMD; membrane position marked by grey bars) and cytoplasmic domain (CTD). YiiP acts as a homodimer (yellow and blue for each protomer). DxxxD/HxxxD domains underlined in red. Cysteine residue C287 from each protomer labelled (yellow and blue spheres) move together after Zn (pink spheres) binds to protein to stabilise dimer at cytoplasmic domain. Zn (pink sphere) binds to 3 sites, A, B and C within each protomer. Site A is mediated by D/H residues in TMDs 2 and 5 forming tetrahedral complex around Zn ion; see insert. Site C is mediated by 2 key histidines at H232 and H248. TMD and CTDs connected by TMD-CTD hinge, red. Adapted from Lu, et al., 2009. B) Amino acid sequence of Ec YiiP aligned to At MTP8. Black boxes, predicted TMDs, labelled I-VI. Key residues important for Zn binding and function, highlighted in part A, are labelled on the sequence to show conserved or substituted residues. Alignment: (*), positions with a single, fully conserved value. (:), conservation between amino acids of strongly similar properties.

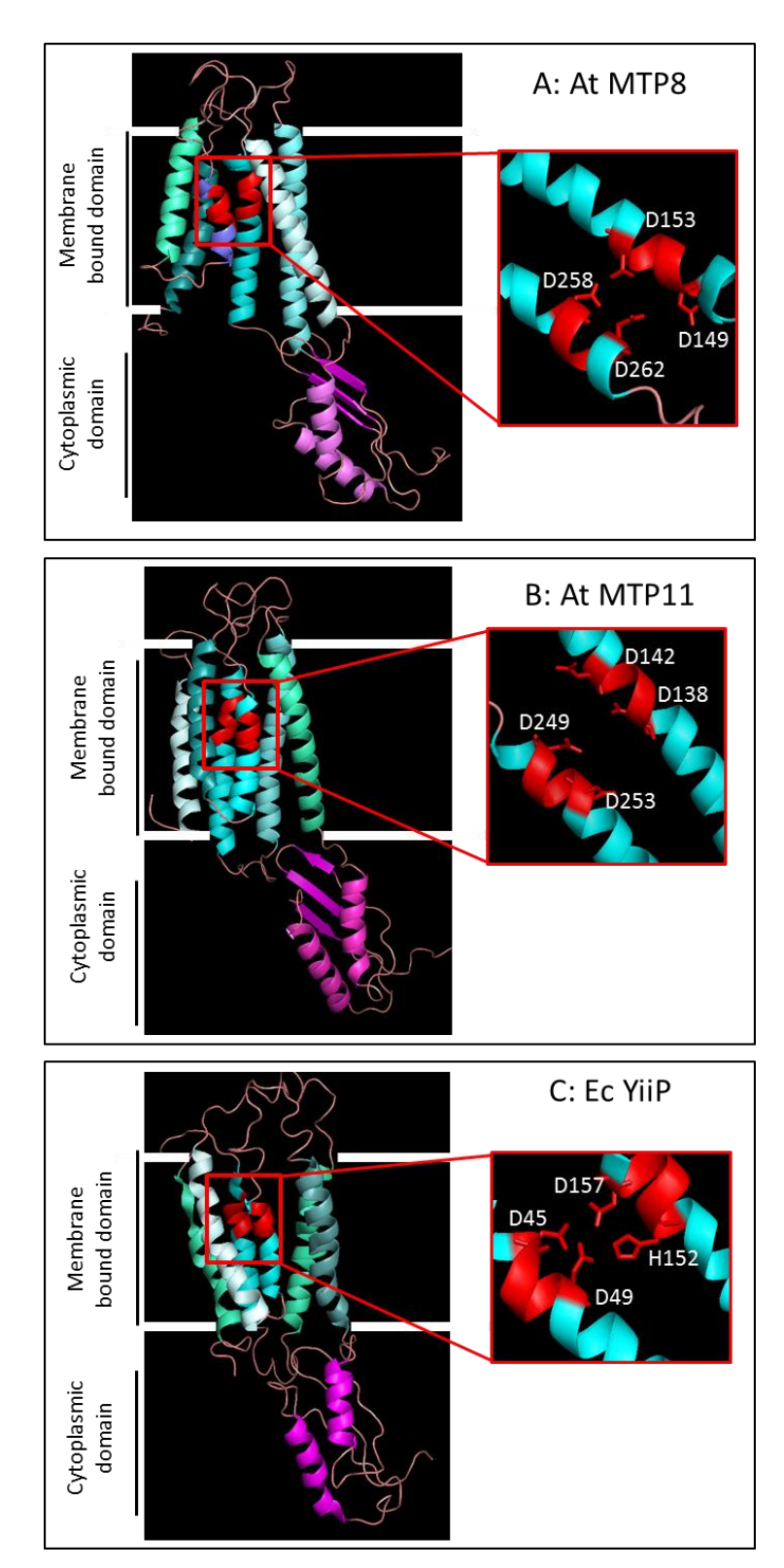


Figure 5.21. Predicted tertiary structure of Ec YiiP, At MTP8 and At MTP11 generated using Swissmodel (Biasini, et al., 2014) with Ec YiiP as a homology model template.

Blue spirals, α helices spanning 6 transmembrane domains (TMDs). Pink spirals and arrows, α helices and β sheets forming cytoplasmic domain. Red, positioning of DxxxD domains on TMD 2 and 5 in tertiary structure. White bars show predicted positioning of membrane with respect to protein, based on findings of Ec YiiP (Wei & Fu, 2005; Li & Fu, 2007; Li, et al., 2009) and TMD predictions, resulting in membrane-bound and cytoplasmic domains. Inset: Zoom in of DxxxD domains with aspartate (D) residues labelled.

Chapter 5

MTP10 and MTP11 to the secretory system or the Golgi. Although the values for MTP8 did not reach the threshold value to be predicted to target these organelles in plants, these values were still positive and not as low as predicted for MTP9. It is therefore possible that MTP8 possesses a motif that results in an increased likelihood of targeting the Golgi when expressed in yeast.

5.3.2 MTP8 and MTP10 are strong Mn transporters

Both MTP8 and MTP10 are able to restore tolerance of pmr1 to that of the WT up to at least 20 mM Mn. This is higher than the 6 mM previously been tested for MTP8 (Eroglu, et al., 2016) or the 8 mM tested for the most closely related protein to MTP10, Bm MTP10 (Erbasol, et al., 2013). MTP11 still confers tolerance to pmr1 but not to the same extent as MTP8 and MTP10; perhaps MTP8 and MTP10 show different kinetic properties for Mn compared to MTP11. The alignment of Figure 5.20 and the 3D model proposed in Figure 5.21 suggests MTP8 shares a similar structure with Ec YiiP, with a cytoplasmic domain connected to a distinct transmembrane domain by a 'hinge' region. It should be noted, however, that Ec YiiP was used as the homology template, so the model is likely biased. One hypothetical reason for the difference in Mn transport by MTP8 and MTP11 could be this hinge region. Ec YiiP was originally proposed to function as a metallochaperone; however, the flexibility of this hinge allows for a rapid transfer of Zn across the membrane, with a turnover rate of several magnitudes higher than that of metallochaperones (Lu, et al., 2009). As highlighted in Figure 5.20B, the LDRALP motif at this hinge region in Ec YiiP is substituted for a IGQSAP motif in At MTP8, maintaining similar charge and properties in 3 out of 6 residues. Of particular note is the proline at the end, which in transmembrane domains can serve as a helix breaker, disrupting folded structures like helices and sheets and forcing a kink in the protein chain, possibly aiding flexibility of this hinge. This proline is conserved in the IGRSAP motif of MTP10, but is substituted for R in the VGKSAR of MTP11. Site-directed mutagenesis studies relating to this hinge region may be an interesting place to start when determining why MTP8 and MTP10 are better at transporting Mn than MTP11.

That MTP8 targets the Golgi rather than the vacuole possibly masks the ability to interpret the determination of its specificity. Expression of MTP8 in *ccc1* increases sensitivity to Fe compared to the empty vector. It is therefore possible that MTP8 is capable of transporting Fe, but is conferring increased sensitivity to Fe by transporting it into the Golgi rather than into the vacuole, as it would *in planta*. Tolerance to Fe-deficiency in *fet3 fet4* was not restored by expression of either Mn-MTP, but this does not necessarily rule out the ability to transport Fe; *fet3 fet4* lacks routes for Fe uptake (Eide, et al., 1996; Li & Kaplan, 1998) so it is likely a protein must provide Fe uptake, rather than intracellular Fe transport, to rescue this phenotype. MTP11 is the only transporter

tested to confer tolerance to Fe when expressed in ccc1, a finding that has not been previously been explored.

The GFP tag interferes with transport function for both MTP10 and MTP11; this is most obvious for MTP10 in *pmr1* and MTP11 in *ccc1*. If MTP10 and MTP11 were to function similarly to Ec YiiP, forming a homodimer stabilised by the cytoplasmic domain (Lu & Fu, 2007; Lu, et al., 2009), it is possible that the bulky GFP could interfere with this connection and impair protein function. It would be interesting to generate an N-terminal construct to compare.

5.3.3 DxxxD domains play important roles in Mn-MTP function

The presence of conserved residues between key regions of MTP8 and YiiP may suggest these proteins share a similar structure-function relationship. The DD-HD complex of Ec YiiP coordinates Zn-binding at site A, as shown in the insert of Figure 5.20A (Lu, et al., 2009; Gupta, et al., 2014); it is hypothesised that the DxxxD motifs of MTP8 fold to form a Mn-binding DD-DD complex at site A (Figure 5.21). It was hypothesised that the residues of these motifs would play an important role in maintaining transport function and specificity. Indeed, substituting the HD-HD complex in the Zn-transporting Os MTP1 for DD-HD (mutation H90D) abolishes Zn transport but increases affinity for Fe (Menguer, et al., 2013). Substituting aspartate for histidine in MTP8 (mutations D149H/D258H) and MTP11 (D138H/D247H), forming a HD-DD or DD-HD coordination site in place of DD-DD, seems to abolish Mn transport. This is conclusive for MTP11; unfortunately MTP8-D149H routinely failed to grow comparably to unmutated MTP8 on the galactose control plate in pmr1, so it is not entirely conclusive, but growth was clearly further inhibited with addition of Mn. These mutations in MTP8 appear to confer a slight resistance to Zn and Co in zrc1cot1, which may suggest a small increase in affinity for Zn and Co transport. A very slight increase in Fe sensitivity is also observed in ccc1. As discussed in Section 5.3.2, MTP8 may be able to transport Fe in yeast, causing an increase in sensitivity in ccc1 compared to the empty vector by sequestering Fe into the Golgi; D149H and D247H mutations also increase Fe sensitivity of ccc1 relative to the unmutated MTP8, which may suggest an enhancement of Fe transport, although this is inconclusive. Neither of these mutations affects the Zn-, Co- or Fe-tolerance compared to the unmutated version of MTP11, although it is noted that the MTP11-D138H mutation did not grow on the zrc1 cot1 galactose plate. The DD-DD domain has also very recently been shown to be important for maintaining function of Os MTP8.1; substituting either of the D residues for A abolishes Mn tolerance in pmr1, but a change in specificity was not tested (Chen, et al., 2016).

The D153A and D142A mutations also appear to abolish Mn transport in MTP8 and MTP11, respectively. It is again acknowledged that MTP8-D153A did not grow comparably on the *pmr1*

Chapter 5

galactose plate, but growth is clearly inhibited with addition of Mn. These mutations would result in a DA-DD complex in place of DD-DD at the hypothetical Mn-binding site A, possibly disturbing its ability to bind Mn. Substituting aspartate (D) for alanine (A) loses the negative side chain, likely important for binding the positive charge of Mn. Although loss-of-function mutations can imply a breakdown in tertiary structure or blocking of a transport pore, alanine is quite small and with a non-reactive side chain, so does not tend to cause large alterations to protein structure and conformation (Betts & Russell, 2003). The loss of Mn-transport in this mutation may therefore highlight the importance of residue D153, conserved in all CDFs and MTPs identified to date (Montanini, et al., 2007; Gustin, et al., 2011), in maintaining the metal binding site A; the equivalent mutation in At MTP1 (D94A; Kawachi, et al., 2012) and in Os MTP11 (D162A, Williams, et al., unpublished data) also abolishes Zn and Mn transport, respectively.

The very slight change in sensitivity to Zn and Fe conferred by D149H and D258H in MTP8 might imply the residues coordinating the DD-DD complex affect specificity of site A. Recent studies compared two human CDFs, Zn-transporting ZnT1 and Mn-transporting SLC30A10, generating chimeric proteins to indicate both the TMD- and cytoplasmic-regions of the proteins are essential for function, but only the TMD-region, which contains the binding site A, is essential for maintaining specificity (Zogzas, et al., 2016; Nishito, et al., 2016). However, based on similarities and differences in the alignment of Ec YiiP and MTP8, it is proposed that additional residues in the cytoplasmic domain of MTP8, in particular those surrounding hypothetical binding site C, may also play a role in maintaining specificity. The conserved and non-conserved residues are highlighted in Figure 5.20B and it is hypothesised that a more obvious change in specificity of MTP8 might be observed when residues at both site A and site C are mutated simultaneously. Of particular interest are the Zn-binding histidines at site C of Ec YiiP, H261 and H283, which are substituted for D339 and D355 in MTP8. The equivalent residues in Os MTP8.1 have recently been shown to be important for Mn transport, but Zn transport was not tested (Chen, et al., 2016). It may be interesting to generate D339H and D355H mutations in combination with D149H and D258H, which may increase the affinity of MTP8 to bind and transport Zn, in place of Mn.

Other residues which suggest MTP8 possesses a Mn-binding site C are the conserved neighbouring histidines and aspartate (Lu & Fu, 2007; Lu, et al., 2009); H232, H248 and D285 in Ec YiiP are proposed to form a network of hydrogen-bonds to stabilise site C, and are conserved in MTP8 as H368, H390 and D392. Additionally, dimerization of Ec YiiP further stabilises site C and is coordinated by the cysteine at C287 (Lu, et al., 2009); this is conserved at C395 in MTP8, as highlighted in Figure 5.209B, which may suggest MTP8 also forms a homodimer at the C-terminal, cytoplasmic domain of the protein. Throughout the course of this project, efforts have been made to optimise the purification process of At MTP8, in collaboration with the Oxford Protein

Production Facility at the Research Complex at Harwell (data not shown). Following purification it may be interesting to analyse the structure of MTP8 further, using non-denaturing or native gel electrophoresis and gel filtration chromatography, to determine whether MTP8 exists mostly as a dimer or a protomer. Further, it would be very interesting to eventually perform crystallography studies on purified MTP8, to determine its tertiary structure, including whether Mn-binding sites A, B and C are present.

Chapter 6: The Roles of At ECA3, At NRAMP1 and At NRAMP2 in Mn Deficiency

6.1 Introduction

The main focus of this thesis so far has been on Mn toxicity, but Mn deficiency is an equally important stress condition for plants. This chapter will focus on some of the transporters involved in alleviating Mn deficiency. Playing a key role in this process is At NRAMP1, a plasma membrane transporter that has been shown to transport both Mn and Fe into the cell (Curie, et al., 2000; Cailliatte, et al., 2010). The *nramp1-1* T-DNA insertion mutant was previously shown to be sensitive to Mn deficiency conditions (Cailliatte, et al., 2010). Here, *nramp1-1* is investigated alongside *nramp1-2* and *nramp1-3*, two additional mutants identified and isolated prior to the start of this project (Williams, et al., unpublished data). This chapter aims to further characterise the different *nramp1* mutants to increase understanding of the NRAMP1 structure and function relationship. This will be related to the structure of Sca DMT, from *Staphylococcus capitis*, one of the few NRAMP family members to have its structure determined through crystallography studies (Ehrnstorfer, et al., 2014).

Of the six Arabidopsis NRAMP members, At NRAMP2 remains one of the last remaining to be functionally characterised, although it has been shown not to rescue the Fe-deficient yeast mutant *fet3 fet4*, defective in Fe uptake (Curie, et al., 2000). While At NRAMP1 clusters into the 'Plant 1' clade of the NRAMP phylogenetic tree, At NRAMP2 clusters into the 'Plant 2' clade, with At NRAMP3 and NRAMP4; the Plant 2 clade also clusters more closely with the animal clade (Figure 1.11; Pottier, et al., 2015). The majority of proteins clustering near At NRAMP2 are able to transport both Fe and Mn (Lanquar, et al., 2005; Lanquar, et al., 2010); for example, the related human protein DMT1 has a relatively broad substrate range, coupling transport of Mn, Fe, Ni, Pb, Zn, Co, Cu and Cd with proton-exchange (Gruenheid, et al., 1995; Gunshin, et al., 1997; Ehrnstorfer, et al., 2014). This chapter therefore aims to characterise the role of At NRAMP2 in Mn homeostasis of Arabidopsis, including beginning to elucidate its specificity. The first step in this process is to identify and isolate T-DNA insertion mutants for *nramp2* to determine whether any metal-dependent phenotype is observed when At NRAMP2 is non-functional. Additionally, this chapter aims to clone At NRAMP2 for expression in tobacco, to determine its subcellular localisation, and in yeast, to determine its transport properties.

Chapter 6

At ECA3 is a P-type ATPase Ca-pump proposed to be of importance in alleviating Mn deficiency (Mills, et al., 2008). However, it has also been implicated to function under Mn toxicity (Li, et al., 2008). Because At MTP11 is also known to function in alleviating Mn toxicity (Delhaize, et al., 2007; Peiter, et al., 2007), a double mutant *eca3 mtp11* was isolated prior to the start of this project (Williams, et al., unpublished data). This chapter aims to characterise the *eca3 mtp11* double mutant under Mn extremes, using normal Ca conditions and the low Ca regime introduced in Chapter 3, to determine the role of At ECA3 in Mn homeostasis. Further, as described in the General Introduction, the subcellular localisation of At ECA3 has been disputed, targeting either the Golgi (Mills, et al., 2008) or the pre-vacuolar compartment or endosome (Li, et al., 2008). This chapter aims to resolve this discrepancy by transiently expressing an ECA3::YFP construct in tobacco, with a range of subcellular markers. Determining where a transporter functions is a key step in providing a model for its physiological role; as both At MTP11 and At ECA3 have been implicated in Mn toxicity, it will be interesting to see if they co-localise at the subcellular level.

6.1.1 Aims

- 1. To isolate T-DNA insertion mutants for At NRAMP2 and characterise any Mn-dependent characterisation
- 2. To compare three independent *nramp1* mutants under Mn deficiency
- 3. To characterise the *eca3-1 mtp11-1* double mutant using plate- and hydroponics-based assays to determine the role of At ECA3 in Mn deficiency and toxicity
- 4. To transiently express At ECA3 in tobacco to determine its subcellular localisation, especially in relation to At MTP11
- 5. To clone the At NRAMP2 coding sequence for subcellular localisation studies in tobacco
- 6. To isolate and characterise double and triple mutants for *eca3-1*, *nramp1-1* and *nramp2-1* to determine their relative contribution to Mn deficiency

6.2 Results

6.2.1 Three nramp1 mutants display different levels of sensitivity to Mn deficiency

An alignment of At NRAMP1 with Sca DMT in shown in Figure 6.1, with predicted transmembrane domains (TMDs) highlighted. The predicted TMDs for NRAMP1 are based on an output from AramTmConsens, a consensus TMD prediction programme (Schwacke, et al., 2003). While Sca DMT has 11 TMDs confirmed by crystallography (Erhnstorfer, et al., 2014), here At NRAMP1 is predicted to have an additional 12th TMD, in the elongated 3' end compared to the sequence of Sca DMT. Also included in Figure 6.1 are small regions of alignment with *E. coli* NRAMP family

member, MntH. The alignment includes key residues which have been shown to be important for maintaining the structure, and thus function, of Sca DMT and Ec MntH (Courville, et al., 2008; Ehrnstorfer, et al., 2014; Cellier, et al., 2016). For example, the DPGN motif of TMD 1, the AxxMxH motif of TMD 6 and the CTM domain are each conserved in At NRAMP1. Additionally, key asparagine (N) residues which support the structure of MntH by maintaining inter-helix contacts between neighbouring TMDs (Courville, et al., 2008) are also conserved in At NRAMP1, at residues N282 and N446. Finally, the M226 of Sca DMT has been shown to be important for maintaining transport specificity, by selecting against alkaline earth metals, such as Mg and Ca, in favour of transition metals; this M is conserved in NRAMP1 at M236. The predicted TMDs of NRAMP1 are also visualised in Figure 6.2B.

Three insertion mutants are available for nramp1 and were provided for use in this project; their insertion sites were confirmed by sequencing, as visualised in Figure 6.2A. While nramp1-1 and nramp1-3 insertions fall in the 9th exon of NRAMP1, nramp1-2 falls within the 6th exon. These mutants display differential sensitivities to Mn deficiency. In addition to the plate-based assay used in earlier chapters, a hydroponics growth system was developed throughout the course of this project. Unlike the ½ MS media using in plate assays, hydroponic plants are grown on liquid Modified Hoaglands (MH) media (see Table 2.3 for comparison of components). A benefit of this hydroponic system is that it enables plants to be exposed to different conditions throughout the experiment, also allowing growth of seedlings to more mature stages of development. The nramp1 mutants were grown hydroponically under two different Mn deficiency regimes: exposure to deficiency from day 0 of the experiment, for the full 42 days (Figure 6.3) or growth on control media for 29 days before transfer to deficiency for the remaining 48 days of the experiment (Figure 6.4). When exposed to Mn deficiency from day 0, all nramp1 mutants are significantly stunted compared to the WT. However, nramp1-2 displays an intermediate level of stunting and is not as affected as nramp1-1 and nramp1-3 (Figure 6.3). Similarly, nramp1-2 displays an intermediate phenotype in the delayed-exposure regime, but the level of stunting is not significantly different compared to the WT. Both nramp1-1 and nramp1-3 are significantly stunted under Mn deficiency delayed-exposure regime (Figure 6.4). It should be noted, however, that nramp1-1 and nramp1-3 are also smaller than WT under control conditions in Figure 6.3.

Given the positions of the inserts (Figure 6.2), it is possible that the different sensitivities of the *nramp1* mutants are due to the translation of a truncated but still semi-functional protein in *nramp1-2*. The confirmatory gel in Figure 6.5 compares the presence of *NRAMP1* transcript in WT, *nramp1-1* and *nramp1-2*. Primers which span the insertion site for *nramp1-2* do not amplify a product in line with that of the WT, suggesting the full *NRAMP1* transcript is not present in *nramp1-2* (Figure 6.5B). However, using primers which bind further downstream of the insert site

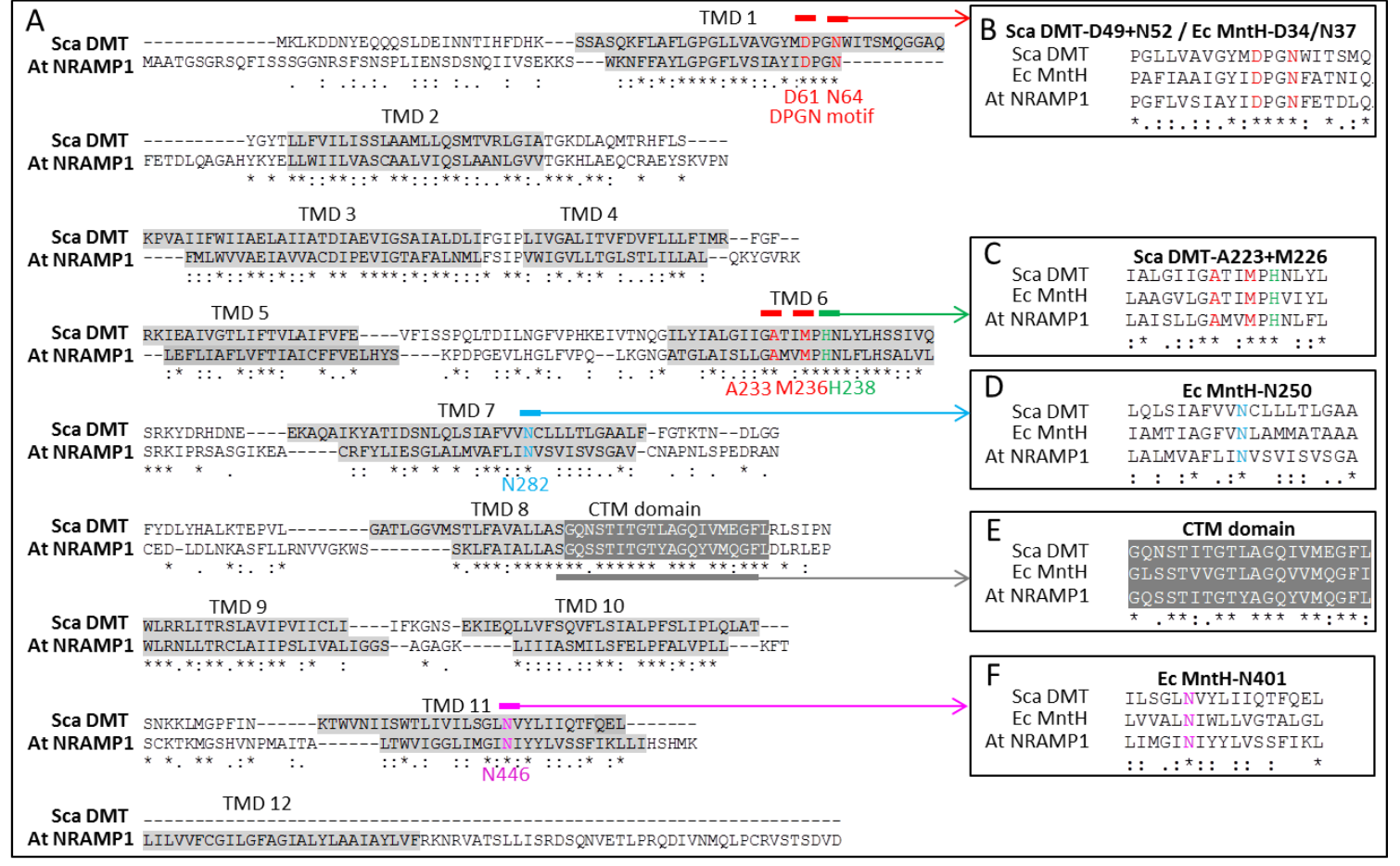
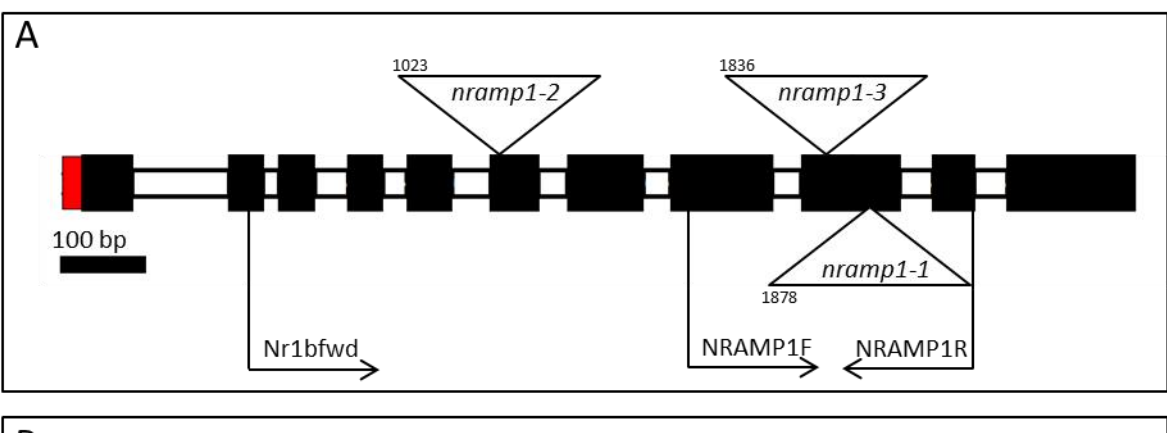


Figure 6.1. Alignment of At NRAMP1 with Staphylococcus capitis DMT (Sca DMT) and E. coli MntH, two prokaryotic NRAMP homologs.

Alignment adapted from output from Clustal Omega (Sievers, et al., 2011). A) Grey highlight, predicted transmembrane domains (TMDs): NRAMP1 TMDs based on output from AramTmConsens (Scwacke, et al., 2003) and this alignment; Sca DMT TMDs based on findings by Erhnstorfer, et al. (2014). DPGN motif labelled (Haemig & Brooker, 2004). Key residues highlighted proposed to be important for function based on findings for Ec MntH by Courville, et al. (2008) and for Sca DMT by Erhnstorfer, et al. (2014): B+C) Sca DMT residues D49 and N52, and A223 and M226 (red), in TMD 1 and 6, respectively, are conserved in At NRAMP1 and MntH; H211 of MntH TMD 6 (green) is conserved in At NRAMP1 and Sca DMT. D) N250 of MntH TMD 7 (blue) is conserved in Sca DMT and At NRAMP1. E) The Consensus Transport Motif (grey with white writing; Curie, et al., 2000) is conserved in each protein analysed here. F) N401 of MntH TMD 11 (pink) is conserved in Sca DMT and At NRAMP1. Residue identification in NRAMP1 listed below alignment in (A). A-F) (*), fully conserved residues between sequences; (:), conservation of residues with strongly similar properties; (.), conservation of residues with weakly similar properties.



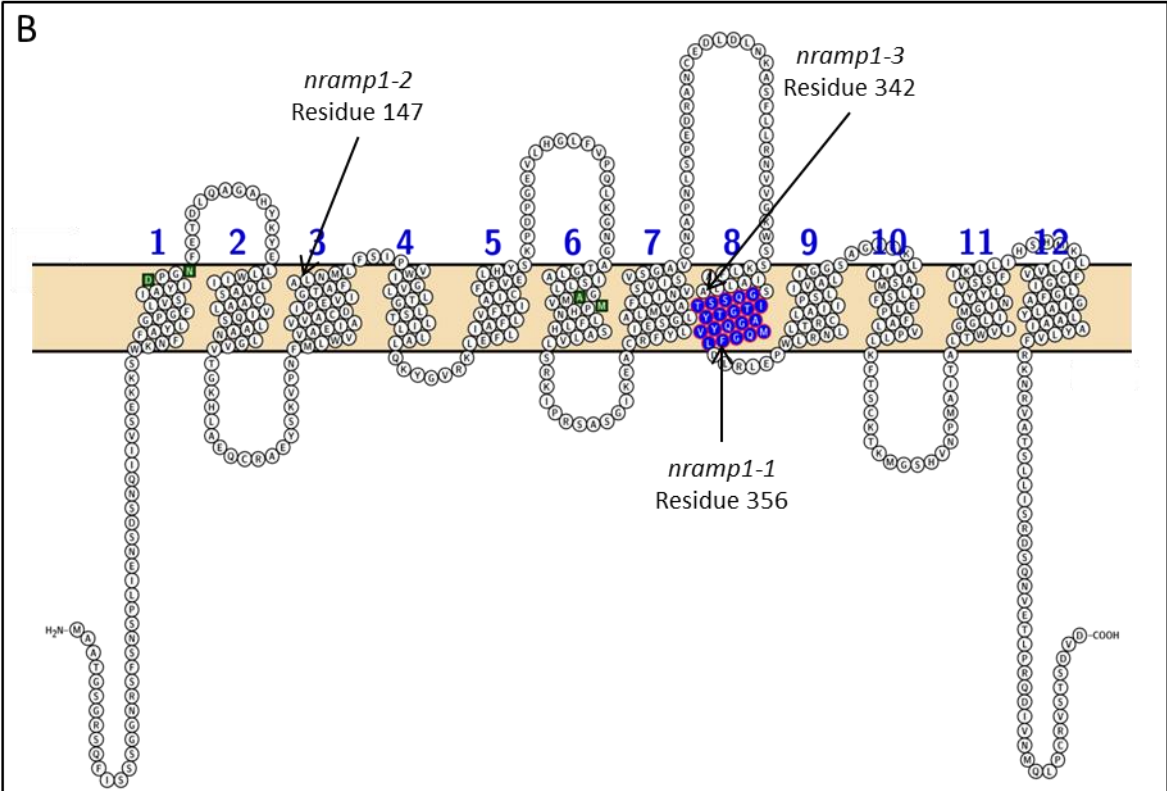


Figure 6.2. At NRAMP1 genomic structure and predicted membrane topology.

A) Intron-exon structure of *NRAMP1*. Black bar, exon; white bar, intron; red bar, predicted 5'-UTR. Black scale bar, 100 base pairs (bp). Confirmed insertion sites for 3 *nramp1* T-DNA insertion mutants are labelled as bp after ATG in the genomic sequence: *nramp1-1*, N553236 (Cailliatte, et al., 2010); *nramp1-2*, N579653; *nramp1-3*, N679062. B) Predicted transmembrane domain (TMD) structure of NRAMP1, predicted by AramTmConsens (Schwacke, et al., 2003) and alignment with ScaDMT; visualised by Protter (Omasits, et al., 2014). Relative insertion sites for three *nramp1* mutants are included, labelled at the final uninterrupted codon before the insertion site. Blue residues, CTM domain. Green residues, D61, N64, A233 and M236, which are conserved in NRAMP homologs, Sca DMT and Ec MntH.

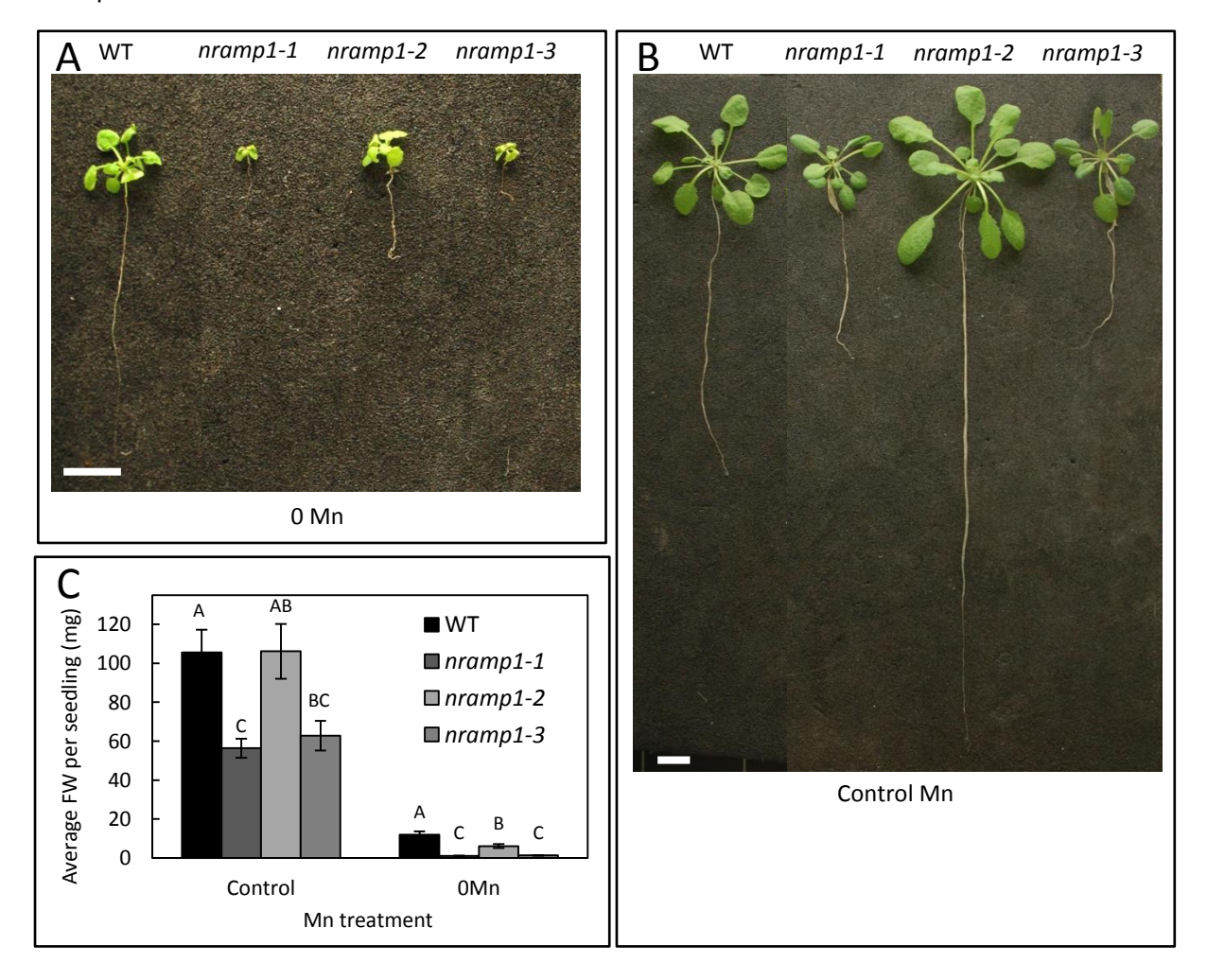


Figure 6.3. Sensitivity to Mn deficiency of three different *nramp1* mutants, when grown hydroponically and exposed to Mn deficiency from day 0.

A and B) Images displaying growth of Col8 wild type (WT) and three nramp1 mutants after being grown hydroponically for 42 days on media supplemented with either no Mn (A; 0 Mn) or 1.8 μ M Mn (B; control). White bar = 1 cm. C) Average fresh weight (FW) per seedling under control or Mn deficiency treatments. Data shows mean FW (mg) per seedling calculated for 24 seedlings (\pm SE). As determined by 2-way ANOVA, there is a significant effect of [Mn] (F_{1, 120} = 1476.33, p<0.001), genotype (F_{3, 120} = 73.31, p<0.001) and interaction between [Mn] and genotype (F_{3, 127} = 24.65, p<0.001) on FW. Means not sharing a letter at a particular concentration are significantly different, according to Tukey post hoc test.

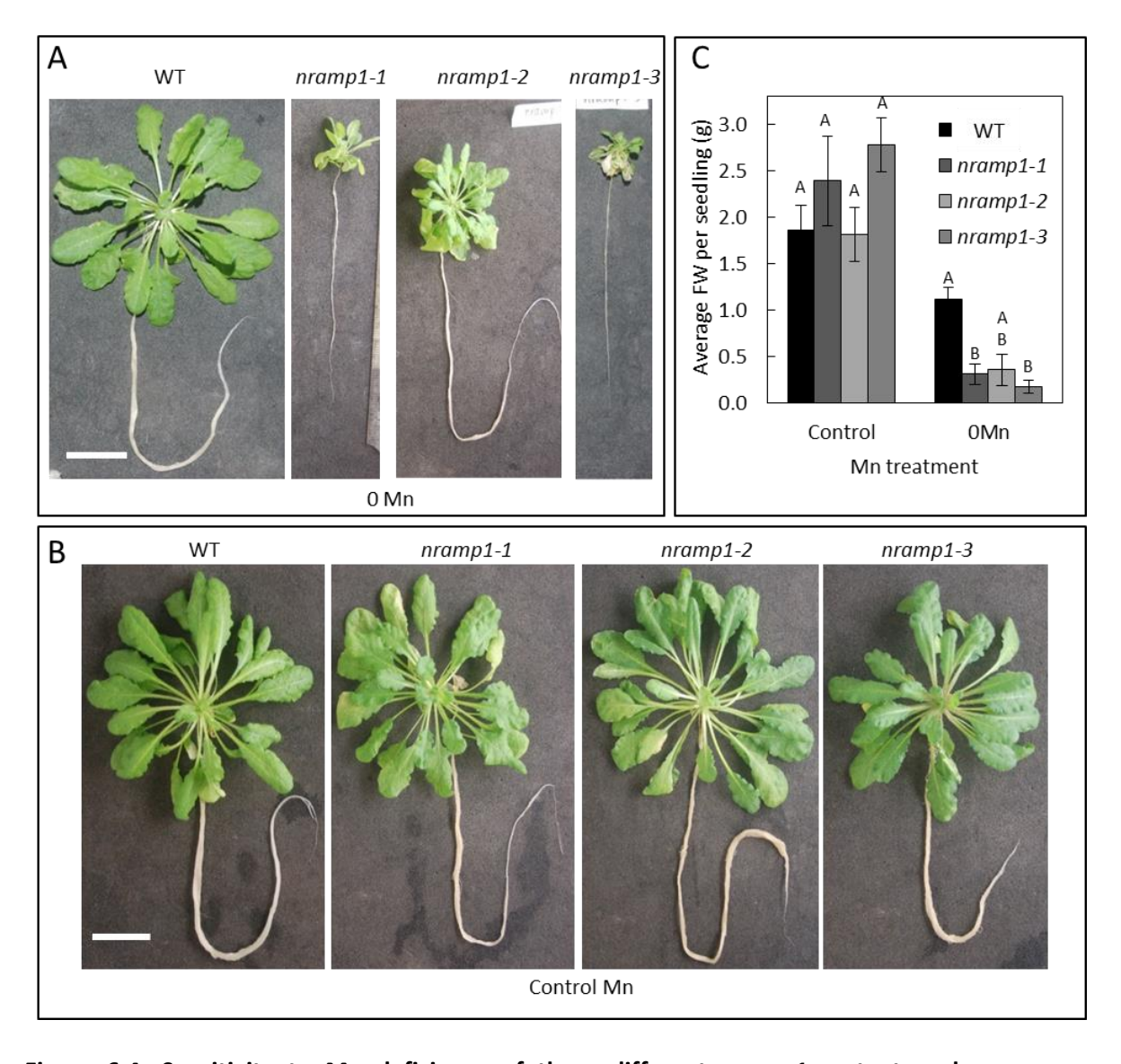


Figure 6.4. Sensitivity to Mn deficiency of three different *nramp1* mutants, when grown hydroponically and exposed to Mn deficiency from day 29.

A and B) Images displaying growth of Col8 wild type (WT) and three nramp1 mutants after being grown hydroponically for 77 days; all seedlings were grown on control media (1.8 μ M Mn) for 29 days before 0 Mn regime seedlings were transferred to Mn deficiency for a further 48 days. A) Mn deficiency seedlings; B) control seedlings. White bar = 3 cm. C) Average fresh weight (FW) per seedling under control or Mn deficiency treatments. Data shows mean FW (mg) per seedling calculated for 15 to 8 seedlings (\pm SE). As determined by GLM, there is a significant effect of [Mn] (F_{1,31} = 70.91, p<0.001), genotype (F_{3,31} = 3.64, p=0.023) and interaction between [Mn] and genotype (F_{3,38} = 5.31, p=0.005) on FW. Means not sharing a letter at a particular concentration are significantly different, according to Tukey post hoc test.

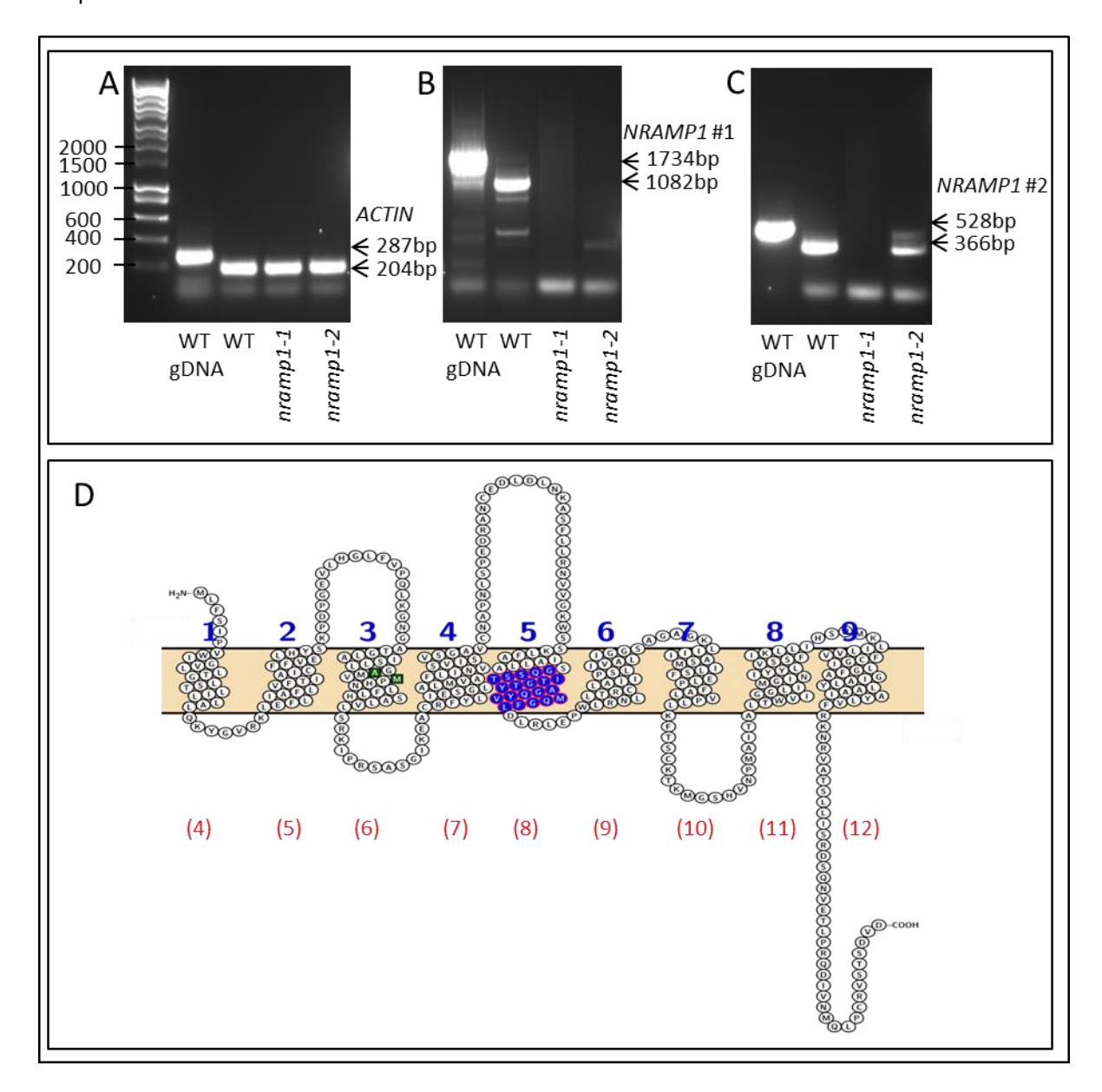


Figure 6.5. NRAMP1 transcript exists at the 3' end of nramp1-2 but not of nramp1-1.

Amplification of different products from templates: wild type (WT) gDNA, WT cDNA and cDNA from *nramp1-1* (N553236) and *nramp1-2* (N579653). A) *ACTIN* primers amplify products of 287 base pairs (bp) from wild type (WT) gDNA, and 204 bp from WT, *nramp1-1* (N553236) and *nramp1-2* (N579653) cDNA, indicating cDNA is of good quality with no gDNA contamination. B) *NRAMP1* primers (#1; Nr1bfwd + NRAMP1R) which span the insert site of both *nramp1-1* and *nramp1-2* amplify a product of 1734 bp from WT gDNA and 1082 bp from WT cDNA; no product of this size is amplified from *nramp1-1* or *nramp1-2*. C) *NRAMP1* primers (#2; NRAMP1F + NRAMP1R) which span the insert site of *nramp1-1* but not of *nramp1-2* amplify a product of 528bp from WT gDNA and 366 bp from WT cDNA and *nramp1-2* cDNA; no product amplified from *nramp1-1*. Gel provided for comparison in this project by Dr. L. E. Williams. Primers labelled in schematic of Figure 6.2. D) Hypothetical secondary structures of truncated NRAMP1 post-insertion site of *nramp1-2*. Sequence is translated from the first in-frame ATG after the confirmed insertion site to the stop codon. Blue residues, CTM domain. Green residues, A233 and M236, which are conserved in NRAMP homologs, Sca DMT and Ec MntH. Red numbers in brackets indicate the numbering of the original NRAMP1 TMDs. Based on prediction from AramTmConsens and alignment with ScaDMT; visualised with Protter (Omasits, et al., 2014).

amplifies a product in *nramp1-2* cDNA, in line with the 366 bp product amplified from WT (Figure 6.5C). No product is amplified from *nramp1-1* using either primer set; primers locations are highlighted in Figure 6.2. Taken together, these findings suggest a truncated NRAMP1 may be translated from the transcript at the 5' side of the *nramp1-2* insertion site. Based on the predicted membrane topology of NRAMP1 (Figure 6.2), Figure 6.5D shows the corresponding truncated protein that could hypothetically be translated, from the first in-frame ATG after the insertion site to the stop codon. If this is accurate, the final 9 TMDs could be translated, which includes the CTM and AxxMxH domains of TMDs 8 and 6, respectively, although would not include the DPGN domain of TMD 1. The next step in confirming this is to determine the level of 3' transcript expression in *nramp1-2* compared to WT, *nramp1-1* and *nramp1-3* using qPCR.

As described in previous chapters, the Mn-dependent phenotypes of mtp11-1 and mtp8-2 are exacerbated under low Ca conditions. To determine whether the Mn deficiency response of nramp1 is also Ca-dependent, nramp1-1 and nramp1-3 were compared to WT in a plate assay with 0 or 50 μ M Mn (deficiency and basal Mn) and 100 or 1495 μ M Ca (low and basal Ca) (Figure 6.6). Both mutants are significantly inhibited by Mn deficiency under both Ca regimes, in terms of chlorophyll; significant differences between WT and nramp1 FW values are only seen under basal Ca.

6.2.2 At NRAMP2 is involved in alleviating Mn deficiency

An alignment of At NRAMP1 and At NRAMP2 is presented in Figure 6.7A. Similarly to At NRAMP1, At NRAMP2 is predicted to have 12 TMDs, based on this alignment and the output from AramTmConsens; this is visualised in Figure 6.7B. Also highlighted on the alignment is the conservation of certain motifs: the DPGN motif and CTM domain are conserved in TMDs 1 and 8 of At NRAMP2, while N250 and N401, of TMD 7 and 11 of Ec MntH, are also conserved. The AxxMxH motif of TMD 7 of At NRAMP1, Sca DMT and Ec MntH is substituted for CxxMxH in At NRAMP2.

Two insertion mutants are available for *nramp2*, predicted by T-DNA Express (Alonso, et al., 2003) to fall within the first and third of four exons. The insertion site for *nramp2-1* is confirmed at the RNA level in Figure 6.8, with an insertion site in the third exon, as confirmed by sequencing. The *nramp2-2* mutant is confirmed at the gDNA level to carry an insert in the promoter, up to 60bp upstream of the *NRAMP2* start codon. The *nramp2* mutants were screened hydroponically under Mn deficiency from day 0, using *nramp1-1* as a control for a Mn-dependent phenotype. The *nramp2-1* displays high levels of stunting under Mn deficiency, similarly to *nramp1-1*.

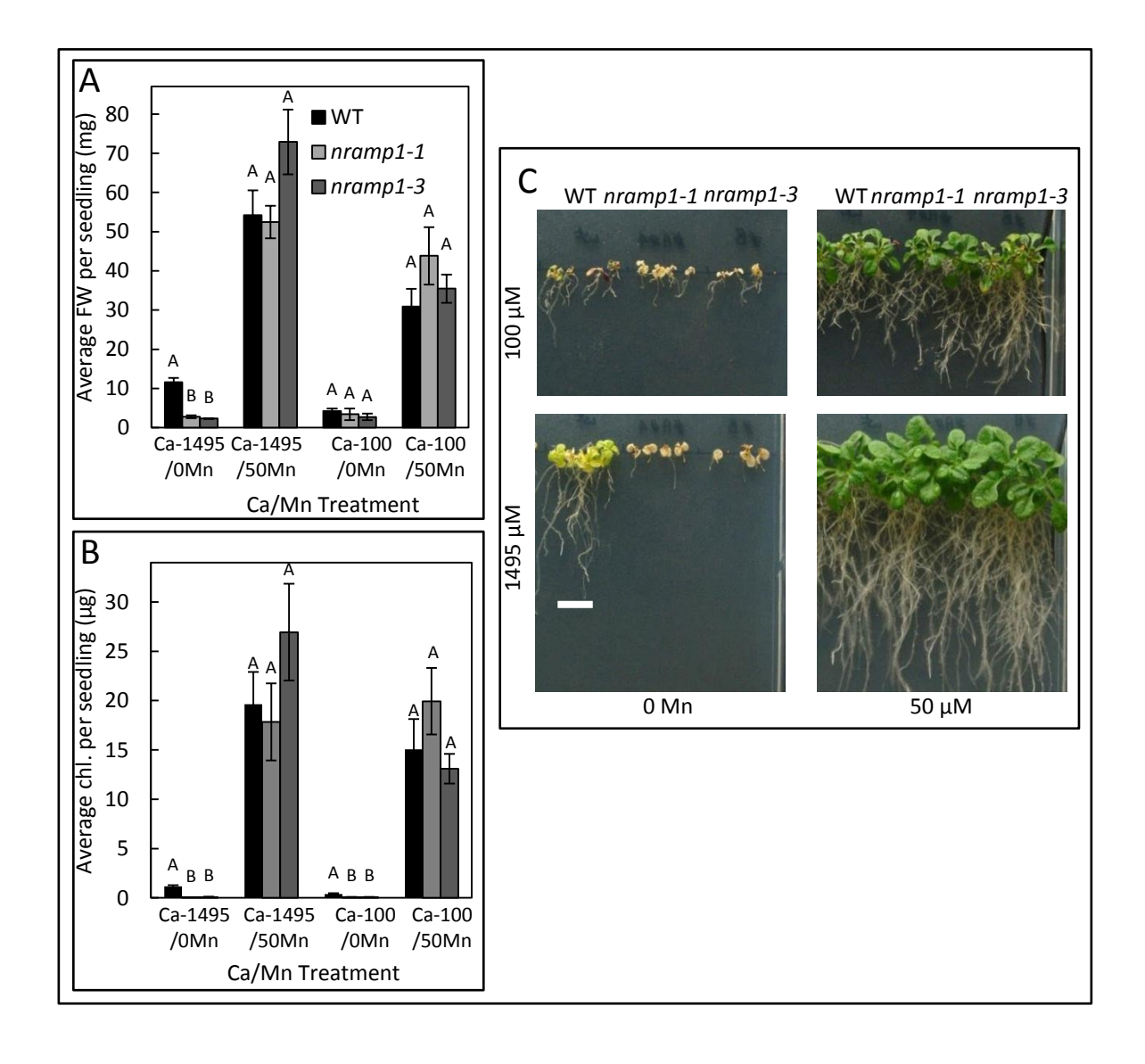
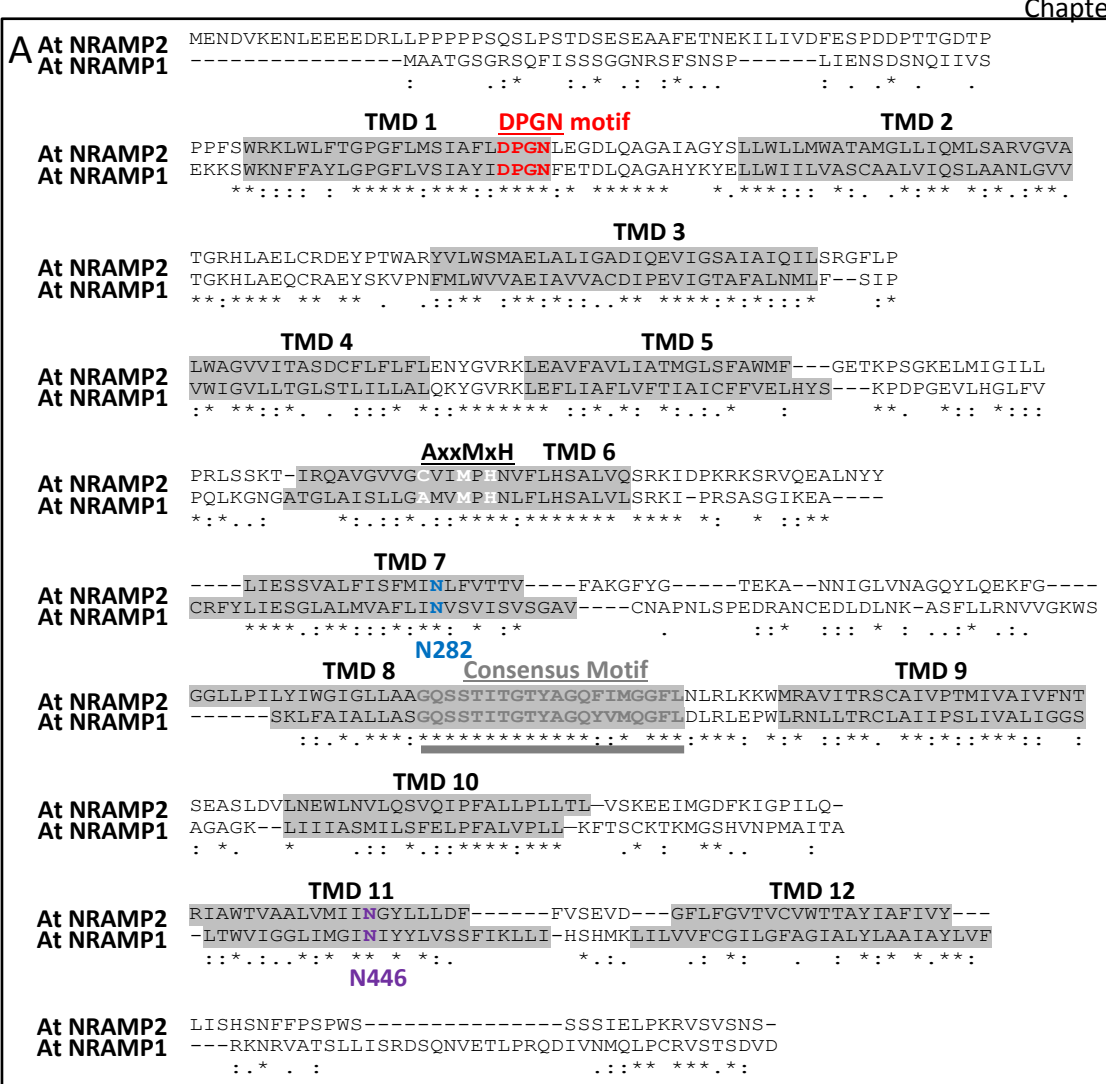


Figure 6.6. Mn deficiency phenotypes of two *nramp1* mutants when grown on plates under two Ca regimes.

A) average fresh weight (FW) and B) chlorophyll (chl) per seedling of Col8 wild type (WT), nramp1-1 and nramp1-2 when grown for 25 days on ½ MS supplemented with either 1495 μ M Ca (Ca-1495) or 100 μ M Ca (Ca-100), and either 0 Mn (0Mn) or 50 μ M Mn (50Mn), supplied as CaCl₂ and MnSO₄, respectively. Data shows mean value per seedling calculated for 6 plates, with 4 seedlings per genotype per plate (\pm SE). Means not sharing a letter at a particular condition are significantly different, according to MANOVA and Tukey post-hoc test. C) Image displaying growth under each condition tested. White bar = 1 cm.

<u>Chapte</u>r 6



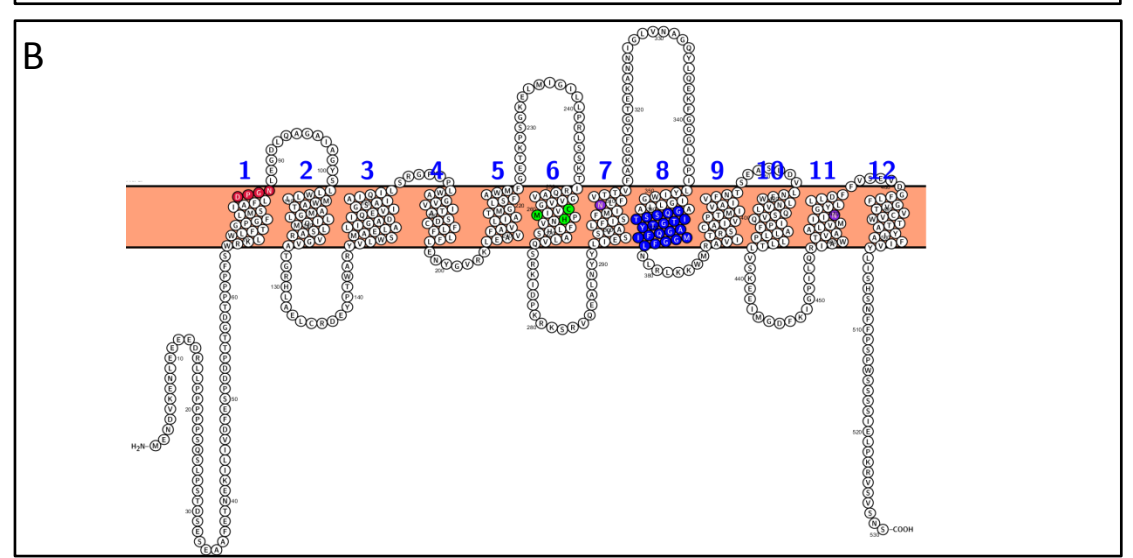


Figure 6.7. Alignment of At NRAMP1 and At NRAMP2.

A) Alignment adapted from output from Clustal Omega (Sievers, et al., 2011). Grey highlight, predicted transmembrane domains (TMD), based on output from AramTmConsens (Schwacke, et al., 2003) and alignment of At NRAMP1 with Sca DMT in Figure 6.1. Red, DPGN motif (Haemig & Brooker); blue and purple, N282 and N446 conserved in At NRAMP1 and NRAMP2. AxxMxH motif of At NRAMP1 conserved as CxxMxH motif in At NRAMP2. Consensus motif (CTM; grey underline) is conserved in TMD8. (*), fully conserved residues between sequences; (:), conservation of residues with strongly similar properties; (.), conservation of residues with weakly similar properties. B) Predicted membrane topology of At NRAMP2 with these key motifs highlighted; visualised by Protter (Omasits, et al., 2014).

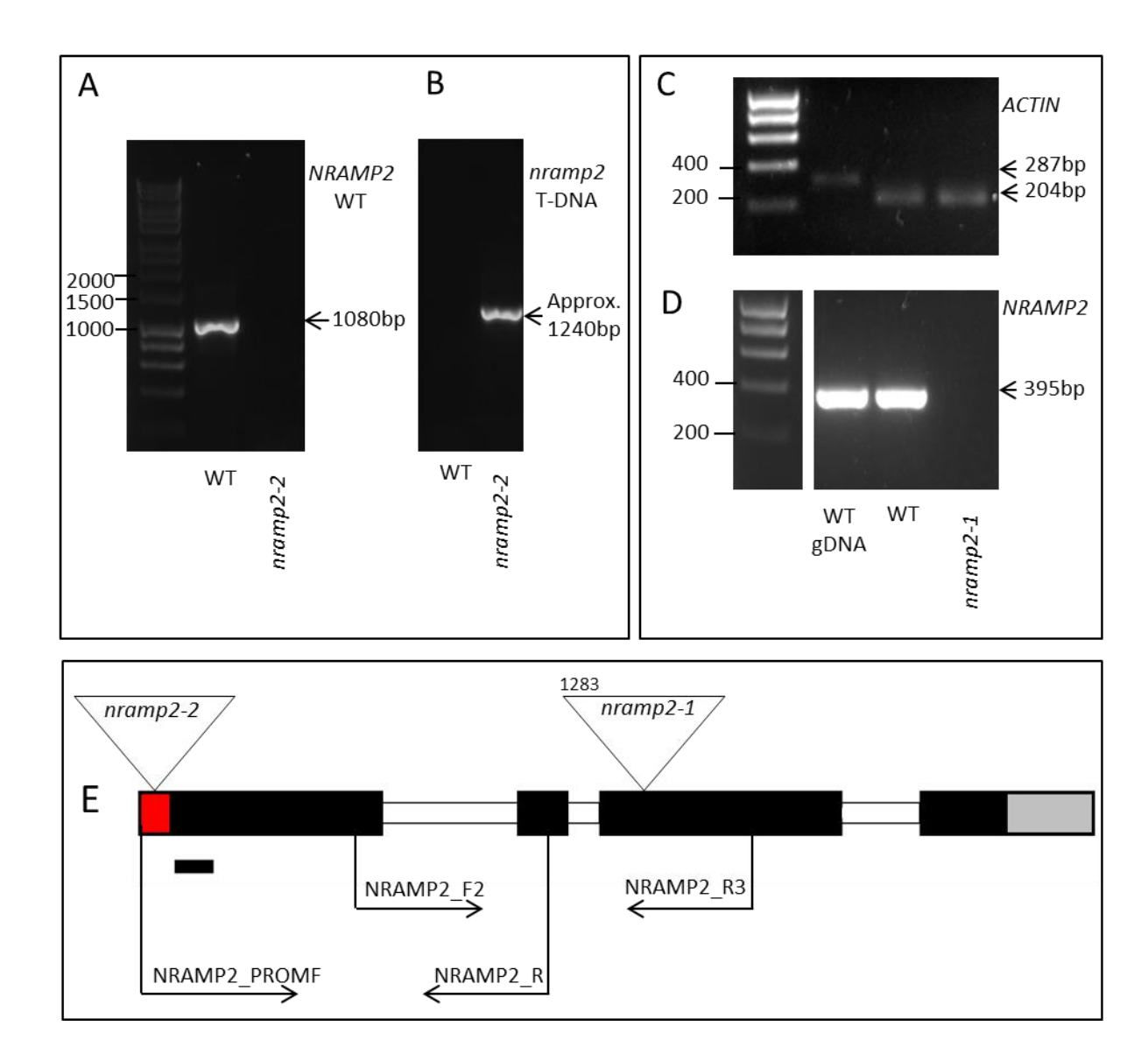


Figure 6.8. Isolation of T-DNA insertion mutants for *nramp2*.

A+B) Isolation of *nramp2-2*, GABI__306A04, at the genomic level, using wild type (WT) and *nramp2-2* gDNA as template. A) Primers NRAMP2_promF and NRAMP2_R span *nramp2-2* insert site in promoter and amplify produce of 1080 base pairs (bp) from WT but no product from *nramp2-2*. B) Primers amplify fragment of pAC161 T-DNA in *NRAMP2* gene from *nramp2-2* but not from WT; product size is approx. 1240bp. C+D) Confirmation of *nramp2-1*, N900414, at the RNA level, using WT gDNA, WT cDNA and *nramp2-1* cDNA as template. C) Primers for *ACTIN* amplify product of 287bp from gDNA and 204bp from cDNA indicating cDNA is of good quality and not contaminated with gDNA. D) Primers NRAMP2_F2 and NRAMP2_R3 amplify a product of 395bp from both WT gDNA and cDNA but no product from *nramp2-1* indicating a knockout at the RNA level. A-D) Gels have predicted amplicon sizes on right and molecular weight markers labelled on left. E) Schematic of *NRAMP2* gDNA. Red, promoter; black, exon; white, intron; grey, 3' untranslated region; coding sequence confirmed with sequencing, promoter and UTR information obtained from TAIR. Black scale bar represents 100bp. Arrows mark insert positions for T-DNA mutants, *nramp2-1* and *nramp2-2*; *nramp2-1* confirmed by sequencing.

Contrastingly, *nramp2-2* is not sensitive under Mn deficiency, also growing better than *nramp1-1* and *nramp2-1* under control conditions, 1.8 µM Mn (Figure 6.9A-B). While *nramp1-1* and *nramp2-1* are found in the Columbia 8 background, *nramp2-2* is found in the Columbia 0 background. As such, both Columbia WTs were included when comparing *nramp2* mutants in a plate-grown assay (Figure 6.9C-D). While all genotypes grew similarly under control conditions, *nramp2-1* was again sensitive to Mn deficiency, with reduced fresh weight (FW) and a chlorotic appearance. The *nramp2-2* mutant was not confirmed at the RNA level; based on the lack of sensitivity, it appears *nramp2-2* is not a knockout, although the level of expression is still to be determined.

To explore the specificity of the *nramp2-1* response, it was grown alongside *nramp1-1*, and in one case *eca3-1*, under different metal extremes. While *nramp2-1* values were consistently smaller than WT under Mn toxicity, this was not significant; additionally, neither *eca3-1* nor *nramp1-1* were affected by Mn toxicity (Figure 6.10A-B). Further, neither *nramp1-1* nor *nramp2-1* were inhibited under Zn or Fe deficiency, although it is noted that *nramp2-1* grew significantly better than the WT under control conditions in these experiments (Figure 6.10 C-F). Taken together, these findings suggest the sensitivity of *nramp1-1* and *nramp2-1* is specific to Mn deficiency.

6.2.3 At NRAMP2 targets the cis-Golgi when expressed in tobacco

As the next step in functionally characterising At NRAMP2, its coding sequence was amplified and cloned into the pENTR/D-TOPO cloning system. It was not possible to amplify the full sequence in one step, and instead a two-step amplification approach was used, as summarised in Figure 6.11A and B. The Gateway cloning system was used to generate constructs P35S::NRAMP2::mRFP and P35S::NRAMP2::GFP for expression in plants; a positive digest is shown in Figure 6.11C. The NRAMP2 coding sequence was identical to that reported on The Arabidopsis Information Resource (TAIR), as confirmed by two independent sequencing reads.

At NRAMP2 displays a punctate expression pattern when transiently expressed in tobacco. This does not overlap with that of TGN-marker ST::RFP or ECA3::YFP, but their foci sit adjacent to each other and move around the cell at the same rate (Figure 6.12A-F). Unfortunately it was not possible to co-express At NRAMP2 with cis-Golgi marker Manl, due to poor expression of the Manl construct in tobacco. However, At NRAMP2 does give strong overlap with MTP11 (Figure 6.12G-I), a protein which has been shown to colocalise with Manl (Chapter 4). Based on these findings, it is concluded that At NRAMP2 targets the cis-Golgi.

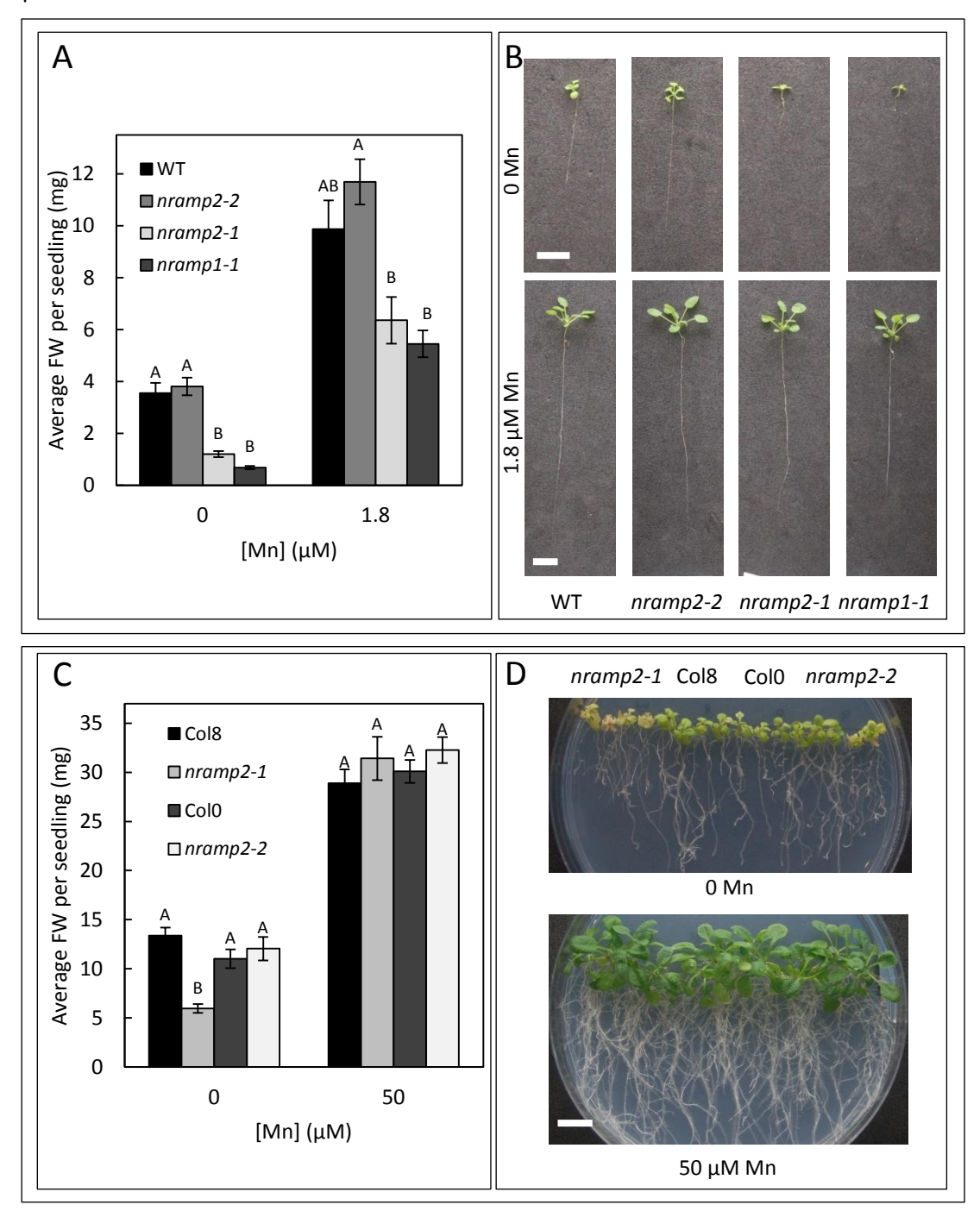


Figure 6.9. Sensitivity of nramp2-1 to Mn deficiency.

Comparison of Columbia 8 wild type (Col8/WT) with nramp2-1 and nramp2-1, and additionally A-B) nramp1-1 or C-D) Columbia 0 WT under Mn deficiency. A-B) Seedlings grown hydroponically for 35 days on Modified Hoaglands media supplemented eith either 0 or 1.8 μ M MnSO₄ . A) Data shows mean FW (mg) per seedling (\pm SE) calculated for 24 seedlings per genotype per condition. As determined by 2-way ANOVA, there is a significant effect of [Mn] ($F_{(1,184)} = 273.21$; p<0.001), genotype ($F_{(3,184)} = 45.1$; p<0.001) and interaction between [Mn] and genotype ($F_{(3,191)} = 4.1$; p=0.008) on FW. C-D) Seedlings grown on plates for 21 days on ½ MS supplemented with either 0 or 50 μ M MnSO₄. Mean FW calculated for 6 plates per condition, with 4 seedlings per genotype per plate. C) According to two-way AVOVA, there is a significant effect of [Mn] ($F_{(1,40)} = 493.04$, p<0.001), genotype ($F_{(3,40)} = 11.98$, p<0.001) and interaction between [Mn] and genotype ($F_{(3,47)} = 14.56$, p<0.001) on FW. Genotypes which do not share a letter at a particular concentration are significantly different, according to Tukey's post hoc test. B+D) Image displaying representative plant growth under basal and deficient Mn conditions. White bar = 1 cm.

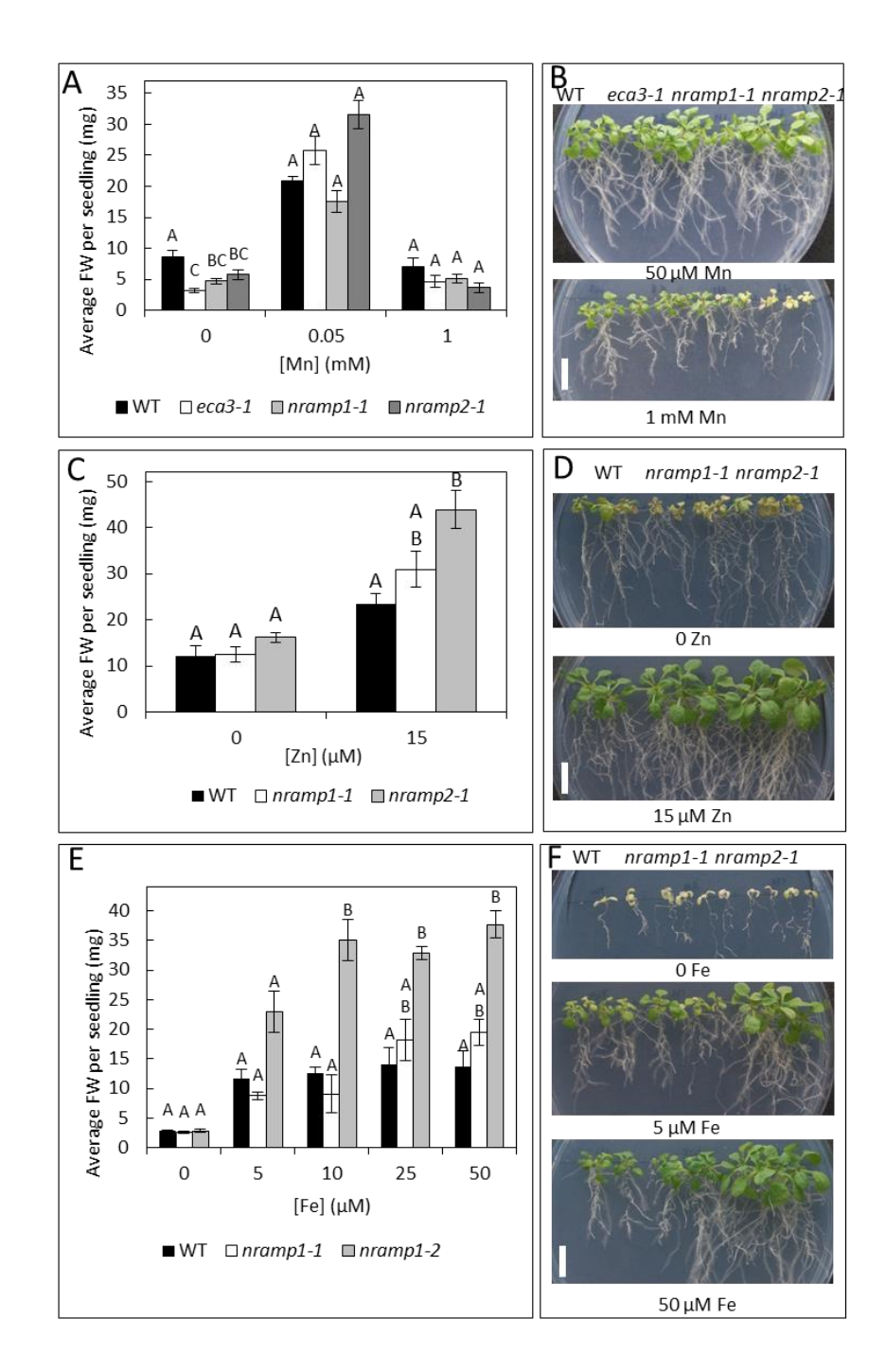


Figure 6.10. Sensitivity of nramp2-1 is specific to Mn-deficiency.

Comparison of wild type (WT), nramp1-1 and nramp2-1, and eca3-1 seedlings in A-B, when grown for 21 days on ½ MS exposed to A-B) a range of Mn concentrations from deficiency to toxicity, supplied as MnSO₄, C-D) Zn-deficient or Zn-replete conditions, 15 μ M ZnSO₄, or E-F) a range of Fe concentrations from deficiency to basal 50 μ M Fe, supplied as FeNaEDTA. A, C, E) Data shows mean fresh weight (FW; mg) per seedlin (\pm SE) calculated for 6 plates per condition, with 4 seedlings per genotype per condition. A) According to GLM, there is a significant effect of genotype (F_{3,60} = 6.15, p=0.001), [Mn] (F_{2,60} = 186.51, p<0.001) and interaction between genotype and [Mn] (F_{6,71} = 6.31, p<0.001) on FW. C) There is a significant effect of genotype (F_{2,30} = 8.65, p=0.001) and [Zn] (F_{1,30} = 103.61, p<0.001) on FW, but no significant interaction effect (F_{2,35} = 0.81, p=0.456). E) There is a significant effect of genotype (F_{2,72} = 39.21, p=0.001), [Fe] (F_{4,72} = 54.14, p<0.001) and interaction between genotype and [Fe] (F_{8,86} = 3.72, p<0.001) on FW. Means not sharing a letter at a particular concentration are significantly different, according to Tukey's post-hoc test. B, D, F) photos showing representative plant growth under different conditions. White scale bar = 1cm.

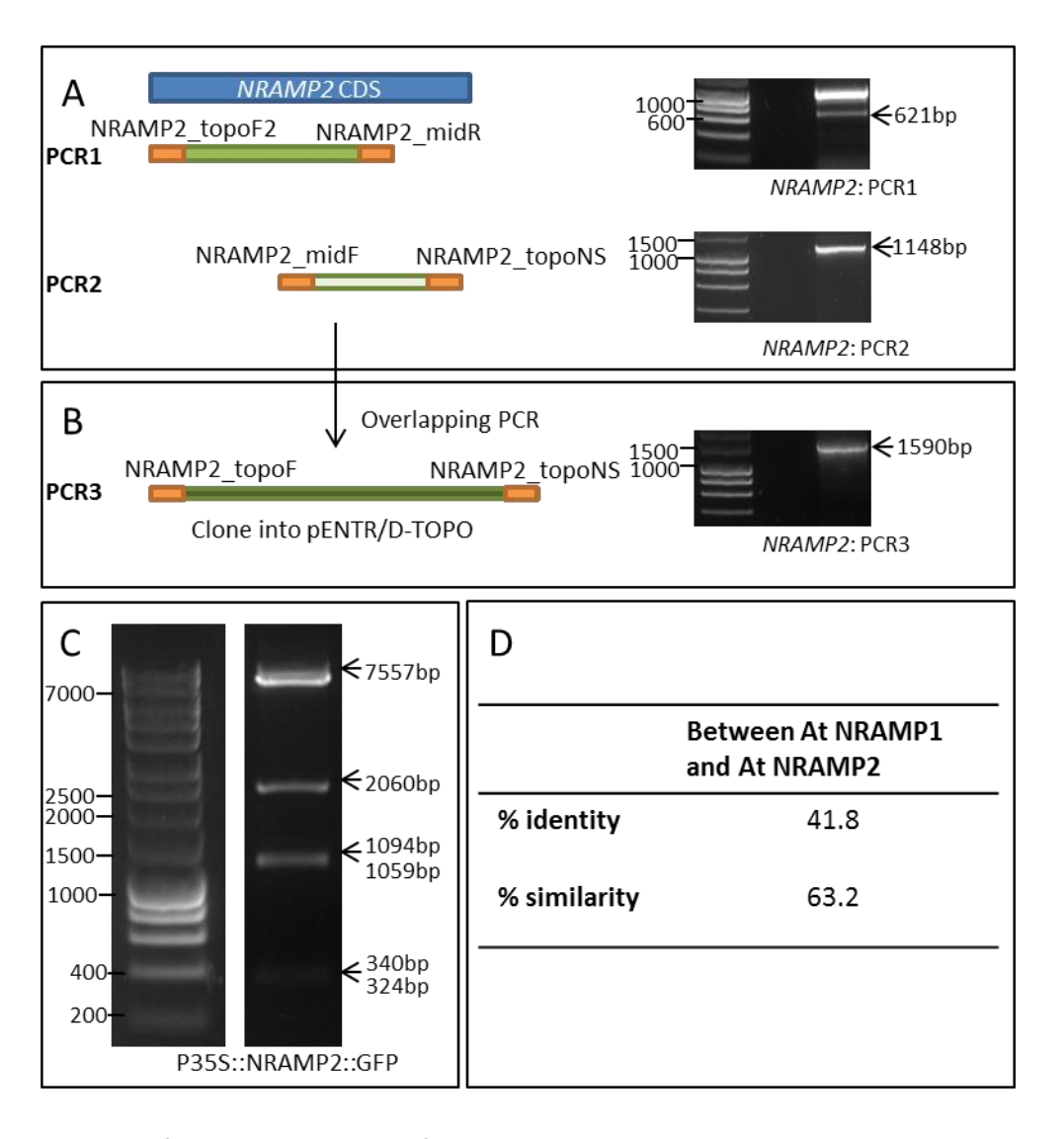


Figure 6.11. Amplification and cloning of At NRAMP2.

A-B) Overlapping PCR process to amplify full-length *NRAMP2* without stop codon (NS; no stop). A) Two independent PCRs (1 and 2) amplify from *NRAMP2* coding sequence (CDS) to amplify products of 621 base pairs (bp) and 1148 bp. B) These are gel extracted and combined in overlapping PCR (3) to amplify full length *NRAMP2* without stop codon. Successful amplification shown on right of schematic. This is cloned into pENTR/D-TOPO vector (not shown) for Gateway cloning into destination vectors: C) Restriction digestion analysis of NRAMP2 in pMDC83 vector, creating construct *P35S::NRAMP2::GFP*, using Xbal and Xhol to give predicted fragment sizes of 324, 340, 1059, 1094, 2020 and 7557 bp. A-C) predicted product sizes listed on right of gel; molecular weight markers labelled on left. D) Percentage similarity and identity between At NRAMP1 and At NRAMP2, calculated using EMBOSS Matcher.

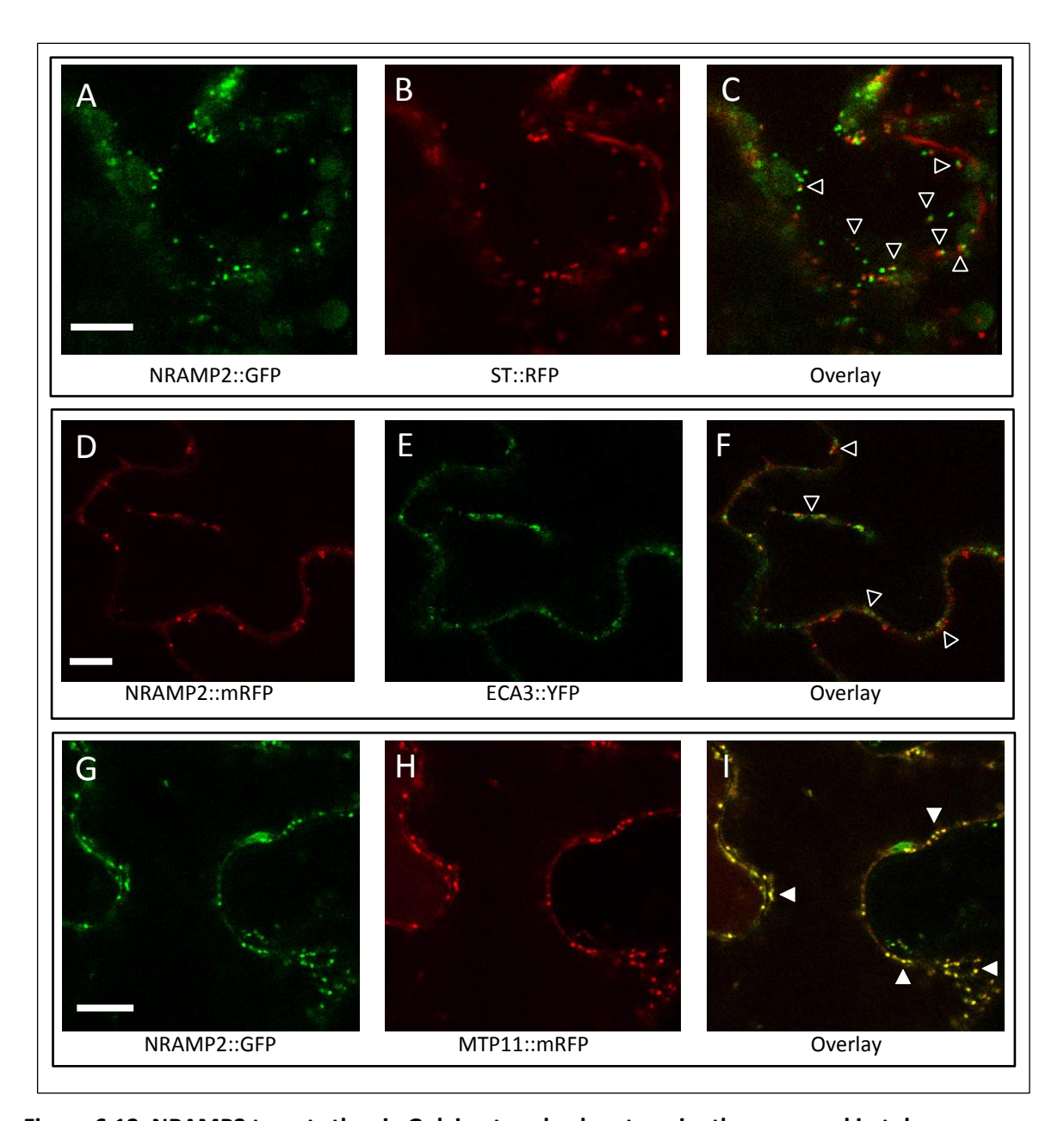


Figure 6.12. NRAMP2 targets the cis-Golgi network when transiently expressed in tobacco.

A-C) Punctate signal of NRAMP2::GFP (A, green signal) co-expressed with ST::mRFP (B, red signal) sit adjacent to each other and move around cell at same rate but do not overlap; unfilled arrows, areas of adjacent signal that do not overlap. D-F) Signal of NRAMP2::mGFP (D, red signal) co-expressed with ECA3::YFP (E, green signal) move sit adjacent to each other and move around cell at same rate but do not fully overlap; unfilled arrows, areas of adjacent signal that do not overlap. G-I) Strong overlap of NRAMP2::GFP (G, green signal) co-expressed with MTP11::mRFP (H, red signal); areas of yellow signal in overlay (I) indicate overlapping signals (filled arrows). White scale bar = 10 µm.

6.2.4 Elucidating the function of ECA3 in Mn homeostasis

The eca3-2 mutant is not sensitive compared to WT under elevated Mn under basal Ca (Figure 6.10A; Figure 6.16) or low Ca (Figure 6.17). However, both eca3-1 and eca3-2 are stunted and chlorotic compare to WT under Mn deficiency, under both Ca conditions. These findings suggest ECA3 is a major Mn transporter contributing to growth under Mn-deficient conditions, independent of Ca levels (Figure 6.13). To explore this further, eca3-1 and mtp11-1 were grown hydroponically under Mn deficiency, when exposed to treatment from day 0 and when transferred to deficiency after 29 days growth on control conditions (Figure 6.14). The sensitivity of eca3-1 was observed when exposed to Mn deficiency from day 0 but was not apparent when exposed to deficiency at a later stage of development. It should be noted that this experiment had a relatively low n number per genotype (n = 5 to 6 and n = 24, for exposure to deficiency at day 29 and day 0, respectively) but may suggest ECA3 plays a more important role in Mn deficiency at earlier stages of development. To clarify this, Genevestigator was used to determine differences in ECA3 expression during development. This is shown in Figure 6.15; based on microarray data from Genevestigator (Hruz, et al. 2008), ECA3 expression remains quite stable throughout development, eventually dropping from medium to low expression levels during senescence. However, it should be noted that this was performed on control tissue; microarray information is not available for developmental expression patterns under Mn deficiency.

To further explore the possibility that ECA3 may also play a role in Mn toxicity, a double mutant eca3-2 mtp11-1 was isolated, prior to the start of this project. The Mn-dependent phenotype of mtp11-1 is exacerbated when less Ca is available in the media (Chapter 3). As such, eca3-2 mtp11-1 was compared to WT, eca3-2 and mtp11-1 on plates, across a range of Mn conditions from deficiency to toxicity, both standard Ca (1495 μ M Ca; Figure 6.16) and low Ca (100 μ M Ca; Figure 6.17). All single and double mutants grew similarly to WT plants under basal Mn conditions. Again, eca3-2 displayed significantly reduced FW and chlorophyll values compared to WT under Mn deficiency; mtp11-1 remained unaffected. The eca3-2 mtp11-1 double mutant did not display additive sensitivity under Mn deficiency.

Under elevated Mn, *mtp11-1* displayed a hypersensitive phenotype, as observed previously. An additive sensitive phenotype is displayed by *eca3-2 mtp11-1* at certain concentrations, significantly more stunted and with reduced chlorophyll production compared to *mtp11-1*. This is true for both Ca regimes, but was more apparent under basal (Figure 6.16). This additive sensitivity suggests ECA3 does play a minor role in alleviating Mn toxicity, but this is only apparent when MTP11 is non-functional. It was therefore important to determine whether ECA3 and MTP11 co-localise at the subcellular level. Findings in Chapter 4 suggest MTP11 targets the cis-

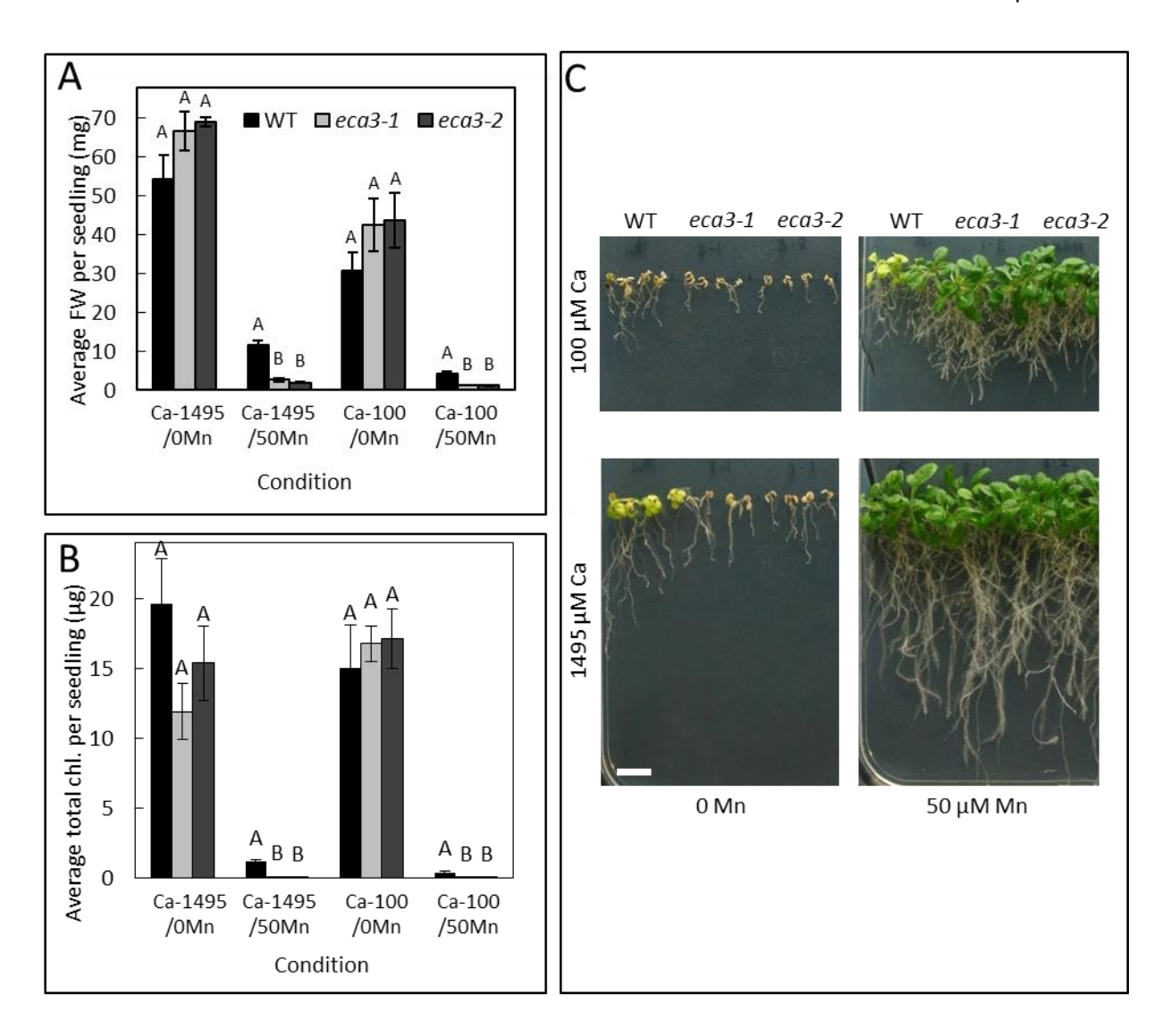


Figure 6.13. Mn deficiency phenotypes of two *eca3* mutants when grown on plates under two Ca regimes.

A) average fresh weight (FW; mg) and B) chlorophyll (chl; μ g) per seedling of Col8 wild type (WT), eca3-1 and eca3-2 when grown for 25 days on ½ MS supplemented with either 1495 μ M Ca (Ca-1495)or 100 μ M Ca (Ca-100), and either 0 Mn (0Mn) or 50 μ M Mn (50Mn), supplied as CaCl₂ and MnSO₄, respectively. Data shows mean value per seedling calculated for 6 plates, with 4 seedlings per genotype per plate (\pm SE). Means not sharing a letter at a particular condition are significantly different, according to MANOVA and Tukey post-hoc test. C) Image displaying growth under each condition tested. White bar = 1 cm.

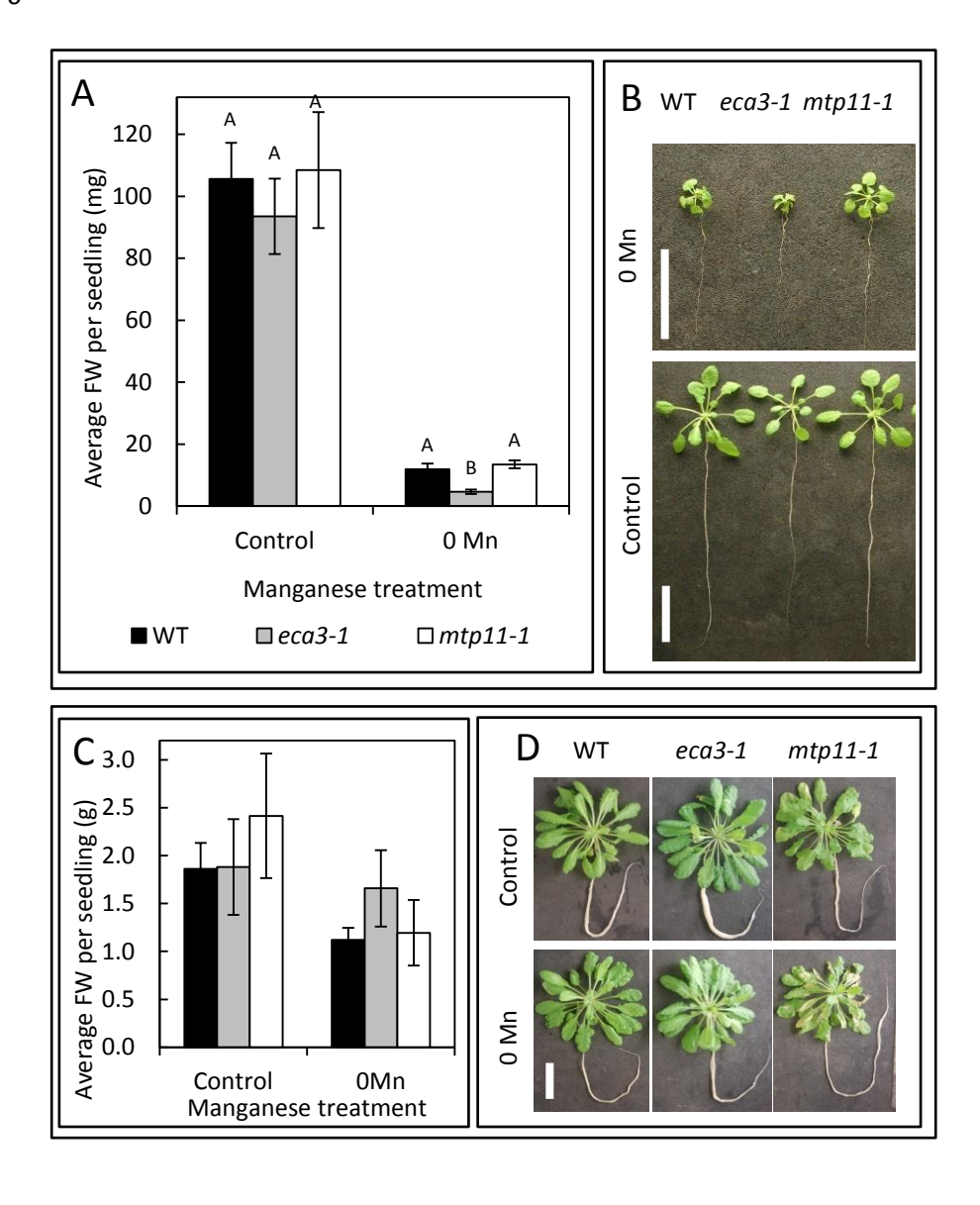


Figure 6.14. Differential Mn-deficient phenotype of *eca3-1 1* when exposed to treatment at different stages of development.

Comparison of Columbia 8 wild type (WT), eca3-1 and mtp11-1 when grown hydroponically on Modified Hoagland's solution for A-B) 48 days, exposed to Mn deficiency from day 0, or C-D) 77 days, exposed to Mn deficiency at age 29 days after initial growth on control media. Control media contains 1.8 μ M MnSO₄. A+C) Data shows mean fresh weight (FW) per seedling, calculated for A) 24 seedlings or C) 5-6 seedlings per genotype per condition. A) As determined by 2-way ANOVA, there is no significant effect of [Mn] (F_(1,90) = 527.7; p<0.001), genotype (F_(2,90) = 13.56; p<0.001) or interaction between [Mn] and genotype (F_(3,95) = 8.93; p<0.001) on FW. Genotypes which do not share a letter at a particular concentration are significantly different, according to Tukey's post hoc test. C) As determined by GLM there is no significant effect of [Mn] (F_(1,24) = 1.78; p=0.194), genotype (F_(2,24) = 0.01; p=0.989) or interaction between [Mn] and genotype (F_(2,29) = 0.83; p=0.447) on FW. There is no significant difference between any genotype at either concentration, according to Tukey's test. B+D) Image displaying representative plant growth under Mn deficient and replete conditions. White bar = 3 cm.

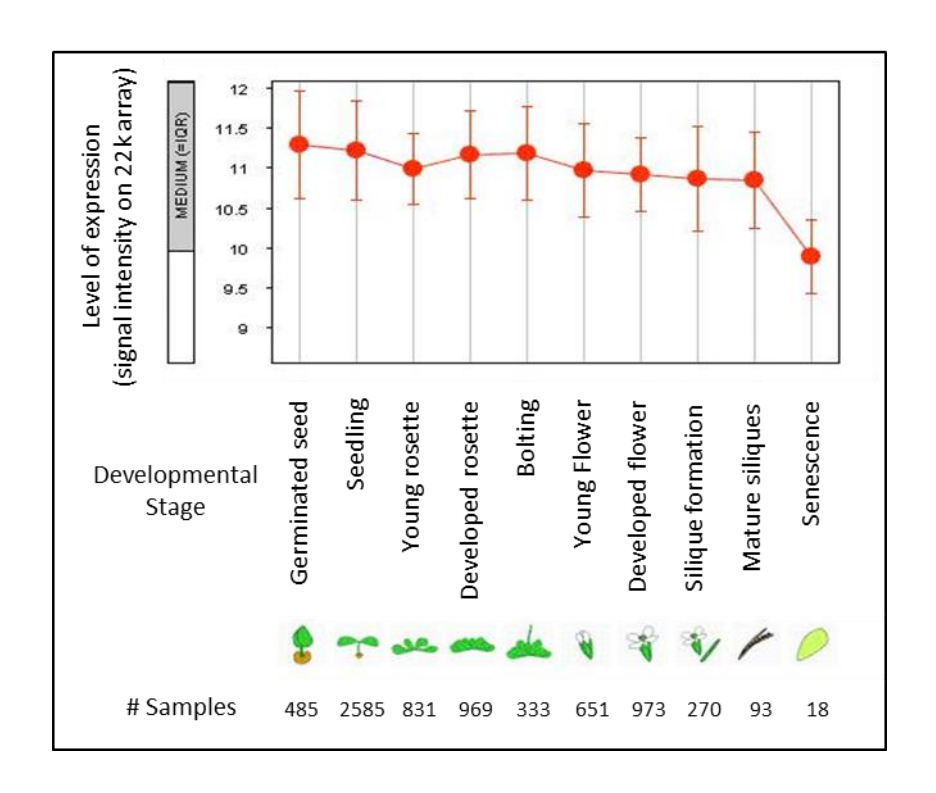


Figure 6.15. Pattern of At ECA3 (At1g10130) expression in Arabidopsis plants across a range of developmental stages.

Absolute expression levels calculated from signal intensity on a 22k affymetrix array; medium expression is defined as the interquartile range. Created with Genevestigator (Hruz, et al., 2008).

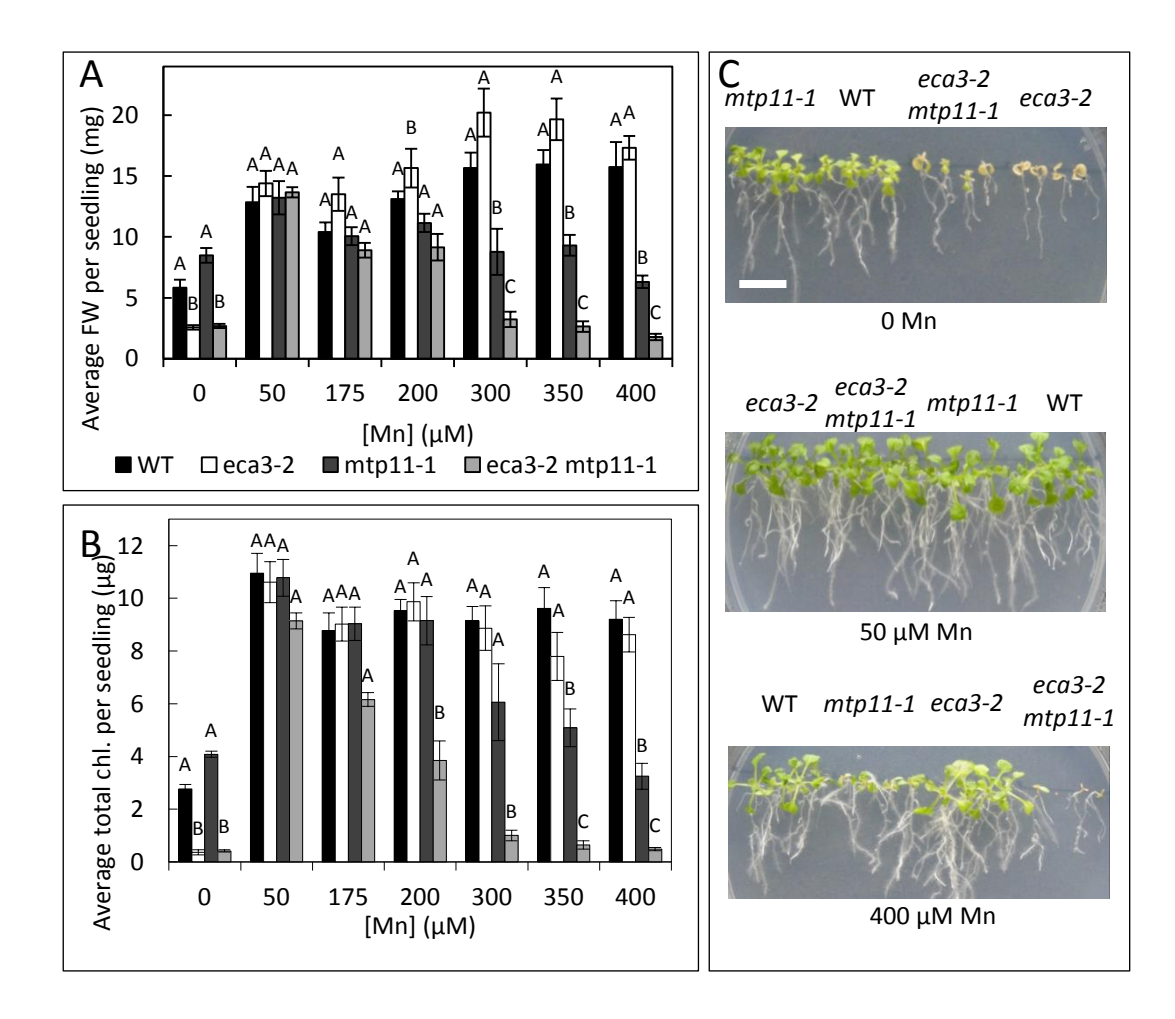


Figure 6.16. Additive phenotype of *eca3-2 mtp11-1* under Mn toxicity when grown under standard Ca conditions.

A) average fresh weight (FW; mg) and B) chlorophyll (chl; μ g) per seedling of Col8 wild type (WT), *eca3-2*, *mtp11-1* and *eca3-2 mtp11-1* when grown for 19 days on ½ MS supplemented with a range of Mn conditions supplied as MnSO₄. Data shows mean value per seedling calculated for 6 plates, with 4 seedlings per genotype per plate (\pm SE). According to 2-way ANOVA, there is a significant effect of genotype (F $_{(3,140)}$ = 114.04, p<0.001), [Mn] (F $_{(6,140)}$ = 40.27, p<0.001) and interaction of genotype and [Mn] (F $_{(18,167)}$ = 18.63, p<0.001) on FW. There is a significant effect of genotype (F $_{(3,140)}$ = 209.28, p<0.001), [Mn] (F $_{(6,140)}$ = 125.35, p<0.001) and interaction between genotype and [Mn] (F $_{(18,167)}$ = 27.65, p<0.001 on chlorophyll. Means not sharing a letter at a particular condition are significantly different, according to Tukey post-hoc test. C) Image displaying growth deficient, basal and elevated Mn conditions. White bar = 1 cm. Data provided for this project by Dr. Lorraine E. Williams and analysed as part of this thesis.

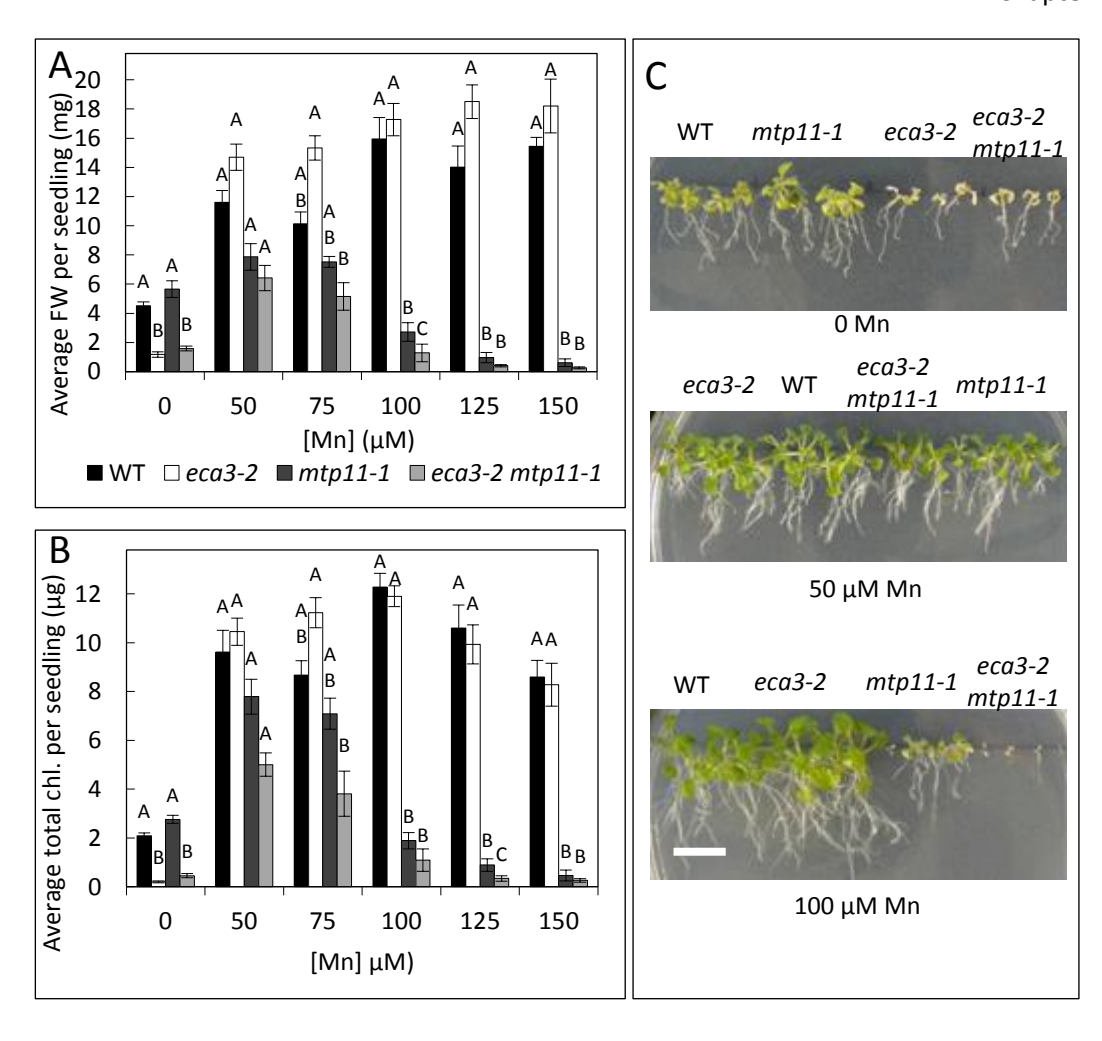


Figure 6.17. Additive phenotype of *eca3-2 mtp11-1* under Mn toxicity when grown under low Ca conditions.

A) average fresh weight (FW; mg) and B) chlorophyll (chl; μ g) per seedling of Col8 wild type (WT), *eca3-2*, *mtp11-1* and *eca3-2 mtp11-1* when grown for 20 days on ½ MS containing 100 μ M CaCl₂, supplemented with a range of Mn conditions supplied as MnSO₄. Data shows mean value per seedling calculated for 6 plates, with 4 seedlings per genotype per plate (±SE). According to 2-way ANOVA, there is a significant effect of genotype (F _(3,90) = 209.6, p<0.001), [Mn] (F_(5,90) = 10.4, p<0.001) and interaction of genotype and [Mn] (F_(15,143) = 26.78, p<0.001) on FW. There is a significant effect of genotype (F_(3,90) = 132.9, p<0.001), [Mn] (F_(5,90) = 70.88, p<0.001) and interaction between genotype and [Mn] (F_(18,143) = 25.17, p<0.001 on chlorophyll. Means not sharing a letter at a particular condition are significantly different, according to Tukey post-hoc test. C) Image displaying growth under each condition tested. White bar = 1 cm. Data provided for this project by Dr. Lorraine E. Williams and analysed as part of this thesis.

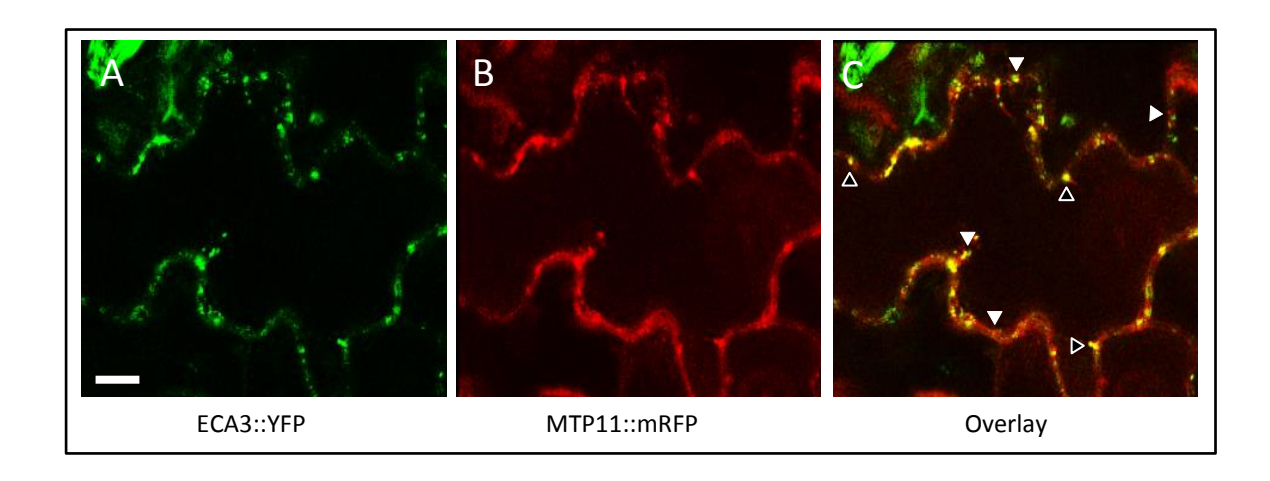
Chapter 6

Golgi when expressed in Arabidopsis and tobacco. ECA3 has been proposed to target the Golgi (Mills, et al., 2008) or the PVC or another endosomal compartment (Li, et al., 2008). Here, they were co-expressed in tobacco to further resolve this issue. The punctate foci of ECA3::YFP and MTP11::mRFP expression share areas of distinct but incomplete overlap that travel around the cell together and at the same rate (Figure 6.18A-C). Correspondingly, ECA3 shows strong, consistent overlap with trans-Golgi network marker ST::RFP (Figure 6.18D-F). It appears, therefore, that ECA3 and MTP11 target the trans- and cis-Golgi, respectively. Targeting of these proteins to distinct Golgi compartments may contribute to the additive Mn-dependent phenotype observed when both transporters are non-functional in Arabidopsis.

6.2.5 Exploring the contribution of At ECA3, At NRAMP1 and At NRAMP2 in Mn deficiency

The use of single mutants in this chapter indicates At ECA3, At NRAMP1 and At NRAMP2 each play important roles under Mn deficiency. A key aim of this thesis is to evaluate how different transporters work together in Mn homeostasis; as such, the single mutants were directly compared under Mn deficiency (Figure 6.19). While all mutants are stunted by Mn deficiency compared to WT, eca3-1 is significantly more affected than nramp1-1 and nramp2-1.

To explore whether they share any functional redundancy, double mutants were made for each combination of eca3-1, nramp1-1 and nramp1-2. Each of these genes are found on chromosome 1, with NRAMP1 and ECA3 at opposite ends of the chromosome and NRAMP2 in the centre. According to Mendelian genetics, in a normal cross between homozygous single mutants where genes are found on different chromosomes, the likelihood of finding a double homozygous mutant at the F2 generation is 1/16. The chance of isolating a double homozygous mutant is usually reduced if both genes are found on the same chromosome, due to spontaneous crossing over events during meiosis. The recombination frequency can be estimated based on the distance separating the genes of interest: 1 centiMorgan, cM, is around 217000 bp. The chance of isolating a homozygous mutant is 1% for every 1 cM; this is only approximate because the linkage of different regions on chromosomes will vary. The distances and corresponding likelihoods of obtaining a double mutant for each combination are summarised in Table 6.1, calculated from the stop codon of the first gene, to the start codon of the second gene. Based on these reduced chances of obtaining a double homozygous plant, more plants were sown at the F2 generation. As shown in the confirmation gels in Figures 6.20, double mutants were successfully isolated and confirmed homozygous at the RNA level for eca3-1 nramp1-1, eca3-1 nramp1-2 and nramp1-1 nramp1-2. A triple mutant was then generated by crossing double mutants for eca3-1 nramp2-1 and *nramp1-1 nramp2-1*; this is confirmed at the RNA level in Figure 6.21.



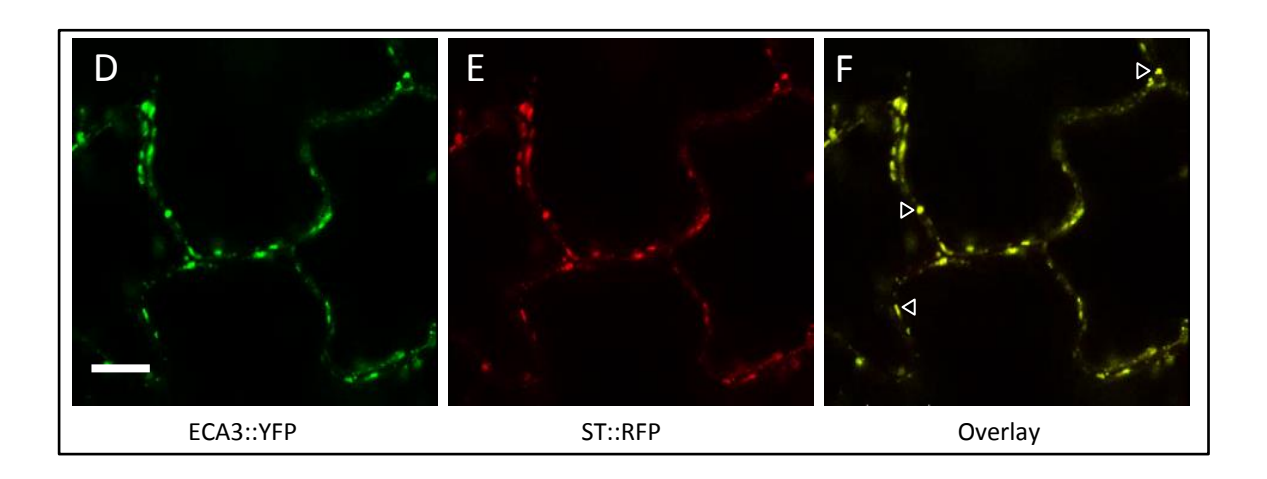
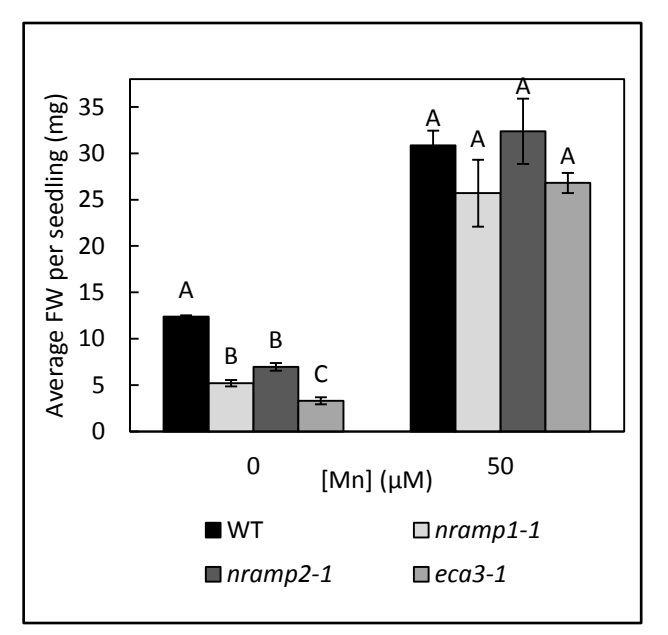


Figure 6.18. ECA3 targets the trans-Golgi network when transiently expressed in tobacco.

Partial overlap of ECA3::YFP (A, green signal) with MTP11::mRFP (B, red signal); areas of yellow in C indicate overlapping of signals (unfilled arrows) whereas areas of expression remaining red or green indicate the signals do not fully overlap (filled arrows). D-F) Overlap of ECA3::YFP (D; green signal) with trans-Golgi marker ST::RFP (E; red signal); areas of yellow in F indicate overlapping signals (unfilled arrows). White scale bar = $10 \mu m$.

Chapter 6



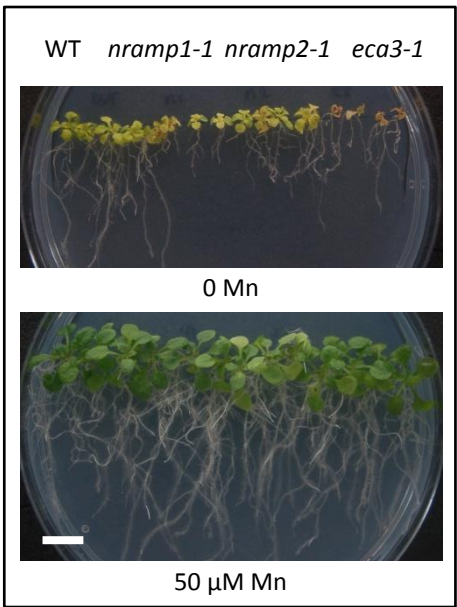


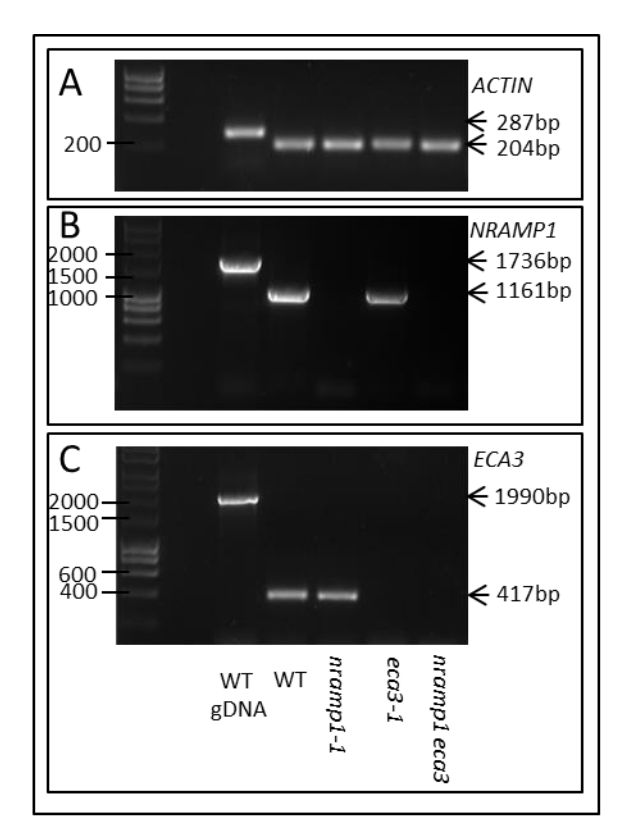
Figure 6.19. Comparison of eca3-1, nramp1-1 and nramp2-1 single mutants under Mn deficiency.

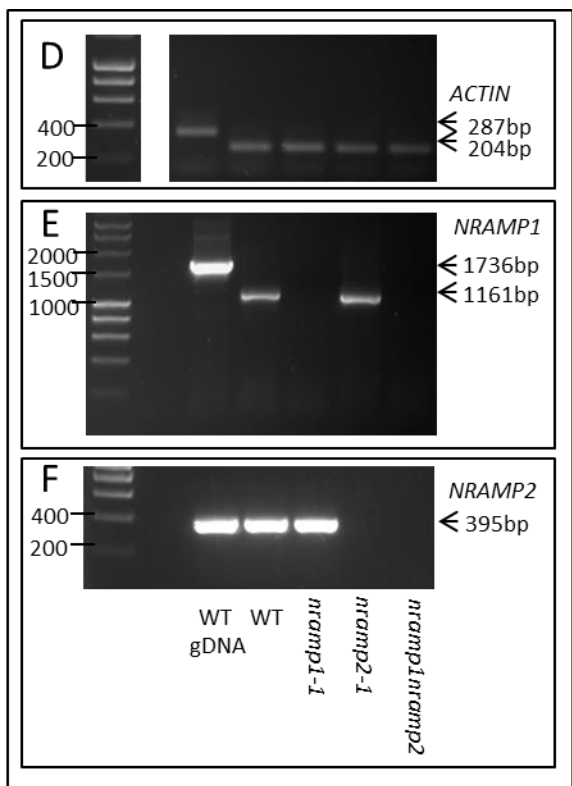
Comparison of Columbia 8 wild type (WT) with single mutants of eca3-1, nramp1-1 and nramp2-1 when grown for 21 days on ½ MS supplemented with either 0 or 50 μ M MnSO₄. A) Data shows mean fresh weight (FW) per seedling (\pm SE) calculated for 6 plates per condition, with 4 seedlings per genotype per plate. A) According to two-way AVOVA, there is a significant effect of [Mn] ($F_{(1,40)}$ = 880.48, p<0.001), genotype ($F_{(3,40)}$ = 104.54, p<0.001) and interaction between [Mn] and genotype ($F_{(3,47)}$ = 126.27, p<0.001) on FW. B) There is a significant effect of [Mn] ($F_{(1,40)}$ = 710.27, p<0.001), genotype ($F_{(3,40)}$ = 35.49, p<0.001) and interaction between [Mn] and genotype ($F_{(3,47)}$ = 19.4, p<0.001) on FW. Means not sharing a letter at a particular concentration are significantly different, according to Tukey's post-hoc test. B) Photo show representative plant growth at 0 and 50 μ M Mn; white bar = 1 cm.

Table 6.1. Likelihoods of generating double homozygous mutants between *eca3*, *nramp1* and *nramp2*.

Distances between *ECA3* (At1g10130), *NRAMP2* (At1g47240) and *NRAMP1* (At1g80830) on *Arabidopsis thaliana* chromosome 1, measured in centiMorgans (cM); % chance for isolating a double homozygous mutant increases by approx. 1% for every 1 cM. Likelihood is based on this % chance in relation to the normal 1/16 likelihood of isolating double mutant at F2 generation, based on Mendelian genetics.

Cross	Distance (cM)	% chance	Likelihood of isolating
			double mutant at F2
eca3 nramp1	124.65	100	1/16
eca3 nramp2	60.19	60.2	1/27
nramp1 nramp2	64.45	64.5	1/25





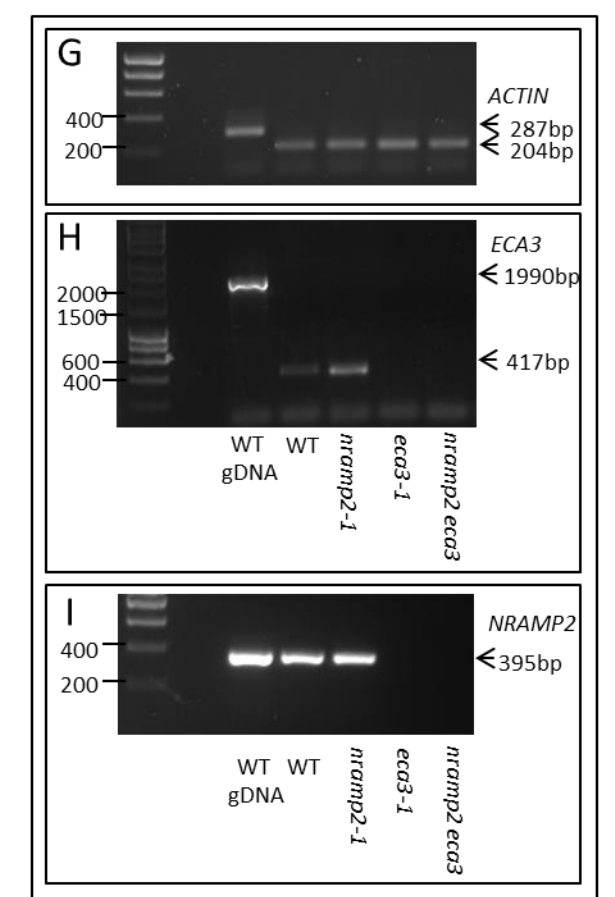


Figure 6.20. Confirmation of *nramp1-1*, *nramp1-2* and *eca3-1* double mutants at RNA level.

Confirmation of A-C) nramp1-1 eca3-1, D-F) nramp1-1 nramp2-1 and G-I) nramp2-1 eca3-1 using wild type (WT) gDNA, WT cDNA, single mutant nramp1-1, nramp2-1 and eca3-1 cDNA and corresponding double mutant cDNA as template. A, D, G) ACTIN primers amplify products of 287 base pairs (bp) from WT gDNA and 204bp from all cDNA, indicating cDNA is of good quality with no genomic contamination. B, D) NRAMP1 primers amplify product of 1736bp from WT gDNA and 1161bp from nramp2-1 and eca3-1, but not from nramp1-1 or double mutants indicating knockout at RNA level. C, H) ECA3 primers amplify products of 1990bp from WT gDNA and 417 bp from WT, nramp1-1 and nramp2-1 cDNA, but no product from eca3-1 or double mutants, indicating knockout at RNA level. F, I) NRAMP2 primers amplify product of 395bp from WT gDNA and WT, nramp1-1 and eca3-1 cDNA, but not from nramp2-1 or double mutant, indicating knockout at RNA level. A-I) Gels labelled with predicted amplicon sizes at right and molecular weight markers at left of gel.

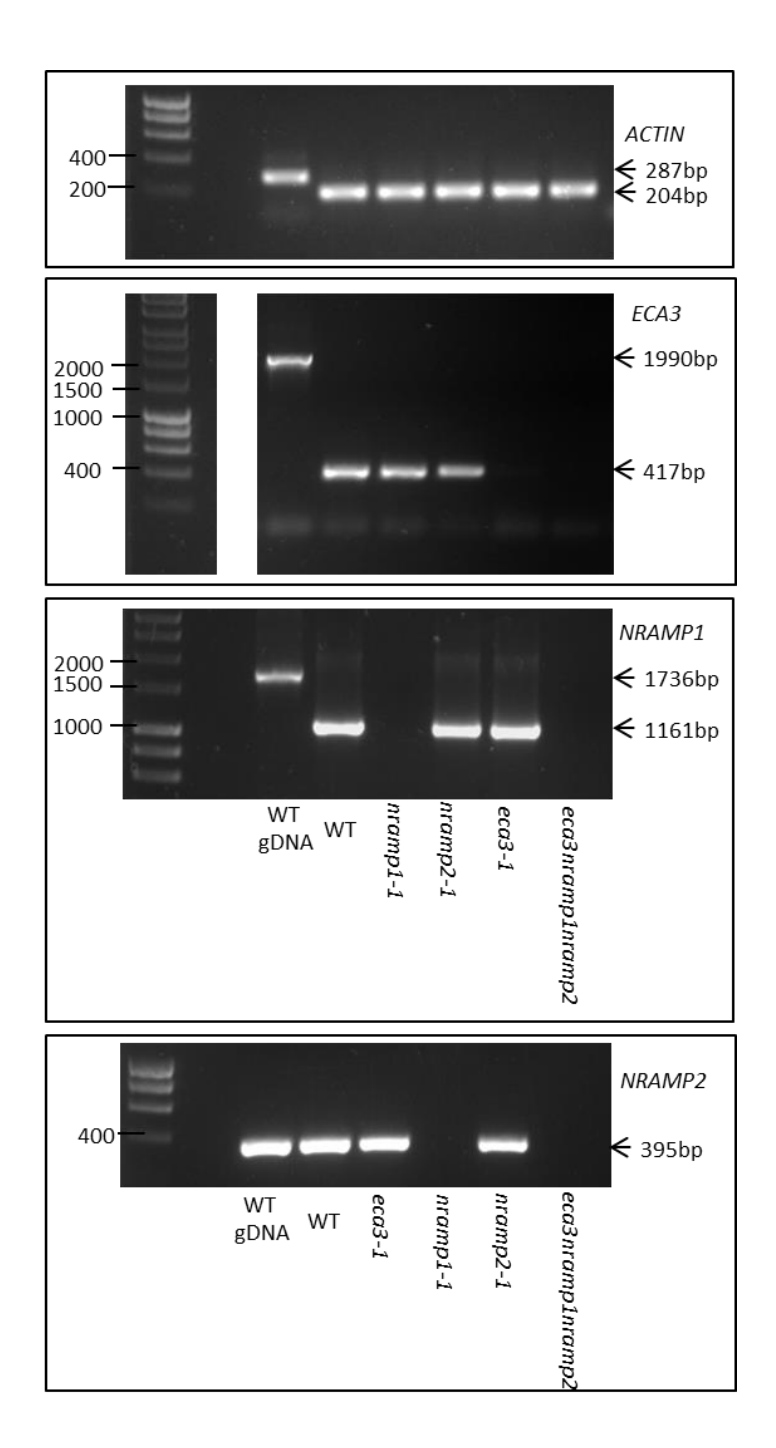


Figure 6.21. Confirmation of eca3-1 nramp1-1 nramp2-1 triple mutant at RNA level.

Confirmation at RNA level using using wild type (WT) gDNA, WT cDNA, single mutant *nramp1-1*, *nramp2-1* and *eca3-1* cDNA and corresponding triple mutant cDNA as template. A) *ACTIN* primers amplify products of 287 base pairs (bp) from WT gDNA and 204bp from all cDNA, indicating cDNA is of good quality with no genomic contamination. B) *ECA3* primers amplify products of 1990bp from WT gDNA and 417 bp from WT, *nramp1-1* and *nramp2-1* cDNA, but no product from *eca3-1* or triple mutant. C) *NRAMP1* primers amplify product of 1736bp from WT gDNA and 1161bp from *nramp2-1* and *eca3-1*, but not from *nramp1-1* or triple mutant. D) *NRAMP2* primers amplify product of 395bp from WT gDNA and WT, *nramp1-1* and *eca3-1* cDNA, but not from *nramp2-1* or triple mutant. Together these findings demonstrate *eca3-1 nramp1-1 nramp2-1* is knockout at RNA level. A-D) Gels labelled with predicted amplicon sizes at right and molecular weight markers at left of gel.

As shown in Figure 6.22, each double mutant eca3-1 nramp1-1, eca3-2 nramp2-2 and nramp1-1 nramp2-2 display additive sensitivities under Mn deficiency compared to the corresponding single mutants. All grew similarly under WT conditions. Additionally, each double mutant displays a different level of sensitivity to Mn deficiency: nramp1-1 eca3-1 is most detrimentally affected, followed by nramp2-1 eca3-1, followed by nramp1-1 nramp2-1 (Figure 6.23 A-B). Rather than display a further additive phenotype, the eca3-1 nramp1-1 nramp2-1 triple mutant is less sensitive than nramp1-1 eca3-1, displaying sensitivity to Mn deficiency that corresponds with that of nramp2-1 eca3-1 (Figure 6.23 C+D).

6.3 Discussion

6.3.1 The intermediate sensitivity of *nramp1-2* to Mn-deficiency may be due to translation of a truncated At NRAMP1

At NRAMP1 and NRAMP2 are predicted to possess 12 transmembrane domains (TMDs), correlating with previous hypotheses for At NRAMP1 (Curie, et al., 2000; Vatensever, et al., 2016) and other related eukaryotic NRAMP homologs (Chen, et al., 2006; Xiao, et al., 2008); most prokaryotic homologs characterised to date possess 11 TMDs (Courville, et al., Erhnstorfer, et al., 2014; Cellier, et al., 2016). This is highlighted in Figure 6.1 and 6.7; At NRAMP1 has a longer C-terminal domain than Sca DMT, containing a predicted 12th TMD. Also highlighted on these alignments are the conservation of the Consensus Transport Motif (CTM) domain in At NRAMP1, At NRAMP2, Sca DMT and Ec MntH, which is also conserved in a range of other plant and non-plant NRAMPs (Chen, et al., 2006; Vatansever, et al., 2016). Based on sequence similarity between At NRAMP1 and bacterial ATP-driven transport proteins, Curie, et al. (2000) originally proposed the CTM domain functions as an ATP-binding site to drive active transport. However, NRAMP family members characterised to date are not ATP-driven transporters, functioning instead as proton antiporters or symporters (Jabado, et al., 2000; Goswami, et al., 2001; Courville, et al., 2008; Erhnstorfer, et al., 2014; Cellier, et al., 2016). Due to its high level of conservation between species, it is therefore likely that the CTM domain functions in an as-yet-unidentified mechanism.

Certain multidrug transporters, such as Ec LeuT, have been proposed to function with an inward-facing structure, supported by inverted repeat regions of sequence (Pornillos & Chang, 2006). Based on low levels of sequence similarity with these proteins, Ec MntH, Sca DMT and homologous Dra MntH, from *Deinococcus radiodurans*, have also been proposed to form an inward-facing conformation, placing TMD 1 and TMD 6 together in the centre of the tertiary structure (Courville, et al., 2008; Ehrnstorfer, et al., 2014; Bozzi, et al., 2016). Key residues are conserved on these TMDs, as shown in Figure 6.1 and 6.7, including the DPGN domain on TMD 1

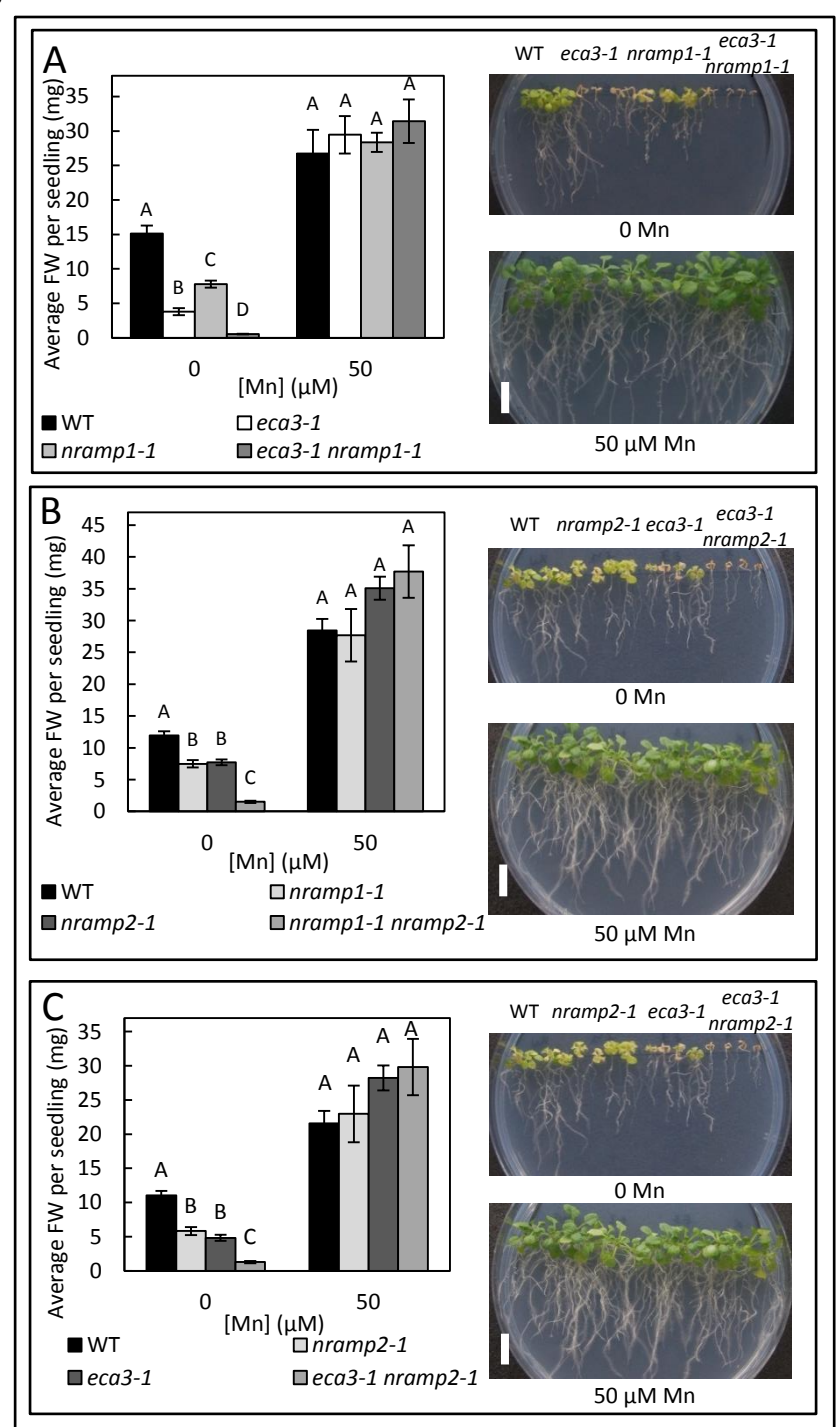


Figure 6.22. Additive sensitivity of eca3-1, nramp1-1 and nramp2-1 double mutants under Mn deficiency.

Comparison of Columbia 8 wild type (WT) with single mutants of eca3-1, nramp1-1 and nramp2-1 and corresponding double mutants A) eca3-1 nramp1-1, B) nramp1-1 nramp2-1 and C) eca3-1 nramp2-1 when grown for 21 days on ½ MS supplemented with either 0 or 50 μ M MnSO₄. Data shows mean fresh weight (FW) per seedling (\pm SE) calculated for 6 plates per condition, with 4 seedlings per genotype per plate. A) According to two-way AVOVA, there is a significant effect of [Mn] (F_(1,40) = 880.48, p<0.001), genotype (F_(3,40) = 104.54, p<0.001) and interaction between [Mn] and genotype (F_(3,47) = 126.27, p<0.001) on FW. B) There is a significant effect of [Mn] (F_(1,39) = 800.78, p<0.001), genotype (F_(3,39) = 46.07, p<0.001) and interaction between [Mn] and genotype (F_(3,46) = 74.05, p<0.001) on FW. C) There is a significant effect of [Mn] (F_(1,28) = 495.34, p<0.001), genotype (F_(3,28) = 24.22, p<0.001) and interaction between [Mn] and genotype (F_(3,35) = 43.72, p<0.001) on FW. Means not sharing a letter at a particular concentration are significantly different, according to Tukey's post-hoc test. Photos show representative plant growth at 0 and 50 μ M Mn; white bar = 1 cm.

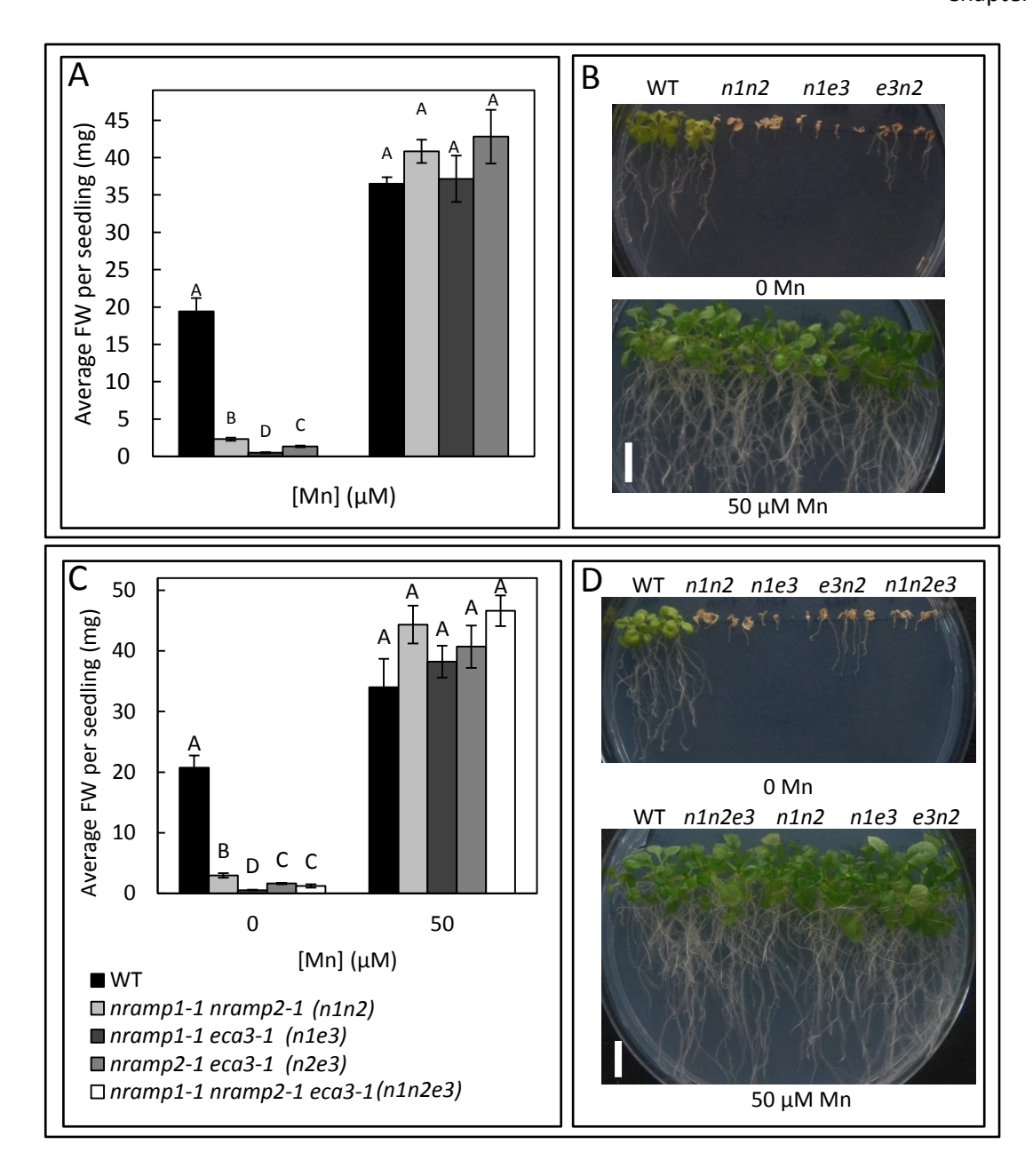


Figure 6.23. Comparison of *nramp1-1 nramp2-1 eca3-1* double and triple mutants under Mn deficiency.

A-B) Comparison of Columbia 8 wild type (WT) with double mutants nramp1-1 nramp2-1, nramp1-1 eca3-1 and eca3-1 nramp2-1 and C-D) with addition of triple mutant eca3-1 nramp1-1 nramp2-1, when grown for 21 days on ½ MS plates containing either 0 or 50 μ M MnSO₄. A + C) Data shows mean fresh weight (FW) per seedling (\pm SE) calculated for 6 plates per condition, with 4 seedlings per genotype per plate. A) According to two-way AVOVA, there is a significant effect of [Mn] ($F_{(1,40)} = 1934.02$, p<0.001), genotype ($F_{(3,40)} = 143.23$, p<0.001) and interaction between [Mn] and genotype ($F_{(3,47)} = 149.36$, p<0.001) on FW. C) There is a significant effect of [Mn] ($F_{(1,45)} = 1362.81$, p<0.001), genotype ($F_{(4,45)} = 55.87$, p<0.001) and interaction between [Mn] and genotype ($F_{(4,54)} = 71.57$, p<0.001) on FW. Means not sharing a letter at a particular concentration are significantly different, according to Tukey's post-hoc test. Photos show representative plant growth at 0 and 50 μ M Mn; white bar = 1 cm.

Chapter 6

and the AxxMxH domain on TMD 6; this is substituted for CxxMxH in At NRAMP2. Mutational studies have shown these domains are essential for function in prokaryotic NRAMPs Sca DMT and Ec MntH and the human DMT1, with studies generally investigating changes in the ability of mutated proteins to transport Cd. Mutations in the DPGN domain drastically reduce but do not fully abolish Cd transport, while mutations in TMD 6 can potentially abolish Cd transport (Courville, et al., 2008; Erhnstorfer, et al., 2014). These residues line the ion-transport pathway but are generally shown to be important for maintaining structure and function, rather than directly binding protons or metal cations (Cellier, et al., 2016). The DPGN domain maintains the structure of the surrounding TMDs (Haemig & Brooker, 2006; Courville, et al., 2008) while the conserved histidine of the TMD 6 AxxMxH domain mediates conformational change after proton binding. Additionally the conserved Ns of TMD 1, 7 and 11 do not interact directly with cations, but facilitate the overall structure by maintaining inter-helix contacts between neighbouring TMDs (Courville, et al., 2008). Rather than directly binding substrate ions, the conserved M in the AxxMxH/CxxMxH of TMD 6 is proposed to confer selectivity against alkaline earth metals such as Ca and Mg, in favour of transition metal ions (Bozzi, et al., 2016).

Metal-sensitivity assays comparing nramp1 T-DNA insertion mutants provide further evidence that At NRAMP1 is involved in alleviating Mn deficiency (Cailliatte, et al., 2010), but also identifies nramp1-2 as displaying an intermediate level of Mn sensitivity. This differential response could be due to an additional unidentified mutation in the nramp1-2 background. However, due to the presence of low-levels of transcript at the 3' end of At NRAMP1, it is hypothesised that nramp1-2 translates a truncated, semi-functional At NRAMP1 protein. Based on the position of the nramp1-2 insertion site, it is possible that the final 9 TMDs of At NRAMP1 could be translated in this truncated protein. The knowledge obtained from aligning NRAMP1 with Sca DMT and Ec MntH suggests this truncated protein would still possess the CTM domain in TMD 8, as well as the conserved AxxMxH of TMD 6, and N residues on TMD 7 and 11. However, this truncated protein would be lacking the first 3 TMDs of NRAMP1, including the DPGN domain. Therefore, it is hypothesised that the ability to transport Mn can be maintained by only the final nine TMDs of NRAMP1, but at a lower rate, affinity or conformational turnover than if all the structurallyimportant residues of TMD 1 were present. It is hypothesised that it is this difference that causes the intermediate sensitivity of nramp1-2, relative to WT and nramp1-1 and nramp1-3 under Mn deficiency. To explore this further, quantitative PCR should be utilised to determine whether there is indeed a level of transcript still expressed in nramp1-2. Further, it would be interesting to clone this truncated protein and express in deficient yeast mutants to compare the level of functional complementation relative to the full length NRAMP1, which can functionally complement the Mn-deficient phenotype of *smf1 smf2* (Thomine, et al., 2000).

6.3.2 NRAMP2 is involved in alleviating Mn deficiency at the cis-Golgi

Phenotypic analysis of *nramp2-1* suggests NRAMP2 is involved in alleviating Mn deficiency, with stunted growth observed under Mn deficiency in both plate- and hydroponically-grown assays. When grown hydroponically, both *nramp2-1* and *nramp1-1* grow less well than WT under control conditions of 1.8 µM Mn. The nutrient components of Modified Hoagland's solution are generally at lower concentrations than in ½ MS (see Table 2.5 for comparison); it appears that 1.8 µM Mn is sufficiently low, in combination with the other nutrients present, to induce a Mn-deficiency response in *nramp1-1* and *nramp2-1*. It might be interesting to compare these mutants across a range of Mn concentrations to determine at which point the Mn deficiency response is initiated. This sensitivity appears to be specific to Mn deficiency, although it is noted that *nramp2-1* grew significantly better than WT under control conditions in both the Zn- and Fe-deficiency experiments. It would be useful to isolate another *nramp2* allele to ensure the Mn sensitivity of *nramp2-1* is not due to an additional, unidentified insertion elsewhere in the genome. Unfortunately the only other currently available allele, *nramp2-2*, is homozygous for an insertion in the *NRAMP2* promoter, but this does not seem sufficient to cause a knockout. This has not been confirmed at the RNA level and the level of expression could be determined using qPCR.

Transient expression in tobacco suggests At NRAMP2 is expressed at the cis-Golgi. This correlates with the increased sensitivity to Mn deficiency when *nramp2* is knocked out in addition to *eca3* or *nramp1*, which would favour targeting to different subcellular membranes. It is therefore proposed that At NRAMP2 functions to alleviate Mn deficiency by sequestering Mn into the cis-Golgi. To further assess its specificity and function, At NRAMP2 should be expressed in sensitive yeast mutants *smf1 smf2* and *zrt1 zrt2*, to determine whether it is capable of rescuing Mn- and Zn-deficient phenotypes, respectively. At NRAMP2 expression does not restore the Fe-deficiency phenotype of *fet3 fet4*, defective in Fe uptake pathways (Curie, et al., 2000). However, the ability to transport Fe should not be ruled out as targeting an intracellular membrane may not be sufficient to complement a mutant defective in Fe uptake.

6.3.3 At ECA3 is a transporter with a major role in alleviating Mn deficiency, and a minor role in Mn toxicity

A major aim of this project was to improve understanding of how At ECA3 and At MTP11 contribute to Mn homeostasis; the role of ECA3 has been disputed, with reports suggesting it functions in either Mn deficiency (Mills, et al., 2008) and toxicity (Li, et al., 2008). Here, the *eca3-1* and *eca3-2* mutants display clear growth defects under Mn deficiency, both at low and standard Ca, thus confirming an important role for ECA3 under low Mn conditions. No additive phenotype

Chapter 6

is observed under Mn deficiency when *mtp11-1* is knocked out in addition to ECA3; this indicates that, in terms of contributing positively to Mn efficiency, ECA3 plays a more important role than MTP11.

The sensitivity of *eca3-1* to Mn deficiency is observed when grown hydroponically under Mn deficient conditions from day 0, but not when transferred to Mn deficiency after 29 days on control media. Contrastingly, *nramp1-1* displays sensitivity to Mn deficiency under both exposure regimes. This may suggest ECA3 has a more important role in alleviating Mn deficiency at an earlier stage of development. However, results from Genevestigator suggest *ECA3* expression remains fairly stable throughout development, although this microarray data was performed on control tissue; additionally, qPCR data suggests expression does not change under Mn deficiency in the root or shoot of 15 day old seedlings (Mills, et al., 2008). It may be interesting to collect Mn-deficient tissue from a range of developmental stages to determine whether *ECA3* is expressed at higher levels at very early stages of development.

No significant detrimental effect was observed under Mn toxicity in *eca3-1*, tested here at 1 mM Mn. Li, et al. (2008) report a strong inhibition of root growth in *eca3-4* mutants, exhibiting reductions of 50-60% compared to WT at 50 µM Mn. A direct replication of this experiment did not demonstrate any significant reductions in root length, FW or chlorophyll in *eca3-1*, *eca3-2* nor *eca3-4* under Mn toxicity (Williams, et al., unpublished data). It appears, therefore, that MTP11 is more important than ECA3 under Mn toxicity. However, enhanced stunting and chlorosis is observed in the *eca3-2 mtp11-1* double mutant, suggesting ECA3 does play a minor role in alleviating Mn toxicity, but that this is only apparent when MTP11 is also non-functional. The susceptibility of *eca3-2 mtp11-1* to Mn also appears to be Ca-dependent; the sensitive phenotype is apparent at lower Mn concentrations when Ca is less available, although it is more obvious under basal Ca.

This additive phenotype may suggest ECA3 and MTP11 participate in Mn homeostasis at different pathways. Indeed, co-expression of ECA3 and MTP11 in tobacco, together and with different cellular markers, suggests ECA3 targets the trans-Golgi network, while MTP11 targets the cis-Golgi. This finding favours reports by Mills, et al. (2008) as opposed to targeting of the PVC proposed by Li, et al. (2008), although it is recognised that different plant systems have been used for localisation studies. This could imply ECA3 functions primarily under Mn deficiency, supplying Mn to key enzymes within the Golgi, but could also confer a benefit under Mn toxicity by sequestering Mn into this compartment; the dual role of ECA3 in Mn homeostasis, functioning under both Mn deficiency and toxicity, is easier to explain if ECA3 targets the Golgi rather than the PVC. Golgi-sequestration is also the mechanism proposed by Peiter, et al. (2007) as the route by which

MTP11 alleviates Mn toxicity, leading to vesicular trafficking and exocytosis as a route for detoxification. Specific Mn pathways around the cell are beginning to be elucidated; for example, Mn is remobilised from the vacuole by At NRAMP3 and At NRAMP4, preferentially providing Mn to PS-II in the chloroplast instead of Mn-SOD in the mitochondria; this is possibly sequestered into the chloroplast by At PAM71 (Lanquar, et al., 2005; Lanquar, et al., 2010; Schneider, et al., 2016). It is possible that, while MTP11 sequesters Mn into the Golgi for eventual efflux from the cell, sequestration by ECA3 may target a different pathway that does not lead to an eventual efflux pathway, tolerating low-to-moderate levels of Mn, but not excess Mn; thus, ECA3 only plays a minor role in alleviating Mn toxicity. Further investigation is needed to test this functional hypothesis for ECA3, however.

6.3.4 Exploring the relative importance of At NRAMP1, At NRAMP2 and At ECA3 in Mn homeostasis

Each of the *nramp1-1*, *nramp2-1* and *eca3-1* mutants are sensitive to Mn deficiency, but *eca3-1* displays the strongest level of stunting when directly compared. Additionally, the corresponding double mutants are each additive under Mn deficiency. The additive sensitivities corresponds with the finding that each protein targets a different subcellular membrane, with At NRAMP1 targeting the plasma membrane (Cailliatte, et al., 2010), At ECA3 targeting the trans-Golgi network (Figure 6.18; Mills, et al., 2008) and At NRAMP2 targeting the cis-Golgi network (Figure 6.12). These findings suggest At NRAMP1 is responsible for Mn uptake at the plasma membrane, alongside other uptake transporters with Mn affinity such as At IRT1 (Vert, et al., 2002); once within the cell, Mn is proposed to be sequestered into distinct compartments of the Golgi by At ECA3 and At NRAMP2, potentially supplying Mn to key enzymes. This is summarised in the model shown in Figure 6.24A.

The double mutants display differential sensitivities to Mn deficiency when directly compared, with eca3-1 nramp1-1 showing greater sensitivity than nramp1-1 nramp2-1, even though both double mutants have lost a route for sequestration into the Golgi, that may provide Mn to key enzymes and proteins. This might suggest either that At ECA3 is more important than At NRAMP2 in alleviating Mn deficiency, or alternatively that the route into the trans-Golgi is more important than the route into the cis-Golgi when sequestering Mn under deficiency conditions. Rather than displaying an additive sensitivity, the eca3 nramp1 nramp2 triple mutant is less stunted than nramp1-1 eca3-1. This could be because, although having lost an uptake pathway, the triple mutant has also lost two sequestration pathways, potentially meaning any residual Mn, or Mn remobilised from the vacuole and other stores, are retained in the cytoplasm longer than if it

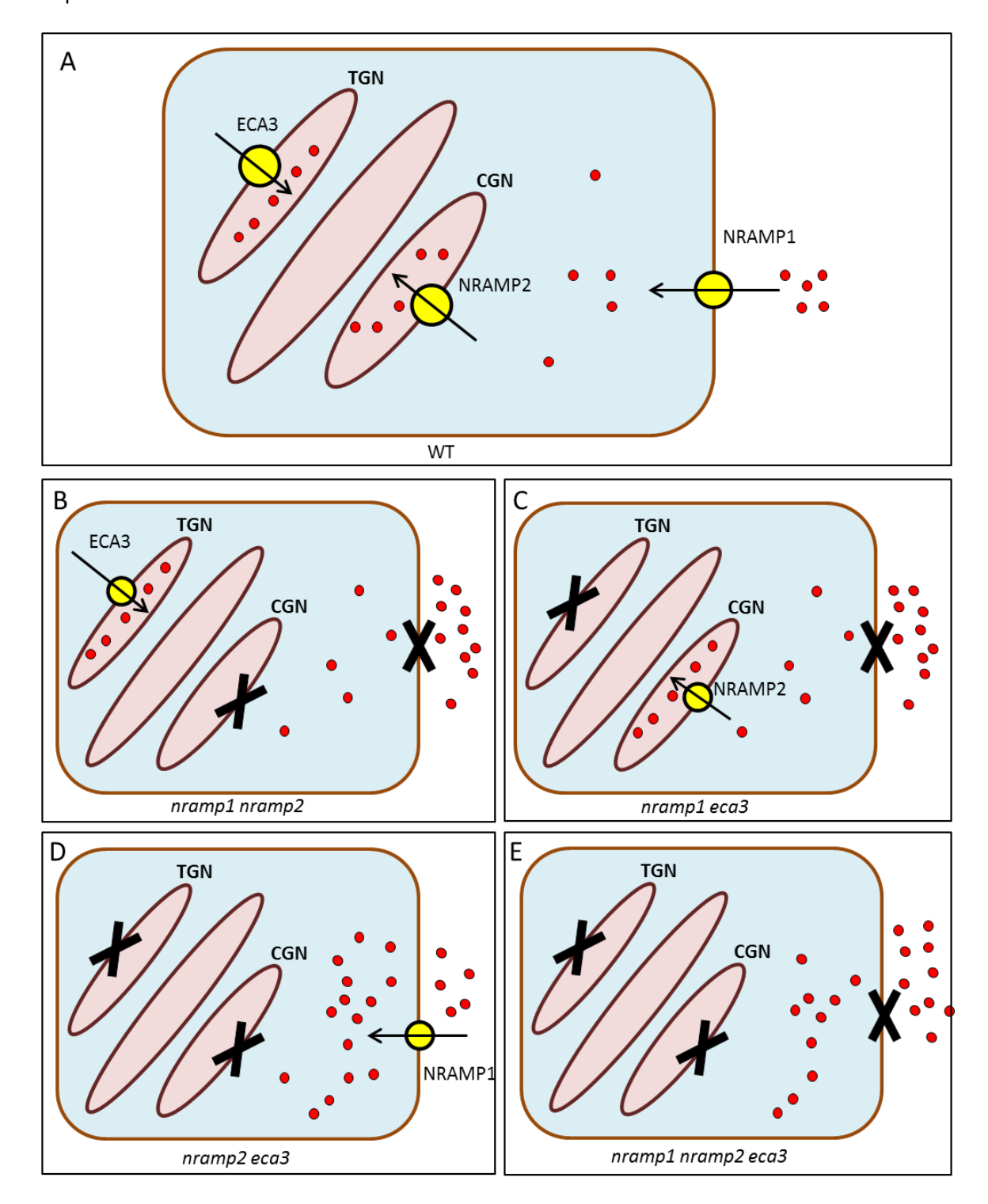


Figure 6.24. Proposed model of At NRAMP1, At NRAMP2 and At ECA3 contributing to alleviating Mn deficiency.

A) Function and proposed localisation of ECA3, NRAMP1 and NRAMP2 (triangles) in typical Arabidopsis cell. TGN, trans-Golgi network; CGN, cis-Golgi network; red circles, Mn ions. B-D) proposed effect on Mn distribution in plant cell when different transporters are knocked out in double m utants. E) proposed effect on Mn distribution in plant cell when all transporters are knocked out in the *nramp1 nramp2 eca3* triple mutant. X, lost transporter in a mutant.

were immediately sequestered into the Golgi, for use elsewhere in the cell. Figure 6.24B-E summarises the hypothetical models for each of these double and triple mutants.

While NRAMP1 expression is limited mostly to the root (Cailliatte, et al., 2010), ECA3 is expressed across the whole plant (Mills, et al., 2008) and the tissue-specificity of NRAMP2 is as-yet-unknown. It is unclear whether these transporters function together or independently, but determining whether these transporters function in the same cells within the plant would be a useful strategy. The use of double and triple mutants provide an interesting starting point for determining their relative importance in alleviating Mn deficiency.

Chapter 7: General Discussion

7.1 At MTP8, MTP10 and MTP11 all contribute to Mn tolerance

7.1.1 At MTP8 sequesters excess Mn into the vacuole

A key result of this project confirms findings that At MTP8 sequesters Mn into the vacuole. When expressed in Arabidopsis and tobacco cells, fluorescence is characteristic of the tonoplast: the At MTP8 signal runs in a continuous signal that does not enclose the chloroplasts, and forms transvacuolar strands to enable passage of the Golgi and contents of the cytoplasm across the cell. This localisation corresponds with all plant MTP8 proteins characterised so far (Delhaize, et al., 2003; Chen, et al., 2013; Migocka, et al., 2015; Eroglu, et al., 2016), except for Hv MTP8.1 and Hv MTP8.2, which target the Golgi (Pedas, et al., 2014). Expression of At MTP8 confers considerable tolerance to the Mn-sensitive yeast mutant pmr1, enabling growth comparable to the WT at concentrations up to 20 mM Mn; this appears to be quite specific for Mn, although the ability to transport Fe should not be ruled out. Site-directed mutagenesis indicates the conserved DxxxD domains in transmembrane domain (TMD) 2 and 5 of the Mn MTPs are critical for maintaining Mn-transporting ability of both MTP8 and MTP11. These domains have very recently been shown to be important for maintaining the function of Os MTP8.1 (Chen, et al., 2016). Although the exact residues are not strictly conserved, these domains are similarly important for function in MTPs transporting different substrates (Kawachi, et al., 2008; Podar, et al., 2012; Menguer, et al., 2013) and CDFs from different phyla (Zogzas, et al., 2016; Nishito, et al., 2016; Martin and Giedroc, 2016).

The role of At MTP8 in Mn-homeostasis is further confirmed by the Mn-hypertolerance when overexpressed in Arabidopsis, and the Mn-hypersensitivity of *mtp8* knockout mutants. At MTP8 has also recently been implicated in alleviating Mn/Fe antagonism by sequestering Mn in the vacuole, preventing Mn-dependent inhibition of components of the Fe deficiency response (Eroglu, et al., 2016). Hypersensitivity and hypertolerance to pH-induced low Fe bioavailability conditions, in knockout mutants and overexpressing lines, respectively, also confirms this finding. Moreover, At MTP8 is shown to be the only Mn-MTP involved in this process. Other transporters localised to the tonoplast have been shown to sequester Mn in the vacuole, such as At CAX2 (Connorton, et al., 2012) and At CCX3 and Os CCX3 (Morris, et al., 2008; Yadav, et al., 2015). It may be interesting to determine whether *ccx* or *cax* mutants display any sensitivity to low Fe bioavailability, or whether transcript levels change in response to these conditions; this may

determine whether vacuolar sequestration for alleviation of Mn/Fe antagonism is specific to At MTP8, or if it is conserved in other tonoplast transporters.

Another mutant, the EMS mutant 954-12, also displays a very similar phenotype to *mtp8* under elevated Mn and on low Fe bioavailability conditions. Additionally, 954-12 features enhanced Mn accumulation in the shoot, as identified by analysing data available from the PiiMS database (Baxter, et al., 2007), similarly to *mtp8* mutants (Eroglu, et al., 2016). Although this mutant does not feature any polymorphic differences in the At *MTP8* coding sequence, it would be interesting to determine whether polymorphisms exist elsewhere in the 954-12 genome; this may identify potentially important parts of the transcriptional regulation of *MTP8*, or other unidentified components of Mn homeostasis. For example, it may be useful to compare the coding sequence of *FIT* in 954-12 and WT, as this transcription factor has been shown to upregulate *MTP8* under Mn toxicity and low Fe bioavailability (Eroglu, et al., 2016). Alternatively, sequencing the 954-12 genome would identify any other polymorphisms.

7.1.2 At MTP10 and At MTP11 detoxify Mn at different subcompartments of the Golgi.

Although two localisation and functional hypotheses have previously been proposed for At MTP11 (Delhaize, et al., 2007; Peiter, et al., 2007), findings here align with the hypothesis proposed by Peiter, et al. (2007), with At MTP11 targeting the cis-Golgi (CGN). Additionally, MTP10 is proposed to target the trans-Golgi (TGN). The restoration of Mn tolerance in pmr1 also indicates MTP10 and MTP11 are involved in Mn detoxification; when expressed in yeast, At MTP8 and At MTP10 confer greater levels of tolerance than At MTP11. However, although the contributions of At MTP8 and At MTP11 in Mn detoxification are revealed in single knockout mutants, the role of At MTP10 is only evident in the mtp8 mtp10 mtp11 triple mutant, which is more adversely affected by Mn toxicity than the double mutants. This project therefore highlights the importance of using double and triple mutants to assess the relative contribution of transporters in Mn homeostasis, as it can reveal any compensatory function and activity. The severe sensitivity of the triple mutant is likely because three important routes of detoxification are lost, increasing amounts of free Mn in the cytoplasm: sequestration into the vacuole by At MTP8, and sequestration into the cis- and trans-Golgi by At MTP11 and At MTP10, respectively, potentially losing a pathway of vesicular trafficking to the plasma membrane for exocytosis from the cell (Peiter, et al., 2007). Findings may also suggest At MTP11 is one of the more important contributors to Mn detoxification, and that At ECA3 and At MTP10 may serve compensatory mechanisms for Golgi sequestration when MTP11 is non-functional, at the TGN.

At *MTP9* and *MTP10* are found on the same chromosome and share a high % identity and similarity. Additionally, the single *mtp9* and *mtp10* mutants do not display any Mn-dependent phenotype; it was originally hypothesised, therefore, that these proteins may share a functional redundancy. However, while At MTP10 is shown here to transport Mn at the TGN, homologous proteins to At MTP9 in cucumber and rice, Cs MTP9 (Migocka, et al., 2015) and Os MTP9 (Ueno, et al., 2015), localise to the plasma membrane to export Mn from the cell. Although efforts were made to clone At *MTP9*, this resulted in a construct with *MTP9* in the wrong orientation. Future work should involve a different strategy to clone At *MTP9*, enabling expression in different systems for further protein characterisation. It is hypothesised that the *mtp9 mtp10* double mutant would display an additive phenotype to excess Mn, if both are indeed involved in mediating Mn detoxification; however, it is possible that MTP11 would compensate for loss of MTP10, as in the *mtp10* and *mtp8 mtp10* backgrounds. Future work should determine whether the amiRNA plants generated in Chapter 3 do indeed downregulate *MTP9* in the *mtp10* mutant background, and if so, whether any Mn-dependent phenotype is observed.

7.2 Susceptibility to Mn depends on Ca availability

Exposure to elevated Ca has previously been shown to alleviate symptoms of Mn toxicity, including Mn-induced Fe deficiency (Gunes, et al., 1998; Bekker, et al., 1994; Alam, et al., 2006). Here it is shown that Mn toxicity symptoms are correspondingly exacerbated by a reduction in Ca availability: Mn-hypersensitive mutants (including mtp8, mtp11 and eca3 mtp11) become sensitive to Mn at a lower concentration under low Ca conditions (100 μ M Ca) than under basal Ca conditions (1495 μ M Ca). Additionally, the germination of mtp8 mtp11 and mtp8 mtp10 mtp11 mutants is inhibited at relatively low Mn concentrations under low Ca conditions, a phenomenon that is not observed under basal Ca conditions.

The mechanism of this Mn/Ca antagonism is not well understood. A variety of transport proteins are able to transport Ca, to control Ca signalling across the cell. As chemical homologs, some transporters have affinity for Mn in addition to Ca, as summarised in Table 1.3, although affinity for Mn is not always tested. Therefore it is possible that under low Ca availability Mn competes with Ca for transport into the cytoplasm, contributing to cytoplasmic toxicity and exacerbating Mn toxicity symptoms. Alternatively, Mn could compete with or displace Ca from active sites on other key proteins and enzymes. Although there is little information regarding Mn/Ca displacement, Ca can be displaced from its position in the water splitting/oxygen evolving complex of PSII, Mn₄CaO₅, by lanthanides (Ghanotakis, et al., 1985); displacement of Ca does not necessarily alter the core structure, but Ca is essential for proper function of this protein due to its role in organising the surrounding water network (Lohmiller, er al., 2012).

7.3 At ECA3, At NRAMP1 and At NRAMP2 play major roles in Mn deficiency

ECA3 appears to play a minor role in Mn toxicity, but this is only apparent when MTP11 is non-functional. Instead, the major role of ECA3 appears to be in alleviating Mn deficiency, as proposed by Mills, et al. (2008). Transient expression in tobacco suggests ECA3 targets the TGN, also supporting the localisation proposed by Mills, et al. (2008), rather than the PVC as proposed by Li, et al. (2008), with strong colocalisation with trans-Golgi marker sialyl transferase (ST), and partial overlap with MTP11. Targeting the Golgi also favours the hypothesis that ECA3 could feasibly act under both deficiency and toxicity, providing Mn to important enzymes and proteins under deficiency and physiological conditions, whilst also sequestering Mn at low levels under Mn toxicity. This 'dual function' hypothesis would be harder to explain if ECA3 targeted the PVC. Based on the physiological provision of Mn to the Golgi, it would be interesting to see whether any particular proteins are specifically dependent on this Mn provision by ECA3, for example to determine whether any proteins are particularly affected in the *eca3* mutant, or whether ECA3 serves a general Mn-provision mechanism to the TGN.

NRAMP2 is also shown here to play a key role in alleviating Mn deficiency, proposed to sequester Mn into the CGN. Future investigation into this protein should clarify any tissue specificity of expression, through promoter analysis and determining changes in *NRAMP2* expression in response to Mn extremes. Expression in Fe- and Mn-deficiency yeast mutants, *fet3 fet4* and *smf1 smf2*, would also be useful to further determine its metal transport properties. Additionally, it may be interesting to further explore the structure-function relationship of NRAMP1 and NRAMP2. The differential sensitivity of *nramp1-2* to Mn deficiency, compared to the hypersensitive *nramp1-1*, is possibly due to translation of a truncated NRAMP1 in *nramp1-2*, although it is possible there is an unidentified background insertion causing this phenotype. The truncated NRAMP1, and the equivalent truncation in NRAMP2, would still possess key domains such as the AxMxxH and CTM motifs of TMD6 and TMD8, but would lack the DPGN motif of TMD1, based on an alignment with Sca DMT, crystallised by Ehrnstorfer, et al. (2014). Characterising these proteins, for example comparing the ability of truncated NRAMP1 and NRAMP2 to rescue metal-sensitive yeast mutants relative to the full length protein, may provide further insight into the structure-function relationship of NRAMP family members.

7.4 An updated overview of Mn homeostasis in the plant cell

Figure 7.1A shows a typical Arabidopsis cell with a simplistic subcellular model of the transporters investigated in this report. Under Mn deficiency, At NRAMP1 imports Mn at the plasma

membrane (Cailliatte, et al., 2010), which is transported into the TGN and CGN, by At ECA3 and NRAMP2, respectively, possibly to provide Mn to functional sites in important enzymes and proteins. Under Mn-replete conditions but when Fe is limiting, At MTP8 sequesters Mn into the vacuole to prevent Mn/Fe antagonism; this is also an important detoxification mechanism to alleviate cytotoxicity under elevated Mn conditions. At MTP11 and At MTP10 also play important roles in alleviating Mn toxicity, by sequestering Mn into the CGN and TGN, respectively. Direct comparison of the single, double and triple mutants isolated in this thesis may expose ECA3 as the most important player in alleviating Mn deficiency at the TGN, perhaps due to a higher Mn affinity or faster conformational turnover than At NRAMP2. Contrastingly, MTP11 has been highlighted as the key player in Mn toxicity at the CGN, potentially leading to exocytosis from the cell (Peiter, et al., 2007); compensatory mechanisms exist when At MTP11 is non-functional, with At MTP10 and At ECA3 sequestering Mn into the TGN.

Therefore, this thesis work begins to highlight the importance of the Golgi in both extremes of Mn homeostasis, a finding that has previously been under-reported in the literature. Additionally, it may be possible that the TGN is more important for alleviating Mn deficiency, while the CGN is more important for alleviating Mn toxicity. The intricacies of specific Mn homeostatic pathways are beginning to be elucidated. For example, At NRAMP3 and NRAMP4 are responsible for Mn remobilisation under deficiency conditions, specifically to target PS-II in the chloroplast, instead of other Mn-requiring enzymes in the cell (Lanquar, et al., 2005; Lanquar, et al., 2010). It is therefore possible that specific pathways exist in the Golgi, depending on the transporter and compartment utilised for Mn-loading.

Corresponding with this hypothesis is the notion that the barley MTP8s, Hv MTP8.1 and Hv MTP8.2, function at the Golgi in non-overlapping roles: Hv MTP8.1 is upregulated in the roots under Mn toxicity, implying a detoxification role, while Hv MTP8.2 is downregulated, potentially playing a role under Mn deficiency (Pedas, et al, 2014). Proteins that supply Mn to the Golgi under deficiency and physiological conditions often function to provide key enzymes and proteins with Mn. For example, correct N- and O-linked glycosylation is dependent on Golgi-loading of Mn by P_{2A}-type ATPase PMR1 in yeast (Durr, et al., 1998); in plants, important proteins such as Os MSD1, the Mn-SOD1 of rice, are reliant on Golgi-based N-glycosylation (Kang, et al., 2015; Shiraya, et al., 2015). Also a P_{2A}-type ATPase, it is possible At ECA3 loads Mn into the TGN for a similar purpose, playing a more important role in this process than At NRAMP2 at the CGN, and thus *eca3* suffers a more detrimental phenotype under Mn deficiency.

Therefore, it is hypothesised that the sequestration pathway by At ECA3 leads to loading of Mn into the TGN for physiological purposes. However, this pathway can function in a compensatory

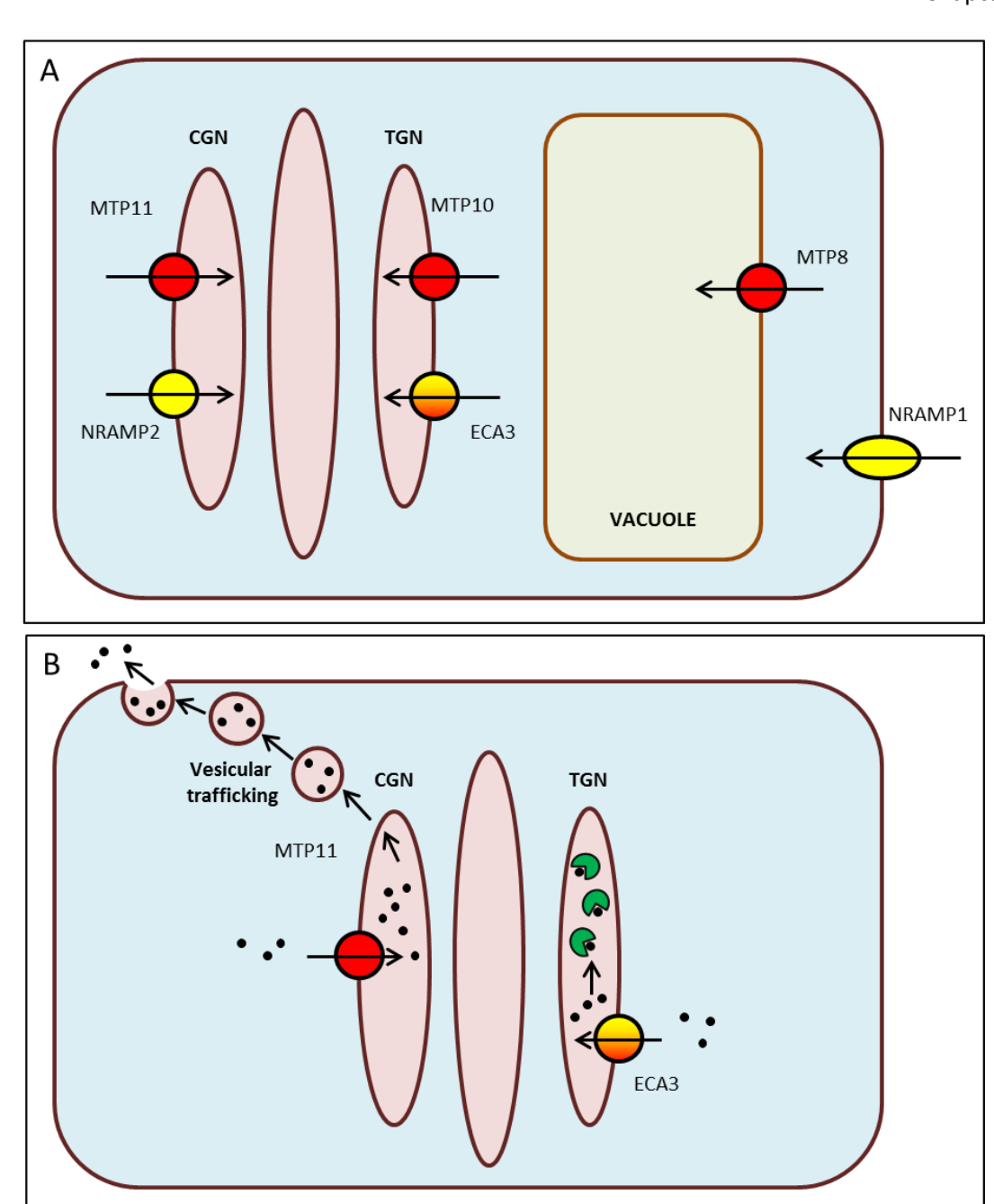


Figure 7.1. Schematic for subcellular localisation of transporters characterised in this study.

A) Subcellular localisation of At MTP8, MTP10, MTP11, NRAMP1 (Cailliatte, et al., 2010), NRAMP2 and ECA3 at the plasma membrane, vacuole, trans-Golgi network (TGN) or cis-Golgi network (CGN) in a plant cell. Red, involved in sequestration to alleviate Mn toxicity; yellow, involved in sequestration or uptake to alleviate Mn deficiency. ECA3 is proposed to be involved in both Mn deficiency and toxicity. Arrow shows proposed direction of Mn transport with respect to the membrane. B) Hypothetical functional roles of ECA3 and MTP11 in relation to Mn homeostasis at the Golgi. ECA3 sequesters Mn (black circles) into the TGN for incorporation into and proper glycosylation of important enzymes and proteins (green pie shapes). MTP11 sequesters Mn into the CGN which initiates vesicular trafficking to the plasma membrane for efflux from the cell, as proposed by Peiter, et al. (2007).

way for Mn detoxification. There is little information regarding Golgi-storage of Mn in plants. However, the Golgi network in rat dopaminergic cells is able to store physiological-to-moderately-toxic levels of Mn until a certain threshold concentration, at which point Mn accumulates in the cytoplasm and nucleus, eventually resulting in cell death (Carmona, et al., 2010). A mammal protein, GPP130 (Golgi phosphoprotein 4), has been identified as a CGN-specific Mn-sensor, responsible for sensing elevated Mn in the CGN and leading to vesicle-trafficking from the Golgi under Mn-toxic conditions (Mukhopadhyay, et al., 2010; Masuda, et al., 2013). Vesicular trafficking of Mn from the Golgi, leading to efflux from the cell, is the mode of detoxification proposed after Golgi-sequestration by At MTP11 (Peiter, et al., 2007). It would be interesting to see if a homologous protein to GPP130 exists in Arabidopsis, which is also CGN-specific, as this may provide insight into the enhanced detoxification by MTP11 compared to ECA3, and provide more evidence of specific subcellular pathways for Mn homeostasis. The proposed mechanisms for ECA3 and MTP11 are summarised in Figure 7.1B.

The models proposed here are simplistic, focussing on expression in a single, hypothetical cell. While At NRAMP1 and At MTP8 are shown to function specifically in the root (Cailliatte, et al., 2010; Eroglu, et al., 2016), At ECA3 shows quite broad tissue-specificity (Mills, et al., 2008), and At MTP11 is expressed in tissues across the plant, although not in epidermal cells and trichomes (Peiter, et al., 2007). The tissue-specificity of At MTP10 and At NRAMP2 are yet to be determined. It is therefore possible that these proteins do not all function in the same cell. The time-, exposure- and developmental-specific expression of these genes should be determined and compared to provide a representative model of Mn homeostasis in Arabidopsis.

7.5 Potential applications of knowledge and future outlook

Chapter 1 highlights the detrimental symptoms of crop plants growing under both Mn toxic and deficient conditions, including stunting and chlorosis of the leaf, which can lead to large agricultural yield losses in cereal plants (Palmgren, et al., 2008). Additionally, Fe deficiency is a global problem, both for plant growth on poor soils, and for human nutrition (Wessells & Brown, 2012). Although Arabidopsis is a very useful model organism for determining protein function, it is important to relate this knowledge to more agriculturally relevant species. Here it is shown that, similarly to At MTP11, Os MTP11 also targets a Golgi compartment when expressed in tobacco and Arabidopsis, and is capable of rescuing the Mn-dependent phenotype of *mtp11*. Additionally, its expression in yeast can restore Mn tolerance of *pmr1* (Williams, et al., unpublished data). Although overexpression of At MTP8 confers Mn-hypertolerance, tolerance is not enhanced by expression of At MTP11 or Os MTP11 under the constitutive 35S promoter in the WT; it might be interesting to determine whether a feedback mechanism or post-translational

modification exists for MTP11 in rice and Arabidopsis that prevents conference of hypertolerance. It appears that the Golgi-based Mn detoxification mechanism of At MTP11 is conserved in Arabidopsis and rice, although Os MTP11 targets the CGN while At MTP11 targets the TGN. It would, therefore, also be interesting to also investigate the function and subcellular localisation of Os MTP11.1.

Phylogenetic analysis has also identified homologous transporters to At MTP8: Ta MTP8 and MTP8.1. An RNAi construct was generated to target all three homeologues of both Ta *MTP8* and *MTP8.1*; this has been confirmed by qPCR to downregulate Ta *MTP8.1*, and also appears to downregulate Ta *MTP8* based on semi quantitative PCR. The next step in this analysis would be to use the hydroponics system in Chapter 3 to expose RNAi-transformed wheat plants to elevated Mn, or to low Fe availability induced by high pH, to determine whether downregulating Ta *MTP8* and *MTP8.1* has any impact on tolerance to these conditions. Certainly, disruption of Os MTP8.1 in rice leads to inhibited growth and chlorophyll production under elevated Mn (Chen, et al., 2013). Despite many efforts to amplify Ta *MTP8* and *MTP8.1* for expression in yeast, tobacco and Arabidopsis for further functional analysis, it was not possible to amplify the full length sequence. Although the predicted coding sequences for these genes possess key motifs, such as the two DxxxD domains found in all plant Mn-MTPs, and the CDF signature sequence (Montanini, et al., 2007; Gustin, et al., 2011), it is possible that the intron/exon predictions towards the 3' and 5' termini need to be further resolved to aid correct amplification of the coding sequences. This may be clarified with release of additional genomic sequencing information for *Triticum aestivum*.

The majority of transporters investigated for their role in Mn homeostasis have been studied independently. However, it is important to determine whether they function individually or together in particular pathways, to create a full understanding of Mn homeostasis and distribution around the plant. For example, Os NRAMP5 and Os MTP9 are involved in uptake and efflux of Mn, respectively, at polar ends of root cells, to mediate Mn root-to-shoot translocation (Sasaki, et al., 2012; Ueno, et al., 2015). It would be interesting to see whether enhancing this uptake system, perhaps through altering the native promoters, would enhance uptake from the soil to improve Mn efficiency. This project has isolated and characterised double and triple Arabidopsis mutants to begin to determine the relative contribution of different transporters in Mn homeostasis. The knowledge obtained here may be a useful starting point for developing plants that are more tolerant to poor soils and thus achieve higher yields. For example, a slight growth improvement is seen under Mn deficiency in Arabidopsis in the *mtp8 mtp11* double mutant. It might also be interesting to create knockouts for MTP8 and MTP11 in either rice or wheat to determine whether the corresponding crop plant is more tolerant to Mn deficiency, a key problem for UK soils (Roques, et al., 2013).

Further applications of this knowledge include phytoremediation and biofortification. Phytoremediation may provide an option to improve soils for future crop growth; metal toxicities in the soil, such as Mn and Cd, can be highly detrimental to plant growth and difficult to rectify (Adams, 1981). Phytoremediation aims to detoxify soils by engineering plants that can take up higher levels of contaminants from the soil for sequestration in the aerial tissues. This process would require a greater understanding of how plants uptake metals from the soil, including Mn, for distribution around the plant, and may require further investigation into the mechanisms behind hypertolerant and hyperaccumulating species.

Alternatively, biofortification aims to enhance certain elements, often micronutrients, in the edible part of the plant to improve human nutrition. Micronutrient deficiencies, in particular Zn and Fe, are huge global problems that may in turn lead to cognitive impairment, growth retardation and immune defects (Benoist, et al., 2008; Bailey, 2015). Genetic biofortification aims to develop self-fortifying seeds, a sustainable system implicitly targeting the global poor (Nestel, et al., 2006). Conventional plant breeding to biofortify cereal grains is currently in progress; a cultivar of pearl millet has recently been bred through traditional breeding to contain higher Fe density in the grain, with higher Zn density in the grain as an associated trait (Rai, et al., 2013). This is currently undergoing dietary clinical trials in young children to determine any changes in Fe markers of blood and plasma, and whether they correspond to changes in immune function and cognition (Tako, et al., 2015). Although breeding strategies are useful for developing more efficient crops, biofortification through genetic engineering may provide an advantage over traditional breeding, allowing a more efficient, targeted approach. The knowledge obtained from this study, and other related studies, may be important starting points developing biofortified plants. For example, At MTP8 sequesters Mn into the vacuole; investigation of its promoter and transcriptional control may enable targeting of MTP8 to the grain for sequestration of Mn into the vacuole. Additionally, further investigation into the structure/function relationship of MTP8, such as the DxxxD domains, may provide mutational targets that enhance sequestration of other favourable metals in the grain, in addition to Mn.

Appendix A

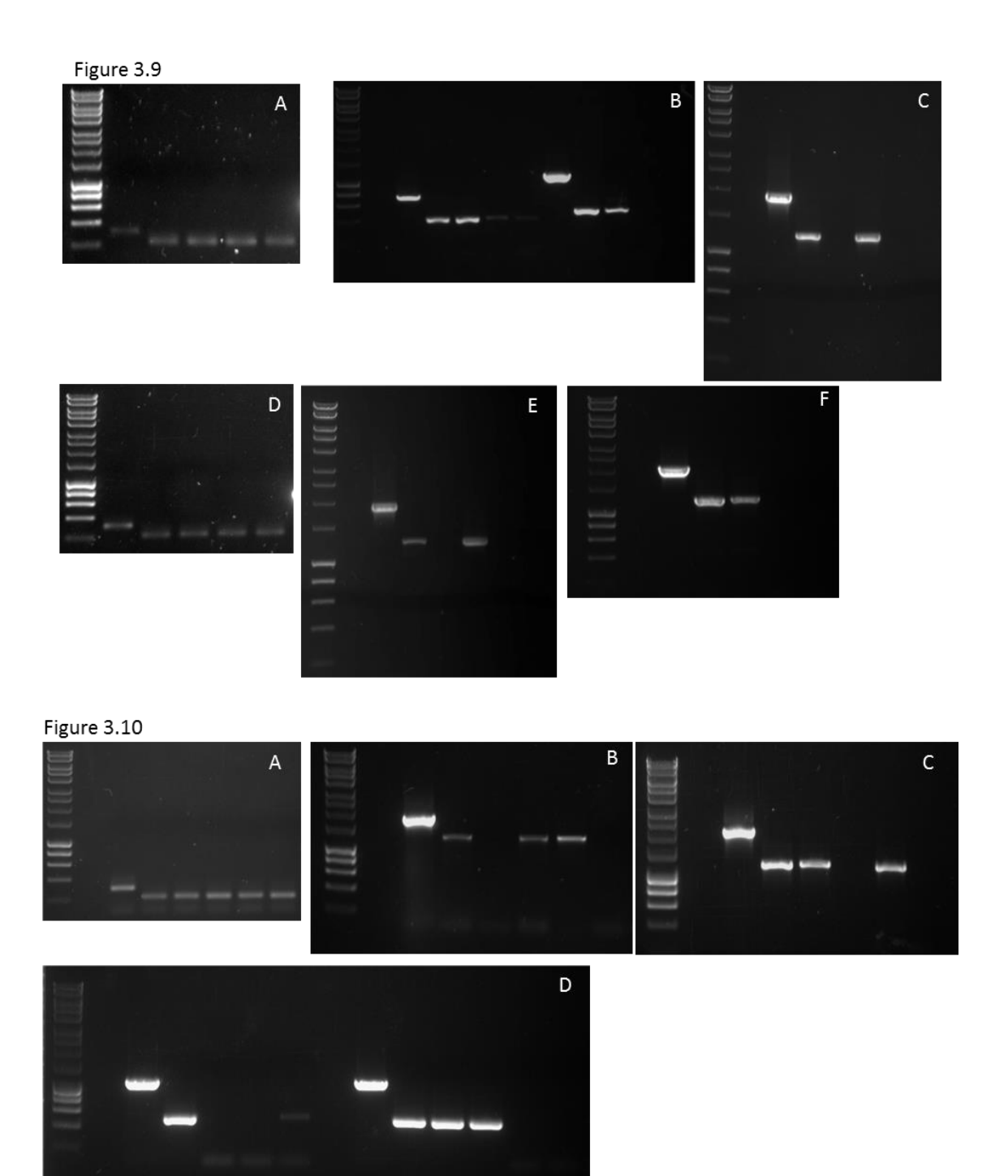
Accession numbers for protein sequences used in phylogenetic analysis, and where obtained. TAIR, The Arabidopsis Information Resource. IBSC, the International Barley Consortium Database; RGAP, Rice Genome Annotation Project

Species	notation Project Accession number	Gono nama (if anu)	Where obtained
Species Arabidopsis thaliana		Gene name (if any) AtMTP10	TAIR
Arabidopsis thaliana Arabidopsis thaliana	At3g58060 At1g79520	AtMTP10	TAIR
	_		
Arabidopsis thaliana	At1g16310	AtMTP10 AtMTP11	TAIR TAIR
Arabidopsis thaliana	At2g39450	AtMTP11	TAIR
Arabidopsis thaliana	At2g46800 At2g47830	AtMTP6	TAIR
Arabidopsis thaliana Arabidopsis thaliana	At1g51610	AtMTP7	TAIR
•	LOC_Os02g53490	OsMTP8	Phytozome9.1, RGAP
Oryza sativa Oryza sativa	LOC_0s02g33490 LOC_0s03g12530	OsMTP8.1	Phytozome9.1, RGAP
Oryza sativa	LOC_0s03g12330 LOC_0s01g03914	OsMTP9	Phytozome9.1, RGAP
Oryza sativa	LOC_Os01g63914 LOC_Os01g62070	OsMTP11	Phytozome9.1, RGAP
Oryza sativa	LOC_Os05g38670	OsMTP11.1	Phytozome9.1, RGAP
Populus trichocarpa	POPTR_0003s21540	PtMTP8.1	Phytozome9.1
Populus trichocarpa	POPTR 0001s04740	PtMTP8.2	Phytozome9.1
Populus trichocarpa	POPTR 0001s04740	PtMTP8.3	Phytozome9.1
Populus trichocarpa	POPTR 0008s08310	PtMTP9	Phytozome9.1
Populus trichocarpa	POPTR_0010s17950	PtMTP10.1	Phytozome9.1
Populus trichocarpa	POPTR 0010s17960	PtMTP10.2	Phytozome9.1
Populus trichocarpa	POPTR 0010s17980	PtMTP10.3	Phytozome9.1
Populus trichocarpa	POPTR_0010s18000	PtMTP10.4	Phytozome9.1
Populus trichocarpa	POPTR 0010s21810	PtMTP11.1	Phytozome9.1
Populus trichocarpa	POPTR_0008s04940	PtMTP11.2	Phytozome9.1
Brachyposium	Bradi3g57420		Phytozome9.1
distachyon			, -
Brachyposium	Bradi2g02050		Phytozome9.1
distachyon	<u> </u>		•
Brachyposium	Bradi2g23070		Phytozome9.1
distachyon	-		•
Brachyposium	Bradi2g54410		Phytozome9.1
distachyon			
Sorghum bicolor	Sb04g034705	SbMTP8	Phytozome9.1
Sorghum bicolor	Sb01g041820	SbMTP8.1	Phytozome9.1
Sorghum bicolor	Sb03g007250	SbMTP9	Phytozome9.1
Sorghum bicolor	Sb03g039220	SbMTP11	Phytozome9.1
Brassica rapa	Bra007377		Phytozome9.1
Brassica rapa	Bra014588		Phytozome9.1
Brassica rapa	Bra003316		Phytozome9.1
Brassica rapa	Bra035123		Phytozome9.1
Brassica rapa	Bra026067		Phytozome9.1
Brassica rapa	Bra026723		Phytozome9.1
Zea mays	ZmGRMZM5G862882_T		Phytozome9.1
_	02		
Zea mays	ZmGRMZM2G118497_T		Phytozome9.1
_	02		
Zea mays	ZmGRMZM2G014454_T		Phytozome9.1
	01		

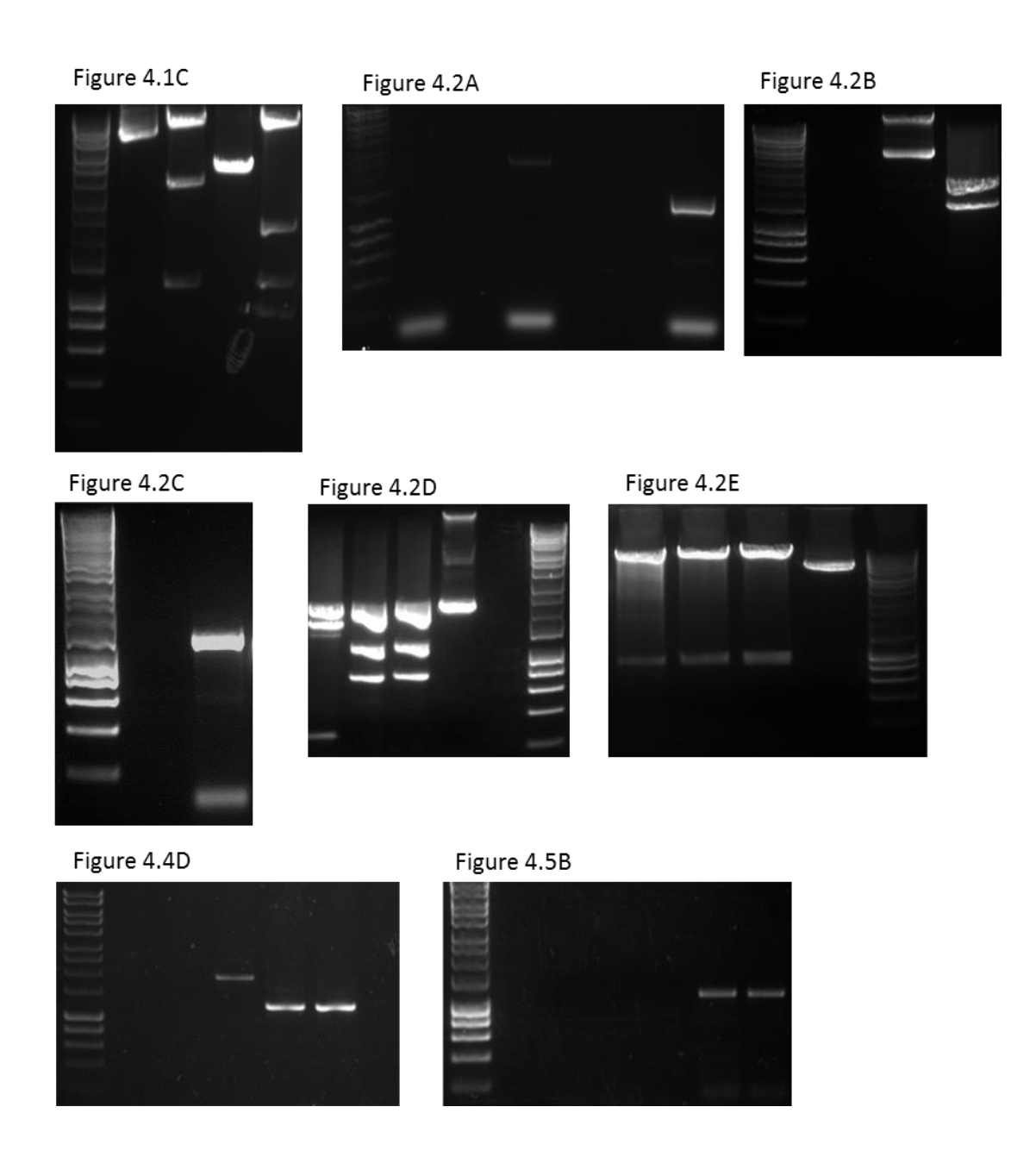
Appendix

Beta vulgaris spp. maritima	AEP40484.1	BmMTP10	GenBank
Beta vulgaris spp. maritima	AEP40483.1	BmMTP11	GenBank
Hordeum vulgare	MLOC_65324.1	HvMTP8.1	IBSC
Hordeum vulgare	MLOC_55775.1	HvMTP8.2	IBSC
Hordeum vulgare	HvAK372762.1	HvMTP11	IBSC
Cucumbis sativa	ACHR01011125	Cs MTP8	Migocka, et al., 2014
Cucumbis sativa	ACHR01003497	Cs MTP9	Migocka, et al., 2014
Cucumbis sativa	ACHR01009952	Cs MTP11	Migocka, et al., 2014

Appendix B

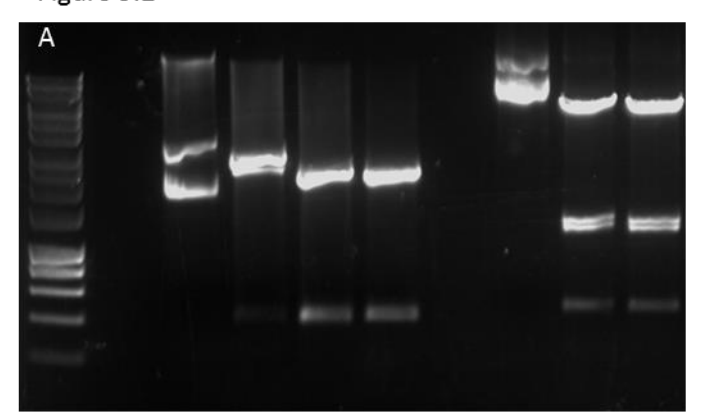


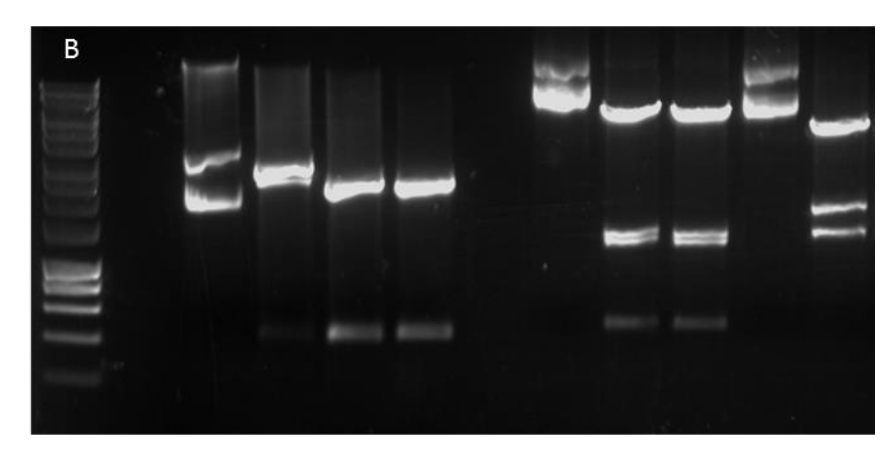
Appendix B. Uncropped gels from various figures throughout thesis. Cont. on next page.

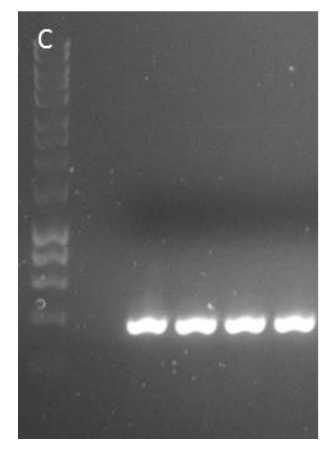


Appendix B. Uncropped gels from various figures throughout thesis. Cont. on next page.

Figure 5.2







Appendix B. Uncropped gels from various figures throughout thesis. Cont. on next page.

Figure 6.8D

Figure 6.11C

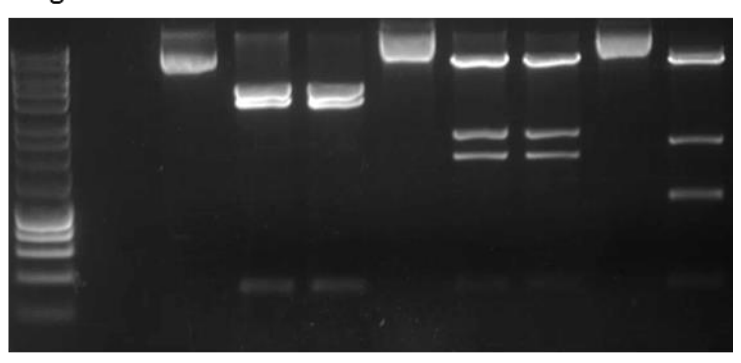


Figure 6.20D

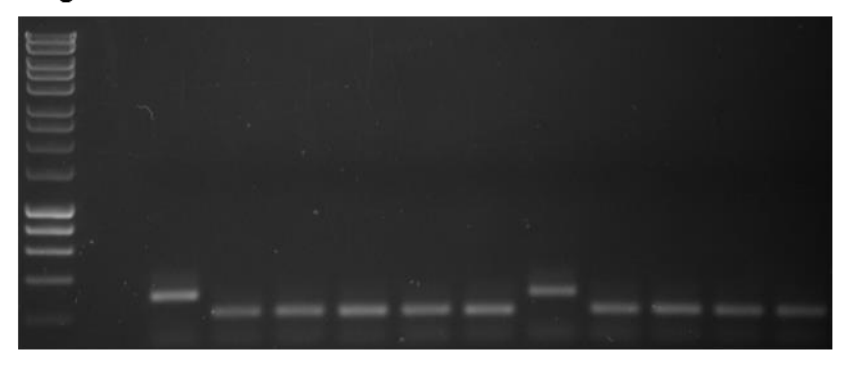
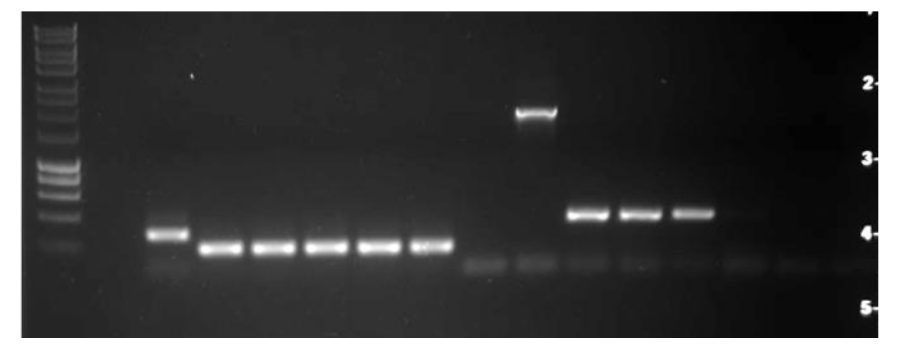


Figure 6.21B



Appendix B. Uncropped gels from various figures throughout thesis.

Adams, F., 1981. Nutritional imbalances and constraints to plant growth on acid soils. *Journal of Plant Nutrition*, 4, 81-87.

Alam, S., Kodama, R., Akiha, F., Kamei, S. & Kawai, S., 2006. Alleviation of manganese phytotoxicity in barley with calcium. *Journal of Plant Nutrition*, 29, 59-74.

Albers, R. W., 1967. Biochemical aspects of active transport. *Annual Review of Biochemistry*, 36, 727-756.

Allen, G., Chu, S.P., Harrington, C.L., Schumacher, K., Hoffman, T., Tang, Y.Y., Grill, E. & Schoeder, J.I., 2001. A defined range of guard cell calcium oscillation parameters encodes stomatal movements. *Nature*, 411, 1053-1057.

Allen, M., Kropat, K. T. & Merchant, S., 2007. Manganese deficiency in *chlamydomonas* results in loss of Photosystem II and MnSOD function, sensitivity to peroxides, and secondary phosphorus and iron deficiency. *Plant Physiology*, 143, 263-277.

Alonso, J., Stepanova, A., Leisse, T., Kim, C., Chen, H., Shinn, P., Stevenson, D., Zimmerman, J., Barajas, P., Cheuk, R., Gadrinab, C., Heller, C., Keske, A., Koesema, E., Meyers, C., Parker, H., Prednis, L., Ansari, Y., Choy, M., Deen, H., Geralt, M., Hazari, N., Hom, E., Karnes, M., Mulholland, C., Ndubaku, R., Schmidt, I., Guzman, P., Aguilar-Henonin, L., Schmid, M., Weigel, D., Carter, D., Marchand, T., Risseeuw, E., Brogden, D., Zeko, A., Crosby, W., Berry, C. & Ecker, J., 2003. Genome-wide insertional mutagenesis of *Arabidopsis thaliana*. *Science*, 301, 653-657

Anton, A., Gross, C., Reissmann, J., Pribyl, T. & Nies, D.H., 1999. CzcD is a heavy metal ion transporter involved in regulation of heavy metal resistance in Ralstonia sp. Strain CH34. *Journal of Bacteriology*, 181, 861-879.

Arrivault, S., Senger, T. & Kraemer, U., 2006. The Arabidopsis metal tolerance protein AtMTP3 maintains metal homeostasis by mediating Zn exclusion from the shoot under Fe deficiency and Zn oversupply. *The Plant Journal*, 45, 861-879.

Arya, S. & Roy, B., 2011. Manganese induced changes in growth, chlorophyll content and antioxidants activity in seedlings of broad bean (*Vicia faba* L.). *Journal of Environmental Biology,* Volume 32, 707-711.

Assunção, A., Herrero, E., Lin, Y.F., Huettel, B., Talukdar, S., Smaczniak, C., Immink, R.G.H., van Eldick, M., Fiers, M., Schat, H. & Aarts, M.G.M., 2010. *Arabidopsis thaliana* transcription factors

bZIP19 and bZIP23 regulate the adaptation to zinc deficiency. *Proceedings of the National Academy of Sciences of the United States of America*, 107, 10296-10301.

Au, C., Benedetto, A., Anderson, J., Labrousse, A., Erikson, K., Ewbank, J. & Aschner, M., 2009. SMF-1, SMF-2 and SMF-3 DMT1 orthologues regulate and are regulated differentially by manganese levels in *C. elegans. PLoS One*, 18., e7792.

Axelsen, K. & Palmgren, M., 1998. Evolution of substrate specificities in the P-Type ATPase superfamily. *Journal of Molecular Evolution*, 46, 84-101.

Baker, A. & Brooks, R., 1989. Terrestrial higher plants which hyperaccumulate metallic elements - a review of their distribution, ecology and phytochemistry. *Biorecovery*, 1, 81-126.

Barabasz, A., Mills, R.F., Trokamowska, E., Williams, L.E. & Antosiewicz, D.M., 2011. Expression of AtECA3 in tobacco modifies its responses to manganese, zinc and calcium. *Environmental and Experimental Botany*, 72, 202-209.

Barber, 1995. Soil Nutrient Bioavailability: a Mechanistic Approach. 2nd ed. Canada: John Wiley and Sons, Inc.

Bashir, K., Inoue, H., Nagasaka, S., Takahashi, M., Nakanishi, H., Mori, S., & Nishizawa, N. K., 2006. Cloning and characterization of deoxymugineic acid synthase genes from graminaceous plants. *Journal of Biological Chemistry*, 281, 32395-32402.

Bassham, D.C. & Raikhel, N.V., 2000. Unique features of the plant vacuolar sorting machinery. *Current Opinions in Cell Biology*, 12, 491-195

Bayle, V., Arrighi, J. F., Creff, A., Nespoulous, C., Vialaret, J., Rossignol, M., Gonzalez, E., Paz-Ares, J., & Nussaume L., 2011. *Arabidopsis thaliana* high-affinity phosphate transporters exhibit multiple levels of posttranslational regulation. *The Plant Cell*, 23, 1523-1535.

Baxter, I., Ouzzani, M., Orcu, S., Kennedy, B., Jandhyala, S. & Salt, D., 2007. Purdue ionomics information management system. An integrated functional genomics platform. *Plant Physiology*, 143, 600-611

Bekker, A., Hue, N., Yapa, L. & Chase, R., 1994. Peanut growth as affected by liming, Ca-Mn interactions, and Cu plus Zn applications to oxidic Samoan soils. *Plant and Soil*, 164, 203-211.

Bell, S. & Vallee, B., 2009. The metallothionein/thionein system: an oxidoreductive metabolic zinc link. *Chembiochem*, 10, 55-62.

Benoist, B., McLean, E., Egli, I. & Cogswell, M., 2008. *Worldwide prevalence of anaemia 1993-2005: WHO global database on anaemia*, Geneva: World Health Organization.

Betts, M.J. & Russell, R.B., 2003. Amino Acid Properties and Consequences of Substitutions, in: *Bioinformatics for Geneticists*. Ed: Barnes, M.R. & Gray, I.C. John Wiley & Sons, Ltd.

Biasini, M., Bienert, S., Waterhouse, A., Arnold, K., Studer, G., Schmidt, T., Kiefer, F., Gallo Cassarino, T., Bertoni, M., Bordoli, L. & Schwede, T., 2014. SWISS-MODEL: modelling protein tertiary and quaternary structure using evolutionary information. *Nucleic Acids Research*, 42, W252-258

Bidwell, S., Woodrow, I., Batianoff, G. & Sommer-Knusden, J., 2002. Hyperaccumulation of manganese in the rainforest tree *Austromyrtus bidwillii* (Myrtaceae) from Queensland, Australia. *Functional Plant Biology*, 29, 899-905.

Blaudez, D., Kohler, A., Martin, F., Sanders, D. & Chalot, M., 2003. Poplar metal tolerance protein 1 confers zinc tolerance and is an oligomeric vacuolar zinc transporter with an essential leucine zipper motif. *The Plant Cell*, 15, 2911-2928.

Bonaventure, G., Gfeller, A., Rodríguez, V. M., Armand, F., & Farmer, E. E., 2007. The *fou2* gain-of-function allele and the wild-type allele of Two Pore Channel 1 contribute to different extents or by different mechanisms to defense gene expression in Arabidopsis. *Plant Cell Physiology*, 48, 1775-1789.

Bonifacino, J.S. & Traub, L.M., 2003. Signals for sorting of transmembrane proteins to endosomes and lysosomes. *Annual Reviews of Biochemistry*, 72, 395-447

Bonza, M. C., Morandini, P., Luoni, L., Geisler, M., Palmgren, M. G., & De Michelis, M. I., 2000. At *ACA8* encodes a plasma membrane-localized calcium-ATPase of Arabidopsis with a calmodulin-binding domain at the N terminus. *Plant Physiology*, 123, 1495-506.

Borrello, S., de Leo, M. & Galeotti, T., 1993. Defective gene expression of MnSOD in cancer cells. *Molecular Aspects of Medicine*, 14, 253-258.

Borrill, P., Connorton, J., Balk, J., Miller, A., Sanders, D. & Uauy, C., 2014. Biofortification of wheat grain with iron and zinc: integrating novel genomic resources and knowledge from model crops. *Frontiers in Plant Science*, 5, 1-8

Boutigny, S., Sautron, E., Finazzi, G., Rivasseau, C., Frelet-Barrand, A., Pilon, M., Rolland, N. & Seigneurin-Berny, D., 2014. HMA1 and PAA1, two chloroplast-envelope P_{IB}-ATPases, play distinct roles in chloroplast copper homeostasis. *Journal of Experimental Botany*, 65, 1529–1540,

Bowler, C., Slooten, L., Vandenbranden, S., De Rycke, R., Botteman, J., Sybesma, C., Van Montagu, M. & Inze, D. 1991. Manganese superoxide dismutase can reduce cellular damage mediated by oxygen radicals in transgenic plants.. *EMBO Journal*, 10, 1723-1732.

Bozzi, A.T., Bane, L.B., Weihofen, W.A., McCabe, A., Singharoy, A., Chipot, C., Schulten, K. & Gaudent, R., 2016. Conserved methionine dictates substrate preference in Nramp-family divalent metal transporters. *PNAS*, 113, 10310-10315

Bragg, J., Wu, J., Gordon, S.P., Guttman, M.E., Thilmony, R., Lazo, G.R., Gu, Y.Q. & Vogel, J.P., 2012. Generation and characterization of the Western Regional Research Center Brachypodium T-DNA insertional mutant collection. *PLOS One*, 7(9), 1-14.

Braulke, T. & Bonifacino, J.S., 2009. Sorting of lysosomal proteins. *Biochimica Biophysica Acta*, 1793, 605-614

Brown, P., Welch, R. & Cary, E., 1987. Nickel: a micronutrient essential for higher plants. *Plant Physiology*, 85, 801-803.

Butterworth, R. F., 2000. Complications of cirrhosis III. Heptatic encephalopathy. *Journal of Hepatology*, 32, 171-180.

Cailliatte, R., Lapeyre, B., Mari, S. & Curie, C., 2009. The NRAMP6 metal transporter contributes to cadmium toxicity. *Biochemistry Journal*, 422, 217-228.

Cailliatte, R., Schikora, A., Briat, J.R., Mari, S. & Curie, C., 2010 . High-affinity manganese uptake by the metal transporter NRAMP1 Is essential for Arabidopsis growth in low manganese conditions. *The Plant Cell*, 22, 904-917.

Cakmak, I. & Marschner, H., 1988. Enhanced superoxide radical production in roots of Zn deficient plants. *Journal of Experimental Botany*, 39, 1449-1469.

Cárdenas, L., 2009. New findings in the mechanisms regulating polar growth in root hair cells. *Plant Signaling & Behavior*, 4, 4-8.

Carl, G., Blackwell, L.K., Barnett, F.C., Thompson, L.A., Kissinger, C.K., Olin, K.L., Critchfield, J.W., Keen, C.L. & Gallagher, B.B, 1993. Manganese and epilepsy: brain glutamine synthetase and liver arginase activities in genetically epilepsy prone and chronically seizured rats. *Epilepsia*, 34, 441-446.

Carl, G., Keen, C.L., Gallagher, B.B., Clegg, S., Littleton, W.H., Flannery, D.B. & Hurley, L.S. 1986. Association of low blood manganese concentrations with epilepsy. *Neurology*, 32.

Carmona, A., Deves, G., Roudeau, S., Cloetens, P., Bohic, S. & Ortega, R., 2010. Manganese accumulates within golgi apparatus in dopaminergic cells as revealed by synchrotron x-ray fluorescence nanoimaging. *ACS Chemical Neuroscience*, 1, 194-203

Carter, C., Pan, S., Zouhar, J., Avila, E.L., Girke, T. & Raikhel, N.V., 2004. The vegetative vacuole proteome of *Arabidopsis thaliana* reveals predicted and unexpected proteins. *Plant Cell*, 16, 3285-3303.

Cellier, M. F. M., 2016. Evolutionary analysis of Slc11 mechanism of proton-coupled metal-ion transmembrane import. *AIMS Biophysics*, 3, 286-318.

Cellier, M. F., Courville, P., & Campion, C., 2007. *Nramp1* phagocyte intracellular metal withdrawal defense. *Microbes and Infection*, 9, 1662-1670.

Chakrabarty, R., Banerjee, R., Chung, S., Farman, M., Citovsky, V., Hogenhout, S., Tzfira, T. & Goodin, M., 2007. pSITE vectors for stable integration or transient expression of autofluorescent protein fusions in plants: probing *Nicotiana benthamiana*-virus interactions. *Molecular Plant-Microbe Interactions*, 20, 740-750

Chandra, S., Kable, E.P., Morrison, G.H. & Webb, W.W., 1991. Calcium sequestration in the Golgi apparatus of cultured mammalian cells revealed by laser scanning confocal microscopy and ion microscopy. *Journal of Cell Science*, 100, 747-752.

Chen, S., Wang, Z., Xu, M. & Gui, J., 2006. Molecular identification and expression analysis of natural resistance associated macrophage protein (Nramp) cDNA from Japanese flounder (*Paralichthys olivaceus*). Fish & Shellfish Immunology, 20, 365-373

Chen, Z., Fujii, Y., Yamaji, N., Masuda, S., Takemoto, Y., Kamiya, T., Yusuyin, Y., Iwasaki, K., Kato, S., Maeshima, M., Ma, J. F., & Ueno, D., 2013. Mn tolerance in rice is mediated by MTP8.1, a member of the cation diffusion facilitator family. *Journal of Experimental Botany*, 64, 4375-4387.

Chen, X., Li, J., Wang, L., Ma, G. & Zhang, W., 2016. A mutagenic study identifying critical residues for the structure and function of rice manganese transporter OsMTP8.1. *Scientific Reports*, 6, DOI: 10.1038/srep32073

Cheniae, G. & Martin, I., 1968. Sites of manganese function in photosynthesis. *Biochimica et Biophysica Acta*, 153, 819-837.

Chiu, J. C., Brenner, E. D., De Salle, R., Nitabach, M. N., Holmes, T. C., & Coruzzi, G. M., 2002. Phylogenetic and expression analysis of the glutamate-receptor-like gene family in *Arabidopsis thaliana*. *Molecular Biology & Evolution*, 19, 1066-82.

Clemens, S., 2001. Molecular mechanisms of plant metal tolerance and homeostasis. *Planta*, 212, 475-486.

Clough, S. & Bent, A., 1998. Floral dip: a simplified method for Agrobacterium-mediated transformation of *Arabidopsis thaliana*. *Plant Journal*, 16, 735-743

Colangelo, E. P., & Guerinot, M. L., 2004. The essential basic helix-loop-helix protein *FIT1* is required for the iron deficiency response. *The Plant Cell*, 16, 3400-3412.

Conklin, D., McMaster, J., Culbertson, M. & Kung, C., 1992. COT1, a gene involved in cobalt accumulation in *Saccharomyces cerevisiae*. *Molecular and Cellular Biology*, 12, 3678-3688.

Conn, S., & Gilliham, M., 2010. Comparative physiology of elemental distributions in plants. *Annals of Botany*, 105, DOI: 10.1093/aob/mcq027.

Connolly, E. L., Campbell, N. H., Grotz, N., Prichard, C. L., & Guerinot, M. L., 2003. Overexpression of the *FRO2* ferric chelate reductase confers tolerance to growth on low iron and uncovers posttranscriptional control. *Plant Physiology*, 133, 1102–1110.

Connorton, J., Webster, R., Cheng, N. & Pittman, J., 2012. Knockout of multiple arabidopsis cation/H⁺ exchangers suggests isoform-specific roles in metal stress response, germination and seed mineral nutrition. *PLOS One*, 7.

Coudray, N., Valvo, S., Hu, M., Lasala, R., Kim, C., Vink, M., Zhou, M., Provasi, D., Filizola, M., Tao, J., Fang, J., Penczek, P. A., Ubarretxena-Belandia, I., & Stokes, D. L., 2013. Inward-facing conformation of the zinc transporter YiiP revealed by cryoelectron microscopy. *PNAS*, 110, 2140-5.

Courville, P., Urbankova, E., Rensing, C., Chaloupka, R., Quick., M. & Cellier, M., 2008. Solute carrier 11 cation symport requires distinct residues in transmembrane helices 1 and 6. *Journal of Biological Chemistry*, 283, 9651-9658

Covey, S., Turner, D., Lucy, A. & Saunders, K., 1981. Host regulation of the cauliflower mosaic virus multiplication cycle. *PNAS*, 87, 1633-1637

Crossgrove, J. & Zheng, W., 2004. Manganese toxicity upon overexposure. *NMR in Biomedicine*, 17, 544-553.

Cubillas, C., Vinuesa, P., Tabche, M. & los Santos, A., 2013. Phylogenomic analysis of Cation Diffusion Facilitator proteins uncovers Ni²⁺/Co²⁺ transporters. *Metallomics*, *5*, 1634-1643

Curie, C., Alonso, J.M., le Jean, M., Ecker, J.R. & Briat, J.F., 2000. Involvement of NRAMP1 from *Arabidopsis thaliana* in iron transport. *Biochemistry Journal*, 347, 749-755.

Curtis, M.D. & Grossniklaus, U., 2003. A gateway cloning vector set for high-throughput functional analysis of genes in planta. *Plant Physiology*, 133, 462-469

Da Silva, L., Foresti, O. & Denecke, J., 2008. Targeting of the plant vacuolar sorting receptor BP80 is dependent on multiple sorting signals in the cytosolic tail. *Plant Cell*, 18, 1477-1497

Damaegd, D., Foulquier, F., Colinet, A.S., Gremillon, L., Legrand, D., Mariot, P., Peiter, E., Van Schaftinger, E., Matthijs, G. & Morsomme, P., 2013. Newly characterized Golgi-localized family of proteins is involved in calcium and pH homeostasis in yeast and human cells. *PNAS*, 110, 6859-6864

Damaegd, D., Colinet, A.S., Deschamps, A. & Morsomme, P., 2014. Molecular evolution of a novel family of putative calcium transporters. *PLoS One*, p, e100851

De la Luz Mora, M., Roasa, A., Ribera, A. & Rengel, Z., 2009. Differential tolerance to Mn toxicity in perennial ryegrass genotypes: involvement of antioxidative enzymes and root exudation of carboxylates. *Plant Soil*, 320, 79-89.

Delhaize, E., 1996. A metal-accumulator mutant of *Arabidopsis thaliana*. *Plant Physiology*, 111, 849-855.

Delhaize, E., Gruber, B.D., Pittman, J.K., White, R.G., Leung, H., Miao, Y., Jiang, L., Ryan, P.R. & Richardson, A.E., 2007. A role for the AtMTP11 gene of Arabidopsis in manganese transport and tolerance. *The Plant Journal*, 51, 198-210.

Delhaize, E., Kataoka, T., Hebb, D.M., White, R.G. & Ryan, P.R., 2003. Genes encoding proteins of the Cation Diffusion Facilitator family that confer manganese tolerance. *The Plant Cell*, 15, 1131-1142.

Desbrosses-Fonrouge, A., Voigt, K., Schroder, A., Arrivault, S., Thomine, S. & Kraemer, U., 2005. *Arabidopsis thaliana* MTP1 is a Zn transporter in the vacuolar membrane which mediates Zn detoxification and drives leaf Zn accumulation. *FEBS Letters*, 579, 4165-4174.

Dietrich, R., Richberg, M., Schmidt, R., Dean, C. & Dangl, J., 1997. A novel zinc finger protein is encoded by the Arabidopsis *LSD1* gene and functions as a negative regulator of plant cell death. *Cell*, 88, 685-694.

Digonnet, C., Aldon, D., Leduc, N., Dumas, C. & Rougier, M., 1997. First evidence of a calcium transient in flowering plants at fertilization. *Development*, 124, 2867-2874.

Dixon, N., Gazzola, C., Blakeley, R. & Zerner, B., 1975. Jack-Bean urease, a metalloenzyme. A simple biological role for nickel. *Journal of the American Chemical Society*, 97, 4131-4133.

Doncheva, S., Poschenrieder, C., Stovanova, Z., Georgieva, J., Velichkova, M. & Barcelo, J., 2009. Silicon amelioration of manganese toxicity in Mn-sensitive and Mn-tolerant maize varieties. *Environmental and Experimental Botany*, 65, 189-197.

Dunkel, M., Latz, A., Schumacher, K., Muller, T., Becker, D. & Hedrich, R., 2008. Targeting of vacuolar membrane localized members of the TPK channel family. *Molecular Plant*, 1, 938-949

Durr, G., Strayle, J., Plemper, R., Elbs, S., Klee, S.K., Catty, P., Wolf., D.H. & Rudolph, H.K., 1998. The medial-Golgi ion pump Pmr1 supplies the yeast secretory pathway with Ca²⁺ and Mn²⁺ required for glycosylation, sorting, and endoplasmic reticulum-associated protein degradation. *Molecular Biology of the Cell*, 9, 1149-1162.

Earley, K., Haag, J., Pontes, O., Opper, K., Juehne, T., Song, K. & Pikaard, 2006. Gateway-compatible vectors for plant functional genomics and proteomics. *The Plant Journal*, 45, 616-629

Edmond, C., Shigaki, T., Ewert, S., Nelson, M. D., Connorton, J. M., Chalova, V., Noordally, Z., Pittman, J. K., 2009. Comparative analysis of *CAX2*-like cation transporters indicates functional and regulatory diversity. *Biochemical Journal*, 15, 145-154.

Ehrnstorfer, I. A., Geertsma, E. R., Pardon, E., Steyaert, J., & Dutzler, R., 2014. Crystal structure of a SLC11 (NRAMP) transporter reveals the basis for transition-metal ion transport. *Nature Structural & Molecular Biology*, 21, 990-996.

Eide, D., 2006. Zinc transporters and the cellular trafficking of zinc. *Biochimica et Biophysica Acta* – *Biomembranes*, 1763, 711-722.

Eide, D., Broderius, M., Fett, J., & Guerinot, M. L., 1996. A novel iron-regulated metal transporter from plants identified by functional expression in yeast. *PNAS*, 93, 5624-5628.

Elbashir, S., Harborth, J., Lendeckel, W., Yalcin, A., Weber, K. & Tuschl, T., 2001. Duplexes of 21-nucleotide RNAs mediate RNA interference in cultured mammalian cells. *Nature*, 411, 494-498

Erbasol, I., Bozdag, G. O., Koc, A., Pedas, P., & Karakaya, H. C., 2013. Characterization of two genes encoding metal tolerance proteins from *Beta vulgaris* subspecies *maritima* that confers manganese tolerance in yeast. *Biometals*, 26, 795-804.

Eren, E. & Arguello, J.M., 2004. Arabidopsis HMA2, a divalent heavy metal-transporting P_{IB}-Type ATPase, is involved in cytoplasmic Zn²⁺ homeostasis. *Plant Physiology*, 136, 3712-3723

Eroglu, S., Meier, B., von Wirén, N., & Peiter, E., 2016. The vacuolar manganese transporter MTP8 determines tolerance to iron deficiency-induced chlorosis in Arabidopsis. *Plant Physiology*, 170, 1030-1045.

Eyster, C., Brown, T., Tanner, H. & Hood, S., 1958. manganese requirement with respect to growth, Hill reaction and photosynthesis. *Plant Physiology*, 33, 235-241.

Fan, H., Zhang, Z., Wang, N., Cui, Y., Sun, H., Liu, Y., Wu, H., Zheng, S., Bao, S., & Ling, H. Q., 2014. SKB1/PRMT5-mediated histone *H4R3* dimethylation of Ib subgroup bHLH genes negatively regulates iron homeostasis in *Arabidopsis thaliana*. *The Plant Journal*, 77, 209-221.

Farh, K., Grimson, A., Jan, C., Lewis, B., Johnston, W., Lim, L., Burge, C. & Bartel, D., 2005. The widespread impact of mammalian microRNAs on mRNA repression and evolution. *Science*, 310, 1817-1821

Feldmen, M. & Levy, A., 2001. Genome evolution due to allopolyploidization in wheat. *Genetics*, 192, 763-774

Fernando, D., Batianoff, G., Baker, A. & Woodrow, I., 2006. In vivo localisation of manganese in the hyperaccumulator *Gossia bidwillii* (Benth.) N. Snow & Guymer (Myrtaceae) by cryo-SEM/EDAX. *Plant cell and the environment*, 29, 1012-1020.

Ferreira, K. N., et al., 2004. Architecture of the photosynthetic oxygen-evolving center. *Science*, 303, 1831-1838.

Fischer, R. & Hsiao, T., 1968. Stomatal opening in isolated epidermal strips of *Vicia faba II*. Responses to KCl concentration and the role of Potassium absorption. *Plant Physiology*, 43, 1953-1958.

Foster, A. W., Osman, D., & Robinson, N. J., 2014. Metal preferences and metallation, *The Journal of Biological Chemistry*, 289, 28095-28103.

Foy, C., Fleming, A. & Armiger, W., 1969. Differential tolerance of cotton varieties to excess manganese. *Agronomy Journal*, 61, 690-692.

Foy, C., Weil, R. & Coradetti, C., 1995. Differential manganese tolerances of cotton genotypes in nutrient solution. *Journal of Plant Nutrition*, 18, 685-706.

Frei dit Frey, N., Mbengue, M., Kwaaitaal, M., Nitsch, L., Altenbach, D., Häweker, H., Lozano-Duran, R., Njo, M. F., Beeckman, T., Huettel, B., Borst, J. W., Panstruga, R., & Robatzek, S., 2012. Plasma membrane calcium ATPases are important components of receptor-mediated signaling in plant immune responses and development. *Plant Physiology*, 159, 798-809.

Friedman, B. J., Freeland-Graves, J.H., Bales, C. W., Behmardi, F., Shorey-Kutschke, R. L., Willis, R. A., Crosby, J. B., Trickett, P. C., & Houston, S. D., 1987. Manganese balance and clinical observations in young men fed a manganese-deficient diet. *Journal of Nutrition*, 117, 133-143.

Fritsche, G., Nairz, M., Libby, S. J., Fang, F. C., & Weiss, G., 2012. Slc11a1 (Nramp1) impairs growth of *Salmonella enterica* serovar *typhimurium* in macrophages via stimulation of lipocalin-2 expression. *Journal of Leukocyte Biology*, 92, 353–359.

Führs, H., Behrens, C., Gallien, S., Heintz, D., Van Dorsselaer, A., Braun, H. P., & Horst, W. J., 2010. Physiological and proteomic characterization of manganese sensitivity and tolerance in rice (*Oryza sativa*) in comparison with barley (Hordeum vulgare). *Annals of Botany*, 105, 1129-1140.

Fujiwara, T., Kawachi, M., Sato, Y., Mori, H., Kutsuna, N., Hasezawa, S., & Maeshima, M., 2015. A high molecular mass zinc transporter MTP12 forms a functional heteromeric complex with MTP5 in the Golgi in *Arabidopsis thaliana*. *FEBS Journal*, 282, doi:10.1111/febs.13252.

Furiuchi, T., Cunningham, K. W., & Muto, S., 2001. A putative Two Pore Channel AtTPC1 mediates Ca²⁺ flux in Arabidopsis leaf cells. *Plant Cell Physiology*, 42, 900-905.

Gao, F., Han, X., Wu, J., Zheng, S., Shang, Z., Sun, D., Zhou, R., & Li, B., 2012. A heat-activated calcium-permeable channel--Arabidopsis cyclic nucleotide-gated ion channel 6--is involved in heat shock responses. *The Plant Journal*, 70, 1056-1069.

Geer, L., Marchler-Bauer, A., Geer, R., Han, L., He, J., He, S., Liu, C., Shi, W. & Bryant, S., 2010. The NCBI BioSystems database. *Nucleic Acids Research*, 38, D492-496

Geisler, M., Axelsen, K., Harper, J. & Palmgren, M., 2000. Molecular aspects of higher plant P-type Ca²⁺-ATPases. *Biochimica et Biophysica Acta, Biomembranes*, 1465, 52-78.

Ghanotakis, D. F., Babcock, G. T., &Yocum, C. F., 1985. Structure of the oxygen-evolving complex of photosystem II: calcium and lanthanum compete for sites on the oxidizing side of photosystem II which control the binding of water-soluble polypeptides and regulate the activity of the manganese complex. *Biochimica Biophysica Acta*, 809, 173–180.

Gomi, M., Sonoyama, M., & Mitaku, S., 2004. High performance system for signal peptide prediction: SOSUIsignal. *Chem-Bio Informatics Journal*, 4, 142-147

Goodstein, D., Shu, S., Howson, R., Neupane, R., Hayes, R., Fazo, J., Mitros, T., Dirks, W., Hellsten, U., Putnam, N. & Rokshar, D., 2012. Phytozome: a comparative platform for green plant genomics. *Nucleic Acids Research*, 40, D1178-1186

Gorrell, J. M., et al., 1997. Occupational exposures to metals as risk factors for Parkinson's disease. *Neurology*, 48, 650-658.

Goswami, T., Bhattacharjee, A., Babal, P., Searle, S., Moore, E., Li, M., & Blackwell, J. M., 2001. Natural-resistance-associated macrophage protein 1 is an H⁺/bivalent cation antiporter. *Biochemical Journal*, 354, 511–519.

Granick, S., 1961. Magnesium Protoporphyrin Monoester and Protoporphyrin Monomethyl Ester in Chlorophyll Biosynthesis. *Journal of Biological Chemistry*, 236, 1168-1172.

Greene, E., Codomo, C., Taylor, N., Henikoff, J., Till, B., Reynolds, S., Enns, L., Burtner, C., Johnson, J., Odden, A., Comai, L. & Henikoff, S., 2003. Spectrum of chemically induced mutations from a large-scale reverse-genetic screen in Arabidopsis. *Genetics*, 164, 731-740

Greger, J., 1999. Nutrition versus toxicology of manganese in humans: evaluation of potential biomarkers. *Neurotoxicology*, 20, 205-212.

Greie, J-C., & Altendorf, K., 2007. The K^+ -translocating KdpFABC complex from *Escherichia coli*: A P-type ATPase with unique features. *Journal of Bioenergetics and Biomembranes*, 39, 397-402.

Gruenheid, S., Canonne-Hergaux, F., Gauthier, S., Hackam, D. J., Grinstein, S., & Gros, P., 1999. The iron transport protein NRAMP2 is an integral membrane glycoprotein that colocalizes with transferrin in recycling endosomes. *The Journal of Experimental Medicine*, 189, DOI: 10.1084/jem.189.5.831.

Guest, C., Schulze, D., Thompson, I. & Huber, D., 2002. Correlating manganese x-ray adsorption near-edge structure spectre with extractable soil manganese. *Soil Science Society of America*, 66, 1171-1182.

Guffanti, A., Wei, Y., Rood, S. & Krulwich, T., 2002. An antiport mechanism for a member of the cation diffusion facilitator family: divalent cations efflux in exchange for K⁺ and H⁺. *Molecular Microbiology*, 45, 145-153.

Gunes, A., Alpaslan, M., & Inal, A., 1998. Critical nutrient concentrations and antagonistic and synergistic relationships among the nutrients of NFT-grown young tomato plants. *Journal of Plant Nutrition*, 21, 2035-2047.

Gunshin, H., Mackenzie, B., Berger, U., Gunshin Y., Romero, M., Boron, W., Nussberger, S., Gollan, J. & Hediger, M., 1997. Cloning and characterization of a mammalian proton-coupled metal-ion transporter. *Nature*, 388, 482-488.

Guo, K. M., Babourina, O., Christopher, D. A., Borsics, T., & Rengel, Z., 2008. The cyclic nucleotide-gated channel, AtCNGC10, influences salt tolerance in *Arabidopsis*. *Plant Physiology*, 134, 499-507.

Guo, K. M., Babourina, O., Christopher, D. A., Borsic, T., & Rengel, Z., 2010. The cyclic nucleotide-gated channel AtCNGC10 transports Ca²⁺ and Mg²⁺ in Arabidopsis. *Plant Physiology*, 139, 303-312.

Gupta, S., Chai, J., Cheng, J., D'Mello, R., Chance, M. & Fu, Dax., 2014. Visualizing the kinetic power stroke that drives proton-coupled Zn(II) transport. *Nature*, 512, 101-114

Gustin, J., Zanis, M. & Salt, D., 2011. Structure and evolution of the plant cation diffusion facilitator family of ion transporters. *BMC Evolutionary Biology*, 11.

Hachez, C., et al, 2011. Short-term control of maize cell and root water permeability through plasma membrane aquaporin isoforms. *Plant, Cell & Environment*, 35, 185-198.

Haemig, H.A. & Brooker R.J., 2004. Importance of conserved acidic residues in MntH, the Nramp homolog of *Escherichia coli*. *Journal of Membrane Biology*, 20, 97-107

Hansen, E., 1990. Phytophthora root rot. In: P. Hamm, S. Campbell & E. Hansen, eds. *Growing healthy seedlings: identification and management of pests in Northwest forest nurseries*. Pacific Northwest Region: US Dept of Agriculture, 17-21.

Happel, N., Honing, S., Neuhaus, J.M., Paris, N., Robinson, D.G. & Holstein, S.E., 2004. Arabidopsis mu A-adaptin interacts with the tyrosine motif of the vacuolar sorting receptor VSR-PS1. *Plant Journal*, 37, 678-693

Hebbern, C. A., et al, 2005. Genotypic differences in manganese efficiency: field experiments with winter barley (*Hordeum vulgare L.*). *Plant and Soil*, 272, 233-244.

Hebbern, C. A., et al, 2009. Latent manganese deficiency increases transpiration in barley (*Hordeum vulgare*). *Physiologia Plantarum: An International Journal for Plant Biology,* 135, 307-316.

Hirschi, K. D., Korenkov, V. D., Wilganowski, N. L., & Wagner, G. J., 2000. Expression of Arabidopsis *CAX2* in tobacco. Altered metal accumulation and increased manganese tolerance. *Plant Physiology*, 124, 125–134.

Horiguchi, T., 1987. Mechanism of manganese toxicity and tolerance in plants. II. Deposition of oxidised manganese in plant tissues. *Journal of Soil Science and Plant Nutrition*, 33, 595-606.

Horst, W., 1988. The physiology of Mn toxicity. In: R. Graham, R. Hannam & N. Uren, eds. *Manganese in Soils and Plants*. Dordrecht, The Netherlands: Kluwer Academic Publishers, 175-188.

Hruz, T., Laule, O., Szabo, G., Wessendorp, F., Bleuler, S., Oertle, L., Widmayer, P., Gruissem, W. & Zimmerman, P., 2008. Genevestigator V3: a reference expression database for the meta-analysis of transcriptomes. *Advances in Bioinformatics*, 420747

Hubert, N., & Hentze, M. W., 2002. Previously uncharacterized isoforms of divalent metal transporter (*DMT*)-1: implications for regulation and cellular function. *PNAS*, 99, 12345-12350.

Hue, N., 1988. A possible mechanism for manganese phytotoxicity in Hawaii soils amended with a low-manganese sewage sludge. *Journal of Environmental Quality*, 17, 472-479.

Huo, N., Vogel, J., Lazo, G., You, F., Ma, Y., McMahon, S., Dvorak, J., Anderson, O., Luo, M. & Gu, Y., 2009. Structural characterization of *Brachypodium* genome and its syntenic relationship with rice and wheat. *Plant Molecular Biology*, 70, 47-61.

Husted, S., Laursen, K. H., Hebbern, C. A., Schmidt, S. B., Pedas, P., Haldrup, A., & Jensen, P. E., 2009. Manganese deficiency leads to genotype-specific changes in fluorescence induction kinetics and state transitions. *Plant Physiology*, 150, 825-833.

Ikeda, J.S., Janakiraman, A., Kehres, D. G., Maguire, M. E., & Slauch, J. M., 2005. Transcriptional regulation of ABCD of *Salmonella enterica* serovar Typhimurium by MntR and Fur. *Journal of Bacteriology*, 187, 912-922.

Illing, A. C., Shawki, A., Cunningham, C. L., & Mackenzie, B., 2012. Substrate profile and metal-ion selectivity of human Divalent Metal-ion Transporter-1. *Journal of Biological Chemistry*, 287, 30485–30496.

Isernia, C., Bucci, E., Leone, M., Zaccaro, L., Di Lello, P., Digilio, G., Esposito, S., Saviano, M., Di Blasio, B., Pedone, C., Pedone, P.V. & Fattorusso, R., 2003. NMR structure of the single QALGGH zinc finger domain from the *Arabidopsis thaliana* SUPERMAN protein. *Chembiochem*, 4, 171-180.

Ishii, T. & Matsunaga, T., 1996. Isolation and characterization of a boron-rhamnogalacturonan-II complex from cell walls of sugar beet pulp. *Carbohydrate Research*, 284, 1-9.

Ishimaru, Y., Takahashi, R., Bashir, K., Shimo, H, Senoura, T., Sugimoto, K., Ono, K., Yano, M., Ishikawa, S, Arao, T., Nakanishi, H., & Nishizawa, N. K., 2012. Characterizing the role of rice NRAMP5 in Manganese, Iron and Cadmium Transport, *Scientific Reports*, 2, 286.

Islam, M. M., Munemasa, S., Hossain, M. A., Nakamura, Y., Mori, I. C., & Murata, Y., 2011. Roles of AtTPC1, vacuolar two pore channel 1, in Arabidopsis stomatal closure. *Plant Cell Physiology*, 51, 302-311.

Jabado, N., Jankowski, A., Dougaparsad, S., Picard, V., Grinstein, S., & Gros, P., 2000. Natural Resistance to Intracellular Infections. *The Journal of Experimental Medicine*, 192, 1237-1248.

Jahn, T., Schulz, A., Taipalensuu, J. & Palmgren, M.G., 2001. Post-translational modification of plant plasma membrane H⁺-ATPase as a requirement for functional complementation of a yeast transport mutant. *Journal of Biological Chemistry*, 277, 6353-6358

Jansen, E., Jang, R., Albersheim, P. & Bonner, J., 1960. Pectic metabolism of growing cell walls. *Plant Physiology*, 35, 87-97.

Jardetzky, O., 1966. Simple allosteric model for membrane pumps. Nature, 211, 969-970.

Jensen, L. T., Ajua-Alemanji, M., & Culotta, V. C, 2003. The *Saccharomyces cerevisiae* high affinity phosphate transporter encoded by PHO84 also functions in manganese homeostasis. *Journal of Biological Chemistry*, 278, 42036-42040.

Jensen, A-M. L., Sørensen, T. L-M., Olesen, C., Møller, J. V., & Nissen, P., 2006. Modulatory and catalytic modes of ATP binding by the calcium pump. *The EMBO Journal*, 25, 2305-2314.

Jiang, W., 2006. Mn use efficiency in different wheat cultivars. *Environmental and Experimental Botany*, 57, 41-50.

Johnston, M., 1987. Genetic evidence that zinc is an essential co-factor in the DNA binding domain of GAL4 protein. *Nature*, 328, 353-355.

Kamano, S., Kume, S., Iida, K., Lei, K-J., Nakano, M., Nakayama, Y., & Iida, H., 2015. Transmembrane topologies of Ca²⁺-permeable mechanosensitive channels MCA1 and MCA2 in *Arabidopsis thaliana*. *The Journal of Biological Chemistry*, DOI: 10.1074/jbc.M115.692574

Kamiya, T. & Maeshima, M., 2004. Residues in internal repeats of the rice cation/H⁺ exchanger are involved in the transport and selection of cations. *Journal of Biological Chemistry*, 279, 812-819

Kang, J., Mehta, S., & Turano, F. J., 2004. The putative glutamate receptor 1.1 (AtGLR1.1) in *Arabidopsis thaliana* regulates abscisic acid biosynthesis and signaling to control development and water loss. *Plant Cell Physiology*, 45, 1380-1389.

Kang, B., Baek, J., Macoy, D., Chakraborty, R., Cha, J., Hwang, D., Lee, Y., Lee, S., Kim, W. & Kim, M., 2015. N-Glycosylation process in both ER and Golgi plays pivotal role in plant immunity, *Journal of Plant Biology*, 58, 374-382

Katoh, S. & Takamiya, A., 1994. Nature of copper-protein binding in spinach plastocyanin. *The Journal of Biochemistry*, 55(4), 378-387.

Kawachi, M., Kobae, Y., Mimura, T. & Maeshima, M., 2008. Deletion of a histidine-rich loop of AtMTP1, a vacuolar Zn²⁺/H⁺ antiporter of *Arabidopsis thaliana*, stimulates the transport activity. *The Journal of Biological Chemistry*, 283, 8374-8383.

Kawahara, Y., de la Bastide, M., Hamilton, J., Kanamori, H., McCombie, W., Outang, S., Schwartz, D., Tanaka, T., Wu, J., Zhou, S., Childs, K., Davison, R., Lin, H., Quesada-Ocampo, L., Vaillancourt, B., Sakai, H., Lee, S., Kim, J., Numa, H., Itoh, T., Buell, R. & Matsumoto, T., 2013. Improvement of the *Oryza sativa* Nipponbare reference genome using next generation sequence and optical map data. *Rice*, 6, doi:10.1186/1939-8433-6-4

Kehres, D. G., Janakiraman, A., Slauch, J. M., & Maguire, M. E., 2002. Regulation of *Salmonella enterica* serovar Typhimurium MntH transcription by H_2O_2 , Fe^{2+} , and Mn^{2+} . *Journal of Bacteriology*, 184, 3151-3158.

Keller, O., Kollmar, M., Stanke, M. & Waack, S., 2011. A novel hybrid gene prediction method employing protein multiple sequence alignments. *Bioinformatics*, 27, 757-763

Kern, J. & Renger, G., 2007. Photosystem II: Structure and mechanism of the water:plastoquinone oxidoreductase. *Photosynthesis Research*, 94, 183-202.

Kim, S. A., Punshon, T., Lanzirotti, A., Li, L., Alonso, J. M., Ecker, J. R., Kaplan, J., Guerinot, M. L., 2006. Localization of iron in *Arabidopsis* seed requires the vacuolar membrane transporter VIT1. *Science*, 314, 1295-1298.

Kliebenstein, D., Monde, R.A. & Last, R.L., 1998. Superoxide dismutase in Arabidopsis: An eclectic enzyme family with disparate regulation and protein localization. *Plant Physiology*, 118, 637-650

Kobae, Y., Uemura, T., Sato, M. H., Ohnishi, M., Mimura, T., Nakagawa, T., & Maeshima, M., 2004. Zinc transporter of *Arabidopsis thaliana* At*MTP1* is localized to vacuolar membranes and implicated in zinc homeostasis. *Plant Cell Physiology*, 45, 1749-1758.

Kovalchuk, I., Kovalchuk, O. & Hohn, B., 2000. Genome-wide variation of the somatic mutation frequency in transgenic plants. *EMBO Journal*, 19, 4431-4438

Kraemer, U., Talkelna, N. & Hanikenne, M., 2007. Transition metal transport. *FEBS Letters*, 581, 2263-2272.

Krysan, P., Young, J. & Sussman, M., 1999. T-DNA as an insertional mutagen in Arabidopsis. *The Plant Cell*, 11, 2283-2290

Kuhlbrandt, W., 2004. Biology, structure and mechanism of P-type ATPases. *Nature reviews molecular biology*, 5, 282-295.

Kurihara, Y. & Watanabe, Y., 2004. Arabidopsis micro-RNA biogenesis through Dicer-like 1 protein functions. *PNAS*, 101, 12753-12758

Lahner, B., Gong, J., Mahmoudian, M., Smith' E. L., Abid' K. B., Rogers, E. E., Guerinot' M. L., Harper' J. F., Ward' J. M., McIntyre, L., Schroeder, J. I., & Salt, D. E., 2003. Genomic scale profiling of nutrient and trace elements in *Arabidopsis thaliana*. *Nature Biotechnology*, 21, 1215-1221.

Lanquar, V., Lelièvre, F., Bolte, S., Hamès, C., Alcon, C., Neumann, D., Vansuyt, G., Curie, C., Schröder, A., Krämer, U., Barbier-Brygoo, H., & Sebastien Thomine, 2005. Mobilization of vacuolar iron by *AtNRAMP3* and *AtNRAMP4* is essential for seed germination on low iron. *The EMBO Journal*, 24, 4041-4051.

Lanquar, V., Ramos, M. S., Lelièvre, F., Barbier-Brygoo, H., Krieger-Liszkay, A., Krämer, U., & Thomine, S., 2010. Export of vacuolar manganese by AtNRAMP3 and AtNRAMP4 is required for optimal photosynthesis and growth under manganese deficiency. *Plant Physiology*, 152, 1989-1999.

Laohavisit, A., Shang, Z., Rubio, L., Cuin, T. A., Véry, A-A., Wang, A., Mortimer, J. C., Macpherson, N., Coxon, K. M., Battey, N. H., Brownlee, C., Park, O. K., Sentenac, H., Shabala, S., Webb, A. A. R., & Davies, J. M., 2012. *Arabidopsis* Annexin1 mediates the radical-activated plasma membrane Ca²⁺- and K⁺-Permeable conductance in root cells. *The Plant Cell*, 24, 1522-1533.

Larisch, N., Schulze, C., Galione, A. & Dietrich, P., 2012. *Traffic*, 13, 1012-1022

Lee, J., 2000. Manganese intoxication. Archives of Neurology, 57, 597-599.

Lee, Y., Kim, M., Han, J., Yeom, K., Lee, S., Baek, S. & Kim, V., 2004. microRNA genes are transcribed by RNA polymerase II. *EMBO Journal*, 23, 4051-4060

Lei, Y., Korpelainene, H. & Li, C., 2007. Physiological and biochemical responses to high Mn concentrations in two contrasting Populus cathayana populations. *Chemosphere*, 68, 686-694.

Leyva-Illades, D., Chen, P., Zogzas, C.E., Hutchens, S., Mercado, J. M., Swaim, C. D., Morrisett, R. A., Bowman, A. B., Aschner, M., & Mukhopadhyay, S., 2014. SLC30A10 is a cell surface-localized manganese efflux transporter, and parkinsonism-causing mutations block its intracellular trafficking and efflux activity. *The Journal of Neuroscience*, 15, 14079-14095.

Li, X., Chanroj, S., Wu, Z., Romanowsky, S. M., Harper, J. F., & Sze, H, 2008. A distinct endosomal Ca²⁺/Mn²⁺ pump affects root growth through the secretory process. *Plant Physiology*, 147, 1675-1689.

Li, L., & Kaplan, J., 1998. Defects in the yeast high affinity iron transport system result in increased metal sensitivity because of the increased expression of transporters with a broad transition metal specificity. *Journal of Biological Chemistry*, 273, 22181-22187

Li, L., Chen, O., McVey-Ward, D. & Kaplan, J., 2001. CCC1 is a transporter that mediates vacuolar iron storage in yeast.. *Journal of Biological Chemistry*, 276(31), 29515-29519.

Li, W. & Schmidt, W., 2010. A lysine-63-linked ubiquitin chain-forming conjugase, UBC13, promotes the developmental responses to iron deficiency in Arabidopsis roots. *Plant Journal*, 62, 330-343

Li, Q., Zhao, Y., Yue, M., Xue, Y. & Bao, S., 2016. The Protein Arginine Methylase 5 (*PRMT5/SKB1*) gene is required for the maintenance of root stem cells in response to DNA damage. *Journal of Genetics and Genomics*, 43, pp187-197

Liang, F., Cunningham, K., Harper, J. & Sze, H., 1997. ECA1 complements yeast mutants defective in Ca²⁺ pumps and encodes an endoplasmic reticulum-type Ca²⁺-ATPase in *Arabidopsis thaliana*. *PNAS*, 94, 8579-8584.

Liang, F. & Sze, H., 1998. A high-affinity Ca²⁺ pump, ECA1, from the endoplasmic reticulum is inhibited by cyclopiazonic acid but not by thapsigargin. *Plant Physiology*, 118, 817-825.

Lidon, F., Barreiro, M. & Ramalho, J., 2004. Manganese accumulation in rice: implications for photosynthetic functioning. *Journal of Plant Physiology*, 161, 1235-1244.

Lim, L.P., Lau, N.C., Garrett-Engele, P., Grimson, A., Schelter, J.M., Castle, J., Bartel, D.P., Linsley, P.S. & Johnson, J.M. Microarray analysis shows that some microRNAs downregulate large numbers of target mRNAs. *Nature*, 433, 769-773

Lindsay, W. L., & Schwab, A. P., 1982. The chemistry of iron in soils and its availability to plants. *Journal of Plant Nutrition*, 5, 821-840.

Llave, C., Kasschau, K., Rector, M. & Carrington, J., 2002. Endogenous and silencing-associated small RNAs in plants. *The Plant Cell*, 14, 1605-1619

Lohmiller, T., Cox, N., Su, J., Messinger, J. & Lubitz, W., 2012. The basic properties of the electronic structure of the oxygen-evolving complex of photosystem II are not perturbed by Ca²⁺ removal. *The Journal of Biological Chemistry*, 287, 24721-24733

Long, T., Tzukagoshi, H., Busch, W., Lahner, B., Salt, D. & Benfey, P., 2010. The bHLH transcription factor POPEYE regulates response to iron deficiency in Arabidopsis roots. *The Plant Cell*, 22, 2219-2236

Loth-Pereda, V., Orsini, E., Courty, P. E., Lota, F., Kohler, A., Diss, L., Blaudez, D., Chalot, M., Nehls, U., Bucher, M., & Martin, F., 2011. Structure and expression profile of the phosphate Pht1 transporter gene family in mycorrhizal Populus trichocarpa. *Plant Physiology*, 156, 2141-2154. DOI: 10.1104/pp.111.180646.

Lu, M. & Fu, D., 2007. Structure of the zinc transporter YiiP. Science, 317, 1746-1748.

Lu, M., Chai, J. & Fu, D., 2009. Structural basis for auto-regulation of the zinc transporter YiiP. *Nature Structural & Molecular Biology,* 16, 1063-1067.

Lucchini, R. G., et al., 2012. Neurological impacts from inhalation of pollutants and the nose – brain connection. *NeuroToxicology*, 33, 838-841.

Luscombe, N.M., Greenbaum, D. & Gerstein, M., 2001. What is bioinformatics? A proposed definition and overview of the field. *Methods of Information in Medicine*, 40, 346-358.

MacDiarmid, C., Milanick, M. & Eide, D., 2002. Biochemical properties of vacuolar zinc transport systems of *Saccharomyces cerevisiae*. *Journal of Biological Chemistry*, 277, 39187-39194.

Macfie, S. & Taylor, G., 1992. The effects of excess manganese on photosynthetic rate and concentration of chlorophyll in *Triticum aestivum* grown in solution culture. *Physiologa Plantarum*, 85, 467-475.

MacNicol, R. & Beckett, P., 1985. Critical tissue concentrations of potentially toxic elements. *Plant and Soil*, 85, 107-129.

Madison, S.L. & Nebenfuhr, A., 2011. Live-cell imaging of dual-labeled Golgi stacks in tobacco BY-2 cells reveals similar behaviors for different cisternae during movement and brefeldin A treatment. Molecular Plant, 4, 896-908

Makui, H., Roig, E., Cole, S. T., Helmann, J. D., Gros, P., & Cellier, M. F., 2000. Identification of the *Escherichia coli* K-12 Nramp orthologue (MntH) as a selective divalent metal ion transporter. *Molecular Microbiology*, 35, 1065-78.

Marschner, H., 1995. Mineral Nutrition of Higher Plants. 2 ed. San Diego, CA: Academic Press.

Masuda, M., Bruan-Summargren, M., Crooks, D. & Smith, D.R., 2013. Golgi phosphoprotein 4 (GPP130) is a sensitive and selective cellular target of manganese exposure. *Synapse*, 76, 205-215.

Martin, J. E., & Giedroc, D. P., 2016. Functional determinants of metal ion transport and selectivity in paralogous cation diffusion facilitator transporters CzcD and MntE in *Streptococcus pneumoniae*. *Journal of Bacteriology*, 198, 1066-76.

Martinez, J., Patkaniowska, A., Urlaub, H., Lurhmann, R. & Tuschl, T., 2002. Single-stranded antisense siRNAs guide target RNA cleavage in RNAi. *Cell*, 110, 563-574

Marty, F., 1999. Plant vacuoles. The Plant Cell, 11, 587-599

Mäser, P., Thomine, S., Schroeder, J. I., Ward, J. M., Hirschi, K., Sze, H., Talke, I. N., Amtmann, A., Maathuis, F. J. M., Sanders, D., Harper, J. F., Tchieu, J., Gribskov, M., Persans, M. W., Salt, D. E., Kim, S. A., & Guerinot, M. L., 2001. Phylogenetic relationships within cation transporter families of *Arabidopsis*. *Plant Physiology*, 126, 1646–1667.

Mengel, K., Kirkby, E., Kosegarten, H. & Appel, T., 2001. *Principles of plant nutrition*. Dordrecht: Kluwer Academic.

Menguer, P. K., Farthing, E., Peaston, K. A., Ricachenevsky, F. K., Fett, J. P., & Williams, L.E., 2013. Functional analysis of the rice vacuolar zinc transporter OsMTP1. *Journal of Experimental Botany*, 64, 2871-83.

Michard, E., Lima, P. T., Borges, F., Silva, A. C., Portes, M. T., Carvalho, J. E., Gilliham, M., Liu, L., Obermeyer, G., & Feijó, J. A., 2011. Glutamate receptor–like genes form Ca²⁺ channels in pollen tubes and are regulated by pistil **D**-Serine. *Science*, 332, 434-437.

Migocka, M., Papierniak, A., Maciaszczyk-Dziubińska, E., Poździk, P., Posyniak, E., Garbiec, A., & Filleur, S., 2014. Cucumber metal transport protein MTP8 confers increased tolerance to

manganese when expressed in yeast and *Arabidopsis thaliana*. *Journal of Experimental Botany*, 65. 5367-5384.

Migocka, M., Papierniak A, Kosieradzka A., Posyniak E., Maciaszczyk-Dziubinska, E., Biskup, R., Garbiec A., & Marchewka T., 2015. Cucumber metal tolerance protein CsMTP9 is a plasma membrane H⁺-coupled antiporter involved in the Mn²⁺ and Cd²⁺ efflux from root cells. *The Plant Journal*, 84, 1045-1058.

Millaleo, R., Reyes-Diaz, M., Alberdi, M., Ivanov, A. G., Krol, M., & Hüner, N. P., 2013. Excess manganese differentially inhibits photosystem I versus II in *Arabidopsis thaliana*. *Journal of Experimental Botany*, 64, 343-354.

Mills, R. F., Doherty, M. L., López-Marqués, R. L., Weimar, T., Dupree, P., Palmgren, M. G., Pittman, J. K., & Williams, L. E., 2008. ECA3, a Golgi-Localized P_{2A}-Type ATPase, plays a crucial role in manganese nutrition in Arabidopsis. *Plant Physiology*, 146, 116-128.

Milner, M., Seamon, J., Craft, E. & Kochian, L., 2013. Transport properties of members of the ZIP family in plants and their role in Zn and Mn homeostasis. *Journal of Experimental Botany*, 64, 369-381.

Mizuno, T., Emori, K., & Ito, S., 2013. Manganese hyperaccumulation from non-contaminated soil in Chengiopanax sciadophylloides Franch. et Sav. and its correlation with calcium accumulation. *Soil Science and Plant Nutrition*, 59, 591-602.

Molnar, A., Bassett, A., Thuenemann, E., Schwach, F., Karkare, S., Ossowski, S., Weigel, D. & Baulcombe, D., 2008. Highly specific gene silencing by artificial microRNAs in the unicellular alga *Chlamydomonas reinhardtii*. *Plant Journal*, 58, 165-174

Montanini, B., Blaudez, D., Jeandroz, S., Sanders, D., & Chalot, M., 2007. Phylogenetic and functional analysis of the Cation Diffusion Facilitator (CDF) family: improved signature and prediction of substrate specificity. *BMC Genomics*, 8, DOI: 10.1186/1471-2164-8-107.

Moran, R., 1982. Formulae for determination of chlorophyllous pigments extracted with *N,N*-Dimethylformamide. *Plant Physiology*, 69, 1376-1381

Mori, S., 1999. Iron acquisition by plants. Current Opinion in Plant Biology, 2, 250-253.

Morris, J., Tian, H., Park, S., Sreevidya, C., Ward, J. & Hirschi, K., 2008. AtCCX3 is an Arabidopsis endomembrane H⁺-dependent K⁺ transporter. *Plant Physiology*, 148, 1474-1486

Mossessova, E., Bickford, L.C. & Goldbert, J., 2003. SNARE selectivity of the COPII coat. *Cell*, 1134, 483-495

Muehe, E. M., Weigold, P., Adaktylou, I. J., Planer-Friedrich, B., Kraemer, U., Kappler, A., Behrens, S., 2015. Rhizosphere microbial community composition affects cadmium and zinc uptake by the metal-hyperaccumulating plant *Arabidopsis halleri*. *Applied Environmental Microbiology*, 81, 2173-2181. doi: 10.1128/AEM.03359-14.

Mukhopadhyay, S., Bachert, C., Smith, D. & Linstedt, A., 2010. Manganese-induced trafficking and turnover of the cis-golgi glycoprotein GPP130. *Molecular Biology of the Cell*, 21, 1282-1292

Munro, S. & Pelham, H.R., 1987. A C-terminal signal prevents secretion of luminal ER proteins. *Cell*, 48, 899-907

Murata, Y., et al., 2006. A specific transporter for iron(III)-phytosiderophore in barley roots. *The Plant Journal*, 46, 563-572.

Murashige, T. & Skoog, F., 1962. A revised medium for rapid growth and bio assays with tobacco tissue cultures. *Physiologa Plantarum*, 15, 473-497

Nable, R., Houtz, R. & Cheniae, G., 1988. Early inhibition of photosynthesis during development of Mn toxicity in tobacco. *Plant Physiology*, 86, 1136-1142.

Nakagawa, Y., Katagiri, T., Shinozaki, K., Qi, Z., Tatsumi, H., Furuichi, T., Kishigami, A., Sokabe, M., Kojima, I., Sato, S., Kato, T., Tabata, S., Iida, K., Terashima, A., Nakano, M., Ikeda, M., Yamanaka, T., & Iida, H., 2007. Arabidopsis plasma membrane protein crucial for Ca²⁺ influx and touch sensing in roots. *PNAS*, 104, 3639-44.

Nestel, P., Bouis, H. E., Meenakshi, J. V., & Pfeiffer, W., 2006. Biofortification of staple food crops. *The Journal of Nutrition*, 136, 1064-1067.

Neuberger, A. & Scott, J., 1952. The Basicities of the nitrogen atoms in the porphyrin nucleus; their dependence on some substituents of the tetrapyrrolic ring. *Proceedings of the Royal Society of London. Series A, Mathematical and Physical Sciences*, 213, 307-326.

New Wave Agriculture, 2012. Liming – A biochemical approach to remediating deficiencies in various acidic soil types. [Online] Available at: http://www.newwaveagriculture.com.au/articles/liming-soils [Accessed 6 July 2014].

Nicholas, D. & Nason, A., 1955. Role of molybdenum as a constituent of nitrate reductase from soybean leaves. *Plant Physiology*, 30, 135-138.

Nies, D. & Silver, S., 1995. Ion efflux systems involved in bacterial metal resistances. *Journal of Industrial Microbiology*, 14(2), 186-199.

Nishito, Y., Tsuji, N., Fujishiro, H., Takeda, T., Yamazaki, T., Teranishi, F., Okazaki F., Matsunaga, A., Tuschl, K., Rao, R., Kono, S., Miyajima, H., Narita, H., Himeno, S., & Kambe, T., 2016. Direct comparison of manganese detoxification/efflux proteins and molecular characterization of ZnT10 as a manganese transporter. *Journal of Biological Chemistry*, 291, 14773-14787.

Obara, K., Miyashita, N., Xu, C., Toyoshima, I., Sugita, Y., Inesi, G., & Toyoshima, C., 2005. Structural role of countertransport revealed in Ca²⁺ pump crystal structure in the absence of Ca²⁺. *PNAS*, 102, 14489-14496.

Ogo, Y., Itai, R.N., Nakanishi, H., Kobayashi, T., Takahashi, M., Mori, S. & Nishizawa, N.K., 2007. The rice bHLH protein OsIRO2 is an essential regulator of the genes involved in Fe uptake under Fe-deficient conditions. *Plant Journal*, 51, 366–77

Ogo, Y., Itai, R.N., Kobayashi, T., Aung, M.S., Nakanishi, H. & Nishizawa, N.K., 2011. OsIRO2 is responsible for iron utilization in rice and improves growth and yield in calcareous soil. *Plant Molecular Biology*, 75, 593–605

Olesen, C., Sørensen, T. L-M., Nielsen, R. C., Møller, J. V., & Nissen, P., 2004. Dephosphorylation of the Calcium Pump Coupled to Counterion Occlusion. *Science*, 306, 2251-2255.

Omasits, U., Ahrens, C.H., Muller, S. & Wollscheid, B., 2014. Protter: interactive protein feature visualization and integration with experimental proteomic data. *Bioinformatics*, 30, 884-886

Ossowski, S., Schawb, R. & Weigel, D., 2008. Gene silencing in plants using artificial microRNAs and other small RNAs. *The Plant Journal*, 54, 674-690

Orci, L., Perrelet, A. & Rothman, J.E., 1998. Vesicles on strings: Morphological evidence for processive transport within the Golgi stack. *PNAS*, 95, 2279-2283

Palmgren, M, Clemens, S., Williams, L.E., Kramer, U., Borg, S., Schjorring, J & Sanders, D., 2008. Zinc biofortification of cereals: problems and solutions. *Trends in Plant Science*, 13, 464-473.

Park, J., Song, W., Ko, D., Eom, Y., Hansen, T., Schiller, M., Lee, T., Martinoia, E. & Lee, Y., 2012. The phytochelatin transporters AtABCC1 and AtABCC2 mediate tolerance to cadmium and mercury. *The Plant Journal*, 69, 278-288

Passardi, F., Dobias, J., Valerio, L., Guimil, S., Penel, C. & Dunand, C., 2007. Morphological and physiological traits of three major *Arabidopsis thaliana* accessions. 164, 980-992

Passioura, J.B. & Leeper, G.W., 1963. Soil compaction and manganese deficiency. *Nature*, 200, 29-30

Paulsen, I. & Saier, M., 1997. A novel family of ubiquitous heavy metal ion transport proteins. *The Journal of Membrane Biology*, 156, 99-103.

Pedas, P., et al., 2005. Differential capacity for high-affinity manganese uptake contributes to differences between barley genotypes in tolerance to low manganese availability. *Plant Physiology*, 139(3), 1411-1420.

Pedas, P., Husted, S., Skytte, K., & Schjoerring, J. K., 2011. Elevated phosphorus impedes manganese acquisition by barley plants. *Frontiers in Plant Science*, 2, 1-12.

Pedas, P., Stokholm, M. S., Hegelund, J. N., Ladegard, A. H., Schjoerring, J. K., & Husted, S., 2014. Golgi localized barley MTP8 proteins facilitate Mn transport. *PLoS ONE*, 9, DOI:10.1371/journal.pone.0113759.

Pedersen, C., Axelsen, K., Harper, J., & Palmgren, M., 2012. Evolution of plant P-type ATPases. Frontiers in Plant Science, 3, doi: 10.3389/fpls.2012.00031

Peiter, E., Maathuis, F. J. M., Mills, L. N., Knight, H., Pelloux, J., Hetherington, A. H., & Saunders, D., 2005. The vacuolar Ca²⁺-activated channel TPC1 regulates germination and stomatal movement. *Nature*, 434, 404-408.

Peiter, E., Montanini, B., Gobert, A., Pedas, P., Husted, S., Maathuis, F. J., Blaudez, D., Chalot, M., Sanders, D., 2007. A secretory pathway-localized cation diffusion facilitator confers plant manganese tolerance. *PNAS*, 104, 8532-8537.

Peng, J. & Gong, J., 2014. Vacuolar sequestration capacity and long-distance metal transport in plants. *Frontiers in Plant Science*, doi:10.3389/fpls.2014.00019

Petersen, T., Brunak, S., Heijne, G. & Nielsen, H., 2011. SignalP 4.0: discriminating signal peptides from transmembrane regions. *Nature Methods*, 8, 785-786

Pfaffl, M.W., 2001. A new mathematical model for relative quantification in real-time PCR. *Nucleic Acids Research*, 20, 2002-2007

Podar, D., Scherer, J., Noordally, Z., Herzyk, P., Nies, D., & Sanders, D., 2012. Metal selectivity determinants in a family of transition metal transporters. *Journal of Biological Chemistry*, 287, 3185-96.

Portnoy, M. E., Liu, X. F., & Culotta, V. C., 2000. *Saccharomyces cerevisiae* expresses three functionally distinct homologues of the NRAMP family of metal transporters. *Molecular Cell Biology*, 20, 7893–7902.

Pottier, M., Oomen, R., Picco, C., Giraudat, J., Scholz-Starke, J., Richaud, P., Carpaneto, A., & Thomine, S., 2015. Identification of mutations allowing Natural Resistance Associated Macrophage Proteins (NRAMP) to discriminate against cadmium. *The Plant Journal*, 83, 625-637.

Quadri, M., Federico, A., Zhao, T., Breedveld, G. J., Battisti, C., Delnooz, C., Severijnen, L. A., Di Toro Mammarella, L., Mignarri, A., Monti, L., Sanna, A., Lu, P., Punzo, F., Cossu, G., Willemsen, R., Rasi, F., Oostra, B. A., van de Warrenburg, B. P., Bonifati, V., 2012. Mutations in SLC30A10 cause parkinsonism and dystonia with hypermanganesemia, polycythemia, and chronic liver disease. *American Journal of Human Genetics*, 90, 467-477.

Quiquampoix, H., Loughman, B. & Ratcliffe, R., 1993. A P-NMR study of the uptake and compartmentation of manganese by maize roots. *Journal of experimental botany*, 44(269), 1819-1827.

Rai, K., Yadav, O., Rakpurohi, B., Patil, H., Govindaraj, M., Khairwal, I., Rao, A., Shivade, H., Pawar, V. & Kulkarni, M., 2013. Breeding pearl millet cultivars for high iron density with zinc density as an associated trait. *Journal of SAT Agricultural Research*, 11, 1-7.

Ranf, S., Wünnenberg, P., Lee, J., Becker, D., Dunkel, M., Hedrich, R., Scheel, D., & Dietrich P., 2008. Loss of the vacuolar cation channel, AtTPC1, does not impair Ca²⁺ signals induced by abiotic and biotic stresses. *The Plant Journal*, 53, 287-299.

Rea, P., Li, Z., Lu, Y. & Drozdowicz, Y., 1998. From vacuolar GS-X pumps to multispecific ABC transporters. *Annual Review of Plant Physiology and Plant Molecular Biology*, 49, 727-760

Reeves, R. & Baker, A., 2000. Metal Accumulating Plants. In: I. Raskin & B. Ensley, eds. *Phytoremediation of Toxic Metals: Using Plants to Clean Up the Environment.* New York: John Wiley and Sons.

Reinhart, B., Weinstein, E., Rhoades, M., Bartel, B. & Bartel, D., 2002. MicroRNAs in plants. *Genes and Development*, 16, 1616-1626

Rengel, Z., 2000. Uptake and transport of manganese in plants. In: A. Sigel & H. Sigel, eds. *Metal Ions in Biological Systems*. New York: Marcel Dekker, 57-87.

Rhee, S.W., Starr, T., Forsten-Williams, K. & Storrie, B., 2005. The steady-state distribution of glycosyltransferases between the golgi apparatus and the endoplasmic reticulum is approximately 90:10. *Traffic*, 6, 978-990.

Ricachenevsky, F. K., Menguer, P. K., Sperotto, R. A., Williams, L. E., & Fett, J. P., 2013. Roles of plant metal tolerance proteins (MTP) in metal storage and potential use in biofortification strategies. *Frontiers in Plant Science*, 144, DOI: 10.3389/fpls.2013.00144.

Robinson, N. J., Procter, C. M., Connolly, E. L., & Guerinot, M. L., 1999. A ferric-chelate reductase for iron uptake from soils. *Nature*, 397, 694-697.

Rogers, E. E., & Guerinot, M. L., 2002. *FRD3*, a member of the multidrug and toxin efflux family, controls iron deficiency responses in Arabidopsis. *The Plant Cell*, 14, 1787-1799.

Roques, S., Kendall S., Smith, K., Price, P. N., & Berry, P., 2013. A review of the non-NPKS nutrient requirements of UK cereals and oilseed rape. *Research Review*, 78, 1-108.

Roschzttardtz, H., Séguéla-Arnaud, M., Briat, J. F., Vert, G., & Curie, C., 2011. The *FRD3* citrate effluxer promotes iron nutrition between symplastically disconnected tissues throughout Arabidopsis development. *The Plant Cell*, 23, 2725-2737.

Salt, D., 2004. Update on ionomics. *Plant Physiology,* Volume 136, 2451-2456.

Sanderfoot, A.A., Ahmed, S.U., Marty-Mazars, D., Rapoport, I., Kirchhausen, T., Marty, F. & Raikhel, N.V., 1998. A putative vacuolar cargo receptor partially colocalizes with AtPEP12p on a prevacuolar compartment in Arabidopsis roots. *PNAS USA*, 95, 9920-9925

Sano, T., Yoshihara, T., Handa, K., Sato, M.H., Nagata, T. & Hasezawa, S., 2012. metal ion homeostasis mediated by NRAMP Transporters in plant cells - focused on increased resistance to iron and cadmium ion. In: R. Weigert, ed. *Crosstalk and Integration of Membrane Trafficking Pathways*. Rijeka: InTech, 213-228.

Santi, S., & Schmidt, W., 2009. Dissecting iron deficiency-induced proton extrusion in Arabidopsis roots. *New Phytologist*, 183, 1072-1084.

Sarret, G., Saumitou-Laprade, P., Bert, V., Proux, O., Hazemann, J. L., Traverse, A., Marcus, M. A., & Manceau, A., 2002. Forms of zinc accumulated in the hyperaccumulator Arabidopsis halleri. *Plant Physiology*, 130, 1815-1826.

Sasaki, A., Jamaki, N., Yokosho, K. & Ma, J., 2012. NRAMP5 Is a major transporter responsible for manganese and cadmium uptake in rice. *The Plant Cell*, 24, 2155-2167.

Schaaf, G., Ludewig, U., Erenoglu, B. E., Mori, S., Kitahara, T., & von Wirén, N., 2004. ZmYS1 functions as a proton-coupled symporter for phytosiderophore- and nicotianamine-chelated metals. *Journal of Biological Chemistry*, 279, 9061-9066.

Schiøtt, M., Romanowsky, S. M., Bækgaard, L., Jakobsen, M. K., Palmgren, M. G., & Harper, J. F., 2004. A plant plasma membrane Ca²⁺ pump is required for normal pollen tube growth and fertilization. *PNAS*, 101, 9502-9507.

Schmid, N. B., Giehl, R. F. H., Döll, S., Mock, H-P., Strehmel, N., Scheel, D., Kong, X., Hider, R. B., & von Wirén, N., 2014. Feruloyl-CoA 6'-Hydroxylase1-Dependent Coumarins Mediate Iron Acquisition from Alkaline Substrates in Arabidopsis. *Plant Physiology*, 164, 160-172.

Schneider, A., Steinberger, I., Herdean, A., Gandini, C., Eisenhut, M., Kurz, S., Morper, A., Hoecker, N., Rühle, T., Labs, M., Flügge, U. I., Geimer, S., Schmidt, S. B., Husted, S., Weber, A. P., Spetea, C., & Leister, D., 2016. The evolutionarily conserved protein PHOTOSYNTHESIS AFFECTED MUTANT71 is required for efficient manganese uptake at the thylakoid membrane in Arabidopsis. *The Plant Cell*, 28, 892-910.

Schulte, D., Close, T., Grana, A., Langridge, P., Matsumoto, T., Muehlbauer, G., Sato, K., Schulmann, A., Waugh, R., Wise, R. & Stein, N., 2009. The International Barley Sequencing Consortium—at the threshold of efficient access to the barley genome. *Plant Physiology*, 149(1), 142-147.

Schwab, R., Ossowski, S., Riester, M., Warthmann, N., Weigel, D., 2006. Highly specific gene silencing by artificial microRNAs in *Arabidopsis*. *Plant Cell*, 18, 1121-1133

Schwacke, R., Schneider, A., van der Graaff, E., Fischer, K., Catoni, E., Desimone, M., Frommer, W.B., Flugge, U.I. & Kunze, R., 2003. ARAMEMNON, a novel database for Arabidopsis integral membrane proteins. *Plant Physiology*, 131, 16-26

Searle, S., Bright, N. A., Roach, T. I., Atkinson, P. G., Barton, C. H., Meloen, R. H., & Blackwell, J. M., 1998. Localisation of Nramp1 in macrophages: modulation with activation and infection. *Journal of Cell Science*, 111, 2855-2866.

Shen, J., Zeng, Y., Zhuang, X., Sun, L., Yao, X., Pimpl, P. & Jiang, L., 2013. Organelle pH in the *Arabidopsis* endomembrane system. *Molecular Plant*, 6, 1419-1437

Shenker, M., Plessner, O. & Tel-Or, E., 2004. Manganese nutrition effects on tomato growth, chlorophyll concentration, and superoxide dismutase activity. *Journal of Plant Physiology*, 161(2), 197-202.

Shiraya, T., Mori, T., Maruyama, T., Sasaki, M., Takamatshu, T., Oikawa, K., Itoh, K., Kaneko, K., Ichikawa, H. & Mitsui, T., 2015. Golgi/plastid-type manganese superoxide dismutase involved in heat-stress tolerance during grain filling of rice. *Plant Biotechnology Journal*, 13, 1251-1263.

Sieben, C., Mikosch, M., Brandizzi, F. & Homann, U., 2008. Interaction of the K⁺ channel KAT1 with the COPII coat component Sec24 depends on a diacidic ER export motif. *Plant Journal*, 56, 997-1006

Sieprawska, A., Filek, M., Tobiasz, A., Walas, S., Dudk-Adamska, D. & Grygo-Szymank, E., 2016. Trace elements' uptake and antioxidant response to excess of manganese in in vitro cells of sensitive and tolerant wheat. *Acta Physiologiae Plantarum*, 38, doi:10.1007/s11738-016-2071-4

Sievers, F., Wilm, A., Dineen, D., Gibson, T.J., Karplus, K., Li, W., Lopez, R., McWilliam, H., remmert, M., Soding, J., Thompson, J.D., Higgins, D.G., 2011. Fast, scalable generation of high-quality protein multiple sequence alignments using Clustal Omega. *Molecular Systems Biology*, 7, doi: 10.1038/msb.2011.75.

Slovacek, R., Crowther, D. & Hind, G., 1979. Cytochrome function in the cyclic electron transport pathway of chloroplasts. *Biochimica et Biophysica Acta (BBA) - Bioenergetics*, 547, 138–148.

Sørensen, T. L-M., Møller, J. V., & Nissen, P., 2004. Phosphoryl transfer and calcium ion occlusion in the calcium pump. *Science*, 304, 1672-1675.

Sparkes, I., Runions, J., Kearns, A. & Hawes, C., 2006. Rapid, transient expression of fluorescent fusion proteins in tobacco plants and generation of stably transformed plants. *Nature Protocols*, 1, 2019-2025

Stael, S., Wurzinger, B., Mair, B., Mehlmer, N., Vothknecht, U. C., & Teige, M., 2012. Plant organellar calcium signalling: an emerging field. *Journal of Experimental Botany*, 63, 1525-1542.

Stanke, M., Diekhans, M., Baertsche, R. & Haussler, D., 2008. Using native and syntenically mapped cDNA alignments to improve de novo gene finding. *Bioinformatics*, doi: 10.1093/bioinformatics/btn013

Strause, L. G., Hegenauer, J., Saltman, P., Cone, R., & Resnick, D., 1986. Effects of long-term dietary manganese and copper deficiency on rat skeleton. *Journal of Nutrition*, 116, 135-41.

Su, M. A., Trenor, C. C., Fleming, J. C., Fleming, M. D., & Andrews, N. C., 1998. The G185R mutation disrupts function of the iron transporter Nramp2. *Blood*, 92, 2157-2163.

Supek, F., Supekova, L., Nelson, H., & Nelson, N., 1996. A yeast manganese transporter related to the macrophage protein involved in conferring resistance to mycobacteria. *PNAS*, 93, 5105-5110.

Sylvester, P., 2011. *Manganese deficiency on corn as related to soil organic matter.* [Online] Available at: http://extension.udel.edu/kentagextension/tag/manganese-deficiency/ [Accessed 23 February 2013].

Tagawa, T. & Bonner, J., 1957. Mechanical properties of the avena coleoptile as related to auxin and to ionic interactions. *Plant Physiology*, 32, 207-212.

Tagawa, K., Tsujimoto, H. & Arnon, D., 1963. Role of chloroplast ferredoxin in the energy conversion process of photosynthesis. *Biochemistry*, 49, 567-572.

Takahashi, R., Ishimaru, Y., Senoura, T. & Nishizawa, N., 2011. The OsNRAMP1 iron transporter is involved in Cd accumulation in rice. *Journal of Experimental Botany*, 62, 4843-50

Tako, E., Reed, S., Budiman, J., Hart, J. & Glahn, R., 2015. Higher iron pearl millet (*Pennisetum glaucum* L.) provides more absorbable iron that is limited by increased polyphenolic content. *Nutrition Journal*, 4, DOI: 10.1186/1475-2891-14-11.

Tamura, K., Dudley, J., Nei, M. & Kumar, S., 2007. MEGA4: Molecular Evolutionary Genetics Analysis (MEGA) software version 4.0. *Molecular Biology and Evolution*, 24, 1596-1599

Tanaka, K., Takio, S. & Satoh, T., 1995. Inactivation of the cystolic Cu/Zn superoxide dismutase induced by copper deficiency in suspension cultured cells of Marchantia paleacer var. diptera. *Journal of Plant Physiology*, 146, 361-365.

Tanno, K. & Willcox, G., 2006. How fast was wheat domesticated? Science, 311, 1886

Tapken, D., & Hollmann, M., 2008. *Arabidopsis thaliana* glutamate receptor ion channel function demonstrated by ion pore transplantation. *Journal of Molecular Biology*, 383, 36-48.

Taylor, R., 2010. *Check soybeans for manganese (Mn) deficiency.* [Online] Available at: http://agdev.anr.udel.edu/weeklycropupdate/?p=2091 [Accessed 7 March 2013].

Tchernitchko, D., Bourgeois, M., Martin, M. E., & Beaumont, C., 2002. Expression of the two mRNA isoforms of the iron transporter Nramp2/DMTI in mice and function of the iron responsive element. *Biochemical Journal*, 363, 449-455.

Terry, N. & Ulrich, A., 1974. Photosynthetic and respiratory CO₂ exchange of sugar-beet leaves as influenced by manganese deficiency. *Crop Science*, 14, 502-504.

Thomine, S., Lelièvre, F., Debarbieux, E., Schroeder, J. I., Barbier-Brygoo, H., 2003. AtNRAMP3, a multispecific vacuolar metal transporter involved in plant responses to iron deficiency. *The Plant Journal*, 34, 685-695.

Thomine, S., Wang, R., Crawford, N. & Schroeder, J., 2000. Cadmium and iron transport by members of a plant metal transporter family in Arabidopsis with homology to NRAMP genes. *PNAS*, 97, 4991-4996.

Toyoshima, C., 2009. How Ca²⁺-ATPase pumps ions across the sarcoplasmic reticulum membrane. Biochimica et Biophysica Acta (BBA) – Molecular Cell Research, 1793, 941-946.

Toyoshima, C., & Mizutani, T., 2004. Crystal structure of the calcium pump with a bound ATP analogue. *Nature*, 430, 529-535.

Toyoshima, C., Nakasako, M., Nomura, H., & Ogawa, H., 2000. Crystal structure of the calcium pump of sarcoplasmic reticulum at 2.6 Å resolution. *Nature*, 405, 647-655.

Toyoshima, C., & Nomura, H., 2002. Structural changes in the calcium pump accompanying the dissociation of calcium. *Nature*, 418, 605-611.

Tuschl, K., Clayton, P. T., Gospe, S. M. Jr, Gulab, S., Ibrahim, S., Singhi, P., Aulakh, R., Ribeiro, R. T., Barsottini, O. G., Zaki, M. S., Del Rosario, M. L., Dyack, S., Price, V., Rideout, A., Gordon, K., Wevers, R. A., Chong, W. K., & Mills, P.B., 2012. Syndrome of hepatic cirrhosis, dystonia, polycythemia, and hypermanganesemia caused by mutations in SLC30A10, a manganese transporter in man. *American Journal of Human Genetics*, 90, 457-466.

Ueno, D., Sasaki, A., Yamaji, N., Miyaji, T., Fujii, Y., Takemoto, Y., Moriyama, S., Che, J., Moriyama, Y., Iwasaki, K., & Ma, J. F, 2015. A polarly localized transporter for efficient manganese uptake in rice. *Nature Plants*, 170, DOI: 10.1038/NPLANTS.2015.170.

Van der Zaal, B. J., Neuteboom, L. W., Pinas, J. E., Chardonnens, A. N., Schat, H., Verkleij, J. A., & Hooykaas, P. J., 1999. Overexpression of a novel Arabidopsis gene related to putative zinctransporter genes from animals can lead to enhanced zinc resistance and accumulation. *Plant Physiology*, 119, 1047-55.

Vatansever, R., Filiz, E. & Ozyigit, I., 2016. In silico analysis of Mn transporters (NRAMP1) in various plant species. *Molecular Biology Reports*, 43, 151-163

Verbruggen, N., Hermans, C. & Schat, H., 2009. Molecular mechanisms of metal hyperaccumulation in plants. *New Phytologist*, 181, 759-776.

Vert., G., Grotz, N., Dédaldéchamp, F., Gaymard, F., Guerinot, M. L., Briat, J-F., & Curie, C., 2002. IRT1, an Arabidopsis transporter essential for iron uptake from the soil and for plant growth. *The Plant Cell*, 14, 1223-1233.

Very, A. & Davis, J., 2000. Hyperpolarisation-activated calcium channels at the tip of Arabidopsis root hairs. *PNAS*, 97, 9801-9806.

Villalba, J.M., Palmgren, M.G., Berberian, G.E., Ferguson, C. & Serrano, R., 1992. Functional expression of plant plasma membrane H⁺-ATPase in yeast endoplasmic reticulum. *Journal of Biological Chemistry*, 267, 12341-12349

Violante, A., Ricciardella, M. & Pigna, M., 2003. Adsorption of heavy metals on mixed Fe-Al oxides in the absence or presence or organic ligands. *Water, Air and Soil Pollution*, 145, 289-306.

Vitale, A., Ceriotti, A. & Denecke, J., 1993. The role of the Endoplasmic Reticulum in protein synthesis, modification and intracellular transport. *Journal of Experimental Botany*, 33, 1417-1444

Vlamis, J. & Williams, D., 1964. Iron and manganese relations in rice and barley. *Plant and Soil*, 2, 221-231.

Wang, Y.H., 2008. How effective is T-DNA insertional mutagenesis in Arabidopsis? *Journal of Biochemical Technology*, 1, 11-20.

Wang, X., Cai, Y., Wang, H., Zeng, Y., Zhuang, X., Li, B. & Jiang, L., 2014. Trans-Golgi network-located AP1 gamma adaptins mediate dileucine motif-directed vacuolar targeting in Arabidopsis. *The Plant Cell*, doi: 10.1105/tpc.144.129759

Wang, F., Chen, Z. H., Liu, X., Colmer, T. D., Zhou, M., & Shabala, S., 2016. Tissue-specific root ion profiling reveals essential roles of the CAX and ACA calcium transport systems in response to hypoxia in Arabidopsis. *Journal of Experimental Botany*, 67, 3747-3762.

Warthmann, N., Chen, H., Ossowski, S., Weigel, D. & Herve, P., 2008. Highly specific gene silencing by artificial miRNAs in rice. *PLoS ONE*, 3, e1829.

Wei, Y. & Fu, D., 2005. Selective metal binding to a membrane-embedded aspartate in the Escherichia coli metal transporter YiiP (FieF). *Journal of Biological Chemistry*, 280, 33716-33724.

Weinstein, L. & Robbins, W., 1955. The effect of different iron and manganese nutrient levels on the catalse and cytochrome oxidase activities of green and albino sunflower leaf tissues. *Plant physiology*, 30.

Welch, R.M. & Shuman, L., 1995. Micronutrient Nutrition of Plants. *Critical Reviews in Plant Science*, 14, 49-82.

Wessells, K. & Brown, K., 2012. Global prevalence of zinc deficiency: results based on zinc availability in national food supplies and the prevalence of stunting. *PLoS ONE*, 7.

White, P. & Broadley, M., 2009. Biofortification of crops with seven mineral elements often lacking in human diets – iron, zinc, copper, calcium, magnesium, selenium and iodine. *New Phytologist*, 182, 49-84.

White, P. & Brown, P., 2010. Plant nutrition for sustainable development and global health. *Annals of Botany*, 105, 1073-1080.

Whiting, S., Neumann, P. & Baker, A., 2003. Nickel and zinc hyperaccumulation by *Alyssum murale* and *Thlaspi caerulescens* (Brassicaceae) do not enhance survival and whole-plant growth under drought stress. *Plant, Cell and Environment*, 26, 351-360.

Wolfe, K., Gouy, M., Yang, Y., Sharp, P. & Li, W., 1989. Date of the monocot-dicot divergence estimated from chloroplast DNA sequence data. *PNAS*, 86, 6201-6205

Wu, Z., Liang, F., Hong, B., Young, J. C., Sussman, M. R., Harper, J. F, & Sze, H., 2002. An endoplasmic reticulum-bound Ca²⁺/Mn²⁺ Pump, ECA1, supports plant growth and confers tolerance to Mn²⁺ stress. *Plant Physiology*, 130, 128–137.

Wunschmann, J., Beck, A., Meyer, L., Letzel, T., Grill, E. & Lendzian, K., 2007. Phytochelatins are synthesized by two vacuolar serine carboxypeptidases in *Saccharomyces cerevisiae*. FEBS Letters, 581, 1681-1687

Xie, Z., Allen, E., Fahlgren, N., Calamar, A., Givan, S. & Carrington, J., 2005. Expression of Arabidopsis *miRNA genes*. *Plant Physiology*, 138, 2145-2154

Xing, J., Wang, T., Liu, Z., Xu, J., Yao, Y., Hu, Z., Peng, H., Xin, M., Yu, F., Zhou, D., & Ni, Z., 2015. GENERAL CONTROL NONREPRESSED PROTEIN5-Mediated histone acetylation of FERRIC REDUCTASE DEFECTIVE3 contributes to iron homeostasis in Arabidopsis. *Plant Physiology*, 168, 1309-1320.

Xu, H., Jin, J., De Felice, L. J., Andrews, N. C., & Clapham, D. E., 2004. A spontaneous, recurrent mutation in divalent metal transporter-1 exposes a calcium entry pathway. *PLoS Biology*, 2, E50.

Yadav, A.K., Shankar, A., Kha, S., Kanwar, P., Pandey, A. & Pandey, G.K., 2015. A rice tonoplastic calcium exchanger, OsCCX2 mediates Ca²⁺/cation transport in yeast. *Scientific Reports*, 5, doi:10.1038/srep17117

Yang, X., Chen, W. & Feng, Y., 2007. Improving human micronutrient nutrition through biofortification in the soil–plant system: China as a case study. *Environmental Geochemistry and Health*, 29, 413-428.

Yang, X., Ye, Z. Q., Shi, Ch. H., Zhu, M. L., & Graham, R. D., 1998. Genotypic differences in concentrations of iron, manganese, copper, and zinc in polished rice grains. *Journal of Plant Nutrition*, 21, 1453-1462.

Yang T. J. W., Perry, P. J., Ciani, S., Pandian, S., & Schmidt, W., 2008. Manganese deficiency alters the patterning and development of root hairs in *Arabidopsis*. *Journal of Experimental Botany*, 3453-3464.

Yu, Q., Osborne, L. & Rengel, Z., 1998. Micronutrient deficiency influences plant growth and activities of superoxide dismutase and ascorbate peroxidase in tobacco plants. *Journal of Plant Nutrition*, 21, 1427-1437.

Yu, Q. & Rengel, Z., 1999. Micronutrient deficiency influences plant growth and activities of superoxide dismutase and ascorbate peroxidase in narrow leaf lupines. *Annals of Botany*, 183, 175-182.

Yuan, Z. & Teasdale, R.D., 2002. Prediction of Golgi Type II membrane proteins based on their transmembrane domains. *Bioinformatics*, 18, 1109-1115

Yuan, Y., Wu, H., Wang, N., Li, J., Zhao, W., Du, J., Wang, D., & Ling, H. Q., 2008. FIT interacts with *AtbHLH38* and *AtbHLH39* in regulating iron uptake gene expression for iron homeostasis in Arabidopsis. *Cell Research*, 18, 385-397.

Yuan, L., Yang, S., Liu, B., Zhang, M., & Wu, K., 2012. Molecular characterization of a rice metal tolerance protein, OsMTP1. *Plant Cell Reports*, 31 67-79.

Zhang, G.F., Driouch, A. & Staehelin, L.A., 1993. Effect of monensin on plant Golgi: re-examination of the monensin-induced changes in cisternal architecture and functional activities of the Golgi apparatus of sycamore suspension-cultured cells. *Journal of Cell Science*, 104, 99.819-831

Zhang, J., Zhang, X., Wang, R., & Li, W., 2014. The plasma membrane-localised Ca²⁺-ATPase ACA8 plays a role in sucrose signalling involved in early seedling development in Arabidopsis. *Plant Cell Reports*, 33, 755-766.

Zhou, X., & Yang, Y., 2004. Differential expression of rice *Nramp* genes in response to pathogen infection, defense signal molecules and metal ions. *Physiological and Molecular Plant Pathology*, 65, 235-243.

Zogzas, C. E., Aschner, M., & Mukhopadhyay, S., 2016. Structural Elements in the Transmembrane and Cytoplasmic Domains of the Metal Transporter SLC30A10 Are Required for Its Manganese Efflux Activity. *The Journal of Biological Chemistry*, 291, 15940-15957

Zwiewka, M., Feraru, E., Moller, B., Hwang, I., Feraru, M., Kleine-Vehn, J., Weijers, D. & Friml, J., 2011. The AP-3 adaptor complex is required for vacuolar function in Arabidopsis. *Cell Research*, 21, 1711-1722